

Green Chemistry

Cutting-edge research for a greener sustainable future

www.rsc.org/greenchem

Volume 12 | Number 1 | January 2010 | Pages 1–180



ISSN 1463-9262

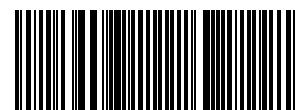
RSC Publishing

Ragauskas *et al.*
Characterization of Kraft lignin

Deetlefs and Seddon
Assessing the greenness of ionic liquid preparations

Thomas, Poliakoff and Benaissi
Solubilisation of α -chymotrypsin

Huisman and Sheldon *et al.*
Green biocatalytic process for atorvastatin



1463-9262(2010)12:1;1-1

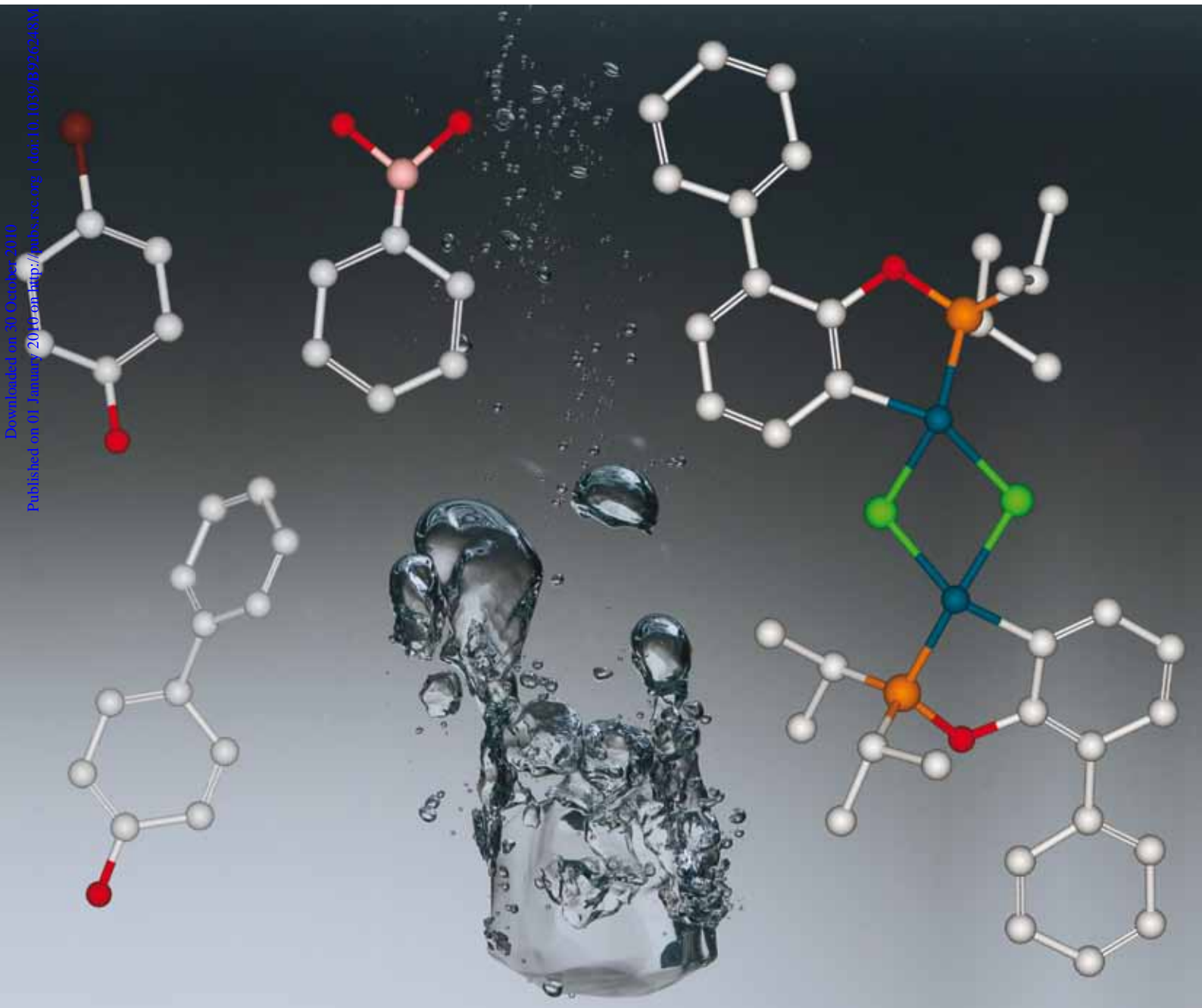
Green Chemistry

Cutting-edge research for a greener sustainable future

www.rsc.org/greenchem

Volume 12 | Number 1 | January 2010 | Pages 1–180

Downloaded on 30 October 2010
Published on 01 January 2010 on http://pubs.rsc.org | doi:10.1039/B926248M



ISSN 1463-9262

RSC Publishing

Eppinger *et al.*
Palladacyclic coupling catalyst

Corma *et al.*
One-pot multistep synthesis of fine
chemicals

Varma *et al.*
Nanoscale zerovalent iron particles

Cadierno, Gimeno and Francos
Ruthenium-catalyzed synthesis of
 β -oxo esters

News from *Green Chemistry* ... the year ahead

DOI: 10.1039/b924137j

Changes to the Editorial Board

At the end of 2009 Janet Scott and Alexei Lapkin finished their terms on our Editorial Board. We would like to thank them for their input into the development of the Journal during their time on the Editorial Board. We also welcome Peter Dunn onto the Editorial Board, who will provide a valuable industry perspective to editorial discussions.

2010 marks the launch of our new Advisory Board for the Journal. This very much enlarged Advisory Board brings together green chemists from across the world to help shape the Journal for the future. We welcome all the new members of the Advisory Board and look forward to working with them.

Editorial policy

From 2010 the Editorial Board has agreed to introduce a new Checklist, which authors must complete when submitting to the Journal. The purpose of the Checklist is to remind authors of the factors that need to be considered when submitting to the Journal. In particular, one of the questions asks the authors to consider the potential environmental impact of the solvents that have been used in their paper—are there greener alternatives that could have been used instead? This question has been added to the Checklist after discussions with the ACS Green Chemistry Institute Pharmaceutical Roundtable, and we would like to thank them for involving the Journal in their discussions. Full details of the new *Green Chemistry* Checklist can be found on the Journal homepage at www.rsc.org/greenchem

Green Chemistry leads the way

In June 2009, Thomson ISI released the 2008 impact factors and *Green Chemistry* has an impact factor of 4.542. Over the

past 4 years the impact factor for the Journal has increased by nearly 40% confirming *Green Chemistry* as the leading Journal in the field. We would like to thank our referees and authors for their contributions to achieving this high impact factor.

1st PACN Green Chemistry Congress

We are very pleased to announce that *Green Chemistry* will be sponsoring the 1st Pan Africa Chemistry Network Green Chemistry Congress that will be held in Ethiopia 15–17th November 2010. This meeting is supported and organised by the RSC, Syngenta and Addis Ababa University. We already have an impressive number of speakers, and we will be adding further speakers over the coming months.

To date, the following green chemists have agreed to speak at the Congress:

Paul Anastas, Yale University, USA
 Colin Brennan, Syngenta, UK
 Bob Crawford, Unilever, UK
 Buxing Han, Chinese Academy of Sciences, Beijing, China
 Walter Leitner, ITMC-RWTH, Germany
 Egid Mubofu, Dar es Salaam, Tanzania
 Vanderlan Bolzani, Sao Paulo State University

Further information about the meeting can be found at www.rsc.org/pacn, and updates will be posted on the Journal homepage.

News from the RSC

New integrated content delivery platform

RSC Publishing is proud to announce the launch of our powerful new content delivery platform that supports multiple content types. Powered by the industry's leading MarkLogic Server, and benefiting from the interactive browsing

functionality offered by RSC's enhanced html mark-up technology, the platform delivers exceptionally fast and precise results. Users can now search 165 years of world-class RSC-hosted content including 20 000 book chapters, 300 000 journal articles and 450 000 database records from a single, simple search. Designed around readers' preferences (identified from a detailed and ongoing user-interview process), our user-friendly platform offers faster browsing, intelligent searching, consistent user experience irrespective of content type sought, and simpler more intuitive navigation. We'll be releasing even more exciting functionality later in the year. Please tell us what you think at rscpublishing@rsc.org

ChemSpider

Last year RSC acquired ChemSpider, the richest single source of structure based chemistry information freely available online, with fast searching of over 21.5 million chemical structures. Alongside the powerful database, the ChemSpider development team brings well over 40 years of additional cheminformatics experience to the RSC, including a chemistry centric document mark-up system capable of finding chemical names and converting to chemical structures and linking to online resources. Integration of this technology with RSC's existing award winning enhanced html mark-up technology, RSC Prospect, will lead to substantial enhancements in semantic enrichment for the chemical sciences. Find out more at www.chemspider.com

Free, fast access to millions of chemical entities

www.chemspider.com



ChemSpider
 Building community for chemists

Continued e-alert success in 2010

2009 saw the launch of the new RSC journal e-alerts; in 2010 we are hoping to see a continued rise in their popularity. The e-alerts are packed with information and links enabling readers to easily view content as soon as it's published, helping them to stay abreast of journal content. The new e-alert registration system has been designed so readers can manage their own subscriptions, tailoring the information they receive and giving them the freedom to unsubscribe at any point. You can find out more information online: www.rsc.org/alerts

New for 2010: the RSC eBook Subject Collections

In response to readers' needs and a testament to the innovation of RSC Publishing, we are pleased to announce the launch of the new RSC eBook Subject Collections.

The nine new RSC eBook Subject Collections, including a Tutorial Chemistry

Texts and Paperbacks package, deliver the high quality content contained in our books into subject specialist packages. With new content being uploaded throughout the year, the new RSC eBook Subject Collections are set to become another key, premier resource. To find out more, please visit www.rsc.org/ebooks

Chemical Science

This new flagship journal will launch in mid-2010, and will publish findings of exceptional significance from across all the chemical sciences. Editor-in-Chief Professor David MacMillan of Princeton leads a dynamic international team of Associate Editors responsible for the scientific development of the journal. Free institutional online access to the entire 2010 and 2011 content of *Chemical Science* will be automatically provided to all existing customers.

Keep in touch with the latest news at www.rsc.org/chemicalscience

...on a related note

RSC is pleased to announce a significant new global symposia series supporting the launch of the *Chemical Science*. The *International Symposia on Advancing the Chemical Sciences (ISACS)* meetings will be held on three continents, over three sequential weeks, focusing on distinct subject areas. More information can be found at: www.rsc.org/isacs

We would like to thank you for your continued support of *Green Chemistry* and wish you a very successful 2010.

Martyn Poliakoff
Editorial Board Chair

Walter Leitner
Scientific Editor

Sarah Ruthven
Editor

Assessing the greenness of some typical laboratory ionic liquid preparations

Maggel Deetlefs* and Kenneth R. Seddon

Received 27th July 2009, Accepted 22nd October 2009

First published as an Advance Article on the web 8th December 2009

DOI: 10.1039/b915049h

The greenness, or lack thereof, of various ionic liquid syntheses and purification methodologies are assessed using a common tool used in strategic planning *viz.* strengths weaknesses opportunities threats (SWOT) analysis, including their adherence to the twelve principles of green chemistry, % atom economies and *E*-factors.

When are ionic liquid syntheses green?

Although ionic liquids still uphold their baptism as 'green', the use of the term, and indeed what constitutes a green ionic liquid synthesis, continues to be misinterpreted. At the heart of the misinterpretation, and many spurious claims, lies the assumption that ionic liquids are green because of their negligible vapour pressure.^{1,2} However, there are many other factors that determine whether an ionic liquid is, or is not, green, particularly the ionic liquid preparation itself (which is generally not considered or reported in the literature). It is also often overlooked that the very designer classification³ of ionic liquids means that they can be engineered to possess distinctly 'non-green' attributes (*viz.* toxicity, explosivity,⁴ non-biodegradability, *etc.*), and they can be (and have been) obtained by distinctly dirty procedures (*e.g.* using harmful organic solvents). In other words, the term 'green' should only be applied to an ionic liquid if both the ionic liquid, and the process used to produce it are green, *i.e.* if all twelve principles of green chemistry apply (Fig. 1).⁵

The twelve principles of green chemistry have been formalised and extensively promoted since the 1990s by their progenitor, Prof. Paul Anastas,^{5,6} and, recently, were elegantly condensed by Prof. Martyn Poliakoff and co-workers into a mnemonic for easy communication, *viz.* PRODUCTIVELY.⁷ Undeniably,

it is challenging for a chemical process to incorporate all twelve principles of green chemistry, but the *sine qua non* is that it must always be crystal-clear whether a reported process is truly green, or whether only parts of it are green. Needless to say, the same overarching green approach should apply to ionic liquid syntheses too, and it must thus be spelled out, especially in the open literature, what exactly is green about the ionic liquid and/or its preparation or use, if anything at all.

Since many excellent reviews^{8–11} already exist that describe various ionic liquid syntheses and purifications, here we have confined ourselves to assessing the 'greenness' of some common, laboratory-scale ionic liquid preparative methods *i.e.* purification procedures (Fig. 2)¹² and synthetic routes (Fig. 3).^{9,12,13} Although it would be desirable to assess ionic liquid preparations conducted at the industrial scale, the information is not available for a credible study. Moreover, we have only assessed the preparative routes themselves and have not considered the fate¹⁴ of the ionic liquid starting materials or products.

In addition, we have also gauged the relative pros and cons of using differing energy sources to promote ionic liquid syntheses, *viz.* conductive (conventional) heating, microwave irradiation, ultrasonic irradiation, and simultaneous microwave and ultrasonic irradiation. For convenience, we have concentrated on ionic liquids containing 1-alkyl-3-methylimidazolium cations, [C_nmim]⁺.

Although many other synthetic routes are also available to prepare ionic liquids, *e.g.* carbene¹⁵ and alkylsulfate^{9,16} routes, the

The QUILL Research Centre, David Keir Building, Stranmillis Road, Belfast, BT9 5AG, UK. E-mail: quill@qub.ac.uk



Maggel Deetlefs

Maggel joined the QUILL Research Centre as a post-doctoral researcher in 2001 and has since advanced to the position of Assistant Director, with the dual-purpose of managing the Centre and maintaining her own research portfolio. Her research interests focus on the green synthesis and applications of ionic liquids, including purpose-specific design and developing simple methods to predict their physical properties.



Ken Seddon

Ken Seddon was appointed as chair of Inorganic Chemistry at the Queen's University of Belfast in 1993, where in 1999, he also co-founded the QUILL Centre with Prof. W. J. Swindall OBE. The QUILL Centre currently has a complement of 89 staff, including 64 research staff, students and technicians, as well as 14 associated academics. For more details about Ken, Maggel, and QUILL see <http://quill.qub.ac.uk>

The Twelve Principles of Green Chemistry

1. It is better to prevent waste than to treat or clean up waste after it has formed.
2. Synthetic methods should be designed to maximise the incorporation of all materials used in the process into the final product.
3. Wherever practicable, synthetic methodologies should be designed to use and generate substances that possess little or no toxicity to human health and the environment.
4. Chemical products should be designed to preserve efficacy of function while reducing toxicity.
5. The use of auxiliary substances (*e.g.* solvents, separation agents *etc.*) should be made unnecessary wherever possible and innocuous when used.
6. Energy requirements should be recognised for their environmental and economic impacts and should be minimised. Synthetic methods should be conducted at ambient temperature and pressure.
7. A raw material of feedstock should be renewable rather than depleting wherever technically and economically practicable.
8. Unnecessary derivatisation (blocking group, protection/deprotection, temporary modification of physical/chemical processes) should be avoided whenever possible.
9. Catalytic reagents (as selective as possible) are superior to stoichiometric reagents.
10. Chemical products should be designed so that, at the end of their function, they do not persist in the environment, and break down into innocuous degradation products.
11. Analytical methodologies need to be further developed to allow for real-time, in-process monitoring and control prior to the formation of hazardous substances.
12. Substances and the form of a substance used in a chemical process should be chosen so as to minimise the potential for chemical accidents, including releases, explosions and fires.

Fig. 1 The twelve principles of green chemistry.⁵

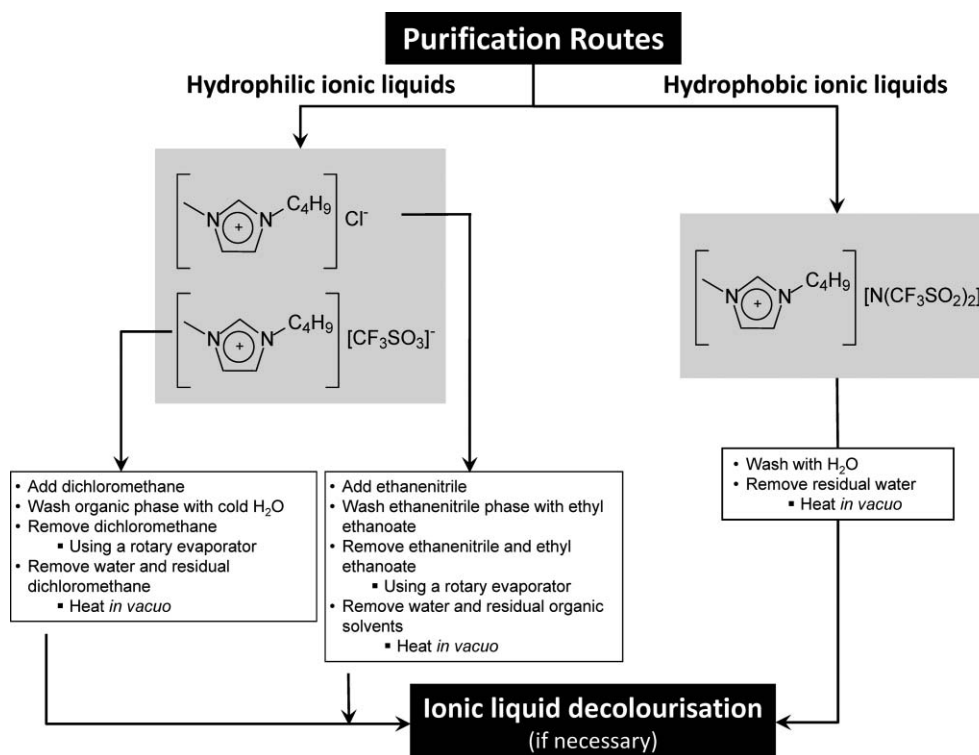


Fig. 2 Typical ionic liquid purification routes.¹²

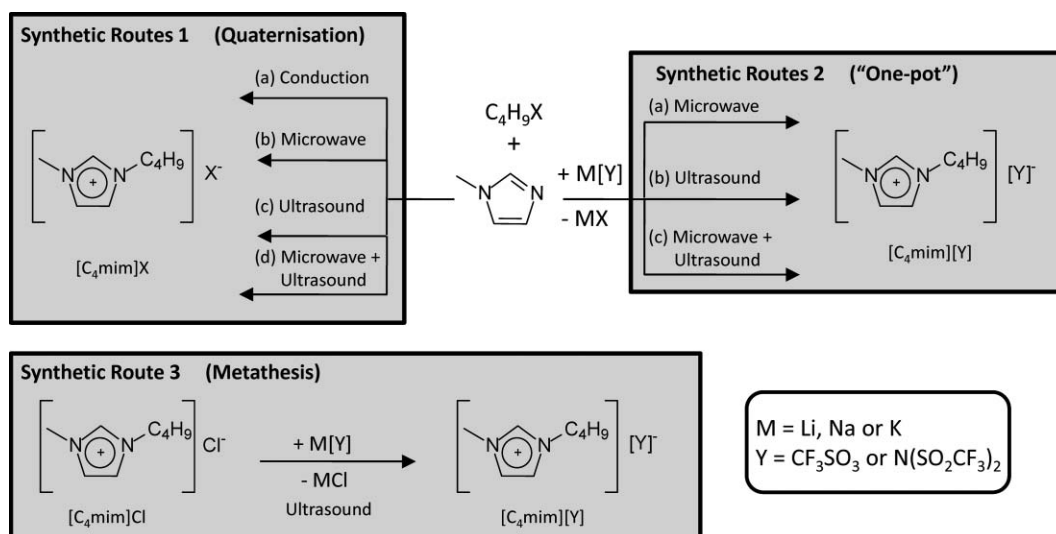


Fig. 3 Typical ionic liquid synthetic routes.

general principles outlined here apply only to the hydrophobic and hydrophilic synthetic procedures discussed, but the method of analysis could be applied.

The scales of justice

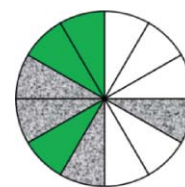
The assessment of the greenness of ionic liquid syntheses is a question of scale, and size really matters! This is because the greenness factors associated with laboratory-scale ionic liquid preparations are quite different than those that are relevant to industrial-scale syntheses. For example, in industrial-scale processes, excess 1-haloalkanes are typically recycled, whereas in the laboratory they are usually discarded. Another example is that on an industrial scale, the use of conductive heating (e.g. superheated steam) is more convenient, energy efficient and economical than employing microwave irradiation, while the opposite is true for laboratory-scale preparations.¹⁷ Therefore, according to the 6th principle of green chemistry, industrial-scale ionic liquid preparations are greener than their laboratory-scale cousins.

It is important to re-emphasise that in this paper, all greenness arguments are focussed solely on the preparative steps of laboratory-scale ionic liquid preparations (<2 kg). Although our approach will be expanded in the future to include a cradle-to-grave approach for both small and large scales preparations, our primary aim was to first develop a user-friendly greenness assessment protocol. As more information becomes available for large scale ionic liquid syntheses, our evaluation protocol will be extended to gauge the greenness of industrial scale ionic liquid preparations by including, for example, the twelve principles of green engineering⁶ in our assessments, as well as quantitative considerations of energy efficiency using different heating sources. Ultimately, we envisage that our greenness analyses will also incorporate life cycle assessments, which take into account the greenness of ionic liquid starting materials plus the ionic liquid product itself.

What principles of green chemistry are relevant to typical ionic liquid preparations?

Of the twelve principles of green chemistry, the 4th, 7th, 9th and 10th principles⁵ are irrelevant to the laboratory-scale ionic liquid preparations discussed here. This is because the 4th, 7th and 10th principles of green chemistry apply to the ionic liquid product itself rather than the procedure, while the 9th principle is associated with catalytic methodologies and hence is also not relevant to the typical ionic liquid preparations summarised in Fig. 2 and 3. In contrast, the 8th, 11th and 12th principles of green chemistry apply to all the ionic liquid syntheses discussed here since (i) derivatisation (8th principle) is not used in any of the ionic liquid syntheses, (ii) in-process monitoring (11th principle), although currently under development (e.g. lab-on-a-chip),¹⁸ is not yet ready for implementation, and (iii) ionic liquids, by virtue of their negligible vapour pressure, minimise the potential for chemical accidents such as fires and explosions (12th principle). To summarise, only eight of the twelve principles of green chemistry are relevant to the synthetic procedures discussed here, *viz.* 1st, 2nd, 3rd, 5th, 6th, 8th, 11th and 12th.

Although, strictly speaking, the twelve principles of green chemistry only apply to synthetic procedures, the 1st, 5th, 6th and 12th principles are relevant to ionic liquid purification procedures and, therefore, we have assessed the purification of the salts according to these four principles too.



Atom economy and the E-factor

In addition to applying the twelve principles of green chemistry to evaluate the green credentials of ionic liquid syntheses and purifications, these methods can also be assessed using two additional measures, *viz.* atom economy¹⁹ and the *E*-factor.²⁰

Atom economy (also known as atom efficiency) provides, for a given reaction, the ratio between the mass of the atoms

making up the final product(s) and the mass of the atoms that are incorporated in all the reactants, eqn (1). It should be noted that the atom economy is a theoretical construct based solely on the stoichiometry of a given reaction, and assumes 100% yield. Stated more simply, atom economy measures how many of the atoms present in the starting materials form part of the final product, and is reported as a percentage value with those values closest to 100% reflecting superior atom economies. For example, the preparation of 1-alkyl-3-methylimidazolium halide salts using quaternisation (Routes 1(a)–(d), Fig. 2) are 100% atom efficient, regardless of the yield obtained, since no by-products are formed. On the other hand, ionic liquids prepared using one-pot (Routes 2(a)–(c), Fig. 2) or metathesis reactions (Route 3, Fig. 2) will be <100% atom efficient since a stoichiometric amount of MCl waste is generated.

$$\% \text{Atom economy} = \frac{\text{Molecular weight of desired product(s)}}{\text{Sum of molecular weight of all reagents}} * 100 \quad (1)$$

The problem with employing atom economy to evaluate the green credentials of a reaction is that it does not take into account that some reactions with favourable stoichiometries require large excesses of reagents, give poor yields, and often generate large amounts of unwanted by-products. This, of course, highlights the basic flavour in the atom economy concept, *viz.* it is necessary but not sufficient, since a reaction giving 0.5% yield can still be described as 100% atom efficient. As a result, the *E*-factor concept was introduced, where all compounds that are not product are classified as waste. The nature of the *E*-factor equation, eqn (2), dictates that the greenest chemical reactions have *E*-factor values close to zero. In brief, the *E*-factor gives a much truer reflection of the greenness of a chemical reaction than atom economy, since all generated waste is accounted for.

$$E\text{-factor} = \frac{\text{Amount of waste produced in the process/kg}}{\text{Amount of the desired product(s) produced in the process/kg}} \quad (2)$$

The ‘ideal’ *E*-factor is reflected in the 2nd principle of green chemistry that states: ‘*Synthetic methods should be designed to maximise the incorporation of all materials used in the process into the final product*’.⁵ In other words, for a chemical process to have an *E*-factor of zero, all materials used in a process (and not just the reagents) should be contained in the final product if the process is truly green.

If we necessarily assume the process of producing an ionic liquid is the process of producing a pure, isolated ionic liquid, then the *E*-factor for the process, which combines Fig. 2 and Fig. 3, must be considered. Although every chemical reaction will have its own unique % atom economy and *E*-factor, to simplify discussion, the atom economies and *E*-factors associated with ionic liquid preparations and purifications (Fig. 2 and 3) have respectively been designated as low/medium/high and poor/good/excellent, since the literature has rarely given enough detail to allow definitive values to be assigned.

Strengths, weaknesses, opportunities and threats (SWOT) analyses

In order to simultaneously assess the green credentials of the selected synthetic and purification procedures of ionic liquids in terms of the twelve principles of green chemistry, atom economy, and the *E*-factor, we have applied a common tool used in strategic planning, *viz.* strengths, weaknesses, opportunities, threats (SWOT) analysis.²¹ For ionic liquid preparation and purification methods, SWOT analyses involve specifying the objective(s) of a given procedure (*e.g.* obtaining an ionic liquid that is >99% pure) and identifying the internal and external factors that are favourable and unfavourable to achieving that objective. Thus, SWOT analyses give an overview of the relative advantages or disadvantages of ionic liquid syntheses and purifications. In brief, the SWOT analyses provided here (represented skeletally in Fig. 4) give a measure of the balance between good and bad for some common ionic liquid preparation and purification procedures, and indicate potential directions for improving these methods.

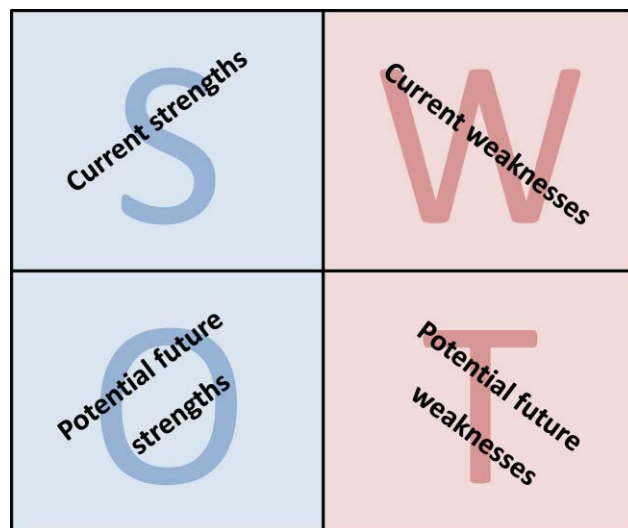


Fig. 4 Skeletal strengths weaknesses opportunities threats (SWOT) analysis.

Greenness assessment: traditional synthesis of 1-alkyl-3-methylimidazolium halide salts

It is safe to say that the methods used to prepare 1-alkyl-3-methylimidazolium halide salts¹¹ have changed very little since they were first reported in 1982;²² most reported syntheses still involve reaction of 1-methylimidazole with an excess of 1-haloalkane and are promoted using conductive heating, Route 1(a), Fig. 2. However, from a green chemistry perspective, much room for improvement exists in the syntheses of 1-alkyl-3-methylimidazolium halide salts, particularly regarding the use of more efficient energy sources and reducing/eliminating the need for organic solvents during both synthesis and purification; all these issues are discussed below.

The literature shows that the vast majority of 1-alkyl-3-methylimidazolium halide salt preparations are executed using traditional heating under reflux, although nowadays an atmo-

sphere of dry dinitrogen is sometimes used since it has been found to promote the production of colourless ionic liquids¹¹ and also prevents the formation of hydrated halide salts from adventitious water.²³

Almost without exception, reported preparations of 1-alkyl-3-methylimidazolium halide salts use an excess of 1-haloalkane,²⁴ which means that the reactions are not in line with the 2nd principle of green chemistry that states: 'Synthetic methods should be designed to maximize the incorporation of all materials used in the process into the final product'.⁵ It also means that although the preparations of the halide salts are 100% atom efficient, with every atom of the starting materials being incorporated into the final product, their *E*-factors are very poor, since excess 1-haloalkane is required to promote completion of the reactions at a reasonable rate. It also follows that the smaller the excess of 1-haloalkane, the lower the *E*-factor value will be, provided no organic solvent is used during the preparation. For example, the *E*-factors for the preparation of [C₄mim]Cl (molar mass = 174.1 g mol⁻¹) are 0.106 and 0.005 when 20% and 1% mol excesses of 1-chlorobutane (molar mass = 92.56 g mol⁻¹) are employed, respectively.

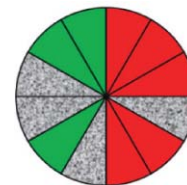
Some reported syntheses of 1-alkyl-3-methylimidazolium halide salts also make use of an organic solvent;²⁵ to reduce the viscosity of the reaction mixture and thus improve mass transfer, but also to control the reaction temperature and prevent product scrambling.²⁶ However, the employed molecular solvent, as well as the employed excess of 1-haloalkane, require removal and subsequent disposal, which also do not comply with the 1st principle of green chemistry that states: 'It is better to prevent waste than to treat or clean up waste after it has formed'.⁵ Therefore, the practice of employing an organic solvent during the preparation of 1-alkyl-3-methylimidazolium halide salts further increases the *E*-factor and is highly undesirable. For example, if 100 g of toluene is used during the synthesis of [C₄mim]Cl (and using a 20 mol% excess of 1-chlorobutane), the *E*-factor increases from 0.106 to 0.681.

The 5th principle of green chemistry states that: 'The use of auxiliary substances (e.g. solvents, separation agents, etc.) should be made unnecessary wherever possible and innocuous when used',⁵ which means that, ideally, no solvent should be used during preparation, but if a solvent is to be used, it must be green and recycled. In order to align with the 1st, 2nd and 5th principles of green chemistry, and have low *E*-factor values, neither an excess of 1-haloalkane nor organic solvent should be used during the synthesis of 1-alkyl-3-methylimidazolium halide salts.

The use of conductive heating (usually an oil bath or heating mantle) to prepare 1-alkyl-3-methylimidazolium halide salts is also in opposition with the 6th principle of green chemistry that states: 'Energy requirements should be recognized for their environmental and economic impacts and should be minimised. Synthetic methods should be conducted at ambient temperature and pressure'.⁵ Therefore, since conductive heating is slow, it is also energy inefficient because the transfer of heat from the heat source to the reaction mixture depends on the thermal conductivities of all the materials that must be penetrated such as the flask and solvent. In contrast, microwave-promoted ionic liquid preparations require lower (heating) energy inputs since microwaves penetrate the reaction mixture directly and are not limited by the thermal conductivities of the reaction

flask, for example. Therefore, microwave-promoted preparations align better with the 6th principle of green chemistry than conventionally-heated ionic liquid syntheses.

When all the above-mentioned negative factors associated with the traditional syntheses of 1-alkyl-3-methylimidazolium halide ionic liquids are considered, it is safe to say that their preparations are not green. Indeed, of the eight relevant principles of green chemistry, they only comply with three principles (*viz.* the 8th, 11th and 12th) which apply to all the ionic liquid syntheses discussed here anyway. On the other hand, the *E*-factors for the preparations fall between good and excellent, provided excess 1-haloalkane is kept to a minimum and no harmful organic solvent is used during the preparation, and any solvent that is used is recycled. As a whole, however, the conductively-heated preparations of 1-alkyl-3-methylimidazolium halide salts possess a lot of room for improvement, as indicated by their SWOT analysis (*vide infra*).



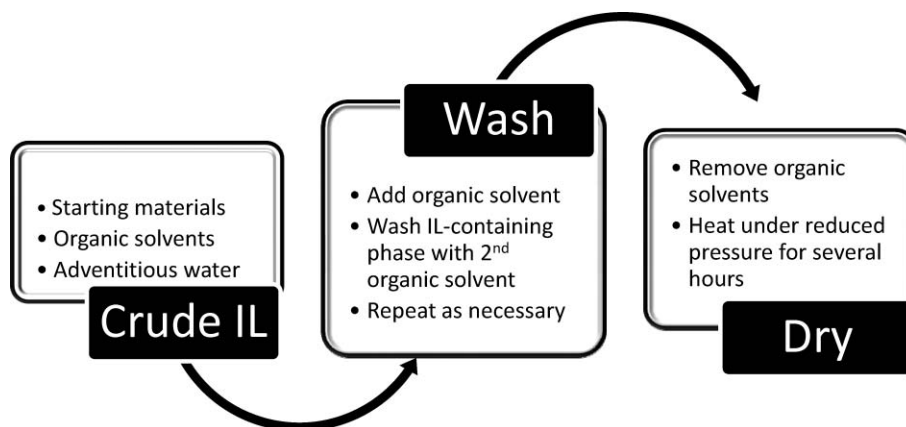
Greenness assessment: purification of 1-alkyl-3-methylimidazolium halide salts

The purifications of 1-alkyl-3-methylimidazolium halide salts (Scheme 1) are generally dirty, with poor *E*-factors, since the excess 1-haloalkane, unconverted 1-methylimidazole, as well as any solvent used during their preparation, require removal and are thus out of line with the 5th principle of green chemistry.⁵

In our laboratories, removal of the excess 1-haloalkane and unconverted 1-methylimidazole is typically achieved by first adding a solvent such as ethanenitrile to the crude ionic liquid mixture and then repeatedly washing this phase with ethyl ethanoate. Once the washing process is complete, the two organic solvents are removed under reduced pressure (using a rotary evaporator). Since the amount of organic solvent used for the purification, as well as the excess of reagents, are classified as waste in the *E*-factor equation, the more of each that is used, the higher the *E*-factor will be for a given purification procedure.

In less experienced groups, the purification of 1-alkyl-3-methylimidazolium halide salts is often performed on the bench, and thus the salts absorb water from the atmosphere, that also requires removal. It must be noted, however, that this adventitious water cannot be completely removed from ionic liquids containing halide anions (especially chloride), as they form, typically, very stable hydrates (see, for example, Fig. 5).²³

Therefore, if water-free ionic liquids containing halide ions are desired, their preparation and purification must be conducted under strictly anhydrous conditions from start to finish, *e.g.* using Schlenk techniques, with rigorously predried reagents. Nevertheless, some adventitious water can be removed by heating 1-alkyl-3-methylimidazolium halide salts under reduced pressure at *ca.* 70 °C for several hours. Almost needless to say, removing water in this way requires a large energy input and thus contributes further to the green inefficiency (*via* non-compliance with the 6th principle of green chemistry)⁵ of the purification of 1-alkyl-3-methylimidazolium halide salts. Indeed, the purification of 1-alkyl-3-methylimidazolium halide salts, as



Scheme 1 Schematic for the purification of [C₄mim]X ionic liquids.

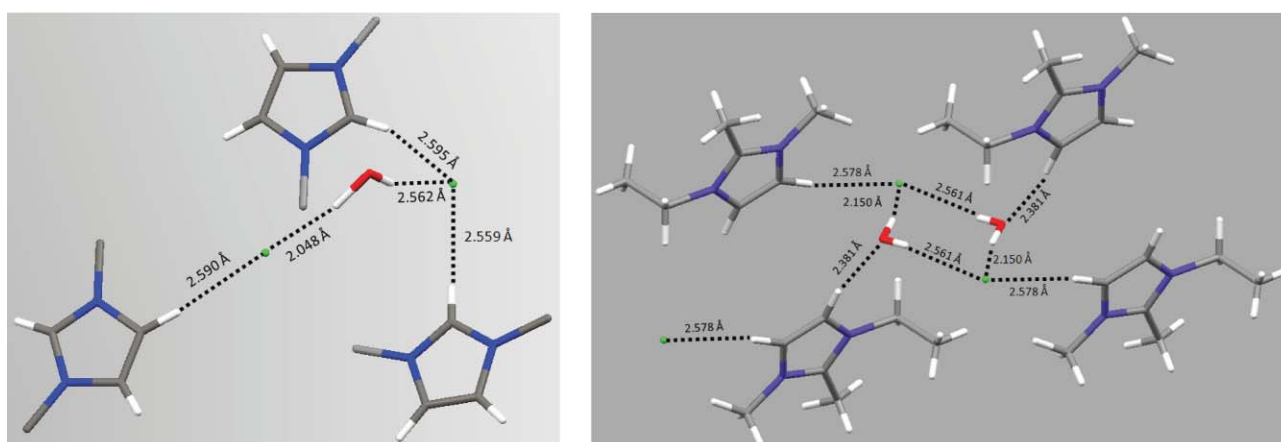


Fig. 5 Structures of 1,3-dimethylimidazolium chloride hemihydrate (left) and 1,2-dimethyl-3-ethylimidazolium chloride hemihydrate (right) showing hydrogen bonding (dashed lines), as determined by single crystal X-ray diffraction.²³

summarised in Scheme 1, complies with none of the relevant principles of green chemistry *viz.* the 1st, 5th, 6th and 12th.

SWOT analysis: conductively-heated preparation of 1-alkyl-3-methylimidazolium halide salts and their subsequent purification

Examination of the SWOT analysis for the preparation of 1-alkyl-3-methylimidazolium halide salts using conductive heating and their subsequent purification (Fig. 6) shows that the overall methodology is dirty. Nevertheless, the procedure possesses some strengths, *viz.* the processes are well-established, simple, can be performed in even the most basic of laboratories to produce the salts on a small to medium scale (<1 kg), and possess 100% atom economies. On the other hand, both the preparations and purifications share the weakness of poor *E*-factors, since extensive purification is necessary to remove the excess of 1-haloalkane employed, which generates large volumes of solvent waste. Further weaknesses are that large-scale preparations (>1 kg) and purifications are laborious, and the use of conductive heating to promote the reactions, as well as to remove some residual water and organic solvents, is slow and energy inefficient. All the aforementioned weaknesses show that opportunities exist to develop a greener methodology to prepare pure 1-alkyl-3-

<p>i. Well-established methodology</p> <p>ii. Simple</p> <p>iii. Useful for laboratory scale preparations</p> <p>iv. High atom economy</p>	<p>i. Long syntheses</p> <p>ii. Excess 1-haloalkane used</p> <p>iii. Poor E-factor</p> <p>iv. Inconvenient for large-scale procedures</p> <p>v. Laborious purification</p> <p>vi. Large volumes of waste solvent generated</p>
<p>i. Green process development</p> <p>ii. Eliminate/reduce use of organic solvents</p> <p>iii. Identify green solvent replacements</p>	<p>i. REACH legislation</p> <p>ii. Starting material cost rises</p>

Fig. 6 SWOT analysis: conductively-heated preparation of 1-alkyl-3-methylimidazolium halide salts and their subsequent purification.

methylimidazolium halide salts using conductive heating, and thus reduce the costs of their manufacture, especially on large scales.

At present, the implementation of REACH (registration, evaluation, authorisation and restriction of chemicals)²⁷ legislation is a threat to the continued low-cost manufacturer of many chemicals, but especially for new products, since they require a large initial financial investment. Therefore, research scientists aiming to develop any new industrial-scale ionic liquid synthesis need to be extremely familiar with REACH legislation in order to achieve their aim. A further threat that exists for the synthesis of 1-alkyl-3-methylimidazolium halide salts using conductive heating is that starting material costs will undoubtedly rise and, therefore, the challenge facing chemists is to render preparations greener and concomitantly cheaper.

Greenness assessment: ionic liquid syntheses promoted by microwave irradiation

It has long been recognised that much more efficient energy sources exist to promote chemical reactions than conductive heating. In particular, microwave irradiation,^{13,28–31} has started to attract attention for the preparation of ionic liquids (Routes 1(b) and 2(a), Fig. 3), and a wide variety of ionic liquids have been prepared to date using microwave reactors.³²

The promotion of 1-alkyl-3-methylimidazolium halide syntheses using microwave irradiation is favoured by an ionic conduction heating mechanism.³⁰ This is because ionic liquids absorb microwave irradiation not only by a dipole rotation mechanism, but they also oscillate back and forth under the influence of the electric field of the microwave.^{13,30} These 'ionic oscillations' result in collisions with neighbouring ions and molecules, which generate heat, and thus speed up the reaction. In other words, the more ionic liquid product that has formed during a given preparation, the faster the reaction will proceed. In brief, microwave irradiation repre-

sents a far more efficient mode of heating to prepare ionic liquids than conductively-heated syntheses. In other words, ionic liquids represent a superlative method for microwave heating.

At present, the implementation of microwave irradiation to prepare ionic liquids continues to evolve, but a question that remains unanswered is: how much greener are microwave-promoted preparations than traditional methods? From a very simplistic standpoint, tremendous energy savings have already been demonstrated for laboratory-scale ionic liquid syntheses,^{13,29} since microwave-promoted reactions occur far more rapidly than the same preparations performed using conductive heating. This strongly aligns with the 6th principle of green chemistry⁵ by keeping the energy input of the syntheses to a minimum.

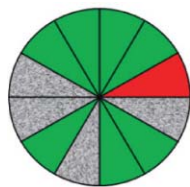
The first papers describing microwave syntheses of ionic liquids employed domestic microwave ovens that offered no temperature and pressure control and thus gave irreproducible results.^{31–33} Since then, more reliable results have been obtained using commercial microwave reactors (Fig. 7), which have allowed the temperature and pressure of reactions to be moderated, rendering the procedures far safer and more reproducible than their domestic predecessors.³⁴

It is worth noting that while the first reports describing microwave-assisted ionic liquid syntheses focussed on their preparation *via* quaternisation (Route 1(b), Fig. 3), later reports^{33,35,36} showed that a one-pot approach (Route 2(a), Fig. 3) could also be used. Since the microwave-assisted procedures require much smaller 1-haloalkane excesses (~1 mol%) compared to conventional preparations (up to 400 mol%),²⁴ they align well with the 1st principle of green chemistry and their *E*-factors are far superior to traditional synthetic routes, especially conducted in the absence of additional solvent. In other words, if no organic solvent is used during the synthesis, the

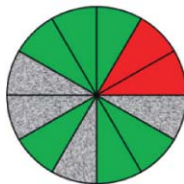


Fig. 7 Commercially available microwave reactors for batch synthesis (left) and for continuous flow synthesis (right). Photographs courtesy of Milestone s.r.l., Sorisole, BG, Italy.

preparations also align with the 2nd principle of green chemistry and the best *E*-factors for the preparations are obtained. In brief, the microwave-assisted syntheses of 1-alkyl-3-methylimidazolium halide salts comply with seven of the eight relevant principles of green chemistry (*viz.* the 1st, 2nd, 5th, 6th, 8th, 11th and 12th) while the analogous one-pot microwave-assisted syntheses align with six (*viz.* the 1st, 5th, 6th, 8th,



11th and 12th). It must be noted that although the one-pot microwave-assisted ionic liquid syntheses generate a stoichiometric amount of MX waste (*e.g.* NaCl), the waste salt is far less harmful/toxic and straightforward to dispose of compared to 1-haloalkane waste and thus the methodology aligns reasonably well with the 1st principle of green chemistry too.



Microwave-assisted *vs.* traditional ionic liquid preparations

The superior *E*-factors and energy efficiencies of microwave-assisted syntheses of ionic liquids show that they are far greener than conductively-heated preparations. However, the 'degree of greenness' depends on (i) the type of quaternisation being performed, since the kinetics of the reaction typically follow the order: $C_nH_{2n+1}Cl < C_nH_{2n+1}Br < C_nH_{2n+1}I$, (ii) the 1-haloalkane excess required to achieve complete conversion to product, (iii) the scale of the reaction, and (iv) whether any solvent is necessary to reduce the viscosity and/or reduce product scrambling.²⁶ The proviso for the use of solvent in terms of green chemistry is that the solvent itself will have to be green (*e.g.* ethanol) and/or recycled to uphold the overall green credentials of a given preparation.

The preparation of ionic liquids on scales >2 kg also requires special consideration, as this is moving from bench scale to semi-pilot plant scales. However, at semi-pilot plant scale, the twelve principles of green engineering⁶ must also be considered, but this falls outside the scope of this review. Nevertheless, current indications are that continuous flow reactors (see Fig. 7) represent the way forward in producing ionic liquids on large scales.^{32,37}

SWOT analysis: microwave-promoted syntheses of ionic liquids

The SWOT analysis for the preparation of ionic liquids using microwave irradiation is shown in Fig. 8.

The greatest green strengths of performing microwave-assisted ionic liquid preparations on a laboratory scale are the energy reduction by virtue of reduced reaction times and low 1-haloalkane excesses. Further strengths are that (i) different microwave reactors³⁰ can be employed to execute the preparations on different scales,³² (ii) syntheses can be performed solvent-free, (iii) the reactions are 100% atom efficient and (iv) have excellent (low) *E*-factor values compared to traditional

<p>S</p> <ul style="list-style-type: none"> i. Rapid ii. Energy efficient iii. Flexible reaction scales iv. Solvent-free synthesis v. High atom economy vi. Excellent E-factor 	<p>W</p> <ul style="list-style-type: none"> i. Lack of energy efficiency data ii. Expensive apparatus iii. Ionic liquid discolouration iv. Ionic liquid decomposition v. Mass transfer issues vi. Scale-up very expensive
<p>O</p> <ul style="list-style-type: none"> i. Green process development ii. Quantitative energy input data iii. Reactor design iv. Intellectual property 	<p>T</p> <ul style="list-style-type: none"> i. Expensive operation ii. <i>In-situ</i> reaction monitoring iii. Safety controls

Fig. 8 SWOT analysis for the preparation of ionic liquids using microwave irradiation.

preparations. All these strengths render the microwave-promoted syntheses of ionic liquids very green indeed.

Weaknesses associated with microwave-assisted preparation of ionic liquids are:

- Currently, there is a lack of energy efficiency data for syntheses *vs.* other methodologies
- Microwave reactors are expensive compared to traditional synthetic apparatus
- Discoloured ionic liquids are sometimes obtained at temperatures >75 °C³⁸
- Ionic liquids decompose if overheated^{13,26,39}
- The high viscosity of ionic liquids can produce mass transport problems during synthesis
- The scale-up of the syntheses is very expensive.

Despite the weaknesses mentioned above, opportunities exist for the development of green microwave reactor technology to produce ionic liquids. One major opportunity is green process development by establishing quantitative energy input data to definitively assess the greenness of microwave-assisted preparations *vs.* other methodologies. Another opportunity is the design and manufacture of custom-made reactors to produce ionic liquids on large scales.³⁷ Both these opportunities may generate valuable intellectual property and could also reduce the cost of producing ionic liquids on large scales.

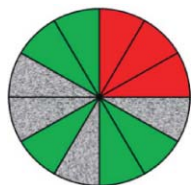
The largest threat to the development of microwave technology to produce ionic liquids on large scales by continuous flow is that it proves too expensive. Further threats include the inability, *via* design constraints, to incorporate *in situ* reaction monitoring (which aligns with the 11th principle of green chemistry) and the inability (albeit unlikely) to incorporate safety controls in industrial reactors to produce ionic liquids on large scales (which aligns with the 12th principle of green chemistry). Also, the low penetration of microwaves limits the size of the reactor; syntheses of over 2 kg will require a flow system.

Greenness assessment: syntheses of ionic liquids promoted by ultrasonic irradiation

At about the same time that the first reports describing the microwave-assisted preparations of ionic liquids were published, reports also began to appear describing ultrasound-promoted preparations of ionic liquids.^{40,41}

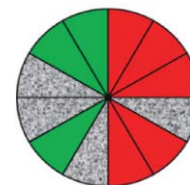
The promotion of chemical reactions with ultrasound is due to a physical phenomenon known as cavitation, which is the formation, growth, and implosive collapse of bubbles in a liquid.⁴² The collapse or implosion of such bubbles results in some fascinating physical effects, which include the formation of localised 'hotspots' in an elastic liquid and reduction of bubble size.⁴³ In terms of ionic liquid synthesis, the formation of hotspots favours quaternisations (Route 1(c), Fig. 3), while the reduction of bubble size favours both quaternisations and metathesis (Route 3, Fig. 3)⁴⁰ since improved mass transport overcomes the viscosity issues generally associated with ionic liquid syntheses. Hotspot formation, bubble size reduction and the reduced preparation times compared to traditional methods all combine to speed up ionic liquid syntheses, and thus represent a significant green advantage, especially if the preparations are performed solvent-free. Indeed, it is worth noting that at present, the majority of papers describing ultrasound-promoted syntheses of ionic liquids have focussed on 'one-pot' reactions (Route 2(b), Fig. 3).

Despite the apparent green advantages of ultrasound-assisted ionic liquid preparations, a phenomenon which renders these preparations inadequate is that, almost without exception, ionic liquids discolour and decompose when exposed to ultrasonic irradiation for the time required to obtain acceptable conversions.^{44,45} Needless to say, this decomposition of ionic liquids is a severe disadvantage to the successful and widespread implementation of the technology and, from a green chemistry perspective, does not align with the 1st principle of green chemistry, since very dirty purification and decolourisation of the salts is required, which also gives very poor *E*-factors. In addition, in a recent review, the highest reported tabulated yields to produce 1-alkyl-3-methylimidazolium halides and similar salts without halide anions are 95 and 90%, respectively.⁴⁶ This contrasts with yields of >99% obtained by thermally-induced and microwave-assisted preparations, rendering ultrasound-assisted ionic liquid syntheses far less green.



Although ultrasound-assisted syntheses of 1-alkyl-3-methylimidazolium ionic liquids (Route 1(c) and 2(b), Fig. 3) comply with five of the eight relevant principles of green chemistry (*viz.* the 5th, 6th, 8th, 11th and 12th), they do not follow the 1st and 2nd principles, since they give poor yields (compared to thermal and microwave routes), and the ionic liquid products require extensive purification. This is especially true for ionic liquids prepared by anion exchange under the influence of ultrasonic irradiation (Route 3, Fig. 3), which only comply with three of the eight (*viz.* 8th, 11th and 12th) principles of green chemistry, and these are met by all ionic liquid preparations anyway. All the ultrasound-assisted ionic

liquid syntheses considered here have poor *E*-factors too and thus are not as green as their microwave-assisted analogues.



SWOT analysis: ultrasound-promoted syntheses of ionic liquids

The SWOT analysis for the preparation of ionic liquids promoted by ultrasonic irradiation (Fig. 9) reveals that its unique strength (compared to traditional and microwave-assisted syntheses) is improved mass transport. However, almost without exception, the preparations have very poor *E*-factors due to the discoloured ionic liquid products, which require extensive purification and decolourisation efforts that produce large volumes of organic solvent and solid waste (*vide supra*). In addition to the major weakness of a poor *E*-factor, other weaknesses of ultrasound-assisted ionic liquid syntheses include the lack of quantitative energy efficiency data, the cost of the apparatus, and the lack of demonstrated large-scale production. It must be pointed out that ionic liquid discolouration is far more severe under ultrasonic conditions than under microwave irradiation and, furthermore, the salts decompose under even mild ultrasonic conditions.⁴⁴

<p>S</p> <ul style="list-style-type: none"> i. Rapid ii. Energy efficient iii. Good mass transport iv. Solvent-free synthesis v. High atom economy 	<p>W</p> <ul style="list-style-type: none"> i. Lack of energy efficiency data ii. Expensive apparatus iii. Ionic liquid discolouration iv. Ionic liquid decomposition v. Scale-up not demonstrated vi. Poor <i>E</i>-factor
<p>O</p> <ul style="list-style-type: none"> i. Green process development ii. Quantitative energy input data iii. Reactor design iv. Intellectual property 	<p>T</p> <ul style="list-style-type: none"> i. Ionic liquid discolouration ii. Ionic liquid decomposition iii. <i>In-situ</i> reaction monitoring iv. Safety controls

Fig. 9 SWOT analysis for the preparation of ionic liquids using ultrasonic irradiation.

The greatest opportunities that exist for ultrasound-promoted ionic liquid syntheses are (i) to develop green procedures that do not lead to the discolouration and decomposition of ionic liquids, and (ii) to determine the true energy efficiency of the preparations compared to other methodologies by collecting quantitative energy input data, thus creating the opportunity for (iii) reactor design and (iv) generating valuable intellectual property.

It must be reiterated that ultrasound-assisted ionic liquid preparation will probably only find commercial application if its

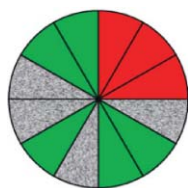
severe shortcomings (or threats in terms of the SWOT analysis) are overcome by future research and development efforts. Such research and development efforts will, similarly to microwave-assisted preparations, have to include safety controls and *in situ* reaction monitoring to align with the 11th and 12th principles of green chemistry.

Greenness assessment: simultaneous use of microwave and ultrasonic irradiation to prepare ionic liquids

Recent studies have shown that the simultaneous use of microwave and ultrasonic irradiation can be used to promote ionic liquid syntheses by one-step (Route 1(d), Fig. 3), two-step (Routes 1(a) then Route 3, Fig. 3), as well as one-pot (Route 2(c), Fig. 3) procedures.^{36,46,47}

The simultaneous use of microwave and ultrasonic irradiation to prepare ionic liquids should offer the cumulative benefits of the individual irradiations, *viz.* excellent coupling of microwaves with ionic liquids plus improved mass transport. Therefore, the time and energy saved using microwave and ultrasonic irradiation simultaneously would represent a significant green advantage, especially if the syntheses are solvent-free. However, using this technology to prepare 1-alkyl-3-methylimidazolium halide salts (Route 1(d), Fig. 3) gives very poor yields (<5%) and can also take significantly longer than using microwave or ultrasound irradiation alone.³⁶ Therefore, the combined use of microwave and ultrasonic irradiation to prepare 1-alkyl-3-methylimidazolium halide salts has a very poor *E*-factor, and uses significantly more energy than using the individual types of irradiation alone, rendering the syntheses dirty. In addition, a major problem that is anticipated for all ionic liquid syntheses using microwave and ultrasonic irradiation simultaneously is that discoloured ionic liquid products will be obtained, requiring extensive decolourisation, which will have a further negative effect on the *E*-factors.

Although the simultaneous microwave/ultrasound-assisted preparations of 1-alkyl-3-methylimidazolium halide (Route 1(d), Fig. 3) and non-halide (Route 2(c), Fig. 3) salts comply with five of the eight relevant principles of green chemistry (*viz.* the 5th, 6th, 8th, 11th and 12th), they do not follow the 1st and 2nd principles, since they give poor yields (compared to thermal and microwave routes) and the ionic liquid products require extensive purification. In addition, the *E*-factors of the preparations are poor due to the need to decolourise the ionic liquid products.



SWOT analysis: simultaneous use of microwave and ultrasonic irradiation to prepare ionic liquids

The simultaneous use of microwave and ultrasonic irradiation to prepare ionic liquids offers both the best and worst of the individual technologies (A Tale of Two Technologies?), and the SWOT analysis shows that this is indeed true (Fig. 10).

The expected strengths of the technology include (i) rapid preparations with (ii) good energy efficiencies compared to traditional methods, (iii) improved mass transport (*vs.* con-

i. Rapid ii. Energy efficient iii. Good mass transfer iv. Solvent-free synthesis v. High atom economy	i. Ionic liquid discolouration ii. Ionic liquid decomposition iii. Extremely specialised apparatus iv. Expensive apparatus v. Lack of energy efficiency data vi. Scale-up not demonstrated vii. Poor E-factor viii. Low yield
i. Green process development ii. Quantitative energy input data iii. Reactor design iv. Intellectual property	i. Ionic liquid discolouration ii. Ionic liquid decomposition iii. <i>In-situ</i> reaction monitoring iv. Safety controls

Fig. 10 SWOT analysis for the preparation of ionic liquids using simultaneous ultrasound and microwave irradiation.

ductive heating and microwave-assisted preparations), (iv) the potential to perform the transformations solvent-free, and (v) high atom economies. At present, however, the limited number of studies describing syntheses have shown that the technology works best for one-pot preparations (Route 2(c), Fig. 3), and is less successful for preparing ionic liquids containing halide anions.³⁶ The SWOT analysis clearly shows, without labouring the point, that at present, the combined microwave/ultrasound irradiation technology has both obvious advantages and severe disadvantages.

Greenness assessment: purification of ionic liquids with non-halide anions

Ionic liquid purification procedures can be divided into two main categories, *viz.* purification of hydrophobic ionic liquids and purification of hydrophilic ionic liquids (Fig. 2). To simplify discussion for the former and latter categories, we have selected two stereotypical salts as representatives, *viz.* 1-butyl-3-methylimidazolium bis{(trifluoromethyl)sulfonyl}-amide, [C₄mim][NTf₂], and 1-butyl-3-methylimidazolium trifluoromethanesulfonate, [C₄mim][OTf]. It must be noted that 1-alkyl-3-methylimidazolium halide salts fall in the above-mentioned hydrophilic category, but their purification and associated green performance have already been discussed (*vide supra*).

On examination of the twelve principles of green chemistry, it is clear that only the 1st, 5th, 6th and 12th principles are relevant to ionic liquid purification. This is because the remaining principles of green chemistry only address synthetic methodologies.

Regardless of whether a one- or two-step methodology is employed to prepare [C₄mim][NTf₂] or [C₄mim][OTf] (Fig. 3), a stoichiometric amount of MX waste (usually NaCl) is generated. If not removed from the ionic liquid product, the presence of the metal halide waste will severely affect the physical properties of the ionic liquid.^{10,12} The removal of MX from both

[C₄mim][NTf₂] and [C₄mim][OTf] is achieved by washing the crude ionic liquid product with water, although the ease with which this is achieved, and the respective green performances, vary considerably.

Although a stoichiometric amount of MX waste is generated during two-step ionic liquid syntheses, it is not toxic waste, and thus does not require incineration. Furthermore, the metal halide waste is not contaminated with organics, which means that both one- and two-step syntheses to produce [C₄mim][NTf₂] and [C₄mim][OTf] closely align with the 1st principle of green chemistry.⁵

Greenness assessment: purification of hydrophobic vs. hydrophilic ionic liquids

In order to remove MX from hydrophilic [C₄mim][OTf], dichloromethane, a dense solvent, is usually added to the crude ionic liquid mixture. The dichloromethane is added since the ionic liquid preferentially dissolves therein, allowing repeated washing of the ionic liquid-containing phase with cold water to remove the MX waste more easily. The residual dichloromethane, as well as the water that remains in the ionic liquid as a result of the washing procedure, require removal that is achieved by first using a rotary evaporator and then drying the salt *in vacuo* at ~70 °C for many hours, which is extremely energy inefficient. Almost needless to say, the use of dichloromethane to purify [C₄mim][OTf] is an extremely dirty practice, since it is a toxic solvent that is detrimental to both humans and the environment.⁴⁸ Furthermore, the larger the volume of dichloromethane used, the poorer the *E*-factor of the procedure.

The removal of MX from hydrophobic [C₄mim][NTf₂] is far easier than its removal from [C₄mim][OTf] because it does not readily mix with water and, therefore, washing the salt with water to extract MX is both faster and more efficient. This purification is also greener, since no organic solvent is required, as is the case for hydrophilic salts, to aid with the removal of MX. In principle, the water phase can also be recycled by distillation and

reused, although some contaminated ionic liquid, now severely contaminated with MX, will remain, since even hydrophobic ionic liquids exhibit mutual solubility with water.² Moreover, the water must be removed in order to obtain the pure salt; this is achieved by drying the salt *in vacuo* at ~70 °C for many hours, which is extremely energy inefficient.

In brief, the purification procedure of [C₄mim][OTf] is far less efficient than that of its [C₄mim][NTf₂] cousin, since a significant amount of the ionic liquid is 'lost' to the organic phase and higher levels of MX also remain in the purified ionic liquid. This is evidenced by the lower chloride content levels achievable for [C₄mim][NTf₂]⁴⁹ than for [C₄mim][OTf].^{12,50} In addition, less energy is required to remove residual water from [C₄mim][NTf₂] than for [C₄mim][OTf] by heating the salts *in vacuo*, as the former should, by definition, hold less water than the latter. Although the purification of these ionic liquids does not comply with the relevant principles of green chemistry (*viz.* the 1st, 5th, and 6th), the hydrophobic ionic liquid processes are much greener than the hydrophilic, both in total isolated yield and avoidance of organic solvents.

SWOT analyses: purification of hydrophobic and hydrophilic ionic liquids

The SWOT analyses for the purification of [C₄mim][NTf₂] and [C₄mim][OTf] show that the former procedure is the greener (Fig. 11). This is mainly due to the purification of [C₄mim][OTf] requiring the use of dichloromethane, which is an extremely harmful compound. Another major reason why the purification of [C₄mim][OTf] is dirty, is because much greater losses of the ionic liquid to the water phase occur compared to the purification of [C₄mim][NTf₂] and it also requires longer heating *in vacuo* to remove residual water.

Decolourisation of ionic liquids

All practicing ionic liquid synthetic chemists know that the salts are sometimes obtained as pale yellow to black prod-


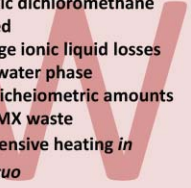

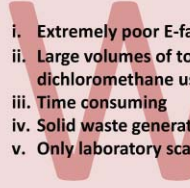



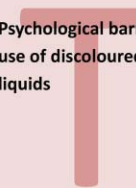
<p>i. Simple</p> 	<p>i. Poor E-factor ii. Toxic dichloromethane used iii. Large ionic liquid losses to water phase iv. Stoichiometric amounts of MX waste v. Extensive heating <i>in vacuo</i> vi. Laboratory scale only</p> 	<p>i. Simple ii. Efficient</p> 	<p>i. Extremely poor E-factor ii. Large volumes of toxic dichloromethane used iii. Time consuming iv. Solid waste generated v. Only laboratory scale use</p> 
<p>i. Process optimisation ii. Scale-up</p> 	<p>i. Waste disposal</p> 	<p>i. Explore greener alternatives ii. Identify chromophore</p> 	<p>i. Psychological barrier to use of discoloured ionic liquids</p> 

Fig. 11 SWOT analyses for the purification of [C₄mim][NTf₂] (left) and [C₄mim][OTf] (right).

Table 1 How green is my procedure?

Methodology	<i>E</i> -factor	Atom economy	Principles of green chemistry upheld ^a	$\frac{x}{8}$
Route 1 (a)	Good–excellent	High	3 (8th, 11th, 12th)	
Route 1 (b)	Excellent	High	7 (1st, 2nd, 5th, 6th, 8th, 11th, 12th)	
Route 1 (c)	Poor	Low–high	5 (5th, 6th, 8th, 11th, 12th)	
Route 1 (d)	Poor	High	5 (5th, 6th, 8th, 11th, 12th)	
Route 2 (a)	Poor–good	Low–medium	7 (1st, 2nd, 5th, 6th, 8th, 11th, 12th)	
Route 2 (b)	Poor	Low–medium	5 (5th, 6th, 8th, 11th, 12th)	
Route 2 (c)	Very poor	Low–medium	5 (5th, 6th, 8th, 11th, 12th)	
Route 3	Poor	Low–medium	3 (8th, 11th, 12th)	

^a The 4th, 7th, 9th and 10th principles of green chemistry do not apply.

ucts. Ionic liquids containing halide anions are particularly susceptible to discolouration, and the cause of the colour can be transferred to derived ionic liquids prepared by metathesis (Route 3, Fig. 3). Although intense chromophores (extinction coefficients $> 10^6 \text{ mol l}^{-1} \text{ cm}^{-1}$) are the suspected discolouration culprits,⁵¹ the true cause (and indeed the types of chromophores responsible) remains a mystery. To date, attempts to isolate the chromophores by column chromatography have failed to provide enough material for identification. This failure indicates

the extremely low levels of the chromophores in ionic liquids (probably ppb levels). It is worth noting that even some of the most intensely coloured ionic liquids are usually analytically pure to NMR spectroscopy and mass spectrometric techniques.

The colour of an ionic liquid is usually not detrimental when using the salts as solvents (provided that they contain minimal levels of other impurities such as chloride and/or water), but colourless ionic liquids are essential for spectroscopic studies, in order to eliminate interference from the suspected chromophoric

impurity resonances that usually appear in the UV-Vis spectra; the impurity is also often strongly luminescent.

Conclusions

In conclusion, we believe this is the first critical assessment of the greenness of the synthetic procedures and purification methodologies commonly used for the synthesis of ionic liquids, which are summarised in Table 1.

To maintain green credibility, ionic liquids must be both green in application and in their synthesis. The above discussions clearly illustrate that laboratory-scale ionic liquid synthesis and purification can certainly be considered as green if microwave-assisted synthesis is employed. It is also clear that the purification of hydrophobic ionic liquids is intrinsically greener than hydrophilic ionic liquids. However, it is important to emphasise that for industrial scale ionic liquid preparations, we will have to readdress how to determine greenness.

With current trends towards the design of non-toxic, biodegradable ionic liquids, the new challenges become to develop improved purification procedures for hydrophilic ionic liquids alongside a universal requirement for development of *in situ* on-line analytical monitoring for industrial scale syntheses. Overall, the judgement provided here for the synthesis and purification of ionic liquids is: 'Green, but not green enough'.

Acknowledgements

M.D. and K.R.S. gratefully acknowledge the EPSRC for funding under their Portfolio Partnership Scheme (Grant no. EP/D029538/1) and also thank Milestone, particularly Dr. Mauro Iannelli, for the supply of their microwave units to QUILL. M.D. thanks Drs J. D. Holbrey and M. Nieuwenhuysen for help in generating the images for Fig. 5 and Prof. Chris Strauss for helpful discussions. K.R.S. also wishes to thank the Institute of Chemical Sciences and Engineering at the EPFL (Switzerland) for providing the opportunity for tranquil meditation.

Notes and references

- M. J. Earle, J. M. S. S. Esperança, M. A. Gilea, J. N. C. Lopes, L. P. N. Rebelo, J. W. Magee, K. R. Seddon and J. A. Widegren, *Nature*, 2006, **439**, 831–834; L. P. N. Rebelo, J. N. C. Lopes, J. M. S. S. Esperança and E. Filipe, *J. Phys. Chem. B*, 2005, **109**, 6040–6043.
- M. Deetlefs and K. R. Seddon, "Ionic liquids: fact and fiction", *Chim. Oggi – Chem. Today*, 2006, **24**, 16–17, 20–23.
- M. Freemantle, "Designer solvents - Ionic liquids may boost clean technology development", *Chem. Eng. News*, 1998, **76**, 32–37.
- A. R. Katritzky, S. Singh, K. Kirichenko, J. D. Holbrey, M. Smiglak, W. M. Reichert and R. D. Rogers, *Chem. Commun.*, 2005, 868–870.
- P. T. Anastas and M. M. Kirchhoff, *Acc. Chem. Res.*, 2002, **35**, 686–694; P. T. Anastas, and J. C. Warner, *Green Chemistry: Theory and Practice*, Oxford University Press, New York, 1998.
- P. T. Anastas and J. B. Zimmerman, *Environ. Sci. Technol.*, 2003, **37**, 94A.
- S. Tang, R. Bourne, R. Smith and M. Poliakoff, *Green Chem.*, 2008, **10**, 268–269.
- J. H. Davis Jr., C. M. Gordon, C. Hilgers, and P. Wasserscheid, in *Ionic Liquids in Synthesis*, eds. P. Wasserscheid and T. Welton, Wiley-VCH, Weinheim, 2003, pp. 7–21; P. Wasserscheid and W. Keim, *Angew. Chem., Int. Ed.*, 2000, **39**, 3772–3789.
- A. J. Carmichael, M. Deetlefs, M. J. Earle, U. Fröhlich and K. R. Seddon, in *Ionic Liquids as Green Solvents: Progress and Prospects*, eds. R. D. Rogers and K. R. Seddon, American Chemical Society, Washington D.C., 2003, pp. 14–31.
- A. Stark, and K. R. Seddon, in *Kirk-Othmer Encyclopaedia of Chemical Technology*, ed. A. Seidel, John Wiley & Sons, Inc., Hoboken, New Jersey, 2007, pp. 836–920.
- C. M. Gordon, and M. J. Muldoon, in *Ionic Liquids in Synthesis*, eds. P. Wasserscheid and T. Welton, Wiley-VCH, Weinheim, 2008, pp. 7–25.
- K. R. Seddon, A. Stark and M.-J. Torres, *Pure Appl. Chem.*, 2000, **72**, 2275–2287.
- M. Deetlefs and K. R. Seddon, *Green Chem.*, 2003, **5**, 181–186.
- D. Kralisch, A. Stark, S. Koersten, G. Kreisel and B. Ondruschka, *Green Chem.*, 2005, **7**, 301–309; D. Reinhardt, F. Ilgen, D. Kralisch, B. Koenig and G. Kreisel, *Green Chem.*, 2008, **10**, 1170–1181.
- M. J. Earle and K. R. Seddon, Preparation of imidazole carbenes and the use thereof for the synthesis of ionic liquids, *WO Pat.* 2001077081 (2001).
- P. Wasserscheid, R. van Hal and A. Boesmann, *Green Chem.*, 2002, **4**, 400–404; P. Wasserscheid, R. van Hal, A. Bosmann, J. Esser, and A. Jess, in *Ionic Liquids as Green Solvents: Progress and Prospects*, eds. R. D. Rogers, and K. R. Seddon, American Chemical Society, Washington D.C., 2003, pp. 57–69.
- C. R. Strauss, *Org. Process Res. Dev.*, 2009, **13**, 915–923.
- G. McHale, C. Hardacre, R. Ge, N. Doy, R. W. K. Allen, J. M. MacInnes, M. R. Bown and M. I. Newton, *Anal. Chem.*, 2008, **80**, 5806–5811.
- B. M. Trost, *Science*, 1991, **254**, 1471–1477.
- R. A. Sheldon, *Chem. Ind.*, 1992, **23**, 903–906; R. A. Sheldon, *Green Chem.*, 2007, **9**, 1273–1283.
- R. C. Appleby, *Modern Business Administration*, Pearson Education Ltd., 1994.
- J. S. Wilkes, J. A. Levisky, R. A. Wilson and C. L. Hussey, *Inorg. Chem.*, 1982, **21**, 1263–1264; A. A. Fannin, D. A. Floreani, L. A. King, J. S. Landers, B. J. Piersma, D. J. Stech, R. L. Vaughn, J. S. Wilkes and J. L. Williams, *J. Phys. Chem.*, 1984, **88**, 2614–2621.
- A. E. Elaiwi, Mass Spectrometry of Organic and Chlorometallated Salts, *D. Phil. Thesis*, University of Sussex, Sussex (1994).
- G. P. Smith, A. S. Dworkin, R. M. Pagni and S. P. Zingg, *J. Am. Chem. Soc.*, 1989, **111**, 525–530.
- P. Bonhôte, A.-P. Dias, N. Papageorgiou, K. Kalyanasundaram and M. Grätzel, *Inorg. Chem.*, 1996, **35**, 1168–1178.
- A. J. Jeapes, R. C. Thied, K. R. Seddon, W. R. Pitner, D. W. Rooney, J. E. Hatter and T. Welton, Process for recycling ionic liquids, *WO Pat.* 2001015175 (2001).
- Health and Safety Executive, *REACH (Registration, Evaluation, Authorisation & restriction of CHemicals)*, <http://www.hse.gov.uk/reach/index.htm>, 2008.
- R. S. Varma and V. V. Nambodiri, *Pure Appl. Chem.*, 2001, **73**, 1309–1331.
- B. M. Khadilkar and G. L. Rebeiro, *Org. Process Res. Dev.*, 2002, **6**, 826–828.
- N. E. Leadbeater, and H. M. Torenius, in *Microwaves in Organic Synthesis*, ed. A. Loupy, Wiley-VCH, Weinheim, 2006, pp. 327–361.
- R. S. Varma and V. V. Nambodiri, *Chem. Commun.*, 2001, 643–644.
- È. Boros, K. R. Seddon and C. R. Strauss, Chemical processing with microwaves and ionic liquids, *Chim. Oggi – Chem. Today*, 2008, **26**, 28–30.
- V. V. Nambodiri and R. S. Varma, *Tetrahedron Lett.*, 2002, **43**, 5381–5383.
- B. A. Roberts and C. R. Strauss, *Acc. Chem. Res.*, 2005, **38**, 653–661.
- D. Q. Xu, B. Y. Liu, S. P. Luo, Z. Y. Xu and Y. C. Shen, *Synthesis*, 2003, 2626–2629.
- G. Cravotto, C. Gaudino Emanuela, L. Boffa, J.-M. Lévêque, J. Estager and W. Bonrath, *Molecules*, 2008, **13**, 149–156.
- T. Erdmenger, R. M. Paulus, R. Hoogenboom and U. S. Schubert, *Aust. J. Chem.*, 2008, **61**, 197–203.
- C. G. Begg, M. R. Grimmett and P. D. Wethey, *Aust. J. Chem.*, 1973, **26**, 2435–2438.
- A. K. Abdul-Sada, P. W. Ambler, P. K. G. Hodgson, K. R. Seddon and N. J. Stewart, Ionic liquids of imidazolium halide for oligomerization or polymerization of olefins, *World Pat. WO* 95 21871 (1995).

- 40 J.-M. Lévêque, J.-L. Luche, C. Pétrier, R. Roux and W. Bonrath, *Green Chem.*, 2002, **4**, 357–360.
- 41 V. V. Namboodiri and R. S. Varma, *Org. Lett.*, 2002, **4**, 3161–3163.
- 42 E. A. Nepparis, *Phys. Rep.*, 1980, **61**, 159–251.
- 43 *Synthetic Organic Sonochemistry*, ed. J.-L. Luche, Plenum Press, New York, 1998.
- 44 J. D. Oxley, T. Prozorov and K. S. Suslick, *J. Am. Chem. Soc.*, 2003, **125**, 11138–11139.
- 45 X. Li, J. Zhao, Q. Li, L. Wang and S. C. Tsang, *Dalton Trans.*, 2007, 1875–1880.
- 46 J.-M. Lévêque, J. Estager, M. Draye, G. Cravotto, L. Boffa and W. Bonrath, *Monatsh. Chem.*, 2007, **138**, 1103–1113.
- 47 G. Cravotto and P. Cintas, *Chem.–Eur. J.*, 2007, **13**, 1902–1909.
- 48 Scorecard – The Pollution Information Site, Dichloromethane, http://www.scorecard.org/chemical-profiles/summary.tcl?edf_substance_id=75-09-2, 2005.
- 49 G. W. Driver, Physical Chemistry and Thermodynamics of Ionic Liquids and Ionic Liquid Solutions, *PhD Thesis*, The Queen's University of Belfast, Belfast (2006).
- 50 C. Villagrán, M. Deetlefs, W. R. Pitner and C. Hardacre, *Anal. Chem.*, 2004, **76**, 2118–2123.
- 51 M. J. Earle, C. M. Gordon, N. V. Plechkova, K. R. Seddon and T. Welton, *Anal. Chem.*, 2007, **79**, 758.

Characterization of CO₂ precipitated Kraft lignin to promote its utilization

Máté Nagy,^{†a} Matyas Kosa,^{†a} Hans Theliander^b and Arthur J. Ragauskas^{*a}

Received 8th July 2009, Accepted 25th September 2009

First published as an Advance Article on the web 14th October 2009

DOI: 10.1039/b913602a

Converting pulp mills into forest biorefineries to produce biopower and biomaterials can decrease their environmental impact and increase feasibility at the same time. One of the key challenges to reach this goal is the recovery of lignin from process streams for subsequent utilization in a variety of innovative green processes. This study examines the fundamental chemical structure of lignin recovered from Kraft pulping streams by an acid precipitation/washing methodology. Functional group analysis and molecular weight profiles were determined by NMR and SEC with promising results for future conversions; such as low hydroxyl (oxygen) contents and low molecular weights (~3000 g mol⁻¹).

Continuously developing new technologies that allow for a more efficient utilization of resources including biomass is crucial in all industries for reasons like sustainability and higher profit. The pulp and paper industry is also constantly searching for alternative solutions to valorize its Kraft cycle – like the process detailed below – mainly by trying to find ways to recover lignin and sell it as a higher value material.

During chemical pulping, lignin is chemically degraded and extracted from wood in an aqueous environment in a pressure reactor at pH values of 13–14 and temperatures of 140–170 °C.^{2,3} These conditions remove 85–93% of the lignin and approximately 56–71% of the hemicelluloses.^{1–3} The approach when NaSH is used in the cooking process along with caustic to delignify wood is referred to as Kraft pulping. In the United States alone, the pulp and paper industry collects and processes ~108 million tonnes of pulpwood for the production of pulp, paper and paperboard annually.¹ In turn, the paper industry produces over 50 million tons of residual lignin per year worldwide in a form of a caustic sidestream.¹ Currently, this material is burned in a low efficiency Thompson recovery furnace to recover energy and cooking chemicals. A continuing interest in this field is the desire to recover fractions of lignin from the Kraft cooking liquors for biopower, biochemical and biomaterial utilizations. Recently, a green process referred to as “LignoBoost” provides a viable separation of lignin from these cooking liquors by employing carbon-dioxide to precipitate lignin from alkaline solutions.^{4–8} The application of this process involves acidification of an alkaline cooking liquor with CO₂,

precipitation, filtration and washing.^{9–11} Process integration and mill trials have tested this process from an engineering and economic point of view.^{8,9,12}

The lignin recovered by the LignoBoost process has been shown to be valuable green resource for biopower production.¹³ This method enables lignin to be exported in the form of a solid biofuel and also gives the opportunity to transform it into materials of higher value.^{13–15}

Recognizing the possibilities in recovering lignin from black liquor *via* CO₂ precipitation and washing, we became interested in the detailed chemical composition and structure of the isolated lignin; anticipating that this data could facilitate future applications of this bioresource. Herein, we wish to report the characterization of LignoBoost derived lignin in terms of molecular weight profiles and functional group properties.

Experimental

Lignin separation from a commercial Scandinavian softwood Kraft pulping liquor was accomplished following published methods.^{5,10,16} In brief; Kraft cooking liquor (BL) was collected in a reaction vessel then treated with pressurized CO₂ (1500 kPa)⁴ until the solution's pH reached 10.5, causing some of the lignin to precipitate. The suspension was subsequently separated by filtration giving a precipitate (P) and a filtrate (F) part. This process was done on two separate occasions with two different final pHs: 10.5 and 9.5, resulting the following samples: P 10.5, P 9.5 (precipitates) and F 10.5, F 9.5 (filtrates). Solids were obtained from the F and BL solutions by evaporation, then all samples were freeze dried and kept frozen until purification.⁴

Detailed structural analysis of the lignin in the above samples required additional purification. The initial LignoBoost samples were diluted in distilled water to 5 wt% solid content. Next EDTA-2Na⁺ was added to the aqueous solution (5.00 g L⁻¹) to facilitate metal-ion removal and the pH was adjusted to a value of 6 with aqueous sulfuric acid (2 M) and stirred for 1 h. Subsequently, the pH was further lowered to a value of 3 facilitating lignin precipitation.^{4,17} The resulting samples were frozen (–20 °C) overnight, thawed and filtered through a medium sintered glass funnel at 0 °C.^{9,14,16} Retentates were dissolved in pH 3 aqueous sulfuric acid solution up to 5 wt% and the filtration process was repeated three times for effective salt removal. All filtrates were collected, the solvent was removed under reduced pressure and the remaining solid provided the salt fraction (SF). Retentates were air dried, extracted with pentane to remove free sulfur and dissolved in dioxane : water (9 : 1) solution (1 g L⁻¹).¹⁷ After filtration through a medium sintered glass funnel the solvent was removed under reduced pressure. The resulting solid

^aSchool of Chemistry and Biochemistry, Georgia Institute of Technology, Atlanta, GA 30332, USA.

E-mail: Art.Ragauskas@chemistry.gatech.edu; Fax: +1-404-894-4778; Tel: +1-404-894-9701

^bChalmers University of Technology, Göteborg, SE-41296, Sweden

[†] Contributed equally to this work.

provided purified lignin samples which were stored in a freeze dried form at ($-20\text{ }^{\circ}\text{C}$) until further use.

All NMR spectral data reported in this study was recorded with a 400 MHz DMX Bruker spectrometer (Billerica, MA, USA) at $25\text{ }^{\circ}\text{C}$. Qualitative ^1H and ^{13}C -NMR spectra were acquired on lignin samples (80–120 mg) dissolved in dimethyl sulfoxide (DMSO-d_6) (450 μL).¹⁸ Quantitative ^1H -NMR spectra were acquired on dry lignin samples ($\sim 20\text{ mg}$) dissolved in dry DMSO-d_6 (450 μL) using pentafluorobenzaldehyde ($\sim 1\text{ mg mL}^{-1}$) as internal standard.^{18,19} ^{31}P -NMR lignin spectra were acquired on dry samples ($\sim 25\text{ mg}$) that were derivatized with 2-chloro-4,4,5,5-tetramethyl-1,3,2-dioxaphospholane (TMDP) and analyzed by ^{31}P -NMR.^{18,20}

For size exclusion chromatography (SEC), purified lignin (20 mg) was acetylated by stirring with acetic anhydride : pyridine 1 : 1 (2 mL) at room temperature for 72 h. The solvent mixture was then removed under vacuum at $50\text{ }^{\circ}\text{C}$, the acetylated lignin was dissolved in chloroform (50 mL) and washed with deionised water (20 mL). The organic fraction was dried over anhydrous MgSO_4 and the chloroform was removed under reduced pressure. The dried acetylated lignin was dissolved in tetrahydrofuran (1 mg mL^{-1}) for analysis.^{18,21}

Results and discussion

After purification of the unwashed samples, the lignin content of the initial LignoBoost samples could be determined. The mass balance data showed that the initial unpurified dry samples had various amounts of lignin as the following (in wt%): 25.8% in BL, 73.3% in P 9.5, 71.3% in P 10.5, 11.1% in F 9.5 and 20.0% in F 10.5. This data clearly shows that treatment of the pulping liquor with CO_2 yields a lignin rich stream and a filtrate fraction that is enriched in salts. The pH 9.5 treatment condition resulted in a better separation of lignin. Results of the elemental analysis are consistent with the mass balance data and shows that the purified lignin samples contain only organic elements up to 97.1%.

To evaluate the primary components present in the initial LignoBoost fractions and in their purified samples, qualitative

^1H - and ^{13}C -NMR measurements were conducted (Fig. 1) following literature methods.^{17,18,22-24} Qualitative NMR data shows that during the purification step, sugars and fatty acids were removed with salts and salt-EDTA complexes from the initial LignoBoost samples and ended up in the SF. With the lignin purification method used in this study, the chemicals used earlier to bring lignin into solution can be separated from the crude samples. This allows the process chemicals to be returned to the main stream and reused, while it also produces lignin with 95–97% purity, resulting in a higher environmental and economic efficiency.

To selectively follow the structural changes of the lignin biopolymer on the molecular level, quantitative ^1H -NMR measurements were conducted on the purified fractions. The differences between the process fractions and the changes in the distribution of selected lignin moieties at different final pHs are shown in Table 1. Quantitative ^1H -NMR shows that the F lignin has more carboxylic and phenolic groups, while P is enriched in methoxyl moieties. The hydroxyl group content of the lignin plays a crucial role in determining its solubility.^{2,3} Selective phosphitylation of the hydroxyl groups on the lignin polymer with TMDP, followed by quantitative ^{31}P -NMR measurement provides facile monitoring of the changes in the hydroxyl content throughout the process.¹⁸

The pK_a values of phenolic lignin groups fall between 9.4 and 10.8,⁴ hence at pH 9.5 and 10.5 these groups get protonated consequently affecting the solubility of the polymer by determining – lowering – its charge. A polymer with a higher total hydroxyl and carboxyl content will have more sites that can stay deprotonated causing better solubility. Our ^{31}P -NMR results in Table 2 confirm the above logic by showing that both hydroxyl and carboxyl contents of F lignins are higher than in their analogous P lignins; this is also consistent with the results from ^1H -NMR analysis. F lignins have almost double the amount of carboxylic hydroxyl groups that contribute significantly to their ability to stay in solution despite the decreasing pH. Moreover, the quantities of guaiacyl phenolic groups are also almost doubled in F lignins meaning more free hydroxyls compared

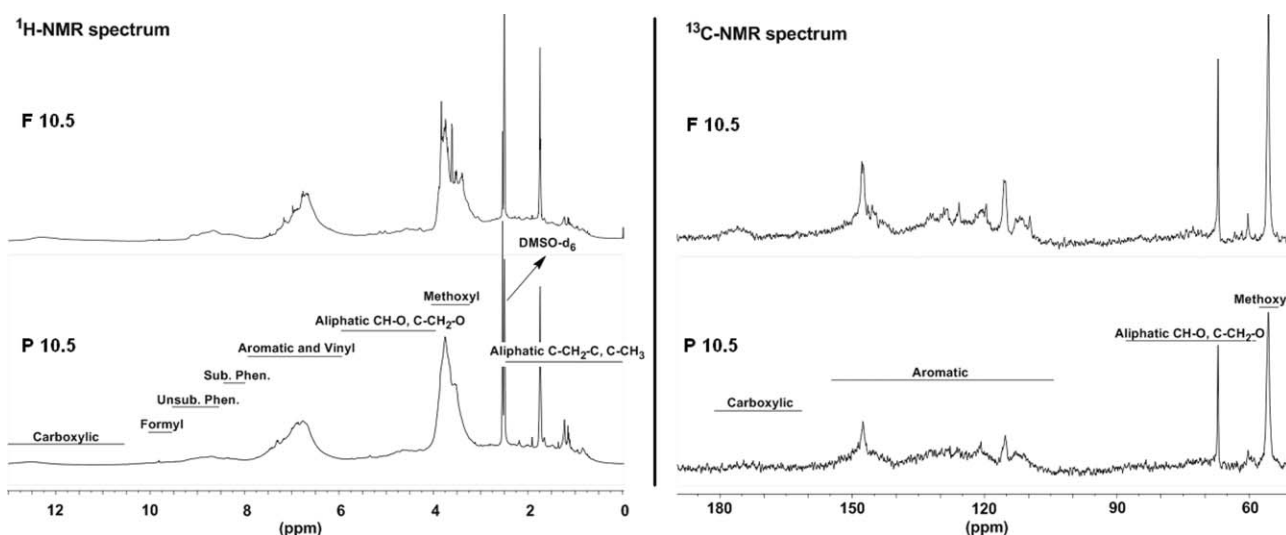


Fig. 1 Qualitative ^1H and ^{13}C -NMR spectrum of purified P and F 10.5 LignoBoost samples, measured in dimethyl sulfoxide (DMSO-d_6) as solvent. Abbreviations: Sub. = substituted, Unsub. = unsubstituted.

Table 1 Partial hydrogen content [mol mol⁻¹]^a of different lignin functional groups in the ratio of all H containing functional groups as determined by quantitative ¹H-NMR

Sample name	Hydrogen content of selected groups (mol mol ⁻¹ % relative to all H containing groups)						
	Carboxylic acid	Formyl	Phenolic	Aromatic, vinyl	Aliphatic	Methoxyl	Aliphatic
	(13.50–10.50) ppm	(10.10–9.35) ppm	(9.35–8.00) ppm	(8.00–6.00) ppm	(6.00–4.05) ppm	(4.05–3.45) ppm	(2.25–0.00) ppm
	–C(O)OH	–C(O)H	=HC–OH	CH=CH	CH–O	–OCH ₃	C–CH ₂ –C
				CH ₂ =CH	C–CH ₂ –O		C–CH ₃
Black liquor	1.26	1.50	6.73	20.22	8.44	45.84	14.42
P 9.5	1.06	0.90	4.19	18.75	5.92	52.42	16.70
P 10.5	0.81	0.98	3.66	19.69	8.22	49.16	16.04
F 9.5	1.71	1.61	6.16	19.82	7.89	41.25	17.35
F 10.5	1.22	1.67	5.73	19.58	6.78	44.58	16.87

Table 2 Hydroxyl content of different LignoBoost fractions determined by quantitative ³¹P-NMR after derivatization with TMDP

Sample name	Hydroxyl content of selected groups/μmol mg ⁻¹				
	Total –OH content/μmol mg ⁻¹ (149.0–133.8) ppm ^a	Aliphatic hydroxyl (149.0–145.6) ppm ^a	Condensed phenolic (144.4–140.4) ppm ^a	Guaiacyl phenolic (140.4–137.6) ppm ^a	Carboxylic hydroxyl (136.0–133.8) ppm ^a
Black liquor	6.37	1.49	1.73	2.46	0.69
P 9.5	4.30	1.11	1.14	1.47	0.59
P 10.5	3.18	0.91	0.85	1.03	0.39
F 9.5	6.74	1.27	1.80	2.55	1.11
F 10.5	5.76	1.22	1.57	2.20	0.78

^a All samples were referenced to an internal standard of cyclohexanol at 144.9 ppm.

to their P analogs that most likely contain etherified units in most of these positions.

Changes in the polymer structure of the lignin were followed by molecular mass distribution analysis with SEC on the purified fractions using acetylated lignin samples.^{4,8,18} Polystyrene equivalent weight average molecular weight (M_w), number average molecular weight (M_n) and polydispersity (PD) were determined using calculation strategies from Baumberger for whole curve integration.²¹ M_w/M_n gives a PD that directly shows how accurate it is to evaluate a peak as one and not as a sum of multiple peaks. SEC data shows that P samples were enriched in the lower M_w fraction in the 200–300 g mol⁻¹ region, which represents a lignin DP of 1–2 units.^{1,18,25} Their peaks were recognizable and easy to separate from the main peak resulting from the higher M_w lignin fractions.^{18,21} While on the contrary, in the case of F and BL samples, no additional peaks were recognizable in the lower M_w region and their SEC curves were integrated as one peak, and as a result their respective PD's were 2–3 times larger than in case of the precipitates. These results are consistent with previous research data of Wallmo.⁴ Table 3 shows all main peak data obtained by SEC.

It is noteworthy that the polydispersity of all separated lower M_w peaks fell between 1.02 and 1.12 (data not shown), which confirms the validity of the calculation strategy used.

In conclusion, the entering BL separates into fraction P which is enriched in lignin and into fraction F which is enriched in salts and also contains some sugars and short chain acids. It is noteworthy that a lower final pH resulted in a better lignin separation. SEC data obtained on the purified P phase showed that the fraction is enriched in the ~3000 g mol⁻¹ –

Table 3 SEC results for purified and acetylated samples

Sample	M_w	M_n	PD
BL	3601	812	4.44
P 10.5	2939	1694	1.73
F 10.5	2718	795	3.42
P 9.5	2979	1795	1.66
F 9.5	2101	735	2.86

Polystyrene standards were used with M_w 1200–195 000 g mol⁻¹.

low degree of polymerization (DP) – and in the 200–300 g mol⁻¹ monomer regions. Quantitative NMR data showed that F contains almost two times the amount of carboxylic and phenolic groups causing its better solubility in water. Low DP together with low quantities of oxygen containing functional groups make both P 9.5 and P 10.5 viable starting feedstocks for future biofuel (or biomaterial) production. Ongoing pyrolysis experiments showed promising oil yields (~40% based on dry weight of purified lignin from P 9.5 sample), however much more analytical data need to be obtained for the determination of these products, which is the goal in the continuation of this project.

Acknowledgements

Authors thank the support of the AtlanTICC Alliance and its member universities and the doctoral grant of MN and MK. AJR also wishes to thank the support of the Fulbright Fellowship program for the support of his Chair in Alternative Energy.

Notes and references

- 1 A. J. Ragauskas, M. Nagy, D. H. Kim, C. A. Eckert, J. P. Hallett and C. L. Liotta, *Ind. Biotechnol.*, 2006, **2**, 55.
- 2 J. Gullichsen, and C.-J. Fogelholm, *Chemical Pulping* 1999 TAPPI Press.
- 3 C. W. Dence, and D. W. Reeve, *Pulp Bleaching, Principles and practice*, TAPPI Press, 1996.
- 4 H. Wallmo, T. Richards and H. Theliander, *Paperi ja Puu*, 2007, **89**, 436.
- 5 F. Öhman, H. Wallmo and H. Theliander, *Nord. Pulp Pap. Res. J.*, 2007, **22**, 9.
- 6 F. Öhman, H. Wallmo and H. Theliander, *Nord. Pulp Pap. Res. J.*, 2007, **22**, 188.
- 7 A. Moosavifar, P. Sedin and H. Theliander, *Nord. Pulp Pap. Res. J.*, 2006, **21**, 180.
- 8 A. Moosavifar, P. Sedin, H. Brelid and H. Theliander, *Nord. Pulp Pap. Res. J.*, 2006, **21**, 493.
- 9 H. Luotfi, B. Blackwell and V. Uloth, *Tappi Journal*, 1991, **74**, 203.
- 10 F. Öhman, H. Theliander, P. Tomani and P. Axegard, *Patent WO 2006/031175 A1*, 2006.
- 11 R. Alén, E. Sjöström and P. Vaskikari, *Cellulose Chemistry Technol.*, 1985, **19**, 537.
- 12 M. Olsson, E. Axelsson and T. Berntsson, *Nord. Pulp Pap. Res. J.*, 2006, **21**, 476.
- 13 U. Wising, J. Algehed, T. Berntsson and L. Delin, *Tappi Journal*, 2006, **5**, 3.
- 14 F. Öhman and H. Theliander, *Paperi ja Puu*, 2006, **88**, 287.
- 15 C. Laaksometsä, E. Axelsson, T. Berntsson and A. Lundström, *Clean Technol. Environ. Policy*, 2009, **11**, 77.
- 16 F. Öhman, H. Wallmo and H. Theliander, *Filtration*, 2007, **7**, 309.
- 17 P. Froass, A. J. Ragauskas and J. E. Jiang, *Holzforschung*, 1998, **52**, 385.
- 18 M. Nagy, K. David, G. Britovsek and A. J. Ragauskas, *Holzforschung*, 2009, **63**, 513.
- 19 T. M. Runge and A. J. Ragauskas, *Holzforschung*, 1999, **53**, 623.
- 20 Y. Pu and A. J. Ragauskas, *Can. J. Chem.*, 2005, **83**, 2132.
- 21 S. Baumberger, A. Abaecherli, M. Fasching, G. Gellerstedt, R. Gosselink, B. Hortling, J. Li, B. Saake and E. de Jong, *Holzforschung*, 2007, **61**, 459.
- 22 F. Chakar and A. Ragauskas, *Ind. Crops Prod.*, 2004, **20**, 131.
- 23 E. Sjöström, *Wood Chemistry: Fundamentals and applications*, Academic press, Orlando, 1981.
- 24 J. Gierer, *Wood Sci. Technol.*, 1980, **14**, 241.
- 25 L. B. Davin and N. G. Lewis, *Curr. Opin. Biotechnol.*, 2005, **16**, 407.

Facile palladium catalyzed Suzuki–Miyaura coupling in air and water at ambient temperature†

Alexander N. Marziale,^a Stefan H. Faul,^a Thomas Reiner,^b Sven Schneider^b and Jörg Eppinger^{*a}

Received 29th July 2009, Accepted 24th September 2009

First published as an Advance Article on the web 7th October 2009

DOI: 10.1039/b915436a

A new palladacyclic catalyst yields high activities in aqueous Suzuki–Miyaura coupling at room temperature. Using an optimized protocol, a broad range of products can be isolated in good to excellent yields and high purity by simple filtration.

The application of water as an environmentally benign and economically favourable alternative to organic solvents has developed into an highly active field of research addressing current requirements in synthetic chemistry and catalysis.^{1–4} In contrast to common organic reaction media it is non-toxic, non-flammable and cheap.⁵ Particularly, catalytic cross-coupling reactions have been successfully applied in the aqueous phase.^{5,7} Regarding functional group tolerance and scope of application, Suzuki–Miyaura reactions have become one of the most powerful tools to selectively generate biaryls.⁸ During the last decade several groups described biphasic protocols for Suzuki–Miyaura couplings commonly based on water-soluble catalysts, including contributions by Buchwald,⁹ Beller,¹⁰ Miyaura,¹¹ Plenio,^{12,13} Shaughnessy,¹⁴ Genet,¹⁵ and Leadbeater.⁶ Lipshutz and co-workers reported room temperature couplings in water utilizing nonionic amphiphiles or micelle forming additives.¹⁶ Alternatively, phase-transfer catalysis¹⁷ or mixtures of water and organic co-solvents have been employed.^{17,18} Further approaches include heating by microwave irradiation^{6,19–21} or application of supported catalysts.^{22–24} Yet, despite a variety of advantageous features, aqueous cross-coupling protocols typically necessitate co-solvents, high catalyst loading,^{25–27} elevated temperatures²⁸ and/or tedious product work-up by column chromatography.^{6,13–28}

Arguably the greatest advantage of performing cross-coupling reactions in neat aqueous buffer represents the possibility of facile separation of the phase, which is formed by solid lipophilic biaryl coupling products, yet such examples remain scarce.^{29,12} In this communication we present an ambient temperature protocol for aqueous Suzuki–Miyaura couplings based on a newly developed Bedford-type³⁰ catalyst **4**, facilitating product isolation by simple filtration. Such a protocol meets the criteria of “click-reactions”, which were defined by Sharpless to tolerate

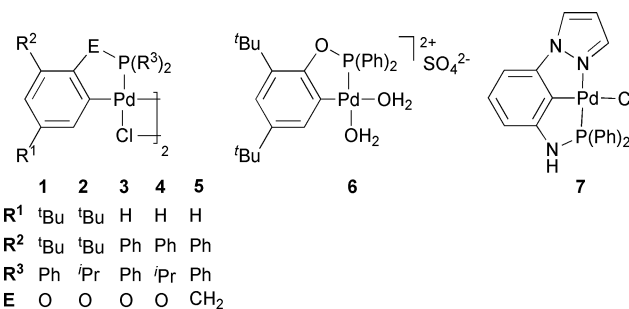


Fig. 1 Catalysts tested in aqueous Suzuki–Miyaura cross-coupling.

Table 1 Catalyst screening

Entry	Catalyst	Yield (%) ^a
1	1	42
2	2	73
3	3	33
4	4	91
5	5	30
6	6	32
7	7	64
8	(NBu ₄) ₂ [Pd ₂ Br ₆] (8)	35
9	(NBu ₄) ₂ [Pd ₂ Br ₆]/P(OH) ⁱ Pr ₂ (9) ^b	39
10	Pd(OAc) ₂ /P(OH) ⁱ Pr ₂ (10) ^b	56

Reaction conditions: 2 mmol (1 eq.) of 4-bromophenol, 1.0 eq. phenylboronic acid, 20 ml buffer (1.0 M, NaOH/NaHCO₃, pH = 11), r.t., 16 h, air, cat. ([Pd] = 0.02 mol%).^a Yields were determined by GC.
^b [Pd]:HP(O)ⁱPr₂ = 1:1.

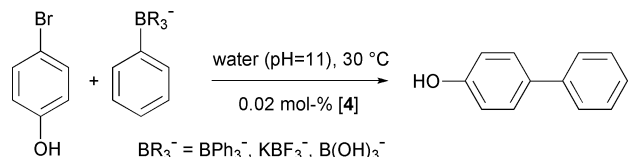
a broad scope of substrates, exhibit high yields, no or only inoffensive byproducts, insensitivity against air and water, no or only benign solvents and – most importantly – ease of product isolation.^{31,32} Hence, we systematically tested a variety of palladium catalysts known to be active in aqueous cross-coupling reactions.^{30,29,33} Based on the pH-dependence for catalyst activities in Suzuki reactions, which was established by Ogo *et al.*,³³ conversion of bromophenol with phenylboronic acid at pH = 11 (carbonate buffer) was chosen as test reaction (Table 1). Reaction temperatures had to be kept slightly above room temperature (30 °C) to guarantee reproducible results. Under the desired conditions (aqueous buffer without any additives, room

^aBio- & Organometallic Catalysis Laboratories, KAUST Catalysis Center, 4700 King Abdullah University of Science and Technology, Thuwal, 23955-6900, Kingdom of Saudi Arabia.

E-mail: jorg.eppinger@kaust.edu.sa

^bTechnische Universität München, Department Chemie, Lichtenbergstr. 4, D-85747, Garching, Germany

† Electronic supplementary information (ESI) available: Experimental details and analytical data. See DOI: 10.1039/b915436a

Table 2 Optimization of reaction conditions


Entry	Parameters	Yield (%)	
1	[4]/mol% ^{a,c,e,f}	0.005	48
2		0.01	91
3		0.02	≥99
4	[Ar-Br]/mol L ⁻¹ ^{a,b,c,e}	0.05	84
5		0.1	≥99
6		0.25	74
7	reaction time/h ^{a,b,e,f}	0.5	76
8		2	83
9		16	≥99
10	BR ₃ ⁻ ^{a,b,c,f}	B(OH) ₃ ⁻	≥99
11		BF ₃ ⁻	90
12		BPh ₃ ⁻	0
13	[Ar-BR ₃ ⁻]/[Ar-Br] ^{b,d,e,f}	1	83
14		1.5	81

Reaction conditions: 20 ml buffer (1.0 M, NaOH/NaHCO₃, pH = 11), r.t., air.^a 1.0 eq. of borane nucleophile. ^b [4] = 0.04 mol%. ^c Reaction time 16 h. ^d Reaction time 2 h. ^e Ar-BR₃⁻ = phenylboronic acid. ^f [Ar-Br] = 0.1 mol L⁻¹.

temperature, vessel open to air, palladium loading <0.05 mol%, product isolation by simple filtration), water soluble catalyst precursors including typical palladium salts with (**9**, **10**) or without (**8**) stabilizing water-soluble phosphine ligand and cationic palladacycles (**6**) delivered only poor to moderate yields after 16 hrs of reaction time. Non-ionic palladium complexes proved to be more efficient catalysts under these reaction conditions. Improved yields were found for the asymmetric pincer complex **7**, which has recently been applied by Domínguez and co-workers under similar conditions,²⁹ yet working at high catalyst loadings (2 mol%). Best cross-coupling results were achieved using Bedford-type palladacyclic catalysts³⁰ after optimizing the substitution pattern. In particular, the phosphine substituents proved to be of high influence with *iso*-propyl groups being most beneficial. Correspondingly, the new palladacycle **4** achieved 91% yield.

Having identified this catalyst as a possible candidate for a cross-coupling “click-chemistry” protocol, we investigated the influence of various reaction parameters on product yields (Table 2). A catalyst loading of [Pd] = 4 × 10⁻² mol L⁻¹ proved to be necessary to achieve quantitative conversion, while at [Pd] = 2 × 10⁻² mol L⁻¹ the best TON (4550) was achieved. Examination of the dependence of isolated yields on substrate concentration revealed an optimal concentration of bromophenol of 0.1 mol L⁻¹. While a decrease in yield for lower substrate concentrations seems to reflect the typical reaction profile of cross-coupling catalysis (1st order in aryl halide), reduced yields at higher substrate concentrations can be attributed to the formation of a solid product phase at low conversions. After this phase has been formed, the lipophilic compounds (aryl halide and catalyst) are trapped since mixing is hampered. Thus, the substrate concentration has to be chosen such that formation of the product layer, which facilitates work-



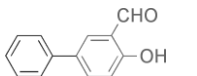
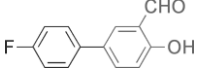
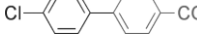
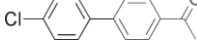
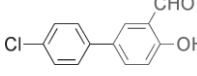
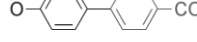
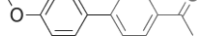
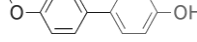
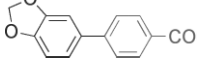
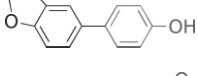


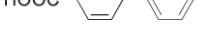
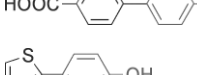
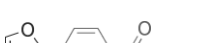
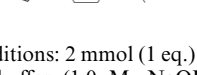
up by filtration, occurs at close to quantitative conversion only. This interpretation is supported by the marked decrease in reaction rate after the solid layer has started to form. Using catalyst **4**, 76% yield can be isolated after 30 min, surpassing the 16 hrs value of all other catalysts tested under the same conditions (Table 1). Interestingly, an excess of boronic acid also leads to decreased yields due to enhanced formation of the undesired homocoupling by-product. Among the different boron nucleophiles tested, quantitative conversion could only be achieved for phenylboronic acid. Potassium phenyltrifluoroborate can also well be used under these conditions yielding 90% of the coupling product, while no conversion is observed for sodium tetraphenylborate.

The substrate range of catalyst **4** in the Suzuki–Miyaura cross-coupling reaction was tested under the optimized reaction conditions using a combination of four different aryl bromides and nine boronic acids. Among all possible combinations 16 biphenylic coupling products precipitated during the reaction and were isolated in good to excellent yields and selectivities by filtration (Table 3, entries 1–16). Formation of boronic acid homocoupling by-products has been attributed to palladium peroxy complexes, which are generated in the presence of oxygen during catalysis.³⁴ Although cross-coupling reactions were carried out in an open vessel under an atmosphere of air, less than 1% of homocoupling was observed. Correspondingly, washing the residue twice with desalinated water was sufficient to obtain pure products,³⁵ as determined by ¹H NMR spectroscopy and elemental analysis. Various functionalities are tolerated for the aryl bromide, including aldehyde, ketone, carboxylic and hydroxylic groups. Furthermore, a broad variety of arylboronic acids bearing methyl, chlorine, fluorine, carboxylic, methoxy, and 3,4-methylenedioxy residues were coupled successfully. Hence, the optimized protocol is applicable to electron-rich and electron-poor aryl bromides and arylboronic acids. The heteroaromatic boron substrates 2-furyl and 2-thiophenyl boronic acid (Table 3, entries 17 and 18) could only be converted in moderate yields using aryl iodides. Hence, in these cases, isolation of products by filtration was not practical. Aryl chlorides in general and non-polar aryl bromides, such as bromobenzene or bromoanisole, could not be converted at 30 °C. Notably, the reactivity difference established for aryl bromides and chlorides can be used for selective couplings as demonstrated for the reaction of 4-Cl-phenylboronic acid with 4-bromophenol (Table 3, entry 5–7).

Conclusions

In conclusion, we have developed a simple protocol for Suzuki–Miyaura cross-coupling catalysis at room temperature in pure aqueous buffer, facilitating isolation of a broad variety of cross-coupling products by simple filtration in excellent yields and purity. Hence, this protocol meets all the criteria associated with “click-reactions”. In particular, avoiding the addition of organic additives, which are usually difficult to separate from the desired product offers the ability to beneficially exploit solubility differences. We are currently investigating possibilities to broaden this concept to other catalytic reactions.

Table 3 Results for aqueous Suzuki cross-coupling protocol

Entry	Product ^a	Isolated yield (%)
1		≥ 99
2		83
3		≥ 99
4		65
5		≥ 99
6		83
7		72
8		90
9		≥ 99
10		93
11		83
12		81
13		≥ 99
14		≥ 99
15		93
16		88
17		49 ^{b,c}
18		31 ^{b,c}

Reaction conditions: 2 mmol (1 eq.) 4-bromophenol, 1.0 equiv. boronic acid, 20 ml buffer (1.0 M, NaOH/NaHCO₃, pH = 11), air, cat. (0.02 mol% palladacycle **4**). Reaction times not optimized.^a Carboxylic acids isolated as corresponding sodium salts. Note on product representation: arene on right side originates from aryl bromide, arene on left side from boronic acid. ^b Purification by column chromatography necessary. ^c The corresponding aryl iodide has been used.

Experimental

General procedure for the Suzuki cross-coupling: 0.2 ml of a catalyst stock solution (0.002 mol L⁻¹) containing palladacycle **4** (4.0 mg, 4.7 μmol) in 2.34 ml of dichloromethane were placed in a Schlenk tube. The solvent was removed *in vacuo* and 2 mmol (1 eq.) of the according aryl bromide in 20 ml of a NaHCO₃/NaOH buffer (pH = 11, c = 1.0 M) were added. The reaction was vigorously stirred for 10 min at r.t. Subsequently 2 mmol (1 eq.) of the respective boronic acid were added. The reaction mixture was stirred for 16 h at 30 °C before the product was filtered. After washing the residue twice with 5 ml of deionized water, the analytically pure product was obtained.

Acknowledgements

We are grateful to the Stifterverband für die deutsche Wissenschaft (Projekt-Nr. 11047 (ForschungsDozentur Molekulare Katalyse), J.E.), the DFG (Emmy-Noether Programm (SCHN950/2-1), S.S.), the Elitenetzwerk Bayern (graduate fellowship for A.N.M. and T.R.), and the IDK NanoCat for funding of this project.

Notes and references

- I. T. Horváth, *Green Chem.*, 2008, **10**, 1024–1028; C.-J. Li, *Acc. Chem. Res.*, 2002, **35**, 533–538.
- B. H. Lipshutz and S. Ghorai, *Aldrichim. Acta*, 2008, **41**, 59–72; F. Alonso, I. P. Beletskaya and M. Yus, *Tetrahedron*, 2008, **64**, 3047–3101.
- A. R. Sheldon, *Green Chem.*, 2005, **7**, 267–278.
- S. Liu and J. Xiao, *J. Mol. Catal. A: Chem.*, 2007, **270**, 1–43.
- Organic Reactions in Aqueous Media*, ed. C.-J. Li and T.-H. Chan, Wiley, New York, 1997; *Organic Synthesis in Water* ed. P. A. Grieco, Academic Press, Dordrecht, The Netherlands, 1997; *Aqueous-Phase Organometallic Catalysis*, ed. B. Cornils and W. A. Herrmann, Wiley-VCH, Weinheim, 2nd edn, 2004; K. H. Shaughnessy and R. B. DeVasher, *Curr. Org. Chem.*, 2005, **9**, 585.
- N. E. Leadbeater, *Chem. Commun.*, 2005, 2881.
- C. J. Li, *Chem. Rev.*, 2005, **105**, 3095–3165; I. P. Beletskaya, A. V. Cheprakov, in *Handbook of Organopalladium Chemistry for Organic Synthesis*, ed. E. Negishi, Wiley, New York, 2002, vol. 2, pp. 2957–3006.
- N. Miyaura and A. Suzuki, *Chem. Rev.*, 1995, **95**, 2457–2483.
- K. W. Anderson and L. Buchwald, *Angew. Chem., Int. Ed.*, 2005, **44**, 6173–6177.
- M. Beller, J. G. E. Krauter, A. Zapf and S. Bogdanovic, *Catal. Today*, 1999, **48**, 279–290; M. Beller, J. G. E. Krauter and A. Zapf, *Angew. Chem., Int. Ed. Engl.*, 1997, **36**, 772–774.
- M. Ueda, M. Nishimura and N. Miyaura, *Synlett*, 2000, **6**, 856–858.
- C. A. Fleckenstein and H. Plenio, *Green Chem.*, 2007, **9**, 1287–1291.
- C. A. Fleckenstein, S. Roy, S. Leuthäuser and H. Plenio, *Chem. Commun.*, 2007, 2870–2872; C. A. Fleckenstein and H. Plenio, *Chem.–Eur. J.*, 2007, **13**, 2701–2716; C. A. Fleckenstein and H. Plenio, *J. Org. Chem.*, 2008, **73**, 3236–3244; C. A. Fleckenstein and H. Plenio, *Chem.–Eur. J.*, 2008, **14**, 4267–4279.
- L. R. Moore and K. H. Shaughnessy, *Org. Lett.*, 2001, **3**, 2757–2759; L. R. Moore and K. H. Shaughnessy, *Org. Lett.*, 2004, **6**, 225–228; R. Huang and K. H. Shaughnessy, *Organometallics*, 2006, **25**, 4105–4112; L. R. Moore, E. C. Western, R. Craciun, J. M. Spruell, D. A. Dixon, K. P. O'Halloran and K. H. Shaughnessy, *Organometallics*, 2008, **27**, 576–593.
- J. P. Genêt, A. Linquist, E. Blart, V. Mouriès and M. Savignac, *Tetrahedron Lett.*, 1995, **36**, 1443–1446; C. Dupuis, K. Adiey, L. Charrault, V. Michelet, M. Savignac and J. P. Genêt, *Tetrahedron Lett.*, 2001, **42**, 6523–6526.
- B. H. Lipshutz, T. B. Petersen and A. R. Abela, *Org. Lett.*, 2008, **10**, 1333–1336; B. H. Lipshutz and A. R. Abela, *Org. Lett.*, 2008, **10**, 5329–5332.

- 17 C. Nájera, J. Gil-Moltó, S. Karlström and L. R. Falvello, *Org. Lett.*, 2003, **5**, 1451–1454; C. Nájera, J. Gil-Moltó and S. Karlström, *Adv. Synth. Catal.*, 2004, **346**, 1798–1811; L. Botella and C. Nájera, *Angew. Chem., Int. Ed.*, 2002, **41**, 179–181; K. Botella and C. Nájera, *Angew. Chem.*, 2002, **114**, 187–189; D. A. Alonso, C. Nájera and M. C. Pacheco, *J. Org. Chem.*, 2002, **67**, 5588–5594; L. Botella and C. Nájera, *J. Organomet. Chem.*, 2002, **663**, 46–57; D. A. Alonso, L. Botella, C. Nájera and M. C. Pacheco, *Synthesis*, 2004, **10**, 1713–1718.
- 18 R. B. DeVasher, L. R. Moore and K. H. Shaughnessy, *J. Org. Chem.*, 2004, **69**, 7919–7927; R. B. DeVasher, J. M. Spruell, D. A. Dixon, G. A. Broker, R. D. Rogers and K. H. Shaughnessy, *Organometallics*, 2005, **24**, 962–971.
- 19 R. K. Arvela and N. E. Leadbeater, *Org. Lett.*, 2005, **7**, 2101–2104.
- 20 K. M. Dawood, *Tetrahedron*, 2007, **63**, 9642–9651.
- 21 V. Polackova and S. Toma, *Chem. Pap.*, 2007, **61**, 41–45; V. Polackova, M. Hutka and S. Toma, *Ultrason. Sonochem.*, 2005, **12**, 99–102.
- 22 K. Worm-Leonhard and M. Meldal, *Eur. J. Org. Chem.*, 2008, 5244–5253.
- 23 M. Mora, C. Jiménez-Sanchidrián and J. R. Ruiz, *J. Mol. Catal. A: Chem.*, 2008, **285**, 79–83.
- 24 M. Meise and R. Haag, *ChemSusChem*, 2008, **1**, 637–642.
- 25 L. Liu, Y. Zhang and B. Xin, *J. Org. Chem.*, 2006, **71**, 3994–3997.
- 26 Y. Han, H. V. Huynh and G. K. Tan, *Organometallics*, 2007, **26**, 6581–6585.
- 27 T. Brendgen, M. Frank and J. Schatz, *Eur. J. Org. Chem.*, 2006, 2378–2383.
- 28 A. M. Sheloumov, P. Tundo, F. M. Dolgushin and A. A. Koridze, *Eur. J. Inorg. Chem.*, 2008, 572–576.
- 29 B. Inés, R. SanMartin, F. Churrua, E. Domínguez, M. K. Urtiaga and M. I. Arriortua, *Organometallics*, 2008, **27**, 2833–2839; B. Inés, I. Moreno, R. SanMartin and E. Domínguez, *J. Org. Chem.*, 2008, **73**, 8448–8451.
- 30 R. B. Bedford and S. L. Welch, *Chem. Commun.*, 2001, 129–130; R. B. Bedford, S. L. Hazelwood (née Welch) and M. E. Limmert, *Chem. Commun.*, 2002, 2610–2612; R. B. Bedford, C. S. J. Cazin and S. L. Hazelwood (née Welch), *Angew. Chem., Int. Ed.*, 2002, **41**, 4120–4122; R. B. Bedford, S. L. Hazelwood (née Welch), P. N. Horton and M. B. Hursthouse, *Dalton Trans.*, 2003, 4164–4174; R. B. Bedford and M. E. Blake, *Adv. Synth. Catal.*, 2003, **345**, 1107–1110; R. B. Bedford, *Chem. Commun.*, 2003, 1787–1796.
- 31 H. C. Kolb, M. G. Finn and K. B. Sharpless, *Angew. Chem., Int. Ed.*, 2001, **40**, 2004–2021; S. Narayan, J. Muldoon, M. G. Finn, V. V. Fokin, C. Kolb and K. B. Sharpless, *Angew. Chem., Int. Ed.*, 2005, **44**, 3275–3279.
- 32 E. J. Moses and A. D. Moorhouse, *Chem. Soc. Rev.*, 2007, **36**, 1249–1262.
- 33 S. Ogo, Y. Takebe, K. Uehara, T. Yamazaki, H. Nakai, Y. Watanabe and S. Fukuzumi, *Organometallics*, 2006, **25**, 331–338.
- 34 C. Adamo, C. Amatore, I. Ciofini, A. Jutand and H. Lakmini, *J. Am. Chem. Soc.*, 2006, **128**, 6829–6836.
- 35 While the products received by our procedure are pure enough for general synthesis, they are likely to contain trace amounts of Pd, which would need to be removed for medicinal applications to meet the allowable level in drug substances of 5 ppm. See: C. E. Garrett and K. Prasad, *Adv. Synth. Catal.*, 2004, **346**, 889–900.

Aerobic oxidative carboxylation of olefins with metalloporphyrin catalysts†

Dongsheng Bai and Huanwang Jing*

Received 5th August 2009, Accepted 19th October 2009

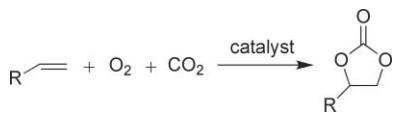
First published as an Advance Article on the web 27th October 2009

DOI: 10.1039/b916042f

Dioxo(tetraphenylporphyrinato)ruthenium(vi) and quaternary onium salt were successfully developed as catalysts to initiate a three component reaction of olefin, O₂, and CO₂ at ambient temperature under low pressure. The reaction can be carried out under solvent-free or solvent conditions. Styrene carbonate was obtained in 76% yield with 100% selectivity using 4 mol% of catalyst under optimized conditions.

The catalytic transformation of carbon dioxide into useful organic compounds has attracted much attention during the last two decades due to economic and environmental benefits arising from the utilization of renewable sources and a growing concern about the greenhouse effect.^{1,2} The preparation of cyclic carbonates (CC) *via* cycloaddition of CO₂ with epoxides is one of the methodologies for CO₂ fixation^{3–11} in terms of their valuable uses such as organic synthetic intermediates, monomers, aprotic polar solvents, pharmaceutical/fine chemical intermediates.^{12–20}

The direct oxidative carboxylation of olefins seems to be an efficient method for the synthesis of cyclic carbonates (Scheme 1). Aresta *et al.* reported the one-pot synthesis of styrene carbonate from styrene, CO₂ and molecular oxygen as an oxidant with homogeneous rhodium complex catalysts^{21,22} or metal oxide,²³ which, however, suffer from high pressure, low yields of the desired carbonates and by-products such as benzaldehyde, benzoic acid, acetophenone, phenylacetaldehyde and styrene oxide. Srivastava *et al.* used titanasilicate catalysts for the direct synthesis of cyclic carbonate from styrene in a single reactor; initially they conducted the epoxidation of olefin with H₂O₂ or *tert*-butyl hydroperoxide (TBHP) at 60 °C and then added CO₂ and a co-catalyst with an organic base at a temperature of 120 °C. The yield of carbonate was not high although the reaction conditions were optimized.²⁴ Arai *et al.* used TBHP as an oxidant to synthesize carbonates from styrene and CO₂. The yield of carbonate was higher than in the literature above,



Scheme 1 The synthesis of carbonate from olefins.

State Key Laboratory of Applied Organic Chemistry, College of Chemistry and Chemical Engineering, Lanzhou University, 730000, Lanzhou, Gansu, China. E-mail: hwjing@lzu.edu.cn; Fax: (+) 86 931 891 2582; Tel: 18919992189

† Electronic supplementary information (ESI) available: Experimental details and spectra of IR, ¹H NMR, GC-MS and GC trace. See DOI: 10.1039/b916042f

but it also suffers from high pressure, high temperature and by-products such as benzaldehyde and benzoic acid.^{25–30} Li *et al.* developed a catalytic system of *N*-bromosuccinimide (NBS) together with 1,8-diazabicyclo[5.4.0]undec-7-ene (DBU) to synthesize carbonate with aqueous H₂O₂ as an oxidant under high pressure and temperature.³¹

In the search for an alternative homogeneous catalyst for this aerobic oxidative carboxylation approach and expanding our own efforts toward the development of efficient catalysts for cycloaddition of CO₂ to epoxides,³ we initiated our investigations using metalloporphyrin catalysts following the principle that ruthenium porphyrin catalysts can catalyze the epoxidation of alkenes without reductive aldehyde additives.^{32,33} Herein, we demonstrate a convenient route to synthesize cyclic carbonates by an aerobic oxidative carboxylation of olefins using O₂ as an oxidant and CO₂ as a carboxylation reagent with 100% selectivity and high yield under lower pressure at ambient temperature.

We have discovered that dioxo(tetraphenylporphyrinato)ruthenium(vi) [Ru(TPP)(O)₂](1)/quaternary onium salt can effectively catalyze the aerobic oxidative carboxylation of olefins at ambient temperature under 1.6 MPa pressure of oxygen and carbon dioxide. Styrene reacts with 2 equivalents of TBAB in the presence of 0.4 mol% of catalyst **1** to generate styrene carbonate (SC) in 19.7% yield within 48 h at 30 °C under solvent-free conditions. It is noteworthy that this three component reaction does not lead to any by-products. Moreover, with catalyst loading as low as 0.1 mol%, NMR monitoring of the reaction showed a slight conversion in the product after 48 h. These results outshine the use of heterogeneous catalysts of metal oxide or homogeneous rhodium complex catalysts which require higher temperature and pressure.

The analysis and identification of products were performed by GC-MS, ¹H NMR, and IR *etc.* As shown in Table 1, these attractive reactions can be carried out under solvent-free conditions or with solvent. The ruthenium catalyst **1** combined with tetrabutylammonium bromide (TBAB) was found to be the best catalyst for this three component reaction (Entries 1–10). Any additives diminished the reaction rate (Entries 7, 8–10). The cocatalyst of CrO₃/CrCl₃ induced many by-products of benzaldehyde and benzoic acid (Entry 10). In dichloromethane, the reaction was carried out very well to yield the desired SC in about 76% yield with 100% selectivity (Entry 13) using 2 equivalents of tetrabutylammonium iodide (TBAI) as cocatalyst. More or less cocatalyst loading decelerated the reaction rate under both solvent-free conditions and with solvent (Entries 1, 3 and 12–14). Surprisingly, this reaction can be achieved in air (Entry 20) and can also be accomplished in other solvents such as ethanol (Entry 21) and THF (Entry 22). The common

Table 1 Aerobic oxidative carboxylation of styrene^a

Entry	Co-catalyst	Styrene	Time/h	SC Yield (%) ^b
1	1TBAB	250 ^b	48	trace
2	2TBAB	250 ^b	48	19.7
3	3TBAB	250 ^b	48	<1
4	2TBAF	250 ^b	48	trace
5	2TBAC	250 ^b	48	2.2
6	2TBAI	250 ^b	48	1.5
7	2TBAB/imidazole	250 ^b	48	trace
8	2TBAB/V ₂ O ₅	250 ^b	120	4.6
9	2 PTAT	250 ^b	48	<1
10	2CrO ₃ /CrCl ₃	250 ^b	120	trace
11	2TBAI	50	48	23.9
12	1TBAI	25	48	9.8
13	2TBAI	25	48	76
14	3TBAI	25	48	7.1
15	2TBAI	10	48	79.3
16	2TBAF	25	48	14.7
17	2TBAC	25	48	8.3
18	2TBAB	25	48	17.5
19	2PTAT	25	48	50.5
20	2TBAI	25 ^c	72	7.5
21	2TBAI	25 ^d	60	89
22	2TBAI	25 ^e	48	14.5
23	2TBAI	25 ^f	48	3.6
24	<i>m</i> -CPBA/TBAI	25 ^g	48	40.7

^a Catalyst **1** 37.5 mg (0.05 mmol), cocatalyst 1-3 equivalents of catalyst, styrene 10-250 equivalents of catalyst, $P(\text{O}_2)$ 0.5 MPa, $P(\text{CO}_2)$ 1.1 MPa, CH_2Cl_2 5 ml, T 30 °C. ^b Neat. ^c $P(\text{air})$ 2.0 MPa. ^d Ethanol 5 ml. ^e THF 5 ml. ^f Catalyst Fe(TPP)Cl. ^g Catalyst Ru(Salen)(PPh₃)₂. ^h Determined by ¹H NMR

Table 2 Aerobic oxidative carboxylation of olefins^a

Entry	Olefin	Co-catalyst	Yield (%) ^b of CC
1	3-Chloropropylene	TBAI	56.7
		PTAT	4.6
2	1-Hexene	TBAI	11.1
		PTAT	28.6 ^c
3	1-Octene	TBAI	<1
		PTAT	78.4 ^c
4	Cyclohexene	TBAI	6.8 ^d
		PTAT	30.5 ^{c,d}
5	Cyclooctene	TBAI	1.8
		PTAT	49.8 ^{c,e}

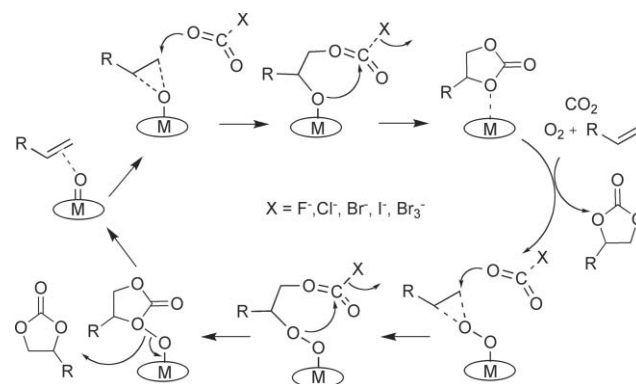
^a Catalyst **1** 37.5 mg (0.05 mmol), cocatalyst 0.1 mmol, olefin 1.25 mmol (25 equivalents). $P(\text{O}_2)$ 0.5 MPa, $P(\text{CO}_2)$ 1.1 MPa, CH_2Cl_2 5 ml, T 30 °C, 48 h. ^b Determined by ¹H NMR. ^c Combined bromination by-products indicated by GC-MS. ^d Some branched carbonate by-product can be found by IR. ^e Some epoxide by-product can be found by GC-MS.

biomimetic catalyst of Fe(TPP)Cl can lead to styrene carbonate formation in poor yield (3.6%) accompanied by benzoic acid (55.3%) and benzaldehyde (37.5%) as major products because of its good oxidative property and poor coupling property from epoxide to cyclic carbonate (Entry 23). Meanwhile, the *in situ* catalyst of Ru(Salen)(O) generated from Ru(Salen)(PPh₃)₂ by oxidation with *m*-CPBA can convert styrene to styrene carbonate in considerable yield (40.7%) with a little benzaldehyde (2.3%) as a by-product (Entry 24).

The best catalysts were thus found to be **1**/TBAB under solvent-free conditions and **1**/TBAI in dichloromethane for styrene and 3-chloropropylene (Table 2, entry 1). To expand the scope of the reaction, various olefins were used with this

green reaction. The results are listed in Table 2 and reveal that the cocatalyst of phenyltrimethylammonium tribromide (PTAT) was more active than TBAI (Entry 2-5) for 1-hexene, 1-octene, cyclohexene, and cyclooctene *etc.* The best example is that 1-octene can be transformed to cyclic carbonate in 78.4% yield when the ratio of 1-octene to catalyst was 25 (Entry 3). Under these reaction conditions, some branched carbonates of cyclohexene and bromination addition species of other olefins were found as by-products. It is well known that the cyclohexene is easily converted to polycarbonate in the presence of catalyst.² For example, the vibration of the carbonyl group of polycarbonate formed from cyclohexene appeared at 1746 cm⁻¹ whereas the carbonyl group of cyclic carbonate appeared at 1793 cm⁻¹. A little cyclooctene oxide was also detected by GC-MS in the presence of PTAT as cocatalyst.

Hence it is evident that the cocatalyst plays an important role in initiating the reaction. These findings impelled us to propose a mechanism for this attractive green reaction (Scheme 2). The formation of the target is rationalized by the transfer of an oxygen atom from the catalyst to form the epoxide intermediate which is attacked by active carbon dioxide. The intermediate then undergoes intramolecular cyclization to yield the cyclic carbonate and metalporphyrin that reacts immediately with oxygen and olefin to form a new intermediate. The new intermediate is attacked by active carbon dioxide to regenerate the oxo-metalporphyrin catalyst accompanied by another molecule of target compound, which completes the catalytic cycle.

**Scheme 2** Proposed mechanism of aerobic oxidative carboxylation of olefins.

In summary, we have developed a one-pot, highly selective synthetic method for forming cyclic carbonate using Ru(TPP)(O)₂ as catalyst and quaternary onium salt as cocatalyst. The most important feature of this methodology can be attributed to the use of 4 mol% of catalyst providing a high yield of product. Thus, this simple methodology would be a novel protocol to directly approach the cyclic carbonate from various alkenes. To the best of our knowledge, this is the first example of a homogenous protocol towards the formation of styrene carbonate with 100% selectivity at ambient temperature under low pressure reported in the literature. The investigation of this reaction mechanism and optimization of catalyst systems to enhance their catalytic efficiency are under way in our laboratory.

Acknowledgements

This research was supported by the National Natural Science Foundation of China (No. 20843005, 20973086).

Notes and references

- D. J. Darensbourg and M. W. Holtcamp, *Coord. Chem. Rev.*, 1996, **153**, 155.
- D. J. Darensbourg, R. M. Mackiewicz, A. L. Phelps and D. R. Billodeaux, *Acc. Chem. Res.*, 2004, **37**, 836.
- L. L. Jin, H. W. Jing, T. Chang, X. L. Bu, L. Wang and Z. L. Liu, *J. Mol. Catal. A: Chem.*, 2007, **262**, 261.
- K. Nakano, T. Kamada and K. Nozaki, *Angew. Chem., Int. Ed.*, 2006, **45**, 7274.
- H. S. Kim, J. J. Kim, J. J. S. D. Lee, M. S. Lah, D. Moon and H. G. Jang, *Chem.–Eur. J.*, 2003, **9**, 678.
- X. B. Lu, S. Lei, Y. M. Wang, R. Zhang, Y. J. Zhang, X. J. Peng, Z. C. Zhang and B. Li, *J. Am. Chem. Soc.*, 2006, **128**, 1664.
- Y. Shen, W. L. Duan and M. Shi, *Adv. Synth. Catal.*, 2003, **345**, 337.
- H. W. Jing and S. T. Nguyen, *J. Mol. Catal. A: Chem.*, 2007, **261**, 12.
- Y. J. Kim and R. S. Varma, *J. Org. Chem.*, 2005, **70**, 7882.
- Y. M. Shen, W. L. Duan and M. Shi, *J. Org. Chem.*, 2003, **68**, 1559.
- J. L. Jiang, F. X. Gao, R. M. Hua and X. Q. Qiu, *J. Org. Chem.*, 2005, **70**, 381.
- J. W. Huang and M. Shi, *J. Org. Chem.*, 2003, **68**, 6705.
- W. N. Sit, S. M. Ng, K. Y. Kwong and C. P. Lau, *J. Org. Chem.*, 2005, **70**, 8583.
- M. Alvaro, C. Baleizao, D. Das, E. Carbonell and H. Garcia, *J. Catal.*, 2004, **228**, 254.
- A. G. Shaikh and S. Sivaram, *Chem. Rev.*, 1996, **96**, 951.
- R. L. Paddock and S. T. Nguyen, *J. Am. Chem. Soc.*, 2001, **123**, 11498.
- V. Caló, A. Nacci, A. Monopoli and A. Fanizzi, *Org. Lett.*, 2002, **4**, 2561.
- H. Yang, Y. Gu, Y. Deng and F. Shi, *Chem. Commun.*, 2002, 274.
- T. Yano, H. Matsui, T. Koike, H. Ishiguro, H. Fujihara, M. Yoshihara and T. Maeshima, *Chem. Commun.*, 1997, 1129.
- R. L. Paddock and S. T. Nguyen, *Chem. Commun.*, 2004, 1622.
- M. Aresta and E. Quaranta, *J. Mol. Catal.*, 1987, **41**, 355.
- M. Aresta, A. Dibenedetto and I. Tommasi, *Appl. Organomet. Chem.*, 2000, **14**, 799.
- M. Aresta and A. Dibenedetto, *J. Mol. Catal. A: Chem.*, 2002, **182**, 399.
- R. Srivastava, D. Srinivas and P. Ratnasamy, *Catal. Lett.*, 2003, **91**, 133.
- J. M. Sun, S. I. Fujita, B. Bhanage and M. Arai, *Catal. Commun.*, 2004, **5**, 83.
- J. M. Sun, S. I. Fujita, B. Bhanage and M. Arai, *Catal. Today*, 2004, **93–95**, 383.
- J. M. Sun, S. I. Fujita, B. Bhanage and M. Arai, *J. Organometal. Chem.*, 2005, **690**, 3490.
- J. M. Sun, S. I. Fujita, X. F. Zhao, M. Hasegawa and M. Arai, *J. Catal.*, 2005, **230**, 398.
- Y. L. Wang, J. M. Sun, D. Xiang, L. Wang, J. M. Sun and F. S. Xiao, *Catal. Lett.*, 2009, **129**, 437.
- J. M. Sun, Y. L. Wang, X. J. Qu, D. Z. Jiang, F. S. Xiao, M. Hasegawa and M. Arai, *Chem. J. Chin. Univ.*, 2006, **27**, 1522.
- N. Eghbali and C. J. Li, *Green Chem.*, 2007, **9**, 213.
- J. T. Groves and R. Quinn, *J. Am. Chem. Soc.*, 1985, **107**, 5790.
- J. L. Zhang, J. S. Huang and C. M. Che, *Chem. Eur. J.*, 2006, **12**, 3020.

Amidine-mediated delivery of CO₂ from gas phase to reaction system for highly efficient synthesis of cyclic carbonates from epoxides

Balaka Barkakaty, Kazuhide Morino, Atsushi Sudo and Takeshi Endo*

Received 7th August 2009, Accepted 6th October 2009

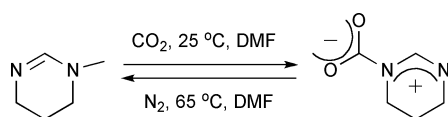
First published as an Advance Article on the web 29th October 2009

DOI: 10.1039/b916235f

A novel, efficient synthesis of cyclic carbonates from the reaction of epoxides and gaseous CO₂ under mild conditions (1 atm, rt to 45 °C) was achieved in reasonable yields (65–83%) by using *N*-methyltetrahydropyrimidine (MTHP) that facilitated efficient delivery of CO₂ from the gas phase to the reaction system.

Introduction

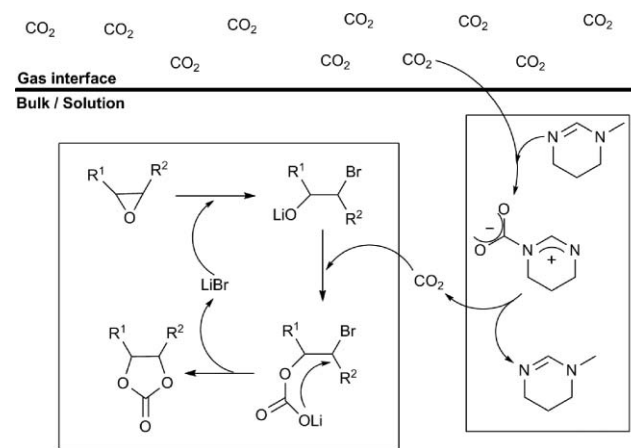
Innovation of novel methods for easy and economical chemical fixation of CO₂ and its use as a C1 resource for synthesis of valuable target molecules is the need of this century for the sustenance of life on earth.¹ Recently, the synthesis of five-membered cyclic carbonates from epoxides using CO₂ has gained much attention, owing to its increased importance as a building block in polymer synthesis, electrolytes, aprotic polar solvents and precursors for pharmaceuticals.² For this reaction, various catalysts, including metal complexes,³ smectites,⁴ titanosilicates,⁵ zeolites,⁶ metal oxides,⁷ organic bases,⁸ alkali metal halides⁹ and ionic liquids,¹⁰ have already been developed and reported. However, high pressure and/or high temperature are important pre-requisites for high efficiency in these catalytic systems, and some of them suffer from the formation of poly(carbonate) as a by-product. Endo and coworkers have reported that alkali metal salts such as lithium bromide catalyzed the reaction at 1 atm pressure to give five-membered cyclic carbonates in high yields and without the formation of poly(carbonate).⁹ However, in order to achieve a satisfactory rate of reaction, heating the system to 100 °C was required. In other words, catalysis of the reaction at 1 atm and at near ambient temperature is still a highly challenging endeavour. Recently, Endo and coworkers have reported a reversible system for efficient trap-and-release of CO₂(g) by *N*-methyltetrahydropyrimidine (MTHP) and its analogous functionality attached to polymer side chains (Scheme 1).¹¹



Scheme 1 Reversible fixation-release of CO₂ by amidine (MTHP).

Molecular Engineering Institute, Kinki University, 11-6 Kayanomori, Iizuka, Fukuoka, 820-8555, Japan.
E-mail: tendo@mol-eng.fuk.kindai.ac.jp; Fax: +81-948-22-7210;
Tel: +81-948-22-7210

This intrinsic nature of MTHP prompted us to design a new system for converting epoxides into the corresponding carbonates under milder temperature conditions and at atmospheric pressure, which relies on utilization of MTHP that can naturally capture CO₂ molecules from the gas phase and deliver them to the reactive site in a reversible cycle (Scheme 2).

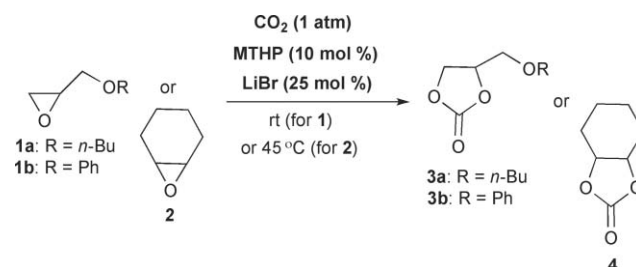


Scheme 2 Delivery of CO₂ by amidine and its insertion reaction with epoxide.

Herein, we report our achievement of a highly efficient utilization of CO₂ at low temperature (<45 °C) and under 1 atm, which was facilitated by participation of MTHP as a “CO₂ deliverer”.

Results and discussion

For the present study, two monosubstituted epoxides, *n*-butyl glycidyl ether (**1a**), glycidyl phenyl ether (**1b**), and one sterically hindered disubstituted epoxide, cyclohexene oxide (**2**), were employed as substrates (Scheme 3). The reactions were carried out at 25 or 45 °C, which were much lower than the previously



Scheme 3 Amidine catalyzed synthesis of cyclic carbonates from epoxides under mild conditions.

Table 1 Synthesis of cyclic carbonates from epoxides^a

Entry	Substrate/ product	Amount of MTHP/mol%	Time/h	<i>T</i> /°C	Yield/% ^b
1	1a / 3a	0	6	25	48
2	1a / 3a	10	6	25	100 (77)
3 ^c	1a / 3a	10	6	25	0
4 ^d	1b / 3b	0	96	25	45
5 ^d	1b / 3b	10	24	25	35
6 ^d	1b / 3b	10	96	25	100 (83)
7	2 / 4	0	72	45	12
8	2 / 4	10	12	45	25
9	2 / 4	10	24	45	68
10	2 / 4	10	48	45	84
11	2 / 4	10	72	45	95 (65)

^a Conditions: [epoxide]₀: [MTHP]: [LiBr] = 100:10:25. ^b Determined by ¹H NMR. Isolated yields are shown in parentheses. ^c Reaction carried out in the absence of LiBr. ^d Reaction carried out in NMP, the initial concentration of epoxide was 1 M.

reported temperature (100 °C)⁹ for the efficient transformation of epoxide into the corresponding carbonate by using lithium bromide as catalyst under 1 atm CO₂. The results are summarized in Table 1.

The reaction of **1a** was studied first. As a reference experiment, the reaction was performed in the absence of MTHP (entry 1); when a bulk mixture of **1a** and LiBr (25 mol%) was stirred at room temperature in a reaction vessel equipped with a 1 atm CO₂ balloon, **1a** was slowly converted into the corresponding cyclic carbonate **3a**, and after 6 h, its yield, determined by ¹H NMR analysis of the resulting mixture, had reached 48%. On the other hand, the addition of 10 mol% MTHP under similar conditions remarkably improved the efficiency of the reaction to allow complete conversion of **1a** into **3a** after 6 h (entry 2). However, use of LiBr was mandatory for the reaction; in its absence, the reaction fails to proceed (entry 3).

This remarkable acceleration was also observed on adding MTHP in the reaction of epoxide **1b** (entry 4 vs. entry 5). In this case, use of a solvent was required, because the intrinsically high crystallinity of the corresponding carbonate product **3b** prevented efficient progress of the reaction in the bulk state. *N*-Methylpyrrolidone (NMP) was used as a suitable solvent which allowed the reaction to proceed in the homogeneous system.⁹ In the absence of MTHP, only 45% yield of the corresponding cyclic carbonate **3b** was achieved, even though the reaction time was prolonged to 96 h (entry 4). In contrast, by adding MTHP, the reaction was greatly accelerated to achieve 100% yield of **3b** under the same reaction conditions (entry 6).

These successful results at low temperature encouraged us further to apply the MTHP-mediated system for the reaction of cyclohexene oxide **2** (Table 1, entries 8–11). So far, transformation of such 1,2-disubstituted epoxides into the corresponding carbonates by conventional systems has been rather difficult due to steric hindrance.^{3d,3g,8c,10a,10e} For example, when cyclohexene oxide **2** was heated in NMP (at 100 °C, for 24 h) under 1 atm CO₂, the reaction was quite slow, leading to only 35% yield of the carbonate **4**. This poor efficiency implied the intrinsic low reactivity of **2**, and, in fact, its bulk reaction at 45 °C in the absence of MTHP was also very slow, giving the corresponding carbonate **4** in only 12% yield after 72 h (entry 7). In contrast, by adding MTHP, the efficiency of the reaction was improved

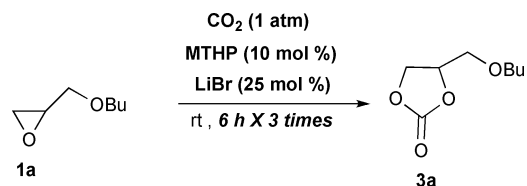
Table 2 Reusability of MTHP–LiBr system

Entry	Recycle number	Yield/% ^a
1	Fresh	100
2	Recycle 1	46
3	Recycle 2	22

^a Determined by ¹H NMR.

markedly. The yield of **4** reached 25% after 12 h (entry 8), followed by a smooth progress of the reaction to achieve 95% yield at 72 h (entries 8–11).

However, the catalytic efficiency of the catalysts showed a gradual decrease when recycled (Scheme 4, Table 2). This might be attributed to the gradual decrease of LiBr concentration during the process of product separation by filtration and repeated washing with diethyl ether. Since Li salts are known to have a high affinity for carbonate and ether compounds,¹² successive formation of carbonate products followed by further treatment with diethyl ether probably removes substantial amounts of the required LiBr catalyst from the reaction system, resulting in lower yields of the desired products when the same loadings of catalysts were reused.

**Scheme 4** Synthesis of butylglycidyl carbonate from recycled catalysts.

Conclusion

In summary, a highly efficient synthesis of cyclic carbonates from the corresponding epoxides was designed and achieved by utilizing only a catalytic amount of natural CO₂ fixer like MTHP along with the conventional LiBr catalyst. This system broadens the scope of such reactions by outlining a key concept to overcome the high activation barrier which is faced by these reactions when using conventional methodologies employing high temperature and high pressure techniques. The reported method can be operated successfully at atmospheric pressure and at 25–45 °C, which allows less energy-demanding and more environmentally friendly chemical fixation of CO₂ into valuable compounds. The successful results imply that addition of MTHP as a “CO₂ deliverer” might be a versatile strategy to improve the efficiency of various reaction systems which use CO₂ as a reactant.

Experimental

a) The experimental procedure for the synthesis of **3a**

CO₂(g) from a gas balloon (purchased from AS ONE, code 9-086-01) was allowed to react with 10 mol% of MTHP (25 mg, 0.25 mmol) at room temperature for 25 min, after which the liquid MTHP turned into white solid. Then, 25 mol% of LiBr (55 mg, 0.64 mmol) followed by 2.55 mmol of *n*-butyl glycidyl

ether (**1a**, 0.36 ml) were added to the reaction mixture and the reaction was allowed to stir at room temperature under CO₂ atmosphere (1 atm) for another 6 h. ¹H NMR of the crude reaction mixture in CDCl₃ showed 100% conversion of the starting epoxide to the desired carbonate compound after 6 h. Diethyl ether (5 ml) was then added to the reaction mixture and the reaction mixture was allowed to stir for around 10 min in the open air, the liquid part was then separated from the suspension by simple filtration. The residue in the reaction vessel was scratched with a spatula and washed several times with diethyl ether and filtered to ensure removal of any carbonate product trapped in the white solid suspension. Then, the combined filtrate was evaporated to obtain 360 mg of pure *n*-butyl glycidyl carbonate (**3a**) in 81% yield.¹³

b) The experimental procedure for the synthesis of **3b**

CO₂(g) from a gas balloon (purchased from AS ONE, code 9-086-01) was allowed to react with 10 mol% of MTHP (25 mg, 0.25 mmol) in 2.5 mL of NMP at room temperature for 25 min. Then, 25 mol% of LiBr (55 mg, 0.64 mmol) followed by 2.55 mmol of phenyl glycidyl ether (**1b**, 0.35 ml) were added to the reaction mixture and the reaction was allowed to stir at room temperature under CO₂ atmosphere (1 atm) for another 96 h. ¹H NMR of the crude reaction mixture in CDCl₃ after 96 h showed 100% conversion of the starting epoxide to the desired carbonate compound. The reaction mixture was then poured into 100 mL of water and the precipitate was washed thoroughly with water. The crude cyclic carbonate was then recrystallized from ethanol to obtain 411 mg of pure phenyl glycidyl carbonate (**3b**) in 83% yield.^{9a}

c) The experimental procedure for the synthesis of **4**

CO₂(g) from a gas balloon (purchased from AS ONE, code 9-086-01) was allowed to react with 10 mol% of MTHP (200 mg, 2.04 mmol) at room temperature for 25 min, after which the liquid MTHP turned into white solid. Then, 25 mol% of LiBr (443 mg, 5.1 mmol) followed by 20.04 mmol of cyclohexene oxide (**2**, 2.0 ml) were added to the reaction mixture and the reaction was allowed to stir at 45 °C under CO₂ atmosphere for 72 h. After 72 h, the reaction mixture turned into a gel-like precipitate. ¹H NMR of the crude reaction mixture in CDCl₃ after 72 h showed 95% conversion of the starting epoxide to the desired carbonate compound. Then, the crude reaction mixture was extracted with EtOAc–H₂O followed by a further three extractions of the aqueous layer with EtOAc. The combined organic layers were dried over anhydrous MgSO₄ and concentrated *in vacuo*. The residue was purified by column chromatography [hexane–EtOAc (3/2, v/v)] to give 1.85 g of **4** (65% yield).¹⁴

Acknowledgements

This research was financially supported by the JSR Corporation. We are thankful to Dr. Bungo Ochiai from Yamagata University for providing us with MTHP to carry out our initial investigations.

Notes and references

- (a) M. Yoshida, Y. Komatsuzaki and M. Ihara, *Org. Lett.*, 2008, **10**, 2083; (b) Y. Sugawara, W. Yamada, S. Yoshida, T. Ikeno and T. Yamada, *J. Am. Chem. Soc.*, 2007, **129**, 12902; (c) M. Yoshida, Y. Ohnawa, K. Sugimoto, H. Tokuyama and M. Ihara, *Tetrahedron Lett.*, 2007, **48**, 8678; (d) T. Mizuno, M. Mihara, T. Nakai, T. Iwai and T. Ito, *Synthesis*, 2007, 2524; (e) M. Murakami, N. Ishida and T. Miura, *Chem. Commun.*, 2006, 643; (f) K. Shimizu, M. Takimoto, Y. Sato and M. Mori, *Org. Lett.*, 2005, **7**, 195; (g) G. S. Andrade, J. E. Berkner, C. L. Liotta, C. Eckert, D. A. Schiraldi, A. Andersen and D. M. Collard, *Synth. Commun.*, 2003, **33**, 3643; (h) P. Munshi, D. J. Heldebrant, E. P. Mckoon, P. A. Kelly, C.-C. Tai and P. G. Jessop, *Tetrahedron Lett.*, 2003, **44**, 2725; (i) E. R. Perez, M. O. da Silva, V. C. Costa, P. R.-F. Ubirajara and D. W. Franco, *Tetrahedron Lett.*, 2002, **43**, 4091; (j) T. Mizuno and Y. Ishino, *Tetrahedron*, 2002, **58**, 3155; (k) M. Takimoto and M. Mori, *J. Am. Chem. Soc.*, 2001, **123**, 2895; (l) W. McGhee, D. Riley, K. Christ, Y. Pan and B. Parnas, *J. Org. Chem.*, 1995, **60**, 2820; (m) H. Hoberg and M. Minato, *J. Organomet. Chem.*, 1991, **406**, C25; (n) H. Hoberg, Y. Peres, C. Krueger and Y. H. Tsay, *Angew. Chem.*, 1987, **99**, 799.
- (a) A.-A. G. Shaikh and S. Sivaram, *Chem. Rev.*, 1996, **96**, 951; (b) J. H. Clements, *Ind. Eng. Chem. Res.*, 2003, **42**, 663; (c) J. P. Parrish, R. N. Salvatore and K. W. Jung, *Tetrahedron*, 2000, **56**, 8207; (d) J. Bayardon, J. Holz, B. Schaffner, V. Andrushko, S. Verevkin, A. Preetz and A. Borner, *Angew. Chem., Int. Ed.*, 2007, **46**, 5971.
- (a) R. L. Paddock and S. T. Nguyen, *J. Am. Chem. Soc.*, 2001, **123**, 11498; (b) H. S. Kim, J. J. Kim, B. G. Lee, O. S. Jung, H. G. Jang and S. O. Kang, *Angew. Chem., Int. Ed.*, 2000, **39**, 4096; (c) S.-S. Wu, X.-W. Zhang, W.-L. Dai, S.-F. Yin, W.-S. Li, Y.-Q. Ren and C.-T. Au, *Appl. Catal., A*, 2008, **341**, 106; (d) H. Jing and S. T. Nguyen, *J. Mol. Catal. A: Chem.*, 2007, **261**, 12–15; (e) T. Chang, H. Jing, L. Jin and W. Qiu, *J. Mol. Catal. A: Chem.*, 2007, **264**, 241; (f) W.-L. Wong, K.-C. Cheung, P.-H. Chan, Z.-Y. Zhou, K.-H. Lee and K.-Y. Wong, *Chem. Commun.*, 2007, 2175; (g) F. Li, C. Xia, L. Xu, W. Sun and G. Chen, *Chem. Commun.*, 2003, 2042.
- B. M. Bhanage, S. Fujita, Y. Ikushima, K. Torii and M. Arai, *Green Chem.*, 2003, **5**, 71.
- R. Srivastava, D. Srinivas and P. Ratnaswamy, *Catal. Lett.*, 2003, **91**, 133.
- M. Tu and R. J. Davis, *J. Catal.*, 2001, **199**, 85.
- (a) K. Yamaguchi, K. Ebitani, T. Yoshida, H. Yoshida and K. Kaneda, *J. Am. Chem. Soc.*, 1999, **121**, 4526; (b) H. Yasuda, L.-N. He and T. Sakakura, *J. Catal.*, 2002, **209**, 547.
- (a) H. Kawanami and Y. Ikushima, *Chem. Commun.*, 2000, 2089; (b) Y.-M. Shen, W.-L. Duan and M. Shi, *Adv. Synth. Catal.*, 2003, **345**, 337; (c) A. Barbarini, R. Maggi, A. Mazzacani, G. Mori, G. Sartori and R. Sartorio, *Tetrahedron Lett.*, 2003, **44**, 2931.
- (a) N. Kihara, N. Hara and T. Endo, *J. Org. Chem.*, 1993, **58**, 6198; (b) N. Kihara and T. Endo, *Macromolecules*, 1992, **25**, 4824.
- (a) J. Sun, S. Zhang, W. Cheng and J. Ren, *Tetrahedron Lett.*, 2008, **49**, 3588; (b) V. Calo, A. Nacci, A. Monopoli and A. Fanizzi, *Org. Lett.*, 2002, **4**, 2561; (c) Y. J. Kim and R. S. Varma, *J. Org. Chem.*, 2005, **70**, 7882; (d) H. Kawanami, A. Sasaki, K. Matsui and Y. Ikushima, *Chem. Commun.*, 2003, 896; (e) Y. Xie, Z. Zhang, T. Jiang, J. He, B. Han, T. Wu and K. Ding, *Angew. Chem., Int. Ed.*, 2007, **46**, 7255.
- (a) T. Endo, D. Nagai, T. Monma, H. Yamaguchi and B. Ochiai, *Macromolecules*, 2004, **37**, 2007; (b) B. Ochiai, K. Yokota, A. Fujii, D. Nagai and T. Endo, *Macromolecules*, 2008, **41**, 1229; (c) E. R. Perez, R. H. A. Santos, M. T. P. Gambardella, L. G. M. de Macedo, U. P. Rodrigues-Filho, J.-C. Launay and D. W. Franco, *J. Org. Chem.*, 2004, **69**, 8005; (d) P. G. Jessop, D. J. Heldebrant, X. Li, C. A. Eckert and C. L. Liotta, *Nature*, 2005, **436**, 1102; (e) Y. Liu, P. G. Jessop, M. Cunningham, C. A. Eckert and C. L. Liotta, *Science*, 2006, **313**, 958; (f) T. Yamada, P. J. Lukac, T. Yu and R. G. Weiss, *Chem. Mater.*, 2007, **19**, 4761; (g) T. Yamada, P. J. Lukac, M. George and R. G. Weiss, *Chem. Mater.*, 2007, **19**, 967.
- (a) A. M. Belostotskii, E. Markevich and D. Aurbach, *J. Coord. Chem.*, 2004, **57**, 1047; (b) W. H. Meyer, *Adv. Mater.*, 1998, **10**, 439.
- T. Nishikubo, T. Iizawa, M. Iida and N. Isobe, *Tetrahedron Lett.*, 1986, **27**, 3741.
- M. Suzuki and T. Sugai, *Bull. Chem. Soc. Jpn.*, 2004, **77**, 1217.

An efficient approach to homocoupling of terminal alkynes: Solvent-free synthesis of 1,3-diynes using catalytic Cu(II) and base†

Dong Wang, Jihui Li, Na Li, Tingting Gao, Sihua Hou and Baohua Chen*

Received 24th August 2009, Accepted 19th October 2009

First published as an Advance Article on the web 30th October 2009

DOI: 10.1039/b917448f

We report an environmentally friendly, efficient method for transforming terminal acetylenes into 1,3-diynes based on catalytic amounts of a Cu(II) salt and base under solvent-free conditions. The developed process conforms to the principles of 'green' chemistry and addresses the shortage of such methods for the synthesis of 1,3-diynes. The reaction is quite general and results in good yields. Interestingly, the system also allows the synthesis of unsymmetric 1,3-diynes by cross-coupling of two different terminal alkynes. Finally, the catalyst can also be recycled.

Introduction

One of the challenges facing chemists this century is to develop new transformations that are not only efficient, selective, and high-yielding but that are also environmentally benign.¹ During the last decade, the topic of 'green' chemistry has received increasing attention.^{1,2} 'Green' chemistry aims at the total elimination (or at least the minimization) of waste, and the implementation of sustainable processes.^{1a} The utilization of nontoxic chemicals, renewable materials and solvent-free conditions are the key issues in a green synthetic strategy. In the present work, we describe a green approach towards the synthesis of conjugate 1,3-diyne.

Conjugate 1,3-diyne derivatives are very important materials in the fields of biology and materials science, because they can be converted into various structural entities, especially substituted heterocyclic compounds.³ Traditional methods for the synthesis of 1,3-diynes include Glaser oxidative dimerization of terminal alkynes,^{4a} various improved Glaser oxidative homocoupling reactions of terminal alkynes,^{4b-c} and Sonogashira coupling.^{4f} The catalyst system used commonly is the Pd,⁵ which involves Cu(I) salts as co-catalyst. Although Pd catalysts play a crucial role because of their mild, efficient and selective properties, they are expensive and often require phosphine or amine reagents.^{5e,5g,6} To address this, several groups have reported homocoupling reactions of terminal alkynes using a Pd-free catalytic system.⁷ For example, D. F. Li *et al.* described the reaction in the presence of CuI/I₂,⁸ and H. F. Jiang *et al.* reported the Cu(II)-promoted oxidative homocoupling reaction of terminal alkynes

in supercritical carbon dioxide.⁹ These Pd-free catalytic systems are efficient and economic, but their imperfections include the requirements of stoichiometric amounts of amine reagents, high pressure, high temperature, utilization of a co-catalyst and an oxygen atmosphere.^{5h,7b,7c,10} Moreover, it should be pointed out that the classical syntheses of conjugate 1,3-diynes (including the Pd-catalyzed and the Pd-free systems) generally involve organic solvents such as methanol, acetone, pyridine, methyl cellosolve (2-methoxyethanol) and toluene. Use of organic solvents is environmentally unfriendly, and so it is highly desirable to develop more environmentally friendly and economic methodologies for synthesizing conjugate 1,3-diynes. To achieve this, we report an environmentally friendly, economic, efficient and simple solvent-free system that allows the homocoupling reactions of terminal alkynes based on catalytic amounts of CuCl₂ and triethylamine at 60 °C in air. The method is also useful for the synthesis of unsymmetric 1,3-diynes by cross-coupling of two different terminal alkynes. The results are summarized below.

Results and discussion

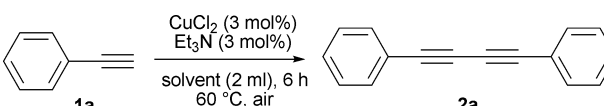
In order to identify the optimal reaction conditions, phenylacetylene was chosen as a test substrate. In this preliminary experiment, the homocoupling of phenylacetylene was carried out in various solvents, with CuCl₂ (3 mol%) as a catalyst and Et₃N (3 mol%) as a base, in air at 60 °C for 6 h (Table 1). It was found that the reaction proceeded perfectly in toluene or benzene (Table 1, entries 1 and 2), but that the yields decreased when the reaction was carried out in other solvents (Table 1, entries 3–11). However, the reaction surprisingly proceeded in excellent yields (>96%) under solvent-free conditions (Table 1, entry 12). The pure product was purified by column chromatography or reduced-pressure distillation. Considering our goal of an economic and environmentally friendly reaction, these solvent-free conditions are clearly the most favorable.

Then we examined the influence of the catalysts on the yields. The reaction did not occur without a catalyst (Table 2, entry 1), and CuCl₂ was more efficient than other Cu(0), Cu(I) and Cu(II) catalysts (Table 2, entries 2–12). It was noted that Cu(OH)₂/TiO₂ produced the desired product in 65% yield in the absence of base at 100 °C under an oxygen atmosphere (entry 2).

In the third set of experiments, we performed the reaction with various bases under solvent-free conditions in air (Table 3). As can be seen, the reaction could not be performed without a base (Table 3, entry 1). Organic bases including primary amines, secondary amines and tertiary amines were more effective than inorganic bases, with triethylamine being the best. There was

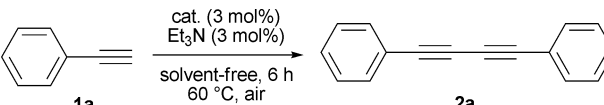
Key Laboratory of Nonferrous Metal Chemistry and Resources Utilization of Gansu Province, Lanzhou, 730000, P. R. China; State Key Laboratory of Applied Organic Chemistry, Lanzhou University, Lanzhou, 730000, P. R. China. E-mail: chbh@lzu.edu.cn

† Electronic supplementary information (ESI) available: Additional experimental information. See DOI: 10.1039/b917448f

Table 1 Preliminary survey of solvents for the homocoupling reaction of phenylacetylene catalyzed by CuCl₂^a


Entry	Catalyst	Solvent	Yield (%) ^b
1	CuCl ₂	Toluene	99
2	CuCl ₂	Benzene	98
3	CuCl ₂	Water	3
4	CuCl ₂	Methanol	14
5	CuCl ₂	THF	16
6	CuCl ₂	Acetonitrile	12
7	CuCl ₂	Ethanol	8
8	CuCl ₂	DMF	40
9	CuCl ₂	DMSO	42
10	CuCl ₂	Dioxane	72
11	CuCl ₂	Acetone	25
12	CuCl ₂	None	>96

^a The reaction was carried out using **1a** (1 mmol) and Et₃N (0.03 mmol) in the presence of CuCl₂ (0.03 mmol) in the solvent (2 ml) at 60 °C in air. ^b Isolated yields after column chromatography.

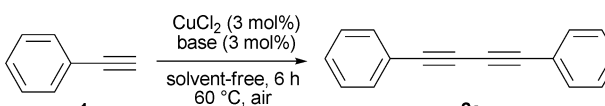
Table 2 Screening of catalysts for the homocoupling reaction of phenylacetylene^a


Entry	Catalyst	Yield (%) ^b
1	None	0
2	Cu(OH) _x /TiO ₂ ^c	65
3	CuCl	16
4	CuBr ₂	8
5	Cu(OAc) ₂ ·H ₂ O	7
6	CuI	Trace
7	Cu(OTf) ₂	7
8	Cu	4
9	Cu(PPh ₃) ₃ Cl	2
10	CuCl ₂ ·2H ₂ O	49
11	Cu(PPh ₃) ₂ NO ₃	15
12	Cu(acac) ₂	Trace

^a The reaction was carried out using **1a** (1 mmol) and Et₃N (0.03 mmol) in the presence of catalyst (0.03 mmol) at 60 °C in air. ^b Isolated yields after column chromatography. ^c Cu(OH)_x/TiO₂ (Cu = 5 mol%).

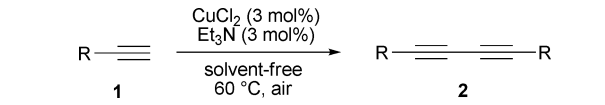
also a good yield with n-butylamine as base (Table 3, entry 5). Therefore, the optimal solvent-free system for this reaction involves Et₃N (3 mol%) and CuCl₂ (3 mol%).

Encouraged by the efficiency of the reaction protocol described above, we investigated the substrate scope. A variety of terminal alkynes including aromatic and aliphatic acetylenes were tested under the optimized conditions. The results show that the solvent-free CuCl₂-catalyzed homocoupling reaction tolerates a variety of functional groups. As shown in Table 4, the catalytic oxidative homocoupling of phenylacetylenes **1a–h**, which contain electron-donating as well as electron-withdrawing substituents, proceeded readily to afford the corresponding diyne derivatives **2a–h** in 50–99% yields (entries 1–8). The reaction of the heteroatom-containing alkyne **1i** also proceeded efficiently (entry 9), but the desired product of the heteroatom-

Table 3 Screening of bases for the homocoupling reaction of phenylacetylene catalyzed by CuCl₂^a


Entry	Base	Yield (%) ^b
1	None	0
2	Triethylamine	>96
3	Diethylamine	69
4	Pyridine	12
5	n-butylamine	90
6	K ₂ CO ₃	24
7	KO ^t Bu	10
8	Piperidine	38
9	Diisopropylamine	35
10	<i>tert</i> -Butylamine	18
11	NaOH	14
12	TMEDA	70 ^c
13	K ₃ PO ₄ ·3H ₂ O	7

^a The reaction was carried out using **1a** (1 mmol) and base (0.03 mmol) in the presence of CuCl₂ (0.03 mmol) at 60 °C in air. ^b Isolated yields after column chromatography. ^c TMEDA = tetramethylethylenediamine.

Table 4 Solvent-free synthesis of various conjugate 1,3-diyne by CuCl₂^a


Entry	R	Time/h	Product	Yield (%) ^b
1	Phenyl (1a)	6	2a	>96
2	4-CH ₃ OC ₆ H ₄ (1b)	6	2b	99
3	3-CH ₃ C ₆ H ₄ (1c)	6	2c	>98
4	4-FC ₆ H ₄ (1d)	6	2d	80
5	Naphthalen-1-yl (1e)	6	2e	88
6	2-ClC ₆ H ₄ (1f)	6	2f	85
7	3-NH ₂ C ₆ H ₄ (1g)	4	2g	50
8	4-n-C ₅ H ₁₁ OC ₆ H ₄ (1h)	6	2h	>98
9	Thiophen-3-yl (1i)	6	2i	90
10	Pyridine-2-yl (1j)	4	2j	70
11	BrCH ₂ (1k)	6	2k	60
12	n-C ₄ H ₉ (1l)	6	2l	75
13	HOC(CH ₃) ₂ (1m)	6	2m	40
14	HOCH ₂ (1n)	6	2n	45
15	Ferrocenyl (1o)	10	2o	99 ^c

^a The reaction was carried out using RC≡CH (1 mmol) and Et₃N (0.03 mmol) in the presence of CuCl₂ (0.03 mmol) at 60 °C in air.

^b Isolated yields after column chromatography. ^c The reaction was carried out using **1o** (1 mmol) and Et₃N (2 mmol) in the presence of CuCl₂ (0.03 mmol) at 100 °C in air for 10 h.

containing alkyne **1j** was isolated in 70% yield, due to the partial carbonization of the substrate (entry 10). When aliphatic acetylenes were used, the yields were somewhat lower (entries 11 and 12). Alkynes based on propargylic alcohols also gave the corresponding diynes, but the yields were low (entries 13 and 14). Interestingly, we successfully extended the procedure to higher-boiling alkynes such as ferrocenylacetylene, and the yield of the obtained product being 99% (entry 15). In addition, the crude products of symmetric 1,3-diyne can be purified by

Table 5 Solvent-free synthesis of various unsymmetric conjugate 1,3-diynes by catalytic amounts of Cu(II) salt and base^a

$\text{R}_1\text{—C}\equiv\text{C} + \text{C}\equiv\text{C—R}_2 \xrightarrow[\text{solvent-free 10 h, 60 }^\circ\text{C, air}]{\text{CuCl}_2 (3 \text{ mol}\%), \text{Et}_3\text{N} (3 \text{ mol}\%)} \text{R}_1\text{—C}\equiv\text{C—C}\equiv\text{C—R}_2$				
Entry	R ₁	R ₂	Product	Yield (%) ^b
1	4-CH ₃ OC ₆ H ₄	C ₆ H ₅	3a	70
2	HOCH ₂	C ₆ H ₅	3b	35
3	4-CH ₃ OC ₆ H ₄	3-CH ₃ C ₆ H ₄	3c	55
4	4-n-C ₅ H ₁₁ OC ₆ H ₄	C ₆ H ₅	3d	72
5	HOC(CH ₃) ₂	C ₆ H ₅	3e	32
6	4-CH ₃ OC ₆ H ₄	Thiophen-3-yl	3f	56
7	n-C ₄ H ₉	C ₆ H ₅	3g	Trace
8	n-C ₄ H ₉	4-CH ₃ OC ₆ H ₄	3h	Trace

^a The reaction was carried out using R¹C≡CH (0.5 mmol), R²C≡CH (3 mmol) and Et₃N (0.03 mmol) in the presence of CuCl₂ (0.03 mmol) at 60 °C in air. ^b Isolated yields after column chromatography.

reduced pressure distillation (except 1,4-diferrocenylbuta-1,3-diyne **2o**) – reduced pressure distillation is simpler and more environmentally friendly than column chromatography.

The cross-coupling of two different terminal alkynes was also investigated in the catalytic system by using an excess of one of the terminal alkyne substrates. As shown in Table 5, unsymmetric 1,3-diynes were produced in 32–72% yield. Phenylacetylene **1a** successfully cross-coupled with some alkynes including alkoxy alkynes (entries 1 and 4), propargylic alcohols (entries 2 and 5); *p*-methoxyphenylacetylene **1b** could also be cross-coupled with aromatic acetylenes (entries 1 and 3) and a heteroatom-containing alkyne (entry 6), although the yields were somewhat lower. The reaction between **1l** and **1a** (or **1b**) only gives trace product (entries 7 and 8). It should be noted that the crude products of unsymmetric 1,3-diynes only can be purified by column chromatography – reduced pressure distillation does not work for these compounds.

Finally, we examined the recovery and reuse of CuCl₂. The catalyst can be recovered by filtration, acidification, and drying under vacuum, and can then be reused. After five recycles, the activity of the recovered catalyst decreased slightly to 85%. The average catalyst recovery was about 80% (Table 6).

Table 6 Recovery and reuse of CuCl₂

$\text{C}_6\text{H}_5\text{—C}\equiv\text{C} \xrightarrow[\text{solvent-free, 6 h, 60 }^\circ\text{C, air}]{\text{CuCl}_2 (3 \text{ mol}\%), \text{Et}_3\text{N} (3 \text{ mol}\%)} \text{C}_6\text{H}_5\text{—C}\equiv\text{C—C}\equiv\text{C—C}_6\text{H}_5$		
Run	Product yield (%)	Catalyst recovery (%)
1	96	75
2	90	78
3	90 ^b	80
4	88 ^b	82
5	85 ^b	85

^a Isolated yields after reduced-pressure distillation. ^b The reaction time was 10 h.

Conclusion

In conclusion, we have developed an environmentally friendly, economical and efficient method for transforming terminal acetylenes into 1,3-diynes under solvent-free conditions with catalytic amounts of CuCl₂ and triethylamine. The procedure is suitable for many substrates, and various conjugate 1,3-diynes can be produced conveniently with excellent yields. This catalytic system can also be used for the synthesis of unsymmetrical 1,3-diynes, although the yields are not perfect. The catalyst can also be recycled five times with only a moderate reduction in activity, making it acceptable for industrial-scale production.

Experimental

General

Solvents were dried and degassed by standard methods, and all alkynes are readily available. Flash column chromatography was performed using silica gel (300–400 mesh). Analytical thin-layer chromatography was performed using glass plates pre-coated with 200–400 mesh silica gel impregnated with a fluorescent indicator (254 nm).

Typical experimental procedure for the homocoupling reaction under solvent-free conditions

Typical reaction procedure: to a mixture of CuCl₂ (3.0 mol%) and Et₃N (3.0 mol%), phenylacetylene (1.0 mmol) was added. The mixture was stirred at 60 °C under air for 6 h.

Purification of crude product by Method 1. After cooling to room temperature, the mixture was diluted with ethyl acetate and filtered. The filtrate was removed under reduced pressure to give the crude product, which was further purified by silica gel chromatography (petroleum ether–ethyl acetate as eluent) to yield the corresponding 1,3-diynes.

Purification of crude product by Method 2. After cooling to room temperature, the mixture was diluted with dichloromethane and filtered. The filtrate was washed with water and the organic phase was dried using MgSO₄. Dichloromethane and unreacted phenylacetylene were removed under reduced pressure to give the purified product.

Acknowledgements

We are grateful to the project sponsored by the Scientific Research Foundation for the State Education Ministry (No. 107108) and the Project of the National Science Foundation of P. R. China (No. J0730425).

References

- (a) P. T. Anastas and T. C. Williamson, *Green Chemistry: Frontiers in Benign Chemical Syntheses and Processes*, Oxford Science Publications, New York, 1998; (b) J. M. DeSimone, *Science*, 2002, **297**, 799–803; (c) S. J. Jeon, H. M. Li and P. J. Walsh, *J. Am. Chem. Soc.*, 2005, **127**, 16416–16425.
- (a) M. Poliakoff and P. T. Anastas, *Nature*, 2001, **413**, 257; (b) A. S. Matlack, *Introduction to Green Chemistry*, Marcel Dekker, Inc., New York, 2001; (c) R. A. Cross and B. Kalra, *Science*, 2002, **297**, 803–807.
- (a) F. Bohlmann, T. Burkhardt and C. Zdero, *Naturally Occurring Acetylenes*, Academic Press, London, 1973; (b) L. Hansen and P. M.

- Boll, *Phytochemistry*, 1986, **25**, 285; (c) H. Matsunaga, M. Katano, H. Yamamoto, H. Fujito, M. Mori and K. Takata, *Chem. Pharm. Bull.*, 1990, **38**, 3480.
- 4 (a) C. Glaser, *Ber. Dtsch. Chem. Ges.*, 1869, **2**, 422; (b) A. S. Hay, *J. Org. Chem.*, 1962, **27**, 3320; (c) E. Valenti, M. A. Pericas and F. Serratos, *J. Am. Chem. Soc.*, 1990, **112**, 7405; (d) P. Cadiot and W. Chodkiewicz, in *Chemistry of Acetylene*, H. G. Viehe, Marcel Dekker, New York, 1969, p. 597; (e) G. Eglinton and R. Galbraith, *J. Chem. Soc.*, 1959, 889; (f) K. Sonogashira, Y. Tohda and N. Hagihara, *Tetrahedron Lett.*, 1975, **16**, 4467.
- 5 (a) M. Vlassa, I. Ciocan-Tarta, F. Margineanu and I. Oprean, *Tetrahedron*, 1996, **52**, 1337; (b) Q. Liu and D. J. Burton, *Tetrahedron Lett.*, 1997, **38**, 4371; (c) A. Lei, M. Srivastava and X. Zhang, *J. Org. Chem.*, 2002, **67**, 1969; (d) I. J. S. Fairlamb, P. S. B. auerlein, L. R. Marrison and J. M. Dickinson, *Chem. Commun.*, 2003, 632; (e) A. S. Batsanov, J. C. Collings, I. J. S. Fairlamb, J. P. Holland, J. A. K. Howard, Z. Y. Lin, T. B. Marder, A. C. Parsons, R. M. Ward and J. Zhu, *J. Org. Chem.*, 2005, **70**, 703; (f) J. H. Li, Y. Liang and X. D. Zhang, *Tetrahedron*, 2005, **61**, 1903; (g) J. H. Li, Y. Liang and Y. X. Xia, *J. Org. Chem.*, 2005, **70**, 4393; (h) M. Shi and H. X. Qian, *Appl. Organomet. Chem.*, 2006, **20**, 771.
- 6 (a) P. Siemsen, R. C. Livingston and F. Diederich, *Angew. Chem., Int. Ed.*, 2000, **39**, 2632; (b) V. D. Subhash, S. Dong and P. H. Lee, *J. Org. Chem.*, 2003, **68**, 7085.
- 7 (a) C. Z. Bing and Z. Xuan, *Appl. Organomet. Chem.*, 2007, **21**, 345; (b) K. Keigo, Y. Syuhei, K. Miyuki, Y. Kazuya and M. Noritaka, *Angew. Chem., Int. Ed.*, 2008, **47**, 2407–2410; (c) J. S. Yadav, B. V. S. Reddy, K. Bhaskar Reddy, K. U. Gayathri and A. R. Prasad, *Tetrahedron Lett.*, 2003, **44**, 6493; (d) A. Sharifi, M. Mirzaei and M. R. N. Jamal, *Monatsh. Chem.*, 2006, **137**, 213; (e) G. W. Kabalka, L. Wang and R. M. Pagni, *Synlett*, 2001, 108–110.
- 8 D. F. Li, K. Yin, J. Li and X. S. Jia, *Tetrahedron Lett.*, 2008, **49**, 5918.
- 9 (a) J. H. Li and H. F. Jiang, *Chem. Commun.*, 1999, 2369; (b) H. F. Jiang, J. Y. Tang, A. Z. Wang, G. H. Deng and S. R. Yang, *Synthesis*, 2006, 1155.
- 10 T. Oishi, T. Katayama, K. Yamaguchi and N. Mizuno, *Chem. Eur. J.*, 2009.

A facile synthesis of alkylated nitrogen heterocycles catalysed by 3D mesoporous aluminosilicates with cage type pores in aqueous medium†

Rajashree Chakravarti,^{a,b} Pranjal Kalita,^a S. Tamil Selvan,^a Hamid Oveisi,^a V. V. Balasubramanian,^a M. Lakshmi Kantam^b and Ajayan Vinu^{*a}

Received 21st July 2009, Accepted 19th October 2009

First published as an Advance Article on the web 4th November 2009

DOI: 10.1039/b914628h

Friedel–Crafts alkylation of nitrogen heterocycles such as indoles and pyrroles with epoxides has been efficiently carried out using cage-type mesoporous aluminosilicates as recyclable catalysts in water under environmentally benign and mild conditions.

Alkylated nitrogen heterocycles such as indoles and pyrroles have been receiving much attention in modern pharmaceutical, biological and synthetic chemistry because of their antibiotic and anticancer activities.^{1,2} The alkylated nitrogen heterocycles are generally prepared by the ring opening of various epoxides with nitrogen heterocycles using highly corrosive acidic or basic catalysts.³ Lewis acids such as lanthanide triflates⁴ and indium salts have also been used as catalysts for the ring opening of epoxides with nitrogen heterocycles.⁵ Recently, highly enantioselective addition of indoles with aromatic epoxides has been carried out using chromium salen complexes as catalysts.⁶ Although the catalysts are highly efficient, they cannot be recovered and reused, which may create a large amount of environmentally hazardous and toxic wastes.

Environmental and economic considerations have recently raised a strong interest in redesigning commercially important processes so that the use of harmful substances and the generation of toxic waste can be avoided.⁷ In this respect, heterogeneous catalytic processes are more favorable over their homogeneous counterparts in the production of fine chemicals, owing to their ease of handling, simple workup procedures and, most importantly, their reusability. Heterogeneous catalysts such as nanocrystalline titanium(IV) oxide,⁸ fluoroboric acid adsorbed on silica gel⁹ and sulfated zirconia¹⁰ have been widely used in the alkylation of nitrogen heterocycles with epoxides. Very recently, Kantam *et al.* have reported the ionic liquid [bmim][OTf] as an efficient promoter for the Friedel–Crafts alkylation of indoles and pyrrole derivatives.¹¹ Friedel–Crafts alkylation of indole and pyrrole derivatives has been reported with carbonyl compounds and nitroalkenes in water.¹² Unfortunately, however, these heterogeneous catalysts suffer from poor textural characteristics

and a disordered porous structure which limit the efficiency of these catalysts in the above transformation.

Ordered mesoporous materials with tunable pore size in the range of 2–50 nm have attracted a great deal of attention owing to their unique structures with organized porosity, high surface area and pore volume, and potential applications, mainly in the field of catalysis, adsorption, separation, sensors, and fuel cells. Among the porous materials, mesoporous silica materials consisting of an interconnected large-pore cage-type mesoporous system with three-dimensional (3D) porous networks are highly interesting and believed to be more advantageous than porous materials having a hexagonal pore structure with a one-dimensional array of pores. Very recently, Vinu *et al.* have reported the preparation of 3D mesoporous cage-type aluminosilicate materials (AIKIT-5) with different pore diameters, aluminium contents and morphologies.¹³ AIKIT-5 materials possess a highly-ordered cage-type mesoporous structure with cubic *Fm3m* close packed symmetry, a high surface area, narrow pore size distribution, a high specific pore volume and well-distributed tetrahedral aluminium atoms in the silica framework which provide a high acidity.¹³ It was also reported that the activity of the AIKIT-5 catalysts in the acetylation of veratrole and other organic transformations was superior to zeolites and AIMCM-41 catalysts.¹³ These exciting catalytic properties of AIKIT-5 materials stimulated us to utilize them in various other acid-catalyzed organic transformations for the production of value-added products.

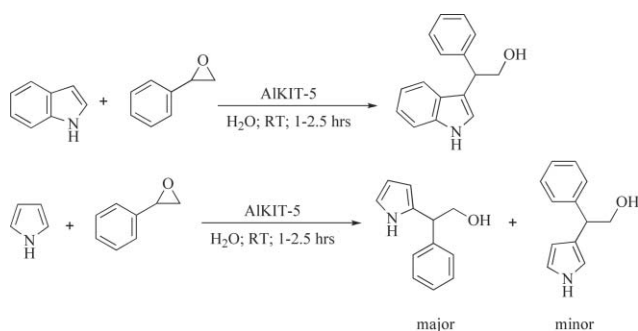
In this communication, we report, for the first time, the catalytic performance of AIKIT-5 materials in the Friedel–Crafts alkylation of nitrogen heterocycles such as indoles and pyrroles with epoxides, which are important intermediates and building blocks in organic synthesis and are readily decomposed under acidic conditions in water.¹⁴ The reactions were conducted in water at room temperature. The catalyst was found to be highly active, affording the corresponding alkylated derivatives of indoles and pyrroles in good yields (Scheme 1).

During the screening process of the catalysts for this reaction, a major emphasis was laid on the zeolites and mesoporous aluminosilicate catalysts due to their characteristic structural and chemical features, which were synthesized by the procedures reported in the literature.¹⁵ In order to find out the best catalytic system suited to the synthesis of alkylated nitrogen heterocycles, the reactions were carried out using various zeolite catalysts such as MOR, BEA, MFI and FAU, and mesoporous catalysts, namely AISBA-15 and AIMCM-41. Recently, the ring-opening reactions of epoxides or aziridines with various types of

^aInternational Centre for Materials Nanoarchitectonics, WPI Research Centre, National Institute for Materials Science, 1-1 Namiki, Tsukuba, 305-0044, Japan. E-mail: vinu.ajayan@nims.go.jp; Fax: +81-29-860-4667; Tel: +81-29-860-4563

^bInorganic and Physical Chemistry Division, Indian Institute of Chemical Technology, Uppal Road, Hyderabad, 500 607, India

† Electronic supplementary information (ESI) available: HRTEM images, N₂ adsorption–desorption isotherms and powder XRD patterns of AIKIT-5 catalysts, before and after use. See DOI: 10.1039/b914628h



Scheme 1 Alkylation of indole and pyrrole with styrene oxide

nucleophiles have been studied.¹⁶ Several methods with different catalysts employed water as the solvent, and it was believed that water was essential for the success of the reactions.¹⁷ Therefore, water and dichloromethane were used as solvents in the catalyst screening experiments in order to understand the effect of water. Comparatively better results were obtained when water was used as the reaction medium. Finally the reaction results were compared with the AIKIT-5 catalysts which are shown in Table 1. Among the catalysts studied, as can be seen in Table 1, the AIKIT-5 catalysts showed superior performance over the zeolites and other mesoporous catalysts used in this study.

The higher activity of AIKIT-5 catalysts could be mainly attributed to their excellent structural order with 3D pore symmetry and highly dispersed active sites on the uniform pore surface, which are easily accessible for the reactant molecules (Fig. S1, ESI†). As the AIKIT-5 catalyst was found to be the best catalyst used in this study, it was selected for use in further studies. It should be pointed out that when the reaction was carried out without any catalyst, no product was formed (Table 1, entry 10) even after prolonged reaction times. The effect of the Al content of the AIKIT-5 catalysts in the alkylation of indoles was also studied. A series of AIKIT-5 catalysts having different $n_{\text{Si}}/n_{\text{Al}}$ ratios was used in this study. As expected, the activity of the catalyst increases with increasing Al content in the silica framework of AIKIT-5 (Table 1, entries 1–3). Of the AIKIT-5 catalysts studied, AIKIT-5 with $n_{\text{Si}}/n_{\text{Al}} = 10$ showed the best performance, affording a yield of *ca.* 88% thanks to

Table 1 Screening of different catalysts for the alkylation of indole by styrene oxide^a

Entry	Catalyst	Time/h	Yield (%) ^{b,c}
1	AIKIT-5(10)	1.5	88, 65
2	AIKIT-5(28)	1.5	85
3	AIKIT-5(44)	1.5	80
4	AlMCM-41	1.5	42
5	MOR	1.5	35
6	BEA	1.5	25
7	MFI	1.5	20
8	FAU	1.5	20
9	AlSBA-15	1.5	—
10	—	1.5, 24	0, 2

^a Reaction conditions: indole (1.2 mmol, 140 mg), styrene oxide (1.0 mmol, 120 mg), catalyst (50 mg), solvent (2 mL) stirred at room temperature for 1.0 h. ^b Yields determined by GC. ^c Yield using dichloromethane as solvent.

Table 2 Screening of different solvents for the alkylation of indole with styrene oxide^a

Entry	Solvent	Time/h	Yield (%) ^b
1	H ₂ O	1.5	88
2	CH ₂ Cl ₂	1.5	65
3	CHCl ₃	1.5	42
4	CH ₃ CN	1.5	42
5	Toluene	1.5	—
6	Benzene	1.5	—

^a Reaction conditions: indole (1.2 mmol, 117 mg), styrene oxide (1 mmol, 120 mg), catalyst AIKIT-5(10) (50 mg), solvent (2 mL), stirred at room temperature for 1.5 h. ^b Isolated yields.

having the highest number of active sites on the surface (Table 1, entry 1).

Different solvents were used for the alkylation of indole with styrene oxide. It was found that AIKIT-5 is very efficient in water, affording an excellent yield of the corresponding product in a shorter reaction time (Table 2, entry 1) compared to other, organic solvents such as dichloromethane, chloroform, acetonitrile, toluene and benzene (Table 2, entries 2–6). The reaction was also carried out under solvent-free conditions but the catalyst was not effective in the absence of any solvent. This observation can be accounted for by the co-ordinating nature of water as a solvent which may act as a tool for facile ring opening of epoxides to form the corresponding products. The tendency of epoxides to decompose under acidic water conditions also provides an added advantage for the completion of the reaction in shorter times.^{14,18}

The reaction was also carried out using a wide variety of structurally-diverse indoles and pyrroles, with several epoxides, to form the corresponding alkylated products using AIKIT-5(10) in water. The differences in the yields of the corresponding alkylated products formed depend on the intrinsic properties of the substituted indoles and pyrroles used.

It was evident from the NMR spectral data that the aryl epoxides underwent cleavage at the benzylic position in the case of indoles to selectively give the primary alcohol product. No trace of the secondary alcohol product was detected. Moreover, in the case of all the substituted indoles used, it was found that the 3-alkylated indole products are formed selectively; no traces of the 2-alkylated products were detected in the reaction mixture. In all cases, the reactions proved to be faster than most of those reported earlier in the literature,^{5,8,9,10} and the yields of the products were also found to be comparable. The regioselectivities of the resulting products are in complete agreement with the earlier reports.^{8,9,11}

The general trend noticed in case of these reactions is that the indoles bearing electron-donating groups afforded the corresponding alkylated products in good yields (Table 3, entries 3 & 4). On the other hand, electron withdrawing groups being present on the indole moiety drastically decreases the rate of the reaction and the yield of the product formed is also very low, even after prolonged reaction times (Table 3, entries 8 & 9) when 5-nitroindole was used in the reaction. It was observed that in the case of 1-methylindole, the reaction proceeds in a significantly more facile manner to afford the corresponding

Table 3 Alkylation of indoles and pyrroles with epoxides over AIKIT-5(10)^a

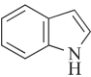
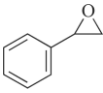
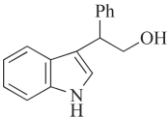
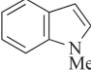
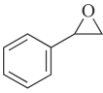
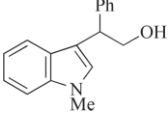
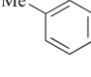
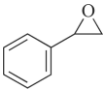
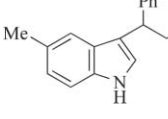
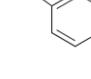
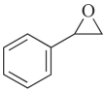
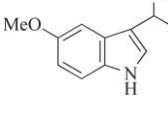
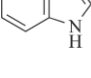
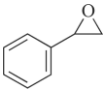
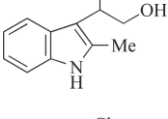
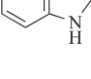
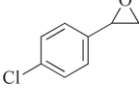
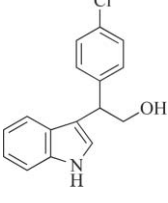
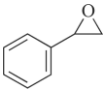
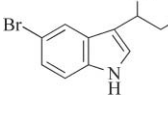
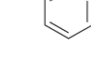
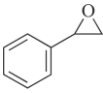
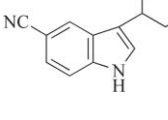
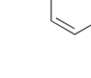
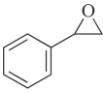
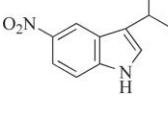
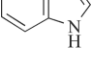
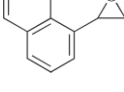
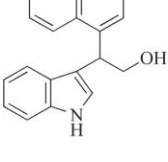
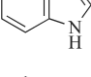
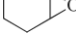
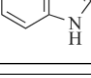

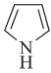
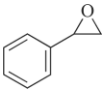
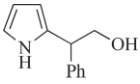
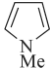
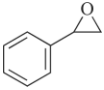
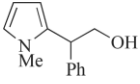
Entry	Nucleophile	Epoxide	Product	Time/h	Yield (%) ^b
1				1.5	88, 85 ^c
2				1.5	85
3				1.0	88
4				1.0	88
5				1.0	90
6				1.0	80
7				2.5	78
8				24	18
9				24	10
10				1.5	78
11			No reaction	24	—
12			No reaction	24	—

Table 3 (Contd.)

Entry	Nucleophile	Epoxide	Product	Time/h	Yield (%) ^b
13				2.5	65, 15 ^d
14				2.5	60, 13 ^d

^a Reaction conditions: indole/pyrrole (1.2 mmol), epoxide (1 mmol), AIKIT-5(10) (50 mg), water (2 mL) stirred at room temperature for an appropriate time. ^b Isolated yield of the product. ^c Yield after five cycles. ^d Isolated yields of 2-alkyl and 3-alkyl pyrroles, respectively.

product in greater yield than in the reaction of unsubstituted indole.

In contrast, in the case of pyrroles, the alkylation reaction results in the corresponding product mixture of 2-alkylated and 3-alkylated pyrroles, in which the 2-alkylated pyrrole is the major one.¹¹

It was observed from the spectroscopic data that the epoxide ring opens by the attack of the nucleophile at the benzylic position, to afford the primary alcohol. In this case, the preferred site for electrophilic attack being the 2-position of the pyrrole ring, the reaction proceeds to yield mostly the 2-alkylated product (Table 3, entry 10). This reveals that the reaction was highly regioselective, affording only primary alcohols.

The aryl epoxides having an electron-withdrawing substituent underwent the reaction comparatively faster (Table 3, entry 6) than the unsubstituted ones. Later, the reaction was carried out on a gram scale to test its effectiveness on a larger scale. In this reaction, 1 g of styrene oxide was reacted with 1.2 g of indole in the presence of AIKIT-5 in water. Interestingly, even in this case, the reaction proceeds smoothly to give 85% yield of the product. All the reactions proceeded smoothly at ambient temperature and pressure in water with high regioselectivity to afford good yields of the products in short periods. It should be pointed out that N-alkylation of the indoles and pyrroles does not take place under the optimized mild reaction conditions.

The use of water as a solvent is not only advantageous in being the most 'green' solvent available but also allows a simple, efficient and robust system for the recycling of the catalyst. In fact, after the completion of the reaction, the aqueous solution containing the catalyst and the products was extracted with ethyl acetate. To the remaining aqueous solution containing the dispersed AIKIT-5 catalyst, fresh substrates were added and the process was repeated for five cycles. The catalyst was found to be highly stable and the activity of the catalyst was not much changed even after repeated cycles (Table 3, entry 1).

In order to understand the influence of the aqueous media and the reactants on the structural order of AIKIT-5, the catalyst was dried, calcined at 540 °C, and subjected to nitrogen physisorption and X-ray diffraction (XRD) analysis after the fifth cycle (Fig. S2 and S3, ESI[†]). Although the shape of the nitrogen adsorption isotherm, the XRD pattern, and the pore size of the AIKIT-5(10) catalyst used are similar to that of the fresh catalyst, a slight reduction in the surface area and pore volume was observed. This could be due to a slight

deterioration of the structure of the catalyst after the reaction and the activation of the catalyst at higher temperature.

In summary, a simple and an efficient protocol for a highly regio- and chemoselective alkylation of indoles and pyrroles with epoxides has been described. The reaction occurs in aqueous media and requires only a catalytic amount of AIKIT-5 catalyst. No other promoters or additives are required to obtain a good yield of the product. The catalyst AIKIT-5 dispersed in water forms a robust and recyclable catalytic system, which can be reused several times without any regeneration, thus reducing the amount of disposed waste considerably. Further, the recycling of the heterogeneous catalyst makes the process of separation simpler and cheaper. The reaction has also been extended to the gram scale to prove its industrial usefulness, which could pave the way to replace the existing toxic, corrosive and expensive homogenous catalysts currently used in the industry.

Experimental section

AIKIT-5 catalysts with different n_{Si}/n_{Al} ratios were synthesized using the procedure reported in the literature.¹³ The various zeolites used were also synthesized using reported procedures.¹³

A typical experimental procedure

To a stirred solution of indole (1.2 mmol, 140 mg) and styrene oxide (1 mmol, 120 mg) in water (2 mL), AIKIT-5 (50 mg) was added. The reaction mixture was stirred at room temperature for an appropriate time (Table 3). After completion of the reaction, as monitored by TLC, the aqueous phase containing the catalyst was recovered quantitatively *via* simple extraction of the product with ethyl acetate (3 × 10 mL). The organic extracts were then dried over anhydrous sodium sulfate and concentrated under reduced pressure. The resulting product was then purified by column chromatography on silica gel (100–200 mesh) with ethyl acetate–*n*-hexane (1 : 4) as eluent to afford pure 2-(3-indolyl)-2-phenylethanol (Table 3, entry 1). ¹H NMR (300 MHz, CDCl₃): δ = 1.60 (br, 1 H), 4.18–4.23 (m, 2 H), 4.50 (t, *J* = 6.7 Hz, 1 H), 7.01–7.45 (m, 10 H), 8.11 (br, 1 H) ppm. MS (EI): *m/z* = 237 (25), 206 (100), 178 (30), 128 (15), 102 (10), 77 (15), 63 (5), 51 (11).

Other known products were identified by comparison with the data in the literature.^{5,9,11}

The aqueous phase containing the catalyst was recycled by the addition of fresh substrates and by continuing the reaction for appropriate times.

Acknowledgements

This work was partially supported by the Ministry of Education, Culture, Sports, Science and Technology (MEXT) under the Strategic Program for Building an Asian Science and Technology Community scheme and the World Premier International Research Center (WPI) Initiative on Materials Nanoarchitectonics, MEXT, Japan. One of the authors, R.C., thanks CSIR, India for a research fellowship and NIMS for offering the internship.

Notes and references

- (a) *The Alkaloids*, Specialist Periodical Reports; The Chemical Society, London, 1971; (b) J. E. Saxton, *Nat. Prod. Rep.*, 1989, **6**, 1; (c) R. A. Glennon, *J. Med. Chem.*, 1997, **40**, 1; (d) M. E. Jung and F. Slowinski, *Tetrahedron Lett.*, 2001, **42**, 6835; (e) T. Walsh, R. B. Toupenca, F. Ujjainwala, J. R. Young and M. T. Goulet, *Tetrahedron*, 2001, **57**, 5233; (f) M. G. N. Russell, R. J. Baker, L. Barden, M. S. Beer, L. Bristow, H. B. Howard, B. Broughton, M. Knowles, G. McAllister, S. Patel and J. L. Castro, *J. Med. Chem.*, 2001, **44**, 3881; (g) H.-C. Zhang, H. Ye, A. F. Moretto, K. K. Brumfield and B. E. Maryanoff, *Org. Lett.*, 2000, **2**, 89; (h) B. H. Lipshutz, *Chem. Rev.*, 1986, **86**, 795.
- (a) M. Hasse, *Alkaloid Chemistry*, Wiley, New York, 1978; (b) G. A. Cordell, *Introduction to Alkaloids: A Biogenetic approach*, Wiley, New York, 1981; (c) T. L. Gilchrist, *Heterocyclic Chemistry*, Pitman, London; (d) M.-L. Bannasar, B. Vidal and J. Bosch, *J. Org. Chem.*, 1997, **62**, 3597; (e) R. F. Raffauf, T. M. Zennie, K. D. Onan and P. W. LeQuesne, *J. Org. Chem.*, 1984, **49**, 2714; (f) P. Magnus, *J. Chem. Soc., Chem. Commun.*, 1983, 26; (g) R. A. Jones, G. P. Bean, *The Chemistry of Pyrroles*, Academic Press, London.
- (a) *Organic High Pressure Chemistry*, W. J. le Noble, Ed.; Elsevier; (b) K. Matsumoto, A. Sera and T. Uchida, *Synthesis*, 1985, 1; (c) H. Kotsuki, M. Nishiuchi, S. Kobayashi and H. Nishizawa, *J. Org. Chem.*, 1990, **55**, 2969; (d) H. Kotsuki, K. Hayashida, T. Shimanouchi and H. Nishizawa, *J. Org. Chem.*, 1996, **61**, 984.
- S. P. Tanis and J. W. Raggon, *J. Org. Chem.*, 1987, **52**, 819.
- (a) H. Kotsuki, M. Teraguchi, N. Shimomoto and M. Ochi, *Tetrahedron Lett.*, 1996, **37**, 3727; (b) M. Bandini, P. G. Cozzi, P. Melchiorre and A. Umani-Ronchi, *J. Org. Chem.*, 2002, **67**, 5386; (c) J. S. Yadav, B. V. S. Reddy, S. Abraham and G. Sabitha, *Synlett*, 2002, 1550.
- M. Bandini, P. G. Cozzi, P. Melchiorre and A. Umani-Ronchi, *Angew. Chem., Int. Ed.*, 2004, **43**, 84.
- A. Taguchi and F. Schuth, *Microporous Mesoporous Mater.*, 2005, **77**, 1.
- M. L. Kantam, S. Laha, J. Yadav and B. Sreedhar, *Tetrahedron Lett.*, 2006, **47**, 6213.
- B. P. Bandgar and A. V. Patil, *Tetrahedron Lett.*, 2007, **48**, 173.
- B. Das, P. Thirupathi, R. A. Kumar and K. R. Reddy, *Catal. Commun.*, 2008, **9**, 635.
- M. L. Kantam, R. Chakravarti, B. Sreedhar and S. Bhargava, *Synlett*, 2008, 1449.
- (a) W. Zhuang and K. A. Jorgensen, *Chem. Commun.*, 2002, 1336; (b) N. Azizi, F. Arynasab and M. R. Saidi, *Org. Biomol. Chem.*, 2006, **4**, 4275.
- (a) P. Srinivasu, S. Alam, V. V. Balasubramanian, S. Velmathi, D. P. Sawant, W. Bohlmann, S. P. Mirajkar, K. Ariga, S. B. Halligudi and A. Vinu, *Adv. Funct. Mater.*, 2008, **18**, 640; (b) V. V. Balasubramanian, P. Srinivasu, C. Anand, R. R. Pal, K. Ariga, S. Velmathi, Sher Alam and A. Vinu, *Microporous Mesoporous Mater.*, 2008, **114**, 303.
- (a) S. Azoulay, K. Manabe and S. Kobayashi, *Org. Lett.*, 2005, **7**, 4593; (b) P. A. Grieco, *Organic Synthesis in Water*, Blackie Academic & Professional, London, 1998; (c) C. J. Li, T. H. Chan, *Organic Reactions in Aqueous Media*, John Wiley, New York, 1997.
- (a) A. Breda, M. Signoreto, E. Ghedini, F. Pinna and G. Cruciani, *Appl. Catal., A*, 2006, **308**, 216; (b) P. Moreau, A. Finiels and P. Meric, *J. Mol. Catal. A: Chem.*, 2000, **154**, 185; (c) M. Sasidharan and R. Kumar, *J. Catal.*, 2003, **220**, 326.
- J. G. Smith, *Synthesis*, 1984, 629.
- (a) F. Fringuelli, O. Piermatti, F. Pizzo and L. Vaccaro, *J. Org. Chem.*, 1999, **64**, 6094; (b) R.-H. Fan and X.-L. Hou, *J. Org. Chem.*, 2003, **68**, 726.
- C.-J. Li, *Chem. Rev.*, 1993, **93**, 2023.

Solubilisation of α -chymotrypsin by hydrophobic ion pairing in fluoruous systems and supercritical carbon dioxide and demonstration of efficient enzyme recycling

Karima Benaissi,^{a,b} Martyn Poliakoff^{*a} and Neil R. Thomas^{*b}

Received 10th March 2009, Accepted 21st August 2009

First published as an Advance Article on the web 29th September 2009

DOI: 10.1039/b904761a

Hydrophobic ion-pairing (HIP) with the fluorinated surfactant KDP 4606 (KDP) was used to extract the protein α -chymotrypsin (CMT) into perfluoromethylcyclohexane (PFMC). The diameter of the solubilised CMT-KDP complexes formed in PFMC was determined by dynamic light scattering (DLS) to be 25 nm which suggested the formation of a protein aggregate containing ~100 protein molecules surrounded by KDP 4606 surfactant molecules per particle. The catalytic activity of the protease CMT either solubilised by HIP or as the suspended native enzyme has been investigated in both a fluoruous biphasic system (FBS) and a supercritical carbon dioxide (scCO₂) batch reactor. Transesterification of *N*-acetyl-L-phenylalanine ethyl ester (APEE) with *n*-butanol or *rac*-2-butanol was catalysed by the protease in the FBS hexane-PFMC or scCO₂ at 40 °C. Under comparable conditions, the amount of transesterification of the solubilised protease-surfactant (CMT-KDP) complex in PFMC (6–10%) was shown to be significantly higher than that of the suspended protease (1–3%) in either hexane-PFMC or scCO₂. This suggested the formation of a catalytically active CMT-KDP aggregate in PFMC. The CMT-KDP complex which is retained in the fluoruous phase on cooling the solution was successfully reused over four cycles with no loss of activity.

Introduction

The lipids, esters, acids and alcohols that are widely used as starting materials for the commercial production of important pharmaceuticals, cosmetics and food products, are often poorly soluble in water. Therefore, biocatalysis in non-aqueous media to produce these materials has attracted considerable attention in recent decades.¹ Given the move to replace hydrocarbon solvents with more environmentally benign alternatives, one area of significant research activity is the identification of new solvents and reaction systems that are compatible with the use of enzymes.¹

Different strategies, such as the suspension of the enzyme in an organic solvent,² lipid-coated enzymes,³ microencapsulation of enzymes in reverse-micelles,⁴ immobilisation of enzymes on a microgel-matrices or within membranes,⁵ covalent attachment of polymers (pegylation) to the enzyme,⁶ stabilisation of enzymes forming cross-linked enzyme crystals (CLECs[®])⁷ or cross-linked enzyme aggregates (CLEAs[®]),^{7,8} aimed at increasing the stability and active site accessibility of enzymes have been employed to enhance enzymatic activity in organic media. However, the effect on the catalytic activity of these modified enzyme forms

is unpredictable and modifications can result in a considerable loss of enzymatic activity.^{3,4,6–11}

The technique of hydrophobic ion-pairing (HIP) has previously been reported to solubilise proteins in hydrocarbon solvents by forming ion pairs with anionic organic surfactants such as Aerosol-OT (AOT) (see Fig. 1 for structure).¹² In some cases, including with protease α -chymotrypsin (CMT),^{1,13–16} an increase in catalytic activity was observed with these anionic surfactant-enzyme complexes in the organic solvent.^{1,13–19} The use of HIP to solubilise enzymes using anionic fluorinated surfactants such as KDP 4606 (see Fig. 1 for structure) and Krytox 157 FSL developed from these studies.^{10,13,19} In the case of CMT, the enzyme-CO₂-philic surfactant complex formed has been shown to be active and dispersible in CO₂.^{10,13}

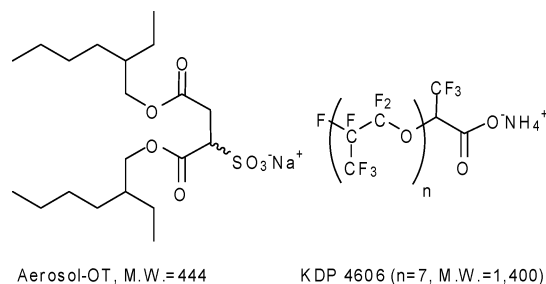


Fig. 1 Structures of the anionic surfactants sodium bis(2-ethylhexyl) sulfosuccinate (Aerosol-OT, AOT) and KDP 4606 (DuPont[®]).

In this paper we describe the use of both a fluoruous biphasic system (FBS) and supercritical carbon dioxide (scCO₂) as solvents for a transesterification catalysed by CMT.

^aClean Technology Group, School of Chemistry, University of Nottingham, University Park, Nottingham, NG7 2RD, United Kingdom. E-mail: martyn.poliakoff@nottingham.ac.uk

^bCentre for Biomolecular Sciences, School of Chemistry, University of Nottingham, University Park, Nottingham, NG7 2RD, United Kingdom. E-mail: neil.thomas@nottingham.ac.uk

Only a few examples of biocatalysis under FBS conditions have been reported.^{9,10,13} *Candida rugosa* lipase (CRL) suspended in hexane was used to catalyse the separation of *rac*-2-methylpentanoic acid *via* fluorinated tagging of one of the two enantiomers using a highly fluorinated alcohol.⁹ This promising approach was shown to allow easy separation and recovery of both product and catalyst. This approach was recently developed further through the use of enzymes solubilised in fluorous solvents by HIP to allow a homogeneous reaction to be achieved in a fluorous biphasic system,¹⁰ the enzyme was retained in the fluorous phase allowing easy recycling.

This paper reports new data on the solubilisation of CMT using HIP and describes efficient recycling of the HIP solubilised protease for transesterification reactions catalysed in both a FBS and scCO_2 .

Materials and methods

α -Chymotrypsin (CMT, type II from bovine pancreas, 51 U mg^{-1}) was obtained from Aldrich. Chemicals: *N*-acetyl-L-phenyl alanine ethyl ester (APEE), *n*-butanol and *rac*-2-butanol were purchased from Aldrich. The organic surfactant sodium bis(2-ethyl-2-hexyl)succinate (AOT) was purchased from Fluka and the fluorinated surfactant KDP 4606 was kindly donated by DuPont®. Perfluoromethylcyclohexane (PFMC) was purchased from Fluorochem. All organic solvents were purchased at the highest purity available from Aldrich. All commercially available reagents and solvents were used without further purification. High purity CO_2 was purchased from CryoService. Gases hydrogen, helium and air were purchased from BOC Gases.

Safety note

Experiments with scCO_2 involve high pressures and should only be carried out in equipment with the appropriate pressure rating and safety operating procedures.

Solubilisation of CMT-KDP in PFMC

The preparation of protein–surfactant complexes has been described previously.¹³ CMT (51 U, 0.02 mM) dissolved in sodium phosphate buffer (1 mL, 10 mM, pH 6.9), 5 mM CaCl_2 (1 mL) was stirred with AOT (2.3 mM) in hexane (1 mL) or KDP (0.7 mM) in PFMC (1 mL) at room temperature at 500 rpm for 10 min and centrifuged at 8000 rpm (4600g) for 2 min to allow phase separation to occur. The lower fluorous phase was then collected and diluted ten-fold in PFMC (1 mL) and the UV absorbance of the protein was measured at 280 nm (value^{20,21} of $\epsilon_{280} = 50\,585 \text{ M}^{-1} \text{ cm}^{-1}$) using an Agilent 8453 UV spectrophotometer. Comparable experiments were set up using AOT (1 mg mL^{-1} , 2.3 mM) in hexane (1 mL) and the amount of CMT-AOT in hexane was determined by UV spectroscopy. All experiments were performed in triplicate.

Determination of the critical micellar concentration (CMC) of KDP 4606 in PFMC

The method used to determine the critical micellar concentration (CMC) of the fluorinated surfactant by UV-visible spectroscopy has been described previously.²² Solutions of KDP in the range

5 mM to 70 mM in PFMC (1 mL) were stirred with 1 ml of sodium phosphate buffer (10 mM, pH 6.9) or sodium acetate buffer (10 mM, pH 3.8) at 500 rpm for 10 min and centrifuged at 8000 rpm (4600g) for two min to allow phase separation to occur. The lower fluorous phase was then collected and the concentration of surfactant analyzed by measuring the absorbance at 240 nm ($\epsilon_{240} = 59.4 \text{ M}^{-1} \text{ cm}^{-1}$),¹⁰ as described above. This measurement was repeated in triplicate.

Dynamic light scattering (DLS)

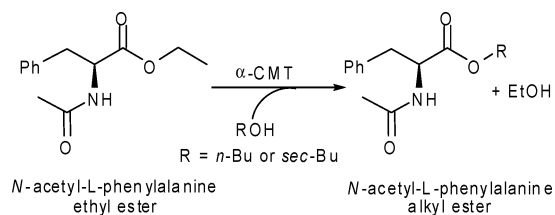
DLS measurements were carried out at 25 °C on a Zetasizer Nano S at Malvern Instruments. The particle size was taken as a mean value of three measurements. CMT dissolved in aqueous buffer; AOT and CMT-AOT dissolved in hexane; and CMT-KDP and KDP dissolved in PFMC were measured at 0.02 mM, 2.3 mM, 0.02 mM, 0.7 mM and 0.02 mM, respectively. The data was analyzed with the following fixed parameters:²³ refractive index 1.333, 1.372, 1.277, 1.39, 1.4 and 1.45 (water, hexane, PFMC, AOT, KDP and protein respectively) and viscosity (cP) 1.0019, 0.294 and 1.561 (water, hexane and PFMC respectively).

Estimation of water content using coulometric Karl Fisher titration

The water content of hexane, PFMC, CMT-AOT in hexane, and CMT-KDP in PFMC based on coulometric Karl Fisher titration was estimated using a Mitsubishi moisture meter CA-100 following the manufacturer's method. Samples (2 to 10 mg) were added into the titration solution using a syringe and the mass of sample introduced was indicated to the titrator. Titration with iodine was performed under stirring at 700 rpm. The percentage of water in the samples was measured in triplicate. The sensitivity of the Coulometric Karl Fisher titrator is 1 ppm water content.²⁴

Transesterification of *N*-acetyl-L-phenylalanine ethyl ester

Transesterification of *N*-acetyl-L-phenylalanine ethyl ester (APEE) with *n*-butanol or *rac*-2-butanol was catalysed by the protease α -chymotrypsin (CMT, MW = 51 000). The protein was used either in solubilised form as its HIP complex (CMT-AOT in hexane or CMT-KDP in PFMC) or as the suspended native form in hexane, hexane-PFMC (v/v 1 : 1) or scCO_2 (100 bar) at 40 °C for two hours. The reaction studied is shown in Scheme 1.



Scheme 1 Transesterification of *N*-acetyl-L-phenylalanine ethyl ester (APEE) (4.2 mM) with *n*-butanol or *rac*-2-butanol (0.45 M) was catalysed by α -chymotrypsin (CMT, 102 U, 0.04 mM) in hexane or hexane–PFMC v/v 1 : 1 (2 mL) or scCO_2 (100 bar, 8.5 mL) at 40 °C for two hours.

CMT (51 U, 1 mg) solubilised in PFMC (1 mL) was added to the substrates *N*-acetyl-L-phenylalanine ethyl ester (APEE) (8.5 μ mol, 2 mg) and *n*-butanol (0.9 mmol, 80 μ L) or *rac*-2-butanol (0.9 mmol, 80 μ L) in hexane or hexane/PFMC v/v 1 : 1 (2 mL). A comparable reaction was set up in scCO₂ (100 bar, 8.5 mL) and the system was left stirring at 40 °C for two hours. When the reaction was finished, the system was cooled down to 0 °C in an ice bath to allow phase separation to occur. Aliquots of the upper organic phase were collected and analyzed as described above. A fresh batch of substrates was then added to the lower fluoruous phase and the reaction was repeated as described above. The yields of products were determined using a Shimadzu GLC-2010 GLC equipped with an AOC 20i autosampler and fitted with a RTX5-FAST column (fused silica, crossbond 5% diphenyl–95% dimethyl polysiloxane, 10 m \times 0.1 mm \times 0.1 μ m) from Restek. A temperature programme was used for each run; the oven temperature was increased from 100 °C to 250 °C at 25 °C per minute and held at 250 °C for two minutes. Samples of 1.0 μ L were injected onto the column with a split ratio of 75 : 1. The injector temperature was 250 °C and the FID temperature was 350 °C.

Batch reactions

Enzymatic reactions in organic solvents and PFMC were carried out in 2 mL septum-sealed Supelco glass micro reaction vessels equipped with magnetic stirrer bars and stirred at 500 rpm in a silicon oil bath thermostated to the indicated temperature using a Yellowline MST basic hot plate equipped with a Yellowline TC1 thermostat.

Reactions in scCO₂ were performed in a stainless-steel high pressure batch reactor specially designed at the University of Nottingham.²⁵ The batch reactor (autoclave) equipped with a magnetic stirrer bar has an internal volume of 8.5 mL and was placed on an IKA Labortechnik RCT basic stirring plate. Solid substrates and reactants and stirrer bar were added into the reactor prior to sealing. Liquid substrates and reactants were added using a Gilson Pipetman micropipette into the autoclave then sealed using a safety valve. A band heater, thermocouple, input and output pressure pipes were then connected to the reactor to enable temperature and pressure control of the system. The system was then heated to the desired temperature and liquid CO₂ was pumped into the reactor using a high pressure NWA PM-101 Pickel pump until the desired pressure was achieved. The reaction mixture was stirred for the period of time specified and the system was then depressurised by placing the autoclave in a dry ice–acetone bath. The residual mixture in the autoclave was dissolved in acetone (3 mL) and centrifuged for 2 min. at 8000 rpm (4600g).

Aliquots (50 μ L) were diluted in acetone (1 mL) and substrates and products were analyzed by gas-liquid chromatography (GLC) using a Shimadzu GC 2010 chromatograph equipped with a Shimadzu AOC-20Si autosampler using helium as the carrier gas. The structure of products was further identified using GLC and GLC-MS by comparing the retention times and fragmentation patterns with those of authentic samples. GLC-MS was performed using a ThermoFinnegan Polaris-Q trap GC-MS equipped with a DB-5 (30 \times 0.25 \times 0.25 μ m film thickness) fused silica column. Helium was used as a carrier gas

Table 1 Solubilisation of CMT-AOT in hexane and CMT-KDP in PFMC

Concentration of CaCl ₂ in buffer (mM)	Complexation efficiency ^a (%)	
	CMT-AOT in hexane	CMT-KDP in PFMC
0	68 \pm 3	29 \pm 4
5	96 \pm 3	51 \pm 4

^a Complexation efficiency (%) = [mass of protein solubilised in organic (or fluoruous) phase]/[initial mass of protein] \times 100

and sample ionisation was carried out using electron impact (EI) at 70 eV.

Results and discussion

Solubilisation of CMT-KDP in PFMC

There are suggestions in the literature that the presence of a salt, such as CaCl₂ in the aqueous buffer from which an enzyme is extracted strongly influences both the solubility and activity of the enzyme in the receiving organic solvent.^{12,16,26} It has been postulated that at high salt concentrations, that the salt matrix may act as a rigid structure that would protect the enzyme from the organic solvent.²⁶ Also, the salt matrix, being highly polar, might help to maintain the native structure of the enzyme in organic media.²⁶

CMT was therefore dissolved in a sodium phosphate buffer (10 mM, pH 6.9) with or without addition of 5 mM CaCl₂. The protein was then extracted into hexane using AOT or into PFMC using KDP and the complexation efficiency of CMT-AOT in hexane and CMT-KDP in PFMC were estimated by measuring the UV absorbance of the protein at 280 nm. The results obtained are summarised in Table 1.

Adding CaCl₂ to the aqueous buffer was observed to facilitate the extraction of the protein into the organic (or fluoruous) phase since the complexation efficiency was observed to be increased by about 40–50% in both cases. Under comparable conditions, the amount of enzyme solubilised in hexane using AOT (96% of the starting material) was higher than that obtained using KDP in PFMC (51%).

The differences in complexation efficiencies observed between the two surfactants tested may be due to the structure of the surfactants (see Fig. 1). Parameters such as the size, polarity and hydrophobicity¹² of the fluorinated tail on the surfactant are likely to influence the contact between surfactant and protein.

Determination of the critical micelle concentration (CMC) of KDP 4606 in PFMC

By plotting absorbance against concentration of KDP¹⁰ it was possible to determine the CMC of KDP in PFMC as 48 mM at room temperature (maximum on the graph shown in Fig. 2).

The concentration of KDP (0.7 mM) used to solubilise CMT in PFMC in our experiments is far below the measured CMC (48 mM) which suggests that the solubilisation process used does not lead to the formation of micelles.

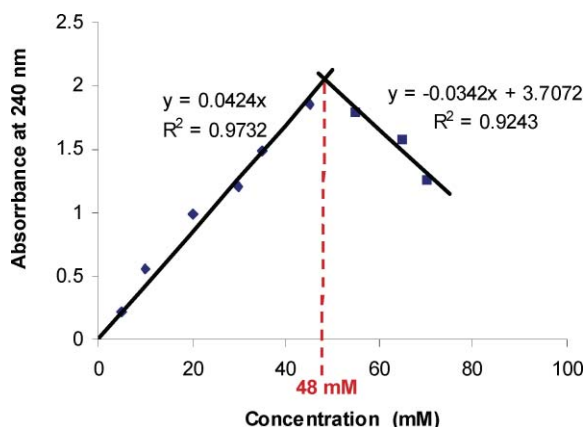


Fig. 2 UV absorbance *versus* concentration for KDP 4606 at 240 nm for the determination of the critical micelle concentration (CMC), indicated by dashed line.

Dynamic light scattering (DLS)

The particle size of CMT solubilised in phosphate buffer (10 mM, pH 6.9), CMT-AOT complexes in hexane and CMT-KDP complexes in PFMC were determined using DLS. The results are shown in Fig. 3.

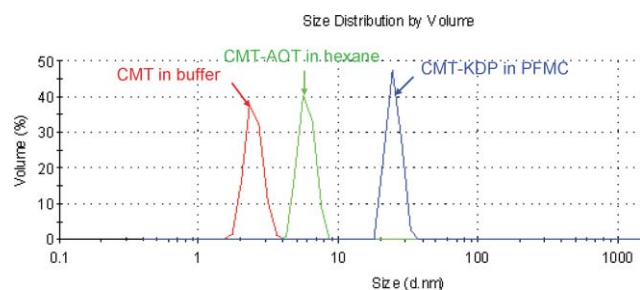


Fig. 3 DLS traces showing different particle sizes of CMT in different media (native CMT in buffer, CMT-AOT in hexane and CMT-KDP in PFMC), indicating that CMT-KDP is clustered under these conditions.

The particle diameter of CMT dissolved in aqueous buffer was determined to be 2.5 nm; consistent with the size of a single molecule of CMT. The diameter of CMT-AOT particles in hexane was found to be around 6.0 nm which is similar to the size of a single molecule of CMT (2.5 nm) plus two molecules of AOT (size of AOT 1.2 nm).¹⁵ This suggests the presence of individual CMT particles surrounded by the surfactant AOT in hexane.

Particles of CMT-KDP in PFMC were found to have a diameter of 25 nm which would correspond to the formation of an aggregate of about 100 protein molecules surrounded by the surfactant KDP in PFMC. KDP is estimated to have a length of ~1.4 nm. The aggregation observed for the solubilised CMT in PFMC might be related to the very low water content of the hydrophobic fluorinated solvent.²⁷

Estimation of water content using coulometric Karl Fisher titration

The water content of hexane; AOT in hexane and CMT-AOT in hexane; PFMC; KDP in PFMC; and CMT-KDP in PFMC were determined using the coulometric Karl Fisher titration.

Table 2 Water content of hexane, AOT and CMT-AOT in hexane, PFMC, KDP and CMT-KDP in PFMC estimated using coulometric Karl Fisher titration

Sample	Water content (ppm)
Hexane	34 ± 4
AOT in hexane	45 ± 5
CMT-AOT in hexane	41 ± 8
PFMC	<1 ^a
KDP in PFMC	<1 ^a
CMT-KDP in PFMC	<1 ^a

^a Sensitivity of the coulometric Karl Fisher Titrator 1 ppm.²⁴

The experiments were performed in triplicate and the results obtained were reproducible as shown in Table 2.

Less than 50 ppm water was detected in a sample of CMT-AOT in hexane which is mainly due to the water content of hexane. The amount of water in the PFMC samples was below the detection limit of the instrument (1 ppm).²⁴ To ensure that the fluorinated solvent PFMC was not interfering with the detection of Karl Fisher titration, known quantities of water were purposely added to PFMC and the water content was measured using Karl Fisher titration. In these cases, the amount of water added was accurately detected by the machine.

The very low amount of water detected for CMT-KDP in PFMC may explain the formation of protein aggregates observed by DLS (Fig. 3). In a recent paper, Akbar *et al.* describe the solubilisation of subtilisin Carlsberg and CALB in isooctane with or without extraction from an aqueous buffer solution.²⁷ They observed that the proteins directly solubilised in a solution of AOT in isooctane containing 0.2% of water would form clusters/aggregates in the organic solvent. However, the enzymes dissolved by extraction from an aqueous buffer solution would appear as single proteins surrounded by the surfactant in isooctane.

These results are in agreement with our own observation that proteins tend to form aggregates when the amount of water is limited in their environment, such as the in very hydrophobic fluorinated solvent PFMC. Akbar *et al.* suggested that this aggregation might provide physical protection of the enzymes, thus maintaining them in an active form and able to catalyse the transesterification of a natural product with vinyl butyrate in different organic solvents. In their case, the enzyme aggregates seemed to be more active for the reaction than the single protein extracted from the buffer.

It seems clear that both protein aggregation and water content are key parameters in determining the enzyme activity. In order to assess if the CMT-KDP HIP complexes formed in PFMC are catalytically active, a CMT catalysed transesterification reaction was studied.

Transesterification of *N*-acetyl-L-phenylalanine ethyl ester

The activity of α -chymotrypsin (CMT) solubilised in either hexane (CMT-AOT) or hexane-PFMC (CMT-KDP) for the transesterification of *N*-acetyl-L-phenylalanine ethyl ester (APEE) with *n*-butanol or *rac*-2-butanol was investigated. The activity of the solubilised protein was compared to that

of the suspended protease (native CMT) and control reactions with only the surfactants: AOT in hexane; or KDP in PFMC were also set up. The results are summarized in Fig. 4.

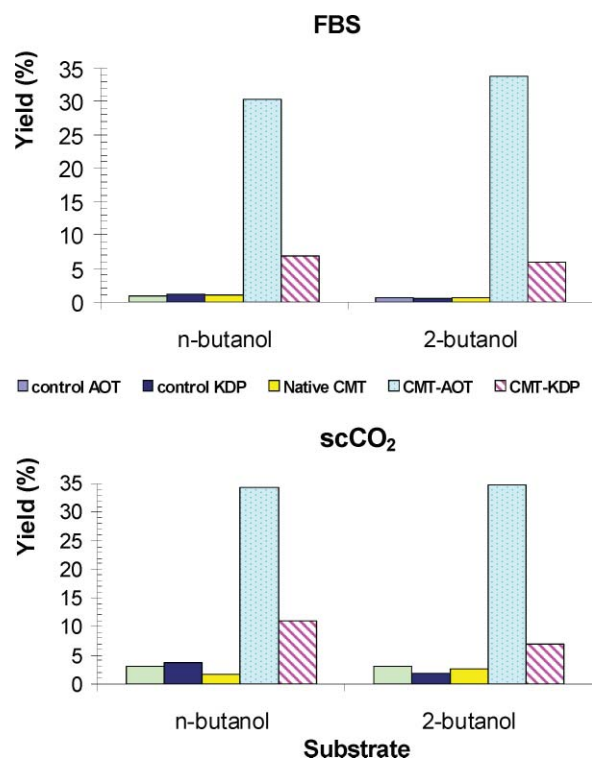


Fig. 4 Transesterification of APEE (4.2 mM) with either *n*-butanol or *rac*-2-butanol (0.42 mM) catalysed by surfactant AOT only (□) or KDP only (■) or native CMT (▨) or solubilised CMT-AOT (▧) or CMT-KDP (▩) (0.01 mM) at 40 °C with stirring for two hours in the FBS hexane-PFMC v/v 1 : 1 in a 2 mL septum sealed glass vessel or in scCO₂ (100 bar) in a 8.5 mL high pressure stainless steel batch reactor. Yields were estimated by GLC equipped with a RTX-5 Fast column. Note that although CMT-KDP is not as active as CMT-AOT, it has higher activity than the native enzyme. However, unlike CMT-AOT, CMT-KDP can be recycled.

The HIP solubilised CMT exhibited higher activity than the suspended enzyme for the transesterification of APEE with the two alcohols tested in both a FBS and scCO₂. Under homogeneous conditions (hexane–PFMC and scCO₂), the dispersion of the enzyme–surfactant complexes into the reaction medium as well as the contact between the enzyme and the substrates are believed to be increased, thus enhancing the yield of the reaction.¹³ With both alkyl alcohols tested, the yields of the ester products are slightly higher in scCO₂ compared to the hexane–PFMC which might be due to better mass transfer of substrates to the enzyme active site in scCO₂.

The CMT-AOT complexes in hexane appear to be around three times more active than the CMT-KDP complexes in PFMC and this trend was observed in both scCO₂ and hexane–PFMC. It is believed that the protein adopts an active configuration^{14,16,17} in both media tested and that the difference in activity observed between CMT-AOT and CMT-KDP could be due to a difference in the accessibility of the active sites in

the enzyme complexes formed with AOT and with the larger surfactant KDP restricting access more.

As explained above (see Fig. 3), particles of CMT-KDP in PFMC were found to form aggregates of a diameter of 25 nm, whereas the estimated size for CMT-AOT complexes (6.0 nm) suggested the presence of individual CMT molecules surrounded by the surfactant AOT in hexane. This difference in the particle size might explain the higher activity observed for CMT solubilised in hexane when compared to that in PFMC, as the number of accessible active sites in the latter will be much reduced as it is aggregated.

In the paper published by Akbar *et al.*, however, subtilisin Carlsberg or CALB enzyme aggregates formed were found to be more active than individual molecules extracted from the buffer for the transesterification of bergenin with vinyl butyrate in different organic solvents.²⁷ Their study and our results both demonstrate that solubilised enzymes aggregates can be more active than the suspended protein. Possibly, aggregation may provide a physical protection of the enzymes, thus maintaining them in an active form.²⁷

The water content of enzyme–surfactant preparations is also a key factor in the activity of enzymes in non-aqueous media. This was determined using coulometric Karl Fisher titrations (see Table 2) and less than 1 ppm of water was detected for CMT-KDP in PFMC compared to about 50 ppm for CMT-AOT in hexane. The higher water content of CMT-AOT particles might also lead to the higher catalytic activity observed compared to CMT-KDP. Interestingly, our results suggest that an amount of water less than 1 ppm is sufficient to permit the formation of catalytically active protein–surfactant (CMT-KDP) particles.

The reusability of CMT-KDP dissolved in PFMC was investigated for the transesterification reaction in the fluorine biphasic system (hexane–PFMC) and in scCO₂ (100 bar) for 2 hours at 40 °C. The results achieved are presented in Fig. 5. The solubilised protease CMT-KDP in PFMC was successfully reused for the transesterification of APEE with both alcohols tested, and no loss of activity was observed over four cycles in the hexane–PFMC biphasic system or in scCO₂. CMT-KDP in PFMC exhibited good stability in both media investigated; in particular, its activity in scCO₂ did not appear to be affected by the pressurisation and depressurisation procedures.¹³

Conclusions

The technique of hydrophobic ion pairing (HIP) has been successfully used to solubilise α -chymotrypsin (CMT) using fluorinated surfactant KDP in PFMC. The transesterification of APEE catalysed by the HIP solubilised protease has been investigated in FBS and scCO₂. Under comparable conditions, we have shown that CMT solubilised in either hexane or PFMC *via* HIP gives higher product yields than the suspended enzyme. The CMT-KDP surfactant enzyme complexes which form catalytically active CMT-KDP aggregates in PFMC retain their activity over at least four reaction cycles, suggesting long-term recyclability.

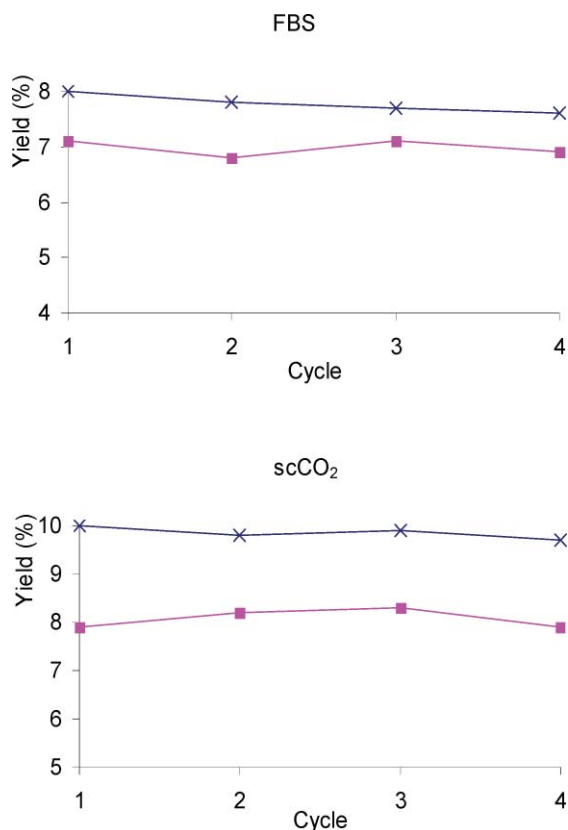


Fig. 5 Demonstration of the efficient recycling of CMT-KDP in PFMC for the transesterification of APEE with *n*-butanol (x) or *rac*-2-butanol (■) in the FBS hexane–PFMC and scCO₂ (100 bar) at 40 °C for two hours. Yields of were estimated by GLC equipped with a RTX5-Fast column.

Acknowledgements

We wish to thank Dr Helen R. Hobbs for the preliminary work performed on this project. We are also grateful to all our colleagues in the Clean Technology Group at the University of Nottingham, the School of Chemistry Workshop, Mark Guyler and Paul Hamley for their help and technical support. Finally, we thank Marie Curie Programme SubClean Probiomat (MEST-CT-2004-007767) for funding.

References

- H. R. Hobbs and N. R. Thomas, *Chem. Rev.*, 2007, **107**, 2786–2820.
- L. A. S. Gorman and J. S. Dordick, *Biotechnol. Bioeng.*, 1992, **39**, 392–397.
- Y. Okahata, A. Hatano and K. Ijro, *Tetrahedron: Asymmetry*, 1995, **6**, 1311–1322.
- A. Gupte, R. Nagarajan and A. Kilara, *Ind. Eng. Chem. Res.*, 1995, **34**, 2910–2922.
- D.-V. Unen, J. F. J. Engbersen and D. N. Reinhoudt, *Biotechnol. Bioeng.*, 2001, **75**, 154–158.
- R. Bovara, G. Carrea, A. M. Gioacchini, S. Riva and F. Secundo, *Biotechnol. Bioeng.*, 1997, **54**, 50–57.
- J. J. Lalonde, C. Govardhan, N. Khalaf, A. G. Martinez, K. Visuri and A. L. Margolin, *J. Am. Chem. Soc.*, 1995, **117**, 6845–6852.
- H. R. Hobbs, B. Kondor, P. Stephenson, R. A. Sheldon, N. R. Thomas and M. Poliakoff, *Green Chem.*, 2006, **8**, 816–821.
- P. Beier and D. O'Hagan, *Chem. Commun.*, 2002, 1680–1681.
- H. R. Hobbs, *PhD Thesis*, 2006, University of Nottingham, UK.
- D.-J. Unen, F. J. Johan and D. N. Reinhoudt, *Biotechnol. Bioeng.*, 2001, **75**, 154–158.
- V. M. Paradkar and J. S. Dordick, *J. Am. Chem. Soc.*, 1994, **116**, 5009–5010.
- H. R. Hobbs, H. M. Kirke, M. Poliakoff and N. R. Thomas, *Angew. Chem., Int. Ed.*, 2007, **46**, 7860–7863.
- J. D. Meyer, B. S. Kendrick, J. E. Matsuura, J. A. Ruth, P. N. Bryan and M. C. Manning, *Int. J. Pept. Protein Res.*, 1996, **47**, 177–181.
- J. D. Meyer, J. E. Matsuura, B. S. Kendrick, E. S. Evans, G. J. Evans and M. C. Manning, *Biopolymers*, 1995, **35**, 451–456.
- V. M. Paradkar and J. S. Dordick, *Biotechnol. Bioeng.*, 1994, **43**, 529–540.
- J. D. Meyer and M. C. Manning, *Pharm. Res.*, 1998, **15**, 188–193.
- M. E. Powers, J. Matsuura, J. Brassell, M. C. Manning and E. Shefter, *Biopolymers*, 1993, **33**, 927–932.
- S. S. Adkins, H. R. Hobbs, K. Benaissi, K. P. Johnston, M. Poliakoff and N. R. Thomas, *J. Phys. Chem. B*, 2008, **112**, 4760–4769.
- The extinction coefficient of the protein was calculated using the ProtParam utility (<http://www.expasy.org/tools/protparam.html>); C. N. Pace, F. Vajdos, L. Fee, G. Grimsley and T. Gray, *Protein Sci.*, 1995, **4**, 2411–2423.
- The X-ray structure is available from the world-wide protein data bank, (www.wwpdb.org): H. M. Berman, K. Henrick and H. Nakamura, *Nat. Struct. Biol.*, 2003, **10**, 980.
- A. Dominguez, A. Fernandez, N. Gonzalez, E. Iglesias and L. Montenegro, *J. Chem. Educ.*, 1997, **74**, 1227–1231.
- D. R. Lide, *CRC Handbook of Chemistry and Physics: A Ready Reference Book of Chemical and Physical Data*, 85th edn, CRC Press, Boca Raton, Florida, USA, 2004.
- http://www.allaboutinstruments.com/pdf/mitsubishi_karl_fisher_moisture.pdf, accessed January 2007.
- S. M. Howdle, P. Grebenik, R. N. Perutz and M. P., *J. Chem. Soc., Chem. Commun.*, **1989**, 1517–1519.
- Y. L. Khmel'nitsky, S. H. Welch, D. S. Clark and J. S. Dordick, *J. Am. Chem. Soc.*, 1994, **116**, 2647–2648.
- U. Akbar, C. D. Aschenbrenner, M. R. Harper, H. R. Johnson, J. S. Dordick and D. S. Clark, *Biotechnol. Bioeng.*, 2007, **96**, 1030–1039.

Toxicity of imidazolium ionic liquids towards algae. Influence of salinity variations

Adam Latała,^a Marcin Nędzi^a and Piotr Stepnowski^{*b}

Received 22nd May 2009, Accepted 4th September 2009

First published as an Advance Article on the web 15th October 2009

DOI: 10.1039/b918355h

This paper reports on a detailed study of the influence of salinity on the biological activity of 1-alkyl-3-methylimidazolium chlorides on two green algae *Oocystis submarina* and *Chlorella vulgaris*, one diatom *Cyclotella meneghiniana* and one blue-green alga *Geitlerinema amphibium*. All these organisms inhabit the Baltic Sea, an environment naturally varying greatly in salinity. The toxicity effects of ILs towards cyanobacterial and algal organisms were tested in fresh water and in water of four different salinities—8, 16, 24 and 32 PSU—reflecting the whole range encountered in the Baltic Sea. Increasing the salinity was found to exert a significant influence on ionic liquid toxicity in all cases. The lower toxicity is probably due to the reduced permeability of ionic liquid cations through the algal cell walls. Higher chloride concentrations offer a good ion-pairing environment for imidazolium cations, which therefore compete with hydroxyl or silanol functional groups in cell-wall structures. The results of this work indicate that at higher salinities algal growth is inhibited to a significantly lesser extent. With the same IL concentration, the toxicity decreases by eight–ten times in the algae or about three times in the cyanobacterium in the 0–32 PSU salinity range.

1. Introduction

First two parts of this series reported on acute toxicity of alkylimidazolium ionic liquids to various algal taxa. Part I concerned planktonic algae, green algae (*Chlorella vulgaris* and *Oocystis submarina*) characteristic for freshwater and brackish environment as well as two marine diatoms (*Cyclotella meneghiniana* and *Skeletonema marinoi*).¹ Part II, diatom *Bacillaria paxillifer* and cyanobacterium *Geitlerinema amphibium*, species characteristic for benthic environment.² For all the organisms studied we have confirmed pronounced alkyl chain effect. The acquired results indicate that sensitivity to ionic liquids decrease in the following order cyanobacterium > diatoms > green algae. It seems that the most important determinant of the observed difference is the cell wall structure; peptidoglycan cell wall in cyanobacterium, silica based cell wall in the case of diatoms and cellulose in the case of green algae. The size of the cells also plays important role in intoxication process; 10 times difference in the cell size resulted in a double more sensitive reaction to ionic liquids within green algae as well as diatom taxonomic groups.

The first report on the toxicity of ionic liquids to algae published by our group demonstrated that growth of two Baltic algae (*Oocystis submarina* and *Cyclotella meneghiniana*) was effectively inhibited even by very low concentrations of alkylimidazolium ionic liquids.³ That study also gave an indication of the moderating influence of salinity on the biological activity of the 1-hexyl-3-methylimidazolium salt in the *Oocystis submarina*

viability assay: the acute toxicity of this compound weakened with increasing ambient salinity.

In the present study we therefore decided to study this effect in detail using two green algae (*Oocystis submarina* and *Chlorella vulgaris*), one diatom (*Cyclotella meneghiniana*) and one blue-green alga (*Geitlerinema amphibium*). All these organisms inhabit the Baltic Sea, an environment that naturally varies greatly in salinity—from about 2–4 PSU (Practical Salinity Unit expressing parts per thousand) in the Bothnian Sea, up to 6–8 PSU in the Baltic Proper and in the Gulf of Gdańsk. In the Baltic straits (the Kattegat and Skagerrak), salinities are from 20 to 30 PSU.

In this study the toxicity effects towards algal organisms were tested in the presence of fresh water and water of four salinities—8, 16, 24 and 32 PSU—reflecting the whole range encountered in the Baltic Sea. In order to precisely assess modifying influence of salinity onto toxicity of ionic liquids, concentrations of compounds used in these experiments were near identical (rounded to decimal values) to those, which in two previous studies of ours^{1,2} were found to cause 50% growth inhibition of organism under investigation.

Results

In order to gain the insight into the salinity effect on toxicity of particular compounds we have chosen concentrations of ionic liquids reflecting their EC₅₀ values for tested species and salinity 8 PSU, found in our two previous studies.^{1,2} Chosen concentrations were rounded to decimal values that made particular dissolutions easier. Our main aim therefore was to

^aFaculty of Oceanography and Geography, University of Gdańsk, Piłsudskiego 46, 81–378, Gdynia, Poland

^bFaculty of Chemistry, University of Gdańsk, Sobieskiego 18/19, 80–952, Gdańsk, Poland. E-mail: sox@chem.univ.gda.pl

firstly clearly recognized the salinity effect rather than establish EC_{50} values for each compound in each salinity point.

Tables 1–4 set out the influence of salinity expressed as a percentage of the growth inhibition of particular algae exposed to 1-ethyl-, 1-butyl-, 1-hexyl-, 1-octyl- and 1-decyl-3-methylimidazolium chlorides, and Fig. 1–4 depict graphically the observed reduction in growth inhibition. The concentrations of ionic liquids used represent the orders of magnitude of the EC_{50} values previously calculated for these species in salinity 8 PSU.^{1,2} The salinity impact on IL toxicity was tested in the range from 0 to 32 PSU. An increase in salinity reduced the toxic effect of ILs to a significant extent in all cases, as found

previously.³ With the lowest salinity (8 PSU), growth inhibition in all four algal organisms fell from 60–70% noted in fresh water to c. 50%; this was achieved with all the compounds under investigation. An increase in salinity to 16 PSU further reduced the toxic effect, but in this case the reduction was especially conspicuous in the case of *O. submarina*, the growth of whose cultures was inhibited by only c. 20–30%. The other three species were more strongly affected by the presence of ILs in the culture media, the levels of growth inhibition being c. 30–40% in *C. vulgaris* and *C. meneghiniana*, and c. 40–50% in *G. amphibium*. The last-mentioned species was the most resistant to toxicity changes also in the higher salinity ranges, its growth being

Table 1 Influence of salinity on IL toxicity expressed as growth inhibition of the green alga *Chlorella vulgaris*

<i>Chlorella vulgaris</i>		Growth inhibition [I%] in different salinities [PSU]									
Substance	concentration [μ M]	0		8		16		24		32	
		%I	SD [%]	%I	SD [%]	%I	SD [%]	%I	SD [%]	%I	SD [%]
EMIMCl	10000	55.91	1.29	38.94	1.19	35.74	2.26	29.79	1.82	5.31	1.35
BMIMCl	1000	66.22	2.77	48.56	4.64	36.36	4.35	8.79	1.98	7.51	1.26
HMIMCl	50	61.47	3.35	51.74	1.63	36.57	2.86	17.65	3.08	6.03	1.93
OMIMCl	5	63.84	1.75	51.76	2.03	25.54	2.34	16.43	2.03	5.41	1.34
DMIMCl	1	68.68	3.93	49.26	1.89	28.85	3.98	34.04	2.77	9.39	1.98

Table 2 Influence of salinity on IL toxicity expressed as growth inhibition of the green alga *Oocystis submarina*

<i>Oocystis submarina</i>		Growth inhibition [I%] in different salinities [PSU]									
Substance	concentration [μ M]	0		8		16		24		32	
		%I	SD [%]	%I	SD [%]	%I	SD [%]	%I	SD [%]	%I	SD [%]
EMIMCl	12 500	70.54	3.20	53.89	0.84	29.21	1.86	15.47	0.82	8.69	1.44
BMIMCl	1 500	67.00	1.65	50.45	0.94	25.73	2.52	11.86	1.55	7.93	0.43
HMIMCl	500	69.55	1.04	53.30	0.48	17.84	0.43	9.99	1.62	8.27	1.62
OMIMCl	75	65.14	1.48	48.65	4.06	19.54	2.06	10.25	1.12	7.92	1.99
DMIMCl	10	63.58	1.86	50.23	0.91	25.21	1.67	13.65	0.89	6.54	2.41

Table 3 Influence of salinity on IL toxicity expressed as growth inhibition of the diatom *Cyclotella meneghiniana*

<i>Cyclotella meneghiniana</i>		Growth inhibition [I%] in different salinities [PSU]									
Substance	concentration [μ M]	0		8		16		24		32	
		%I	SD [%]	%I	SD [%]	%I	SD [%]	%I	SD [%]	%I	SD [%]
EMIMCl	100	66.23	2.06	51.25	1.42	35.21	1.88	16.47	2.04	8.25	1.90
BMIMCl	10	68.21	4.00	52.69	3.03	37.25	0.54	13.68	0.46	7.69	1.88
HMIMCl	1.5	70.30	1.94	49.63	2.20	33.47	0.55	18.65	0.94	8.24	2.17
OMIMCl	0.5	72.23	2.78	50.87	2.92	40.78	1.49	12.58	0.48	7.65	2.49
DMIMCl	0.1	71.61	1.51	50.69	2.11	38.52	3.76	11.69	4.06	6.84	1.58

Table 4 Influence of salinity on IL toxicity expressed as growth inhibition of the blue-green alga *Geitlerinema amphibium*

<i>Geitlerinema amphibium</i>		Growth inhibition [I%] in different salinities [PSU]									
Substance	concentration [μ M]	0		8		16		24		32	
		%I	SD [%]	%I	SD [%]	%I	SD [%]	%I	SD [%]	%I	SD [%]
EMIMCl	25	70.59	1.55	54.34	2.47	48.94	0.94	39.25	2.65	28.72	0.94
BMIMCl	5	69.75	1.62	53.58	2.36	46.45	0.48	37.46	1.88	26.18	0.48
HMIMCl	1.5	71.43	1.12	53.07	2.06	47.49	1.06	38.06	0.54	27.70	2.06
OMIMCl	0.1	63.91	0.89	50.75	2.00	47.75	2.65	43.37	0.55	28.57	1.85
DMIMCl	0.01	65.97	2.54	53.30	1.94	42.75	2.96	39.23	2.84	24.49	2.54

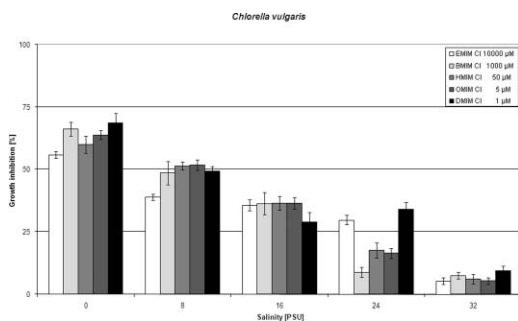


Fig. 1 Influence of salinity on IL toxicity to the green alga *Chlorella vulgaris*.

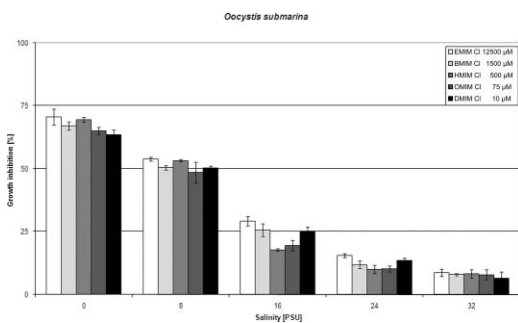


Fig. 2 Influence of salinity on IL toxicity to the green alga *Oocystis submarina*.

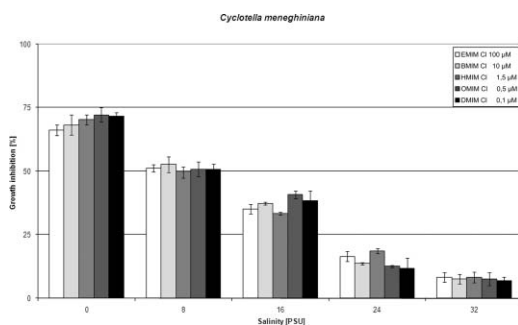


Fig. 3 Influence of salinity on IL toxicity to the diatom *Cyclotella meneghiniana*.

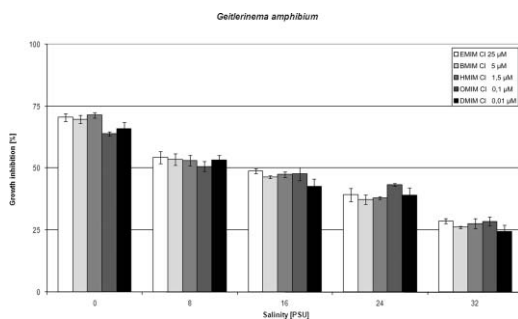


Fig. 4 Influence of salinity on IL toxicity to the blue-green alga *Geitlerinema amphibium*.

inhibited by c. 25–30% at 32 PSU. In the remaining species (*C. vulgaris*, *C. meneghiniana* and *O. submarina*) the highest salinity caused a drop in growth inhibition to 10% and less.

Discussion

The results supply positive evidence that the toxic effects of ILs on algae can be moderated by environmental conditions like salinity. The discovery that the toxicity of ionic liquids is reduced in more saline waters is of major importance for the assessment of the fate of these compounds in marine environments. We had previously hypothesised that the lower toxicity in more saline waters was probably due to the reduced permeability of ionic liquid cations through the algal cell walls.³ It is therefore likely that higher chloride concentrations offer a competitive ion-pairing environment for alkylimidazolium cations, the part of the ionic liquid composition responsible for the toxic mode of action. Paired (or complexed) cations are completely or partially prevented from interacting with peptidoglycan (blue–green alga), silanol (diatom) or cellulose (green alga) functional groups in the cell wall structures. Moreover, a higher salinity implies an elevated concentration of inorganic monovalent cations that are also capable of competing with alkylimidazolium cations for the countercharges available on the algal surfaces.

The results also indicate that there are no significant differences between particular compounds. This very likely provides proof of the identical mode of toxic action of alkylimidazolium ionic liquids regardless of alkyl chain length. It seems, moreover, that the first step in the intoxication process, *i.e.* the interionic interaction between the IL cation and the negatively charged biological membrane component, is as important as the deeper penetration of the membrane by the alkyl moiety of the molecule.

The recorded trend of reduced IL toxicity in conditions of elevated salinity corroborates similar observations made recently by Kulacki and Lamberti.⁴ While studying the effects of imidazolium ILs towards the freshwater alga *Scenedesmus quadricauda*, these authors found that the presence of nutrient media had a mitigating effect on the toxicity of the compounds under investigation. Their explanation of this effect appears, however, to be of an ecological rather than a molecular character: differences in nutrient levels could enable a taxon to cope better with the higher stress levels associated with a particular ionic liquid. They suggest, moreover, that ecotoxicological protocols should be standardised to take into account the abiotic conditions under which an organism is likely to be exposed to a toxic substance. Our study has provided ample evidence that this postulate is absolutely justified if we are to fully understand and predict the real effects of chemicals (including ionic liquids) on the aquatic environment.

The influence of IL toxicity on the limnic green alga *Scenedesmus vacuolatus* has also been studied in the context of mixture and combination effects, when in addition to ionic liquids, these organisms were exposed to cadmium ions.⁵ It was found that when cadmium was present as a background pollutant, the toxic effects were much smaller than those of the fixed ratio mixtures of ILs. This can be explained by the possible complexation of the ILs with the heavy metal, since all these compounds are ionic and have the potential to interact with each other.

Returning to salinity effects, it is well known in the ecotoxicology of heavy metals that the salt content has the potential to modify the toxicity of metallic ions to algal cells.^{6,10} By analogy therefore, we can assume that to some extent at least

we observed a similar effect in our studies, although with much larger cations. The main effect is attributed to the presence of chlorides, which possess a strong complexation potential. Chloride ions are known to be very mobile and capable of stabilising complexes with cationic microelements, thereby diminishing their bioavailability in water.

Conclusions

Obtained results using four different species and five ionic liquids differing in their toxic potential clearly shows a significant impact of salinity variations on algal toxicity. The highest toxicity towards all studied organisms is observed in freshwater, subsequently being reduced while salinity is increasing. All the organisms used in the present study (the green algae *Oocystis submarina* and *Chlorella vulgaris*, the diatom *Cyclotella meneghiniana* and the blue-green alga *Geitlerinema amphibium*) inhabit the Baltic Sea, an environment that naturally varies a great deal in salinity. They therefore constitute a reliable test kit for tracking the differences in toxic responses when exposed to potential contaminants (e.g. ionic liquids) in the presence of various salinities. The results show clearly that the toxic effect of ILs on algae can be moderated by environmental conditions such as salinity. With the same concentration of ILs the toxicity decreased by eight–ten times in the algae and by about three times in the cyanobacterium over a salinity range from 0 to 32 PSU. We therefore assumed that a potential ion-pairing or complexing environment comes into existence with elevated concentrations of chlorides and inorganic cations that prevents alkylimidazolium cations from interacting with the negatively charged biological membranes of algal organisms. This raises a number of issues, the most important of which is a general revision of the approximate data on the toxicity of ILs in various biological test systems, which have so far failed to take into account the composition of the abiotic environment and its variations.

Therefore the main result of this paper presents a significant breakthrough in our understanding of ILs toxicity. For the first time we can see that environment can modulate biological effects of these compounds and often presented threats in regard to ionic liquids should now be deeply refined.

We have compared our results with those obtained for heavy metals; however, this may well be an oversimplification, and the mode of toxic action in the presence of various salinities, pH, and other organic and inorganic toxicants must be studied in detail if we are to gain a full understanding of the prospective fate of ionic liquids in the environment.

Material and methods

Tested organisms

Four taxonomically different algal species were used in this study: the green algae *Oocystis submarina* (BA-0001), *Chlorella vulgaris* BA-0002, diatom *Cyclotella meneghiniana*, BA-0010 and blue-green alga *Geitlerinema amphibium* (BA-0013) They were isolated from coastal waters of the Baltic Sea and maintained as unialgal cultures in the Culture Collection of Baltic Algae

(CCBA) (<http://ocean.univ.gda.pl/~coba/>) at the Institute of Oceanography of the University of Gdańsk.¹¹

The species chosen for study were of euryhaline nature. Therefore, they were not stressed by the salinity range (0–32 PSU) used in the experiments.¹² Moreover, the algae were acclimated to each salinity before testing.

Ionic liquids

All ionic liquids were obtained from Merck (Darmstadt, Germany). They were: 1-ethyl-3-methylimidazolium chloride (EMIM Cl), 1-butyl-3-methylimidazolium chloride (BMIM Cl), 1-hexyl-3-methylimidazolium chloride (HMIM Cl), 1-octyl-3-methylimidazolium chloride (OMIM Cl) and 1-decyl-3-methylimidazolium chloride (DMIM Cl). Applied concentrations for green algae were in the range: EMIM Cl 10000–12500 μM , BMIM Cl 1000–1500 μM , HMIM Cl 50–500 μM , OMIM Cl 5–75 μM , DMIM Cl 1–10 μM and for diatom and cyanobacterium in the range: EMIM Cl 25–100 μM , BMIM Cl 5–10 μM , HMIM Cl 1.5 μM , OMIM Cl 0.1–0.5 μM , DMIM Cl 0.01–0.1 μM .

Batch cultures and toxicity tests

The test algae were batch-cultured in f/2 medium¹³ prepared on distilled water. In cultures salinities of 8, 16, 24, 32 PSU were made on the base of sea salt TropicMarin[®] (Tropic Marin, Wartenberg, Germany).

Stock cultures of the tested organisms were acclimatized in the same salinity media as the experimental salinity for 10 days at 20 °C and illumination by 25 $\mu\text{mol photons m}^{-2} \text{s}^{-1}$ from daylight type fluorescent lamps using an L:D photoperiod of 16:8. Irradiance was measured using a quantum-meter LiCor (LI-189) (LiCor, Lincoln, Nebraska, USA). The data obtained for treated cultures of the tested organisms were normalized to control growth curves obtained for the same salinity environments.

The algal acute toxicity tests of IL's were carried out using modified versions of the methods recommended in the European Committee for Standardization's guidelines.^{14,15} The main modifications were use of f/2 medium, photoperiod and choice of the test strains. The final batch cultures used in the experiments were obtained by mixing a known amount of cells in the log growth phase with sterile medium. The initial cell number was constant and was spectrophotometrically measured as Optical Density (OD) at wavelengths of 665 nm. Density of green algae *C. vulgaris* and *O. submarina* were approximately 0.022/665 nm, diatom *C. meneghiniana* 0.062/665 nm, and *G. amphibium* 0.032/665 nm.

The volumes of 9.5 cm^3 of algal suspension were transferred into glass Erlenmeyer flasks (25 ml). To each of these 0.5 cm^3 of different concentrations of an aqueous ionic liquid solution or distilled water (control cultures) was added. The concentrations of ionic liquids used reflected their EC_{50} values registered for particular algal organisms exposed to these compounds.^{6,7} After 72 h of incubation the number of cells in cultures was determined by OD measurement. All experiments were run in triplicate and the variability of the results did not exceed 5% on the inhibition scale.

Acknowledgements

Financial support was provided by the Polish Ministry of Research and Higher Education under grants: 2P04G 118 29, 2P04F 036 30 and DS 8200–4-0085–9.

References

- 1 A. Latała, N. Nędzi and P. Stepnowski, *Green Chem.*, 2009, **11**, 580–588.
- 2 A. Latała, N. Nędzi and P. Stepnowski, *Green Chem.*, 2009, **11**, 1371–1376.
- 3 A. Latała, P. Stepnowski, M. Nędzi and W. Mroziak, *Aquat. Toxicol.*, 2005, **73**, 91–98.
- 4 K. J. Kulacki and G. A. Lamberti, *Green Chem.*, 2008, **10**, 104–110.
- 5 M. Matzke, S. Stolte, A. Boshen and J. Filser, *Green Chem.*, 2008, **10**, 784–792.
- 6 A. Latała and W. Surosz, *Biologia*, 1998, **53**, 547–555.
- 7 HCh. Hahne and W. Kroontje, *J. Environ. Qual.*, 1973, **2**, 444–450.
- 8 T. M. Florence and J. L. Stauber, *Aquat. Toxicol.*, 1986, **8**, 11–26.
- 9 D. S. McLusky, V. Bryant and R. Campbell, *Oceanogr. Mar. Biol. Ann. Rev.*, 1986, **24**, 481–520.
- 10 D. Y. Lee, C. Fortin and P. G. C. Campbell, *Aquat. Toxicol.*, 2005, **75**, 127–135.
- 11 A. Latała in *Biological Resource Centers and the Use of Microbes*, ed. N. Lima and D. Smith, Micoteca da Universidade do Minho, Braga, Portugal, 2003, pp. 323–345.
- 12 A. Latała, S. Jodłowska and F. Pniewski, *Algological Studies*, 2006, **122**, 137–154.
- 13 R. R. L. Guillard in *Culture of marine invertebrate animals*, ed. W. L. Smith and M. N. Chanle, Plenum Press, New York, 1975, pp. 29–60.
- 14 EN. Water quality–Fresh water algal growth inhibition test with *Scenedesmus subspicatus* and *Selenastrum capricornutum* (ISO 8692:1993). European Committee for Standardization, Brussels, 1993.
- 15 EN ISO. Water quality–Marine algal growth inhibition test with *Skeletonema costatum* and *Phaeodactylum tricorutum* (ISO 10253:1995). European Committee for Standardization, Brussels, 1995.

Immobilization of Pd nanoparticles with functional ionic liquid grafted onto cross-linked polymer for solvent-free Heck reaction

Gang Liu, Minqiang Hou, Jiyuan Song, Tao Jiang, Honglei Fan, Zhaofu Zhang and Buxing Han*

Received 2nd July 2009, Accepted 15th September 2009

First published as an Advance Article on the web 22nd October 2009

DOI: 10.1039/b913182e

1-Aminoethyl-3-vinylimidazolium bromide ([VAIM]Br) grafted on the cross-linked polymer polydivinylbenzene (PDVB) was synthesized. The copolymers were used as a support to immobilize palladium nanoparticles. The catalyst was characterized by Fourier transform infrared spectroscopy (FT-IR), thermogravimetric (TG) analysis, transmission electron microscopy (TEM) and X-ray photoelectron spectroscopy (XPS). The catalytic performance of the copolymer-supported Pd nanoparticles for the Heck arylation of olefins with different aryl iodides was studied under solvent-free conditions. The results demonstrated that the catalyst was very active and stable under solvent-free conditions, and could be reused after simple separation. The reason for the high activity and stability of the catalyst is discussed.

Introduction

Metallic nanoparticles have attracted much attention in the field of catalysis because they can catalyze many organic reactions effectively due to the quantum size effect and high ratio of surface area to volume.^{1–3} However, the naked nanoparticles tend to aggregate to form bulk metal because of the impulse of high surface energy, resulting in a severe decrease in catalytic activity and selectivity. An effective way to solve this problem is to immobilize the metallic nanoparticles on suitable supports, and many methods have been developed for this.^{4–7}

The Heck reaction is a very useful route for the formation of new C–C bonds in a single operational step.^{8–10} The wide functional group tolerance in both reactants allows convenient application in the total synthesis without protecting groups. The Heck reaction has mostly been catalyzed by palladium complexes combined with phosphine ligands in organic solvents under homogeneous conditions. It is known that the homogeneous systems suffer drawbacks in separation, and result in environmental problems, especially in the case of toxic ligands. Therefore, it is desirable to develop cheaper and environmentally benign heterogeneous catalytic systems. It is also known that palladium nanoparticles have high catalytic activity for the Heck reaction.^{11,12} Immobilization of Pd nanoparticles on solid supports to prepare active and stable catalytic systems for the Heck reaction is an interesting topic, and different supports have been used to stabilize the nanoparticles, such as carbon,¹³ hydroxyapatite,¹⁴ molecular sieves,^{7,15} and polymers.^{16,17}

In recent years, ionic liquids (ILs) have been widely studied owing to their unique properties, such as negligible vapor pressure and high thermal stability.¹⁸ Some functionalized

ILs have also been used to stabilize metal nanoparticles. For example, Safavi and coworkers reported highly efficient palladium nanocatalysts supported on a phosphorylated IL modified xerogel, which could be evenly coated on glass slides.¹⁹ Dyson and coworkers synthesized a nitrile-functionalized IL, [C₃CNpy][Tf₂N], which was an effective immobilization solvent for palladium-catalyzed Suzuki and Stille reactions; TEM analysis of the nanoparticles extracted from the catalysis solution showed the stabilizing effect of the IL.²⁰

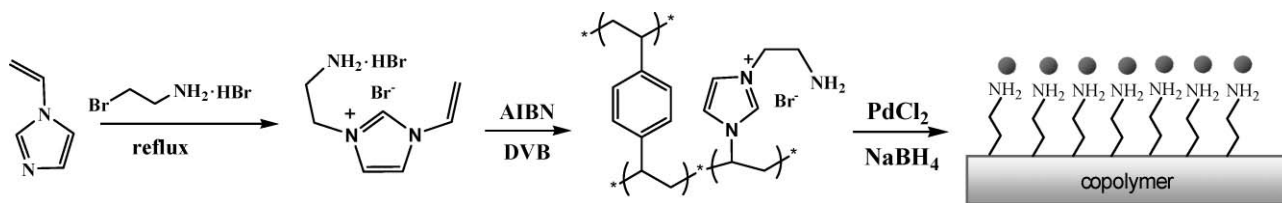
The design and preparation of active and stable catalysts for Heck reactions under solvent-free conditions is highly desirable, and consistent with the requirements of green chemistry. It is well known that amine groups bind strongly to palladium.^{21,22} It can be expected that the ILs with amine groups on solid supports should be effective for stabilizing palladium nanoparticles. Herein we describe the synthesis of a new type of imidazolium IL with an amine group, and its copolymerization with cross-linker divinylbenzene. The prepared copolymer was used for the immobilization of Pd nanoparticles for Heck reaction.

Results and discussion

Preparation and characterization of the catalyst

The route to synthesize the copolymers (PDVB-IL) is presented in Scheme 1, and the procedures were similar to those for the copolymerization of 1-vinyl-3-butylimidazolium chloride and DVB.²³ In brief, the IL with amine group was first prepared by the reaction of 1-vinylimidazole and 2-bromoethylamine hydrobromide to give [VAIM]Br·HBr. This was then copolymerized with DVB using azobisisobutyronitrile (AIBN) as the initiator, and subsequent treatment of the copolymers with NaOH gave the cross-linked copolymer with IL (PDVB-IL). To prepare the copolymer-supported Pd nanoparticles (PDVB-IL-Pd), the copolymer was added to aqueous H₂PdCl₄ solution with vigorous stirring, giving the catalyst after reduction of the Pd(II) on the PDVB-IL with NaBH₄ and drying under vacuum.

Beijing National Laboratory for Molecular Sciences, Institute of Chemistry, Chinese Academy of Sciences, Beijing, 100080, China.
E-mail: hanbx@iccas.ac.cn; Fax: +86-10-62562821;
Tel: +86-10-62562821



Scheme 1 Synthesis of the cross-linked polymer-supported ionic liquid.

The prepared copolymers (PDVB-IL) and neat PDVB were characterized by thermogravimetric analysis. The thermograms are shown in Fig. 1. The small weight loss of PDVB-IL before 220 °C resulted from the loss of the adsorbed water which also occurred in the case of neat PDVB. It can be seen from the two thermograms that the weight loss of PDVB-IL between 220 °C and 380 °C was due to the elimination of the ILs immobilized on the polymers, because there was no weight loss for the neat PDVB. Further weight loss at higher temperature (above 380 °C) was attributed to the decomposition of PDVB. The amount of the IL in the PDVB-IL obtained from the thermal analysis was about 7.0 wt%. The composition of PDVB-IL was also examined by elemental analysis, and the result indicated that the content of IL was 7.4 wt%, which was consistent with the result of thermal analysis. The results of elemental analysis also showed that the molar ratio of N/Br was 3, indicating that

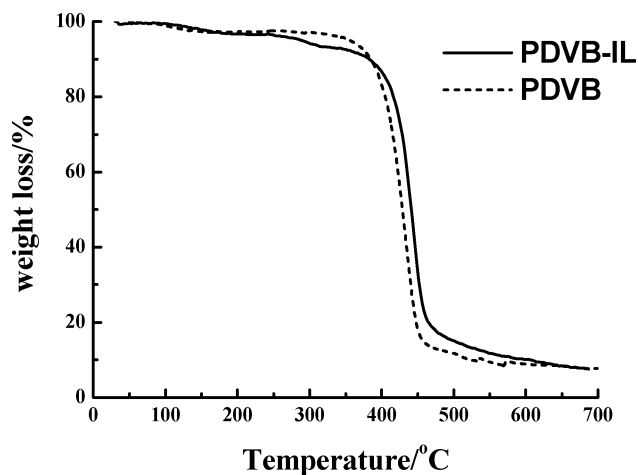


Fig. 1 The thermogram of PDVB-IL and pure PDVB.

the ILs were copolymerized without hydrobromide, and the PDVB-IL had a structure shown in Scheme 1.

Fig. 2 shows the FT-IR spectra of the PDVB-IL and PDVB-IL-Pd. Both spectra showed an asymmetric broad band at around 3435 cm^{-1} , which is attributed to the stretching vibration of the amine groups. It is clear that the band became narrow after the Pd nanoparticles were supported on the polymers, indicating the binding of Pd nanoparticles to the polymers through the amine groups.²¹ The small change in intensity of the band may result from the change of absorption coefficient of the amino groups after interaction with Pd particles.

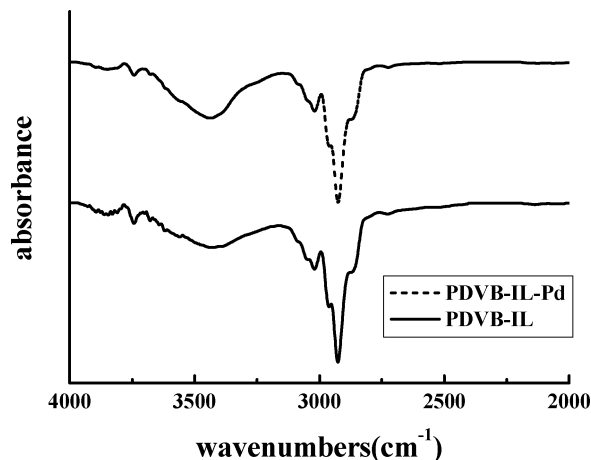


Fig. 2 The FT-IR spectra of PDVB-IL and PDVB-IL-Pd.

Fig. 3 shows the typical SEM and TEM images of the catalyst (PDVB-IL-Pd). The SEM image (Fig. 3A) shows that the catalyst was almost amorphous. The dark spots in the TEM image (Fig. 3B) indicate the presence of palladium nanoparticles that were bound to the copolymers. The diameter of palladium

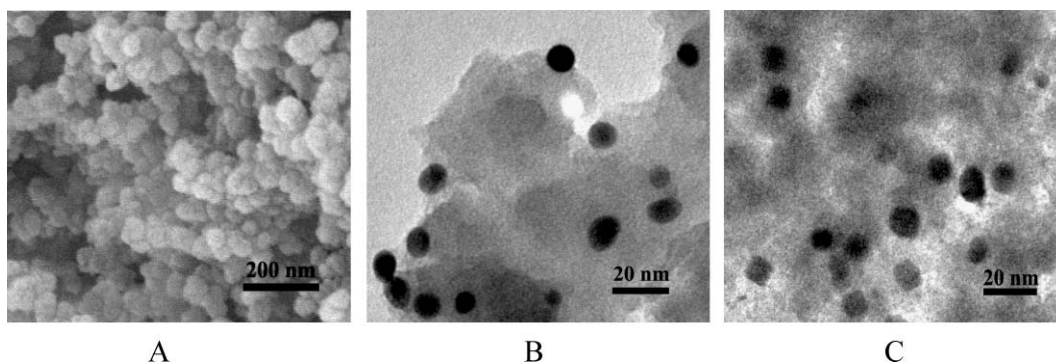


Fig. 3 SEM (A) and TEM (B) images of the PDVB-IL-Pd; the TEM image (C) of the recovered PDVB-IL-Pd after being reused three times.

nanoparticles was in the range 7–8 nm and the size distribution was very narrow.

The catalyst (PDVB-IL-Pd) was also characterized by XPS before reaction, and the results are shown in Fig. 4. It can be seen that the Pd 3d spectrum could be resolved into two spin-orbit pairs with $3d_{5/2}$ binding energies of 335.9 eV and 337.1 eV, respectively. The peak binding energies of 335.9 eV (Pd $3d_{5/2}$) and 341.0 eV (Pd $3d_{3/2}$) correspond to fully reduced Pd nanoparticles, while the peak at 337.1 eV suggests the presence of the unreduced Pd²⁺ ions on the surface of the Pd particles.^{21,24} It can be seen from the XPS spectrum that most of Pd²⁺ was reduced to Pd(0) because the area of the peak of Pd²⁺ ion was relatively small. The content of Pd in the catalyst was 2.3 wt%, as determined by the ICP-AES method.

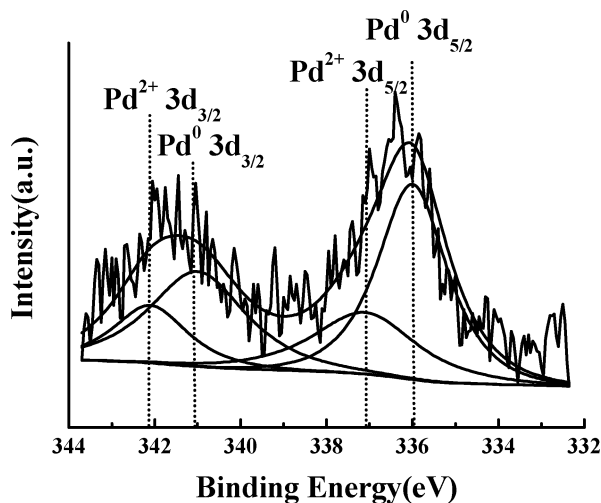


Fig. 4 XPS spectrum of the Pd 3d edge of the PDVB-IL-Pd sample.

Catalytic Heck reactions

The catalytic activity of the PDVB-IL-Pd for Heck reactions was investigated under solvent-free conditions. It is known that a base is required for Heck reactions. The effect of Et₃N and some inorganic bases on the reaction of iodobenzene and methyl acrylate was studied at 120 °C. The results showed that the catalyst was very active and selective for the reaction in the presence of Et₃N (entry 1, Table 1), while the reaction rate was very slow when inorganic bases were used (entries 2–4, Table 1). The main reason for this is that the solubility of the inorganic bases in the reaction system was very poor, while Et₃N is miscible with the substrates. This indicates that the solubility of the bases in the reaction mixture is crucial for the Heck reaction. Using Et₃N as the base, the effect of temperature on the reaction was studied. The results demonstrated that the activity of the catalyst increased with temperature as the temperature increased from 80 to 140 °C (entries 1 and 5–7 of Table 1), with the activity being very high at 120 °C and 140 °C.

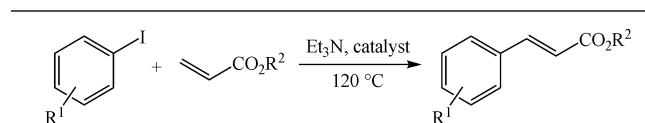
The catalytic activity of the catalyst for the arylation of different olefins with iodobenzene was tested under solvent-free conditions; the results are given in Table 2. The iodobenzene was very active with electron-poor olefins such as methyl, ethyl and butyl acrylate. As the size of the substituted group of acrylate ester increased from methyl to butyl, the reaction time needed for

Table 1 Catalytic performance of the catalyst for Heck reaction between iodobenzene and methyl acrylate^a

Entry	Base	<i>T</i> /°C	Time/h	Yield (%)
1	Et ₃ N	120	4	97
2	NaHCO ₃	120	4	<2
3	CH ₃ COONa	120	4	<2
4	NaOH	120	4	<2
5	Et ₃ N	80	12	<2
6	Et ₃ N	100	12	73
7	Et ₃ N	140	1	98

^a The molar ratio of iodobenzene/methyl acrylate/base/Pd is 1:1.5:1.5:0.0002.

Table 2 Heck reaction of haloarenes with olefins in the presence of PDVB-IL-Pd^{a,b}



Entry	R ¹	R ²	Time/h	Yield (%)
1	H	Me	4	97
2	H	Et	5	94
3	H	Bu	6	95
4	4-F	Me	3	93
5	4-Cl	Me	2	94
6	4-OH	Me	1	98
7	4-OMe	Me	3	96
8	4-Me	Me	6	93
9 ^c	H	Me	4	95
10 ^c	H	Me	4	95
11 ^c	H	Me	4	94

^a The molar ratio of haloarene/olefin/Et₃N/Pd is 1:1.5:1.5:0.0002.

^b The reaction was performed without solvent at 120 °C. ^c Entries 9, 10 and 11 are the results of reusing the catalyst for the second, third and fourth times under the reaction conditions of entry 1.

high conversion increased from 4 h to 6 h (entries 1–3, Table 2). This may be due to the steric hindrance effect that reduced the reaction rate.

In order to investigate the effect of substituted groups of iodobenzene on the Heck reaction, various substituted iodobenzenes were studied. The coupling reaction of both electron-deficient and electron-rich iodobenzenes with olefins can proceed with high yields using the catalyst. Iodobenzenes with electron-donating groups, such as methyl, gave reduced reaction rates, and longer reaction times were required for a high yield. Groups with a lone electron pair (e.g. -OH, -OMe, -F, -Cl) in the iodobenzenes affect the electron cloud density of benzene ring and the coordination of Pd with the benzene ring, ultimately accelerating the reaction rate, as can be seen from entries 1 and 4–8 of Table 2.

The reusability of the catalyst was tested using iodobenzene and methyl acrylate as the substrates. After each run, the catalyst was recovered by filtration, followed by washing with ethanol (10 mL × 3). After drying, the catalyst was reused directly for the next run. The results for the three repeated runs are also presented in Table 2. The activity of the catalyst remained

unchanged after it was reused three times, indicating that the catalyst was not only very active, but also very stable. There are several reasons for the excellent stability of the catalyst. First, the PDVB-IL was not soluble in the reactants and the product because it was a cross-linked polymer; second, it was thermally stable up to about 220 °C (Fig. 1), which was much higher than the reaction temperature; third, the amine groups in the PDVB-IL interacted strongly with Pd particles by coordination, which anchored the Pd nanoparticles stably on the support. The TEM image of the catalyst after being used four times is shown in Fig. 3C. The aggregation of the Pd particles in the used catalyst was not obvious, supporting the argument above.

The mechanism of the Heck reaction employing supported Pd nanoparticles as catalysts has been discussed in the literature.²⁵ Many authors have reported the leaching of Pd during the reaction. In order to investigate the mechanism in our catalytic system, we conducted a filtration test for the Heck reaction between iodobenzene and methyl acrylate using PDVB-IL-Pd as catalyst. After 2 h (the reaction was completed in 4 h), the reaction was stopped and the reaction mixture was centrifuged at 16000 rpm for 20 min. Then the mixture without the solid catalyst was allowed to continue under the same conditions for another 2 h, and the conversion found to increase from 60% to 73%. This suggests that the leaching of active Pd species from the solid supports occurred to some extent, but the dissolved Pd redeposited back onto the polymers after the iodobenzene was completely consumed. This argument was confirmed by our ICP-AES analysis, which showed that the content of Pd in the catalyst before and after reaction was 2.30% and 2.23%, respectively.

Conclusion

We synthesized DVB cross-linked copolymer with chemically supported IL [VAIM]Br. The copolymer was proved to be an effective supporter for palladium nanoparticles. The nanocatalysts immobilized on the copolymers showed high catalytic activity in the Heck reaction for various substrates. The catalyst was very stable and could be easily separated from the products and reused because of the insoluble nature of the cross-linked copolymer and the coordination force between the amine group and the palladium nanoparticles. We believe that this route can be used to support some other metallic nanocatalysts on a highly cross-linked polymer matrix to prepare active, stable catalysts for different reactions.

Experimental

Materials

Azobis(isobutyronitrile) (AIBN), methanol, acetone, acetonitrile, ethanol, PdCl₂, tetrahydrofuran (THF), methyl acrylate, ethyl acrylate, n-butyl acrylate, sodium hydroxide, sodium bicarbonate, sodium acetate, triethylamine, iodobenzene, 4-fluoroiodobenzene, 4-chloro-1-iodobenzene, 4-iodophenyl methyl ether and 4-iodophenol were provided by Beijing Chemical Company. Divinylbenzene (DVB) was purchased from Fluka, and 1-vinylimidazole was provided by Aldrich. AIBN

was recrystallized three times before use. Other chemicals were used as received. All the chemicals were A.R. grade.

Preparation of [VAIM]Br·HBr

To prepare the basic IL [VAIM]Br·HBr, 1-vinylimidazole (9.42 g, 0.10 mol) and acetonitrile (50 mL) were added to a two-necked flask equipped with a magnetic stirrer. The mixture was refluxed at 78 °C under a nitrogen atmosphere. 2-Bromoethylamine hydrobromide (20.50 g, 0.10 mol) was added into the flask stepwise over 24 h. Then, the reaction mixture was cooled down, the liquid was poured out and the solid was washed with anhydrous ethanol three times to remove the unreacted starting materials. After drying under vacuum, 1-aminoethyl-3-vinylimidazolium bromide hydrobromide ([VAIM]Br·HBr) was obtained. ¹H NMR (400 MHz, D₂O) δ: 3.52 (m, 2H), 4.65 (m, 2H), 5.47 (dd, 1H), 5.84 (dd, 1H), 7.17 (dd, 1H), 7.71 (s, 1H), 7.87 (s, 1H), 9.23 (s, 1H). Positive ion ESI-MS: *m/z* 138.1. Anal. Calcd for C₇H₁₃N₃Br₂: N, 14.0; C, 28.1; H, 4.3; Br, 53.5. Found: C, 25.9; H, 4.4; N, 13.2; Br, 54.9.

Our experiment showed that the isolated [VAIM]Br could be obtained by neutralization of [VAIM]Br·HBr by NaOH. In the experiment, [VAIM]Br·HBr (10 mmol) was dissolved in the water (10 mL) and then equimolar NaOH (10 mmol) was added. The solution was stirred for 6 h at r.t. followed by vaporization of the water under vacuum. Then the obtained viscous liquid was dissolved in MeOH (20 mL) with stirring for 1 h. The solution was filtered, and ionic liquid [VAIM]Br was obtained after the MeOH in the filtrate was evaporated. The identity of [VAIM]Br was confirmed by NMR. ¹H NMR (300 MHz, DMSO) δ: 2.78 (m, 2H), 4.12 (m, 2H), 5.27 (dd, 1H), 5.88 (dd, 1H), 7.20 (dd, 1H), 7.79 (s, 1H), 8.11 (s, 1H), 9.47 (s, 1H).

Preparation of PDVB-IL

To prepare the DVB-cross-linked polymers with the supported IL (PDVB-IL), DVB (1.95 g, 15 mmol), AIBN (0.05 g) and [VAIM]Br·HBr (0.45 g, 1.5 mmol) were dissolved in ethanol/water (100 mL, 3 : 1 v/v) under nitrogen. The mixture was refluxed at 100 °C with stirring. After 24 h, a white solid formed was filtrated and was washed with THF, acetone, and methanol. The final product was treated with equimolar NaOH and washed with water before being dried in vacuum at 60 °C for 12 h. Element analysis: C, 84.4; H, 7.8; N, 1.5; Br, 2.7. The PDVB without the ionic liquid was synthesized by direct polymerization of DVB under the same conditions.

Preparation of PDVB-IL-Pd

PdCl₂ (2 mmol) was dissolved in the solution of HCl (0.04 M, 100 mL) with stirring for 24 h. PDVB-IL (1.00 g) was added to the aqueous solution of H₂PdCl₄ (0.02 M, 50 mL) in a 100 mL flask with vigorous stirring. The mixture was stirred for 12 h and then filtered. The solid catalysts were then dispersed in water (20 mL) and reduced by a fresh aqueous solution (10 mL) of NaBH₄ (0.185 g, 5 mmol) at room temperature. The resulting grey catalysts were washed with water (10 mL × 3) and ethanol (10 mL × 3) respectively, then dried under vacuum at 60 °C for 24 h. The content of Pd in the catalyst was 2.30 wt%, which was determined using ICP-AES.

Catalytic reaction

The Heck reaction was carried out in a 6 mL stainless steel reactor with a magnetic stirrer. In the experiment, aryl halide (1 mmol), vinylic substrate (1.5 mmol), triethylamine (1.5 mmol) and Pd catalyst (1.0 mg) were added into the reactor. Then the reactor was heated to the desired temperature in an air bath under stirring. After reaction, the reactor was cooled by a ice bath. The products were collected using DMF as solvent after centrifuging the catalysts from the suspension. The liquid phase was analyzed by GC (Agilent 4890 D) equipped with a flame-ionized detector, and biphenyl was used as the internal standard. The formation of product was confirmed by GC-MS (QP2010). All the reactions were conducted three times and the experimental errors were less than $\pm 2\%$. In the catalyst recycling experiments, the catalyst was reused after washing with ethanol (10 mL \times 3) and drying at 60 °C for 6 h.

Characterization

The FT-IR spectra were collected on a Bruker Tensor 27 spectrometer in KBr pellet form. SEM examination was carried out on a scanning electron microscope (JEOL, JSM-4300) operated in a high-vacuum mode at 15 kV, which provided general textural information of the samples. The SEM sample was sputter-coated with gold before observation. TEM observation was performed on a transmission electron microscope (JEOL, JEM 1011) at an operating voltage of 100 kV, and the images were electronically captured using a CCD camera. X-ray photoelectron spectroscopy data of the as-prepared samples were obtained with an ESCALab220i-XL electron spectrometer from VG Scientific using 300 W MgK α radiation. The base pressure was about 3×10^{-9} mbar. The binding energies were referenced to the C 1s line at 284.8 eV from adventitious carbon. TG measurements were performed on a thermal analyzer (NETZSCH STA 409 PC/PG) with a heating rate of 3 °C min $^{-1}$. The loading content of Pd in the catalysts was determined by ICP-AES (VISTAMPX); the samples were dissolved in aqua regia beforehand. The elemental composition of the polymer was determined using a Flash EA1112 analyzer.

Acknowledgements

The authors are grateful to the National Natural Science Foundation of China (20533010, 20773144) and the

Chinese Academy of Sciences (KJXC2.YW.H16) for financial support.

References

- 1 M. Turner, V. B. Golovko, O. P. H. Vaughan, P. Abdulkin, A. Berenguer-Murcia, M. S. Tikhov, B. F. G. Johnson and R. M. Lambert, *Nature*, 2008, **454**, 981–983.
- 2 A. A. Herzing, C. J. Kiely, A. F. Carley, P. Landon and G. J. Hutchings, *Science*, 2008, **321**, 1331–1335.
- 3 V. Cimpeanu, M. Kocevar, V. I. Parvulescu and W. Leitner, *Angew. Chem., Int. Ed.*, 2009, **48**, 1085–1088.
- 4 D. Astruc, F. Lu and J. R. Aranzas, *Angew. Chem., Int. Ed.*, 2005, **44**, 7852–7872.
- 5 R. W. J. Scott, O. M. Wilson and Richard M. Crooks, *J. Phys. Chem. B*, 2005, **109**, 692–704.
- 6 *Handbook of heterogeneous catalysis*, 2nd edn, ed. G. Ertl, H. Knözinger and J. Weitkamp, Wiley-VCH, 2008.
- 7 V. L. Budarin, J. H. Clark, R. Luque, D. J. Macquarrie and R. J. White, *Green Chem.*, 2008, **10**, 382–387.
- 8 M. T. Reetz and J. G. de Vries, *Chem. Commun.*, 2004, 1559.
- 9 C. Amatore and A. Jutand, *Acc. Chem. Res.*, 2000, **33**, 314–321.
- 10 M. Lombardo, M. Chiarucci and C. Trombini, *Green Chem.*, 2009, **11**, 574–579.
- 11 Y. Wan, H. Y. Wang, Q. f. Zhao, M. Klingstedt, O. Terasaki and D. Y. Zhao, *J. Am. Chem. Soc.*, 2009, **131**, 4541–4550.
- 12 R. T. Tao, S. D. Miao, Z. M. Liu, Y. Xie, B. X. Han, G. M. An and K. L. Ding, *Green Chem.*, 2009, **11**, 96–101.
- 13 T. Maegawa, Y. Kitamura, S. Sako, T. Uduz, A. Sakurai, A. Tanaka, Y. Kobayashi, K. Endo, U. Bora, T. Kurita, A. Kozaki, Y. Monguchi and Hironao Sajiki, *Chem. Eur. J.*, 2007, **13**, 5937–5943.
- 14 K. Mori, T. Hara, T. Mizugaki, K. Ebitani and K. Kaneda, *J. Am. Chem. Soc.*, 2004, **126**, 10657–10666.
- 15 L. Djakovitch and K. Koehler, *J. Am. Chem. Soc.*, 2001, **123**, 5990–5999.
- 16 S. Ko and J. Jang, *Angew. Chem., Int. Ed.*, 2006, **45**, 7564–7567.
- 17 B. Karimi, S. Abedi, J. H. Clark and V. Budarin, *Angew. Chem., Int. Ed.*, 2006, **45**, 4776–4779.
- 18 T. Welton, *Coord. Chem. Rev.*, 2004, **248**, 2459–2477.
- 19 A. Safavi, N. Maleki, N. Iranpoor, H. Firouzabadi, A. R. Banazadeh, R. Azadi and F. Sedaghati, *Chem. Commun.*, 2008, 6155–6157.
- 20 D. B. Zhao, Z. F. Fei, T. J. Geldbach, R. Scopelliti and P. J. Dyson, *J. Am. Chem. Soc.*, 2004, **126**, 15876–15882.
- 21 S. Mandal, D. Roy, R. V. Chaudhari and M. Sastry, *Chem. Mater.*, 2004, **16**, 3714–3724.
- 22 R. M. Crooks, M. Zhao, L. Sun, V. Chechnik and L. K. Yeung, *Acc. Chem. Res.*, 2001, **34**, 181.
- 23 Y. Xie, Z. F. Zhang, T. Jiang, J. L. He, B. X. Han, T. B. Wu and K. L. Ding, *Angew. Chem., Int. Ed.*, 2007, **46**, 7255–7258.
- 24 K. R. Priolkar, P. Bera, P. R. Sarode, M. S. Hegde, S. Emura, R. Kumashiro and N. P. Lalla, *Chem. Mater.*, 2002, **14**, 2120–2128.
- 25 X. M. Ma, Y. X. Zhou, J. C. Zhang, A. L. Zhu, T. Jiang and B. X. Han, *Green Chem.*, 2008, **10**, 59–66.

Production of *p*-cymene and hydrogen from a bio-renewable feedstock—1,8-cineole (eucalyptus oil)

Benjamin A. Leita,^{*a,b} Andrew C. Warden,^a Nick Burke,^b Mike S. O'Shea^a and David Trimm^b

Received 10th August 2009, Accepted 17th September 2009

First published as an Advance Article on the web 23rd October 2009

DOI: 10.1039/b916460j

The catalytic transformation of pure 1,8-cineole was performed in a custom-built down-flow fixed bed pyrolysis rig over various metal-doped alumina pellets controlled at temperatures between 523 K (250 °C) and 873 K (500 °C). Varying amounts of oxygen were added to the feed. Hydrophilic, hydrophobic and gaseous products were analysed separately. The hydrophilic phase was predominantly water, while the composition of the hydrophobic phase varied with catalyst type and contained mainly mixtures of both aromatic and non-aromatic C₁₀ hydrocarbons. The main gases produced were hydrogen, carbon monoxide and carbon dioxide. As the reaction temperature increased, yields of gas phase components increased for all catalysts. The palladium-doped γ -Al₂O₃ catalyst at ~250 °C showed excellent yields and selectivity for the continuous production of *p*-cymene together with hydrogen gas. For the best catalysts and reaction conditions, the process is very atom and carbon efficient, with all ten carbon atoms from the cineole molecule being used in the *p*-cymene product in an oxygen-free environment. The process uses no solvents and the high yields achieved ensure there is no waste clean-up required.

1. Introduction

The volatility of oil prices and the increasing pressure to find sustainable, bio-derived alternatives to petrochemical feedstocks has encouraged researchers to look into an increasingly diverse range of biological materials for chemical precursors. 1,8-cineole (hereafter referred to as cineole) is the main chemical component of eucalyptus oil (~90%) and is obtained *via* steam distillation of eucalyptus leaves¹ (Fig. 1). Most of the world's eucalyptus oil is produced in China as a by-product of the eucalyptus timber plantation industry. The world market for pharmaceutical and domestic use of eucalyptus oil is about 7000 tonne each year.² In recent years, the price has been relatively stable at between US \$4,500 and US \$5,000 per tonne.² However, the potential production of eucalyptus oil has been estimated to be in the millions of metric tonnes per year, globally, with estimates for current Australian eucalyptus plantings alone reaching the level of 800 000 tonnes per year.³ With this volume of eucalyptus oil on the market, the prices can be expected to drop well below current values.⁴

These production figures and lower costs would make cineole a very attractive feedstock for the production of industrial chemicals from a renewable resource. Thus, it is not surprising that cineole has already been regarded as a potentially attractive renewable feedstock for the production of C₁₀ industrial chem-

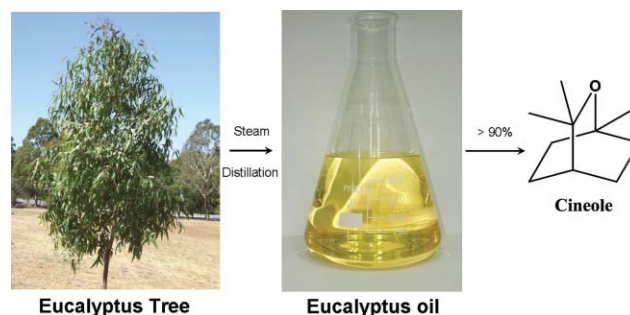


Fig. 1 Production of 1,8-cineole.

icals and chemical precursors such as menthenols, menthenes, menthadiene and *p*-cymene.⁵

p-Cymene (Fig. 2) is of significant interest in that it is already used in the production of *p*-cresol, fragrances, pharmaceuticals, herbicides and fine chemicals.⁶ Currently, commercial

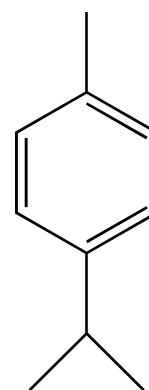


Fig. 2 Structure of *p*-cymene.

^aCSIRO Molecular and Health Technologies, Private Bag 10, Clayton South VIC, 3169, Australia. E-mail: benjamin.leita@csiro.au; Fax: +61 3 95458380; Tel: +61 3 95458130

^bCSIRO Petroleum Resources, Private Bag 10, Clayton South VIC, 3169, Australia. E-mail: david.trimm@csiro.au; Fax: +61 3 95458380; Tel: +61 2 93854340

production of cymenes is from toluene and propylene which are obtained from crude oil. The alkylation and isomerisation steps produce a mixture of the three different isomers of cymene, but primarily yield the *m*- and *p*-isomers.⁷ Further separation to pure *p*-cymene prior to the *p*-cresol conversion is currently achieved using the UOP-developed “Cymex” process, where *m*- and *p*-cymene are subject to chromatography using adsorbing (molecular sieves) and desorbing (toluene) media.⁸

Subsequent production of cresols based on the oxidation of cymenes, or cleavage of isopropyl toluenes into cresols and acetone, are direct extensions of the phenol process from benzene.⁹

There have been investigations into the direct synthesis of pure *p*-cymene using ZSM-5 catalysts for regioselectivity in the alkylation of toluene¹⁰ and some further studies for pure *p*-cymene production using pinenes as a feedstock.⁸

These processes rely on non-renewable crude oil feedstocks and processing. Matsuura and Waki¹¹ studied the pyrolysis of bio-derived cineole over calcium oxide and activated alumina, the latter having a catalytic effect on the reaction starting at 220 °C, while the calcium oxide catalysed the system only at 450 °C. The major liquid hydrophobic product from the activated alumina-catalysed reactions between 250 and 350 °C was found to be dipentene, with some isomerisation due to the rearrangement of the double bond. In contrast, Hügel *et al.* reacted cineole with hydrogen over pumice and silica-supported platinum and palladium catalysts to give mixtures of *cis*- and *trans*-*p*-menthanes at lower temperatures while *p*-cymene was found to be produced at temperatures greater than 350 °C.⁵ Buhl *et al.* investigated the conversion of α -limonene to *p*-cymene over silica-supported Pd catalysts¹² and later from pinenes to *p*-cymene.⁸ A more recent study by Martín-Luengo and co-workers reported 100% batch conversion of limonene to *p*-cymene using mesoporous silica–alumina supports heated by microwave irradiation.¹³

In this study, we have chosen to use continuous flow fixed bed pyrolysis to perform the catalytic transformation of cineole. This approach is advantageous in that we employ a continuous process that provides more scope for mass production at either commercial scales or in smaller, decentralised plants. In addition, the process is very atom and carbon efficient, with all ten carbon atoms from the cineole molecule being used in the *p*-cymene product without the use of any solvents while producing no waste stream requiring costly disposal. For the catalysts, we have used high-surface area γ -Al₂O₃ pellets (200 m² g⁻¹, Saint-Gobain, USA) initially as a slightly acidic catalyst and then as a support where it was doped, *via* the wet impregnation technique, with molybdenum, iron, cobalt, chromium and palladium nitrate solutions.¹⁴ These catalytic materials were subjected to vapour phase pyrolysis of cineole using a down flow fixed bed tubular reactor at atmospheric pressure with varying amounts of blended oxidant.

2. Experimental

2.1. Catalyst preparation

High surface area γ -Al₂O₃ pellets (200 m²g⁻¹) were used as a slightly acidic catalyst and as a solid support for molybdenum,

iron, cobalt, chromium and palladium metals. The metal-doped γ -Al₂O₃ catalysts were prepared by a wet impregnation technique using 1 M aqueous solutions of the appropriate metal salts.

In a typical procedure, 100 mL of 1 M metal nitrate solution was poured over 70 g of γ -Al₂O₃ pellets (Saint-Gobain NorPro, USA) that had been heated in a vacuum oven at 90 °C overnight. The mixture was stirred briefly with a spatula and left to stand at room temperature overnight. The resultant metal-impregnated γ -Al₂O₃ pellets were collected, washed three times with deionised water and dried in a vacuum oven at 90 °C overnight. The coated pellets were then transferred to a crucible and calcined in air at 350 °C for 12 h. As controls, undoped γ -Al₂O₃ pellets were subjected to the same treatment as the metal doped samples before use, and glass beads were used as a blank reaction surface.

2.2. Catalyst characterization

Prior to surface analysis, samples were degassed under vacuum at 300 °C overnight using a VacPrep 061 Degasser. The BET surface area was determined by N₂ adsorption at 77 K using a Micromeritics Tristar 3000. X-Ray diffraction (XRD) measurements were carried out using a Phillips DW 1130 machine with Cu K α (1.542 Å) radiation (40 kV, 25 mA) over the range 5–80° 2 θ at a scan rate of 1° min⁻¹ with 0.1° step size.

2.3. Catalytic activity measurements

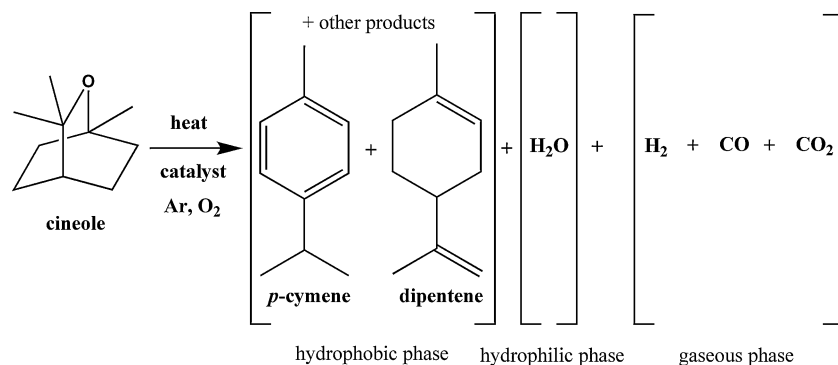
The vapour phase catalytic conversion of cineole was performed using an electrically heated tubular down-flow reactor (13.5 mm internal diameter, 300 mm length) with the catalyst held as a fixed bed at atmospheric pressure. A K-type thermocouple was used to monitor the temperature of the bed. All thermocouples, furnaces, heating bands and mass flow controllers (MFC) were controlled and data were logged using specially designed software.¹⁵

The liquid product was collected at 40 °C in a stainless steel trap. The gaseous products were sent through a second trap at 0 °C to an online gas chromatograph (GC).

In a typical variable temperature experiment, 3 g of catalyst was loaded into a stainless steel mesh basket, which was placed inside the tubular reactor. The furnace was set to an initial temperature of 250 °C and the temperature was allowed to equilibrate for one hour. Cineole was injected upstream of the pre-heater at a rate of 0.5 mL min⁻¹ with an ISCO 500D syringe pump. The carrier gas was a blended mixture of the amount of oxygen required in argon containing a 5.1% helium internal standard; this was fed at a constant rate of 150 mL min⁻¹. Once at equilibrium, gas samples were taken and liquid products collected. The furnace temperature was then raised by 50 °C and the procedure was repeated until the final reaction temperature of 500 °C was reached.

2.4. Analysis of liquid products

The liquid product obtained for the majority of the samples consisted of an oily, hydrophobic phase and an aqueous phase. The analysis of liquid products was performed using a GCMS fitted with an auto sampler. For analysis, 10 μ L of the hydrophobic phase was dissolved in 1.5 mL of acetonitrile (Aldrich) that had been doped with 0.1% mesitylene (Aldrich)



Scheme 1 The catalytic transformation of cineole over metal-doped γ -Al₂O₃ catalysts.

as an internal standard. Chromatographic standards of 1,8-cineole, *p*-cymene and dipentene were run using the same sample preparation method. Major products were also characterised by ¹H and ¹³C NMR. The yield of *p*-cymene was defined as the percentage of *p*-cymene in the whole hydrophobic phase. Selectivity for *p*-cymene is defined as the percentage of *p*-cymene in the non-cineole fraction of the hydrophobic phase. Unless otherwise noted, the non-cineole fraction of the hydrophobic phase was comprised of the products shown in Scheme 1. The hydrophilic phase was found to be mainly water.

2.5. Analysis of gaseous products

Analysis of the reagent and product gases was performed with an online Shimadzu GC 8A fitted with a Valco sampling valve with a 1 mL sample loop. The GC was fitted with a 12 m HAYESEP Q column and a thermal conductivity detector (TCD). The GC was calibrated with a calibration gas mixture containing known concentrations of hydrogen (5.02%), helium (4.92%), carbon monoxide (4.97%) and carbon dioxide (10.20%) (BOC) before each run. Argon was used as the reference gas for the TCD in the GC analyses, allowing for maximum sensitivity to hydrogen. An internal standard gas mixture containing 5.1% helium in argon was used as the carrier gas for the liquid cineole feedstock. Online gas analysis was conducted at the time of collection of liquid samples. Results for the gas phase analysis were accurate to within $\pm 3\%$.

3. Results and discussion

3.1 Catalyst characterization

The XRD patterns of the metal doped γ -Al₂O₃ catalysts prepared by the wet impregnation technique are shown in Fig. 3. The pure γ -Al₂O₃ showed some crystalline nature while the molybdenum-doped catalyst clearly shows a more crystalline nature with intense peaks at $2\theta = 12.9, 23.4, 25.8$ and 27.4° corresponding to α -MoO₃ in the orthorhombic phase.¹⁶ The other metal-doped γ -Al₂O₃ samples display XRD patterns associated with the support material. There is some evidence of added crystallinity in all of the metal-doped samples.

The BET surface areas for all as-prepared catalysts and γ -Al₂O₃ are given in Table 1. The surface area of the γ -Al₂O₃ was the highest while all other catalysts were lower in surface area. Metal doping of the γ -Al₂O₃ using the wet impregnation

Table 1 Surface area and pore volume of fresh (as prepared) metal doped γ -Al₂O₃ catalysts

Catalyst	Surface area/m ² g ⁻¹	Pore volume/cm ³ g ⁻¹	Average pore width/Å
γ -Al ₂ O ₃	247	0.76	12.9
Mo- γ -Al ₂ O ₃	172	0.51	13.1
Cr- γ -Al ₂ O ₃	239	0.71	12.8
Co- γ -Al ₂ O ₃	210	0.66	12.7
Fe- γ -Al ₂ O ₃	216	0.69	12.7
Pd- γ -Al ₂ O ₃	243	0.81	12.4

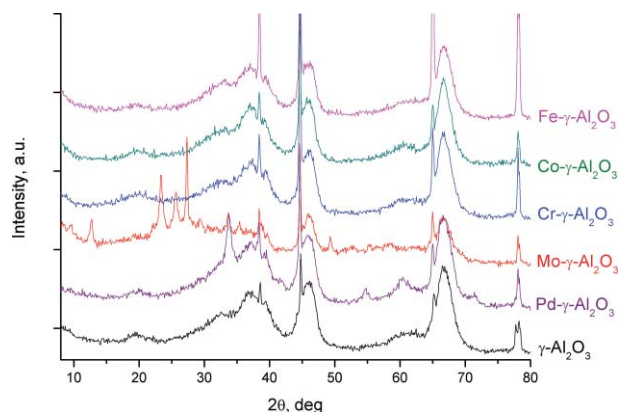


Fig. 3 The XRD patterns of the metal-doped γ -Al₂O₃ catalysts.

technique has shown a minimal amount of surface area loss with the exception of the Mo-doped catalyst.

3.2 Catalytic activity

Products of the pyrolysis process were separated into three phases: hydrophobic and hydrophilic liquid, and gaseous (Scheme 1). Table 2 shows the compositions of the hydrophobic phases produced during the variable temperature experiments using the five metal-doped catalysts and the undoped γ -Al₂O₃ catalyst. Gaseous phase composition is shown in Fig. 7. In all experiments, the only detectable hydrophilic phase component was water, while the hydrophobic phase generally contained a mixture of both aromatic and non-aromatic C₁₀ hydrocarbons with dipentene and *p*-cymene as the major products. The hydrophilic liquids were analysed by NMR and GCMS. The only gases detected were hydrogen, carbon monoxide and carbon

Table 2 Major products in the hydrophobic phase from the conversion of cineole

Catalyst	Furnace T/°C	0% O ₂			7.3% O ₂			14.6% O ₂					
		Bed T/°C	p-Cymene/%	Dipentene/%	Cineole/%	Bed T/°C	p-Cymene/%	Dipentene/%	Cineole/%	Bed T/°C	p-Cymene/%	Dipentene/%	Cineole/%
γ -Al ₂ O ₃	250	214	6	0	93	199	0	0	95	195	6	0	94
	300	212	23	0	76	210	46	0	45	216	18	0	78
	350	262	31	0	65	248	49	0	46	252	42	0	54
	400	285	47	0	35	283	58	0	34	312	51	0	41
	450	357	39	0	20	343	60	0	21	360	51	0	34
Mo- γ -Al ₂ O ₃	500	406	26	0	6	393	50	0	10	397	47	0	24
	250	199	9	0	51	205	9	0	52	228	32	0	19
	300	184	16	0	51	250	54	0	18	266	52	0	25
	350	207	14	0	48	279	52	0	17	292	41	0	41
	400	274	8	0	34	318	52	0	18	325	38	0	48
Cr- γ -Al ₂ O ₃	450	335	33	0	24	356	54	0	22	358	34	0	53
	500	378	56	0	15	393	56	0	25	393	38	0	50
	250	205	11	0	88	200	23	0	42	224	14	0	83
	300	220	18	0	81	225	9	0	91	248	11	0	89
	350	250	2	0	83	265	14	0	85	302	23	0	73
Fe- γ -Al ₂ O ₃	400	293	18	0	40	307	25	0	71	346	36	0	49
	450	344	23	0	24	349	39	0	45	387	46	0	30
	500	394	35	0	13	392	47	0	33	427	55	0	17
	250	224	0	12	87	227	0	61	19	224	0	4	95
	300	228	0	23	76	249	0	41	53	261	0	50	42
Co- γ -Al ₂ O ₃	350	250	0	56	42	282	0	42	54	286	0	48	44
	400	279	0	76	15	321	0	45	46	318	0	51	37
	450	325	0	64	4	363	0	48	40	363	0	52	32
	500	379	0	0	40	408	0	53	35	406	0	58	25
	250	209	0	0	100	233	0	3	97	228	0	34	63
Pd- γ -Al ₂ O ₃	300	229	0	55	42	289	0	4	96	248	0	26	74
	350	267	0	66	26	289	0	10	90	297	0	26	74
	400	315	0	71	15	323	0	26	71	344	0	33	63
	450	361	0	64	8	365	0	44	48	411	0	47	45
	500	411	0	57	7	419	0	55	23	459	0	58	22
Pd- γ -Al ₂ O ₃	250	214	57	0	37	234	89	0	10	293	93	0	5
	300	231	56	0	42	252	91	0	8	301	94	0	5
	350	269	67	0	29	293	95	0	5	317	89	0	5
	400	305	77	0	18	328	94	0	3	350	81	0	4
	450	347	85	0	11	374	68	0	1	393	50	0	2
500	385	88	0	6	425	50	0	2	440	52	0	1	

dioxide. The gas phase composition was dependent on gas feed composition and reaction temperature.

Fig. 4 shows *p*-cymene yield as a function of catalyst bed temperature for all catalysts. Cineole remained relatively unchanged for all experiments using the glass beads. The amount of oxygen blended into the carrier gas had only a mild effect on the hydrophobic phase products. A moderate level of introduced oxygen (7.3%) generally increased the yields of *p*-cymene, while higher levels (14.6%) decreased *p*-cymene yields and increased the formation of CO and CO₂.

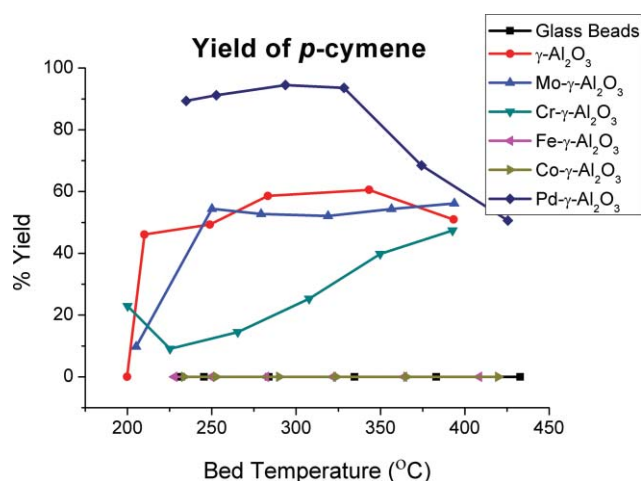


Fig. 4 Yield of *p*-cymene versus bed temperature with 7.3% oxygen.

Experiments performed with the undoped γ -Al₂O₃ pellets showed some formation of *p*-cymene with yields of 47, 60 and 50%, for 0, 7.3 and 14.6% oxygen, respectively at around 400 °C. The selectivity of the undoped γ -Al₂O₃ pellets at this temperature was approximately 70% for *p*-cymene. The major product formed for both the iron- and cobalt-doped γ -Al₂O₃ catalysts was dipentene, with no apparent production of *p*-cymene.

The chromium-doped γ -Al₂O₃ catalyst catalysed the formation of *p*-cymene with a maximum yield of 55% using 14.6% oxygen at ~400 °C. At this bed temperature, the conversion of cineole ranged from 67–87% depending on the amount of oxygen used. The selectivity of this catalyst to *p*-cymene was initially quite high (>95%) but with very little conversion of the cineole (9–15%). At 400 °C, selectivity was again reasonable, being approximately 70% (Fig. 5).

The molybdenum-doped γ -Al₂O₃ catalyst also produced *p*-cymene as the major product with a maximum yield of 56% at 0 and 7.3% oxygen and ~390 °C. At lower temperatures, the selectivity of this catalyst was quite low (<20%) but reached 66% at 378 °C. *p*-Cymene was the major product produced with high selectivity for the palladium-doped γ -Al₂O₃ catalyst. This catalyst gave excellent conversion efficiencies to *p*-cymene at much lower bed temperatures compared to the other catalysts tested. The experiments with this catalyst containing some oxygen in the carrier gas showed almost complete conversion of the cineole while conversion efficiencies to *p*-cymene were 95% at a reaction bed temperature of approximately 250 °C. The selectivity of this catalyst for *p*-cymene was also very high, being >98% at this bed temperature.

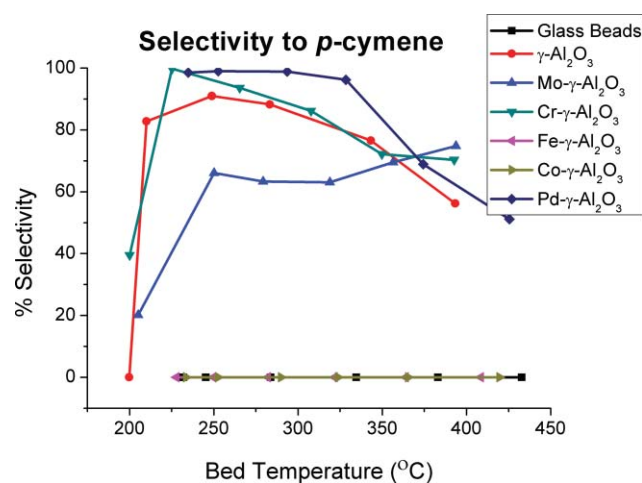


Fig. 5 Selectivity for *p*-cymene versus bed temperature with 7.3% oxygen.

Catalysts such as the undoped alumina and the chromium-based catalyst displayed very high selectivities for *p*-cymene (96 and 100%, respectively) at very low bed temperatures (~220 °C) but had poor overall conversion of cineole (24 and 9%, respectively). The molybdenum catalyst displayed both poor selectivity and overall production of *p*-cymene, whereas the iron and cobalt catalysts produced no *p*-cymene under any of the reaction conditions tested.

There was a general trend towards decreasing selectivity with increasing bed temperatures greater than ~250 °C for most of the catalysts, with the notable exception of the palladium catalyst, which maintained very high selectivity for *p*-cymene in a zero-oxygen environment. Conversion increased from 37% at 214 °C to nearly complete cineole consumption (94%) at 385 °C. Addition of oxygen at moderate levels increased the selectivity to *p*-cymene to 99–100% at low bed temperatures while exhibiting excellent conversion of cineole (>90%).

Interestingly, the undoped alumina, molybdenum, chromium and palladium catalysts produced no dipentene in any of the runs, yet selectivity for dipentene was very high under mild conditions for the iron and cobalt catalysts. Conversion of cineole was poor for cobalt (<10%) but slightly better for iron, reaching a maximum of 58% at 250 °C, with 97% selectivity. As was the case for *p*-cymene, selectivity towards dipentene dropped off past ~250 °C for both the iron and cobalt catalysts. The addition of a moderate level of oxygen during runs with the iron catalyst dramatically improved the conversion level of cineole from 13 to 81% at low bed temperatures. However, additional oxygen past 7.3% reduced cineole conversion to 5%. Selectivity for dipentene was only marginally affected by the varying oxygen levels. The best result for the cobalt catalyst was 74% cineole conversion with 89% selectivity for dipentene at 267 °C with no oxygen.

3.3 Analysis of gas products

The yields of hydrogen for the different catalysts with 7.3% oxygen in the carrier gas are shown in Fig. 6.

The only gas product observed during oxygen-free experiments was hydrogen. Across all catalysts tested, increasing the

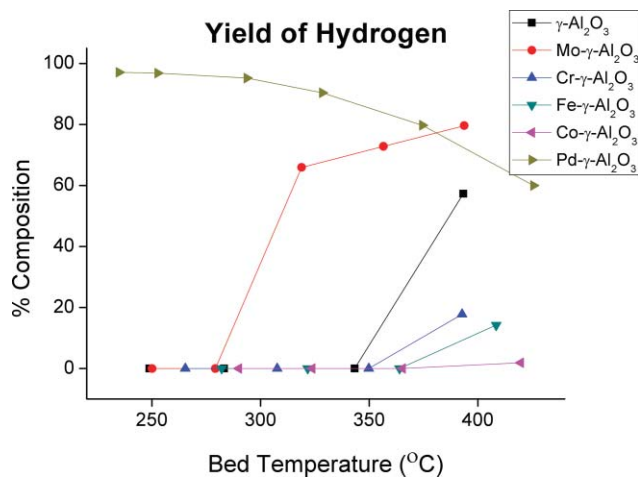


Fig. 6 Yield of hydrogen for experiments with 7.3% oxygen.

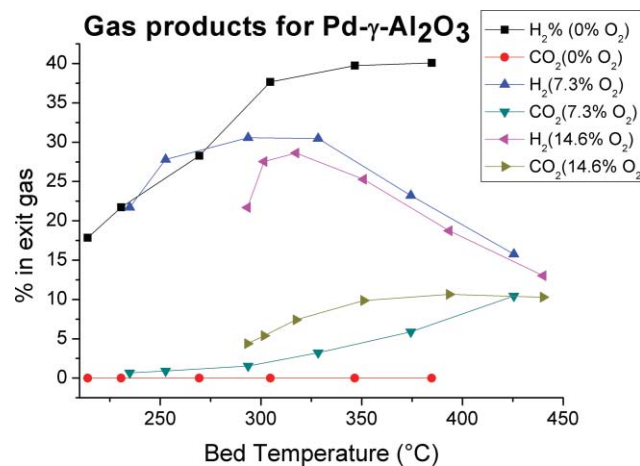


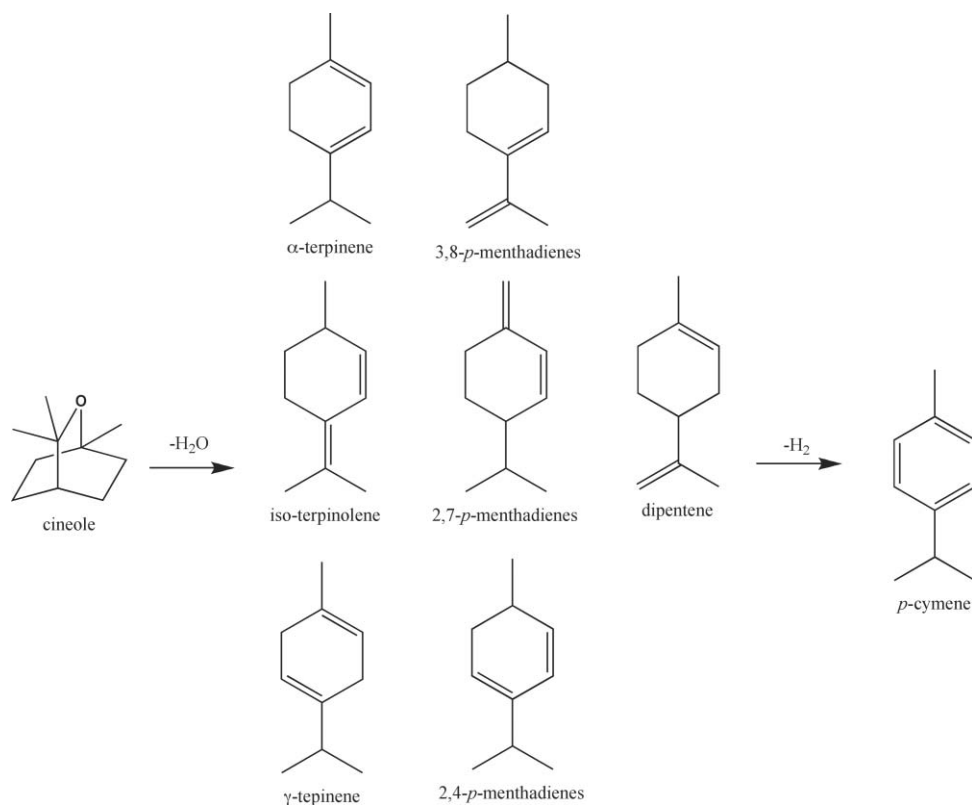
Fig. 7 Gaseous products formed with the palladium doped γ - Al_2O_3 catalyst.

amount of oxygen in the carrier gas increased the production of CO and CO_2 .

The effect of oxygen in the carrier gas stream on the composition of the gas phase produced by the palladium doped γ - Al_2O_3 catalyst is shown in Fig. 7. When oxygen was used in the reaction, the amount of hydrogen produced decreased, while the amount of CO_2 increased. This effect was more pronounced at higher temperatures. The CO production was negligible for all the palladium-doped γ - Al_2O_3 catalyst experiments. Almost total conversion of oxygen was observed during experiments containing oxygen.

3.4 Reaction mechanism

Based on the observed products, a possible reaction mechanism for the conversion of cineole into *p*-cymene over γ - Al_2O_3 supported catalysts is shown in Scheme 2. The reaction consists of a dehydration step followed by a dehydrogenation step. According to the thermophysical and theoretical study undertaken by Leal *et al.*,¹⁷ the weakest bond in the cineole molecule is the oxygen to carbon bond with only one methyl group attached. This bond is broken first, and the dehydration of cineole takes place very rapidly, producing a mixture of doubly unsaturated isomers.



Scheme 2 The proposed reaction sequence for the catalytic transformation of cineole into *p*-cymene.

In the second step, dehydrogenation and rearrangement of the double bonds occurs to produce *p*-cymene.

The undoped γ -Al₂O₃ catalyst was active for both the dehydration and dehydrogenation reactions. The dehydration reaction yielded a mixture of non-aromatic intermediates. This was followed up by the dehydrogenation of these intermediates into the fully aromatic *p*-cymene (Scheme 2). Similar products were also observed for the chromium- and molybdenum-doped γ -Al₂O₃ catalyst. For the cobalt- and iron-doped γ -Al₂O₃ catalyst, there was no observation of *p*-cymene in the products indicating that these catalysts are not able to affect the dehydrogenation step. The major products for both the cobalt- and iron-doped γ -Al₂O₃ catalysts suggest that these catalysts were only capable of performing the dehydration of the cineole while also giving some selectivity towards dipentene. They were not able to perform the dehydrogenation step.

For the palladium-doped γ -Al₂O₃ catalyst, a very high selectivity towards the *p*-cymene was observed. This catalyst is capable of performing both the dehydration of the cineole followed by a rapid dehydrogenation into *p*-cymene. Due to the absence of dehydration products observed when using the palladium-doped γ -Al₂O₃ catalyst, the palladium plays a vital role in the dehydrogenation step. This is not surprising as palladium is a known hydrogenation/dehydrogenation catalyst. The high selectivity of the dehydrogenation step to *p*-cymene over the Pd catalyst suggests this step proceeds at a greater rate than the cineole dehydration step.

4. Conclusions

This study has shown that a continuous synthetic route exists for the conversion of cineole to valuable products. The high temperature catalytic transformation of the bio-renewable feedstock, 1,8-cineole, over a number of metal-doped γ -Al₂O₃ catalysts has shown *p*-cymene to be the major hydrophobic liquid product and hydrogen the major gaseous product. From an industrial perspective, the separation of the liquid products for runs with high selectivity is trivial owing to the *in situ* separation of the aqueous and hydrophobic phases. The results exemplify dual-function catalytic activity (dehydration and dehydrogenation) on a bio-renewable feedstock to produce alkylbenzenes. While cobalt- and iron-doped γ -Al₂O₃ catalysts were only able to

perform the dehydration step, the palladium-doped γ -Al₂O₃ pellets showed the best activity, yielding >90% *p*-cymene while producing large amounts of hydrogen in the exit gas at a bed temperature of ~250 °C. Future work is focusing on studying the palladium catalyst system in more detail including: optimizing the reaction conditions to maximize both conversion of cineole and selectivity to *p*-cymene, and studying catalyst lifetime.

Acknowledgements

The authors wish to thank the CSIRO OCE PDF funding scheme for financial support for this project.

References

- 1 J. L. Simonsen, and L. N. Owen, *The Terpenes* 2nd edn, vol. 1, Cambridge University Press, Cambridge, 1973, p. 423.
- 2 Deeptha Rajkumar *Eucalyptus oil units for dumping duty on Chinese imports* The Hindu Business Line, Thursday, Feb 12, 2004.
- 3 J. Bartle, G. Oslon, D. Cooper and T. Hobbs, *Int. J. Global Energy Issues*, 2007, **27**(2), 115–137.
- 4 G. N. Pain, *Eucalyptus Oil Report*, Verve Energy, 2006.
- 5 H. M. Hügel, W. R. Jackson, C. D. Kachel and I. D. Rae, *Aust. J. Chem.*, 1977, **30**, 1287–1292.
- 6 A. K. Mukhopadhyay, *Industrial Chemical Cresols and Downstream Derivatives*, Marcel Dekker, New York, 2005.
- 7 D. M. Roberge, D. Buhl, J. P. M. Niederer and W. F. Hölderich, *Appl. Catal., A*, 2001, **215**, 111–124.
- 8 R. W. Neuzil, D. H. Rosback, R. H. Jensen, J. R. Teague and A. J. deRosset, *Chemtech*, 1980, **8**, 498.
- 9 H. Fiege, in: *Ullmann's Encyclopedia of Industrial Chemistry*, Vol. A8, VCH, Weinheim, 1985, p. 25.
- 10 J. S. Beck, W. O. Haag, in *Handbook of Heterogeneous Catalysis*, ed. G. Ertl, H. Knözinger and J. Weitkamp, vol. 4, Wiley-VCH, Weinheim, 1996, p. 2123.
- 11 T. Matsuura and T. Waki, *J. Sci. Hiroshima Univ.*, 1957, **20**(3), 177–186.
- 12 D. Buhl, D. M. Roberge and W. F. Hölderich, *Appl. Catal., A*, 1999, **188**, 287.
- 13 M. A. Martín-Luengo, M. Yates, M. J. Martínez Domingo, B. Casal, M. Iglesias, M. Esteban and E. Ruiz-Hitzky, *Appl. Catal., B*, 2008, **81**, 218–224.
- 14 B. Leita, P. Gray, N. Burke, D. Trimm, provisional patent filed 16th July 2009, Australian Provisional Patent Application No. 2009903333.
- 15 ECE Fast, Development of the data logging software 'RAMPX'.
- 16 A. Kido, H. Iwamoto, N. Azuma and A. Ueno, *Catal. Surv. Jpn.*, 2002, **6**, 45.
- 17 S. Aparicio, R. Alcalde, M. J. Da'vila, B. Garcia and J. M. Leal, *J. Phys. Chem. B*, 2007, **111**, 3167–3177.

An unusual common ion effect promotes dissolution of metal salts in room-temperature ionic liquids: a strategy to obtain ionic liquids having organic–inorganic mixed cations

C. Chiappe,^{*a} M. Malvaldi,^a B. Melai,^a S. Fantini,^b U. Bardi^c and S. Caporali^c

Received 5th May 2009, Accepted 7th September 2009

First published as an Advance Article on the web 23rd October 2009

DOI: 10.1039/b919111a

A simple strategy has been reported to prepare new ionic liquids with binary systems of organic–inorganic cations exploiting the common ion effect, *i.e.* dissolving metal salts with organic or inorganic anions (bistriflylimide or nitrate) in ionic liquids bearing the same anions. The resulting concentrated solutions of metal cations in ionic environments, which may have great potential for electrochemical processes, have been characterized by X-Ray photoelectron spectroscopy (XPS) and electropray ionization mass spectrometry (ESI-MS)

Introduction

Transition metals are among the most important elements for chemical and technological industry, with an extremely widespread utility range. Among the possible ways to process these elements, electrodeposition from concentrated solutions of metal salts is used for metal plating and finishing of a wide range of products, improving their environmental resistance and lifetime.

Ionic liquids have received much attention in recent years as promising conductive media for electrodeposition, due to their negligible volatility and large thermal and electrochemical stability.¹ Despite this, the solubility of transition metal salts in ionic liquids is quite limited: Afonso *et al.*² evaluated the solubility of LiCl, HgCl₂ and LaCl₃ in [C_nmim][BF₄] and [C_nmim][PF₆], obtaining solubilities scarcely exceeding 10⁻⁴ wt%. Very limited solubilities were also reported for titanium chlorides in [bmim][Tf₂N]³ and for various other metals.⁴

Concentrated solutions are required for the electrodeposition process,⁵ but these are not easy to obtain. Concentrations of about 50% mol were prepared in some cases;⁵ however, these solutions were obtained by mixing ILs and metal salts in molecular solvents and then removing the solvent (or water), probably obtaining supersaturated solutions or solutions with an appreciable amount of water. Recently, it has been reported that concentrations up to 2.5 mol L⁻¹ have been achieved by dissolving AlCl₃ in [EMIM][TfSA], where a biphasic melt is obtained, going further on adding the aluminium complex.⁶ Similarly, a good solubility is reported for transition metal chlorides in dicyanamide-based ILs;⁷ nevertheless, for some metals, solubility does not exceed 0.01 M. In the above

examples, high solubilities are generally obtained only by means of an ionic liquid based on a strongly complexing anion, probably leading to highly coordinated metal–anion complexes which affect the electrochemical properties of the metal and thus limit the electrodeposition process, as previously noted.⁷

In this work, we report on the possibility of obtaining high concentrations of metal salts in hydrophilic and hydrophobic ILs by simply dissolving the salts in ILs which contain the same anion. Ionic liquids with different cations (based on imidazolium, pyridinium and pyrrolidinium salts) and anions (triflate, bistriflylimide, nitrate, acetate) were tested, in order to ensure that this result can be obtained independently of the chemical nature of the ionic liquid.

Experimental

The metal salts Ag(Tf₂N), Ni(Tf₂N)₂, Al(Tf₂N)₃, Co(Tf₂N)₂, Y(Tf₂N)₃ (Solvionic, 99% pure) and Ag(NO₃), Ni(NO₃)₂, Al(NO₃)₃, Cr(NO₃)₃, AgBF₄, AgPF₆, AgTfO, Cu(TfO)₂ (Aldrich, 99% pure) were always dried (70 °C under vacuum, 2 × 10⁻³ Torr, for 10 h) before use. The ionic liquids 1-butyl-3-methylimidazolium bistriflylimide [bmim][Tf₂N], 1-ethyl-3-methylimidazolium bistriflylimide and 1-butyl-3-methylimidazolium triflate [bmim][TfO] were synthesized as previously reported.⁸ 1-Butyl-3-methylimidazolium nitrate was prepared from 1-butyl-3-methylimidazolium bromide by reaction with AgNO₃ in water. After filtration of the precipitate (AgBr), water was removed by distillation at reduced pressure. The colorless liquid was dissolved in dried acetone and stored at -40 °C for a week. Residual traces of AgBr were removed by filtration of the solution on celite.

The water content of the ionic mixtures was determined by the Karl Fisher technique using an apparatus composed of a standard titrator and a coulometer.

ESI-MS analyses were performed on a Finningan LCQ Advantage (Thermo Finningan, San Jose, CA, USA) ion trap instrument equipped with Excalibur Software.

^aDipartimento di Chimica e Chimica Industriale, Università di Pisa, via Risorgimento 35, 56126, Pisa, Italy. E-mail: cinziac@farm.unipi.it

^bSolvionic, site SNPE, Chemin de la Loge, 31078 Toulouse cedex 4, France

^cDipartimento di Chimica, Università di Firenze, via della Lastruccia 3, 50019 Sesto Fiorentino (FI), Italy

XPS measurements

The X-ray photoelectron spectroscopy (XPS) measurements reported in this paper were performed in a system using a non-monochromated Al K α source (1486.6 eV) and a VSW HAC 5000 hemispherical electron energy analyser.

The sample holder consisted of planar gold foil (dimension 2 \times 2 cm), ground with SiC paper down to 1200 grit, and then carefully degreased using HNO₃ (69.5% for analysis, Carlo Erba) and acetone (ultrapure for spectroscopy, Merck). It was introduced into the UHV system *via* a loadlock under inert gas (N₂) flux, in order to minimize the exposure to air contaminants. The sample thin films were prepared by deposition of one or two drops of IL solution, under nitrogen flux, directly onto the Au foil; the surface tension is enough to cover the surface with a film of liquid, as demonstrated by the absence of peaks attributable to gold. The overall time required for the loading procedure was less than one minute. Before the measurements, the sample was kept in the introduction chamber for at least 12 h, allowing the removal of volatile substances such as water and traces of organic solvents, as confirmed by the pressure value achieved (2×10^{-9} Torr), just above the instrument base pressure.

Photoelectron spectra were acquired in the constant-pass-energy mode at $E_{\text{pas}} = 44$ eV, and the overall energy resolution was 1.2 eV, measured as a full-width at half maximum (FWHM) of the Ag 3d_{5/2} line of a pure silver reference. To vary the measurements probing depth, the spectra were collected at $\theta = 0^\circ$ (normal emission), $\theta = 45^\circ$ and $\theta = 60^\circ$ (grazing angle). The probing depth varies mainly with $\cos \theta$, and since the energy of the collected photoelectrons ranges between 800 and 1300 eV and their inelastic mean free path (imfp) in such compounds is about 2 nm, we can consider that measurements probe 6–7, 4–5 and 2–3 nm at 0, 45 and 60°, respectively. Since the electron distribution within the imidazolium ring is little affected by the counter ion, we correct the energy scale using the N 1s peak (401.6 eV) of the imidazolium ring. Peak positions in different samples were reproduced within 0.2 eV. The recorded spectra were fitted using XPSPeak 4.1 software employing Gauss–Lorentz curves to fit the data after subtraction of a Shirley-type background.

Solubility measurements

Solutions were prepared by adding aliquots of the previously dried metal salt into a calibrated flask containing the weighed ionic liquid (5 mL), previously dried at 70 °C under vacuum (2×10^{-3} Torr) for 10 h. Additions were made at ambient temperature. For slowly solubilizing salts (Cr and Al salts) the flask has been gently heated until complete dissolution was obtained, and then allowed to cool before successive addition. Comparable results have also been obtained by performing the experiments at room temperature using longer dissolution times.

Results and discussion

The results for the solubilities are reported in Tables 1, 2, 3 and 4, where the molar concentration of metal salts solutions that we were able to obtain are reported.

Initially, the solubility of transition metal salts with the nitrate ([NO₃]⁻) and bistriflylimide ([Tf₂N]⁻) anions was measured in

Table 1 Solubilities (M) of nitrate salts in [bmim][NO₃]

Ag(NO ₃)	Ni(NO ₃) ₂	Al(NO ₃) ₃	Cr(NO ₃) ₃
0.670	0.520	0.523	0.609

Table 2 Solubilities (M) of bistriflylimide salts in [bmim][Tf₂N]

Ag(Tf ₂ N)	Ni(Tf ₂ N) ₂	Al(Tf ₂ N) ₃
0.416	1.143	0.404

Table 3 Solubilities (M) of bistriflylimide salts in [emim][Tf₂N]

Al(Tf ₂ N) ₃	Co(Tf ₂ N) ₂	Y(Tf ₂ N) ₃
0.66	1.28	2.12

Table 4 Solubilities (M) of various salts in different ionic liquids. The asterisk (*) indicates that the experiment stopped before the maximum solubility was attained

IL	Salt	Solubility/M
HePyTf ₂ N	Y[Tf ₂ N] ₃	0.847
HePyTf ₂ N	Al[Tf ₂ N] ₃	0.638
[bmim][BF ₄]	Ag[BF ₄]	0.036
[bmim][PF ₆]	Ag[PF ₆]	0.060
[bmim][TfO]	Cu[TfO] ₂	1.108
[bmim][TfO]	Ag[TfO]	0.846
[BMPyrr][Tf ₂ N]	Co[Tf ₂ N]	1.000(*)
[bmim][Ac]	Ag[Ac]	0.5(*)

three ionic liquids having the same anion; specifically, in the hydrophilic [bmim][NO₃] and in the hydrophobic [bmim][Tf₂N] and [emim][Tf₂N].

Data reported in Tables 1–3 show that all the investigated ILs were able to dissolve the metal salts to a high extent, with solubilities greater than 0.4 M. We remark that the concentrations reported do not correspond to the solubility limit concentrations; in fact, many experiments were stopped to prevent the large volume increase of the solution exceeding the vial capacity. In other cases, we found a concentration of about 2 M satisfactory and found no purpose in going further.

As can be seen in Fig. 1, the colors of the nitrate solutions vary—bright green (Ni), yellow–pale green (Al), dark green (Cr), no colour (Ag, Y)—and all the obtained solutions were clear. The solution of Ag(Tf₂N) in [bmim][Tf₂N] is initially light pink, showing a deposition of metallic residues with time. Conversely, solutions of Ni and Al complexes are clear and transparent, with a bright green color (Ni) or no colour (Al). Washing the Ni(Tf₂N)₂ ionic liquid solution with water, a sudden decoloration of the ionic liquid phase is observed, with a



Fig. 1 From left to right: pure [HePy][Tf₂N] and its solution with [Al][Tf₂N]₃, [Ni][Tf₂N]₂ and Y[Tf₂N]₃.

subsequent movement of the green color to the aqueous phase, indicating that the salt is more soluble in water than in the IL.

All the solutions reported in Tables 1–3 were stable; no crystallization was observed, even after prolonged storage at room temperature (three months).

At the same time, we performed dissolution tests on $\text{Al}(\text{NO}_3)_3$ in $[\text{bmim}][\text{Tf}_2\text{N}]$ and of $\text{Al}(\text{Tf}_2\text{N})_3$ in $[\text{bmim}][\text{NO}_3]$; both these tests showed no detectable solubilization of the solid metal complex added, even after heating at the same conditions for times much longer (1 h) than reported for the solutions above.

Water content was determined for some solutions in order to understand if the addition of hygroscopic salts could have affected the dissolution process. We found a moderate water content, ranging from 1.23% for $[\text{bmim}][\text{Tf}_2\text{N}] + \text{Al}[\text{Tf}_2\text{N}]$ to 0.23% for $[\text{bmim}][\text{NO}_3] + \text{Al}[\text{NO}_3]$. We can conclude from this that water intake is not a key point in the dissolution process.

To verify the general character of the dissolution phenomena, further analogous experiments with ILs bearing different cations and/or anions were performed. The solubilities obtained, when the anion of the metal salt is shared with the ionic liquid, are still very high, with the only exceptions being the salts based on BF_4^- and PF_6^- ions.

Even if high solubilities were obtained for mostly all homoanionic solutions, the metals do not share the same solvation structure in all these solutions. This was evident from preliminary X-ray photoelectron spectroscopy analyses, with which we studied the near-surface chemical composition. By performing angle-resolved XPS measurements at three different angles (0° , 45° and 60°) on solutions of Al^{3+} , Ni^{2+} , Cr^{3+} and Ag^+ we found strong differences between the metal ion distribution at the surface.

For Al^{3+} and Ag^+ solutions (see Fig. 2), the metal peak is clearly detectable at all angles, providing evidence of the presence of metal ions up to a depth of no more than 2 nm

from the physical surface. However, for the Cr^{3+} solution (see Fig. 3), the metal peak fades away with increasing take-off angle, showing that metal ions are not present at the physical surface of the liquid. This is also the case for the Ni^{2+} solution. We interpreted this behavior as probably being due to the different coordination spheres of the ions: while Ag^+ and Al^{3+} stand in these solutions as single ions without a strong coordination sphere, independent of the nature of the anion, Cr^{3+} and Ni^{2+} have a strong coordination sphere which does not allow the metal ion to reach the physical surface of the liquid. This creates a strong barrier that shields the photoelectrons generated by the Cr^{3+} and Ni^{2+} ions, preventing them from leaving the surface and being detected. The coordination sphere affects not only the surface properties of these ionic systems, but also the electrochemical properties of the metal cations.

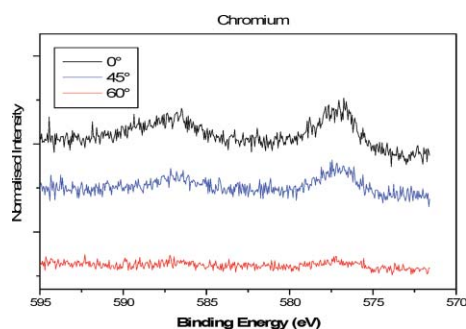


Fig. 3 XPS spectra at varying take-off angles for the Cr(2p) core peak in $[\text{bmim}][\text{NO}_3]$.

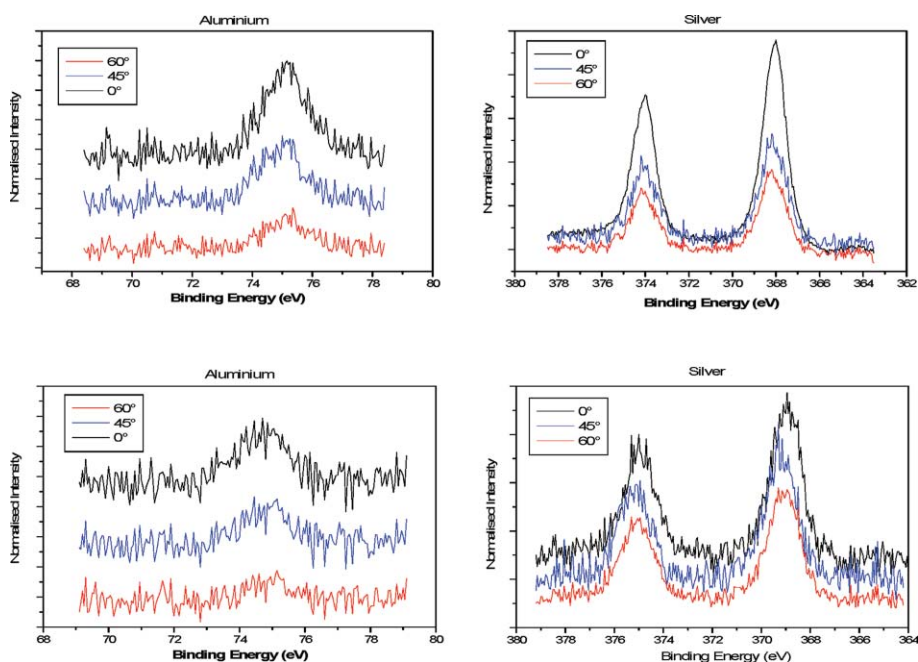


Fig. 2 XPS spectra at varying take off-angle for Al(2p) and Ag(3d) in $[\text{bmim}][\text{NO}_3]$ (top) and $[\text{bmim}][\text{Tf}_2\text{N}]$ (bottom).

temperature, *etc.*) confirmed the different ability of the ionic mixtures to give clusters involving the inorganic cations. While the peak of the charged complex $\text{Ni}[\text{Tf}_2\text{N}]_3^-$ (with mass 897.4 amu) was clearly detectable in the negative ion ESI mass spectrum of the Ni solution, significantly smaller peaks were detected for $\text{Ag}[\text{Tf}_2\text{N}]_2^-$ (668.15 amu) and $\text{Al}[\text{Tf}_2\text{N}]_4^-$ (1147.5 amu) in the corresponding spectra.

All these data led us to infer that the dissolution of a metal salt in an IL having the same anion gives a sort of liquid organic–inorganic mixed salt with structural features not dissimilar to the bulk ionic liquid. This is not an absolute novelty; actually, inorganic (alkali) mixed salts with lower melting points and wider electrochemical windows than the pure components have recently been described in the literature.^{8,9} Nevertheless, the melting points of these inorganic salts are still well above the usual room temperature (about 340 K for LiFSI/KFSI). By solving the inorganic salt in an organic ionic liquid which is already liquid at room temperature, we are still able to obtain a room-temperature liquid phase with a high metal content (about 0.3 in molar fraction for $\text{Ni}(\text{Tf}_2\text{N})$).

If we consider the IL as a solvent, a noticeable aspect of the phenomenon is that it appears to go apparently against the so-called “common ion” effect: the fact that, in aqueous solvents, the solubility of insoluble or sparingly soluble substances will be decreased by the presence of a common ion, leading to the conclusion that a salt will be less soluble if one of its constituent ions is already present in the solution.

Actually, in our experiments, the presence of a common ion leads to a significantly higher solubility of metal cations in ILs, while on the basis of the principle mentioned above, such common-ion salts would have been expected to be scarcely (or not at all) soluble in corresponding-ion liquids, particularly if we consider that these metal salts are sparingly soluble in other ILs. This once again indicates that care must be taken when applying concepts typical of molecular liquids to explain phenomena in the field of ionic liquids.

Conclusions

In conclusion, we have demonstrated that high concentrations of metal salts in both hydrophilic and hydrophobic ionic liquids can be obtained by directly dissolving the salts in ILs which have the same anion. From these results, we may hypothesize that this rather unexpected behavior may be reproduced by many other ionic liquids regardless of their particular chemical nature. This strategy provides the opportunity to prepare new ionic systems with properties, limitations and application possibilities that are currently under investigation.

Acknowledgements

This work has been supported by EC, Project FP6(STREP), Contract No. 517002 (IOLISURF).

References

- 1 T. Welton, P. Wasserscheid, *Ionic Liquids in Synthesis*. Wiley-VCH, Weinheim, 2007.
- 2 L. C. Branco, J. N. Rosa, J. J. M. Ramos and C. A. M. Afonso, *Chem.–Eur. J.*, 2002, **8**, 3671–3677.
- 3 F. Endres, S. Z. El Abedin, A. Y. Saad, E. M. Moustafa, N. Borissenko, W. E. Price, G. G. Wallace, D. R. MacFarlane, P. J. Newman and A. Bund, *Phys. Chem. Chem. Phys.*, 2008, **10**(16), 2189–2199.
- 4 A. E. Visser, R. P. Swatloski, W. M. Reichert, S. T. Griffin and R. D. Rogers, *Ind. Eng. Chem. Res.*, 2000, **39**, 3596–3604.
- 5 F. Endres, A. P. Abbot, D. R. MacFarlane, *Electrodeposition from Ionic Liquids*. Wiley-VCH, Weinheim, 2008.
- 6 S. Zein el Abedin, E. Moustafa, R. Hempelmann, H. Natter and F. Endres, *ChemPhysChem*, 2006, **7**, 1535.
- 7 M.-J. Deng, P.-Y. Chen, T.-I. Leong, I.-W. Sun, J. Chang and W.-T. Tsai, *Electrochem. Commun.*, **10**(2), 213–216.
- 8 R. Bini, C. Chiappe, V. Llopsis Mestre, C. S. Pomelli and T. Welton, *Org. Biomol. Chem.*, 2008, **6**, 2522.
- 9 K. Kubota, T. Nohira, T. Goto and R. Hagiwara, *J. Chem. Eng. Data*, 2008, **53**, 2144–2147; K. Kubota, T. Nohira, T. Goto and R. Hagiwara, *Electrochem. Commun.*, 2008, **10**, 1886–1888.

A green-by-design biocatalytic process for atorvastatin intermediate

Steven K. Ma,^a John Gruber,^a Chris Davis,^a Lisa Newman,^a David Gray,^a Alica Wang,^a John Grate,^a Gjalt W. Huisman^{*a} and Roger A. Sheldon^{*b}

Received 18th June 2009, Accepted 10th September 2009

First published as an Advance Article on the web 23rd October 2009

DOI: 10.1039/b919115c

The development of a green-by-design, two-step, three-enzyme process for the synthesis of a key intermediate in the manufacture of atorvastatin, the active ingredient of the cholesterol lowering drug Lipitor®, is described. The first step involves the biocatalytic reduction of ethyl-4-chloroacetoacetate using a ketoreductase (KRED) in combination with glucose and a NADP-dependent glucose dehydrogenase (GDH) for cofactor regeneration. The (*S*) ethyl-4-chloro-3-hydroxybutyrate product is obtained in 96% isolated yield and >99.5% e.e. In the second step, a halohydrin dehalogenase (HDDH) is employed to catalyse the replacement of the chloro substituent with cyano by reaction with HCN at neutral pH and ambient temperature. The natural enzymes were highly selective but exhibited productivities that were insufficient for large scale application. Consequently, *in vitro* enzyme evolution using gene shuffling technologies was employed to optimise their performance according to predefined criteria and process parameters. In the case of the HDDH reaction, this afforded a 2500-fold improvement in the volumetric productivity per biocatalyst loading. This enabled the economical and environmentally attractive production of the key hydroxynitrile intermediate. The overall process has an E factor (kg waste per kg product) of 5.8 when process water is not included, and 18 if included.

Introduction

Atorvastatin calcium is the active ingredient of Lipitor®, the first drug in the world with annual sales to exceed \$10 billion. Lipitor is a cholesterol-lowering drug, a member of the statin family of so-called HMG-CoA reductase inhibitors that block the synthesis of cholesterol in the liver.¹ The structure of atorvastatin calcium is shown in Fig. 1. In common with other statins, it comprises a chiral 3,5-dihydroxy carboxylate side chain attached to a cyclic nucleus. Atorvastatin is unique in having the side chain attached to nitrogen in the nucleus.

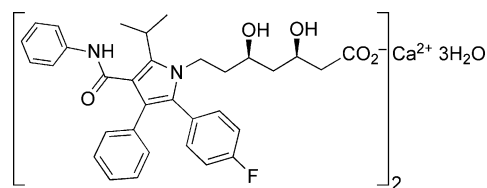


Fig. 1 Structure of atorvastatin calcium.

Atorvastatin's high volume demand coupled with the requirement for high chemical and optical purity has led to extensive efforts towards more economic production of its chirality-setting intermediates.¹ The key chiral building block

in all commercialized syntheses of atorvastatin is ethyl (*R*)-4-cyano-3-hydroxybutyrate **1**, a.k.a. "hydroxynitrile" (see Fig. 2). In the innovator's original commercial process for atorvastatin, the second stereogenic center in atorvastatin (at the 3-hydroxy group) is set by diastereomeric induction, using cryogenic borohydride reduction of a boronate derivative of the 5-hydroxy-3-keto intermediate **2** derived from **1**.²

Previous routes that have been used for the industrial production of **1** are depicted in Fig. 3. Early routes involved kinetic resolutions using microbes, and the use of (*S*)-hydroxy butyrolactone produced from chiral pool raw materials, lactose or malic acid. Later routes have involved asymmetric reduction of ethyl 4-chloroacetoacetate, produced from diketene, using an asymmetric hydrogenation catalyst, microbial cells, or an enzyme. Alternative chemoenzymatic routes have been described, using nitrilases³ or lipases⁴ but they have not, to our knowledge, been commercialized. These processes tend to require high enzyme loadings,¹ making product recovery difficult⁵ and adding significant costs to the process.

The final step to **1** in all of the previous commercial processes involves reaction of an ethyl 3-hydroxy-4-halobutyrate (a.k.a. "halohydrin") with a cyanide ion in alkaline solution at elevated temperatures to form the hydroxynitrile **1**. Alkaline conditions are necessary to form the nucleophilic cyanide anion (the pK_a of HCN is about 9). However, the substrate and product are base-sensitive compounds, resulting in extensive by-product formation. In one report, the reaction with the chlorohydrin was conducted at around 80 °C and pH 10 with a reaction yield of ~85%.⁶ The product is a high-boiling oil and the by-products include many which are close in boiling point.⁶ As a result, a troublesome high-vacuum fractional distillation is required

^aCodexis, Inc, 200 Penobscot Drive, Redwood City, CA, 94603, USA.
E-mail: gjalt.huisman@codexis.com

^bDelft University of Technology, Department of Biotechnology,
Julianalaan 136, 2628, BL, Delft, Netherlands.
E-mail: r.a.sheldon@tudelft.nl

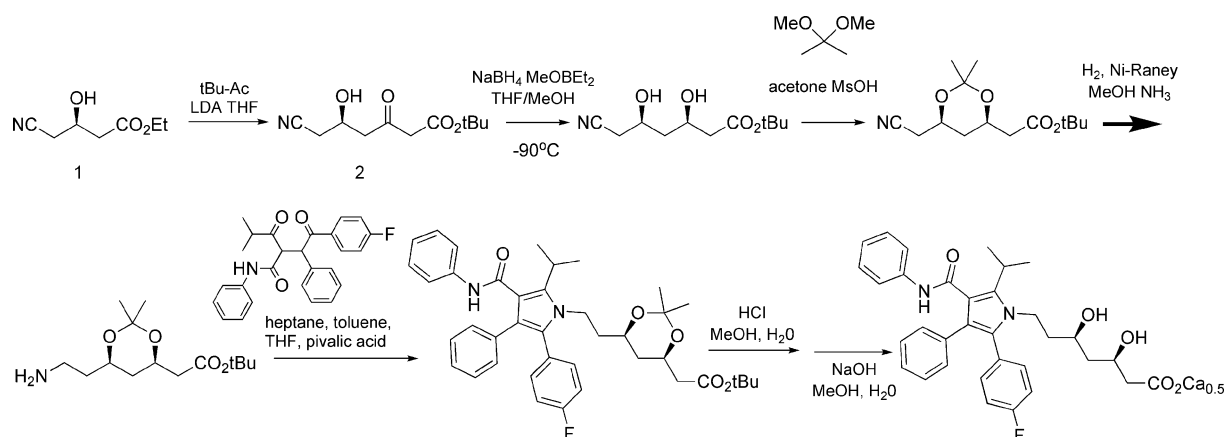


Fig. 2 Synthetic route for atorvastatin calcium.

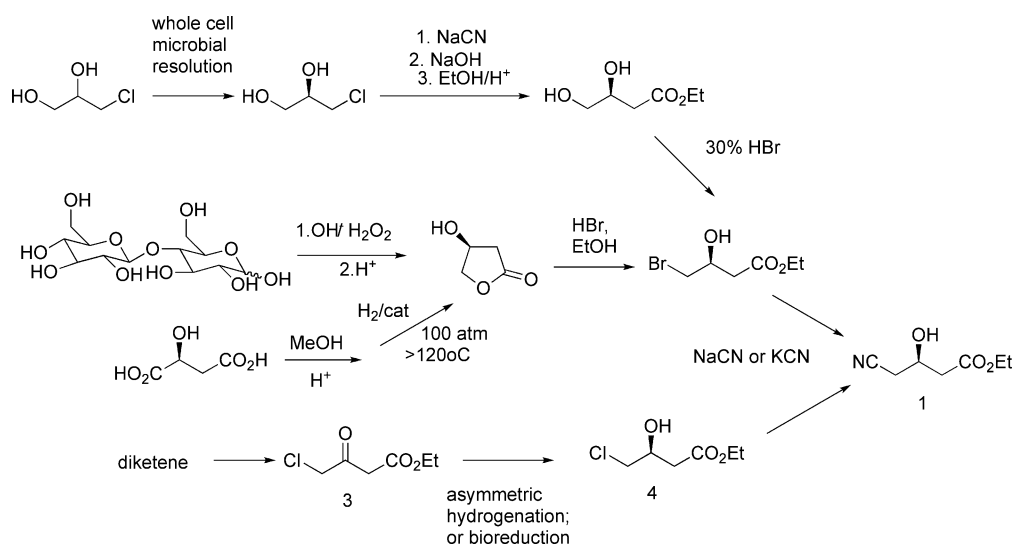


Fig. 3 Previous routes to the hydroxynitrile intermediate 1.

to recover product of acceptable quality, which results in still further yield loss and waste.⁶

Annual demand for **1** is estimated to be in excess of 100 mT, making it highly desirable to reduce the wastes and hazards involved in its manufacture, while reducing its cost and maintaining or, preferably, improving its quality.

It is difficult to imagine a practical process for **1** that does not involve using cyanide, and we are not aware of any that has been proposed. We reasoned that the key to providing a superior process for **1** would be to find and develop a catalyst capable of accomplishing the cyanation reaction under mild conditions at neutral pH, so that by-product formation would be minimized. Enzymes are known that catalyse the enantioselective ring-closing elimination of halohydrins to the corresponding epoxide in a reversible reaction.⁷ These enzymes are often referred to as halohydrin dehalogenases (HHDHs). It is also known, from the work of Nakamura and co-workers^{8,9} that these HHDHs accept cyanide as a non-natural nucleophile leading to the irreversible enantioselective formation of β -hydroxynitriles, under neutral, ambient conditions. More recently, this finding was further elaborated and extended to other non-natural nucleophiles by Janssen and co-workers.^{10–12} The availability of this enzyme

led us to propose the two-step, three-enzyme process for the production of **1** shown in Fig. 4. The key step is the HHDH catalysed reaction of the halohydrin **4** with HCN at neutral pH to produce **1**.

In addition to being highly efficient catalysts that typically exhibit exquisite chemo-, regio-, and stereoselectivities, enzymes have many benefits from the viewpoint of developing green, sustainable processes.¹³ They operate under mild conditions (ambient temperature and pressure as well as neutral pH), with water as the preferred reaction medium. They are produced from renewable raw materials and are nontoxic and biodegradable. Enzymes often provide the opportunity to reduce the number of chemical steps in a synthetic process as there is no need for functional group protection and deprotection. Finally, enzymatic reactions are typically performed in standard multi-purpose manufacturing plants. Notwithstanding all these advantages, the use of enzymes as catalysts in the large-scale production of fine chemicals and pharmaceuticals had been hampered by perceived intrinsic limitations of natural enzymes.^{14,15} Such limitations include insufficient activity towards non-natural substrates, insufficient activity at high substrate loadings due to substrate and/or product inhibition, and low operational stability under

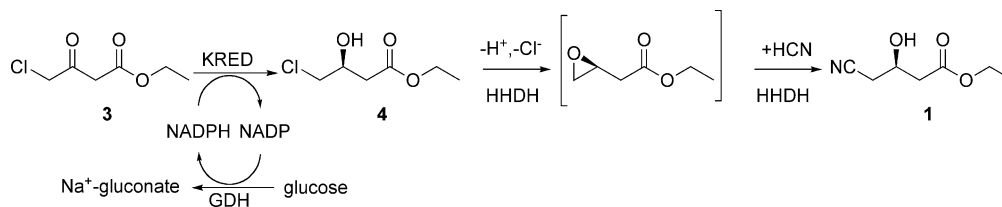


Fig. 4 Two-step, three-enzyme process for hydroxynitrile **1**.

such economically viable conditions. While process engineering solutions might alleviate some of these problems,¹⁶ the optimal solution is to employ *in vitro* directed evolution technologies to generate enzymes that operate effectively with the desired substrate and under the desired, more practical process conditions;¹⁷ instead of following the traditional path of compromising the process to fit the available catalyst, the catalyst is evolved to fit the desired process. This enables the development of a process that is 'green by design'.

Herein, we describe a novel, economically viable and environmentally attractive process for the large-scale synthesis of **1** that includes the laboratory evolution of three enzymes to meet pre-defined process parameters. Details of the enzyme evolution aspects of the HHDH enzyme have been reported elsewhere.¹⁸

Results and discussion

In the process,¹⁹ a ketoreductase (KRED) and glucose dehydrogenase (GDH) are used for the enantioselective reduction of ethyl 4-chloroacetate (**3**), using glucose as reductant, to ethyl (*S*)-4-chloro-3-hydroxybutyrate (**4**). Glucose is oxidized to gluconic acid, which is neutralized by sodium hydroxide *via* a pH-stat. Subsequent to its recovery, **4** is converted to **1** by reaction with HCN ($pK_a \sim 9$) at neutral pH, catalyzed by a halohydrin dehalogenase (HHDH). This reaction releases the H^+ and Cl^- , and must also be pH-statted, which is achieved using aqueous NaCN as the base and source of CN^- .

The activities of natural KRED and GDH for the reduction of **2** to **3** were low (Table 1). With 100 g L^{-1} of **3**, a total of 9 g L^{-1} natural, recombinantly produced KRED (6 g L^{-1}) and GDH (3 g L^{-1}) were required to complete the reaction in 15 h. However, due to emulsion formation, recovery of **4** was problematic. Although the analytical yield of **4** was $>99\%$, the recovered yield, after an hour to allow for some emulsion separation, was

Table 1 Evolution of a KRED/GDH biocatalyst for reduction of **3** to **4**

Parameter	Process design	Initial process	Final process
Substrate loading/ g L^{-1}	160	80	160
Reaction time/h	<10	24	8
Biocatalyst loading/ g L^{-1}	<1	9	0.9
Isolated yield/%	>90	85	95
Chemical purity/%	>98 (GC)	>98	>98
E.e. of 4 /%	>99.5	>99.5	>99.9
Phase separation of organic product phase from aqueous phase containing enzyme/min	<10	>60	<1
Space-time yield/ $\text{g}_{\text{product}} \text{ L}^{-1} \text{ d}^{-1}$	>384	80	480
Catalyst yield ($\text{g}_{\text{product}}/\text{g}_{\text{cat}}$)	>160	9	178

only 85%. To enable a practical large-scale process, the enzyme loadings needed to be drastically reduced.

DNA shuffling technology²⁰ was used to improve the activity and stability of KRED and GDH while maintaining the nearly perfect enantioselectivity exhibited by the natural KRED. DNA shuffling involves the mutation of a gene encoding the enzyme of interest to generate "libraries" of mutants. These libraries are screened in high throughput, under conditions that approximate the desired manufacturing process, and improved mutants are selected for further evolution. Their genes are recombined *in vitro* to create the next generation of libraries to be screened for further improved progeny. The gene libraries are transformed and expressed in a host organism, such as *Escherichia coli*, and screened in high throughput for enzyme variants that exhibit the desired improved properties. DNA shuffling is becoming a proven method to efficiently improve properties of enzymes, such as specific activity, stereoselectivity, optimum pH, organic solvent tolerance, and stability.²¹

Through several generations of such DNA shuffling, GDH activity was improved by a factor of 13 and KRED activity by a factor of 7. The enantioselectivity of the improved KRED remained $>99.5\%$. With the improved enzymes, the reaction was complete in 8 h with an increased loading of **3** to 160 g L^{-1} , reduced KRED loading to 0.57 g L^{-1} , and lowered GDH loading to 0.38 g L^{-1} (Table 1). With a $9.5\times$ lowering of the enzyme loading there were no emulsion problems. Phase separation required less than one minute and provided **4** in $>95\%$ recovered yield of $>99.9\%$ e.e.

The activity improvement for the ketone reduction biocatalysts over the course of evolution compared with the wild type enzyme is shown in Fig. 5.

Similarly, the activity of natural HHDH for cyanation of **4** to **1** (Fig. 6) was extremely low and the enzyme showed poor stability in the presence of the substrate and product. With 20 g L^{-1} of **4** and 30 g L^{-1} of recombinantly-produced natural HHDH, the rate of reaction had virtually approached 0 by 72 h. Product recovery was difficult due to work-up challenges in the filtration and phase separation steps caused by the large amount of enzyme. In addition to the extremely low activity and poor stability of the natural HHDH for the cyanation of **4**, the enzyme was also strongly inhibited by the product. Since **1** is more water-soluble than the substrate **4**, attempts to overcome the inhibition by extraction of product into an organic solvent such as EtOAc, *n*-BuOAc, or MTBE were unsuccessful. However, after many iterative rounds of DNA shuffling, with screening in the presence of iteratively higher concentrations of product, the inhibition was largely overcome and the HHDH activity was increased >2500 -fold compared to the wild-type enzyme.

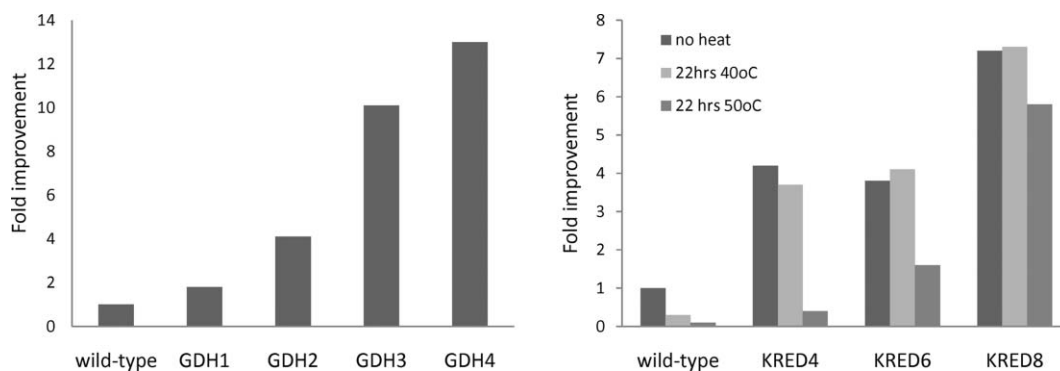


Fig. 5 Improvements in the biocatalysts' performances for the reduction of **3**. The numbers identifying the enzymes represent the number of generations of evolution. The KREDs were exposed to thermal challenges before their assay as indicated in the figure.

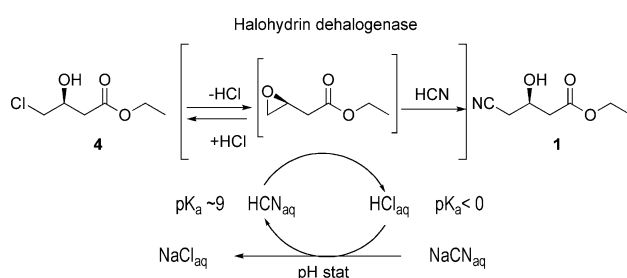


Fig. 6 HHDH-catalyzed cyanation of **4**.

Fig. 7 shows the progress of cyanation reactions, using HHDH catalysts spanning multiple generations of directed evolution. With the improved HHDH, the reaction of 140 g L^{-1} **4** using 1.2 g L^{-1} enzyme was complete in 5 h (Table 2). The product was isolated in 92% yield.

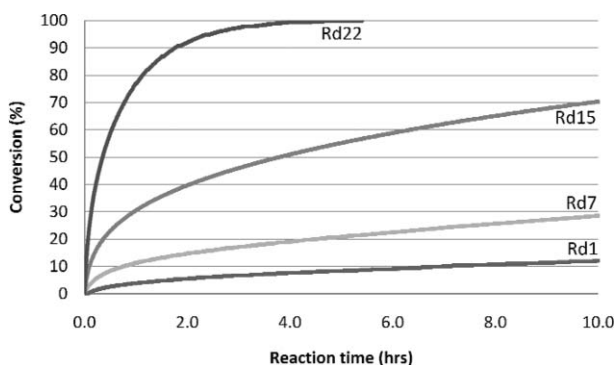


Fig. 7 Progress of cyanation reactions using HHDH catalysts. Substrate : biocatalyst = 100 : 1 (w/w). Rd 1 = expression mutant of wild type enzyme. Rd 22 gave 130 g L^{-1} product.

The dramatic improvement in the activities of three different enzymes demonstrates that DNA shuffling technologies can enable large-scale enzymatic processes that otherwise would not have been economically viable. Our completely enzymatic process has been scaled-up to 2000 L reactors. In addition to this two-step process, running the reactions as a one-pot process, sequentially or concertedly, was demonstrated on a laboratory scale.¹⁹

The green features of the new process

As noted above, previous commercial processes involved kinetic resolution (50% maximum yield), syntheses from chiral pool precursors involving bromine chemistry or asymmetric hydrogenation of **3**. All of these processes ultimately involve substitution of halide by cyanide under warm, alkaline conditions (*e.g.* $80 \text{ }^\circ\text{C}$, pH 10), causing extensive by-product formation and the concomitant need for high-vacuum fractional distillation. The process described here is greener than previous processes when assessed according to the twelve principles of green chemistry.²²

Principle 1: waste prevention. The highly selective biocatalytic reactions afforded a substantial reduction in waste. In the final process, raw material is converted to product with $>90\%$ isolated yield affording product that is more than 98% chemically pure with an enantiomeric excess of $>99.9\%$. Furthermore, the avoidance of alkaline-induced by-products obviates the need for further yield-sacrificing fractional distillation. The highly active evolved biocatalysts are used at such low loadings that countercurrent extraction can be used to minimize solvent volumes. Moreover, the butyl acetate solvent is recycled with an efficiency of 85%. The E factor (kg waste per kg product)²³ for the overall process is 5.8 if process water is excluded (2.3 for the reduction and 3.5 for the cyanation). If process water is included, the E factor for the whole process is 18 (6.6 for the reduction and 11.4 for the cyanation). The main contributors to the E Factor, as shown in Table 3, are solvent (EtOAc and BuOAc) losses which constitute 51% of the waste, sodium gluconate (25%), NaCl and Na_2SO_4 (combined *ca.* 22%). The three enzymes and the NADP cofactor accounted for $<1\%$ of the waste. The main waste streams are aqueous and directly biodegradable.

Principle 2: atom economy. The atom economy²⁴ is only 45%. The use of glucose as the reductant for cofactor regeneration is cost effective but not particularly atom efficient. However, glucose is a renewable resource and the gluconate co-product is fully biodegradable.

Principle 3: less hazardous chemical syntheses. The reduction reaction uses starting materials that pose no toxicity to human health or the environment. It avoids the use of potentially hazardous hydrogen and heavy metal catalysts throughout the process thus obviating concern for their removal from waste streams and/or contamination of the product. While cyanide must be used in the second step, as in all practical routes to HN,

Table 2 Evolution of the enzymatic cyanation catalyst

Parameter	Process design	Initial process	Final process
Substrate loading/g L ⁻¹	≥120	20	140
Reaction time/h	8	72	5
Biocatalyst loading/g L ⁻¹	1.5	30	1.2
Isolated yield/%	>90	67	92
Chemical purity/%	>98	>98	>98
E.e. of 1 /%	>99.5	>99.5	>99.5
Phase separation of organic product phase from aqueous phase containing enzyme/min	<10	>60	<1
Space-time yield/g _{product} L ⁻¹ d ⁻¹	>360	7	672
Catalyst yield (g _{product} /g _{cat})	80	0.7	117

Table 3 Composition of the waste per kg of **1** product in the new process

Waste	Quantity (kg per kg HN)	% Contribution to E (excluding water)	% Contribution to E (including water)
ECAA losses (8%)	0.09	<2	<1
Triethanolamine	0.04	<1	<1
NaCl and Na ₂ SO ₄	1.29	22	ca. 7
Na-gluconate	1.43	ca. 25	ca. 9
BuOAc (85% recycle)	0.46	ca. 8	ca. 3
EtOAc (85% recycle)	2.50	ca. 43	ca. 14
Enzymes	0.023	<1	<1
NADP	0.005	0.1	<0.1
Water	12.250	—	67
E factor	5.8 (18)		

it is used more efficiently (higher yield) and under less harsh conditions compared to previous processes.

Principle 4: design safer chemicals. This principle is not applicable as the hydroxynitrile product is the commercial starting material for atorvastatin.

Principle 5: safer solvents and auxiliaries. Safe and environmentally acceptable butyl acetate is used, together with water, as the solvent in the biocatalytic reduction reaction and extraction of the hydroxynitrile product; no auxiliaries are used. Solvent use is minimized by employing countercurrent extraction.

Principles 6 and 9: design for energy efficiency, and catalysis. In contrast with previous processes, which employ elevated temperatures for the cyanation step and high pressure hydrogenation for the reduction step, both steps in our process are very efficient biocatalytic transformations. The reactions are run at or close to ambient temperature and pressure and pH 7 and the very high energy demands of high vacuum distillation are dispensed with altogether, resulting in substantial energy savings. The turnover numbers for the different enzymes are >10⁵ for KRED and GDH and >5 × 10⁴ for HHDH. Because of the low enzyme concentration used, immobilization of the biocatalyst to make it recyclable is neither practical, nor economic.

Principles 7 and 10: use of renewable feedstocks, and design for degradation. The enzyme catalysts and the glucose co-substrate are derived from renewable raw materials and are completely biodegradable. The by-products of the reaction are gluconate, NADP (the cofactor that shuttles reducing equivalents from GDH to KRED) and residual glucose, enzyme, and minerals and the waste water is directly suitable for biotreatment.

Principle 8: reduce derivatization. The process avoids derivatization steps, *i.e.* it is step-economic²⁵ and involves fewer unit operations than earlier processes, most notably by obviating the trouble-prone product distillation or the bisulfite-mediated separation of dehydrated by-products.²⁶

Principles 11 and 12: real-time analysis for pollution prevention, and inherently safer chemistry. The reactions are run in pH-stat mode at neutral pH by computer-controlled addition of base. Gluconic acid generated in the first reaction is neutralized with aq. NaOH and HCl generated in the second step is neutralized with aq. NaCN, regenerating HCN (pK_a~9) *in situ*. The pH and the cumulative volume of added base are recorded in real time. Feeding NaCN on demand minimizes the overall concentration of HCN affording an inherently safer process.

Conclusions

We have developed and deployed a two-step, three-enzyme, and green-by-design process for the manufacture of the key hydroxynitrile intermediate for atorvastatin. We used directed evolution technologies to optimize the performance of all three enzymes to meet pre-defined process criteria. The overall volumetric productivity per mass catalyst load of the cyanation process was improved ~2500-fold, comprising a 14-fold reduction in reaction time, a 7-fold increase in substrate loading, a 25-fold reduction in enzyme use, and a 50% improvement in isolated yield. Concomitant significant process simplification resulted in an overall reduction in energy use and waste production. These results demonstrate the power of state-of-the-art enzyme optimization technologies in enabling economically viable, green-by-design biocatalytic processes that would otherwise remain mere laboratory curiosities.

Experimental

Materials

Ethyl 4-chloroacetoacetate, ethyl (*S*)-4-chloro-3-hydroxybutyrate (**3**), and ethyl 4-(*R*)-cyano-3-hydroxybutyrate (**1**) were purchased from Sigma-Aldrich. Ketoreductase (KRED; EC1.1.1.184) glucose dehydrogenase (GDH; EC1.1.1.47) and halohydrin dehalogenase (HHDH; EC3.8.1.5) were produced as semi-purified lyophilisates by fermentation using recombinant *E. coli* strains carrying the corresponding genes and subsequent work-up as described. The desired enzymes constitute 30–50% of this material by weight.

Determination of (*S*)-ECHB (**4**) and (*R*)-HN (**1**) by chiral GC

Sample preparation and derivatization. A sample of **4** or **1** was converted to its trifluoroacetyl derivative by reaction with trifluoroacetic anhydride (TFAA). One drop of **4** in a GC sample vial was treated with approximately 0.3 mL of TFAA. The vial was capped and held at room temperature for approximately 30 min. Excess TFAA was removed under a stream of nitrogen. A few drops of methanol were added and blown off. The sample was diluted with hexane (1 mL) and injected (1 μL) into the GC (Agilent 6890 GC and Agilent 19091s-433 GC/MS with a β-cyclodextrin dimethyl (B-DM) column (30 m × 0.25 mm) [Chiraldex (Astec)]). Instrumental parameters: inlet—250 °C,

flow—88 mL min⁻¹, split—60 : 1; temperature program: 80 °C (for **4**) or 100 °C (for **1**) for 30 min, 15 °C min⁻¹, final *T* = 180 °C, held for 5 min; detector: 300 °C; 30 mL min⁻¹ H₂, 400 mL min⁻¹ air; retention times for enantiomers of **4**: *S* at 24 min, *R* at 25 min; retention times for enantiomers of **1**: *R* at 22 min, *S* at 23 min.

Preparative enzymatic reduction of ECAA (**3**) to (*S*)-ECHB (**4**)

A 3 L jacketed three-neck flask equipped with a pH electrode connected to a pH stat (Schott system) was charged with 570 ml of 100 mM triethanolamine. The pH was adjusted to 7 using 96% H₂SO₄ (~5 ml) and D-glucose (298 g; 1.64 M) was added. The temperature was raised to 25 °C. KRED (854 mg) and GDH (578 mg) were charged as lyophilized powders. Then, Na-NADP (98 mg) was added followed by butyl acetate (370 ml). The reaction was started by the addition of **3** (240 g; 1.46 moles) from an addition funnel while maintaining the pH at 6.9 ± 0.05 using the pH stat with 4 N NaOH feeding. The reaction was completed in ~8 h at 25 °C at which point 357 ml 4 N NaOH was consumed. A sample was analyzed by GC to check for completion. The reaction mixture was heated to 50 °C for 30 min and 5 g of Celite was added to facilitate filtration. The reaction mixture was cooled to 25 °C and filtered through a Celite pad. The two layers were separated and the aqueous solution was extracted with 350 mL butyl acetate. The two organic extracts were combined and the solvents were removed to obtain 232.61 g (96%) of **4**, as a light yellow-colored liquid. The enantiomeric excess of **4** was >99.5% (the *R*-enantiomer was not detected).

Preparative enzymatic cyanation of (*S*)-ECHB (**4**) to HN (**1**)

A 1 L jacketed three-neck round bottom flask equipped with a rubber septum, a pH electrode connected to a pH stat, and a mechanical stirrer was charged with 400 ml 500 mM NaCN. The whole system was airtight since gaseous HCN is generated. The pH of the solution was ~11.2. The pH electrode was calibrated at room temperature 20–23 °C before use. The vessel was sealed and the pH was adjusted to ~7.5 using conc. H₂SO₄ (~7 mL). HHDH was charged as an aqueous solution (1.05 g in 20 mL de-ionized water) and the reaction mixture was heated to 40 °C. Then, the pH stat control was started and 70 g (0.42 moles) of **4** was added with a syringe over ~10 min. The pH stat maintained the pH at 7.3 ± 0.05 with the addition of a 25% NaCN solution containing 0.25% NaOH. After ~18 h, 73 mL of NaCN/NaOH solution was consumed. At that point, the progress of the reaction was checked by GC and no ECHB was detected. The pH of the reaction mixture was adjusted to ~3 with conc. H₂SO₄ (~2.5 mL). For safety reasons, the reaction was cooled to 25 °C. The pH electrode and the rubber septum were removed [caution: HCN gas present]. The flask was equipped with a condenser and nitrogen dip tube extending into the liquid. Vacuum (~100 mm Hg) was applied from a diaphragm pump (a caustic trap containing ~4 M NaOH was used to collect the HCN in the off gas). The reaction mixture was heated to 40 °C. A nitrogen bleed was used to facilitate the removal of HCN. After 2.5 h, HCN removal was complete (<5 ppm in the off gas). The mixture was cooled and treated with 3.5 g of Celite and 3.5 mL bleach (containing 6.1% sodium hypochlorite). This mixture was filtered through a Celite pad. The filtrate was extracted four times with 280 mL of ethyl acetate. The combined ethyl

acetate phases were concentrated *in vacuo* to give 61.6 g (93%) of **1**. The chemical purity as determined by GC was 99.5% and the chiral purity was >99.5% e.e. for the *R*-enantiomer (no *S*-enantiomer was detected).

References

- M. Müller, *Angew. Chem., Int. Ed.*, 2005, **44**, 362.
- D. E. Butler, T. V. Le, A. Millar and T. N. Nanninga, *US5155251* (1992).
- G. DeSantis, Z. Zhu, W. A. Greenberg, K. Wong, J. Chaplin, S. R. Hanson, B. Farwell, L. W. Nicholson, C. L. Rand, D. P. Weiner, D. E. Robertson and M. J. Burk, *J. Am. Chem. Soc.*, 2002, **124**, 9024; G. DeSantis, K. Wong, B. Farwell, K. Chatman, Z. Zhu, G. Tomlinson, H. Huang, X. Tan, L. Bibbs, P. Chen, K. Kretz and M. J. Burk, *J. Am. Chem. Soc.*, 2003, **125**, 11476.
- F. H. Hoff and T. Anthonsen, *Tetrahedron: Asymmetry*, 1999, **10**, 1401.
- D. R. Yazbek, C. A. Martinez, S. Hu and J. Tao, *Tetrahedron: Asymmetry*, 2004, **15**, 2757.
- H. Matsuda, T. Shibata, H. Hashimoto and M. Kitai, *U.S. Patent*, 5,908,953, 1999 to Mitsubishi Chemical Corporation.
- M. M. Elenkov, B. Hauer and D. B. Janssen, *Adv. Synth. Catal.*, 2006, **348**, 579.
- T. Nakamura, T. Nagasawa, F. Yu, I. Watanabe and H. Yamada, *Biochem. Biophys. Res. Commun.*, 1991, **180**, 124.
- T. Nakamura, T. Nagasawa, F. Yu, I. Watanabe and H. Yamada, *Tetrahedron*, 1994, **50**, 11821.
- J. H. Lutje Spelberg, L. Tang, M. van Gelder, R. M. Kellogg and D. B. Janssen, *Tetrahedron: Asymmetry*, 2002, **13**, 1083.
- J. H. Lutje Spelberg, J. E. T. van Hylckama Vlieg, L. Tang, D. B. Janssen and R. M. Kellogg, *Org. Lett.*, 2000, **3**, 41.
- G. Hasnaoui, J. H. Lutje Spelberg, E. de Vries, L. Tang, B. Hauer and D. B. Janssen, *Tetrahedron: Asymmetry*, 2005, **16**, 1685.
- R. A. Sheldon, *Chirotechnology; Industrial Synthesis of Optically Active Compounds*, Marcel Dekker, New York, 1993; C. H. Wong and G. M. Whitesides, *Enzymes in Synthetic Organic Chemistry*, Elsevier, Amsterdam, 1994.
- U. T. Strauss, U. Felfer and K. Faber, *Tetrahedron: Asymmetry*, 1999, **10**, 107.
- A. Bommarius and B. Bommarius-Riebel, *Fundamentals of Biocatalysis*, Wiley-VCH, Weinheim, 2005.
- A. Liese, K. Seelbach, and C. Wandrey, *Industrial Biotransformations*, Wiley-VCH, Weinheim, 2000; G. J. Lye, P. A. Dalby and J. M. Woodley, *Org. Process Res. Dev.*, 2002, **6**, 434.
- K. A. Powell, S. W. Ramer, S. B. del Cardayre, W. P. C. Stemmer, M. B. Tobin, P. F. Longchamp and G. W. Huisman, *Angew. Chem., Int. Ed.*, 2001, **40**, 3948; M. T. Reetz and K.-E. Jaeger, *Chem.-Eur. J.*, 2000, **6**, 407; S. B. Rubin-Pitel and H. Zhao, *Combinatorial Chemistry & High Throughput Screening*, 2006, **9**, 247.
- R. J. Fox, S. C. Davis, E. C. Mundorff, L. M. Newman, V. Gavrilovic, S. K. Ma, L. M. Chung, C. Ching, S. Tam, S. Muley, J. Grate, J. Gruber, J. C. Whitman, R. A. Sheldon and G. W. Huisman, *Nat. Biotechnol.*, 2007, **25**, 338.
- US 7125693* and *US 7132267* to Codexis.
- W. P. Stemmer, *Proc. Natl. Acad. Sci. U. S. A.*, 1994, **91**, 10747–51; W. P. Stemmer, *Nature*, 1994, **370**, 389–91; J. E. Ness, M. Welch, L. Giver, M. Bueno, J. R. Cherry, T. V. Borchert, W. P. Stemmer and J. Minshull, *Nat. Biotechnol.*, 1999, **17**, 893–6.
- J. F. Chaparro-Riggers, K. M. Polizzi and A. S. Bommarius, *Biotechnol. J.*, 2007, **2**, 180; R. J. Fox and G. H. Huisman, *Trends Biotechnol.*, 2008, **26**, 132.
- P. Anastas and J. Warner, Eds., *Green Chemistry: Theory and Practice*, Oxford University Press, New York, 1998.
- R. A. Sheldon, *Chem. Ind. (London, UK)*, 1992, 903; R. A. Sheldon, *Chem. Commun.*, 2008, 3352; R. A. Sheldon, *Green Chem.*, 2007, **9**, 1273.
- B. M. Trost, *Science*, 1991, **254**, 1471; B. M. Trost, *Angew. Chem., Int. Ed. Engl.*, 1995, **34**, 259.
- P. A. Wender, M. P. Croatt and B. Witulski, *Tetrahedron*, 2006, **62**, 7505; P. A. Wender, V. A. Verma, T. J. Paxton and T. H. Pillow, *Acc. Chem. Res.*, 2008, **41**, 40.
- US 6,140,527* to Kaneka.

Hydrogenation of nitrile in supercritical carbon dioxide: a tunable approach to amine selectivity

Maya Chatterjee,* Hajime Kawanami,* Masahiro Sato, Takayuki Ishizaka, Toshirou Yokoyama and Toshishige Suzuki

Received 10th July 2009, Accepted 15th September 2009

First published as an Advance Article on the web 23rd October 2009

DOI: 10.1039/b913828e

The use of supercritical carbon dioxide (scCO₂) on the hydrogenation of benzonitrile was investigated over Pd and other metal catalysts. Without any additive, benzonitrile was hydrogenated to benzylamine with high conversion (90.2%) and selectivity (90.9%) using the Pd/MCM-41 catalyst. A strong influence of CO₂ pressure on the conversion and selectivity were observed. As the CO₂ pressure increases, the conversion was increased, and after reaching the maximum at around 8–10 MPa, it decreased. Moreover, simply by tuning the CO₂ pressure, it is possible to obtain benzylamine or dibenzylamine. For instance, at lower pressure CO₂ acts as a protecting agent, leading to the formation of the primary amine, but at higher pressure, the yield of primary amine as well as the solubility of the imine intermediate in CO₂ increases, which results high selectivity for dibenzylamine. A plausible mechanism has been proposed to show the role of CO₂ on the selectivity toward primary and secondary amines. The results confirm that the presence of CO₂ is mandatory for the formation of benzylamine with high selectivity. Furthermore, the other reaction parameters, such as reaction time, H₂ pressure, temperature *etc.*, also affect the conversion as well as selectivity of benzylamine. This process has been extended to the hydrogenation of a series of different nitrile compounds.

Introduction

Supercritical carbon dioxide (scCO₂) is a promising “green” reaction medium for rapid and selective organic synthesis. Over the past few years, a number of heterogeneously-catalyzed reactions have been successfully carried out in scCO₂ medium, often with higher reaction rates and different product distributions, as well as high selectivity, compared to those in conventional organic solvents.¹ The origin of the observed selectivity is of importance in view of the current developments on the understanding of the solvent attributes² and the interesting supramolecular interactions³ reported for CO₂. It has great potential to overcome disadvantages associated with conventional homogeneous and heterogeneous catalysts, such as mass transfer limitation, which frequently occur between reactants in the gas phase and liquid phase. The reactions in CO₂ are tuned mainly by the pressure and temperature. Chemical interaction of CO₂ with substrate or catalyst offers an attractive potential for selectivity control.⁴ For example, amines could react with CO₂ to form carbamic acid or ammonium carbamate. It is thus reasonable to consider the possibility of protecting the amine group, which can improve the selectivity of a reaction, and also prevent catalyst deactivation.

The hydrogenation of nitrile to amine is an industrially important process and generally carried out in the liquid

phase with elevated hydrogen pressure.⁵ Amines are used as intermediates for the pharmaceutical, agrochemical and plastics industries. For example, benzylamine is utilized in several drugs like vitamin H (biotin), in the production of amide, isocyanate, intermediates for photographic material.⁶ On the other hand, dibenzylamine is used as a corrosion inhibitor, production of gasoline additives, pharmaceuticals, and rubber and tire compounding in the manufacture of SBR rubbers.^{7–9}

The hydrogenation of benzonitrile has been studied over homogeneous¹⁰ and heterogeneous¹¹ catalysts. For homogeneous catalysts, the selectivity for the primary amine was high, but involved the difficulty of catalyst/product separation. Compared to the homogeneous catalysts, heterogeneous catalysts exhibit poor selectivity towards the primary amine. Thus, application of NH₃ to increase the selectivity for the primary amine is the most used technique¹² for heterogeneously-catalyzed reactions. However, NH₃ has several disadvantages such as pressurized storage and the amount required is large, which results environmental and economical concern. Furthermore, different acids such as HCl, CH₃COOH, and acid anhydride were used over Pd/C or RANEY® Ni catalysts¹³ to achieve high selectivity for the primary amine. Besides that, high temperature and harsh reaction conditions, and the use of different types of metal like Ni, Co, Fe, Pt, Pd, Ru and Rh are also part of the selectivity enhancement for the primary amine.¹⁴ Volf and Pasek¹⁵ reviewed the hydrogenation of nitrile in the liquid phase and indicated that Ni and Co are the best choices for producing primary amine, but require some additive. Recently, Hegedús *et al.*¹⁵ also accomplished high selectivity of benzylamine (95%) with the use of NaH₂PO₄ as an acidic additive over 10% Pd/C catalyst in

Research Center for Compact Chemical Process, AIST, 4-2-1 Nigatake, Miyagino-ku, Sendai, 983-8551, Japan.

E-mail: c-maya@aist.go.jp, h-kawanami@aist.go.jp;

Fax: 81-22-237-5388; Tel: 81-22-237-5213

dichloromethane–water. Clearly, the use of additives to increase selectivity creates a waste problem (if the additives cannot be recycled), makes the process more expensive, and interferes with product separation, thus reducing the efficiency of the catalyst after certain runs. Hence, it is difficult to implement such a process at an industrial scale.

Instead of the liquid phase hydrogenation, Xie *et al.* used supercritical carbon dioxide at 3 MPa + ethanol (gas expanded liquid) medium, using heterogeneous (solution of NiCl₂/NaBH₄ catalyst) and homogeneous (RhH(P-*i*-Pr₃)₃) catalysts for benzonitrile hydrogenation¹⁶ and explained the protective role of CO₂. It has to be mentioned that the use of expanded solvent enhanced the amount of organic substances used in the reaction (possibly leading to more waste production) but reduces the amount of pressure required and is sometimes preferable for industrial purposes.

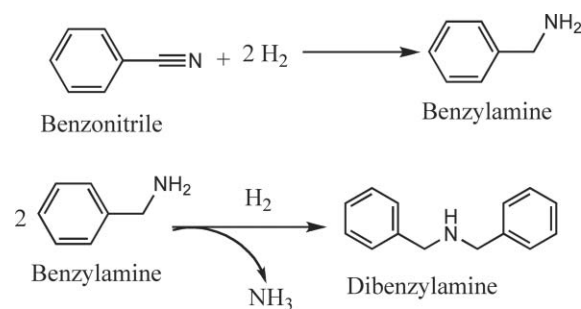
The objective of our work is to carry out the hydrogenation of benzonitrile in supercritical carbon dioxide (scCO₂) over a heterogeneous catalyst, without using any additive or any organic solvent.

Results and discussion

Scheme 1 depicts the possible reaction path of the hydrogenation of benzonitrile in scCO₂. Benzonitrile is hydrogenated to benzylamine followed by the formation of dibenzylamine with the elimination of NH₃, depending on the reaction conditions.

Catalyst screening

The nature of the active metal ion and catalyst supports are the most important parameters to describe the activity and the product distribution of a specific reaction. Thus, at first, the hydrogenation of benzonitrile was carried out over different catalysts, and the results are shown in Table 1. From the results, under the studied reaction conditions (catalysts = 0.1 g, substrate = 1.0 g; P_{CO_2} = 10 MPa, P_{H_2} = 2 MPa, T = 50 °C, reaction time = 4 h), Pd catalysts appear more efficient than any



Scheme 1 Probable reaction path of the hydrogenation of benzonitrile in scCO₂

other metal for benzonitrile hydrogenation. On the other hand, the conversions of benzonitrile on Pt, Rh and Ni catalysts are low, between 15–30% (Table 1, entries 4, 5 and 9), whereas the conversions over Pd catalysts are comparatively high, reaching 100% for Pd/C catalyst (Table 1, entry 1). However, the most impressive selectivity of primary amine (90.9%) was obtained over Pd/MCM-41 (Table 1, entry 3) and secondary amine was formed exclusively over Pd/C. Hence, we have chosen Pd/MCM-41 for further study and the results will be compared with the Pd/C catalyst in the following section. Notably, no reaction proceeded without catalyst.

Effect of CO₂ pressure on benzonitrile hydrogenation

Fig. 1a and b show the effect of CO₂ pressure on the hydrogenation of benzonitrile using Pd/MCM-41 and Pd/C catalysts, respectively, at 50 °C with constant hydrogen pressure of 2 MPa. The results show that increasing CO₂ pressure from 8 to 10 MPa, leads to an increase in the conversion of benzonitrile from 64.9 to 90.2%, but a significant decrease in conversion to 51.5% was observed when the pressure reaches 14 MPa. This scenario can be explained by visual observation of the phase behavior of CO₂ and reactants through the view cell. In the temperature and pressure range considered here, the reaction mixture exists as a gas–liquid (hydrogen and CO₂–substrate) biphasic system.

Table 1 Different catalysts used for the hydrogenation of benzonitrile in scCO₂ medium

Entry	Catalyst	Conversion/%	Selectivity/%		TOF/h ^{-1a}
			Benzylamine	Dibenzylamine	
1	1% Pd/C	100	0.0	100.0	2983
2	5% Pd/Al ₂ O ₃	46.0	50.0	50.0	340.4
3	Pd/MCM-41	90.2	90.9	9.1	4151
4	5% Pt/C	8.5	0.0	100.0	178.8
5	Pt/MCM-41	20.6	19.8	80.2	552.5
6	5% Rh/C	28.8	25.0	75.0	180.6
7	5% Rh/Al ₂ O ₃	21.0	22.4	77.6	291.3
8	Rh/MCM-41	5.1	25.0	75.0	42.4
9	Ni/MCM-41	15.7	37.5	62.5	5.1
Recycle 1	Pd/MCM-41	90.4	91.0	9.0	—
Recycle 2		89.9	90.9	9.1	—
Recycle 3		89.8	90.8	9.2	—
Recycle 4		90.0	90.8	9.2	—
Recycle 5		88.5	90.5	9.5	—
Recycle 1	Pd/C	96.4	0.0	100.0	—
Recycle 2		82.1	0.0	100.0	—

Reaction conditions: catalyst = 0.1 g, substrate = 1.0 g; P_{CO_2} = 10 MPa, P_{H_2} = 2 MPa, T = 50 °C, reaction time = 4 h.^a Turnover frequency (TOF) = number of moles reacted/moles of metal × time.

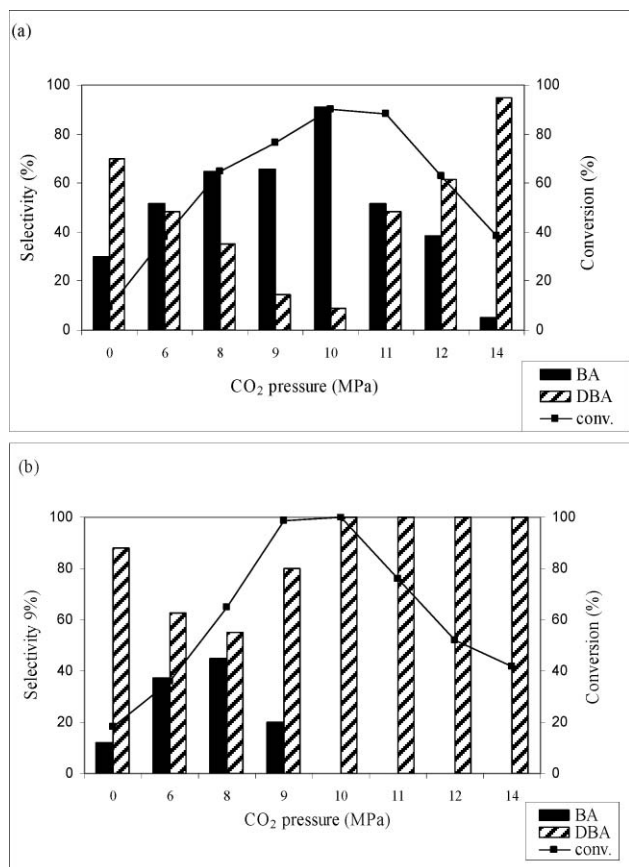
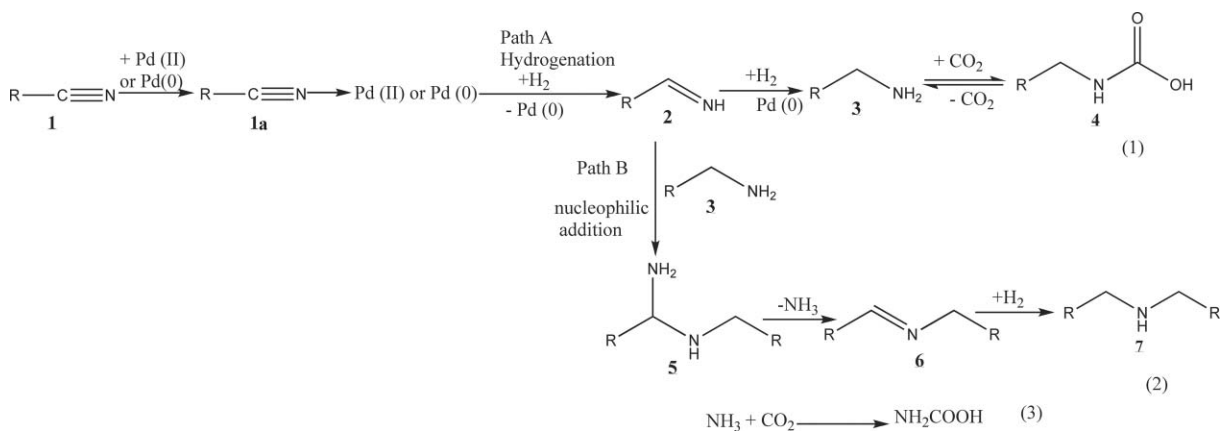


Fig. 1 Effect of CO₂ pressure on the conversion and selectivity of benzonitrile hydrogenation over (a) Pd/MCM-41 and (b) Pd/C. Reaction conditions: catalyst = 0.1 g, substrate = 1.0 g, *T* = 50 °C, *P*_{H₂} = 2 MPa, time = 4 h.

low pressure region, the reactants mainly exist in the liquid phase and mass transfer limitation of H₂ causes low conversion. With increasing CO₂ pressure, the density and solubility of the reactants increase and, accordingly, conversion of benzonitrile increases. However, further increase of the pressure at a constant volume forces more molecules of CO₂ between the reactant molecules, thus mimicking the enhanced dilution effects of the conventional solvent, and conversion decreases. The selectivity

for primary amine was also strongly influenced by the CO₂ pressure. With increasing CO₂ pressure, the selectivity was enhanced from 64 to 90.9% (10 MPa), decreasing to 20%, when the pressure reaches 14 MPa. Thus, in the higher pressure region, the product distribution changes and dibenzylamine becomes the primary product, with ~95% selectivity. The change in selectivity from benzylamine to dibenzylamine with CO₂ pressure can be accounted for as follows. It was proposed that the hydrogenation of nitriles (**1**) occurs in steps:^{15,17} in the first step, the primary amine (**3**) is obtained from the imine intermediate (**2**) followed by the formation of secondary amine (**7**) through the nucleophilic attack of the primary amine (**3**) on the imine (**2**). Here, we propose a reaction scheme to explain the product selectivity depending on the reaction condition, mainly the CO₂ pressure (Scheme 2). To describe the reaction mechanism, the following points need to be considered: (i) results obtained over the Pd/MCM-41 catalyst are the basis for describing the mechanism because of the exclusive formation of **3**, which is the main interest of this work, (ii) the experimental evidence (see Catalyst screening section) showed that the presence of catalyst was essential for the reaction to occur, and (iii) significant information on product selectivity can be obtained from phase behavior studies of **1** and products. It has to be mentioned that after calcination in air, Pd mainly exists as Pd(II) in the Pd/MCM-41 catalyst. From the mechanism perspective, the reaction may start with an oxidative addition between **1** and the catalyst,¹⁸ which results in the formation of chemisorbed species **1a**. The presence of H₂ would afford the generation of catalytically active Pd(0). Now, the phase behavior of **1** revealed that in the lower pressure region, the reaction mixture exists as a gas (CO₂ and H₂)–liquid (substrate) biphasic system. Thus, more **1** was available in the liquid phase rather than in the gas phase. As a result, mass transfer limitations take place and decrease the conversion of **1**. Therefore, the formation of **3** was very low, which can readily react with the imine **2** and **7** was formed. On the other hand, when CO₂ pressure increased, the solubility of **1** in CO₂ was enhanced and the reaction mixture changes from a biphasic to a single phase, where maximum selectivity of **3** was observed. This scenario can be explained by path A of Scheme 2. The phase behavior study of **3** (as described in the Experimental section) suggested the formation of carbamate **4** was preferred when *P*_{CO₂} < 12 (Fig. 4a), which could improve the selectivity



Scheme 2 Proposed reaction mechanism of benzonitrile hydrogenation depending on the reaction conditions.

of **3** by preventing the formation of **7** because **4** cannot act as a nucleophile to interact with **2**. Alternatively, at higher pressure ($P_{\text{CO}_2} \geq 12$ MPa; Fig. 4b), **3** exhibited solubility in CO_2 and favored the nucleophilic addition between **2** and **3** (because the imine also has high solubility in CO_2), followed by the formation of **7** through path B. This observation agrees with the results of Goemz *et al.*, which suggested that the condensation reaction proceeds homogeneously.¹¹ Hence, simply by tuning the CO_2 pressure, it is possible to tune the selectivity from **3** to **7**.

Fig. 1a also depicts the conversion and the selectivity of amines in solvent-free conditions. The conversion of benzylamine was low (~10%) with dibenzylamine as the main product, which is attributed to the presence of CO_2 being necessary for primary amine formation.

Similarly, Fig. 1b reveals that the Pd/C catalyst was selective to the dibenzylamine. The highest selectivity (44.7%) for primary amine was achieved at 8 MPa but decreases to 0.0% as the pressure increases to 14 MPa. Following these results, the reaction was conducted without CO_2 (Fig. 1b) and a striking decrease in the conversion (18%) was evident, probably due to mass transfer limitations.

This difference in activity between the Pd/MCM-41 and Pd/C catalysts under the same reaction conditions may originate from the support effect. It is well-known that a C support is much more acidic compared to MCM-41.¹⁹ The effect of support acidity on the hydrogenation of nitrile is a controversial issue. Some authors have claimed that acidity favors the formation of secondary amine, while others report no effect on selectivity. The results presented here suggest that the effect of CO_2 pressure is more prominent for secondary amine formation when an acidic support was used. Therefore, the role of acid sites to initiate the condensation between primary amine and the imine cannot be ignored.²⁰

Effect of H_2 pressure on benzonitrile hydrogenation

Fig. 2a and b present the effect of change in hydrogen pressure from 1–4 MPa, on the hydrogenation of benzonitrile using Pd/MCM-41 and Pd/C catalysts, respectively. The temperature and CO_2 pressure were kept constant at 50 °C and 10 MPa, respectively, in accordance with the highest observed activity and selectivity. As expected, the conversion of benzonitrile was increased from 44.2 to 95% with an increase in hydrogen pressure from 1 to 4 MPa over Pd/MCM-41, but the selectivity for benzylamine was reduced to 60%. In a similar way, increasing the hydrogen pressure from 1–4 MPa also changes the conversion for the Pd/C catalyst, from 41.9 to 100%. However, the selectivity for benzylamine drops from 70 to 0%. Thus, according to the selectivity for benzylamine, 2 MPa was chosen as optimum pressure for both of the catalysts for benzonitrile hydrogenation.

Reaction time

It is well-known that the product distribution of a reaction is closely related to the working conditions of the catalytic system and the stability of the intermediate species on the catalyst surface. Reaction time is an important parameter which can provide an idea about the kinetics of the reaction. The effect of reaction time has also been studied over Pd/MCM-41 and Pd/C for benzonitrile hydrogenation. Fig. 3a and b show the change in

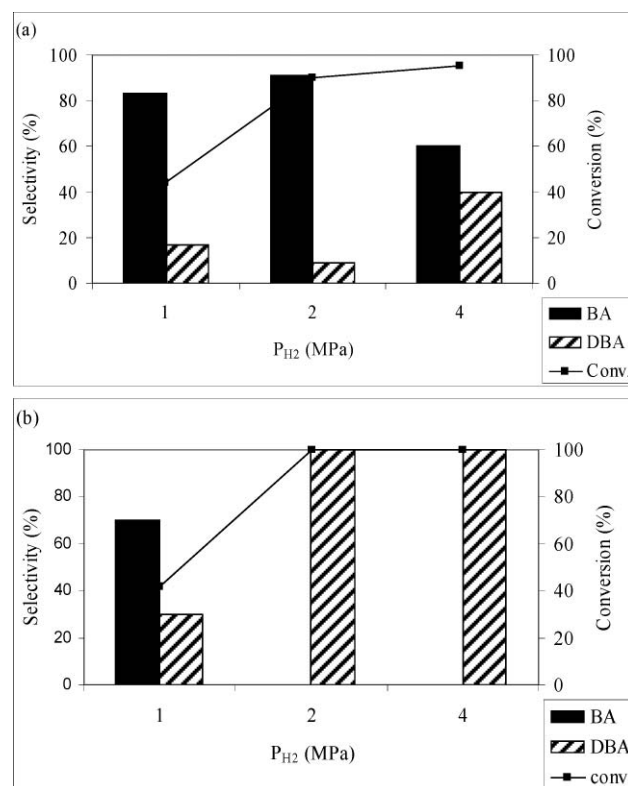


Fig. 2 Effect of variation of H_2 pressure on the hydrogenation of benzonitrile over (a) Pd/MCM-41 and (b) Pd/C. Reaction conditions: catalyst = 0.1g, substrate = 1.0 g, $T = 50$ °C, $P_{\text{CO}_2} = 10$ MPa, time = 4 h.

catalytic activity with time. Evidently, the rate of hydrogenation was faster on Pd/C compared to Pd/MCM-41. For instance, within the fixed reaction time of 2 h, 74 and 44% conversion was achieved over Pd/C and Pd/MCM-41, respectively.

However, the calculation of the turnover frequency (TOF) changes the scenario. The calculated TOF over the Pd/MCM-41 catalyst within 2 h is 4138 h^{-1} , but changes to 4151 h^{-1} after 4 h, whereas the Pd/C catalyst exhibits a TOF of 4445 h^{-1} in 2 h, which decreases to 2983 h^{-1} as the reaction time was extended to 4 h. This decrease in TOF for the Pd/C catalyst during the course of the reaction might be related to the deactivation of the catalyst.

Effect of temperature

The effect of temperature on the hydrogenation of benzonitrile was studied over Pd/MCM-41 and Pd/C catalysts at 35, 50 and 70 °C, with constant H_2 and CO_2 pressures of 4 and 10 MPa, respectively. As expected, the rate of the reaction was enhanced as the temperature changes from 35 to 70 °C, accompanied by decreased selectivity for benzylamine from 91.6 to 40% on Pd/MCM-41. For Pd/C, the conversion of benzonitrile, as well as selectivity for dibenzylamine, also increased along with the temperature.

For both cases, the influence of reaction temperature on conversion and selectivity can be explained by the phase behavior of the substrate–hydrogen– CO_2 system. In scCO_2 , the alteration of temperature changes the density of the medium and

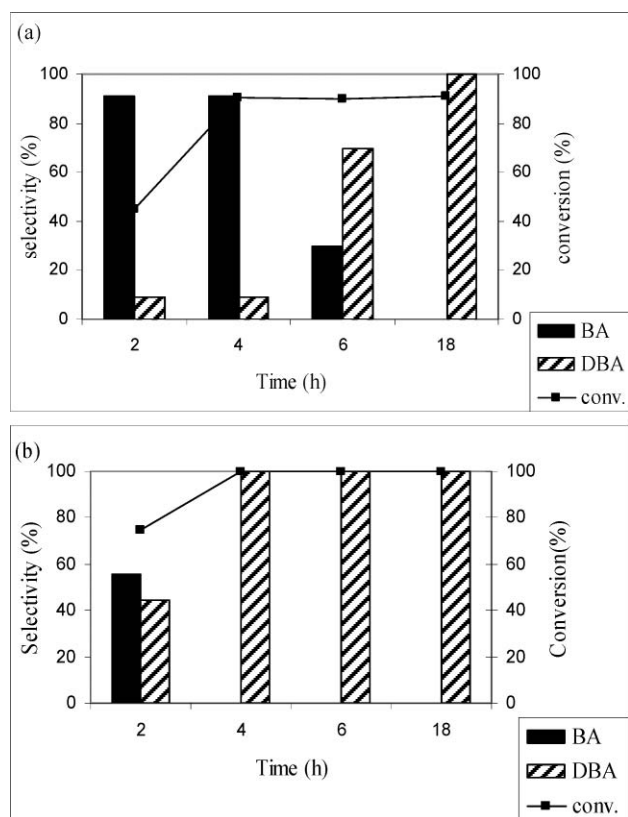


Fig. 3 Effect of variation of reaction time on benzonitrile hydrogenation over (a) Pd/MCM-41 and (b) Pd/C. Reaction conditions: catalyst = 0.1 g, substrate = 1.0 g, $T = 50\text{ }^{\circ}\text{C}$, $P_{\text{CO}_2} = 10\text{ MPa}$, $P_{\text{H}_2} = 2\text{ MPa}$.

there is a possibility of a single phase separating into two phases, because the CO_2 phase become less dense at higher temperatures. Thus, at lower densities, scCO_2 is more gas-like and, therefore, a poorer solvent. The increase in conversion with temperature may be attributed to the dramatic increase in the reaction rate in the liquid phase and also in the gaseous phase, which more than compensates for the negative effect of phase separation.²¹

Hydrogenation of other nitrile substrate

The optimized reaction conditions ($50\text{ }^{\circ}\text{C}$, 4 h, $P_{\text{CO}_2} = 10\text{ MPa}$ and $P_{\text{H}_2} = 4\text{ MPa}$) of benzonitrile has been applied to the hydrogenation of different nitrile substrate and the results are shown in Table 2. These results show that the application of the Pd/MCM-41 catalyst can be extended to nitriles with different functional groups. For example, $-\text{CH}_3$, $-\text{Br}$ and $-\text{OMe}$ (Table 2, entries 1–3) produce the corresponding primary amines with high selectivities, between 65–100%. For aromatic nitriles, a clear trend in conversion and selectivity was found, depending on the presence of electron-withdrawing and electron-donating groups. From the results, it can be seen that in the presence of an electron-donating group, the conversion was high, but the selectivity for the primary amine was low (Table 2, entries 1 and 2). The situation is reversed in the presence of an electron-withdrawing group, however (Table 2, entries 3 and 4). The potential of the catalyst was also described by the hydrogenation of aliphatic nitrile (Table 2, entries 6–8). It has to be mentioned that in comparison with the aromatic nitriles, higher

Table 2 Hydrogenation of different nitrile substrate in scCO_2

Entry	Substrate	Conversion/%	Selectivity of Primary amine/%
1		89.2	82.1
2		80.1	75.2
3		64.5	100.0
4		61.5	100.0
5 ^a		81.5	98.3
6 ^a		94.5	80.1
7		98.6	100.0
8		60.5	100.0

Reaction conditions: catalyst = 0.1 g, substrate = 1.0 g, $T = 50\text{ }^{\circ}\text{C}$, $P_{\text{CO}_2} = 10\text{ MPa}$, $P_{\text{H}_2} = 2\text{ MPa}$, time = 4h.^a $T = 70\text{ }^{\circ}\text{C}$.

temperatures were needed for the conversion of benzyl cyanide and 3-phenylpropionitrile (Table 2, entries 5 and 6) to their corresponding primary amines, with selectivities of 98.3 and 80.1%, respectively. No additive was used to increase the yield of the primary amine for any of the above-mentioned substrates.

Catalyst recycling

As heterogeneous catalysts have claimed to offer the advantage of recycling, we separated the catalysts for reuse by simple filtration. The results up to the fifth recycle are shown in Table 1 and suggest that the reuse of catalyst was possible for Pd/MCM-41. This fact could be justified by considering the high solubility of the imine intermediate in scCO_2 , which is one main reason for catalyst deactivation during nitrile hydrogenation by the blocking of metal sites. However, the Pd/C catalyst shows deactivation after the first recycle.

Conclusions

In conclusion, it has been demonstrated that scCO₂ is a potential medium to facilitate the hydrogenation of benzonitrile to the corresponding primary amine. Without using any additive, high conversion (90.2%) and selectivity for the primary amine (~91%) were achieved over the Pd/MCM-41 catalyst. The product distribution was found to depend on different reaction parameters such as CO₂ and H₂ pressure, temperature and the nature of the support. Simple tuning of the CO₂ pressure resulted in the formation of the secondary amine, dibenzylamine, which was assisted by the interaction of CO₂ with the reactant and also by the acidic support of C, instead of neutral MCM-41. In the studied experimental conditions, Pd/C was deactivated easily, whereas Pd/MCM-41 can be recycled. Preliminary experiments with other substituted nitriles show a strong influence of the nature of the substituted group on the activity and selectivity. The simple methodology presented here could be highly relevant for further development of a clean chemical process for hydrogenation of nitriles.

Experimental

Materials

Benzonitrile (Wako Pure Chemicals) was used as received. Carbon dioxide (>99.99%) was supplied by Nippon Sanso Co. Ltd. The 1% Pd/C, 5% Pd/Al₂O₃, 5% Pt/C and 5% Rh/C were from Aldrich, 5% Rh/Al₂O₃ from Wako Pure chemicals and Pd, Pt, Ni and Rh/MCM-41 were synthesized in our lab.

Catalytic activity

The hydrogenation of benzonitrile was studied at 50 °C over 1% Pd/MCM-41 catalyst. All reactions were carried out in a 50 ml stainless steel batch reactor placed in a hot air circulating oven. The details are given elsewhere.²² Briefly, 0.1 g of catalyst and 1.0 g of the reactant were introduced into the reactor. After the required temperature was attained, H₂, followed by CO₂, was charged into the reactor using a high-pressure liquid pump and then compressed to the desired pressure. The product liquid was separated from the catalyst simply by filtration and identified by NMR and GC-MS, followed by quantitative analysis using a GC (HP 6890) equipped with capillary column and flame ionization detector. For all results reported, the selectivity is as follows: % selectivity = $\frac{\text{concentration of the product}}{\text{total concentration of products}} \times 100$

Phase behavior

The phase behavior of benzonitrile was studied in a 10 ml high pressure view cell fitted with a sapphire window. The cell is placed over a magnetic stirrer and connected to a pressure controller, to regulate the pressure inside the view cell. In addition, a temperature controller was also used to maintain the desired temperature of 50 °C. The substrate was introduced into the view cell at a constant hydrogen pressure of 2 MPa while CO₂ pressure was varied between 7–14 MPa and the phase behavior was monitored. The reaction mixture exhibited a biphasic at $P < 10$ MPa, but with increasing CO₂ pressure the solubility of

benzonitrile increases and a single phase was reached. The phase behavior of benzylamine and dibenzylamine was also checked. Benzylamine showed an interesting behavior as described in Fig. 4, which represents the carbamate formation at $P < 12$ MPa (Fig. 4a) and solubility at higher pressure ($P \geq 12$ MPa; Fig. 4b). Similarly, dibenzylamine also shows solubility in CO₂ at higher pressure.

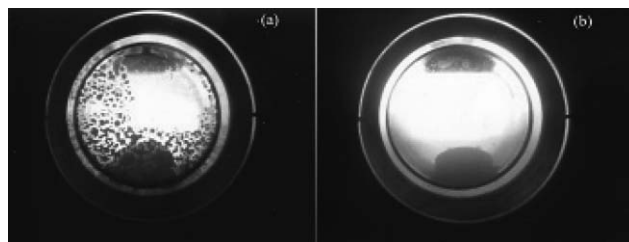


Fig. 4 Phase behavior study of benzylamine (a) $P < 12$ MPa (b) $P \geq 12$ MPa.

Notes and references

- 1 *Green Chemistry using Liquid and Supercritical Carbon Dioxide*, ed. J. M. De Simone, W. Tumas, Oxford Press, 2003; *Modern Solvent in Organic Synthesis*, ed. P. Knochel, Springer, 1999; A. Baiker, *Chem. Rev.*, 1999, **99**, 453; A. Fürstner, L. Ackermann, K. Beck, H. Hori, D. Koch, K. Langeman, M. Liebl, C. Six and W. Leitner, *J. Am. Chem. Soc.*, 2001, **123**, 9000; K. Wittmann, W. Wisniewski, R. Mynott, W. Leitner, C. L. Kranemann, T. Rische, P. Eilbracht, S. Kluwer, J. M. Ernsting and C. J. Elsevier, *Chem.-Eur. J.*, 2001, **7**, 4584; P. Stephenson, B. Kondor, P. Licence, K. Scovell, S. K. Ross and M. Poliakoff, *Adv. Synth. Catal.*, 2006, **348**, 1605; J. R. Hyde and M. Poliakoff, *Chem. Commun.*, 2004, 1482; J. R. Hyde, B. Walsh, P. Singh and M. Poliakoff, *Green Chem.*, 2005, **7**, 357.
- 2 S. G. Kazarian, M. F. Vincent, F. V. Bright, C. L. Liotta and C. A. Eckert, *J. Am. Chem. Soc.*, 1996, **118**, 1729; P. Raveendran and S. L. Wallen, *J. Am. Chem. Soc.*, 2002, **124**, 12590; P. Raveendran, Y. Ikushima and S. L. Wallen, *Acc. Chem. Res.*, 2005, **38**, 478; L. Reynolds, J. A. Gardecki, S. J. V. Frankland, M. L. Horng and M. Maroncelli, *J. Phys. Chem.*, 1996, **100**, 10337; S. Saharay and S. Balasubramanian, *ChemPhysChem*, 2004, **5**, 1442.
- 3 D. M. Rudkevitch, *Angew. Chem., Int. Ed.*, 2004, **43**, 558.
- 4 W. Leitner, *Angew. Chem.*, 1995, **107**, 2391; W. Leitner, *Angew. Chem., Int. Ed. Engl.*, 1995, **34**, 2207; M. Chatterjee, A. Chatterjee, P. Raveendran and Y. Ikushima, *Green Chem.*, 2006, **8**, 445.
- 5 *Ullmann's Encyclopedia of Industrial Chemistry*, fifth rev. edn, Vol. A2, VCH Verlag, Weinheim, 1985, p. 1.
- 6 A. Kleemann, J. Engel, B. Kutscher, D. Reichert, *Pharmaceutical Substances: Syntheses, Patents, Applications*, fourth edn, Stuttgart Georg Verlag, New York, 2001.
- 7 B. Wanderrott, *Z. Metallkd.*, 1965, **56**, 63.
- 8 S. Gomez, J. A. Peters, J. C. Van der Waal, W. Zhou and T. Maschmeyer, *Catal. Lett.*, 2002, **84**, 1.
- 9 D. R. Buehler, G. P. Keister, I. F. Long, Du Pont 1969 US Pat. 3 461 167.
- 10 C. Bianchini, V. Dal Santo, A. Meli, W. Oberhauser, R. Psaro and F. Vizza, *Organometallics*, 2000, **19**, 2433; C. S. Chin and B. N. Lee, *Catal. Lett.*, 1992, **14**, 135; S. Nishimura, *Handbook of Heterogeneous Catalytic Hydrogenation for Organic Synthesis*, John Wiley & Sons, New York, 2001, Chapter 7, p 254; T. Li, I. Bergner, F. Nipa Haque, M. Zimmer De-Iulius, D. Song and R. H. Morris, *Organometallics*, 2007, **26**, 5940; S. Enthalaer, D. Addis, K. Junge, G. Erre and M. Beller, *Chem.-Eur. J.*, 2008, **14**, 9491.
- 11 P. Kukula, M. Studer and H. U. Blaser, *Adv. Synth. Catal.*, 2004, **346**, 1487; H. U. Blaser, C. Malan, B. Pugin, F. Spindler, H. Steiner and M. Studer, *Adv. Synth. Catal.*, 2003, **345**, 103; S. Gomez, J. A. Peters and T. Maschmeyer, *Adv. Synth. Catal.*, 2002, **344**, 1037.

- 12 F. Winnas, *J. Am. Chem. Soc.*, 1939, **61**, 3566; A. M. C. F. Castelijns, P. J. D. Maas, EP Patent 0644177, 1995C. F. Winans, US Patent 2,217,630, 1940.
- 13 W. H. Hartung, *J. Am. Chem. Soc.*, 1928, **50**, 3370; E. Miller, J. M. Sprague, L. W. Kissinger and L. F. McBurney, *J. Am. Chem. Soc.*, 1940, **62**, 2099; W. H. Carothers and G. A. Jones, *J. Am. Chem. Soc.*, 1925, **47**, 3051.
- 14 S. Galvagno, A. Donato, G. Neri and R. Pietropaolo, *J. Mol. Catal., Appl. Catal., A*, 1997, **148**, 405.
- 15 Volf and J. Pasek, *Stud. Surf. Sci. Catal.*, 1986, **27**, 105; L. Hegedűs and T. Máthé, *Appl. Catal., A*, 2005, **296**, 209.
- 16 X. Xie, C. L. Liotta and C. A. Eckert, *Ind. Eng. Chem. Res.*, 2004, **43**, 7907.
- 17 J. von Braun, J. G. Blessing and F. Zobel, *Chem. Ber.*, 1923, **36**, 1988; C. de Bellefon and P. Fouilloux, *Catal. Rev. Sci. Eng.*, 1994, **36**, 459; H. Greenfield, *Ind. Eng. Chem. Prod. Res. Dev.*, 1967, **6**, 142; L. D. Volkova, H. B. Kagaarlickaya and G. D. Zakumbaeva, *Izv. Akad. Nauk Kaz. SSR., Ser. Khim.*, 1970, **23**, 70; J. L. Dallons, A. Van Gysel and G. Jannes, in “*Catalysis of Organic Reactions*” (W. E. Pascoe, Ed.), p. 93, Dekker, New York, 1992.
- 18 Y. Huang, W. M. H. Schtler and J. Catal, *J. Catal.*, 1999, **184**, 247; A. J. Deeming, D. W. Owen and N. I. Powell, *J. Organomet. Chem.*, 1990, **398**, 299; C. M. P. Ferreria, M. F. C. Guedes de Silva, V. Y. Kukushkin, J. J. R. Fraúto da Silva and A. J. L. Pombeiro, *J. Chem. Soc., Dalton Trans.*, 1998, 325; H. Tsutsui and K. Narasaka, *Chem. Lett.*, 1999, 45.
- 19 J. Hájek, N. Kumar, P. Mäki-Arvela, T. Salmi, D. Yu. Murzin, I. Paseka, T. Heikkilä, E. Laine, P. Laukkanen and J. Väyryne, *Appl. Catal., A*, 2003, **251**, 385.
- 20 F. M. Cabello, D. Tichit, B. Coq, A. Vaccari and N. T. Dung, *J. Catal.*, 1997, **167**, 142.
- 21 R. Tschan, R. Wandeler, M. S. Schneider, M. M. Schubert and A. Baiker, *J. Catal.*, 2001, **204**, 219.
- 22 M. Chatterjee, F. Y. Zhao and Y. Ikushima, *Adv. Synth. Catal.*, 2004, **346**, 459; M. Chatterjee, A. Chatterjee and Y. Ikushima, *Green Chem.*, 2004, **6**, 114; M. Chatterjee, F. Zhao and Y. Ikushima, *Appl. Catal., A*, 2004, **262**, 93.

Catalyst-free silylation of alcohols and phenols by promoting HMDS in CH₃NO₂ as solvent†

Santosh T. Kadam and Sung Soo Kim*

Received 8th July 2009, Accepted 17th September 2009

First published as an Advance Article on the web 26th October 2009

DOI: 10.1039/b913398d

An uncatalyzed method for the silylation of alcohols and phenols with HMDS in CH₃NO₂ at rt is developed. A diverse range of aromatic and aliphatic alcohols as well as phenols undergo the silylation in very short reaction time with excellent yield. The uncatalyzed reaction requires neither elevated temperature nor high pressure for the silylation.

Introduction

Functional group protection is at the heart of multifunctional and multistep target molecules. Alcohol and phenol moieties represent one of the most ubiquitous functional groups in nature.¹ The formation of a silyl ether from a hydroxyl group is one of the most popular and widely used methods. It is frequently used as a protection method in multistep reactions due to its stability under a variety of conditions, solubility in non-polar solvents and its ease of removal. Silylation of hydroxyl groups is also utilized in analytical chemistry to prepare volatile derivatives of alcohols and phenols for GC and GC-MS analysis.² Many silylating agents, such as chlorotrimethylsilane,³ hexamethyldisiloxane,⁴ and allylsilane⁵ have been used to introduce silyl groups into a variety of alcohols. Hexamethyldisilazane (HMDS) is a stable, commercially available reagent which gives ammonia as the only by-product. Even though the handling of this reagent is convenient, the main drawback is its poor silylating power which demands the use of catalysts and high temperature.⁶ A variety of catalysts have been reported for the activation of HMDS, such as sulfonic acid-functionalized nanoporous silica,⁷ trichloroisocyanuric acid (TCCA),⁸ InBr₃,⁹ zirconyl triflate,¹⁰ K-10 montmorillonite,¹¹ H-β zeolite,¹² silica-supported perchloric acid,¹³ barbutric acid,¹⁴ iodine,¹⁵ MgBr₂,¹⁶ *N*-bromosuccinimide (NBS)¹⁷ and iron(III) trifluoroacetate.¹⁸

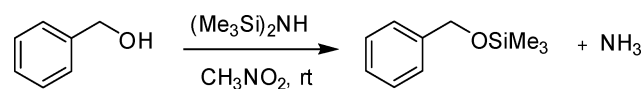
Hence, considering the importance of the silylation reaction, continuous efforts have been made to develop new methodologies involving the application of various catalysts. However, various limitations exist with the reported methodologies, such as long reaction time,¹⁴ high temperature,¹² halogenated solvents,¹⁵ costly catalysts,⁹ toxic metal catalysts¹⁰ and use of excess reagent.²⁵ According to the principle of green chemistry, the synthetic method should be designed to minimize the energy input by running the reaction at ambient temperature and reducing the amount of reagents or catalyst.¹⁹ Thus, with increasing environmental concern, there is a demand for efficient, metal-

or catalyst-free and environmentally benign methods for the silylation of alcohols.

The appropriation of several solvents without intervention of catalyst has been reported for various organic transformations. Watahiki *et al.* have reported DMSO for cyanobenzoylation of aldehydes with benzyl cyanide.²⁰ The combination of DMSO with hexane was employed for the cyanosilylation of aldehyde²¹ as well as synthesis of silyl ether from alcohol and *tert*-butyldimethylsilyl chloride.²² Similarly, Iwanami *et al.* describe the synthesis of cyanohydrin carbonates in DMSO in the presence of molecular sieves.²³ Kumamoto *et al.* show the cyanation of acetal with TMSCN in CH₃NO₂ at 60 °C and high pressure.²⁴ Considering the activity of different silyl reagents in polar solvents, HMDS could be activated in the proper solvent without using catalyst.

Result and discussion

We herein report a novel and simple catalyst-free silylation method of alcohols and phenols under mild conditions (Scheme 1). The effect of various solvents for the silylation of benzyl alcohol is explored (Table 1). The polar aprotic solvents DMF and DMSO produce 20 and 48% of yield, respectively (entries 1 and 2). THF shows a lesser yield (10%) of silylated product (entry 4). Methanol, CH₂Cl₂, dioxane, CH₃CN and hexane give no product (entries 3 and 5–8). Surprisingly, the reaction in CH₃NO₂ results in the desired product with excellent yield in a very short reaction time (10 min). Accordingly, 1 mL of CH₃NO₂ and 1 mmol of HMDS is sufficient for the completion of silylation reaction with alcohols at rt. This could be the first example of uncatalyzed silylation of alcohols with HMDS in CH₃NO₂.



Scheme 1 Silylation of alcohols with HMDS in CH₃NO₂.

A variety of aromatic and aliphatic alcohols have been examined for the silylation in CH₃NO₂ without intervention of any catalyst or promoter (Table 2). Benzyl alcohol and most of its various derivatives undergo the silylation with

Department of Chemistry, Inha University, Incheon, 402-756, South Korea. E-mail: sungsoo@inha.ac.kr

† Electronic supplementary information (ESI) available: Experimental details and ¹H and ¹³C NMR data. See DOI: 10.1039/b913398d

Table 1 Silylation of benzyl alcohol with HMDS in various solvents

Entry	Solvent	Time	Yield/% ^a
1	DMF	6 h	20
2	DMSO	6 h	48
3	1,4-Dioxane	6 h	NR
4	THF	6 h	10
5	MeOH	6 h	NR
6	CH ₂ Cl ₂	6 h	NR
7	CH ₃ CN	6 h	NR
8	Hexane	6 h	NR
9	CH ₃ NO ₂	10 min	99

Reaction conditions: 1 mmol of benzyl alcohol, 1 mmol of HMDS and 1 mL of solvent at rt.^a Isolated yield.

Table 2 Silylation of primary alcohols with HMDS in CH₃NO₂.^a

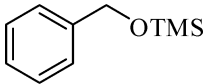
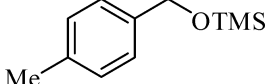
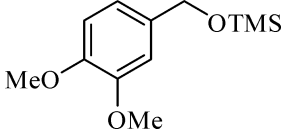
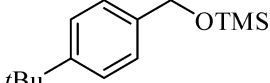
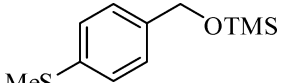
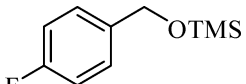
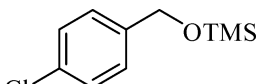
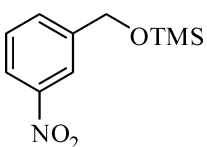
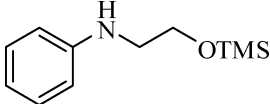
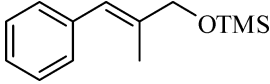
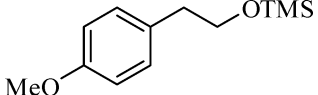
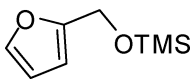
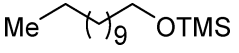
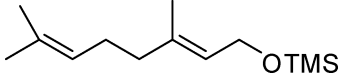
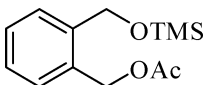
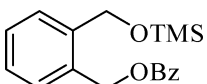
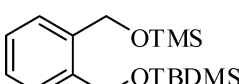
Entry	Products	Yield/% ^b
1		99
2		98
3		99
4		94
5		97
6		96
7		95
8		80 ^c
9		98
10		86 ^c

Table 2 (Contd.)

Entry	Products	Yield/% ^b
11		94
12		87 ^c
13		79 ^c
14		90
15		99
16		99
17		99

^a Reagents and conditions: alcohols (1 mmol), HMDS (1.0 mmol), CH₃NO₂ (1 mL) at rt with 10 min reaction time, unless otherwise mentioned. ^b Isolated yield. ^c 30 min reaction time.

excellent yields within 10 min of reaction time (entries 1–8). Only *m*-nitrobenzyl alcohol reacts rather slowly (30 min) with reduced yield (80%) (entry 8). This could be due to the electron-withdrawing power of the nitro substituent. Anilinoethanol gives the *o*-silylation product with excellent yield (entry 9). This method is also applicable to *trans*-2-methyl-3-phenyl-2-propen-1-ol with relatively lower yield (86%) and longer reaction time (30 min) (entry 10). Methoxyphenylethanol results in the silylation product with very good yield (entry 11). Silylation of heterocyclic furfuryl alcohol (entry 12) and aliphatic primary lauryl alcohol (entry 13) proceed efficiently with good yield in relatively longer reaction time (30 min). Acid-sensitive geraniol is able to produce the silylation product with considerably good yield (entry 14). This uncatalyzed protocol also tolerates presence of acetyl ester, benzoyl ester and TBDMS ether in order to produce excellent yields (entries 15–17).

The silylation reaction is extended to various secondary alcohols and phenols (Table 3). Benzhydrol and 4,4'-dichlorobenzhydrol react smoothly with HMDS, giving excellent yields (entries 1 and 2). Phenylethanol and *p*-tolylethanol deliver the corresponding silylated products with 84 and 99% yield, respectively (entries 3 and 4). *p*-Bromomethylbenzyl alcohol requires a slightly longer reaction time for the production of silylated product (entry 5). 1-Phenyl-1-propanol requires 10 min for the completion of reaction (entry 6).

Propargyl alcohol and secondary aliphatic alcohol undergo the silylation reaction smoothly with slightly lower yield within

Table 3 Silylation of secondary alcohols and phenols with HMDS in CH_3NO_2 .^a

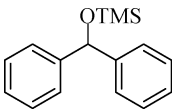
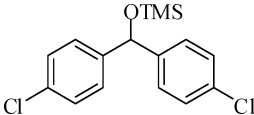
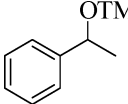
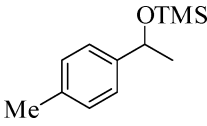
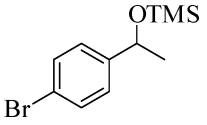
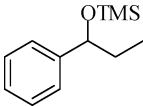
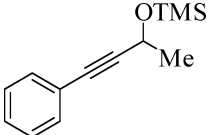
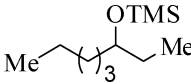
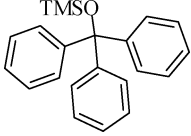
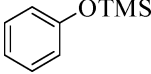
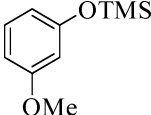
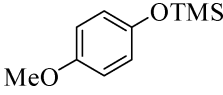
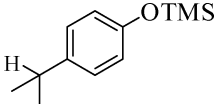
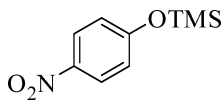
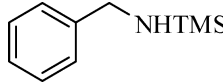
Entry	Products	Time	Yield/% ^b
1		10 min	99
2		10 min	99
3		30 min	84
4		10 min	99
5		30 min	91
6		10 min	93
7		30 min	87
8		30 min	89
9		6 h	NR
10		30 min	80
11		15 min	95
12		15 min	84
13		15 min	92

Table 3 (Contd.)

Entry	Products	Time	Yield/% ^b
14		6 h	NR
15		6 h	NR

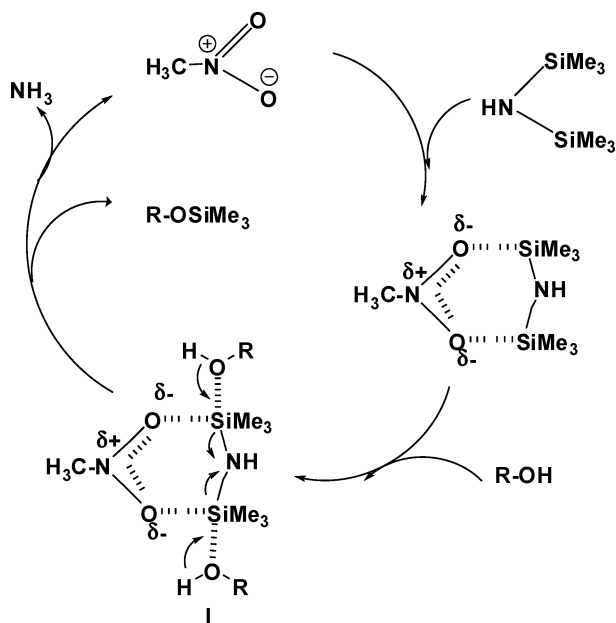
^a Reagents and conditions: alcohols or phenols (1 mmol), HMDS (1.0 mmol), CH_3NO_2 (1 mL) at rt. ^b Isolated yield.

30 min reaction time (entries 7 and 8). The present method is not applicable to tertiary alcohol, even after 6 h reaction time (entry 9). This may indicate that the steric effect is serious enough to prevent the reaction taking place. Interestingly, phenols also undergo the silylation to produce silyl ether in considerably high yields (entries 10–13). Unsubstituted phenol requires a longer reaction time (30 min) relative to electron-donating *p*- and *o*-methoxy and *p*-isopropyl phenol (15 min) (entries 11–13). However, *p*-nitro phenol fails to produce silylation product (entry 14). This result may indicate that the electron-withdrawing ability of the nitro group could reduce the electron density on the oxygen atom that prohibits the silylation. It is very interesting to note that *m*-nitrobenzyl alcohol (entry 8, Table 2) gives a pretty good yield, because no such conjugation could occur here. The reaction of benzyl amine did not produce the corresponding silyl ether, even after 6 h reaction time (entry 15). This may be due to the high affinity of silicon for oxygen atoms compared to the nitrogen of benzyl amine.³⁰ These data demonstrate that HMDS does not interact with amines under the present conditions.

A possible mechanism and the role of CH_3NO_2 are shown in Scheme 2. Several reports have indicated that the oxygen atom of heteroatom oxide can activate the silylating reagent through coordination with the silicon atom.²⁴ Alcohols react with the activated HMDS– CH_3NO_2 (I) complex to produce the O-silyl ether with the liberation of ammonia. The evolution of ammonia is confirmed by its strong and pungent odor and red litmus paper, which turns from red to blue. The cyanation of acetal in CH_3NO_2 as solvent demands high pressure and elevated temperature,²⁴ but the present silylation reaction involves quite mild reaction conditions.

Conclusion

A novel and efficient uncatalyzed method for the silylation of alcohols and phenols is developed. Alcohols (phenols) and HMDS react to give silylated products in CH_3NO_2 as solvent without the aid of a catalyst. The major advantages of the method are mild reaction conditions, easy work up and the absence of catalyst. This could be the most economically convenient method for the silylation of alcohol, compared to other reported catalytic methods. Under the non-metallic and catalyst-free conditions, the reaction becomes “environmentally friendly”.



Scheme 2 Plausible mechanism for the silylation of alcohols with HMDS in CH_3NO_2 .

Experimental section

General

In all cases, the ^1H NMR (400/200 MHz) spectra were recorded with a Varian Gemini 2000 spectrometer. Chemical shifts are reported in ppm in CDCl_3 with tetramethylsilane as an internal standard. ^{13}C NMR data were collected on a Varian Gemini 2000 spectrometer (50 MHz). GC-MS data were recorded with 1200 L Single Quadrupole GC/MS System with 3800GC/Varian.

General procedure for the silylation of alcohols or phenols

To a mixture of alcohol (phenol) (1 mmol) and CH_3NO_2 (1 mL), HMDS (1 mmol) was added at rt. The completion of the reaction was monitored with TLC. After the completion of the reaction, the reaction mixture was concentrated *in vacuo*. The viscous mass was subjected to silica gel flash column chromatography to obtain the pure compound.

^1H , ^{13}C NMR and GC-MS data for new products are given below (Table 2, entries 9, 15, 16, 17 and Table 3, entries 7 and 8). ^1H , ^{13}C NMR and HRMS data for known products are the same as literature values.^{10,13,26-29}

***N*-(2-Trimethylsilyloxy)ethyl)aniline (Table 2, entry 9).** δ_{H} (200 MHz; CDCl_3 ; Me_4Si): 0.00 (s, 9H), 3.09 (t, $J = 7.6$ Hz, 2H), 3.64 (t, $J = 7.6$ Hz, 2H), 3.88 (s, 1H), 6.48–6.61 (m, 3H), 7.00–7.08 (m, 2H). δ_{C} (50 MHz; CDCl_3 , Me_4Si): 0.5, 45.9, 61.0, 113.2, 117.5, 129.2, 148.3. GCMS: $m/z = 209$ [M^+].

2-((Trimethylsilyloxy)methyl)benzyl acetate (Table 2, entry 15). δ_{H} (400 MHz; CDCl_3 ; Me_4Si): 0.15 (s, 9H), 2.09 (s, 3H), 4.75 (s, 2H), 5.18 (s, 2H), 7.25–7.37 (m, 3H), 7.4 (d, $J = 6.8$ Hz, 1H). δ_{C} (CDCl_3 , 400 MHz): –0.4, 20.9, 62.3, 63.8, 127.5, 127.7, 128.47, 129.2, 133.3, 139.2. GCMS: $m/z = 252$ [M^+].

2-((Trimethylsilyloxy)methyl)benzyl benzoate (Table 2, entry 16). δ_{H} (400 MHz; CDCl_3 ; Me_4Si): 0.13 (s, 9H), 4.83 (s, 2H),

5.45 (s, 2H), 7.30–7.35 (m, 5 H), 7.43–7.56 (m, 2H), 8.06–8.08 (m, 2H); δ_{C} (50 MHz; CDCl_3 , Me_4Si): –0.41, 62.49, 64.35, 127.57, 128.43, 128.53, 129.17, 129.71, 130.15, 133.07, 133.44, 139.33, 166.33. GCMS: $m/z = 314$ [M^+].

***tert*-Butyldimethyl 2((trimethylsilyloxy)methyl)benzyloxy)silane (Table 2, entry 17).** δ_{H} (400 MHz; CDCl_3 ; Me_4Si): 0.13 (s, 9H), 0.92 (s, 9H), 4.70 (s, 2H), 4.75 (s, 2H), 7.22–7.24 (m, 2H), 7.36–7.42 (m, 2H); δ_{C} (50 MHz; CDCl_3 , Me_4Si): –5.25, –0.41, 18.40, 25.98, 62.35, 62.77, 126.64, 126.91, 127.03, 127.20, 137.78, 138.46. GCMS: $m/z = 324$ [M^+].

Trimethyl(4-phenylbut-3-yn-2-yloxy)silane (Table 3, entry 7). δ_{H} (200 MHz; CDCl_3 ; Me_4Si): 0.02 (s, 3H), 1.59 (d, $J = 8.2$ Hz, 3H), 4.84 (q, $J = 6.4$ Hz, 1H), 7.33–7.45 (m, 3H), 7.48–7.53 (m, 2H). δ_{C} (50 MHz; CDCl_3 , Me_4Si): 0.1, 25.4, 59.1, 83.6, 91.5, 123.0, 128.8, 128.3, 128.6, 131.7, 131.7. GCMS: $m/z = 218$ [M^+].

(Hexan-3-yloxy)trimethylsilane (Table 3, entry 8). δ_{H} (400 MHz; CDCl_3 ; Me_4Si): 0.14 (s, 9H), 0.79–0.94 (m, 6 H), 1.25–1.51 (m, 8H), 3.52 (qt, $J = 12$ Hz, 1H), δ_{C} (50 MHz; CDCl_3 , Me_4Si): 0.34, 9.93, 13.99, 22.63, 25.35, 30.02, 31.99, 36.89, 73.88. GCMS: $m/z = 174$ [M^+].

Acknowledgements

The authors thank the Centre for Biological Modulators of the KRICT for financial support. Thanks are also due to BK 21 administrated by the Korea Research Council.

References

- (a) T. W. Green and P. G. M. Wuts, in *protective Groups in Organic Synthesis*, 3rd edn, John Wiley & Sons, New York, 1999, p150; (b) S. Otera, *Chem. Rev.*, 1993, **93**, 1449; (c) S. A. Franklin, *J. Chem. Soc., Perkin Trans. 1*, 1998, 2451.
- G. V. Look, G. Smchen and J. Heberle, *Silylation agents*, Fluka, Buchs, Switzerland, 1195.
- B. P. Bandgar, S. N. Chavare and S. S. Pandit, *J. Chin. Chem. Soc.*, 2005, **52**, 125.
- B. E. Cooper, *Chem. Ind.*, 1978, **107**, 794.
- T. Morita, Y. Okamoto and H. Sakurai, *Tetrahedron Lett.*, 1980, **21**, 835.
- C. A. Bruynes and T. K. Jurriens, *J. Org. Chem.*, 1982, **47**, 3966.
- D. Zareyeea and B. Karimi, *Tetrahedron Lett.*, 2007, **48**, 1277.
- A. Khazaei, M. A. Zolfigol, A. Rostami and A. G. Choghamarani, *Catal. Commun.*, 2007, **8**, 543.
- J. S. Yadav, B. V. S. Reddy, A. K. Basak, G. Baishya and A. V. Narsaiah, *Synthesis*, 2006, 3831.
- M. Moghadam, S. Tangestaninejad, V. Mirkhani, I. Mohammadpoor-Baltork, S. Chahardahcheric and Z. Tavakoli, *J. Organomet. Chem.*, 2008, **693**, 2041.
- Z. H. Zang, T. S. Li, F. Yang and C. G. Fu, *Synth. Commun.*, 1998, **28**, 3105.
- V. H. Tillu, V. H. Jadhav, H. B. Borate and R. D. Wakharkar, *Arkivoc*, 2004, 83.
- H. R. Shaterian, F. Shahrekipoor and M. Ghashang, *J. Mol. Catal. A: Chem.*, 2007, **272**, 142 and references cited therein.
- K. Khazaei, M. A. Zolfigol, Z. Tanbakouchian, M. Shiri, K. Niknam and J. Saïen, *Catal. Commun.*, 2007, **8**, 917.
- B. Karimi and B. Golshani, *J. Org. Chem.*, 2000, **65**, 7228.
- M. M. Mojtahedi, H. Abbasi and M. S. Abaee, *J. Mol. Catal. A: Chem.*, 2006, **250**, 6.
- H. R. Shaterian, R. Doostmohammadi and M. Ghashang, *Chin. J. Chem.*, 2008, **26**, 1709.
- H. Firouzabadi, N. Iranpoor, A. A. Jafari and M. R. Jafari, *J. Organomet. Chem.*, 2008, **693**, 2711.
- P. Anastas and J. C. Warner, in *Green Chemistry: Theory and Practice*, Oxford University Press, Oxford, 1998.

- 20 T. Watahiki, S. Ohba and T. Oriyama, *Org. Lett.*, 2003, **5**, 2679.
- 21 F. L. Cabirol, A. E. C. Lim, U. Hanefeld, R. A. Sheldon and I. M. Lyapkalo, *J. Org. Chem.*, 2008, **73**, 2446.
- 22 T. Watahiki, M. Matsuzaki and T. Oriyama, *Green Chem.*, 2003, **5**, 82.
- 23 T. Watahiki, Y. Hinakubo and T. Oriyama, *Tetrahedron Lett.*, 2005, **46**, 5881.
- 24 K. Kumamoto, K. Nakano, Y. Ichikawa and H. Kotsuki, *Synlett*, 2006, **12**, 1968 and references cited therein.
- 25 A. V. Narsaiah, *J. Organomet. Chem.*, 2007, **692**, 3614.
- 26 M. R. Saidi and N. Azizi, *Organometallics*, 2004, **23**, 1457.
- 27 S. T. Kadam and S. S. Kim, *J. Organomet. Chem.*, 2009, **694**, 2562.
- 28 G. Rajagopal, Hanbin Lee and S. S. Kim, *Tetrahedron*, 2009, **65**, 4735.
- 29 J. M. Midgley, S. J. Millership and B. W. Whalley, *J. Chem. Soc., Perkin Trans. 1*, 1976, 1384.
- 30 (a) H. Vorbruggen and K. Krolkiewicz, *Justus Liebigs Ann. Chem.*, 1976, 746; (b) H. Vorbruggen, K. Krolkiewicz and U. Niedballa, *Justus Liebigs Ann. Chem.*, 1975, 988; (c) M. J. Cook, A. R. Katritzky and P. Linda, *Adv. Heterocycl. Chem.*, 1974, **17**, 255; (d) R. A. Singer and M. Dore, *Org. Process Res. Dev.*, 2008, **12**, 1261.

New one-pot multistep process with multifunctional catalysts: decreasing the E factor in the synthesis of fine chemicals†

Maria J. Climent, Avelino Corma,* Sara Iborra, Maria Mifsud and Alexandra Velty

Received 29th April 2009, Accepted 22nd September 2009

First published as an Advance Article on the web 26th October 2009

DOI: 10.1039/b919660a

The synthesis of a series of fine chemicals (4-(4-methoxyphenyl)-2-butanone, 4-(6,6-dimethylbicyclo[3,1,1]hept-2-en-2-yl)-2-butanone, and 2-cyclopentylcyclopentanone) has been performed through a simple process that involves one-pot multi-step reactions (condensation–dehydration–reduction) using multifunctional base–acid–metal catalysts. The E factor for the specific process, as well as for the global process that includes the manufacturing of the reactants, has been calculated and compared with those obtained using conventional methods. In various cases, it is demonstrated that by means of process intensification with multifunctional solid catalysts, it is possible to decrease the E factor by one order of magnitude or more with respect to any of the manufacturing routes reported to date.

Introduction

In the late 1980s, Sheldon¹ introduced the concept of the E (environmental) factor for assessing the environmental impact of manufacturing processes. The E factor is defined as the mass ratio of waste to the desired product (kg waste/kg product). To calculate the E factor, the chemical yield, reagents, solvent losses, all process aids, and even energy consumption (though this is frequently difficult to estimate) are taken into account. The water used in the process is not considered, but water formed is included in the calculations. Catalysis plays an important role in reducing or eliminating waste in chemical processes, particularly for the production of fine chemicals, where the E factors are especially high. Most of the waste generated in the manufacture of fine chemicals is inorganic salts formed by the use of stoichiometric inorganic reagents. Thus, the substitution of conventional stoichiometric methodologies by catalytic processes, combined with the possibility of intensifying processes by combining several catalytic steps into a one-pot catalytic system, provides a means to improve the economical and environmental aspects of chemical processes. In this sense, domino catalytic multi-step reactions with mono- or multifunctional catalysts are very efficient processes in terms of work up and catalyst utilization, with the additional advantage that isolation and purification of intermediates is not required.^{2–12} Moreover, the fact that the same catalyst can catalyze different consecutive steps in a single reaction vessel under the same reaction conditions decreases the operating time and the amount of waste produced. In this way, heterogeneous catalysts containing various active sites on their surface are promising candidates for promoting multiple reactions in a single pot.^{13–18}

Metal supported on alkaline earth layered double hydroxides (LDH) and its mixed oxides have been extensively applied as multifunctional base–acid–metal catalysts for cascade reactions such as the synthesis of methyl isobutyl ketone in one pot from acetone^{19,23} or from 2-propanol^{24–27} and for the preparation of fine chemicals such as 2-methyl-3-phenyl propanal,^{28,29} α -alkylated nitriles,³⁰ and the anti-inflammatory nabumetone.^{11,16}

Here, we present that by means of multifunctional base–acid–metal catalysts (Pd-supported alkaline earth oxides and mixed oxides), it is possible to substitute existing processes for the production of a series of fine chemicals (4-(4-methoxyphenyl)-2-butanone, 4-(6,6-dimethylbicyclo[3,1,1]hept-2-en-2-yl)-2-butanone, and 2-cyclopentylcyclopentanone) by a more simple process that involves one-pot multi-step reactions. We show that by means of process intensification with multifunctional solid catalysts, it has been possible, in various cases, to decrease the E factor by one order of magnitude or more, with respect to any of the manufacturing routes reported up to now. In this work, the E factor for the specific process as well as for the global process that includes the manufacturing of the reactants has been considered.

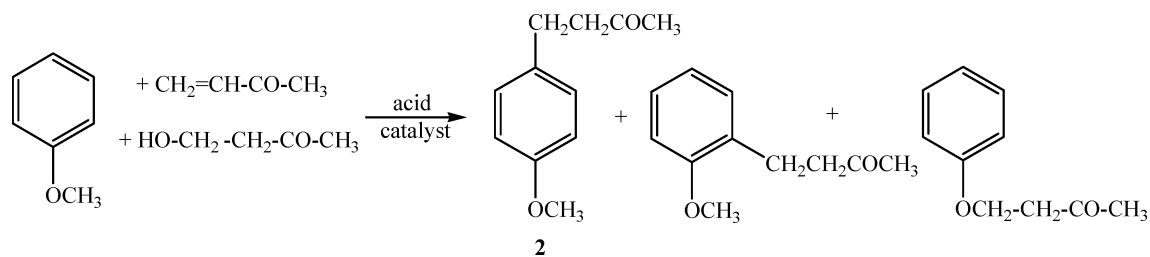
Results and discussion

1. Preparation of 4-(4-methoxyphenyl)-2-butanone (2)

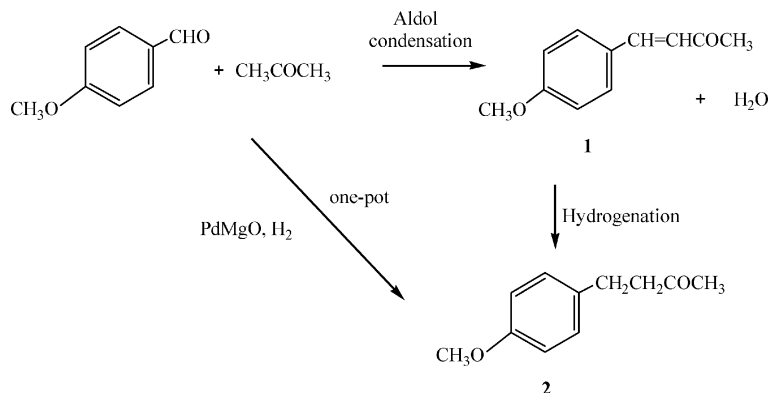
4-(4-Methoxyphenyl)-butan-2-one (**2**) (Scheme 1) is an odorous molecule with a raspberry scent which is extracted from aloe wood, and has been approved by the FDA for food uses at a level of 25 ppm. It has also been utilized as an insect attractant for the scarabaeid family and in the preparation of melanin formation inhibitors.³¹ One route for the preparation of **2** in one step (Scheme 1) is the Friedel–Crafts alkylation of anisole with 4-hydroxybutan-2-one or methyl vinyl ketone using acid catalysts such as H₂SO₄, H₃PO₄, HCl.³² However, many side reactions (transalkylations, isomerization, polyalkylation and polymerization) occur during Friedel–Crafts alkylation in the

Instituto de Tecnología Química, Universidad Politécnica de Valencia, Avda. de los Naranjos s/n, 46022 Valencia, Spain.
E-mail: acorma@itq.upv.es

† Electronic supplementary information (ESI) available: Details of E factor calculations. See DOI: 10.1039/b919660a



Scheme 1



Scheme 2

presence of Lewis or Brønsted homogeneous acid catalyst, resulting in a maximum selectivity for **2** of approximately 70%.

Heterogeneous catalysts, such as exchanged resins (Dowex-50),³³ have also been used for this transformation, however low selectivity for **2** (60–70%) was obtained. Cation exchanged montmorillonite also containing Brønsted acid sites has been utilized, yielding only 25% of **2** at 100 °C after 48 h reaction time.³⁴

There is another route to synthesize **2** (Scheme 2), that involves an aldol condensation between 4-methoxybenzaldehyde and acetone, yielding the α,β -unsaturated compound **1**, which is followed by hydrogenation of the C=C bond in a two-step reaction. When using homogenous catalysts, the condensation step has been carried out with NaOH as catalyst yielding 98% of the α,β -unsaturated ketone (**1**).³⁵ While a one-pot process has been carried out under hydrogen atmosphere, in the presence of NaOH and 5% Pd/C, the two step process yields 80% of 4-(4-methoxyphenyl)-2-butanone (**2**).³⁶

We propose here an alternative one-pot catalytic process to synthesize **2** that consists of reacting 4-methoxybenzaldehyde with acetone under hydrogen atmosphere in the presence of PdMgO catalyst to give an intermediate, **1**, which is hydrogenated to give **2** (Scheme 2). The reaction between 4-methoxybenzaldehyde and acetone was performed using 1 wt% of Pd loaded on the nanocrystalline MgO (see Experimental) at 75 °C. The results in Table 1 show that PdMgO is able to convert 100% of 4-methoxybenzaldehyde, giving 99% yield and 99% selectivity for **2**.

It is known that the selection of the most appropriate type of centres for a given base-catalyzed process has a strong impact on the catalyst activity and selectivity.³⁷ Thus, we have also prepared two Pd catalysts supported on Al/Mg calcined hydrotalcite (PdHTc) and on calcined–rehydrated Al/Mg hydrotalcite

Table 1 Results for the synthesis of **2** using different multifunctional catalysts

Catalysts	$r^o \times 10^4 / \text{mmol min}^{-1} \text{g}^{-1}$	Conversion (%)	Yield 1 (%)	Yield 2 (%)	Selectivity 2 (%)
PdMgO	12.0	100	1	99	99
PdHTc	5.0	89	25	62	68(2)
PdHTr	9.7	95	—	95	100

r^o : rate of disappearance of 4-methoxybenzaldehyde. Reaction conditions: 4-methoxybenzaldehyde (3.8 mmol), acetone (37 mmol); 75 °C, catalyst 38 wt% with respect to anisaldehyde. Conversion and yield at 75 min reaction time. The value in brackets is the percentage of Michael adduct.

(PdHTr) which were tested under the same reaction conditions as PdMgO .

As can be seen in Table 1, PdHTc exhibits lower condensation and hydrogenation rates than PdMgO and, consequently, the yield and selectivity of **2** are lower. Moreover, a secondary product resulting from the Michael addition of acetone to **2** was also detected in minor amounts. When the calcined hydrotalcite containing palladium metal was rehydrated (PdHTr), a twofold increase in initial reaction rate was observed. This result is not surprising since by rehydration, a restoration of the layered structure occurs wherein the CO_3^{2-} counter anions in the interlayer space are replaced by OH^- , resulting in strong Brønsted base catalysts that efficiently catalyze a larger number of reactions.^{38–45} Results in Table 1 indicate that, together with PdMgO , PdHTr is a promising candidate for the preparation of **2**, since 95% yield with 100% selectivity is obtained after 75 min reaction time.

Nevertheless, for a potential industrial implementation of the above catalysts (PdMgO and PdHTr) for the preparation of **2**,

Table 2 Study of the stability of the catalysts

Catalysts	Cycles	Conversion (%)	Yield 1 (%)	Yield 2 (%)	Selectivity 2 (%)
PdHTr	1	95	—	95	100
	2	25	18	7	28
PdMgO	1	100	1	99	99
	2	100	2	98	98
	3	100	1	99	99
	4	100	2	98	98

the possibility of catalyst regeneration has to be considered. To study the reusability of the catalysts, the samples were regenerated after the reaction as described in the Experimental section and the catalyst was used again. As it can be seen in Table 2, an important decrease in activity upon regeneration was found with the PdHTr sample, which is probably due to an incomplete reconstruction and/or a decrease in the number of basic and hydrogenating active sites. In contrast, the PdMgO sample was subjected to four cycles of reaction–regeneration (calcination)–reaction, in all cases achieving 100% conversion and similar selectivity of **2** (Table 2).

In conclusion, we have shown that by using a multifunctional catalyst based on Pd supported on nanocrystalline MgO, it has been possible to develop a new green process for production of **2** in a one-pot cascade reaction. This new process allows yields of 99% with 99% selectivity for **2**. The E factor involved is presented below.

1.1 E factor for the synthesis of 4-(4-methoxyphenyl)-2-butanone (2). We have calculated the E factor for the specific process described above (Scheme 2), as well as the global E factor when starting from primary organics such as methyl phenol or anisole (Scheme 3).

Considering that acetone is an easily recoverable solvent and the hydrogenation process does not produce any waste, the E factor for the one-pot reaction starting from *p*-methoxybenzaldehyde is 0.01, water being the main waste. The E factors for the syntheses of the reagents, acetone and 4-methoxybenzaldehyde, have also been calculated. For the synthesis of acetone we have selected the cumene route starting from benzene and propylene since this is the main industrial method used to produce acetone (see the ESI†). The total E factor for the production of acetone is 0.16.

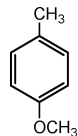
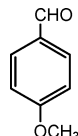

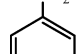
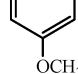
On the other hand, the value for 4-methoxybenzaldehyde has been obtained according to two different routes (Scheme 3):

(i) by methylation of *p*-cresol giving *p*-methoxytoluene followed by catalytic oxidation with air, which has an E factor of 0.82 (see the ESI†).

(ii) by formylation of anisole through a Vilsmeier reaction,⁴⁶ which has an E factor of 2.77 (see the ESI†). If we consider the global process, *via* i and *via* ii, the global E factors are 0.99 and 2.94, respectively (see Table 3).

If we follow the same methodology for the commercially accepted process where the aldol condensation is carried out using a 10% aqueous solution of NaOH³⁵ (see Scheme 3), the specific E factor is 9.69, and when considering the global process, *via* i and *via* ii, the global E factors are 10.67 and 12.62, respectively (see Table 3).

Table 3 Summary of the E factors for the synthesis of **2** through aldol condensation

Compound	E factor (heterogeneous) ^a		E factor (homogeneous) ^a	
	<i>via</i> i	<i>via</i> ii	<i>via</i> i	<i>via</i> ii
	0.78		0.78	
	0.04	2.77	0.04	2.77
	0.16	0.16	0.16	0.16
	0.01	0.01	9.69	9.69
				
2				
Global E factor	0.99	2.94	10.67	12.62

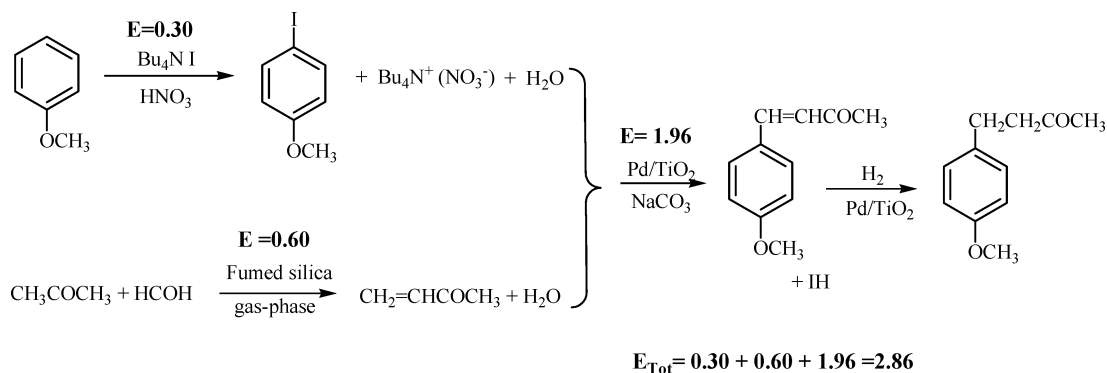
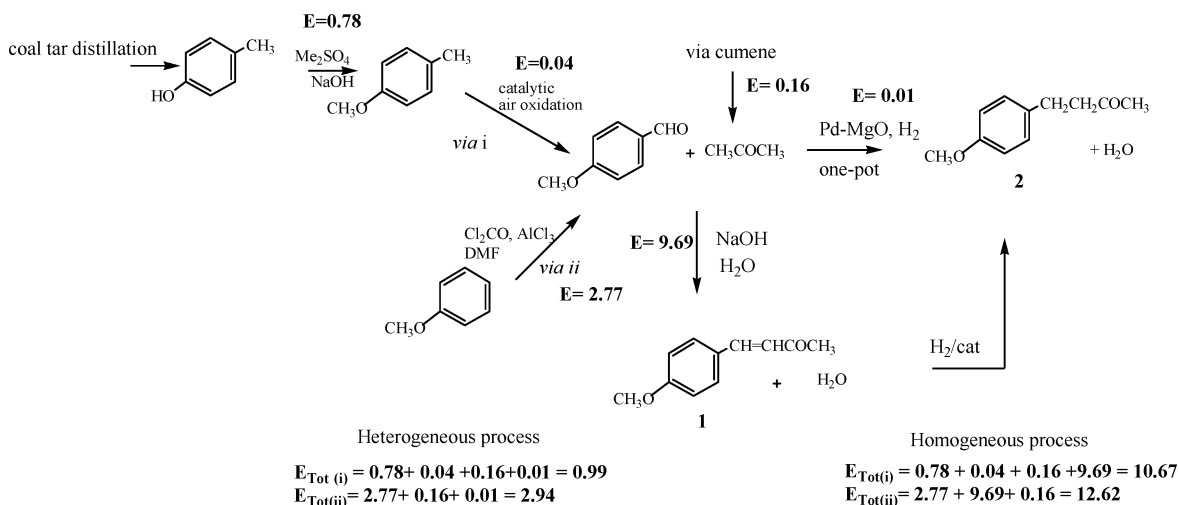
^a Referring to the specific path for the synthesis of **2**

These results indicate that considering the global process starting from *p*-cresol, the E factor for the procedure presented here with PdMgO is one order of magnitude lower than that of the conventional process (see Table 3). In Table 3, the specific E factors of all compounds involved in the production of compound **2** are summarized, as well as the global E factors following routes i and ii, performed using heterogeneous and homogeneous catalysts in the specific path for the synthesis of **2**.

We have also considered here another potential procedure for the synthesis of **2** through two consecutive steps, involving a Heck coupling reaction between *p*-iodoanisole and methyl vinyl ketone (MVK) followed by hydrogenation (see Scheme 4). It has been reported that the synthesis of **2** *via* Scheme 4 could be performed in a one pot, two-step process using palladium supported on titanium dioxide as a catalyst. Under optimized reaction conditions, this catalytic route gave **2** with 97% yield.¹² Thus, for comparison purposes we have calculated the E factor for the synthesis of compound **2** through the Heck coupling reaction under heterogeneous and homogeneous catalysis, and the result, considering that the solvent can be fully recycled, is 1.96 (Scheme 4).

The waste produced during the synthesis of the reagents in Scheme 4 is also considered and, since the synthesis of 4-iodoanisole can be carried out by different methodologies, for calculation of the E factor we have selected a green process recently reported by Earle *et al.*⁴⁷ which has an E factor of 0.30 (see the ESI†) This value is lower than E = 0.80 calculated when the iodation of anisole was performed with *N*-iodosuccinimide⁴⁸ as the iodating agent in acetonitrile as solvent.

The second reactant, *i.e.* methyl vinyl ketone, is produced through the aldol condensation between acetone and



formaldehyde. The process can be carried out in either the gas phase or liquid phase. In the liquid phase,⁴⁹ the E factor is 0.99, while in the gas phase⁵⁰ the E factor is 0.60 (see the ESI†). If we accept the greener, gas phase process for calculating the global E factor for the formation of the 4-(4-methoxyphenyl)-2-butanone *via* Heck coupling, the calculated value is $E = 2.86$ (see the ESI†). When this value is compared to that obtained during the aldol condensation with the solid catalyst (Scheme 3) in a one-pot reaction, it can be concluded that the heterogeneous Heck process produces about three times more waste than the heterogeneous aldol condensation.

Finally, we have considered that the synthesis 4-(4-methoxyphenyl)-2-butanone (**2**) can also be achieved through the Heck reaction by coupling an aryl halide with a α -methylene- β -hydroxy compound in the presence of a Pd complex catalyst (Scheme 5). Specifically, the process involves the reaction between *p*-bromoanisole and methyl-3-hydroxy-2-methylene butyrate using a tetraphosphine palladium complex as a catalyst, in DMF as a solvent and in the presence of K_2CO_3 or $NaHCO_3$. The yield reported for 4-(4-methoxyphenyl)-2-butanone is 87%.⁵¹ The calculated E factor for the specific process, considering the solvent recoverable, is 3.11 (Scheme 5). The E factor involved in the preparation of the tetraphosphine palladium catalyst has not been considered here.

On the other hand, the calculated E factors for the preparation of *p*-bromoanisole and methyl-3-hydroxy-2-methylene butyrate

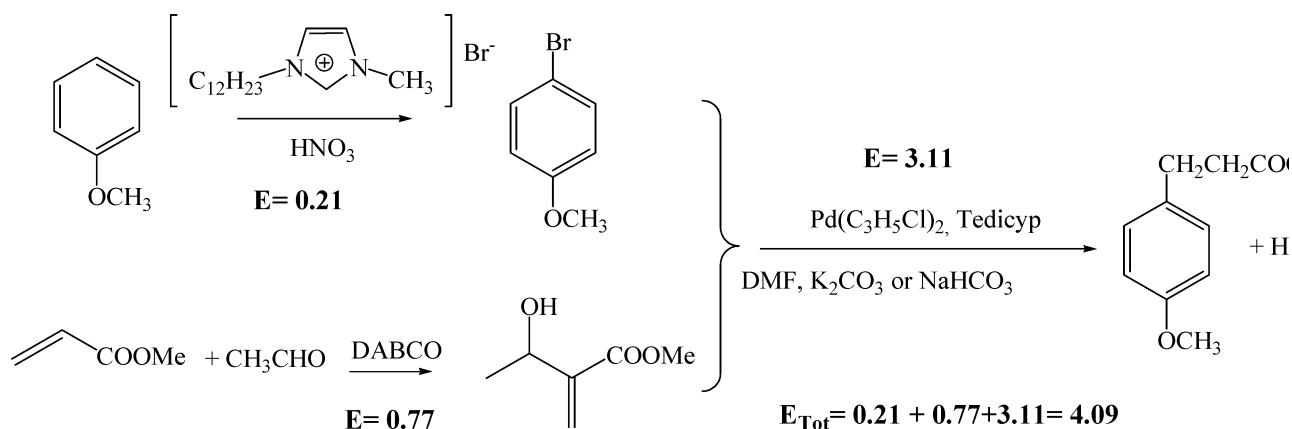
are 0.21 and 0.77, respectively (see the ESI†). Considering these two values, plus the value for the reaction in Scheme 5, the global E factor for the preparation of raspberry scent following Scheme 5 is 4.09. This is about 1.5 \times higher than the heterogeneous process described above, and approximately 5 \times higher than the one-pot process using the PdMgO catalyst.

In Table 4 the specific E factors of each compound involved in the synthesis of **2** are summarized as well as the global E factor for the heterogeneous and homogeneous Heck coupling reaction.

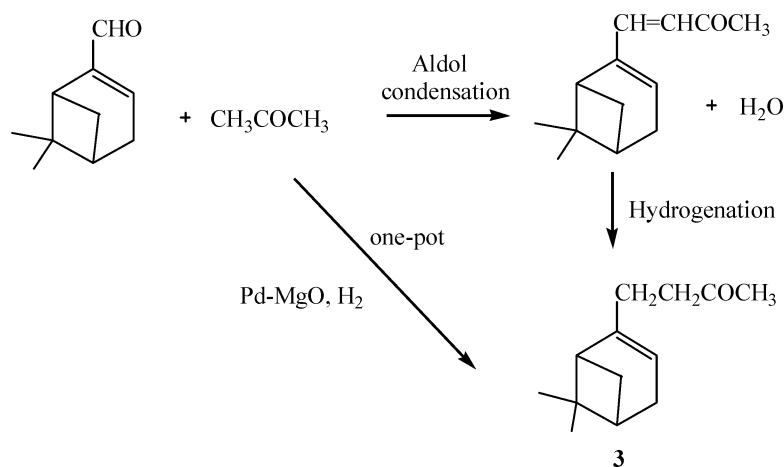
In conclusion, a new synthetic process for 4-(4-methoxyphenyl)-2-butanone with raspberry scent has been outlined that involves a one-pot process with a multifunctional (metal acid–base) solid catalyst and which has a much lower E factor than any reported before.

2. Preparation of 4-(6,6-dimethylbicyclo[3,1,1]hept-2-en-2-yl)-2-butanone (**3**)

Terpenes are important compounds for the fragrance and flavour industry. The terpenic compound 4-(6,6-dimethylbicyclo[3,1,1]hept-2-en-2-yl)-2-butanone (**3**) (Scheme 6), is used as perfume and possesses activity as an insect juvenile hormone.⁵² The conventional preparation of **3** is carried out through the acetoacetic reaction between myrthenyl bromide and ethyl acetoacetate in the presence of stoichiometric amounts of sodium ethoxide at the reflux temperature of ethanol yielding,



Scheme 5



Scheme 6

Table 4 Summary of the E factors for the synthesis of **2** through the Heck coupling reaction

Compound	E factor (heterogeneous) ^a	Reactant	E factor (homogeneous) ^a
	0.30		0.21
$\text{CH}_2=\text{CHCOCH}_3$	0.60		0.77
	1.96		3.11
Global E factor	2.86		4.09

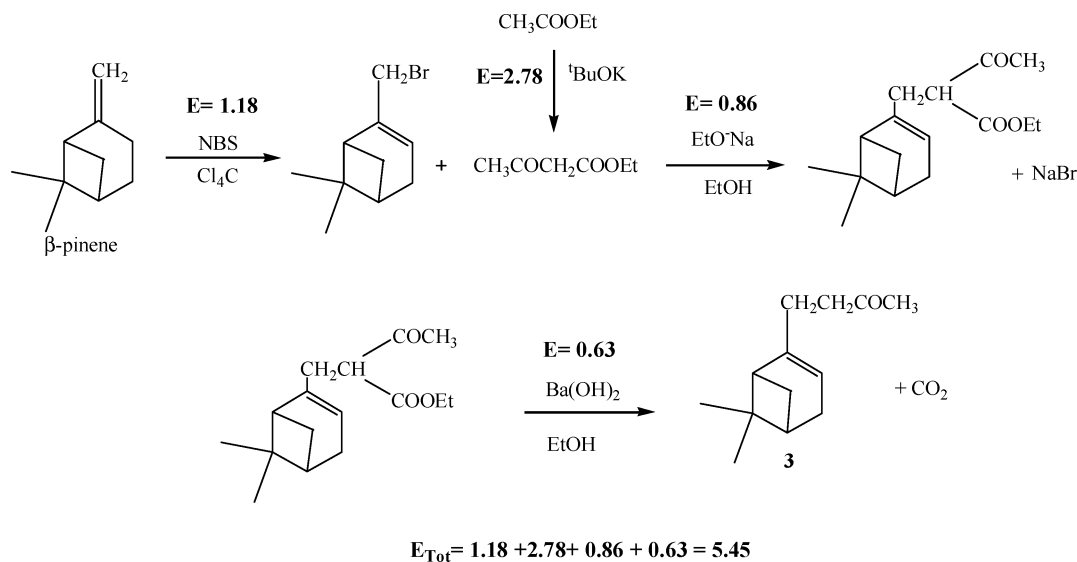
^a Referring to the specific path for synthesis of **2**.

after 4 h, 78% of ethyl 3-oxo-2-(2-pinen-10-yl) butyrate. Thus, in a second synthetic step, the ketoester is decarboxylated by

refluxing for 18 h with barium hydroxide in aqueous ethanol giving **3** in 85% yield.⁵³

We have calculated the E factor of each step of the process given in Scheme 7, starting from β -pinene, whose bromination to myrthenyl bromide can be accomplished with *N*-bromosuccinimide in refluxing CCl_4 , yielding 51% of myrthenyl bromide.⁵⁴ Taking into account that solvent and unreacted β -pinene are recoverable, we have calculated an E factor of 1.18 for the production of myrthenyl bromide. On the other hand, the second reactant involved, *i.e.*, ethyl acetoacetate, can be produced by a solvent-free Claisen condensation of ethyl acetate in the presence of $t\text{BuOK}$ that yields 75% of ethyl acetoacetate. The calculated E factor for this reaction is 2.78. Thus, the E factor of the global process presented in Scheme 7 to prepare the desired product, **3**, is 5.45.

An alternative synthetic approach is presented here (Scheme 8), in which **3** can be prepared in a one-pot cascade reaction which involves an aldol condensation between myrthenal and acetone, followed by dehydration of the aldol formed, and selective double bond hydrogenation. For calculating the E factor of the process, it has been considered that myrthenal can be obtained by oxidation of α -pinene with SeO_2 .⁵⁵ The oxidation of α -pinene is carried out with equimolar amounts of SeO_2 in the presence of a solvent such as ethanol yielding 50% of myrthenal. The E factor for this step (see Scheme 8), considering that both ethanol and the remaining α -pinene can



Scheme 7

be recycled, is 1.3. The E factor for the global process given in Scheme 8 is therefore 1.6. This value is 3.4× lower than the homogeneous process described previously for the preparation 4-(6,6-dimethylbicyclo[3,1,1]hept-2-en-2-yl)-2-butanone (**3**).

3. Preparation of 2-cyclopentylcyclopentanone (**4**)

The product 2-cyclopentylcyclopentanone (**4**) with a jasmine-like smell is used for perfume or flavouring⁵⁶ and as a wood preservative.⁵⁷ 2-Cyclopentylcyclopentanone can be synthesized by different multi-steps methods, for instance by the acyloln condensation of dimethyl glutarate in the presence of sodium (Scheme 9).⁵⁸ However, the preferred method in terms of yield and availability of starting materials, involves the condensation of cyclopentanone in the presence of a basic catalyst (NaOH, KOH or sodium) followed by the hydrogenation of the resulting 2-cyclopentylidene-cyclopentanone in the presence of a hydrogenating catalyst such as Pd/C⁵⁹ (Scheme 10). Thus, by reacting cyclopentanone at 90 °C in the presence of a 10% aqueous solution of NaOH, a 54% yield of 2-cyclopentylidene-cyclopentanone (**5**) was obtained after 3 h reaction time. After purification by distillation at reduced pressure, the compound is hydrogenated using palladium (5 wt%) on activated carbon as catalyst, yielding 89% of 2-cyclopentylcyclopentanone (**4**). The main drawback associated with this methodology is, in general, the low yields of 2-cyclopentylidene-cyclopentanone (**6**) achieved, due to the fact that the self-condensation product can further condense with a second cyclopentanone molecule to form the highly conjugated trimer adduct (2,5-dicyclopentylidene-cyclopentanone) (**6**). Due to the high thermodynamic stability of the conjugated trimer adduct, this compound is formed in important amounts that, depending on reaction conditions, can reach to between 30 and 50%.⁶⁰

It appeared to us that if the reaction was performed in a one-pot system in which the rate of hydrogenation of the condensation product was very high, then the second condensation that leads to formation of the trimer (**6**) could

Table 5 Summary of the E factors for the synthesis of **4**

Compound	E factor (heterogeneous)	E factor (homogeneous)
4	0.10	1.16

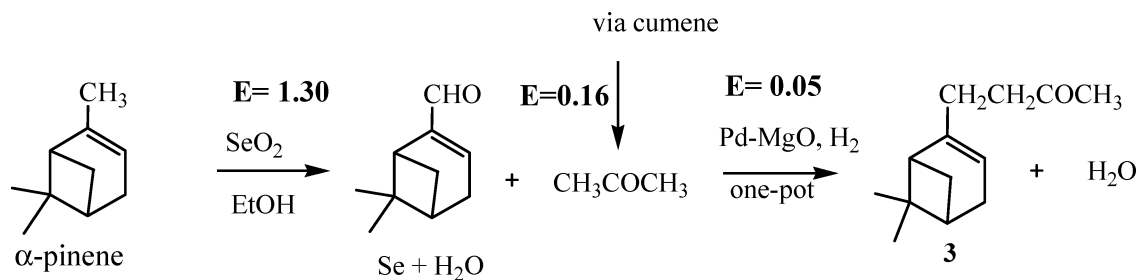
be avoided or, at least, could be strongly diminished, giving a higher final selectivity to 2-cyclopentylcyclopentanone (**5**) (Scheme 10). To do this, cyclopentanone was reacted in the presence of PdMgO under a constant hydrogen pressure at 140 °C. After 8 h reaction time, the conversion was 98% with 91% selectivity for **4**. Under our reaction conditions, the hydrogenated trimer (2,5-dicyclopentylcyclopentanone) (**6**) and 2-cyclopentylcyclopentanol were also detected, with yields of 10 and 2%, respectively. The higher selectivity towards **4** achieved in this case, with respect to the conventional procedure, demonstrates the advantage of the one-pot cascade process using the PdMgO catalyst. In this case, it appears that the fast hydrogenation of the intermediary, 2-cyclopentylidene-cyclopentanone, diminishes the rate of the subsequent aldol condensation that leads to the undesired highly-conjugated trimer.

As shown in Scheme 10, the E factor for the heterogeneous-catalyzed, one-pot cascade process is one order of magnitude lower than the conventional method.

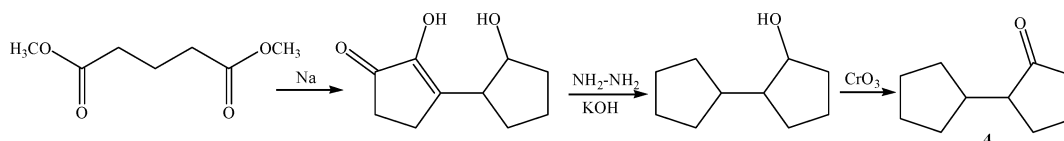
Table 5 summarizes the E factors for the synthesis of **4** using heterogeneous and homogeneous catalysts.

Conclusions

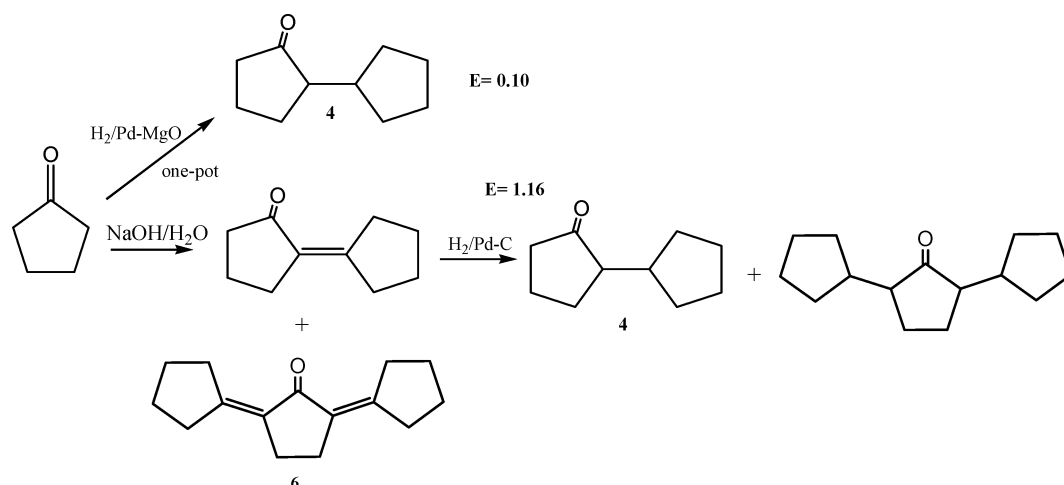
We have illustrated here that process intensification by means of multifunctional solid catalysts that allow one-pot



Scheme 8



Scheme 9



Scheme 10

cascade reactions, opens new, more environmentally benign routes than those currently used for the synthesis of fine chemicals.

Since, in many cases, the new routes proposed require starting from different reactants than the conventional routes, we have also calculated the E factor for the global process starting from the primary products. It has been seen that, in most cases, the new one-pot cascade reactions have E factors which are one order of magnitude lower. The differences in the E factor can be even larger if one considers the energy involved and even the investments, since the one-pot processes do not require intermediate separations.

Finally, it has been shown that, in some cases, higher selectivities can be achieved in the one-pot cascade reactions with multifunctional catalysts, by adjusting the relative rates of the different consecutive steps.

Experimental

Preparation of catalysts

A nanocrystalline MgO sample was purchased from NanoScale Materials Inc.

The magnesium–aluminium layered double hydroxide sample (Mg–Al LDH) was prepared from a gel produced by mixing two solutions, A and B. Solution A contained $(3 - x)$ mol of $\text{Mg}(\text{NO}_3)_2 \cdot 6\text{H}_2\text{O}$ and x mol of $\text{Al}(\text{NO}_3)_3 \cdot 9\text{H}_2\text{O}$ in the (Al + Mg) concentration of 1.5 mol L^{-1} for an Al/(Al + Mg) molar ratio of 0.25. Solution B was formed by $(6 + x)$ mol of NaOH and 2 mol of Na_2CO_3 dissolved in the same volume as solution A. Both solutions were co-added at a rate of 1 mL min^{-1} under vigorous mechanical stirring at room temperature. The gel was aged under autogeneous pressure conditions at 333 K for 12 h. Then, the

hydrotalcite was filtered and washed until pH = 7 and the solid was dried. The Mg–Al mixed oxide (HTc) base catalyst was obtained by calcination of Mg–Al-LDH at 723 K for 6 h in a dry nitrogen flow.

Pd catalysts at 1 wt% loading were obtained by exposing the Mg–Al-LDH or MgO samples to an anhydrous toluene solution with the required amount of palladium acetylacetonate (Pd(OAc)₂) for 12 h. After evaporation of toluene at reduced pressure, the solid was dried overnight at 80 °C in vacuum and then calcined in nitrogen flow at 550 °C for 3.5 h. These samples were denoted as PdHTc (calcined hydrotalcite) and PdMgO

The PdHTc sample was rehydrated at room temperature by direct addition of decarbonated water (MilliQ) (36 wt%) just before their use as catalyst, and was labelled as PdHTr.

Samples of PdMgO and PdHTc were activated before reaction by heating the solid at 450 °C under air for 5 h and then 5 h under nitrogen. Reduction of the Pd(II) was performed by heating the solid at 450 °C in a flow of H₂/N₂ (90/10) for 2 h.

The catalysts prepared were characterized by XRD (Fig. 1), TEM and nitrogen adsorption. N₂ adsorption/desorption isotherms were performed at 77 K in an ASAP 2010 apparatus from Micromeritics, after pre-treating the samples under vacuum at 673 K overnight and the BET surface areas were obtained using the BET methodology. The main characteristics of the catalysts are given in Table 6.

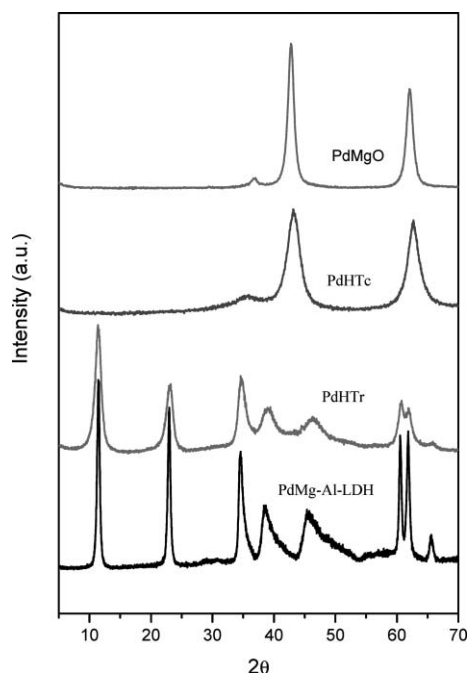


Fig. 1 XRD patterns of the solid catalysts.

Reaction procedure

For a typical experiment, the reactants were placed in a batch slurry reactor which was immersed in a thermostated silicone oil bath and magnetically stirred. When the temperature was reached, the catalyst was added and hydrogen was applied at a constant hydrogen pressure of 5 bar. The course of the reaction was followed by gas chromatography (GC) using a Hewlett

Table 6 Selected physical parameters for the catalysts used in the study

Catalyst	Surface area/m ² g ⁻¹	Total pore volume/cc g ⁻¹	Average pore diameter/Å	Crystallite size/nm ^a
PdHTc	258	0.543	86	< 50
PdHTr	21	—	—	—
PdMgO	670	0.644	39.55	3

^a Crystallite size measured by X-ray diffraction.

Packard GC 5988 A with FID detector and a HP-5 capillary column of 5% phenylmethylsilicone. In all the experiments, dodecane was used as an internal standard. At the end of the reaction, after cooling, the reaction mixture was filtered to remove the catalyst. The solid was extracted thoroughly in a Soxhlet apparatus using methanol as a solvent and the extract considered in the mass balance. The reaction mixture was concentrated under reduced pressure and the reaction products were analyzed by GC-MS (Varian Saturn II, using the same column as GC) and ¹H NMR spectroscopy (Varian Gemini-300 MHz, CDCl₃ as a solvent).

One-pot synthesis of 4-(4-methoxyphenyl)2-butanone (2)

4-methoxybenzaldehyde (3.8 mmol), was reacted with acetone (37 mmol) in the presence of PdMgO (1 wt% of Pd) (38 wt% with respect to 4-methoxybenzaldehyde) under constant hydrogen pressure (5 bar) at 75 °C. After 75 min reaction time, 100% conversion of 4-methoxybenzaldehyde with 99% selectivity for 2 was obtained.

One-pot synthesis of 4-(6,6-dimethylbicyclo[3,1,1]hept-2-en-2-yl)-2-butanone (3)

Myrthenal (3.9 mmol) was reacted with acetone (48 mmol) in the presence of PdMgO (1 wt% of Pd) (34 wt% with respect to myrthenal) under constant hydrogen pressure (5 bar) at 75 °C for 3 h. The target molecule was obtained in 95% yield.

One-pot synthesis of 2-cyclopentylcyclopentanone (4)

Cyclopentanone (10.7 mmol) was reacted in the presence of PdMgO (21 wt%) under a constant hydrogen pressure (5 bar) at 140 °C during 8 h. A 98% conversion of cyclopentanone with 91% selectivity for 4 was achieved.

Regeneration of the catalysts

PdHTr and PdMgO samples were regenerated after each use by calcination of the solids at 450 °C under air atmosphere for 5 h and then under nitrogen for 5 h. Reduction of the Pd was performed by heating the solid at 450 °C in a flow of H₂/N₂ (90/10) for 2 h.

Acknowledgements

The authors thank CICYT for financial support (Project MAT 2006-14274-C02-01). The contribution of Mr Pablo Ramos to the experimental work reported herein is also gratefully acknowledged.

References

- 1 R. A. Sheldon, *Chem. Ind. (London)*, 1992, 903.
- 2 A. Bruggink, R. Schoevaart and T. Kieboom, *Org. Process Res. Dev.*, 2003, **7**, 622.
- 3 N. Hall, *Science*, 1994, **266**, 32.
- 4 K. M. Koeller and C. H. Wong, *Chem. Rev.*, 2000, **100**, 4465.
- 5 F. Gelman, J. Blum and D. Avnir, *J. Am. Chem. Soc.*, 2000, **122**, 11999.
- 6 J. C. Wasilke, S. J. Obrey, R. T. Baker and G. C. Bazan, *Chem. Rev.*, 2005, **105**, 1001.
- 7 A. Corma and M. Renz, *Angew. Chem., Int. Ed.*, 2007, **46**, 298.
- 8 A. Corma, M. Renz and C. Schaverien, *ChemSusChem*, 2008, **1**, 739.
- 9 A. Corma, V. Fornes, S. Iborra, M. Mifsud and M. Renz, *J. Catal.*, 2004, **221**, 67.
- 10 X. Zhang and A. Corma, *Angew. Chem., Int. Ed.*, 2008, **47**, 4358.
- 11 M. J. Climent, A. Corma, S. Iborra and M. Mifsud, *J. Catal.*, 2007, **247**, 223.
- 12 M. J. Climent, A. Corma, S. Iborra and M. Mifsud, *Adv. Synth. Catal.*, 2007, **349**, 1949.
- 13 B. M. Choudary, N. S. Chowdari, S. Madhi and M. L. Kantam, *J. Org. Chem.*, 2003, **68**, 1736.
- 14 F. Zhang, G. Liu, W. He, H. Yin, X. Yang, H. Li, J. Zhu, H. Li and Y. Lu, *Adv. Funct. Mater.*, 2008, **18**, 3590.
- 15 F. X. Felpin and E. Fouquet, *ChemSusChem*, 2008, **1**, 718.
- 16 M. J. Climent, A. Corma and S. Iborra, *ChemSusChem*, 2009, **2**, 500.
- 17 A. Corma, P. Serna and H. Garcia, *J. Am. Chem. Soc.*, 2007, **129**, 6358.
- 18 M. J. Climent, A. Corma, S. Iborra, L. L. Santos, *Chem. A Eur. J.*, in press.
- 19 N. Das, D. Tichit, R. Durand, P. Graffin and B. Coq, *Catal. Lett.*, 2001, **71**, 181.
- 20 R. Unnikrishnan and S. Narayanan, *J. Mol. Catal. A: Chem.*, 1999, **144**, 173.
- 21 Y. Z. Chen, C. M. Hwang and C. W. Liaw, *Appl. Catal., A*, 1998, **169**, 207.
- 22 W. Ferry, A. J. van Pillen and K. P. de Jong, *J. Mol. Catal. A: Chem.*, 2004, **219**, 273.
- 23 M. J. Martínez-Ortiz, D. Tichit, P. Gonzalez and B. Coq, *J. Mol. Catal. A: Chem.*, 2003, **201**, 199.
- 24 J. I. Di Cosimo, G. Torres and C. R. Apesteguía, *J. Catal.*, 2002, **208**, 114.
- 25 C. Carlini, C. Flego, M. Marchionna, M. Novello, A. M. Raspolli Galletti, G. Sbrana, F. Basile and A. Vaccari, *J. Mol. Catal. A: Chem.*, 2004, **220**, 215.
- 26 C. Carlini, C. Flego, M. Marchionna, M. Novello, A. M. Raspolli Galletti, G. Sbrana, F. Basile and A. Vaccari, *J. Mol. Catal. A: Chem.*, 2005, **232**, 13.
- 27 G. Torres, C. R. Apesteguía and J. I. Di Cosimo, *Appl. Catal., A*, 2007, **317**, 161.
- 28 D. Tichit, M. J. Martínez-Ortiz, D. Francova, C. Gerardin, B. Coq, R. Durand, F. Prinetto and G. Ghiotti, *Appl. Catal., A*, 2007, **318**, 170 and references cited therein.
- 29 D. Tichit, B. Coq, S. Cerneaux and R. Durand, *Catal. Today*, 2002, **75**, 197.
- 30 K. Motokura, N. Fujita, K. Mori, T. Mizugapi, K. Ebitani and K. Kaneda, *Tetrahedron Lett.*, 2005, **46**, 5507.
- 31 K. Kasahara, H. Nakanishi, JP Pat., 2002370929, 2002.
- 32 Badische Anilin and Soda Fabrick, A. G. Ger. Offen. Pat., 2145308, 1973.
- 33 Chisso Corp Jpn. Kokai Tokkyo Koho JP Pat. 55151530 (1980).
- 34 J. Tateiwa, H. Horiuchi, K. Hashimoto, T. Yamauchi and S. Uemura, *J. Org. Chem.*, 1994, **59**, 5901.
- 35 S. Paul and M. Gupta, *Synth. Commun.*, 2005, **35**, 213.
- 36 Y. Kido, T. Hamazaki, K. Yoneda and T. Ohnishi, JP Pat., 2000103754, 2000.
- 37 A. Corma and S. Iborra, *Adv. Catal.*, 2006, **49**, 239.
- 38 R. Teissier, D. Tichit, F. Figueras, and J. Kervennal, F Pat., 2729137, 1995.
- 39 M. J. Climent, A. Corma, S. Iborra and A. Velty, *J. Catal.*, 2004, **221**, 474.
- 40 (a) A. Guida, M. H. Lhouty, D. Tichit, F. Figueras and P. Geneste, *Appl. Catal., A*, 1997, **164**, 251; (b) K. K. Rao, M. Gravelle, J. Valente and F. Figueras, *J. Catal.*, 1998, **173**, 115.
- 41 M. J. Climent, A. Corma, S. Iborra and A. Velty, *Catal. Lett.*, 2002, **79**, 157.
- 42 J. A. A. Roelofs, D. J. Lensveld, A. J. van Dillen and K. P. De Jong, *J. Catal.*, 2001, **203**, 184.
- 43 M. J. Climent, A. Corma, S. Iborra and A. Velty, *Green Chem.*, 2002, **4**, 474.
- 44 M. L. Kantam, B. M. Choudary, C. V. Reddy, K. K. Rao and F. Figueras, *Chem. Commun.*, 1998, 1033.
- 45 B. M. Choudary, M. L. Kantam, C. V. Reddy, K. K. Rao and F. Figueras, *J. Mol. Catal. A: Chem.*, 1999, **146**, 279.
- 46 G. Vergne, O. Dabard and F. Cornille, FR Pat., 2824555, 2001 (assigned to Societe Nationale des poudres et explosives).
- 47 M. Earle and S. P. Katdare, WO Pat., 0230852, 2002.
- 48 A. S. Castanet, F. Colobert and P. E. Broutin, *Tetrahedron Lett.*, 2002, **43**, 5047.
- 49 J. Pugach and J. S. Salek, US Pat., 5004839, 1990 (assigned to Aristech Chemical Corp).
- 50 I. Gummin and P. Noesberger, WO Pat., 2007115832, 2007 (assigned to DSM IP ASSETS B.V.).
- 51 F. Berthiol, H. Doucet and M. Santelli, *Tetrahedron*, 2006, **62**, 4372.
- 52 L. Borowiecki, A. Kazubski, E. Reza and W. Wlodzimierz, *Liebigs Ann. Chem.*, 1985, **1985**, 929.
- 53 L. Borowiecki, A. Kazubski and E. Reza Liebigs, *Ann. Chem.*, 1982, 1766.
- 54 G. Zweifel and C. C. Whitney, *J. Org. Chem.*, 1966, **31**, 4178.
- 55 (a) J. A. Retamar, *Bull. Soc. Chim. Fr.*, 1996, 1227; (b) J. A. Retamar, *Essenze Derivati Agrumari*, 1989, **59**, 159.
- 56 S. Shiozaki, M. Senuma, S. Furumai and H. Kawashima, E Pat., 16650, 1980.
- 57 Nippon Zeon Co., Jpn. Kokai Tokkyo Koho JP Pat., 57056401, 1982.
- 58 M. Cordon, J. D. Knight and D. J. Cram, *J. Am. Chem. Soc.*, 1954, **76**, 1643.
- 59 S. Shiozaki, M. Senuma, S. Furumai and H. Kawashima, E Pat., 16650 19801001, 1980.
- 60 (a) P. Rollin, *Bull. Soc. Chim. Fr.*, 1973, **4**, 1509; (b) S. V. Svetozarskii, G. A. Razuvaev, E. N. Zilberman and G. S. Volkov, *Zh. Obshch. Khim.*, 1960, **30**, 2042.

A highly efficient Cu/La₂O₃ catalyst for transfer dehydrogenation of primary aliphatic alcohols

Ruijuan Shi, Fei Wang, Tana, Yong Li, Xiumin Huang and Wenjie Shen*

Received 6th June 2009, Accepted 22nd September 2009

First published as an Advance Article on the web 27th October 2009

DOI: 10.1039/b919807p

La₂O₃-supported copper nanoparticles are sufficiently active for transfer dehydrogenation of primary aliphatic alcohols to aldehydes. When used for 1-octanol, the yield of 1-octanal can be as high as 63%. The catalyst is also highly effective for a wide variety of substrates, such as aromatic, aliphatic, and cyclic alcohols. The yield of the desired products approaches 100% and the turnover frequency is 86.5 h⁻¹. The synergistic effect between the basicity of La₂O₃ and the hydrogen spillover of Cu particle contributes significantly to the extremely high activity of the Cu/La₂O₃ catalyst for transfer dehydrogenation of primary aliphatic alcohols.

Introduction

Catalytic transformation of alcohols to aldehydes or ketones is perhaps the most demanding reaction in organic and green chemistry.¹ Selective oxidation of alcohols using molecular oxygen and/or hydrogen peroxide as green oxidants has been used to replace the conventional oxidation process using stoichiometric quantities of inorganic oxidants (typically, KMnO₄ and K₂Cr₂O₇) which produce enormous amounts of toxic waste.^{2,3} In this field, supported Au, Pd, Pt, and Ru nanoparticles exhibit very high activity for the oxidation of allylic and benzylic alcohols to aldehydes or ketones using molecular oxygen, but they are poorly active for the oxidation of primary aliphatic alcohols.^{3–6} Only Ru-based catalysts afford desirable performance in the oxidation of primary aliphatic alcohols, with the yield of aldehydes in the range 70–90%.^{6–10} However, the oxidation of alcohols using molecular oxygen often causes safety problems linked with the use of flammable organic solvents, particularly in large-scale production processes.^{4–6}

Transfer dehydrogenation of alcohols has been recently proposed to be a green and efficient reaction route, in which the alcohol is directly dehydrogenated to aldehyde or ketone and the readily available unsaturated organic molecule (as a hydrogen acceptor) removes the hydrogen.⁶ Unfortunately, only a few heterogeneous catalysts are known to be effective for this novel process, and they are active only for secondary and allylic/aromatic alcohols.^{11–18} Hayashi and co-workers^{11,12} reported that Pd/C catalyzed the dehydrogenation of allylic and aromatic alcohols with moderate yields (75–86%, 323 K, 2–4 days) using ethylene or nitrobenzene as hydrogen acceptor. Baiker and co-workers¹³ reported that transfer dehydrogenation of aromatic alcohols occurred over a Pd/Al₂O₃ catalyst using cyclohexene as hydrogen acceptor, but this catalyst was nearly inactive for aliphatic and alicyclic alcohols, and the yield of

1-octanal was only 1% in the case of 1-octanol. Ravasio and co-workers^{14,15} revealed that a Cu/Al₂O₃ catalyst was highly active for the transfer dehydrogenation of allylic and alicyclic alcohols, but it was less active for 1-octanol, the yield of 1-octanal being only 4%. Over a Ru/AlO(OH) catalyst at 383 K for 24 h under argon atmosphere, 1-octanol was converted into a complex mixture containing 23% of 1-octanal.¹⁶ More recently, Kaneda and co-workers^{17,18} found that Ag and Cu nanoparticles supported on a basic hydrotalcite (HT) showed excellent catalytic performance for acceptor-free dehydrogenation of benzylic and secondary aliphatic alcohols. However, they were not effective for primary aliphatic alcohols, and the conversion of 1-octanol was only 17%, although the selectivity of 1-octanal was 99% on the Ag/HT catalyst.¹⁷

Clearly, the majority of known catalysts are still poorly active for the dehydrogenation of primary aliphatic alcohols. Here we report that a Cu/La₂O₃ catalyst affords fairly high activity for the transfer dehydrogenation of primary aliphatic alcohols through a synergistic effect between the basicity of the support and the fast hydrogen spillover of Cu nanoparticles.

Experimental

Catalyst preparation

The Cu/La₂O₃ catalyst was prepared by a deposition–precipitation method. 0.55 g copper acetate monohydrate (Cu(CH₃COO)₂·H₂O) was dissolved in 200 ml water, and 1.8 g commercially available La₂O₃ powder was then dispersed into the solution with stirring at room temperature. Subsequently, 40 ml sodium carbonate aqueous solution (0.1 M) was added dropwise to the mixture to achieve a final pH value of 8. The precipitate was further aged in the mother liquid for 2 h. After being filtered and washed thoroughly with water, the resultant solid was dried at 383 K overnight and calcined at 723 K for 4 h in air, giving the CuO/La₂O₃ precursor. 200 mg CuO/La₂O₃ sample was then loaded in a fixed-bed reactor and reduced with pure hydrogen (40 ml min⁻¹) at 573 K for 1 h, yielding the Cu/La₂O₃ catalyst.

State Key Laboratory of Catalysis, Dalian Institute of Chemical Physics, Chinese Academy of Sciences, Dalian, 116023, China.
E-mail: shen98@dicp.ac.cn; Fax: +86-411-84694447;
Tel: +86-411-84379085

Catalyst characterization

The actual loading of copper was measured by inductively coupled plasma atomic emission spectroscopy (ICP-AES) on a Plasma-Spec-II instrument. 20 mg CuO/La₂O₃ was dissolved in concentrated hydrochloric acid and the mixture was diluted with water to meet the detection range of the instrument.

The N₂ adsorption–desorption isotherms were performed using a Micrometrics ASAP 2010 instrument at 77 K. Before the measurement, the sample was degassed at 573 K for 3 h. The surface area was calculated from a multipoint BET analysis of the adsorption isotherm.

The X-ray powder diffraction (XRD) patterns were recorded on a D/MAX 2500/PC powder diffractometer (Rigaku) operated at 40 kV and 200 mA, using Cu-K α (1.5418 Å) radiation. *In situ* XRD measurement for the reduction of the CuO/La₂O₃ sample was performed in a high-temperature chamber installed in the diffractometer. The CuO/La₂O₃ sample was pressed into a flake and mounted in the chamber. After heating to 573 K in the flow of He, pure hydrogen was introduced into the chamber and kept at 573 K for 1 h and the XRD patterns were then recorded.

Transmission electron microscopy (TEM) images were recorded on a FEI Tecnai G² Spirit microscope operated at 120 kV. The specimen was prepared by ultrasonically dispersing the sample powder in ethanol and drops of the suspension were deposited on a clean carbon-coated copper grid and dried in air.

Temperature-programmed reduction (H₂-TPR) was conducted in a U-shape quartz reactor connected to a mass spectrometry (OmniStar 200). 100 mg CuO/La₂O₃ sample was heated to 673 K at a rate of 10 K min⁻¹ under He flow (50 ml min⁻¹) and maintained at this temperature for 1 h. After being cooled to room temperature, a 20 vol.% H₂/He mixture (30 ml min⁻¹) was introduced and the sample was heated to 723 K at a rate of 10 K min⁻¹ and kept at this temperature for 1 h.

The dispersion of copper in the Cu/La₂O₃ catalyst was determined by N₂O chemisorption.¹⁹ 50 mg of the CuO/La₂O₃ sample was loaded in a U-shape quartz reactor and treated with a 20 vol.% O₂/N₂ mixture (30 ml min⁻¹) at 673 K (10 K min⁻¹) for 0.5 h. After being cooled to room temperature, a 5 vol.% H₂/N₂ mixture (30 ml min⁻¹) was introduced and the sample was heated to 673 K at a rate of 5 K min⁻¹. Then, the sample was cooled to 363 K under He flow and further purged for 30 min. Subsequently, the sample was exposed to a 10 vol.% N₂O/He mixture for 30 min at 363 K and then cooled to room temperature under a He flow. A 5 vol.% H₂/N₂ mixture (30 ml min⁻¹) was introduced and the sample was heated to 573 K at a rate of 5 K min⁻¹. The dispersion of copper and the average size of copper particles were calculated by assuming 1.46 × 10¹⁹ copper atoms per m² and a N₂O/Cu ratio of 1:2.

The IR spectra of CO adsorption were recorded on a Bruker vector-22 FTIR spectrometer. The sample powder was pressed into a self-supporting wafer (20 mg) and mounted into the IR cell. The sample was first reduced with pure H₂ (40 ml min⁻¹) at 573 K for 1 h and then evacuated at 673 K (2 × 10⁻² Pa) for 5 h. After acquisition of the background spectrum, the sample was exposed to CO with increasing pressure (5–500 Pa) at room temperature. Then the cell was evacuated and heated from room temperature to 373 K. The spectra of CO adsorption on the

Cu/La₂O₃ catalyst were obtained by subtracting the background spectrum.

The temperature-programmed desorption of CO₂ (CO₂-TPD) was conducted in a U-shape quartz reactor connected to a mass spectrometry (OmniStar 200). 100 mg CuO/La₂O₃ sample was heated at a rate of 10 K min⁻¹ to 723 K under He flow (30 ml min⁻¹) and maintained at this temperature for 1 h in order to remove the surface impurities. Then the sample was reduced with pure H₂ at 573 K for 1 h. After being cooled to room temperature under He flow, the sample was exposed to a mixture of 30 vol.% CO₂/He (20 ml min⁻¹) for 0.5 h. Subsequently, the sample was purged with He (50 ml min⁻¹) for 2 h and then heated to 1073 K at a rate of 10 K min⁻¹. Desorption of CO₂ was monitored by the mass spectrometry.

The X-ray photoelectron spectroscopy (XPS) and Auger electron spectroscopy (AES) were performed on an ESCALAB MK-II X-ray photoelectron spectrometer (VG Scientific Ltd, UK). The CuO/La₂O₃ sample was pressed into a thin disc and mounted on a sample rod placed in a pretreatment chamber, in which the sample was reduced by pure H₂ at 573 K for 1 h. Then the sample was transferred into the analysis chamber where the spectra of Cu 2p, Cu L3VV levels were recorded. The charging effect was corrected by adjusting the binding energy of C 1s to 284.6 eV.

Catalytic test

Transfer dehydrogenation of alcohols was conducted with a stainless steel autoclave (50 ml). Typically, the reaction mixture contained 2 mmol alcohol, 4 mmol styrene (hydrogen acceptor), 200 mg Cu/La₂O₃ catalyst and 8 ml mesitylene. The reaction was performed at 363–423 K for a certain period (0.5–24 h) under N₂ atmosphere. The yield of products was analyzed by Agilent GC-7890T (HP-5 capillary column) using decane as an internal standard. The turnover frequency (TOF) was defined as the moles of product formed per mole of Cu per hour, and the dispersion of copper was determined by N₂O chemisorption measurement.

Results and discussion

Fig. 1 shows the XRD patterns of the samples. Bare La₂O₃ showed typical diffraction peaks of hexagonal structure (JCPDS 05-0602) and the average crystallite size was 94 nm. The

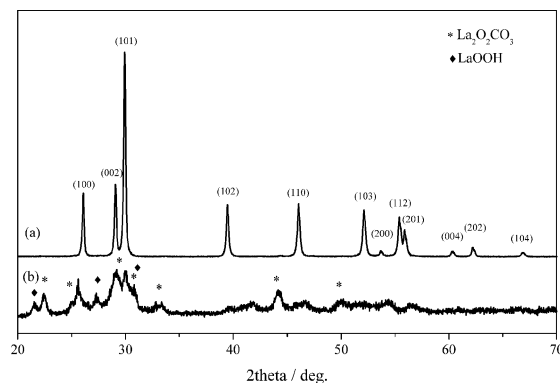


Fig. 1 XRD patterns of La₂O₃ (a) and Cu/La₂O₃ (b).

Cu/La₂O₃ catalyst also exhibited the diffraction peaks of hexagonal La₂O₃, but lanthanum carbonate (La₂O₂CO₃, JCPDS 37-0804) and oxyhydroxide (LaOOH, CPDS 19-0656) phases were also detected. This is caused by the interaction of lanthanum oxide with water and carbon oxide during copper loading and calcination process.²⁰ The absence of diffraction lines of Cu species indicates that they were highly dispersed on the surface of La₂O₃, or they were too small to be detected. The Cu/La₂O₃ catalyst had a surface area of 22 m² g⁻¹, and the copper loading was 8.4 wt%.

Fig. 2 shows the H₂-TPR profiles of bulk CuO and CuO/La₂O₃. The reduction of bulk CuO occurred at 539 K, whereas the reduction of CuO in the CuO/La₂O₃ sample shifted to a much lower temperature region – the main reduction took place at 432 K with a small shoulder at 415 K. The minor reaction peak was ascribed to the reduction of finely dispersed CuO species, while the major peak corresponded to the reduction of CuO species strongly interacting with La₂O₃. The H₂ consumption for the CuO/La₂O₃ sample was estimated as 1.25 mmol g⁻¹, which is very close to the stoichiometric value (1.32 mmol g⁻¹) for the total reduction of CuO species, indicating the sole presence of metallic copper in the Cu/La₂O₃ catalyst.

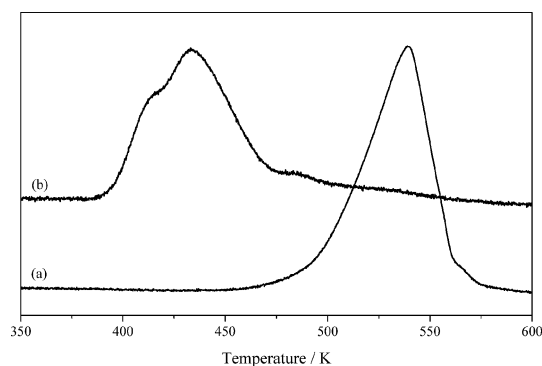


Fig. 2 H₂-TPR profiles of CuO (a) and CuO/La₂O₃ (b).

Fig. 3 shows the TEM images of the Cu/La₂O₃ catalyst. The La₂O₃ support was composed of spherical nanoparticles with an average size of about 30 nm. The Cu particles could not be clearly observed, probably due to the small size and the poor contrast between Cu and La₂O₃. However, the N₂O chemisorption measurement revealed that the mean size of

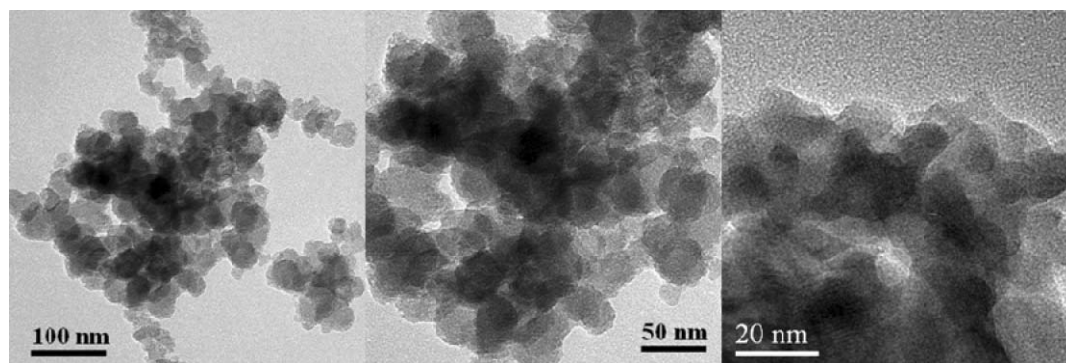


Fig. 3 TEM images of the Cu/La₂O₃ catalyst.

copper particle was about 6 nm, giving a copper dispersion of about 17%.

Fig. 4 shows the FTIR spectra of CO absorption on the Cu/La₂O₃ catalyst. Generally, the band of CO absorption on Cu²⁺ site is above 2140 cm⁻¹; weakly bound CO on Cu⁰ shows a clear stretching frequency below 2110 cm⁻¹; while CO adsorption on Cu⁺ is located between 2110 and 2135 cm⁻¹.²¹ The Cu⁰-CO band is easily decomposed at 298–373 K, but the Cu⁺-CO band is relatively stable and can be present at 373 K.²² CO adsorption at room temperature on the Cu/La₂O₃ catalyst showed a band at 2098 cm⁻¹, indicating the presence of a Cu⁰-CO band. This is similar to the previous observation of CO adsorption on Cu⁰ at 2100 cm⁻¹ on a Cu/TiO₂ catalyst.²³ As the pressure of CO increased, the band slightly shifted to 2102 cm⁻¹ and the intensity was enhanced significantly. Upon heating, the Cu⁰-CO band weakened, and it totally disappeared at 373 K. This further confirms that the copper species are present as Cu⁰ in the Cu/La₂O₃ catalyst.

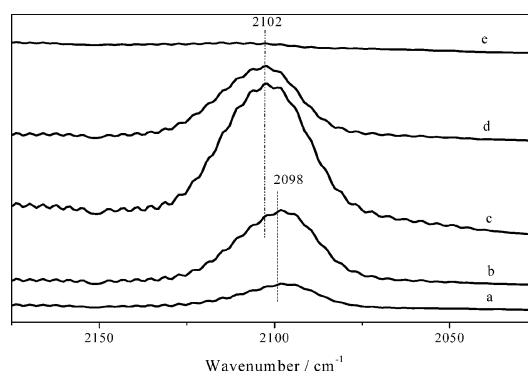


Fig. 4 FTIR spectra of CO adsorbed on the Cu/La₂O₃ catalyst. CO pressure of 5 Pa (a), 20 Pa (b), and 100 Pa (c), followed by evacuation at 323 K (d) and 373 K (e).

Fig. 5 shows the X-ray photoelectron spectra of Cu 2p and Cu L₃VV Auger in the Cu/La₂O₃ catalyst. Obviously, the disappearance of the satellite peak and the binding energy of Cu 2p_{3/2} at 932.0 eV shows that the copper exists as Cu⁰ or Cu⁺ (Fig. 5A). The Cu⁰ and Cu⁺ species cannot be distinguished by the binding energy of Cu 2p_{3/2} because they are almost identical, but they can be easily distinguished from the Cu L₃VV Auger lines, where Cu⁰ and Cu⁺ are separated by 2.0 eV.²⁴ The kinetic energy of Cu L₃VV at 918.3 eV confirmed that Cu⁰ is the main

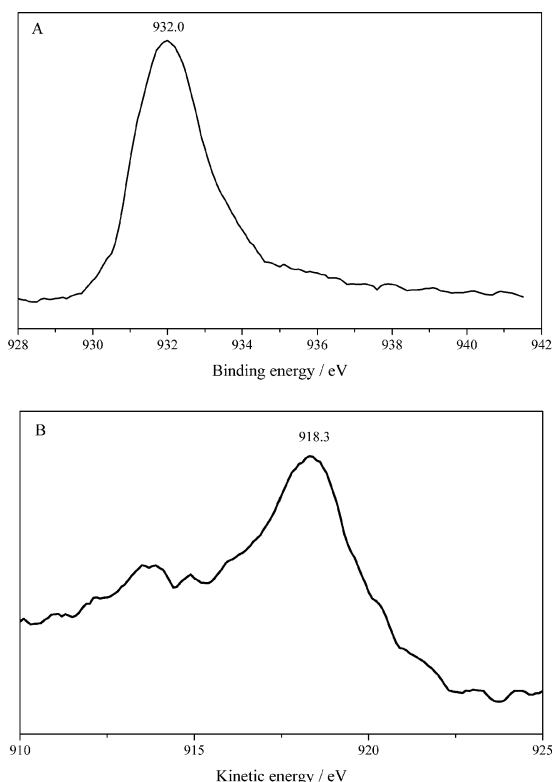


Fig. 5 XPS spectra of Cu 2p (A) and Cu L3VV Auger (B) in the Cu/La₂O₃ catalyst.

species in the Cu/La₂O₃ catalyst.²⁵ These findings are in line with the H₂-TPR and FTIR results, which showed the sole presence of metallic Cu after hydrogen reduction at 573 K.

Fig. 6 shows the CO₂-TPD profile of the Cu/La₂O₃ catalyst. Desorption of CO₂ occurred at 354, 390 and 501 K, and the relative areas were 21, 41 and 38%, respectively. This indicates that there are three types of adsorption sites for CO₂ with different basicity strengths. Previous CO₂-TPD^{26,27} and FTIR^{26–28} studies have readily revealed that the hydroxy groups on the surface of La₂O₃ have a weakly basic character; CO₂ adsorption on the medium strength basic sites (bidentate carbonates) gave CO₂ desorption at intermediate temperature, and CO₂ adsorption on the strong strength basic sites (unidentate carbonates) desorbed

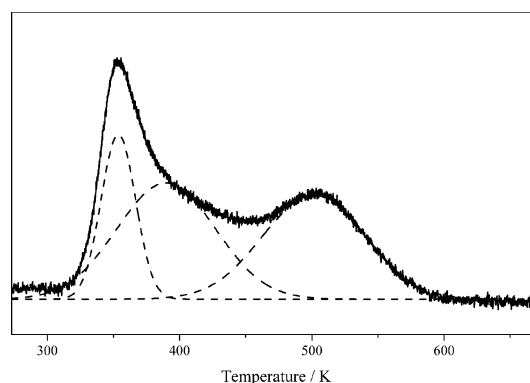


Fig. 6 CO₂-TPD profile of the Cu/La₂O₃ catalyst.

at high temperature. Therefore, the desorption peak at 354 K is ascribed to the weak basic sites (OH groups), while the desorption peak at 390 K and 501 K represents the moderately basic (La–O²⁻ pairs) and strongly basic (O²⁻ ions) sites on the Cu/La₂O₃ catalyst, respectively.

Table 1 summarizes the reaction results of transfer dehydrogenation of alcohols on the Cu/La₂O₃ catalyst. 1-Octanol, which is a representative of aliphatic primary alcohols, was readily and selectively converted into 1-octanal with a yield of about 10% even at 363 K (entry 1). The yield of 1-octanal rapidly increased to 35% at 403 K for 10 h and 63% at 423 K for 2 h (entries 2 and 3). The TOF increased rapidly with temperature, and it reached 13.7 h⁻¹ at 423 K, clearly demonstrating the high activity of the Cu/La₂O₃ catalyst. Here, the TOF is as high as 0.2 h⁻¹ at 363 K, which is almost 20 times larger than that obtained over a Cu/Al₂O₃ catalyst (TOF = 0.01 h⁻¹) at the same reaction temperature.^{14,15} The TOF of 1.5 h⁻¹ at 403 K is about 10 times larger than that obtained over the most active Ru/AlO(OH) (TOF = 0.16 h⁻¹)¹⁶ and Cu/HT (TOF = 0.1 h⁻¹ for heptanol)¹⁸ catalysts. Moreover, the Cu/La₂O₃ catalyst was also highly active for the dehydrogenation of other aliphatic primary alcohols. 1-Hexanol and 1-decanol were selectively converted to 1-hexanal (yield 48%) and 1-decanal (yield 45%) at 423 K (entries 4 and 5). This extremely high activity of the Cu/La₂O₃ catalyst may rely on the active Cu particles and the basic nature of La₂O₃, which favors the effective and selective dehydrogenation of alcohols.

Table 1 Transfer dehydrogenation of alcohols over the Cu/La₂O₃ catalyst^a

Entry	Substrate	Product	T/K	t/h	Conv./%	Sel./%	TOF/h ⁻¹
1	1-Octanol	1-Octanal	363	24	12	97	0.2
2	1-Octanol	1-Octanal	403	10	35	100	1.5
3	1-Octanol	1-Octanal	423	2	63	100	13.7
4	1-Hexanol	1-Hexanal	423	8	48	100	2.6
5	1-Decanol	1-Decanal	423	10	45	100	2.0
6	Benzyl alcohol	Benzaldehyde	423	3	99	100	14.3
7	1-Phenylethanol	Acetophenone	423	0.5	99.5	100	86.5
8	2-Octanol	2-Octanone	423	1	99.5	100	43.3
9	Cyclohexanol	Cyclohexanone	423	1	77	100	33.5

^a Reaction conditions: alcohol (2 mmol), styrene (4 mmol), Cu/La₂O₃ (200 mg), mesitylene (8 ml), N₂ atmosphere.

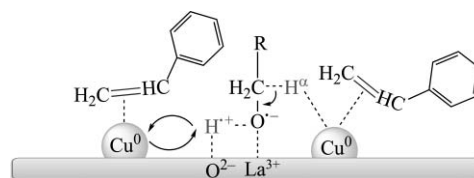
This methodology can also be applied to the conversion of benzylic and secondary aliphatic alcohols. As expected, the Cu/La₂O₃ catalyst was quite active for aromatic alcohols. Benzyl alcohol and 1-phenylethanol were converted to the corresponding aldehydes and ketones quantitatively and the TOFs were much higher than those for primary aliphatic alcohols (entries 6 and 7). When used for benzyl alcohol, 99% yield of benzaldehyde was obtained within 3 h with a TOF of 14.3 h⁻¹. Previously, the reaction of benzyl alcohol using of Pd/C–ethylene system only gave a 43% yield of benzyl aldehyde in 4 days at 323 K,¹¹ and the Pd/Al₂O₃–cyclohexene system gave an 18% yield of benzyl aldehyde within 15 h at 353 K.¹³ Clearly, the reaction rate of Cu/La₂O₃ catalyst is at least 5 times larger than the previous catalysts. In the case of 1-phenylethanol, the yield of acetophenone was 99.5% and the TOF reached 86.5 h⁻¹ (entry 7). This value is also much higher than those reported for Cu catalysts with or without a hydrogen acceptor: Cu/Al₂O₃ (TOF = 8.7 h⁻¹)^{14,15} and Cu/HT (TOF = 4.4 h⁻¹).¹⁸ In addition, the Cu/La₂O₃ catalyst was also highly effective for the dehydrogenation of aliphatic secondary alcohols. 2-Octanol was quantitatively converted to 2-octanone within 1 h (TOF = 43.3 h⁻¹, entry 8). However, this reaction took 15 h at 383 K with a Ru/AlO(OH) catalyst (TOF = 1.5 h⁻¹),¹⁶ 4 h at 353 K with a Cu/Al₂O₃ catalyst (TOF = 1.5 h⁻¹),^{14,15} and 6 h at 403 K with a Cu/HT catalyst (TOF = 2.2 h⁻¹).¹⁸ More importantly, cyclohexanol, which is poorly reactive over noble metals (Pd and Ru) even under aerobic conditions,^{5,6} was converted to cyclohexanone with 77% yield within 1 h (TOF = 33.5 h⁻¹, entry 9). In contrast, the Pd/Al₂O₃–cyclohexene system only gave 1% yield of cyclohexanone within 5 h at 353 K,¹³ and it took 12 h at 353 K over a Ru/AlO(OH) catalyst to achieve total conversion to cyclohexanone.¹⁶

It is well known that the acid–base properties of the catalyst play a central role in alcohol dehydrogenation.^{27,29} In order to facilitate the dehydrogenation of alcohols, organic or inorganic bases are often added to the reaction media as co-catalysts. In particular, strong bases like KOH or NaOH or sodium alkoxides are frequently used as promoters in H-transfer reaction of alcohols for promoting the reaction rates. Meanwhile, the basic component also inhibits over-oxidation of primary alcohols to carboxylic acids under aerobic conditions, improving the selectivity. This can be alternatively achieved by using basic solid oxides, such as MgO, Mg–Al, and Cu–Mg–Al hydrotalcite.^{27,30} Pillai *et al.*³¹ has reported that a palladium catalyst supported on hydrotalcite (a basic MgO-like material) showed comparable performance to that of Pd/MgO, whereas Pd catalysts supported on acidic materials (silica, alumina and zeolite-β) were not active for alcohol oxidation. Probably, the La₂O₃ support here acts as a strong base with a large number of basic sites,³² which favors proton abstraction from the substrate alcohol under anaerobic conditions.

However, a blank test with La₂O₃ alone only gave 1.5% conversion of 1-octanol, implying that La₂O₃ favors the dehydrogenation of alcohol but the finely dispersed Cu particles are also needed to transfer hydrogen species. A mechanistic study on a Cu/Al₂O₃ catalyst for alcohol dehydrogenation revealed that the rate-determining step is the formation of a carbocation-type intermediate by abstracting the OH group in the substrate alcohol.¹⁵ Because the primary carbocation is highly unstable

and the removal of the second hydrogen atom from the α carbon normally does not occur, the primary aliphatic alcohols are almost inactive over the Cu/Al₂O₃ catalyst. Concerning the current Cu/La₂O₃ catalyst, however, the reaction might follow an alternative route. La₂O₃ provides available basic sites for alcohol adsorption and hydrogen abstraction from the substrate alcohol. It is likely that the basic sites of La₂O₃ can display nucleophilic reactivity and abstract a proton from the alcohol to form a reactive negatively charged intermediate (alkoxide). Simultaneously, the Cu particles catalyze the hydrogenation of styrene based on the fast hydrogen spillover and the facile release of hydrogen from its surface. Unlike noble metals, which tend to adsorb hydrogen strongly with the formation of stable metal hydride species,^{13,17} Cu adsorbs hydrogen only weakly and thus favors a fast spillover.

Therefore, it seems reasonable that transfer dehydrogenation of alcohols occurs at the Cu–La₂O₃ boundaries, following a bifunctional process (Scheme 1). The substrate alcohol dehydrogenates to alkoxide on the basic sites of La₂O₃, and then the dissociated hydrogen atom migrates to the nearby Cu. Subsequently, the extraction of α-hydrogen from the alkoxide intermediate occurs on a Cu particle or Cu–La₂O₃ interface, forming the aldehyde or ketone. Finally, hydrogenation of styrene takes place on Cu, yielding ethylbenzene. In summary, the basic sites of La₂O₃ are mainly responsible for proton abstraction from alcohol, while the Cu particles promote the hydrogenation of styrene.



Scheme 1 A possible reaction pathway for transfer dehydrogenation of alcohols on the Cu/La₂O₃ catalyst.

Conclusions

Basic La₂O₃-supported Cu nanoparticles are highly effective for the transfer dehydrogenation of various alcohols, especially aliphatic primary alcohols. When used for 1-octanol, the yield of 1-octanal was as high as 63%. This unique performance is attributed to the synergistic effect between the basicity of La₂O₃ and the efficient spillover effect of Cu particles. The basic sites of La₂O₃ abstract protons from the substrate alcohol, while the Cu particles accelerate the extraction of α-hydrogen from the intermediate and simultaneously catalyze the hydrogenation of styrene.

References

- R. A. Sheldon and J. K. Kochi, *Metal-Catalyzed Oxidations of Organic Compounds*, Academic Press, New York, 1981.
- R. A. Sheldon, I. W. C. E. Arends and A. Dijkstra, *Catal. Today*, 2000, **57**, 157–166.
- B. Z. Zhan and A. Thompson, *Tetrahedron*, 2004, **60**, 2917–2935.
- T. Mallat and A. Baiker, *Chem. Rev.*, 2004, **104**, 3037–3058.

- 5 D. I. Enache, J. K. Edwards, P. Landon, B. Solsona-Espriu, A. F. Carley, A. A. Herzing, M. Watanabe, C. J. Kiely, D. W. Knight and G. J. Hutchings, *Science*, 2006, **311**, 362–365.
- 6 T. Matsumoto, M. Ueno, N. Wang and S. Kobayashi, *Chem. Asian J.*, 2008, **3**, 196–214.
- 7 R. Anderson, K. Griffin, P. Johnston and P. L. Alsters, *Adv. Synth. Catal.*, 2003, **345**, 517–523.
- 8 B. Z. Zhan, M. A. White, T. K. Sham, J. A. Pincock, R. J. Doucet, K. V. R. Rao, K. N. Robertson and T. S. Cameron, *J. Am. Chem. Soc.*, 2003, **125**, 2195–2199.
- 9 K. Yamaguchi, K. Mori, T. Mizugaki, K. Ebitani and K. Kaneda, *J. Am. Chem. Soc.*, 2000, **122**, 7144–7145.
- 10 K. Yamaguchi and N. Mizuno, *Angew. Chem., Int. Ed.*, 2002, **41**, 4538–4542.
- 11 M. Hayashi, K. Yamada, S. Nakayama, H. Hayashi and S. Yamazaki, *Green Chem.*, 2000, **2**, 257–260.
- 12 T. Tanaka, H. Kawabata and M. Hayashi, *Tetrahedron Lett.*, 2005, **46**, 4989–4991.
- 13 C. Keresszegi, T. Mallat and A. Baiker, *New J. Chem.*, 2001, **25**, 1163–1167.
- 14 F. Zaccheria, N. Ravasio, R. Psaro and A. Fusi, *Chem. Commun.*, 2005, 253–255.
- 15 F. Zaccheria, N. Ravasio, R. Psaro and A. Fusi, *Chem. Eur. J.*, 2006, **12**, 6426–6431.
- 16 W.-H. Kim, I. S. Park and J. Park, *Org. Lett.*, 2006, **8**, 2543–2545.
- 17 T. Mitsudome, Y. Mikami, H. Funai, T. Mizugaki, K. Jitsukawa and K. Kaneda, *Angew. Chem. Int. Ed.*, 2008, **47**, 138–141.
- 18 T. Mitsudome, Y. Mikami, K. Ebata, T. Mizugaki, K. Jitsukawa and K. Kaneda, *Chem. Commun.*, 2008, 4804–4806.
- 19 S. Sato, R. Takahashi, T. Sodesawa, K. Yuma and Y. Obata, *J. Catal.*, 2000, **196**, 195–199.
- 20 B. Klingenberg and M. A. Vannice, *Chem. Mater.*, 1996, **8**, 2755–2768.
- 21 A. A. Davydov, *Infrared Spectroscopy of Adsorbed Species on the Surface of Transition Metal Oxides*, New York, 1990.
- 22 V. Z. Fridman and A. A. Davydov, *J. Catal.*, 2000, **195**, 20–30.
- 23 F. Boccuzzi, S. Coluccia, G. Martra and N. Ravasio, *J. Catal.*, 1999, **184**, 316–326.
- 24 G. Moretti, G. Fierro, M. L. Jacono and P. Porta, *Surf. Interface Anal.*, 1989, **14**, 325–336.
- 25 M. Vijayaraj and C. S. Gopinath, *J. Catal.*, 2006, **241**, 83–95.
- 26 S. C. Shen, X. Chen and S. Kawi, *Langmuir*, 2004, **20**, 9130–9137.
- 27 J. I. Di Cosimo, V. K. Diez, M. Xu, E. Iglesia and C. R. Apesteguía, *J. Catal.*, 1998, **178**, 499–510.
- 28 G. Colón, J. A. Navío, R. Monaci and I. Ferino, *Phys. Chem. Chem. Phys.*, 2000, **2**, 4453–4459.
- 29 W. C. Conner and J. L. Falconer, *Chem. Rev.*, 1995, **95**, 759–788.
- 30 P. Haider and A. Baiker, *J. Catal.*, 2007, **248**, 175–187.
- 31 U. R. Pillai and E. S. Demessie, *Green Chem.*, 2004, **6**, 161–165.
- 32 A. Auroux and A. Gervasini, *J. Phys. Chem.*, 1990, **94**, 6371–6379.

In vitro biocompatibility of nanoscale zerovalent iron particles (NZVI) synthesized using tea polyphenols

Mallikarjuna N. Nadagouda,^{†a} Alicia B. Castle,^b Richard C. Murdock,^b Saber M. Hussain^b and Rajender S. Varma^{*a}

Received 7th April 2009, Accepted 9th October 2009

First published as an Advance Article on the web 4th November 2009

DOI: 10.1039/b921203p

A “green” protocol was used for the rapid generation of nanoscale zerovalent iron (NZVI) particles using tea polyphenols. The NZVI particles were subsequently examined for *in vitro* biocompatibility using the human keratinocyte cell (HaCaT) line as a representative skin exposure model. The cells were exposed to NZVI for time periods of 24 and 48 h. Biocompatibility was assessed using the methyl tetrazolium, or MTS, (3-(4,5-dimethylthiazol-2-yl)-5-(3-carboxymethoxyphenyl)-2-(4-sulfophenyl)-2H-tetrazolium)) and lactate dehydrogenase (LDH) assays to determine *in vitro* cytotoxicity. The evaluation of mitochondrial function (MTS) and membrane integrity (LDH) in human keratinocytes showed that these “green” synthesized NZVI particles were nontoxic in the human keratinocytes exposed when compared with control samples synthesized using a borohydride protocol. In fact, in most cases, these “green” nanoparticles induced a prolific response in the cellular function even at the highest concentration (100 µg ml⁻¹).

Introduction

Nanoscale zerovalent iron (NZVI) particles have been found to be effective in degrading various chlorinated organic contaminant hydrocarbons such as trichloroethylene,¹ and trichloroethene (TCE).²⁻⁴ Recent environmental applications include removal of nitrite by ultrasound dispersed NZVI,⁵ dechlorination of dibenzo-P-dioxins,⁶ reduction of chlorinated ethanes,⁷ adsorption of humic acid and its effect on arsenic removal⁸⁻⁹ and hexavalent chromium removal.¹⁰ However, field applications of NZVI have been limited to granular particles used in permeable reactive barriers (PRB).^{4,5} While PRBs are found to be effective for remediation of shallow aquifers, more cost-effective *in situ* technologies are lacking for rapid and complete destruction of chlorinated contaminants in deep aquifers and in source zones.⁶ Recently, there is great interest in testing an *in situ* remediation strategy where reactive NZVI particles are directly delivered into the contaminant source zones compared to passive technologies such as PRB. The *in situ* preparation of the NZVI particles offers unique advantages, such as (i) the applicability to source zones in deep aquifers or to areas where lands are occupied, (ii) a much shorter overall remediation time, (iii) transportation and chemical reactivity and (iv) it helps relieve surface oxidation problems. However,

for this technology to be feasible, the NZVI particles must be small enough to be mobile in the targeted zones, and the transport behaviors (or size) of the nanoparticles in various soils must be controllable. Yet, there has been no technique available for preparing NZVI particles of controlled size and transport properties, and a method is lacking to extend the reactive lifetime of these relatively short-lived nanoparticles. There are several methods which have been employed to prepare NZVI particles including sodium borohydride (NaBH₄),¹¹⁻¹⁴ ethylene glycol¹⁵ and corbothermal synthesis.¹⁰ While NZVI particles have been reported to be attainable by these methods, it was recognized that NZVI particles tend to rapidly agglomerate to form larger aggregates due to Van der Waals and magnetic forces, rendering them undeliverable to the targeted contaminant locations.^{11,12}

To prevent aggregation of metallic nanoparticles, particle stabilization has been commonly practiced by attaching a stabilizer such as a soluble polymer or surfactant onto the nanoparticles.¹³ The stabilizer molecules are designed to provide strong inter-particle electrostatic and/or steric repulsions to outweigh the attractive Van der Waals and magnetic forces. To stabilize NZVI, two general strategies have been employed: (i) Use of stabilizers before the nanoparticles or aggregates are formed or (ii) to mechanically break down the formed nanoparticle agglomerates and add a stabilizer (post-agglomeration stabilization).

We have seen a renewed interest in using green chemistry principles in the preparation of nanomaterials and nanocomposites.¹⁴⁻²⁷ There is a tremendous increase in biological applications of these nanostructures, as well as a continuous interest in using biodegradable polymers or surfactants to cap these nanoparticles that prevent them from aggregation.

^aSustainable Technology Division, National Risk Management Research Laboratory, Environmental Protection Agency, 26 West M. L. K. Drive, MS 443, Cincinnati, 45268, Ohio, USA.

E-mail: varma.rajender@epa.gov

^bApplied Biotechnology Branch, Human Effectiveness Directorate, Air Force Research Laboratory, Wright-Patterson AFB, OH, USA

[†]Present address: Pegasus Technical Services, 46 E Hollister Street, Cincinnati, Ohio 45219.

Table 1 Preparation of nanoscale zerovalent iron (NZVI) particles using tea

Sample Code No	Description
T1	10mL tea extract + 1mL 0.1 N Fe(NO ₃) ₃ solution
T2	5mL tea extract + 5mL 0.1 N Fe(NO ₃) ₃ solution
T3	1mL tea extract + 5mL 0.1 N Fe(NO ₃) ₃ solution
T4	1mL tea extract + 10mL 0.1 N Fe(NO ₃) ₃ solution
T5	5mL tea extract + 4mL 0.1 N Fe(NO ₃) ₃ solution
T6	5mL epicatechin (0.01 N) extract + 1mL 0.1 N Fe(NO ₃) ₃
T7	4mL epicatechin (0.01 N) extract + 4mL 0.1 N Fe(NO ₃) ₃
T8	5mL tea extract + 2mL 0.1 N Fe(NO ₃) ₃ solution
C1	(Control) 2mL Fe(NO ₃) ₃ + 10mL NaBH ₄
C2	(Control) 1mL Fe(NO ₃) ₃ + 10mL NaBH ₄
C3	(Control) 1mL Fe(NO ₃) ₃ + 5mL NaBH ₄

Most of these polymers or surfactants have a tendency to be water soluble and it is of great interest to know how good dispersion or capping can be obtained using these biodegradable polymers or surfactants. The tea extract (poly phenols) was chosen as a reducing agent and stabilizing agent because poly phenols are biodegradable (non toxic) and water soluble at room temperature, unlike other polymers. Second, poly phenols can form complexes with metal ions and thereafter can reduce the metals. Third, tea extract contains molecules bearing alcoholic functional groups which can be exploited for reduction as well as stabilization of the nanoparticles.

In this paper we have synthesized green NZVI which can ideally be utilized for toxicological studies. Control experiments were carried out using the standard NaBH₄ reduction method and results were compared with the new green approach. Favorable conditions to make Fe nanoparticles were established with uniform size and shape.

Experimental procedure

Synthesis of “green” nanoscale zerovalent iron particles (NZVI)

Tea extract preparation: about 2 grams of tea powder (Red label from Tata, India Ltd. 99%) were extracted in 100 mL hot water and were then used to carry out the reaction with 0.1 N Fe(NO₃)₃. The different compositions were prepared at room temperature and are shown in Table 1. Control experiments were carried out using 0.1 N NaBH₄ solutions at room temperature and the compositions are listed in Table 1.

Nanomaterial characterization

Transmission electron microscopy (TEM) characterization was performed to obtain nanoparticle size and morphology on a Hitachi H-7600 tungsten-tip instrument at an accelerating voltage of 100kV. Nanoparticles were examined after suspension in water and subsequent deposition of 5 μ L of solution onto formvar/carbon-coated TEM grids. The AMT software for the digital TEM camera was calibrated for size measurements of the nanoparticles at each magnification level. Information on mean size and standard deviation was calculated from measuring over 100 nanoparticles in random fields of view in addition

to images that show general morphology of the nanoparticles. A Panalytical X-pert diffractometer with a copper K α source was used to identify crystalline phases of the lead precipitates. The tube was operated at 45 kV and 40 mA for the analyses. Scans were performed over a 2-theta ranging from 5 to 70° with a step of 0.02° and a one-second count time at each step. Pattern analysis was performed by following ASTM procedures using the computer software Jade (Versions 8, Materials Data, Inc.), with reference to the 1995-2002 ICDD PDF-2 data files (International Center for Diffraction Data, Newtown Square, PA). UV spectra were recorded using a Varian UV-visible spectrometer (Model Cary 50 Conc).

Keratinocyte (HaCaT) cell culture

HaCaT cells were donated generously by Dr. James F. Dillman III, of the U.S. Army Medical Research Institute of Chemical Defense.²⁸ The HaCaT cells were cultured with RPMI-1640 media with 10% fetal bovine serum and 1% penicillin/streptomycin. The HaCaT line was incubated at 37 °C, 100% humidity, and 5% CO₂. During exposure, the HaCaT line was cultured with RPMI-1640 media with 1% penicillin/streptomycin and no fetal bovine serum (HEM).

Treatment protocol

Cells were seeded to 60-80% confluency in 96 well plates within a growth period of 24-48 h. Upon reaching 80% confluency, typically 48 h, cells were treated with either 0 μ g mL⁻¹, 5 μ g mL⁻¹, 10 μ g mL⁻¹, 25 μ g mL⁻¹, 50 μ g mL⁻¹ or 100 μ g mL⁻¹ concentrations of nanoparticles suspended in HEM. After a 24h or 48h exposure, the nanoparticle biocompatibility was assessed using cytotoxicity assays.

Cytotoxicity assays

The HaCaT cells were exposed to the NZVI at concentrations of 0 μ g mL⁻¹, 5 μ g mL⁻¹, 10 μ g mL⁻¹, 25 μ g mL⁻¹, 50 μ g mL⁻¹ or 100 μ g mL⁻¹ in HEM. After either 24h or 48h incubation with the nanoparticles, cell proliferation was measured using the CellTiter 96® Aqueous One Solution Cell Proliferation Assay (Promega), and membrane leakage was evaluated using the CytoTox 96® Non-Radioactive Cytotoxicity Assay (Promega). The mitochondrial function and membrane leakage were then assessed spectrophotometrically with a Spectra-MAX Plus 190 microplate reader. The data are represented as an average of three independent trials \pm the standard deviation.

Statistical analysis

The data are represented as an average of three independent trials \pm the standard deviation. The cytotoxicity assays were run and any group with a *p* value less than 0.05 was considered significant.

Results and discussion

Typically, nanomaterials possess special properties - chemical, optical, magnetic, and biological, which make them desirable for commercial or medical applications. However, these same

Table 2 Reduction potential of phenoxy and flavonoid radicals

Substance	Reduction Potential/V
Hesperidin	0.72
Rutin	0.60
(+)-Catechin	0.57
(-)-Epigallocatechin	0.43
Quercetin	0.33
Catechol	0.53
Methyl gallate	0.56
3,5-Dihydroxy-anisol	0.84

properties potentially may lead to a response in the human body that is different from and is not directly predicted by the constituent chemicals and compounds. Understanding properties of nanomaterials obtained through different routes is still a challenge. In this context, we found that the preparation of NZVI particles of controlled size and transport properties using benign tea polyphenols is very attractive. The reactive lifetime of these relatively short-lived nanoparticles is extended because the tea polyphenols not only reduce the iron salts but cap the ensuing nanoparticles. The reduction potential of caffeine is 0.3 V *vs.* SCE which is sufficient to reduce metals *viz.* Fe (reduction potential -0.44 V *vs.* SCE). The other polyphenols have reduction potential values²⁹ ranging from 0.3 to 0.8 V (see Table 2 for reduction potential values).

The formation of Fe nanoparticles with caffeine/polyphenols took place *via* the following steps: (1) complexation with Fe

salts, (2) simultaneous reduction of Fe, (3) capping with oxidized polyphenols/caffeine. The reduction of Fe was confirmed using UV spectra and is shown in Fig. 1. The blank extract has an absorption beginning at 500 nm which is similar to the control $\text{Fe}(\text{NO}_3)_3$ solutions. The reaction between $\text{Fe}(\text{NO}_3)_3$ and tea extract was instantaneous and the color of the reaction mixture changed from yellow to dark brown as shown in the inset of Fig. 1. After the reaction the UV spectra had broad absorption at a higher wavelength and there was no sharp absorption at lower wavelengths as shown in the controls.

UV spectra of T1, T2, T3, T4, T5 and T8 (descriptive text codes are given in Table 1) are shown in Fig. 2. All the spectra looked similar in the visible region, but displayed slight differences in the UV region. T1 and T8 did not show strong absorption in the UV range when compared with T2 and T5. The spectra of T3 and T5 had sharp absorption in the UV range when compared with all the others plotted. X-ray diffraction experiments were conducted to confirm the phase formation. Fig. 3 shows the XRD patterns of T1, T2, T3, T4 and T8 samples respectively. Except sample T2, patterns (a) and (e) showed a small 100% intensity peak around 2θ 50° (patterns (c) and (d) were amorphous in nature) and could be indexed to hexagonal Fe (JCPDS No. 00-024-0072). The XRD pattern of T2 showed 100% intensity peak at 2θ , 33.115 which can be indexed to the rhombohedraphase of α Fe_2O_3 with plane (104). Fig. 4 shows TEM images of T1, T2, T3 and T4 samples respectively. Sample T1 yielded spherical particles ranging from 40 to 50 nm

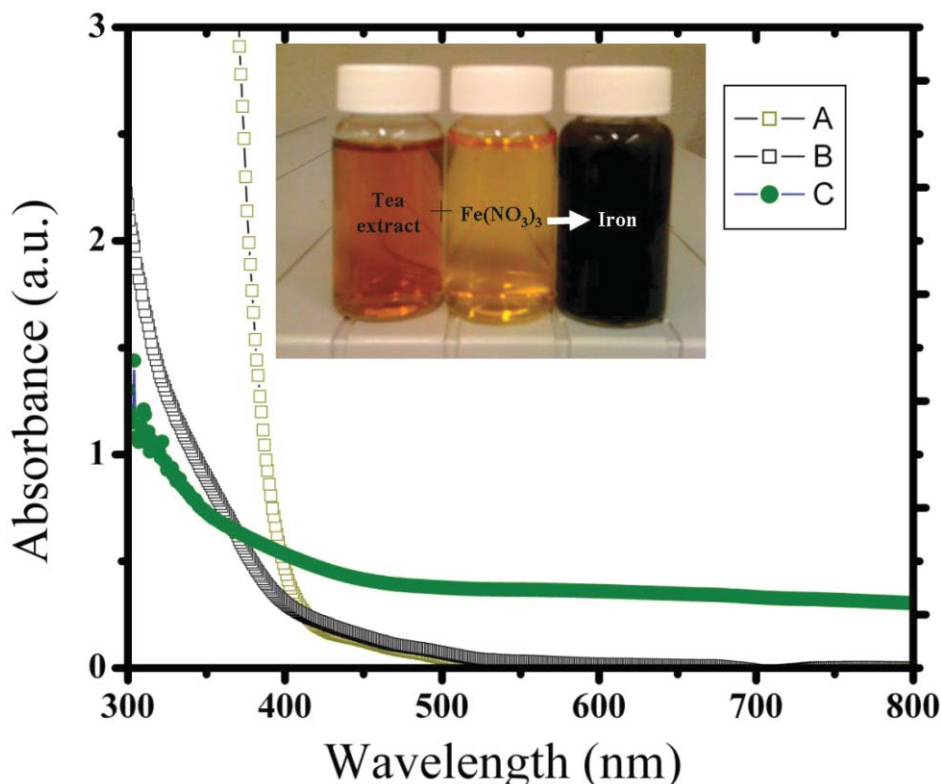


Fig. 1 UV spectra of (a) $\text{Fe}(\text{NO}_3)_3$ control, (b) control tea extract and (c) the reaction product (Fe nanoparticles) obtained from $\text{Fe}(\text{NO}_3)_3$ and tea extract. The inset shows the photographic image of the tea extract, control $\text{Fe}(\text{NO}_3)_3$ solution and after mixing them (from left to right vials).

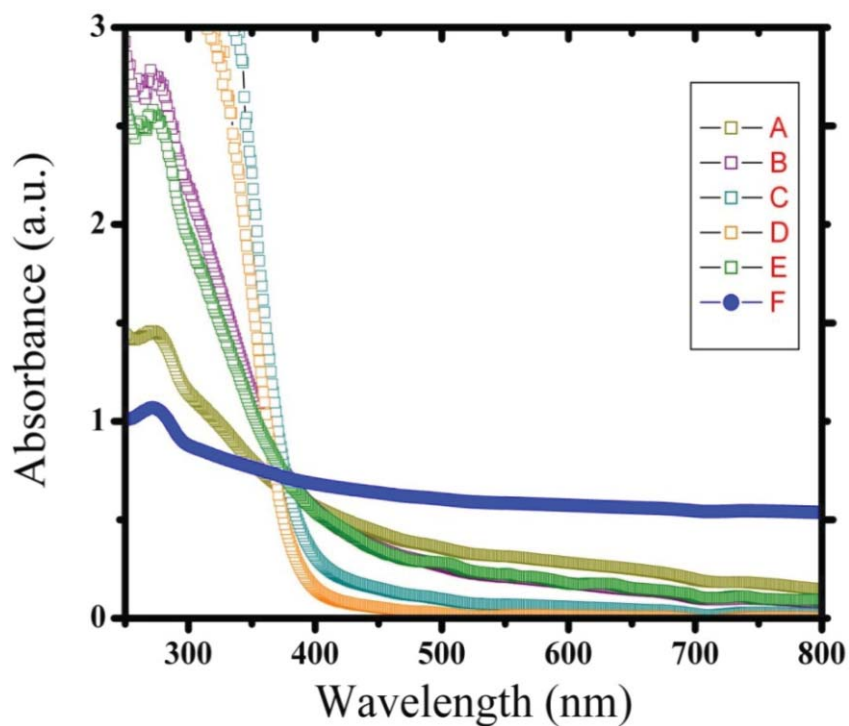


Fig. 2 UV spectra of iron nanoparticles (A) T1, (B) T2, (C), T3, (D) T4, (E) T5 and (F) T8 samples.

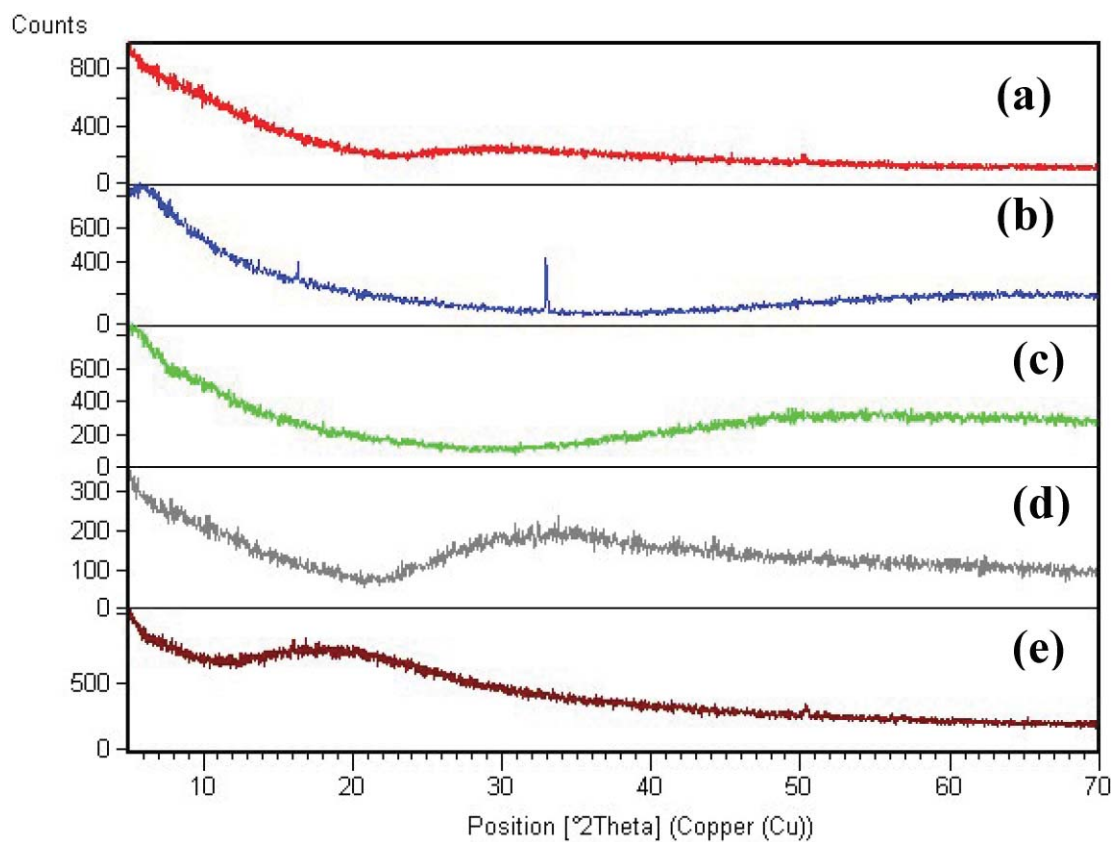


Fig. 3 XRD pattern of iron nanoparticles obtained using different ratios of tea extract and polyphenols; (a) T1, (b) T2, (c) T3, (d) T4 and (e) T8 samples.

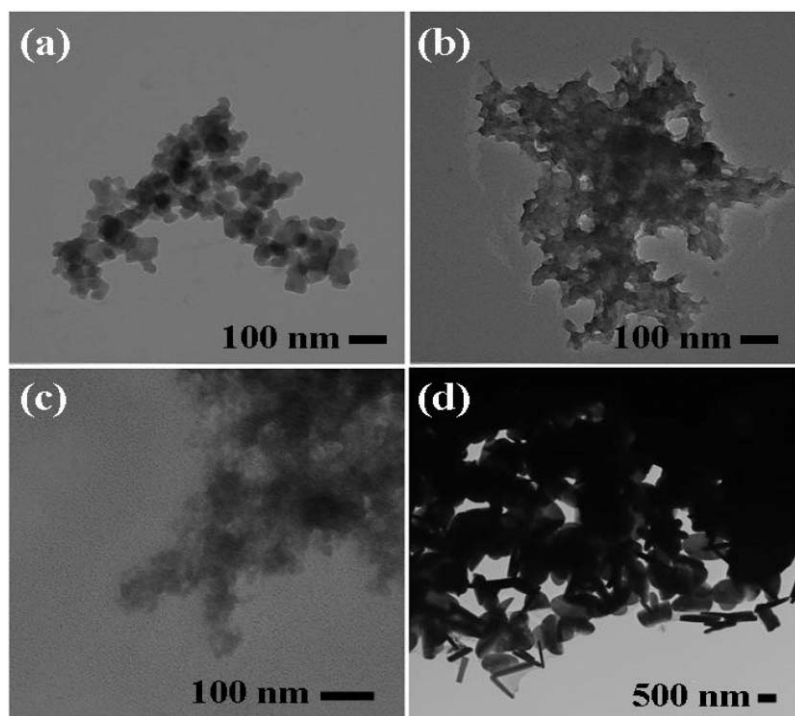


Fig. 4 TEM images of (a) T1, (b) T2, (c) T3 and (d) T4 samples.

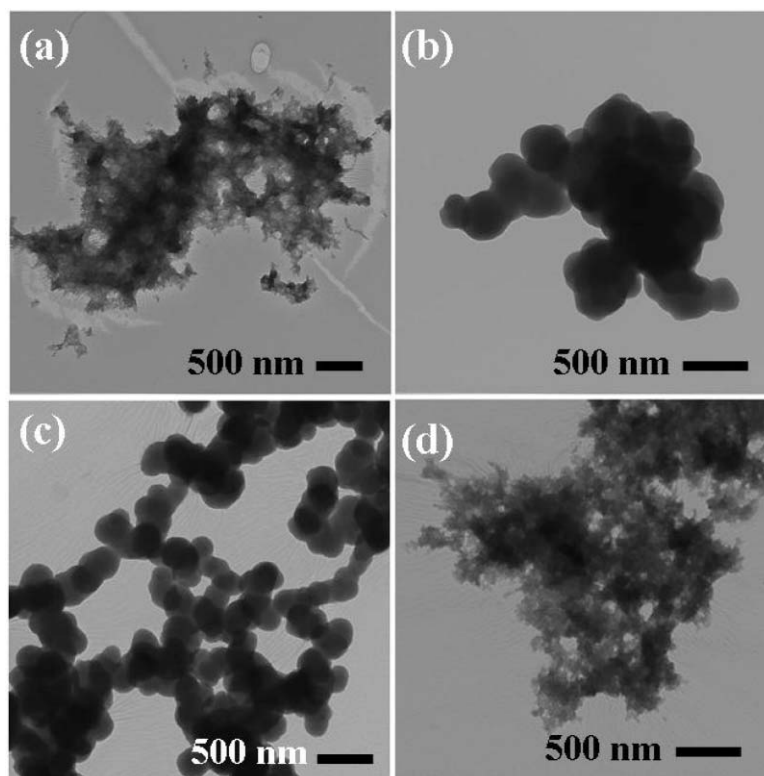


Fig. 5 TEM images of (a) T5, (b) T6, (c) T7 and (d) T8 samples.

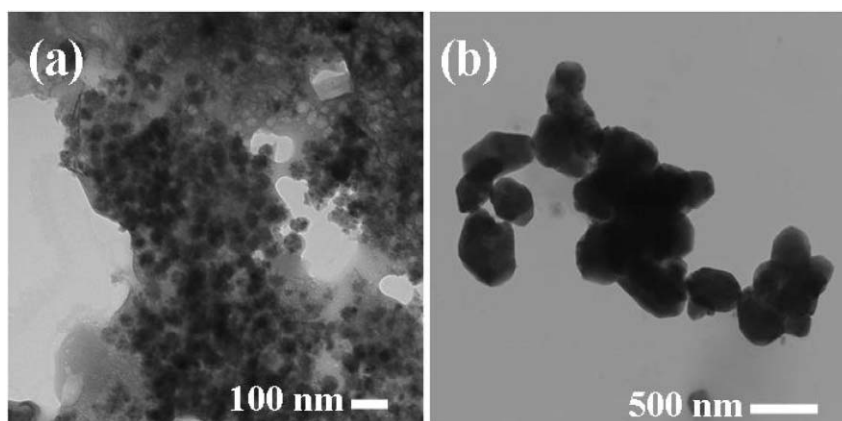


Fig. 6 TEM images of (a) C1 and (b) C2 control samples.

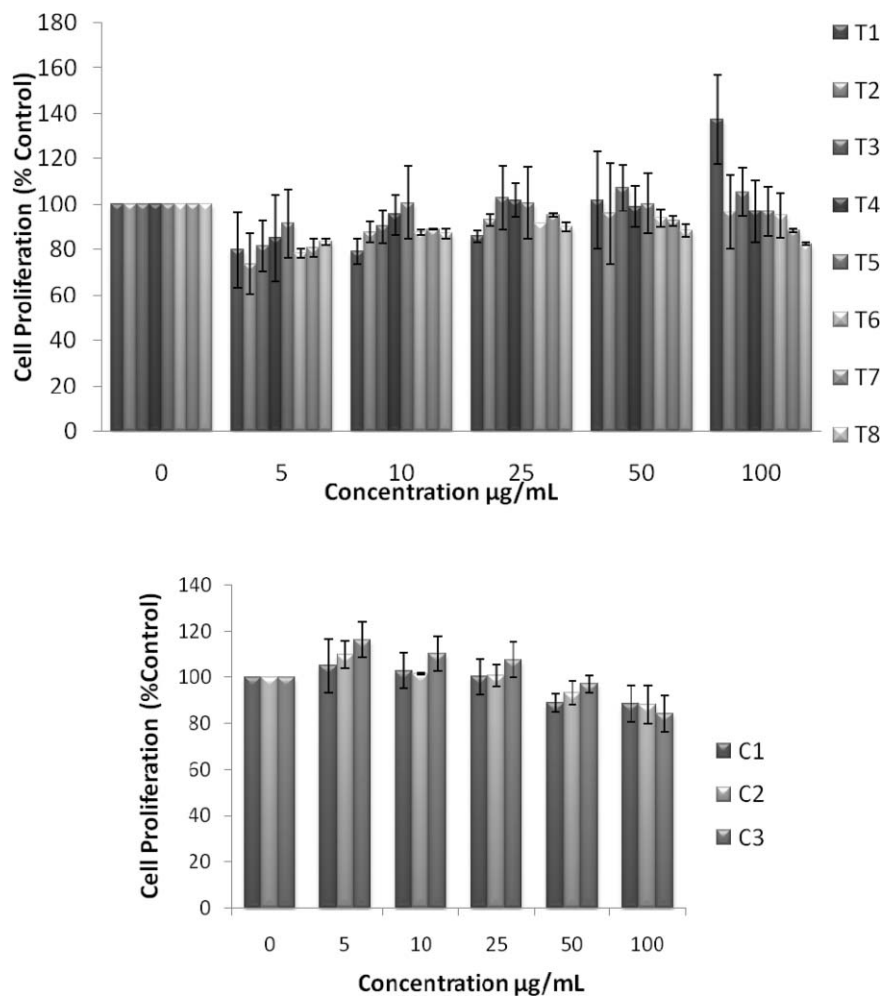


Fig. 7 Effect of NZVI on mitochondrial function after 24h exposure. Mitochondrial function was determined by the MTS assay as described in the Experimental procedure section. Each experimental point is a composite of three independent experiments, with $n \geq 3$ for each point. Top: MTS showing cell proliferation after 24h exposure to various concentrations of NZVI. The figure shows no significant reductions in cell proliferation, but instead increased cell proliferation after 24h. Bottom: MTS showing changes in cell proliferation after 24h exposure to various concentrations of control particles made with sodium borohydride. These particles produced no significant decrease in cell proliferation after 24h.

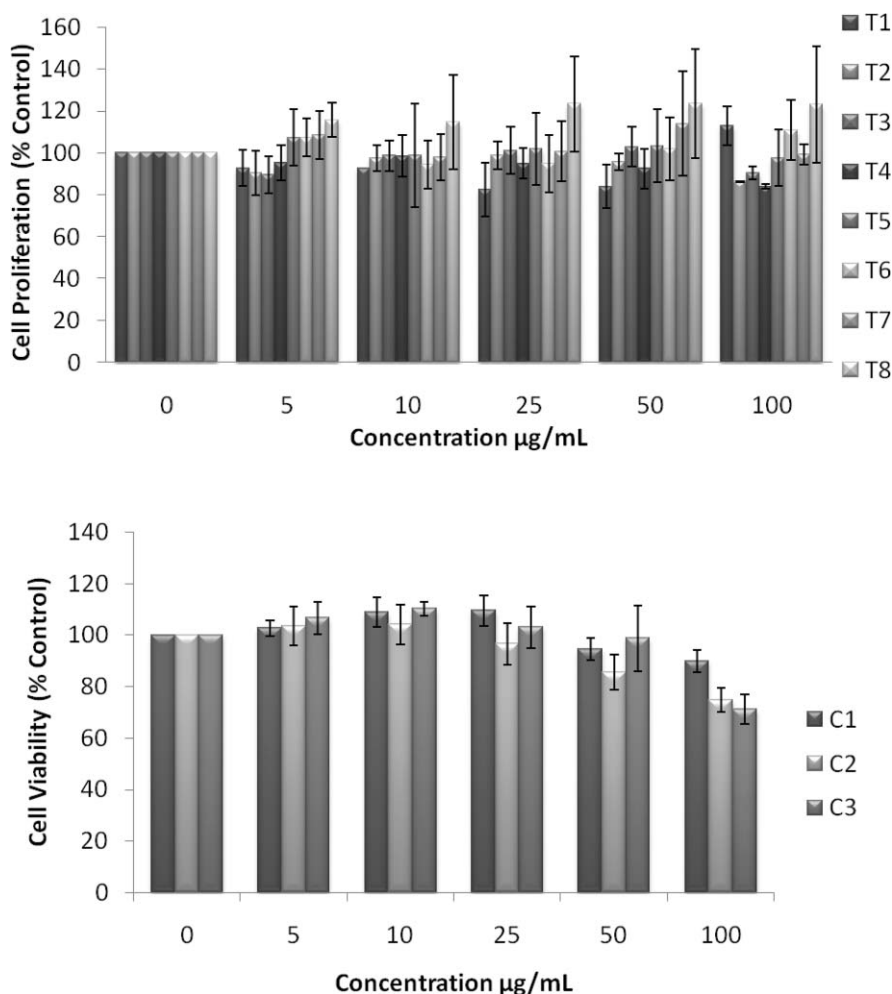


Fig. 8 Effect of NZVI on mitochondrial function after 48h exposure. Mitochondrial function was determined by the MTS assay as described in the Experimental procedure section. Each experimental point is a composite of three independent experiments, with $n \geq 3$ for each point. Top: MTS showing cell proliferation after 48h exposure to various concentrations of NZVI. The figure shows no significant reductions in cell proliferation, but instead increased cell proliferation after 48h. Bottom: MTS showing changes in cell proliferation after a 48h exposure to various concentrations of control particles made with sodium borohydride. These particles produced no significant decrease in cell proliferation after 48h.

whereas T2 and T3 yielded ultra small nanoparticles which are difficult to visualize at this magnification. However, sample T4 showed different structures such as platelets and nanorods. We believe concentration of tea extract plays a key role in dictating the final structures and size of the iron nanoparticles. Sample T4 contained minimal amounts of caffeine/polyphenols hence the larger particle size. Caffeine/polyphenols are important for reducing and capping behavior.²⁰ At higher caffeine/polyphenol concentrations in the reaction mixture we observed a decrease in particle size. From samples T5-T8, particle shapes were found to be spherical and larger in size when compared with T1 to T4 (Fig. 5). The control samples C1 and C2 formed irregular shapes with size varying from 50 nm (control C1) to nearly 500 nm (control C2) (Fig. 6). The MTS assay of all the tested samples at 24 and 48 h showed no decreases in cell proliferation similar to control samples (see Fig. 7 & 8). LDH leakage results after 24h didn't show any discernible difference from control samples except in samples T1, T2, T3, and T4, but

after 48h results were significantly higher when compared with control samples indicating an increase in membrane leakage in HaCaT cells treated with NZVI (see Fig. 9 & 10). T1, T2, T3 and T4 showed increases in LDH leakage when the particle concentrations reached $50 \mu\text{g mL}^{-1}$ and above. The increases in LDH leakage are likely due to the size of the particles created. Increases in LDH are due to stress on the cellular membrane, which could be caused by the larger particle size in this case. Larger particles are not able to enter the cells, but they apply pressure on the cellular membrane while trying to enter leading to cellular membrane stress. As the particles are created in the smaller nano-sizes the membrane leakage will likely decrease. Also we saw higher LDH leakage with higher concentrations of particles. The increase in LDH leakage with increasing particle concentration is due to the cell membrane being stressed by so many particles pushing on the surface and is therefore a result of concentration of the particles rather than the type of particles used.

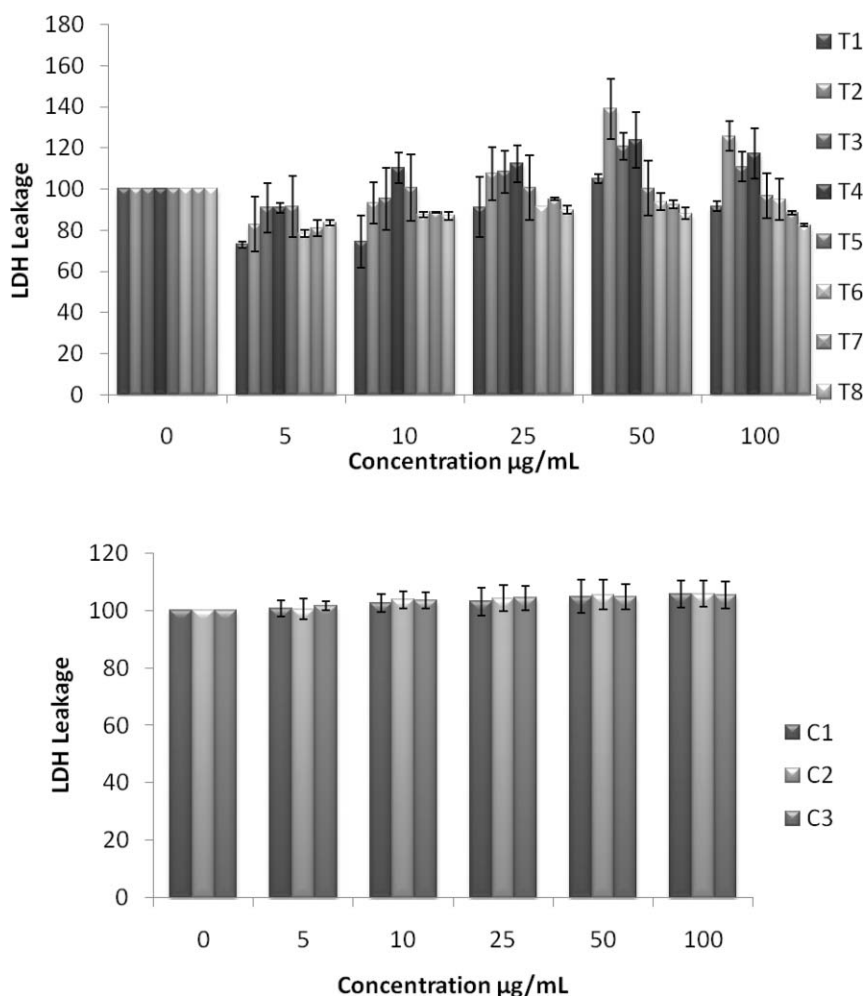


Fig. 9 Effect of NZVI on cellular membrane leakage after 24h exposure. Cellular membrane leakage was determined by the lactate dehydrogenase (LDH) assay as described in the Experimental procedure section. Each experimental point is a composite of three independent experiments, with $n \geq 3$ for each point. Top: LDH leakage after 24h exposure to various concentrations of NZVI. Bottom: LDH leakage after a 24h exposure to various concentrations of control particles made with sodium borohydride.

Conclusions

A “green” one-step approach has been developed for the synthesis of nanoscale zerovalent iron particles at room temperature. The method does not use a typical noxious chemical reducing agent or a surfactant and can be scaled up to bulk level. The “green” synthesized NZVI samples were assessed with MTS and LDH toxicological assays and some of them were found to be nontoxic when compared with control samples prepared using the conventional borohydride reduction protocols. This simple method offers spherical zerovalent iron nanoparticles with unique size and shape when compared with control samples. We anticipate the development of various technological and environmental remediation applications for these stable particles including dechlorination of dibenzo-P-dioxins, reduction of chlorinated ethanes, arsenic and hexavalent chromium removal to name a few.

References

- 1 K.-C. Huang and S. H. Ehrman, *Langmuir*, 2007, **23**, 1419.
- 2 Q. Huang, X. Shi, R. A. Pinto, E. J. Petersen and W. J. Weber Jr., *Environ. Sci. Technol.*, 2008, **42**, 8884.
- 3 L. Guo, Q.-J. Huang, X.-Y. Li and S. Yang, *Langmuir*, 2006, **22**, 7867.
- 4 S. R. Kanel, R. R. Goswami, T. P. Clement, M. O. Barnett and D. Zhao, *Environ. Sci. Technol.*, 2008, **42**, 896.
- 5 F. He and D. Zhao, *Environ. Sci. Technol.*, 2007, **41**, 6216.
- 6 L. B. Hoch, E. J. Mack, B. W. Hydutsky, J. M. Hershman, J. M. Skluzacek and T. E. Mallouk, *Environ. Sci. Technol.*, 2008, **42**, 2600.
- 7 Y. Liu and G. V. Lowry, *Environ. Sci. Technol.*, 2006, **40**, 6085.
- 8 S. R. Kanel, J.-M. Grenche and H. Choi, *Environ. Sci. Technol.*, 2006, **40**, 2045.
- 9 Y. Liu, T. Phenrat and G. V. Lowry, *Environ. Sci. Technol.*, 2007, **41**, 7881.
- 10 A. B. M. Giasuddin, S. R. Kanel and H. Choi, *Environ. Sci. Technol.*, 2007, **41**, 2022.
- 11 H. Song and E. R. Carraway, *Environ. Sci. Technol.*, 2005, **39**(16), 6237.
- 12 J.-H. Kim, P. G. Tratnyek and Y.-S. Chang, *Environ. Sci. Technol.*, 2008, **42**, 4106.
- 13 V. Sarathy, P. G. Tratnyek, J. T. Nurmi, D. R. Baer, J. E. Amonette, C. L. Chun, R. L. Penn and E. J. Reardon, *J. Phys. Chem. C*, 2008, **112**, 2286.
- 14 M. N. Nadagouda and R. S. Varma, *Green Chem.*, 2006, **8**, 516.
- 15 P. Raveendran, J. Fu and S. L. Wallen, *J. Am. Chem. Soc.*, 2003, **125**, 13940.
- 16 M. N. Nadagouda and R. S. Varma, *Green Chem.*, 2007, **9**, 632.

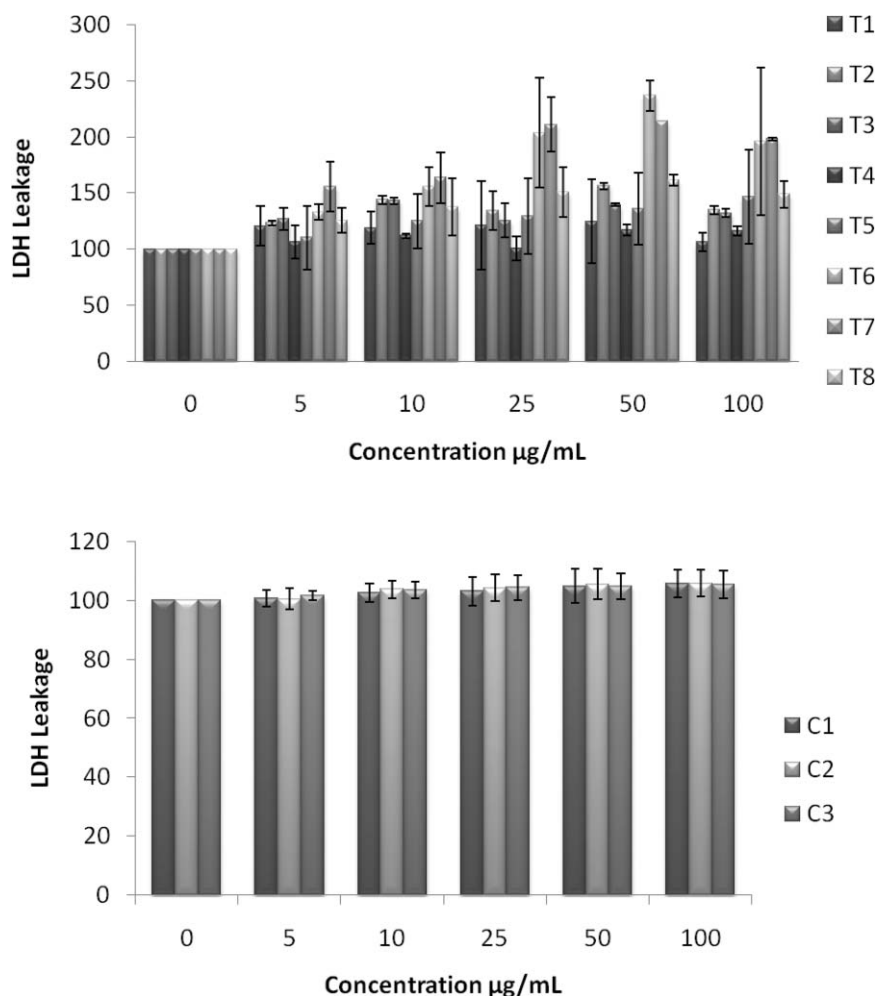


Fig. 10 Effect of NZVI on cellular membrane leakage after 48h exposure. Cellular membrane leakage was determined by the lactate dehydrogenase (LDH) assay as described in the Experimental procedure section. Each experimental point is a composite of three independent experiments, with $n \geq 3$ for each point. Top: LDH leakage after 48h exposure to various concentrations of NZVI. Bottom: LDH leakage after 48h exposure to various concentrations of control particles made with sodium borohydride.

- 17 R. R. Naik, S. J. Stringer, G. Agarwal, S. E. Jones and M. O. Stone, *Nat. Mater.*, 2002, **1**, 169.
- 18 M. N. Nadagouda and R. S. Varma, *J. Nanomaterials*, 2008, DOI: 1155/2008/782358.
- 19 P. Mukherjee, A. Ahmad, D. Mandal, S. Senapati, S. R. Sainkar, M. I. Khan, R. Parishcha, P. V. Ajaykumar, M. Alam, R. Kumar and M. Sastry, *Nano Lett.*, 2001, **1**, 515.
- 20 M. N. Nadagouda and R. S. Varma, *Green Chem.*, 2008, **10**, 859.
- 21 P. T. Anastas, J. C. Warner, *Green, Chemistry: Theory and Practice*, Oxford University Press, Inc. New York, 1998.
- 22 M. N. Nadagouda and R. S. Varma, *Cryst. Growth Des.*, 2008, **8**, 291.
- 23 M. N. Nadagouda and R. S. Varma, *Cryst. Growth Des.*, 2007, **4**, 686.
- 24 M. N. Nadagouda and R. S. Varma, *Biomacromolecules*, 2007, **8**, 2762.
- 25 M. N. Nadagouda and R. S. Varma, *Macromol. Rapid Commun.*, 2007, **28**, 465.
- 26 M. N. Nadagouda, V. Polshettiwar and R. S. Varma, *J. Mater. Chem.*, 2009, **19**, 2026.
- 27 V. Polshettiwar, B. Baruwati and R. S. Varma, *Green Chem.*, 2009, **11**, 127.
- 28 P. Boukamp, R. T. Petrussevska, D. Bretkreutz, J. Hornung, A. Markham and N. E. Fusenig, *J. Cell Biol.*, 1988, **106**, 761.
- 29 *Polyphenols, Wine and Health* Edited by C. Chèze, J. Vercauteren and R. Verpoorte, France, 14–16 April 1999 (Proceedings of the Phytochemical Society of Europe, Volume 48) Springer, Dordrecht, The Netherlands, 2001.

A quantum-chemical-based guide to analyze/quantify the cytotoxicity of ionic liquids†

J. S. Torrecilla,^a J. Palomar,^{*b} J. Lemus^b and F. Rodríguez^a

Received 4th June 2009, Accepted 25th September 2009

First published as an Advance Article on the web 28th October 2009

DOI: 10.1039/b919806g

A COSMO-RS descriptor ($S_{\sigma\text{-profile}}$) has been used in quantitative structure–activity relationship studies (QSARs) based on a neural network for the prediction of the toxicological effect of ionic liquids (ILs) on a leukemia rat cell line (LogEC₅₀ IPC-81) for a wide variety of compounds including imidazolium, pyridinium, ammonium, phosphonium, pyrrolidinium and quinolinium ILs. $S_{\sigma\text{-profile}}$ is a two-dimensional quantum-chemical parameter capable of characterising the electronic structure and molecular size of cations and anions. By using a COSMO-RS descriptor for a training set of 105 compounds (96 ILs and 9 closely related salts) with known biological activities (experimental LogEC₅₀ IPC-81 values), a reliable neural network was designed for the systematic analysis of the influence of structural IL elements (cation side chain, head group, anion type and the presence of functional groups) on the cytotoxicity of ~450 IL compounds. The Quantitative Structure–Activity Map (QSAM), a new concept developed here, was proposed as a valuable tool for (i) the molecular understanding of IL toxicity, by relating LogEC₅₀ IPC-81 parameters to the electronic structure of compounds given by quantum-chemical calculations; and (ii) the sustainable design of IL products with low toxicity, by linking the chemical structure of counterions to the predictions of IL cytotoxicity in handy contour plots. As a principal contribution, quantum-chemical-based QSAM guides allow the analysis/quantification of the non-linear mixture effects of the toxicophores constituting the IL structures. Based on these favorable results, the QSAR model was applied to estimate IL cytotoxicities in order to screen commercially available compounds with comparatively low toxicities.

1. Introduction

Room-temperature ionic liquids (ILs) possess an array of properties that make them attractive for academic studies and industry: extremely low vapour pressure, high thermal and chemical stabilities, non-flammability and high solvent capacity.^{1–3} Thus, ILs have been extensively examined as an alternative to conventional volatile organic solvents in reaction and separation processes.^{4,5} The number of commercial applications of ILs is rapidly growing, and the rate of appearance of patents on IL technology has been rising exponentially for years. Examples of these ILs applications in industry have been reported recently.⁶ ILs have often been frequently considered as an environmentally benign alternative to volatile organic solvents, mainly based on their negligible vapour pressure. However, recently it has been well documented that they can exhibit environmental toxicity (over a wide range) and persistency.^{7–13} Regarding the development of IL risk assessment, Prof. Ranke's group

(UFT Centre for Environmental Research and Sustainable Technology) has performed the most extensive analysis, carried out in single laboratory tests, of the (eco)toxicological hazard potentials of ILs, following the T-SAR (thinking in terms of structure–activity relationships) strategy.^{14,15} By applying the T-SAR approach, a large sample of test IL compounds was selected to evaluate their inhibitory effects on a flexible (eco)toxicological test battery (enzymes, cells, microorganisms and organisms).^{16–23} In order to improve the understanding of toxicity, ILs were subdivided into the cationic size chain,^{17,18} head group^{22,23} and the corresponding anion,^{19,20} to handle the huge structural variability of these compounds. In addition, the test-kits included functionalized side chains and head groups to identify toxicophore elements in ILs.^{22,23} The systematic analysis of structural insights performed by Ranke *et al.* provided very relevant information for the sustainable design of ILs with reduced toxicological hazard potential. However, there are an unmanageable number of possible ILs (>10⁶ simple ion combinations and near-endless potential IL mixtures, >10¹⁸)²⁴ and the experimental quantification of the toxicity of each IL is not possible. As consequence, an important challenge in IL research is the development of reliable models to relate the physicochemical and structural properties of ILs with their biological effects.

A few quantitative structure–activity relationships (QSARs) to predict IL toxicity have been reported in literature. Ranke *et al.*

^aDepartamento de Ingeniería Química, Universidad Complutense de Madrid, 28040, Madrid, Spain

^bSección de Ingeniería Química, Universidad Autónoma de Madrid, Cantoblanco, 28049, Madrid, Spain. E-mail: pepe.palomar@uam.es; Fax: +34 91 497 35 6

† Electronic supplementary information (ESI) available: Nomenclature of ionic liquid units and $S_{\sigma\text{-profile}}$ descriptors for cations and anions. See DOI: 10.1039/b919806g

found a linear correlation between the toxicity of 74 ILs (based on imidazolium, pyrrolidinium, pyridinium, quinolinium, quaternary phosphonium and quaternary ammonium cations) and an empirical HPLC-derived lipophilicity parameter (correlation coefficient of estimated *vs.* real values, $R^2 = 0.78$).²¹ A different approach by Luis *et al.*²⁵ designed an algorithm based on group contribution methods to estimate the aquatic toxicity of 43 imidazolium, pyridinium and pyrrolidinium ILs ($R^2 = 0.92$). Garcia-Lorenzo *et al.*²⁶ built a QSAR model, according to the Topological Sub-Structural Molecular Design (TOP-MODE) approach, which uses graph-based molecular descriptors to predict the cytotoxicity of 15 imidazolium-derived ILs in Caco-2 cells ($R^2 = 0.98$). Recently, Torrecilla *et al.*²⁷ used the empirical formulas (elemental composition) and molecular weights of 153 ILs (ammonium, imidazolium, morpholinium, phosphonium, piperidinium, pyridinium, pyrrolidinium and quinolinium salts) to estimate their toxicity (Log EC₅₀) in a leukemia rat cell line (IPC-81) and acetylcholinesterase (AChE) by multiple linear regression ($R^2 = 0.87$ and 0.81 , respectively) and neural network (NN) models ($R^2 = 0.98$ and 0.97 , respectively).

Molecular simulation based on physically-based models, such as quantum mechanics, molecular dynamics or COSMO-RS, have been much applied as valuable tools to predict physical and thermodynamic properties of ILs, with the main advantage of providing fundamental understanding at the molecular level.²⁸ However, to our knowledge, these reliable methods have hardly been used for the analysis of toxicological effects of ILs. Only one early attempt by Couling *et al.*²⁹ developed a QSAR model for *Vibrio fischeri* toxicity of 25 ILs using molecular descriptors, calculated at low semi-empirical computational level, and genetic function approximations ($R^2 = 0.78$). In this work, we will use a recently proposed COSMO-RS molecular descriptor ($S_{\sigma\text{-profile}}$)³⁰ in a non-linear neural network analysis for the prediction of IL cytotoxicities. The $S_{\sigma\text{-profile}}$ descriptor is an *a priori* quantum-chemical parameter, which quantifies the distribution of the polar electronic charge of a molecular structure on the polarity σ scale, obtained from the histogram function σ -Profile given by COSMO-RS methodology.³¹ We have recently shown its capability to describe qualitatively and quantitatively the electronic structure and molecular size of a wide variety of ionic liquids (IL).³² Specifically, the $S_{\sigma\text{-profile}}$ molecular descriptor has been successfully related by NN to three solvent properties of neat ILs and their mixtures (density, IL solubility in hydrocarbons and partition coefficient of aromatic compounds between aliphatic and IL solvents),³³ properties which depend on the molecular size and the intermolecular interactions of the mixture. In addition, the $S_{\sigma\text{-profile}}$ descriptor has been used in quantitative structure–property relationships (QSPR) based on NN for the prediction of polarity/polarizability scales of pure solvents and their binary and ternary mixtures.³⁴ This study represented the first *a priori* computational approach for a reliable prediction of the non-ideal behavior of solvent effects in mixtures. A remarkable advantage of the $S_{\sigma\text{-profile}}$ parameter is its additive character, since $S_{\sigma\text{-profile}}$ values result from the contribution of the different atomic groups on a σ -range.^{32,33} Thus, the $S_{\sigma\text{-profile}}$ descriptor of a pure IL or a mixture of ILs can be successfully defined as the sum of those $S_{\sigma\text{-profile}}$ values of their independent ions.

In the current study, we will develop a QSAR model to establish the toxicological effects of ILs based on the integration of the powerful $S_{\sigma\text{-profile}}$ descriptor of the cations and anions on NN. In a preliminary section, $S_{\sigma\text{-profile}}$ descriptor was validated by multilinear regression (MLR) relationships to the cytotoxicity of ILs in Leukemia Rat Cell Line (Log EC₅₀ IPC-81).³⁵ For this analysis, the available experimental Log EC₅₀ IPC-81 data for 86 ILs and 9 closely related salts were used,⁷ including 35 different cations (ammonium, imidazolium, phosphonium, pyridinium, quinolinium, and sodium) and 18 different anions. Subsequently, a neural network was designed and optimized to estimate the Log EC₅₀ IPC-81 values of ILs as a function of a restricted number of ten $S_{\sigma\text{-profile}}$ input values (4 for cations and 6 for anions), revealed as statistically significant descriptors in previous MLR analysis. For the development of NN model the Log EC₅₀ IPC-81 sample data were extended to 105 compounds (96 ILs and 9 salts), including additional cations and anions with very high and non-additive cytotoxicological effects. Then, the developed QSAR approach was used for the reliable Log EC₅₀ IPC-81 predictions of ~450 ILs, obtained using 53 cations – with 6 different head groups, different side chains (from 1 to 16 carbon atoms), and functional groups (ether, hydroxyl, benzyl and amino, among others) – and 20 different anions. As a result of this study, the new concept of a Quantitative Structure–Activity Map (QSAM) was established with the following main objectives: (i) the Quantitative Electronic Structure–Activity Map (QSAM-E) approach relates the estimated Log EC₅₀ IPC-81 values to the molecular electronic information of IL compounds given by the COSMO-RS method. As a consequence, QSAM-E allows a deeper insight into the chemical features of toxicophore substructures and the toxicological impacts of ILs; and (ii) the Quantitative Chemical Structure–Activity Map (QSAM-C) approach relates the estimated Log EC₅₀ IPC-81 values to the chemical structure of both cation and anion constituting the IL. Considering the non-linear toxicophore mixture effects,²² which prevent the use of additive predictive models for IL toxicity, QSAM-C is proposed as a useful guide for the prospective design of safer ILs.

Recently, we reported an *a priori* computational design tool to obtain ILs with suitable processing features for specific applications.³³ QSAM approaches were presented as a complementary tool to also take into account the toxicological hazards in the product design of ILs. In this sense, the developed QSAR model was finally applied in this work to screen commercially available ILs in order to select those with comparatively low cytotoxicities.

2. Computational details

2.1 Data set

All toxicity data used for this study was reported in successive works by Prof. Ranke's group and reviewed in ref. 7. The training sample includes the cytotoxicity values of 96 ILs and 9 closely related salts in a leukemia rat cell line (Log EC₅₀ IPC-81). Log EC₅₀ values are base-10 logarithms of EC₅₀ values in μM , the sample data values ranging from -0.19 to 4.30 . The external validation sample consists of Log EC₅₀ IPC-81 values of 15 new

ILs whose types of cation or anion were not previously used for developing the QSAR model.

2.2 Molecular structures

The molecular geometries of independent cationic and anionic species of ILs were optimized at the B3LYP/6-31++G** computational level in the ideal gas phase using the quantum-chemical Gaussian03 package.³⁶ Vibrational frequency calculations were performed for each case to confirm the presence of a minimum energy.

2.3 $S_{\sigma\text{-profile}}$ descriptor

Gaussian03 was used to compute the COSMO files.³⁵ The ideal screening charges on the molecular surface for each species were calculated by the continuum solvation COSMO model using the BVP86/TZVP/DGA1 level of theory. In these calculations, the continuum solvation model COSMO is applied in order to simulate a virtual conductor environment for the molecule, inducing a polarization charge density σ on the interface of the molecule to the conductor, *i.e.* on the molecular surface, generating a more polarized electron density than in vacuum. The 3D distribution of the polarization charges σ of each molecule is converted into a surface composition function (σ -Profile) by the COSMOtherm program.³⁷ Such a σ -Profile gives the relative amount of surface with polarity σ , $p^{\sigma}(\sigma)$, on the surface of the molecule. The $S_{\sigma\text{-profile}}$ molecular descriptors of cations and anions were evaluated by the estimation of the probabilistic surface charge distribution on their σ -Profile at different polarity regions. The σ -Profile values of the IL counterions used in this work are provided as supplementary material, together with the nomenclature used to refer to the cations and anions included in the study.

2.4 Neural network design

Neural networks are composed of neurons (information-processing units), and in each of them non linear algorithms are implemented (*vide infra*). The Multi-Layer Perceptron (MLP) used here has been designed by MATLAB version 7.01.24704 (R14).³⁸ The MLP model is a feed-forward supervised network. Each neuron receives information of all the neurons from the previous layer. Every connection is controlled by parameters (called weights) that modulate the output of the neuron before inputting its numerical content to a neuron in the following layer. The process where the weights are optimized is called the learning or training process.^{38,39} Here, the training algorithm used is based on back-propagation algorithm (BP). As the NN estimates the LogEC₅₀ IPC-81 of ILs using ten values of $S_{\sigma\text{-Profiles}}$, the learning, verification and validation samples consist of eleven rows (one for each $S_{\sigma\text{-Profile}}$ and LogEC₅₀ IPC-81) and as many columns as ILs tested (105 columns). The only difference between the verification and the learning samples is that the latter is composed of 86 columns (81.9% of data) and the former of 19 columns (18.1% of data). Taking into account that every datum of the verification sample should be interpolated within the learning range, the data were randomly distributed between both samples. The external validation sample is made up of the

LogEC₅₀ IPC-81 values of 15 new ionic liquids, specified in the ESI†.

In order to guarantee the reliability of the estimations calculated by these models, the applicability domain has been evaluated selecting the compounds with cross-validated standardized residuals greater than three standard deviations.^{40–42} As the highest cross-validated standardized residual is 2.62 standard deviations (1-hexadecyl-3-methylimidazolium chloride), no set was considered as an outlier.^{40,41}

The MLP model used consists of three layers (input, hidden and output), a topology widely used to deal with several problems.^{27,32–34} The input layer has as many nodes as $S_{\sigma\text{-Profile}}$ used (10 input nodes) and one output neuron to estimate the LogEC₅₀ IPC-81. The hidden neuron number (HNN) should be fixed by optimization techniques (*vide infra*). Given that the range of most $S_{\sigma\text{-Profiles}}$ and the sigmoid function are between 0 and 1, the sigmoid function has been used as the MLP transfer function.^{38,39}

The BP algorithm is based on the Bayesian Regularization (trainBR) training function. It was selected because its generalization power is higher than other training functions and avoids overfitting and overtraining when a small learning sample is used.³⁹ Their specific parameters are learning coefficient (Lc), learning coefficient decrease (Lcd), learning coefficient increase (Lci). The Lc parameter is similar to “h” in Newton’s method (often called the Newton–Raphson method). Lcd and Lci control the value of Lc depending on the MLP model performance. To avoid overfitting of the NN model, learning and verification samples were used (*vide supra*) and the learning process was stopped when the error of prediction (mean square error, MSE) for the verification sample, defined by eqn (1), began to increase. A detailed description of the calculation process is described in the literature.^{43–46}

$$\text{MSE} = \frac{1}{N} \sum_{k=1}^N (r_k - y_k)^2 \quad (1)$$

In eqn 1, N , y_k and r_k are the number of datasets of the database, the response of the output neuron and the corresponding real output response, respectively.

The HNN and NN parameters are optimized by an experimental design based on the Box-Wilson Central Composite Design 2⁴ + Star Points. The experimental factors analyzed were Lc, Lcd (between 1 and 0.001) and Lci (between 2 and 100).⁴⁷ Taking into account the learning sample size, the HNN range was selected between 3 and 10.⁴⁸ The responses of the experimental design were the Mean Prediction Error (MPE), eqn 2, and correlation coefficient (predicted vs. real values, R^2). Both indexes are easily computed and provide a good description of the predictive performance of the NN model.⁴⁹ As the main objective is to have an NN which predicts results with the highest possible accuracy, the considerations taking into account to analyze the experimental design were the need to achieve the least MPE with the highest values of R^2 .

$$\text{MPE} = \frac{1}{N} \sum_{k=1}^N \frac{|r_k - y_k|}{r_k} \times 100 \quad (2)$$

3. Results

3.1 Validation of COSMO-RS descriptor for IL toxicity

Klamt and co-workers³⁰ have developed a quantum chemical approach (COSMO-RS) for the prediction of the thermodynamic properties of fluids using only the surface polarity distributions of individual molecules, which result from quantum chemical calculations. An important advantage of COSMO-RS methodology is that it also provides the 3D charge distribution (σ) on the molecular surface, easily visualized in the histogram function σ -Profile. Based on COSMO-RS methodology, the σ -Profile of one compound includes the main chemical information necessary to predict its possible interactions in a fluid.³⁰ As an example, let us consider the surface polarization charge densities and the resulting σ -Profiles of some cations and anions of common ILs (Fig. 1). The COSMO-RS histogram can be qualitatively divided in three main regions upon next cut-off values: hydrogen bond donor ($\sigma_{\text{HB}} < -0.0082 \text{ e } \text{\AA}^{-2}$) and acceptor ($\sigma_{\text{HB}} > 0.0082 \text{ e } \text{\AA}^{-2}$) regions and non-polar region ($-0.0082 < \sigma < 0.0082 \text{ e } \text{\AA}^{-2}$).³⁰ Thus, the σ -Profile of the negatively charged Cl^- anion corresponds to a single peak located at the strongly negative polar region ($+0.019 \text{ e } \text{\AA}^{-2}$). This characteristic is represented in its polar surface by a deep red colour. Therefore, the chloride anion can be considered a hydrogen bond acceptor segment. Similarly, PF_6^- presents a unique peak in its σ -Profile, but at a less negative polar region ($0.009 \text{ e } \text{\AA}^{-2}$), which is visualized in the polar surface by a light orange colour. It indicates a lower polar character in PF_6^- with respect to Cl^- . NTf_2^- also shows a weak hydrogen bond acceptor fragment (peak located at $0.011 \text{ e } \text{\AA}^{-2}$ corresponding to $-\text{SO}_2$ groups). In addition, NTf_2^- presents an electronic charge located in the non-polar σ regions, *i.e.*, $\pm 0.0082 \text{ e } \text{\AA}^{-2}$, mainly due to the $-\text{CF}_3$ groups of the anion. The surface of these non-polar fragments is represented in green in Fig. 1.

The polarisable surface and the σ -Profiles of the imidazolium, ammonium and quinolinium cations with a common butyl side chain are shown in Fig. 1A. As can be seen, the surface of

the cations is mainly non-polar, *i.e.*, green, with a tendency to blue-green on the more polarized fragments. The σ -Profiles were dominated by a main peak with the charge distribution around zero ($-0.0082 < \sigma < 0.0082 \text{ e } \text{\AA}^{-2}$), corresponding to the aliphatic groups of the cationic alkyl chains. In addition, some unresolved peaks along with low peaks were observed at lower values than the cutoff $-0.0082 \text{ e } \text{\AA}^{-2}$. These peaks are related to the hydrogen atoms of the aromatic ring for the case of imidazolium and quinolinium cations and those of the ammonium cation closest to its nitrogen atom. According to COSMO-RS theory,³¹ these cationic fragments may contribute to hydrogen bonds as donors. These examples manifest how the σ -Profile qualitatively describes the different electronic nature of cations and anions. In fact, we have demonstrated that the charge distribution area ($S_{\sigma\text{-profile}}$) below σ -Profile can be used as a suitable molecular descriptor of solvent properties, with the remarkable advantages of being a quantum-chemical-derived parameter defined in a restricted scale of polarity ($\pm 0.025 \text{ e } \text{\AA}^{-2}$ for most compounds) and presenting an additive character (the σ -Profile of a IL can be reasonably defined as sum of cation and anion contributions).³³

As the first step to develop a QSAR model for establishing IL toxicity based on COSMO-RS information, multilinear regression (MLR) models were constructed for prediction of LogEC_{50} IPC-81 values of ILs. We initially considered the 61 levels of charge distribution [$p^x(\sigma)$] defining the σ -Profile of IL ionic species in the range $\pm 0.03 \text{ e } \text{\AA}^{-2}$, *i.e.*, 61 $S_{\sigma\text{-profile}}$ values. In order to design the best MLR model, the regression model selection (RMS) analysis was used (SPSS software version 15.0.1). The RMS analysis ranked the best subsets of the introduced explanatory variables, using the criteria of best adjusted correlation coefficient and MPE for all possible linear regression models (estimated *vs.* real LogEC_{50} IPC-81 values). Since Ranke *et al.*^{17,18} found a good correlation between the alkyl chain lengths in imidazolium-based ILs and their LogEC_{50} IPC-81 cytotoxicities, we initiated the RMS analysis introducing $S_{\sigma\text{-profile}}$ descriptors of imidazolium cations for a sample data of

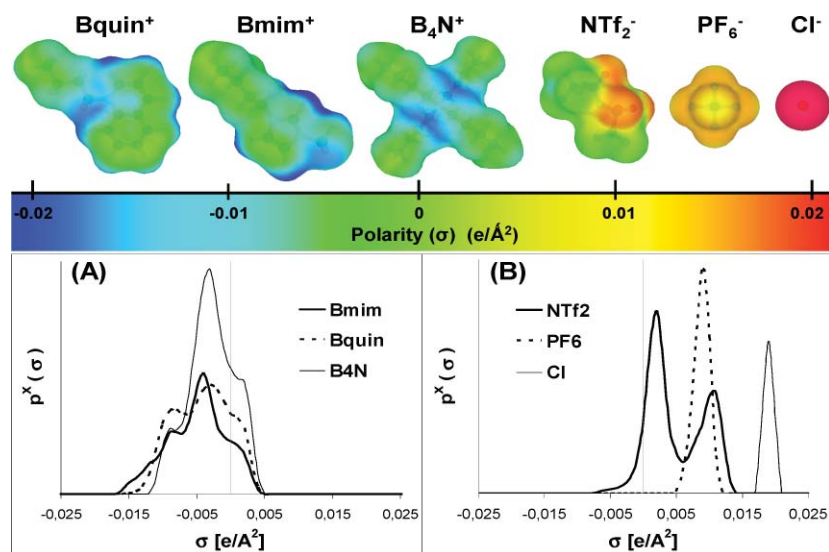


Fig. 1 Surface polarization charge density and σ -Profile of some representative cations (A) and anions (B) of ionic liquids.

Table 1 MLR results for LogEC₅₀ IPC-81 prediction using the S_{σ-profile} molecular descriptors of cation or/and anion obtained from the σ-Profile^a

MLR - Model 1

$$\text{LogEC}_{50} \text{ IPC-81 (Predicted)} = C_0 + \sum_i C_i^{\text{ion}} \cdot S_{\sigma\text{-prof}}^{\text{ion}}(i)$$

Aim/Sample	Eq.	C ₀	C _{-0.011} ^{cation}	C _{-0.008} ^{cation}	C _{-0.006} ^{cation}	C _{-0.002} ^{cation}	C _{-0.002} ^{cation}	C _{0.009} ^{cation}	C _{0.011} ^{cation}	C _{-0.015} ^{cation}	C _{-0.015} ^{cation}	C _{-0.015} ^{cation}	R ²	σ	N
Cation effect / Imidazolium ILs	3	4.8 ± 0.8	0.2 ± 0.1	-0.15 ± 0.03	—	-0.085 ± 0.004	—	—	—	—	—	—	0.90	0.31	60
Anion effect / Imidazolium ILs	4	2.3 ± 0.1	—	—	—	—	-0.012 ± 0.006	0.015 ± 0.006	0.025 ± 0.008	0.047 ± 0.009	0.038 ± 0.007	0.047 ± 0.009	0.91	0.19	15
Cation effect / Imidazolium ILs + toxic anions	5	3.8 ± 0.9	0.3 ± 0.2	-0.13 ± 0.04	—	-0.081 ± 0.005	—	—	—	—	—	—	0.81	0.42	65
Anion effect / 5 head group types of ILs	7	4.9 ± 0.4	-0.03 ± 0.01	-0.12 ± 0.03	0.06 ± 0.02	-0.077 ± 0.004	—	—	—	—	—	—	0.81	0.43	95

MLR - Model 2

$$\begin{aligned} \text{IPC-81 (Predicted)} &= \text{IPC-81}^{\text{cation}} + \text{IPC-81}^{\text{anion}} \\ &= C^{\text{cation}} \cdot \text{IPC-81}_{\text{MLR Model 1}}^{\text{cation}} + \sum_j C_j^{\text{anion}} \cdot S_{\sigma\text{-prof}}^{\text{anion}}(j) \end{aligned}$$

Aim/Sample	Eq.	C ^{cation}	IPC-81 _{MLR Model 1} ^{cation}	C _{-0.002} ^{anion}	C _{0.005} ^{anion}	C _{0.011} ^{anion}	C _{-0.015} ^{anion}	C _{-0.015} ^{anion}	C _{-0.015} ^{anion}	R ²	σ	N
Cation + Anion effects / Imidazolium ILs	6	0.96 ± 0.04	Eq. 5	-0.025 ± 0.006	0.005 ± 0.003	0.002 ± 0.005	0.03 ± 0.01	0.007 ± 0.006	0.013 ± 0.005	0.91	0.31	65
Cation + Anion effects / 5 head group types of ILs	8	0.94 ± 0.03	Eq. 7	-0.022 ± 0.005	0.006 ± 0.003	0.004 ± 0.004	0.034 ± 0.009	0.008 ± 0.004	0.012 ± 0.004	0.90	0.34	95

^a R²: Square correlation coefficient; σ = Standard deviation; N = number of IL in sample data.

60 ILs (MLR Model 1 in Table 1). The RMS analysis revealed that only three S_{σ-profile} of cation were needed to obtain a good MLR model [eqn 3 in Table 1], located at -0.002, -0.008 and -0.011 e Å⁻². The good quality of these simple relationships was indicated by a correlation coefficient R² = 0.90 and a standard deviation of 0.31 (these being parameters based on a logarithmic scale). The results of LogEC₅₀ IPC-81 predictions by eqn 3 are shown in Fig. 2A. As can be seen in Fig. 2C, the S_{σ-profile} descriptors used in eqn 3 were located at the peak maximum for alkyl fragment (-0.002 e Å⁻²) and hydrogen groups linked to head groups (-0.008 and -0.011 e Å⁻²). Interestingly, eqn 3 presents

a negative coefficient for the two cationic S_{σ-profile} descriptors in the non polar range (-0.0082 < σ < 0.0082 e Å⁻²), i.e., the corresponding molecular fragments increase IL toxicity (lower LogEC₅₀ IPC-81 values). In contrast, the coefficient of the S_{σ-profile} descriptor corresponding to the most polarized hydrogen group (-0.011 e Å⁻²) presents a positive signal in eqn 3, i.e. the more acidic groups of cation contribute to the reduction of the IL toxicity. As second step on COSMO-RS descriptor validation, we performed a RMS analysis for the LogEC₅₀ ICP-81 values of 15 ILs with the common cation 1-butyl-3-methylimidazolium, using in this case the 61 S_{σ-profile} values of anions. A good MLR

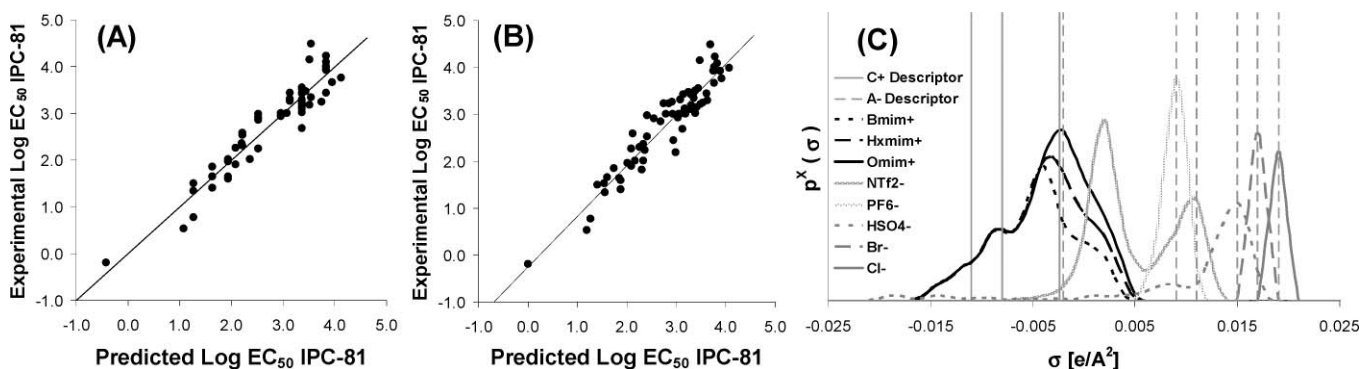


Fig. 2 Comparison of experimental LogEC₅₀ IPC-81 values to those estimated by the MLR model (A) for 60 imidazolium -based ILs, using Eq. 1 with three S_{σ-profile} values of cation, located at -0.002, -0.008 and -0.011 e Å⁻²; and (B) for 65 imidazolium-based ILs, eqn 6 with nine S_{σ-profile} input values (cation: -0.002, -0.008, -0.011 e Å⁻²; and anion: -0.002, 0.009, 0.011, 0.015, 0.017, 0.019 e Å⁻²); and (C) Location of S_{σ-profile} descriptors of cations (used in eqn 3) and anions (used in eqn 4) at σ-Profile polarity range.

model (eqn 4 in Table 1) to describe anion effects was constructed using 6 statistically relevant $S_{\sigma\text{-profile}}$ descriptors of anions, located at -0.002 , 0.009 , 0.011 , 0.015 , 0.017 and 0.019 e \AA^{-2} on their $\sigma\text{-Profile}$ (Fig. 2C). The analysis of eqn 4 indicated that higher polarized anionic fragments result in less toxic ILs. However, the presence of non-polar groups in the anion (see NTf_2^- in Fig. 2C) confers a toxicological effect on ILs, based on the negative coefficient in eqn 4.

The next step was to achieve a general QSAR approach to analyze both cation and anion effects on IL cytotoxicity. For this purpose, we proposed a different MLR, Model 2 (Table 1), which estimates separately the contributions of cation and anion to Log EC_{50} IPC-81 value. The sample data included 65 imidazolium-based ILs, which incorporated anions with considerable toxic effects such as $(\text{C}_2\text{F}_5)_3\text{PF}_3^-$, $\text{N}(\text{CF}_3)_2^-$ and $\text{Co}(\text{CO})_4^-$.¹⁹ Firstly, the main cationic effects were described for the 65 ILs by MLR Model 1 (eqn 5 in Table 1) using 3 $S_{\sigma\text{-profile}}$ descriptors of cations (located at -0.002 , -0.008 and -0.011 e \AA^{-2}). Then, the Log EC_{50} IPC-81 contribution from cation (eqn 5) was included as input in the MLR Model 2 (eqn 6 in Table 1), together with the 6 $S_{\sigma\text{-profile}}$ descriptors of the above-mentioned anion. The predicted Log EC_{50} IPC-81 values by MLR Model 2 (eqn 6) were compared with the experimental values in Fig. 2B. Finally, the scope of the proposed MLR Model 2 was extended to 95 ILs with different head groups (imidazolium, pyridinium, phosphonium, ammonium, pyrrolidinium and sodium, as reference). The RMS analysis, introducing the 61 $S_{\sigma\text{-profile}}$ descriptor of the cation, provided an optimized MLR Model 1 (eqn 7 in Table 1) with four $S_{\sigma\text{-profile}}$ inputs, corresponding to those used in eqn 5, plus an additional input at -0.006 e \AA^{-2} , which presented a significant statistical influence in some head groups such as quinolinium. Then, MLR Model 2 (eqn 8 in Table 1) was constructed to predict both cation and anion effects by including the Log EC_{50} IPC-81 contribution from cation (eqn 7) and the 6 $S_{\sigma\text{-profile}}$ descriptors of anions used in eqn 6.

As can be seen in Fig. 3A, the proposed QSAR approach provided a reasonable prediction of Log EC_{50} IPC-81 values for a wide variety of ILs including 6 different head groups and 19 types of anions. In addition, MLR Model 2 (eqn 8) can be used for a simplistic estimation of cation and anion contribution to IL toxicity. Thus, Fig. 3B showed that the dominant contribution

of cation to IL toxicity increases with the side chain length, in agreement with experimental evidence.^{17,18} On the other hand, current results indicate that most of anions (as Cl^- or HSO_4^-) contribute to the reduction of the IL toxicity, whereas other anions (such as $(\text{C}_2\text{F}_5)_3\text{PF}_3^-$, $\text{N}(\text{CF}_3)_2^-$ or $\text{Co}(\text{CO})_4^-$) were described as strong toxicophores by eqn 8. Similarly, Fig. 3C presented the effect of head group (with common butyl side) on toxicity for some representative IL examples. Quinolinium and pyrrolidinium head groups exhibited, respectively, the highest and lowest hazardous effects, whereas imidazolium and pyridinium cations presented intermediate toxicities, in line with experimental trends with small anions [Experimental Log EC_{50} IPC-81 values: BquinBr (2.32) < BmimBr (3.43) < BpyrrBr (3.77)].⁷ However, the QSAR approach proposed by MLR Model 2 presents significant limitations to predict accurately IL cytotoxicity. For example, it failed to describe the non-linear behaviour of Log EC_{50} IPC-81 values with the alkyl chain length for highly hydrophobic ILs.²¹ In addition, the observed non-additive toxicophore effects for different cation and anion mixtures^{19,23} cannot be described by the QSAR model based on MLR approximation. Therefore, a main aim of this work was the generation of a non-linear model based on NN for the prediction of Log EC_{50} IPC-81 values of ILs using 4 $S_{\sigma\text{-profile}}$ descriptors of cation and 6 $S_{\sigma\text{-profile}}$ descriptors of anions. The sample data contained 105 different compounds, including ILs with very large cations (TetraDmim⁺ or P_{66614}^+) or anions (BBDB⁻). Following the aforementioned optimization process, the NN model was designed using the learning sample. The optimum values of HNN, Lc, Lcd and Lci were 9, 0.001, 1 and 2 respectively (see Table 2). Then, using these parameter values,

Table 2 Optimized parameters of the MLP model

Parameters	
Transfer function	Sigmoid
Input nodes number	10
Hidden neurons number	9
Output neuron number	1
Learning coefficient, Lc	0.001
Learning coefficient decrease, Lcd	1
Learning coefficient increase, Lci	2

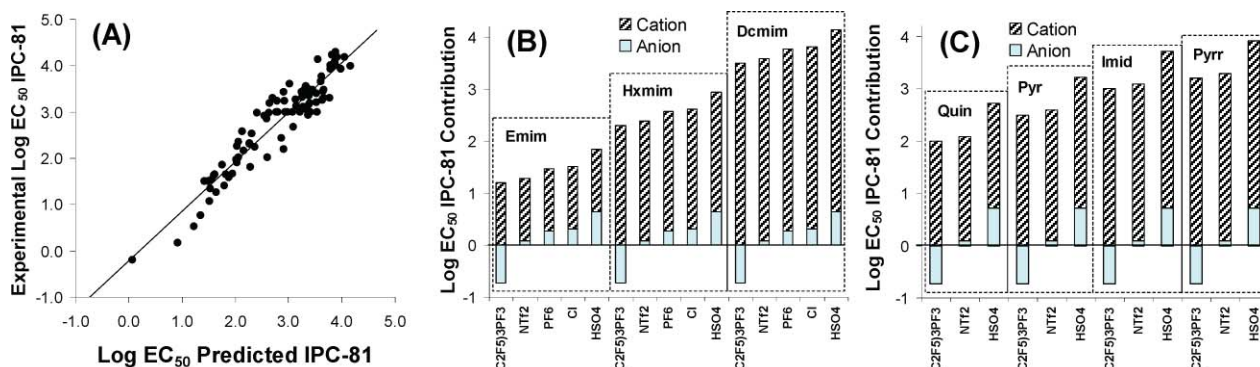


Fig. 3 (A) Comparison of experimental Log EC_{50} IPC-81 values to those estimated by the MLR model for 95 ILs using eqn 8 with ten $S_{\sigma\text{-profile}}$ input values (cation: -0.002 , -0.006 , -0.008 , -0.011 e \AA^{-2} ; and anion: -0.002 , 0.009 , 0.011 , 0.015 , 0.017 , 0.019 e \AA^{-2}); Cation and anion contribution to estimated Log EC_{50} IPC-81 values given by eqn 8 for (B) the 1-alkyl-3-methylimidazolium series and (C) the head group series (with a common butyl side chain).

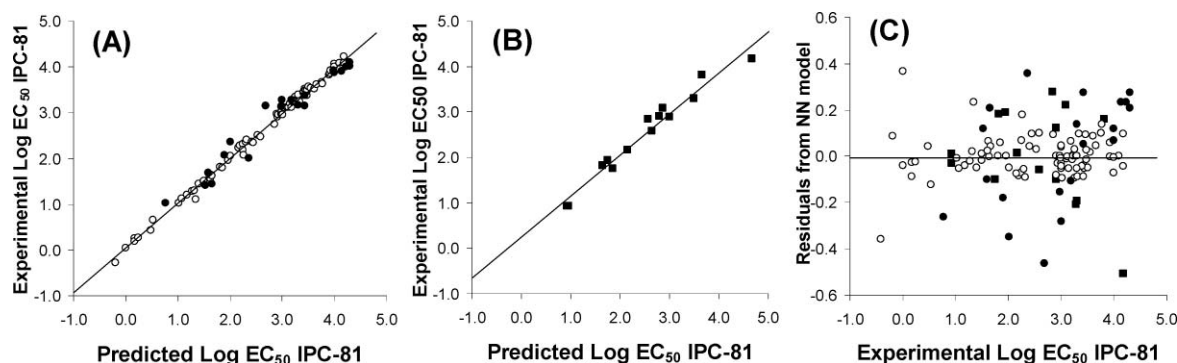


Fig. 4 Comparison of experimental LogEC₅₀ IPC-81 values to those estimated by the NN model for 105 ILs using ten $S_{\sigma\text{-profile}}$ input values (cation: $-0.002, -0.006, -0.008, -0.011 \text{ e \AA}^{-2}$; and anion: $-0.002, 0.009, 0.011, 0.015, 0.017, 0.019 \text{ e \AA}^{-2}$). (A) Learning and verification samples and (B) Validation sample. (C) Graphical analysis of residuals from NN model. (○) Learning sample; (●) Verification sample; (■) External validation sample).

the model was verified. In this process, the model was tested against a verification sample that had not been included in the neural network learning sample. Fig. 4A compared the LogEC₅₀ IPC-81 estimations for learning and verification samples to the experimental values. The correlation coefficient R^2 was obtained higher than 0.996 and MPE and σ were less than 0.47% and 0.12, respectively (these being statistical parameters based on a logarithmic scale of LogEC₅₀ IPC-81). Finally, in order to carry out an external validation process of the optimized model,^{40,50,51} a new validation sample based on experimental data available in literature was employed. Taking into account that the external validation sample range must be within the learning sample range and belong to the same application domain (*vide supra*), the datasets used in the external validation of the MLP model were selected. The mathematical procedure followed was similar to the verification process described above. As can be seen in Fig. 4B, the MLP model presents an acceptable goodness of fit, with $R^2 > 0.96$ and MPE $< 5.7\%$. In terms of external explained variance (Q_{ext}^2), given that this parameter is close to 1 ($Q_{\text{ext}}^2 > 0.94$), the NN model is stable and predictive.^{41,50} Fig. 4C reported the residuals from the NN model. Given that the R^2 between residuals and LogEC₅₀ IPC-81 values is less than 0.07, no mathematical dependence between them can be found. Therefore, in the light of the statistical results, the non-linear NN model (MLP) was adequate to estimate LogEC₅₀ IPC-81 values

of ILs, by only using 10 $S_{\sigma\text{-profile}}$ descriptor values of counterion components, which are derived solely from quantum-chemical COSMO-RS calculations. The diversity of cations (>40) and anions (>20) used to design the NN model, together with the high variability of LogEC₅₀ IPC-81 values (between -0.19 and 4.30), guaranteed the generality of the developed non-linear QSAR model based on NN, validating the *a priori* $S_{\sigma\text{-profile}}$ parameter for the description of IL cytotoxicities.

3.2 Quantitative structure–activity maps (QSAM) for IL toxicity

In this section, the new concept of Quantitative Structure–Activity Map is presented as a systematic way of examining IL compounds from their structural components (alkyl side chain, head group, anion type and linked functional groups) determining their effects on a biological system (leukemia rat cell line, IPC-81). For this purpose, firstly, an extensive screening of IL cytotoxicity for ~ 450 possible cation–anion combinations was performed using the reliable QSAR model based on optimized NN model with 10 $S_{\sigma\text{-profile}}$ descriptors (LogEC₅₀ IPC-81 estimations of ILs were given as ESI†). To establish our hypothesis, Fig. 5A shows the polar charge distribution given by the σ -Profiles of a 1-alkyl-3-methylimidazolium series, which can be represented by a 3-D graph or by a 2-D contour

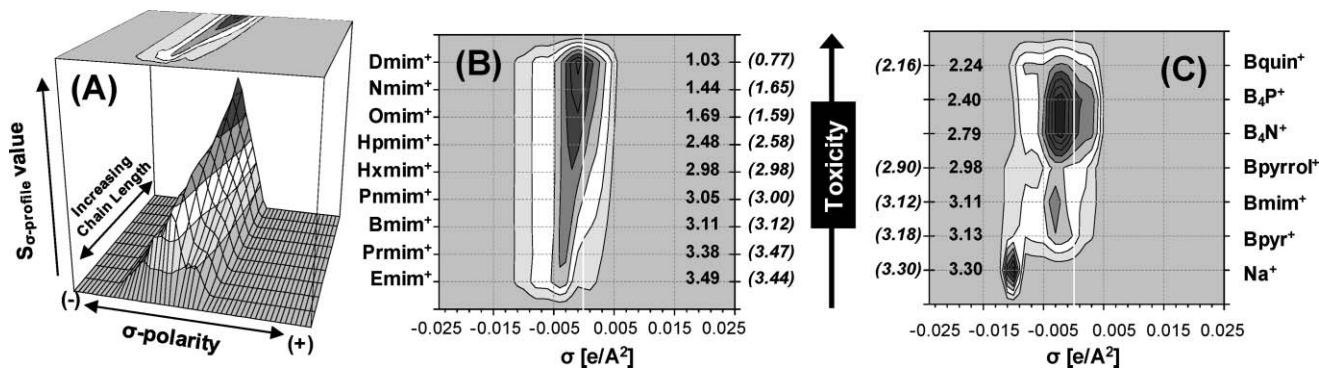


Fig. 5 (A) 3D Graph of σ -Profile for the 1-alkyl-3-methylimidazolium cation series; (B) Quantitative Electronic Structure–Activity Map (QSAM-E) of the alkyl chain effect for the 1-alkyl-3-methylimidazolium tetrafluoroborate series; and (C) QSAM-E of the head-group effect for IL series with a common BF_4^- anion and butyl side chain. Experimental and estimated LogEC₅₀ IPC-81 values are given in parentheses and without parentheses, respectively.

plot. It seems to be clear that the alkyl side effects on the IL toxicities may be rationalized on a molecular basis by relating them to quantum-chemical COSMO-RS information of the cation. With this aim, Fig. 5B proposes a QSAM-E for describing the alkyl chain effects on a series of 1-alkyl-3-methylimidazolium tetrafluoroborate compounds. QSAM-E approach visually relates the estimated LogEC₅₀ IPC-81 values to the electronic polar structure of cation, distributed along the σ -polarity scale. Thus, the progressive increase of IL toxicity with the length of cation side chain can be ascribed to the increasing amount of charge distribution on the non-polar range ($-0.0082 < \sigma < 0.0082 \text{ e } \text{\AA}^{-2}$) of σ -Profile. Continuing the analysis, Fig. 5C presents a QSAM-E for the study of the effect of cationic head group on LogEC₅₀ IPC-81 values for a subset of different core structures, all carrying the common anion (BF_4^-) and butyl side chain. The conclusion of the analysis was again that the increasing addition of non-polar fragments on cation contributes to the hazardous effect of ILs. Interestingly, the more polarized the head group, the less toxic it is. Thus, the reported different behaviour of the quinolinium head group, as a strong toxicophore substructure,²¹ can be assigned to its largely delocalized non-polar electronic charge. Finally, the QSAM-E approach was applied to the systematic study the anion effect on LogEC₅₀ IPC-81 estimations for a series of 1-butyl-3-methylimidazolium compounds (Fig. 6). It was observed that the toxicological effects increased progressively with the loss of anion polarity. In fact, we identified three class of anions in QSAM-E analysis: (i) those with high basicity, *i.e.*, with polar nucleophilic fragments present at $\sigma > 0.015 \text{ e } \text{\AA}^{-2}$, and low toxicophore features, as Cl^- or CH_3SO_3^- , with LogEC₅₀ IPC-81 > 3.4 ; (ii) those with medium basicity, *i.e.*, polar density located in the range $0.005 < \sigma < 0.015 \text{ e } \text{\AA}^{-2}$, and low or intermediate toxicological effects ($3.0 < \text{LogEC}_{50} \text{ IPC-81} < 3.4$); and (iii) those with strong non-polar characteristics, described by charge density located at $\sigma < 0.005 \text{ e } \text{\AA}^{-2}$, and a marked contribution to IL toxicity, as $(\text{C}_2\text{F}_5)_3\text{PF}_3^-$, $\text{N}(\text{CF}_3)_2^-$, $\text{Co}(\text{CO})_4^-$ or BBDB^- , with LogEC₅₀ IPC-81 < 2.5 . To sum up, NN estimations confirmed strong intrinsic cytotoxicity effects of both cation and anion moieties in IL compounds. In fact, the QSAM-E tool seemed to offer a coherent description of IL

toxicity as a function of the polar charge distribution of ionic substructures of the compound.

These results were basically consistent with a previous QSAR model to establish IL toxicity mainly driven by the lipophilicity of the compound.^{19,22} However, the authors reported some cases with significant deviations from the general linear trend between cytotoxicity and lipophilicity: (i) ILs containing anions with clear intrinsic toxicities (as NTf_2^- or BBDB^-); (ii) ILs based on quinolinium or 4-(dimethylamino)pyridinium cations; and (iii) ILs containing very lipophilic cations with very long alkyl chains. In this work, the lipophilicity parameter $\log k_0$, derived from reverse-phase gradient HPLC retention times,²¹ was found to be directly related to the $S_{\sigma\text{-profile}}$ descriptor of the cation located at the non-polar region $\sigma = -0.002 \text{ e } \text{\AA}^{-2}$, as it is shown in Fig. 7A for 32 ILs including 7 different head groups. The amount of charge estimated by $S_{\sigma\text{-profile}}$ ($-0.002 \text{ e } \text{\AA}^{-2}$) was mainly provided by aliphatic fragments of the structure. This result was relevant because it indicated that the lipophilicity estimations by the $\log k_0$ parameter of ILs would be assigned to those aliphatic fragments of the cation. As a consequence, the deviations from the lipophilicity–cytotoxicity relationship^{19–23} must be attributed to the interactions of other toxicophore fragments with biological systems, which seem to be underestimated by lipophilicity parameter $\log k_0$ in HPLC. For example, QSAM-E in Fig. 7B demonstrated that the different behaviour evidenced for the quinolinium head group²¹ must be assigned to the toxicological effects of the aromatic fragment, which presents a strongly delocalized charge in the negative region of low polarity ($-0.0082 < \sigma < -0.002 \text{ e } \text{\AA}^{-2}$). In addition, the greater toxicity of 4-(dimethylamino)pyridinium with respect to the imidazolium head group^{22,23} can be ascribed not only to the higher amount of non-polar groups at $-0.002 \text{ e } \text{\AA}^{-2}$ region but also to the presence of polarized charge density at the σ region between -0.0082 and $-0.002 \text{ e } \text{\AA}^{-2}$. For its part, the intrinsic cytotoxic effects of NTf_2^- , compared to the reference chloride anion,^{19,22} must be ascribed to the presence of non-polar groups in its structure (Fig. 7C and 7D). On the other hand, the observed significant reduction of imidazolium IL toxicity by the introduction of an oxygenated side chain²³ was explained by QSAM-E on the basis of the charge shift of cation structure towards more polarized regions (Fig. 7E), resulting in less toxicophore features.

As noted in the previous section, the current QSAR study confirmed non-additive mixture effects of toxicophores constituting the IL structures. This is shown in Fig. 8, where the general agreement between the experimental and NN estimated values of LogEC₅₀ IPC-81 of ILs contrasted with the results of MLR Model 2. Thus, the increasing side chain lengths generally imply a decrease of LogEC₅₀ IPC-81 values of ILs (higher toxicity), being the non-linear effects due to the well-known biological cut-off effect correctly described by NN model. It is noteworthy, however, that the scope of the alkyl chain effect is strongly modified by the anion nature (Fig. 8A). For example, $(\text{C}_2\text{F}_5)_3\text{PF}_3^-$ clearly behaves as stronger toxicophore than Cl^- (the latter being used as a non-toxic and bio-compatible reference for anions⁵²) for IL with short cationic alkyl chains; however, it presents the opposite behaviour with very long side chains. Mixture effects were also found to be drastically different for different head groups (Fig. 8B). Thus, the contribution to toxicity of different anions is significantly modified by the cationic head group (see

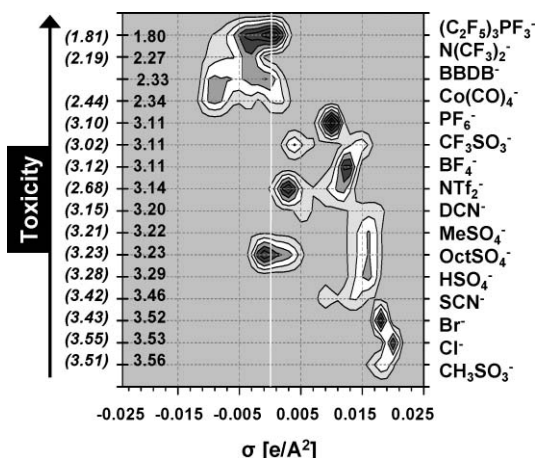


Fig. 6 QSAM-E of the anion effect for the 1-butyl-3-methylimidazolium series. Experimental and estimated LogEC₅₀ IPC-81 values are given in parentheses and without parentheses, respectively.

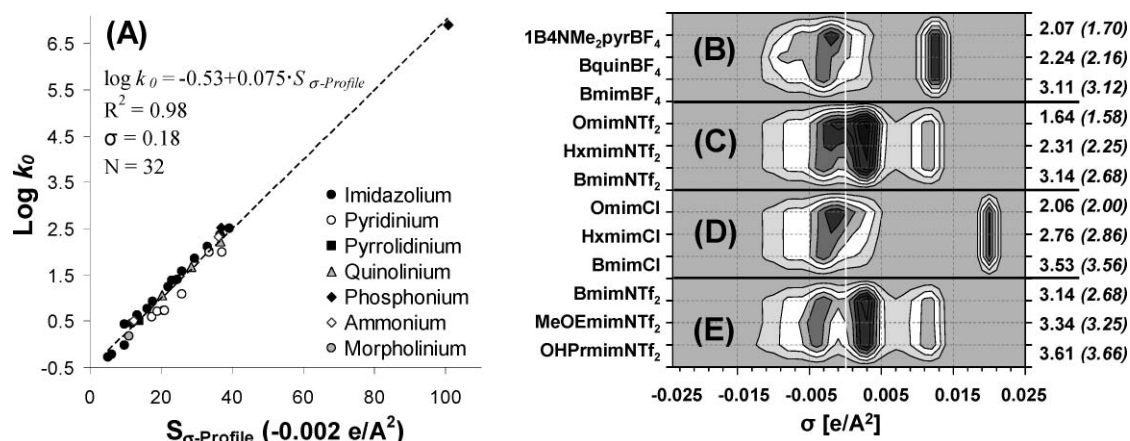


Fig. 7 (A) Comparison of the values for $S_{\sigma\text{-profile}}$ descriptor of cations at $-0.002 \text{ e} \text{ \AA}^{-2}$ against lipophilicity parameter $\log k_0$ derived from reverse-phase gradient HPLC retention times;^{19,22} (B) QSAM-E for ILs with different toxicity-lipophilicity relationships. Experimental LogEC_{50} IPC-81 values are in parentheses.

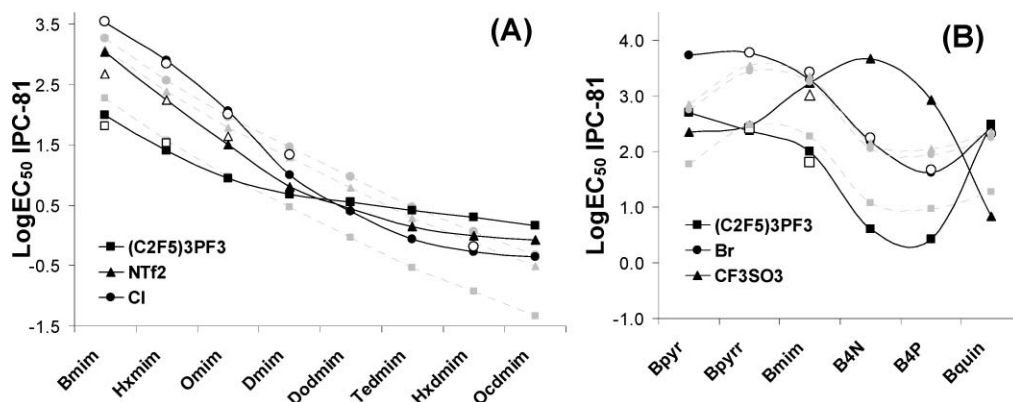


Fig. 8 Non-additive toxicophore effects described by NN estimated (black symbols), MLR estimated (grey symbols) and experimentally available (white symbols) LogEC_{50} IPC-81 values in (A) anion+cation side chain mixture effect and (B) anion+cation head group mixture effects.

the case of CF_3SO_3^- in Fig. 8B). In conclusion, current results show the difficulty of assigning an intrinsic toxicity to an anion, since its toxicophore behaviour is heavily dependent on cationic structure. In other words, a reliable additive treatment based on the intrinsic quantification of cation and anion toxicities is no longer suitable. As a suitable alternative, we proposed the QSAM-C approach to consider the IL cytotoxicity in terms of mixture toxicity. QSAM-C relates the chemical structures of both cation and anion of ILs to the LogEC_{50} IPC-81 estimations in a handy contour plot, as shown Fig. 9 for the families of ILs based on imidazolium (A), pyridinium (B), ammonium (C) and phosphonium (D). The QSAM-C graphics allow a visual quantitative evaluation of IL cytotoxicity in function of the non-linear cation and anion interactions. Firstly, it was clear that the three main structural elements of an IL (cation side chain, cation head group and the kind of anion) have a significant impact on its toxicity, even when the influence of cationic moiety was found to dominate. Thus, the range of LogEC_{50} IPC-81 for a commonly considered low toxic type of IL, such as 1-alkyl-3-methylimidazolium methylsulfate,²² spans from 3.9 to 1.2 by increasing the alkyl side in 7 carbon atoms (Fig. 9A). The non-linear mixture effects were also evident: ILs with intermediate polar anions, such as CF_3SO_3^- or DCN^- , presented the highest

(0.6) and lowest (3.9) toxicity for, respectively, the longest and shortest alkyl imidazolium chains (Fig. 9A). On the other hand, a small anion such as Cl^- seemed to increase its toxicological effects with the length of alkyl chains, whereas a large anion such as BBDB^- presented stronger toxicophore effects in low toxic imidazolium or pyridinium cations, *i.e.*, cations with short side chains (Fig. 9A and 9B). As a general contribution, current QSAM-C revealed that the ammonium-based ILs present lower cytotoxicity than those based on imidazolium, pyridinium or phosphonium head groups, particularly those synthesized with short alkyl chains and alkylsulfate anions (estimated LogEC_{50} IPC-81 values ~ 4.2).

Finally, in order to carry out a useful application, the developed QSAR model was easily used in this work to filter environmentally benign ILs by screening the commercially available compounds, using the criteria of low IL cytotoxicity given in Fig. 6 (LogEC_{50} IPC-81 > 3.4). Table 3 reports 30 ILs with comparatively low hazardous effects, together with their CAS reference number. In fact, 10 commercial ILs in Table 3 were estimated to have lower toxicity than 1-ethyl-3-methylimidazolium ethylsulfate, a compound used in the literature as a reference for low IL toxicity. It should be noted, however, that the examined commercial ILs still have

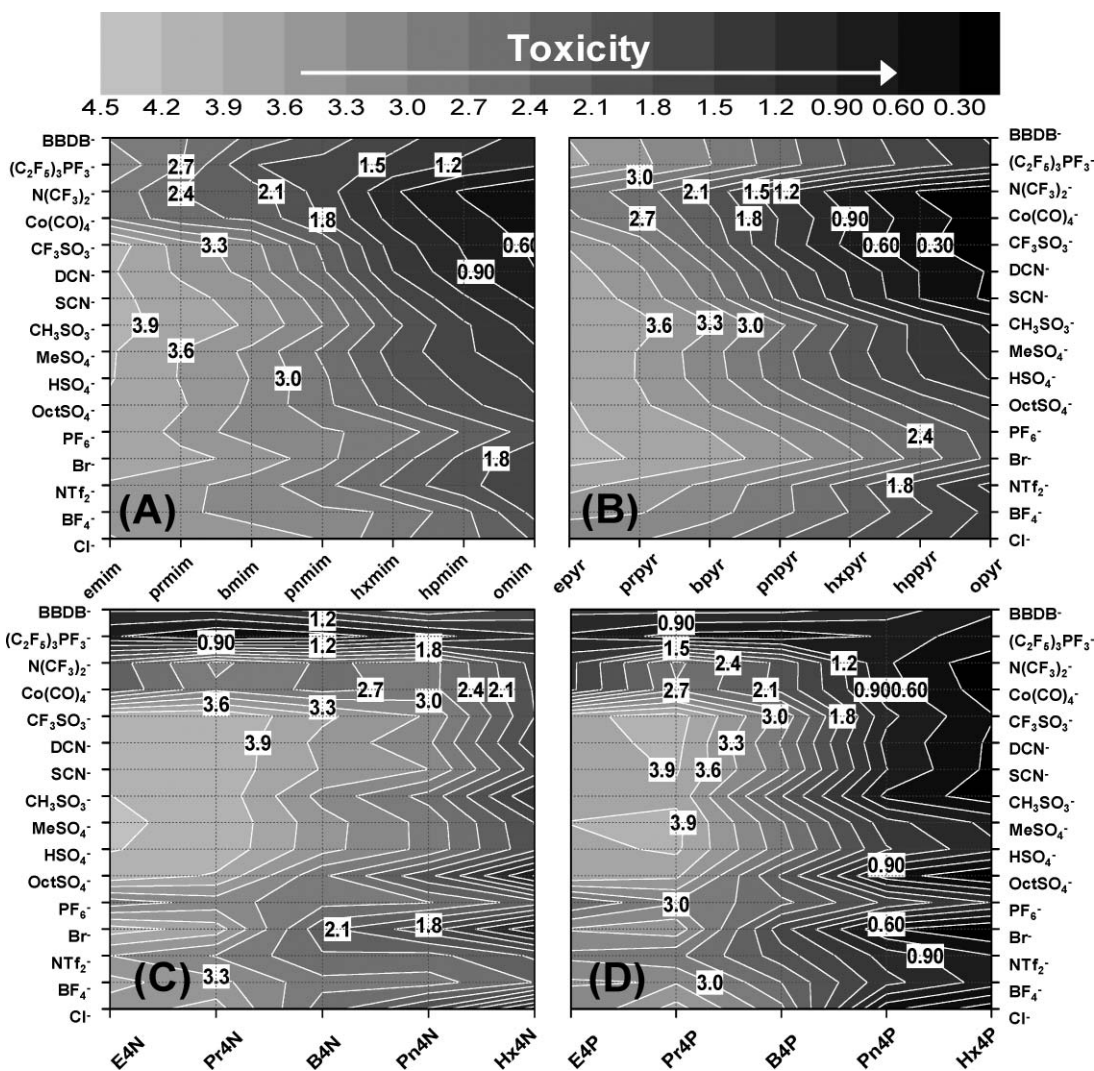


Fig. 9 Quantitative Chemical Structure–Activity Map (QSAM-C) of IL cytotoxicity for (A) 1-alkyl-3-methylimidazolium; (B) 1-alkylpyridinium; (C) tetraalkylammonium and (D) tetraalkylphosphonium series. Estimated LogEC_{50} IPC-81 values for iso-toxicity contour lines are shown with a white background.

cytotoxicities higher than those of common solvents [LogEC_{50} IPC-81 of methyl *tert*-butyl ether (5.6), methanol (6.2) or acetone (6.8)].¹⁷ As a result, further QSAM analysis, based on quantum-chemical data, is currently being performed to select the toxicologically favourable structural elements for designing more sustainable ILs.

4. Conclusions

Predictive relationships between quantum-chemical $S_{\sigma\text{-profile}}$ descriptors of IL compounds and their cytotoxicities (LogEC_{50} IPC-81) were effectively established by non-linear NN analysis for a wide range of cations (>40) and anions (>20), by using a training set of 105 compounds (96 ILs and 9 closely related salts). The reliable non-linear QSAR model was used for the estimation of cytotoxicities of ~450 IL compounds, with the aim of systematically analyzing the toxicological effects of their substructural elements (alkyl side chain, head group and type of anion). As result of this study, the non-additive behaviour of

IL toxicophores was generally observed. This implied that the cytotoxicity of ILs cannot be systematically estimated as the sum of intrinsic toxicities of independent cations and anions. As an alternative predictive model, a new concept of the Quantitative Structure–Activity Map (QSAM) was proposed as a useful tool to design ILs that are not only task-specific, but also inherently safer. Firstly, the QSAM-E approach allowed the analysis of the toxicological behaviour of the components of ILs on a molecular basis, since LogEC_{50} IPC-81 values were understandably related to the polar charge distribution of cations and anions given by the quantum-chemical COSMO-RS method. Secondly, the QSAM-C approach was presented as a simple and reliable graphical guide for the selection of cation and anion, by taking into account the non-linear range of toxicophore mixture effects when the aim is a sustainable computational design of safer ILs. Finally, based on these favourable results, the QSAR model was applied to amplify the current knowledge of IL cytotoxicities by screening commercially available compounds with comparatively low toxicity (LogEC_{50} IPC-81 > 3.4).

Table 3 Estimated LogEC₅₀ IPC-81 of commercially available ionic liquids with comparatively low cytotoxicity (LogEC₅₀ IPC-81 > 3.4)

CAS	Cation	Anion	LogEC ₅₀ IPC-81	
			Estimated	Experimental
479500-35-1	Bpyrr ⁺	Cl ⁻	4.30	—
35895-69-3	E ₄ N ⁺	CF ₃ SO ₃ ⁻	4.19	—
145022-44-2	Emim ⁺	CF ₃ SO ₃ ⁻	4.08	4.09
145022-45-3	Emim ⁺	CH ₃ SO ₃ ⁻	4.03	—
331717-63-6	Emim ⁺	SCN ⁻	4.00	—
1906-79-2	Epyr ⁺	Br ⁻	3.98	—
370865-89-7	Emim ⁺	DCN ⁻	3.94	—
103173-73-5	Epyr ⁺	PF ₆ ⁻	3.94	—
342573-75-5	Emim ⁺	MeSO ₄ ⁻	3.91	3.93
412009-61-1	Emim ⁺	HSO ₄ ⁻	3.92	3.99
65039-08-9	Emim ⁺	Br ⁻	3.89	—
155371-19-0	Emim ⁺	PF ₆ ⁻	3.86	3.92
93457-69-3	Bpyrr ⁺	Br ⁻	3.63	3.77
874-80-6	Bpyr ⁺	Br ⁻	3.73	—
85100-76-1	Prmim ⁺	Br ⁻	3.68	—
712354-97-7	Epyr ⁺	NTf ₂ ⁻	3.68	—
186088-50-6	Bpyr ⁺	PF ₆ ⁻	3.60	—
3878-80-6	Epyr ⁺	CF ₃ SO ₃ ⁻	3.57	—
342789-81-5	Bmim ⁺	CH ₃ SO ₃ ⁻	3.51	3.56
65039-09-0	Emim ⁺	Cl ⁻	3.56	—
174899-82-2	Emim ⁺	NTf ₂ ⁻	3.54	—
79917-90-1	Bmim ⁺	Cl ⁻	3.53	3.55
258273-75-5	B ₁ M ₃ N ⁺	NTf ₂ ⁻	3.52	3.61
85100-78-3	Bmim ⁺	Br ⁻	3.52	3.43
216300-12-8	Prmim ⁺	PF ₆ ⁻	3.51	—
— ^a	Prpyr ⁺	NTf ₂ ⁻	3.50	—
143314-16-3	Emim ⁺	BF ₄ ⁻	3.49	3.44
344790-87-0	Bmim ⁺	SCN ⁻	3.46	3.42
350-48-1	Epyr ⁺	BF ₄ ⁻	3.42	—
216299-72-8	Prmim ⁺	NTf ₂ ⁻	3.40	—

^a Ionic liquid in the Io-Li-Tec catalogue, presented as new without CAS number

Acknowledgements

The authors are grateful to the “Ministerio Ciencia e Innovación” for financial support (projects CTQ2008-01591 and CTQ2008-05641). José S. Torrecilla was supported by a Ramón y Cajal research contract from the “Ministerio Ciencia e Innovación” in Spain. We are very grateful to the “Centro de Computación Científica de la Universidad Autónoma de Madrid” for computational facilities.

References

- 1 T. Welton, *Chem. Rev.*, 1999, **99**, 2071.
- 2 P. Wasserscheid, T. Welton, *Ionic Liquids in Synthesis*, Wiley-VCH, Weinheim, 2003.
- 3 R. D. Rogers and K. R. Seddon, *Ionic Liquids as Green Solvents*, ACS Symposium Series 856, American Chemical Society, 2003.
- 4 R. D. Rogers and K. R. Seddon, *Ionic Liquids IIIB: Fundamentals, Properties, Challenges and Opportunities*, ACS Symposium Series 902, American Chemical Society, 2005.
- 5 X. Han and D. W. Armstrong, *Acc. Chem. Res.*, 2007, **40**, 1079.
- 6 N. V. Plechkova and K. R. Seddon, *Chem. Soc. Rev.*, 2008, **37**, 123–150.
- 7 J. Ranke, S. Stolte, R. Störmann, J. Arning and B. Jastorff, *Chem. Rev.*, 2007, **107**, 2183.
- 8 A. Garcia-Lorenzo, E. Tojo, J. Tojo, M. Teijeira, F. J. Rodriguez-Berrocal, M. P. Gonzalez and V. S. Martinez-Zorzano, *Green Chem.*, 2008, **10**, 508–516.
- 9 K. J. Kulacki and G. A. Lamberti, *Green Chem.*, 2008, **10**, 104–110.
- 10 A. Romero, A. Santos, J. Tojo and A. Rodriguez, *J. Hazard. Mater.*, 2008, **151**, 268–273.

- 11 L. Carson, P. K. W. Chau, M. J. Earle, M. A. Gilea, B. F. Gilmore, S. P. Gorman, M. T. McCann and K. R. Seddon, *Green Chem.*, 2009, **11**, 492–497.
- 12 A. Latala, M. Nedzi and P. Stepnowski, *Green Chem.*, 2009, **11**, 580–588.
- 13 M. Rebros, H. Q. N. Gunaratne, J. Ferguson, K. R. Seddon and G. Stephens, *Green Chem.*, 2009, **11**, 402–408.
- 14 B. Jastorff, R. Stormann and J. Ranke, *Clean: Soil, Air, Water*, 2007, **35**, 399–405.
- 15 B. Jastorff, K. Molter, P. Behrend, U. Bottin-Weber, J. Filser, A. Heimers, B. Ondruschka, J. Ranke, M. Schaefer, H. Schroder, A. Stark, P. Stepnowski, F. Stock, R. Stormann, S. Stolte, U. Welz-Biermann, S. Ziegert and J. Thoming, *Green Chem.*, 2005, **7**, 362–372.
- 16 B. Jastorff, R. Stormann, J. Ranke, K. Molter, F. Stock, B. Oberheitmann, W. Hoffmann, J. Hoffmann, M. Nuchter, B. Ondruschka and J. Filser, *Green Chem.*, 2003, **5**, 136–142.
- 17 J. Ranke, K. Molter, F. Stock, U. Bottin-Weber, J. Poczobutt, J. Hoffmann, B. Ondruschka, J. Filser and B. Jastorff, *Ecotoxicol. Environ. Saf.*, 2004, **58**, 396–404.
- 18 J. Ranke, K. Molter, F. Stock, U. Bottin-Weber, J. Poczobutt, J. Hoffmann, B. Ondruschka, J. Filser and B. Jastorff, *Ecotoxicol. Environ. Saf.*, 2005, **60**, 350–350.
- 19 S. Stolte, J. Arning, U. Bottin-Weber, M. Matzke, F. Stock, K. Thiele, M. Uerdingen, U. Welz-Biermann, B. Jastorff and J. Ranke, *Green Chem.*, 2006, **8**, 621–629.
- 20 M. Matzke, S. Stolte, K. Thiele, T. Juffernholz, J. Arning, J. Ranke, U. Welz-Biermann and B. Jastorff, *Green Chem.*, 2007, **9**, 1198–1207.
- 21 J. Ranke, A. Muller, U. Bottin-Weber, F. Stock, S. Stolte, J. Arning, R. Stormann and B. Jastorff, *Ecotoxicol. Environ. Saf.*, 2007, **67**, 430–438.
- 22 S. Stolte, J. Arning, U. Bottin-Weber, A. Muller, W. R. Pitner, U. Welz-Biermann, B. Jastorff and J. Ranke, *Green Chem.*, 2007, **9**, 760–767.
- 23 J. Arning, S. Stolte, A. Boschen, F. Stock, W. R. Pitner, U. Welz-Biermann, B. Jastorff and J. Ranke, *Green Chem.*, 2008, **10**, 47–58.
- 24 E. F. Borra, O. Seddiki, R. Angel, D. Eisenstein, P. Hickson, K. R. Seddon and S. P. Worden, *Nature*, 2007, **447**, 979–981.
- 25 P. Luis, I. Ortiz, R. Aldaco and A. Irabien, *Ecotoxicol. Environ. Saf.*, 2007, **67**, 423–429.
- 26 A. Garcia-Lorenzo, E. Tojo, J. Tojo, M. Teijeira, F. J. Rodriguez-Berrocal, M. P. Gonzalez and V. S. Martinez-Zorzano, *Green Chem.*, 2008, **10**, 508–516.
- 27 J. S. Torrecilla, J. Garcia, E. Rojo and F. Rodriguez, *J. Hazard. Mater.*, 2009, **164**, 182–194.
- 28 J. Palomar, V. R. Ferro, M. A. Gilarranz and J. J. Rodriguez, *J. Phys. Chem. B*, 2007, **111**, 168–180.
- 29 D. J. Couling, R. J. Bernot, K. M. Docherty, J. K. Dixon and E. J. Maginn, *Green Chem.*, 2006, **8**, 82–90.
- 30 J. Palomar, V. R. Ferro, J. S. Torrecilla and F. Rodriguez, *Ind. Eng. Chem. Res.*, 2007, **46**, 6041–6048.
- 31 A. Klamt, *COSMO-RS: From Quantum Chemistry to Fluid Phase Thermodynamics and Drug Design*, Elsevier, Amsterdam, 1st edn, 2005.
- 32 J. Palomar, J. S. Torrecilla, V. R. Ferro and F. Rodriguez, *Ind. Eng. Chem. Res.*, 2008, **47**, 4523–4532.
- 33 J. Palomar, J. S. Torrecilla, V. R. Ferro and F. Rodriguez, *Ind. Eng. Chem. Res.*, 2009, **48**, 2257–2265.
- 34 J. Palomar, J. S. Torrecilla, J. Lemus, V. R. Ferro and F. Rodriguez, *Phys. Chem. Chem. Phys.*, 2008, **10**, 5967–5975.
- 35 N. Lacaze, G. Gombaudo-Saintonge and M. Lanotte, *Leuk. Res.*, 1983, **7**, 145–154.
- 36 *Gaussian 03, Revision C.02*, M. J. Frisch, G. W. Trucks, H. B. Schlegel, G. E. Scuseria, M. A. Robb, J. R. Cheeseman, J. A. Montgomery, Jr., T. Vreven, K. N. Kudin, J. C. Burant, J. M. Millam, S. S. Iyengar, J. Tomasi, V. Barone, B. Mennucci, M. Cossi, G. Scalmani, N. Rega, G. A. Petersson, H. Nakatsuji, M. Hada, M. Ehara, K. Toyota, R. Fukuda, J. Hasegawa, M. Ishida, T. Nakajima, Y. Honda, O. Kitao, H. Nakai, M. Klene, X. Li, J. E. Knox, H. P. Hratchian, J. B. Cross, V. Bakken, C. Adamo, J. Jaramillo, R. Gomperts, R. E. Stratmann, O. Yazyev, A. J. Austin, R. Cammi, C. Pomelli, J. W. Ochterski, P. Y. Ayala, K. Morokuma, G. A. Voth, P. Salvador, J. J. Dannenberg, V. G. Zakrzewski, S. Dapprich, A. D. Daniels, M. C. Strain, O. Farkas, D. K. Malick, A. D. Rabuck, K. Raghavachari, J. B. Foresman, J. V.

- Ortiz, Q. Cui, A. G. Baboul, S. Clifford, J. Cioslowski, B. B. Stefanov, G. Liu, A. Liashenko, P. Piskorz, I. Komaromi, R. L. Martin, D. J. Fox, T. Keith, M. A. Al-Laham, C. Y. Peng, A. Nanayakkara, M. Challacombe, P. M. W. Gill, B. Johnson, W. Chen, M. W. Wong, C. Gonzalez and J. A. Pople, Gaussian, Inc., Wallingford CT, 2004.
- 37 F. Eckert and A. Klamt, *COSMOtherm*, Version C2.1, Release 01.06, COSMOlogic, Leverkusen, Germany, 2006.
- 38 A. J. Maren, T. Harston and R. P. Pap, *Handbook of neural computing applications*, Academic Press Inc., San Diego, 1990, pp. 323–324.
- 39 H. Demuth, M. Beale and M. Hagan, *Neural Network Toolbox For Use with MATLAB User's Guide*, version 4.0.6, ninth printing, 2005; revised for version 4.0.6; release 14SP3.
- 40 P. Gramatica, E. Giani and E. Papa, *J. Mol. Graphics Modell.*, 2007, **25**, 755–766.
- 41 P. Gramatica, *QSAR Comb. Sci.*, 2007, **26**, 694–670.
- 42 T. I. Netzeva, A. P. Worth, T. Aldenberg, R. Benigni, M. T. D. Cronin, P. Gramatica, J. S. Jaworska, S. Kahn, G. Klopman, C. A. Marchant, G. Myatt, N. Nikolova-Jeliazkova, G. Y. Patlewicz, R. Perkins, D. W. Roberts, T. W. Schultz, D. T. Stanton, J. J. M. van de Sandt, W. D. Tong, G. Veith and C. H. Yang, *Alternatives to Laboratory Animals*, 2005, **33**, 155–173.
- 43 J. S. Torrecilla, M. Deetlefs, K. R. Seddon and F. Rodríguez, *Phys. Chem. Chem. Phys.*, 2008, **10**, 5114–5120.
- 44 J. S. Torrecilla, F. Rodríguez, J. L. Bravo, G. Rothenberg, K. R. Seddon and I. Lopez-Martin, *Phys. Chem. Chem. Phys.*, 2008, **10**, 5826–5831.
- 45 J. S. Torrecilla, L. Otero and P.D. Sanz, *J. Food Eng.*, 2005, **69**, 299–306.
- 46 J. S. Torrecilla, M. L. Mena, P. Yáñez-Sedeño and J. García, *J. Agric. Food Chem.*, 2007, **55**, 7418–7426.
- 47 V. Vacic, *Summary of the training functions in Matlab's NN toolbox*, 2005, http://www.cs.ucr.edu/~vladimir/cs171/nn_summary.pdf.
- 48 Y. Sun, Y. Peng, Y. Chen and A. J. Shukla, *Adv. Drug Delivery Rev.*, 2003, **55**, 1201–1215.
- 49 L. B. Sheiner and S. Beal, *J. Pharmacokinet. Biopharm.*, 1981, **9**, 503–509.
- 50 *Guidance Document on the Validation of (Quantitative) Structure Activity Relationship [(Q)SAR] Models, No. 69* (OECD Series on Testing and Assessment), Organisation of Economic Cooperation and Development, Paris, France, 2007, <http://www.oecd.org>.
- 51 J. C. Dearden, M. T. D. Cronin and K. L. E. Kaiser, *SAR QSAR Environ. Res.*, 2009, **20**, 241–266.
- 52 M. Matzke, S. Stolte, A. Boschen and J. Filser, *Green Chem.*, 2008, **10**, 784–792.

Ruthenium-catalyzed synthesis of β -oxo esters in aqueous medium: Scope and limitations

Victorio Cadierno,* Javier Francos and José Gimeno*

Received 21st July 2009, Accepted 30th September 2009

First published as an Advance Article on the web 28th October 2009

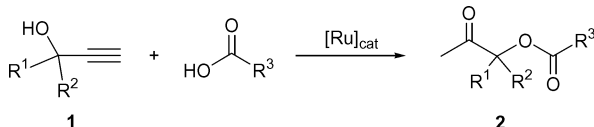
DOI: 10.1039/b914774h

The ability of the hydrosoluble ruthenium(II) complexes $[\text{RuCl}_2(\eta^6\text{-arene})(\text{PTA})]$ **3a–d**, $[\text{RuCl}_2(\eta^6\text{-arene})(\text{PTA-Bn})]$ **4a–d**, $[\text{RuCl}_2(\eta^6\text{-arene})(\text{DAPTA})]$ **5a–d**, $[\text{RuCl}_2(\eta^6\text{-arene})(\text{TPPMS})]$ **6a–d** (arene = C_6H_6 , *p*-cymene, 1,3,5- $\text{C}_6\text{H}_3\text{Me}_3$, C_6Me_6) to promote the atom-economic formation of β -oxo esters, by addition of carboxylic acids to terminal propargylic alcohols in water has been explored. Scope, limitations and catalyst recycling have been evaluated using the most active catalyst $[\text{RuCl}_2(\eta^6\text{-C}_6\text{H}_6)(\text{TPPMS})]$, **6a**.

Introduction

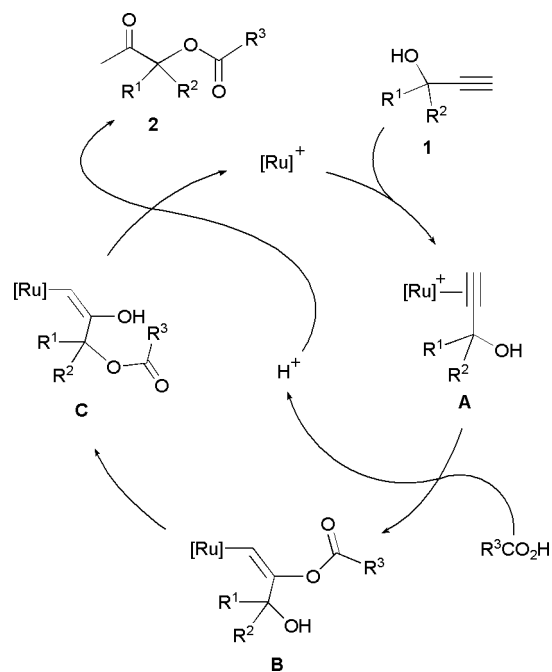
β -Oxo esters are important intermediates in organic synthesis since they can be easily transformed into the corresponding α -hydroxy ketones,¹ which are structural units present in a large variety of biologically active natural products.² Several procedures are presently available to prepare these types of compounds, such as the carbonylation of α -halo ketones,³ the anodic oxidation of enol acetates,⁴ the Cu catalyzed insertion of α -diazo ketones into the O–H bond of carboxylic acids,⁵ the two-step hydration/esterification of propargylic alcohols⁶ or the oxidation of ketones with metal–acetate complexes.⁷ However, the scope of most of these methods is rather low, and they also suffer from environmental problems associated with the use of harmful reagents.

The catalytic addition of carboxylic acids to terminal propargylic alcohols, **1**, represents an appealing and elegant alternative to β -oxo esters, **2** (Scheme 1); an atom-economic transformation that can be efficiently promoted by ruthenium complexes.⁸ Among the different catalysts employed, the best results in terms of activity and selectivity have been described using the mononuclear arene–Ru(II) derivatives $[\text{RuCl}_2(\eta^6\text{-arene})(\text{PR}_3)]$ (arene = *p*-cymene, C_6Me_6 ; PR_3 = PPh_3 , PMe_3 , phosphoramidite),⁹ the dimeric complex $[\{\text{Ru}(\mu\text{-O}_2\text{CH})(\text{CO})_2(\text{PPh}_3)_2\}]$ ¹⁰ and the catalytic system composed of $[\text{Ru}(\eta^5\text{-C}_8\text{H}_{11})_2]$ (C_8H_{11} = cyclooctadienyl), a trialkyl phosphine and maleic anhydride.¹¹



Scheme 1 β -Oxo ester formation by addition of carboxylic acids to terminal propargylic alcohols

From a mechanistic point of view, these catalytic transformations are based on the well-known ability of ruthenium complexes to promote the addition of carboxylic acids to the $\text{C}\equiv\text{C}$ bond of terminal alkynes to afford enol esters.^{12,13} Thus, after the initial Markovnikov addition of the carboxylate anion to the π -alkyne intermediate **A**, intramolecular transesterification of the resulting enol ester complex **B** readily takes place, leading to the alkenyl derivative **C**. Final protonolysis of **C** liberates the β -oxo ester **2** and regenerates the catalytically active ruthenium species (Scheme 2).



Scheme 2 Proposed mechanism for the Ru-catalyzed β -oxo ester formation reactions

On the other hand, a crucial factor in realizing a “green chemical” process involves the choice of a safe, non-toxic and cheap solvent.¹⁴ Water is undoubtedly one of the most appealing candidates.¹⁵ Therefore, the development of organic

Departamento de Química Orgánica e Inorgánica. IUQOEM (Unidad Asociada al CSIC), Universidad de Oviedo, Julián Clavería 8, 33006, Oviedo, Spain. E-mail: vcm@uniovi.es, jgh@uniovi.es; Fax: (34)985103446; Tel: (34)985102985

transformations in aqueous media has become one of the major cornerstones in modern chemistry.¹⁶ Following this general trend, the design of novel transition metal catalysts for organic reactions in water has attracted a growing interest in recent years,¹⁷ disclosing a wide variety of highly efficient and selective synthetic approaches to date.^{16,17} In this context, in the course of our current studies directed toward the application of ruthenium catalysts in aqueous organic synthesis,¹⁸ we have recently reported the preparation of half-sandwich ruthenium(II) complexes $[\text{RuCl}_2(\eta^6\text{-arene})(\text{PR}_3)]$ containing the hydrosoluble phosphine ligands PTA (**3a–d**), PTA-Bn (**4a–d**), DAPTA (**5a–d**) and TPPMS (**6a–d**) (see Fig. 1),¹⁹ also showing that some of them are excellent precatalysts for the selective hydration of organonitriles to amides in aqueous medium under neutral conditions.²⁰ The availability of these compounds, along with the known effectiveness of mononuclear arene–Ru(II) derivatives $[\text{RuCl}_2(\eta^6\text{-arene})(\text{PR}_3)]$ in β -oxo ester formation by addition of carboxylic acids to alkynols,⁹ prompted us to study this atom-economic transformation in water. To the best of our knowledge, no precedents on the use of environmentally benign aqueous media in these catalytic addition reactions have been described previously.

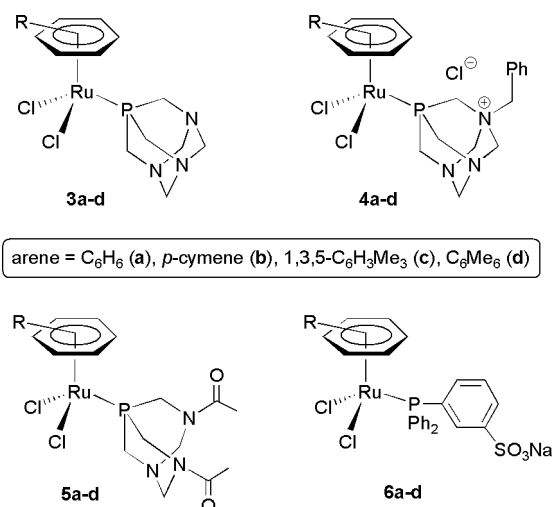


Fig. 1 Structure of the water-soluble ruthenium(II) catalysts used in this study.

Results and discussion

Table 1 provides a summary of our catalyst screening. We used the addition of benzoic acid to the commercially available alkynol 1-phenyl-2-propyn-1-ol **1a** as a model reaction. In a typical experiment, the alkynol (1 mmol) and the acid (1 mmol) were suspended in water (1 mL), under a nitrogen atmosphere, and treated with 2 mol% of the corresponding ruthenium complex **3a–6d** at 60 °C for 24 h. Under these conditions, all the complexes checked were found to be active catalysts in the addition process providing the β -oxo ester 1-phenyl-2-oxopropyl benzoate **2a** in moderate to good yields. Interestingly, the nature of the hydrosoluble phosphine played an important role in both the efficiency and selectivity of the process.²¹ Thus, the best results were obtained with complexes **6a–d**, all bearing the sulfonated ligand TPPMS, which led to the selective formation

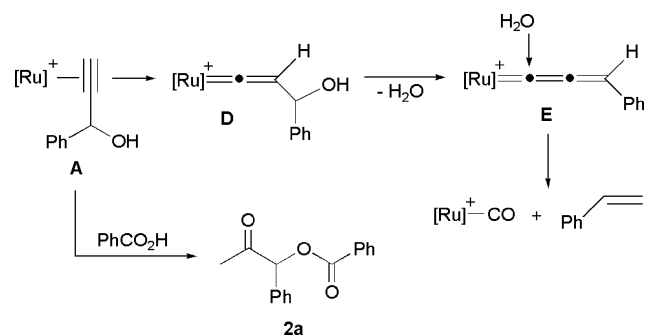
Table 1 Ruthenium-catalyzed synthesis of β -oxo ester **2a** in water^a

Entry	Catalyst	Time/h	Yield ^b / %
1	$[\text{RuCl}_2(\eta^6\text{-C}_6\text{H}_6)(\text{PTA})]$ 3a	24	64 ^c
2	$[\text{RuCl}_2(\eta^6\text{-}p\text{-cymene})(\text{PTA})]$ 3b	24	39 ^d
3	$[\text{RuCl}_2(\eta^6\text{-1,3,5-C}_6\text{H}_3\text{Me}_3)(\text{PTA})]$ 3c	24	54 ^e
4	$[\text{RuCl}_2(\eta^6\text{-C}_6\text{Me}_6)(\text{PTA})]$ 3d	24	71 ^c
5	$[\text{RuCl}_2(\eta^6\text{-C}_6\text{H}_6)(\text{PTA-Bn})]$ 4a	24	38 ^f
6	$[\text{RuCl}_2(\eta^6\text{-}p\text{-cymene})(\text{PTA-Bn})]$ 4b	24	63
7	$[\text{RuCl}_2(\eta^6\text{-1,3,5-C}_6\text{H}_3\text{Me}_3)(\text{PTA-Bn})]$ 4c	24	30
8	$[\text{RuCl}_2(\eta^6\text{-C}_6\text{Me}_6)(\text{PTA-Bn})]$ 4d	24	14
9	$[\text{RuCl}_2(\eta^6\text{-C}_6\text{H}_6)(\text{DAPTA})]$ 5a	24	62 ^g
10	$[\text{RuCl}_2(\eta^6\text{-}p\text{-cymene})(\text{DAPTA})]$ 5b	24	50 ^h
11	$[\text{RuCl}_2(\eta^6\text{-1,3,5-C}_6\text{H}_3\text{Me}_3)(\text{DAPTA})]$ 5c	24	61 ^h
12	$[\text{RuCl}_2(\eta^6\text{-C}_6\text{Me}_6)(\text{DAPTA})]$ 5d	24	56 ^g
13	$[\text{RuCl}_2(\eta^6\text{-C}_6\text{H}_6)(\text{TPPMS})]$ 6a	24	87
14	$[\text{RuCl}_2(\eta^6\text{-}p\text{-cymene})(\text{TPPMS})]$ 6b	24	85
15	$[\text{RuCl}_2(\eta^6\text{-1,3,5-C}_6\text{H}_3\text{Me}_3)(\text{TPPMS})]$ 6c	24	79
16	$[\text{RuCl}_2(\eta^6\text{-C}_6\text{Me}_6)(\text{TPPMS})]$ 6d	24	76
17 ⁱ	$[\text{RuCl}_2(\eta^6\text{-C}_6\text{H}_6)(\text{TPPMS})]$ 6a	3	95

^a Reactions performed under N₂ atmosphere at 60 °C using 1 mmol of 1-phenyl-2-propyn-1-ol (1 M in water) and 1 mmol of benzoic acid. ^b Determined by GC. ^c 5% of styrene is formed. ^d 10% of styrene is formed. ^e 7% of styrene is formed. ^f 1% of styrene is formed. ^g 2% of styrene is formed. ^h 4% of styrene is formed. ⁱ Reaction performed at 100 °C.

of **2a** in 76–87% GC yields (entries 13–16). In contrast, the use of the PTA, PTA-Bn and DAPTA-based catalysts **3a–5d** (entries 1–12) resulted in lower yields of **2a** (14–71%); in most of these reactions the formation of minor amounts of styrene as by-product was also observed (entries 1–5 and 9–11).

Formation of alkene side products, arising from the cleavage of the C≡C bond of the alkynol, has been recently observed in related addition reactions promoted by (η^6 -arene)ruthenium(II)-phosphoramidite catalysts in organic media.^{9b} Such a competitive process involves the generation of a highly reactive allenylidene–ruthenium intermediate **E** (Scheme 3) as the result of an initial tautomerization of the π -alkyne complex **A** into the 3-hydroxy-vinylidene **D**, and subsequent dehydration of **D**. Then, the carbon–carbon cleavage process takes place via nucleophilic addition of water to the electrophilic α -carbon of the allenylidene chain, a well-known transformation in the chemistry of metal–allenylidenes.^{22–24}



Scheme 3 Reaction pathway explaining the formation of styrene

It is known that, due to its π -accepting properties, the allenylidene ligand formation is favored by electron-rich metal fragments.²² This fact could explain why the occurrence of styrene takes place using those catalysts bearing the aliphatic phosphines PTA, PTA-Bn and DAPTA, all of them more basic than the aromatic sulfonated one, TPPMS. From this general catalyst screening, the benzene derivative [RuCl₂(η^6 -C₆H₆)(TPPMS)] **6a** emerged as the top choice due to its selectivity and efficiency (87% GC yield of **2a** after 24 h; entry 13). In addition, both the yield and the rate of the process could be significantly improved by increasing the working temperature from 60 to 100 °C. Under these new reaction conditions, using the same catalyst loading (2 mol% of **6a**), the β -oxo ester **2a** was formed in 95% GC yield after only 3 h (entry 17). No appreciable difference in activity was observed when an organic solvent (toluene) was used instead of water. Subsequent purification by column chromatography on silica gel provided an analytically pure sample of **2a** in 88% isolated yield.

Under these optimized reaction conditions (1 M solution of the alkynol in water; [alkynol]:[**6a**]:[PhCO₂H] ratio = 50:1:50; 100 °C) the ability of **6a** to promote the addition of benzoic acid to a number of other terminal propargylic alcohols was explored. The results are summarized in Table 2. Thus, as observed for

Table 2 Ruthenium-catalyzed synthesis of β -oxo esters in water: generality on the propargylic alcohol^a

Entry	Propargylic alcohol 1	Time/h	Yield of 2 ^b / %
1	R ¹ = H, R ² = Ph 1a	3	2a ; 95 (88)
2	R ¹ = H, R ² = 1-naphthyl 1b	3	2b ; 76 (69) ^c
3	R ¹ = H, R ² = 2-naphthyl 1c	3	2c ; 72 (63) ^d
4	R ¹ = H, R ² = 2-C ₆ H ₄ Cl 1d	6	2d ; 84 (78) ^e
5	R ¹ = H, R ² = 3-C ₆ H ₄ Cl 1e	6	2e ; 75 (63) ^f
6	R ¹ = H, R ² = 4-C ₆ H ₄ Cl 1f	6	2f ; 75 (65) ^g
7	R ¹ = H, R ² = C ₆ F ₅ 1g	6	2g ; 71 (60) ^h
8	R ¹ = H, R ² = 2-C ₆ H ₄ OMe 1h	6	2h ; 57 (48)
9	R ¹ = H, R ² = 3-C ₆ H ₄ OMe 1i	6	2i ; 59 (51)
10	R ¹ = H, R ² = 4-C ₆ H ₄ OMe 1j	6	2j ; 36 (25)
11	R ¹ = H, R ² = Me 1k	3	2k ; 67 (59)
12	R ¹ = H, R ² = CH ₂ Ph 1l	3	2l ; 82 (77) ⁱ
13	R ¹ = H, R ² = CH ₂ CH ₂ Ph 1m	6	2m ; 80 (72)
14	R ¹ = H, R ² = C(H)MePh 1n	6	2n ; 68 (63) ^j
15	R ¹ = R ² = H 1o	3	2o ; 71 (60)
16	R ¹ = Me, R ² = Ph 1p	6	2p ; 65 (55)
17	R ¹ R ² = -(CH ₂) ₄ - 1q	2	2q ; 99 (90)
18	R ¹ R ² = -(CH ₂) ₅ - 1r	3	2r ; 99 (88)
19	R ¹ R ² = -(CH ₂) ₆ - 1s	3	2s ; 92 (85)
20	R ¹ R ² = Adamantane-2,2-diyl 1t	8	2t ; 63 (57) ^k
21	R ¹ = R ² = Ph 1u	3	2u ; 3 ^l
22	R ¹ = R ² = 4-C ₆ H ₄ Cl 1v	3	2v ; 8 ^m

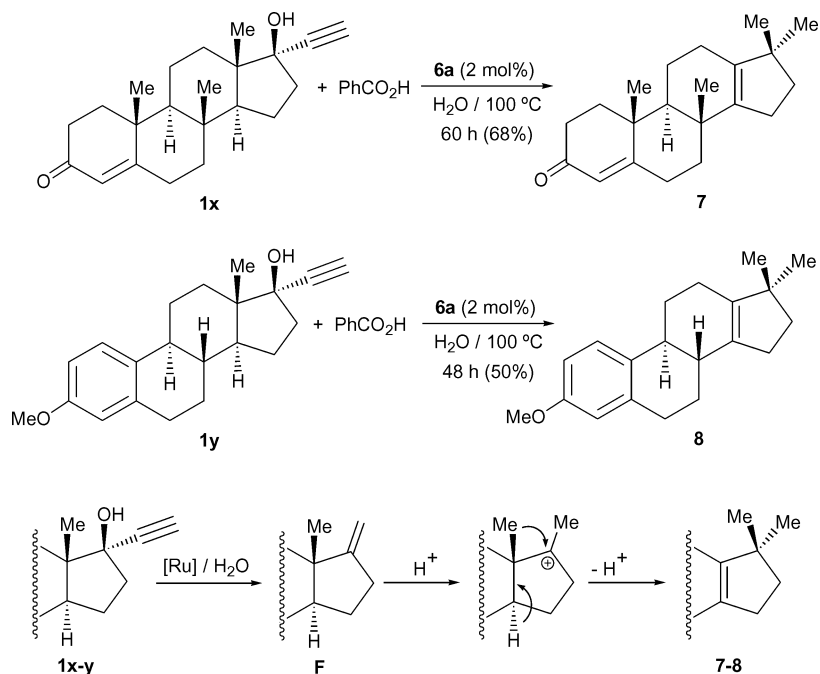
^a Reactions performed under N₂ atmosphere at 100 °C using 1 mmol of the corresponding propargylic alcohol (1 M in water) and 1 mmol of benzoic acid. ^b Determined by GC. Isolated yields are given in brackets. ^c 15% of 1-vinyl-naphthalene is formed. ^d 10% of 2-vinyl-naphthalene is formed. ^e 4% of 2-chloro-styrene is formed. ^f 6% of 3-chloro-styrene is formed. ^g 6% of 4-chloro-styrene is formed. ^h 14% of 2,3,4,5,6-pentafluoro-styrene is formed. ⁱ 7% of allyl-benzene is formed. ^j 4% of (1-methylallyl)-benzene is formed. ^k 5% of 2-methylene-adamantane is formed. ^l 80% of 1,1-diphenyl-ethene is formed. ^m 63% of 1,1-bis(4-chlorophenyl)-ethene is formed.

1a (entry 1), other aromatic (**1b–j**; entries 2–10) and aliphatic (**1k–n**; entries 11–14) secondary alkynols could be converted into the corresponding β -oxo esters **2b–n** in moderate to good yields (36–84% GC yields; 25–78% isolated yields) after 3–6 h of heating. Concerning the aromatic substrates, an influence of the electronic properties of the aryl rings on the efficiency of the process was observed. Thus, alkynols with electron-donating groups showed less reactivity (entries 8–10) compared to substrates with electron-withdrawing functionalities (entries 4–7), even when, in cases of the latter, the minor formation of olefinic by-products, *via* the competitive C \equiv C bond scission process discussed above was observed. As expected,^{9–11} this addition process is not restricted to secondary alkynols. Thus, as shown in entry 15, propargylic alcohol itself, **1o**, can also participate in this transformation leading to the known 2-oxopropyl benzoate (**2o**)^{9a} in 60% isolated yield after only 3 h. Regarding tertiary alcohols (entries 16–22), the best results were obtained with 1-ethynyl-cycloalkanol (**1q–s**; entries 17–19) from which the corresponding β -oxo esters **2q–s** could be synthesized in excellent yields (85–90% isolated yield; entries 17–19). The process is also operative starting from 2-phenyl-3-butyn-2-ol (**1p**; entry 15) and 2-ethynyl-2-adamantanol (**1t**; entry 20). However, its efficiency was found to be lower compared to the precedent cases (55–57% yield). Solvent removal and chromatographic work-up on silica gel provided analytically pure samples of all these β -oxo esters, which were fully characterized by means of standard analytical and spectroscopic techniques (see the Experimental section).

Remarkably, when the addition of PhCO₂H to tertiary diaromatic substrates, such as 1,1-diphenyl-2-propyn-1-ol (**1u**; entry 21) or 1,1-bis(4-chlorophenyl)-2-propyn-1-ol (**1v**; entry 22), was attempted, only trace amounts of the expected β -oxo esters could be detected by GC. In these cases, the reactions gave the major products 1,1-diphenyl-ethene (80%) and 1,1-bis(4-chlorophenyl)-ethene (63%), respectively.

We must also mention that, despite the ability of complex **6a** to promote the addition of benzoic acid to 1-ethynyl-cycloalkanol (**1q–s**; entries 17–19), attempts to synthesize β -oxo esters derived from the hormonal steroids ethisterone, **1x**, and mestranol, **1y**, also failed.²⁵ Thus, we found that treatment of **1x–y** with 1 equivalent of PhCO₂H, under the same catalytic conditions described above, led to the slow formation (48–60 h) of the known 17,17-dimethyl-18-norandrosta-4,13-dien-3-one **7**²⁶ and 3-methoxy-17,17-dimethyl-gona-1,3,5(10),13-tetraene **8**,²⁷ respectively, isolated in moderate yields (50–68%) after appropriate chromatographic workup (Scheme 4). Compounds **7–8** most probably result from the initial ruthenium-catalyzed dehydration and cleavage of the 2-propyn-1-ol function, *via* the corresponding allenylidene intermediates,²⁸ which affords the olefinic intermediates **F**. Then, a classical acid-promoted Wagner–Meerwein rearrangement can take place leading to the final steroids **7–8**.^{26,27} All these results seem to indicate that the competitive π -alkynol to allenylidene rearrangement is governed not only by the electronic nature of the catalyst, but also by the steric requirements of the propargylic alcohol substituents, with bulky substrates clearly favoring this undesirable side reaction.

Once the generality of this aqueous transformation with respect to the propargylic alcohol had been evaluated, the scope regarding the nature of the carboxylic acid was explored. Results are collected in Fig. 2.



Scheme 4 Transformation of ethisterone and mestranol into steroids 7–8

Thus, we have found that using alkynol **1a** as a model compound, several aromatic acids, bearing functional groups such as halide, alkoxy, ketone or sulfonamide, can be successfully employed in this addition process, affording the corresponding β -oxo esters **9a–g** in good isolated yields (63–86%). Interestingly, the reaction is also compatible with heteroaromatic substrates. Thus, carboxylic acids derived from tetrahydrofuran, pyrrole, thiophene, indole or 2-oxo-2H-chromene were efficiently (64–91% yield) converted into the novel β -oxo esters **9h–m**. In addition, the clean formation of **9n–o**, starting from the aliphatic heptanoic and 3-cyclopentyl-propionic acid confirmed the wide scope of this catalytic transformation.

Finally, the catalyst recycling has also been investigated using the addition of benzoic acid to 1-phenyl-2-propyn-1-ol **1a** as model reaction (entry 1 in Table 2). Thus, we have found that after a simple extraction of the final product **2a** with hexane, the aqueous phase, containing $[\text{RuCl}_2(\eta^6\text{-C}_6\text{H}_6)(\text{TPPMS})]$ **6a**, can be re-used in at least two consecutive runs. However, an important decrease of the activity was observed in the third cycle (91% GC yield after 24 h) due to the partial decomposition of the catalyst (release of the C_6H_6 ligand was observed by GC after prolonged periods in solution at 100 °C).

Conclusions

We have demonstrated that β -oxo ester formation, by catalytic addition of carboxylic acids to terminal propargylic alcohols, can be conveniently performed in environmentally benign aqueous medium using the water-soluble ruthenium(II) complex $[\text{RuCl}_2(\eta^6\text{-C}_6\text{H}_6)(\text{TPPMS})]$ **6a**. The process showed a remarkably wide scope, tolerating the presence of several functional groups in the substrates. In fact, its only limitation concerns the use of bulky tertiary alkynols which, under the catalytic conditions employed, undergo hydrolytic cleavage of the $\text{C}\equiv\text{C}$

triple bond instead of the desired addition. In summary, the atom-economic nature of this catalytic transformation, which allows access to valuable synthetic intermediates from readily accessible or commercially available starting materials, along with the remarkable activity of **6a**, confer a genuine potential for practical application in organic chemistry to the aqueous protocol reported herein.

Experimental section

General methods

Infrared spectra were recorded on a Perkin-Elmer 1720-XFT spectrometer. NMR spectra were recorded on a Bruker DPX-300 instrument at 300 MHz (^1H), 75.4 MHz (^{13}C) or 282.4 (^{19}F). The chemical shift values (δ) are given in parts per million and are referred to the residual peak of the deuterated solvent used (CDCl_3). DEPT experiments have been carried out for all the compounds reported. GC/MS measurements were performed on a Agilent 6890 N equipment coupled to a 5973 mass detector (70eV electron impact ionization) using a HP-1MS column. ESI-TOF high-resolution mass spectra were provided by the mass spectrometry service of the University of Santiago de Compostela. Elemental analyses were performed with a Perkin-Elmer 2400 microanalyzer. Flash chromatography was performed using Merck silica gel 60 (230–400 mesh). Propargylic alcohols **1a–y** were obtained from commercial suppliers or synthesized by following the classical Midland's procedure.²⁹ Ruthenium(II) complexes **3a–6d** were prepared by following the methods reported in the literature.^{20,30}

General procedure for the catalytic reactions. Under nitrogen atmosphere, water (1 cm^3), the corresponding propargylic alcohol (1 mmol), carboxylic acid (1 mmol), and the ruthenium catalyst **6a** (12 mg, 0.02 mmol) were introduced into a sealed tube

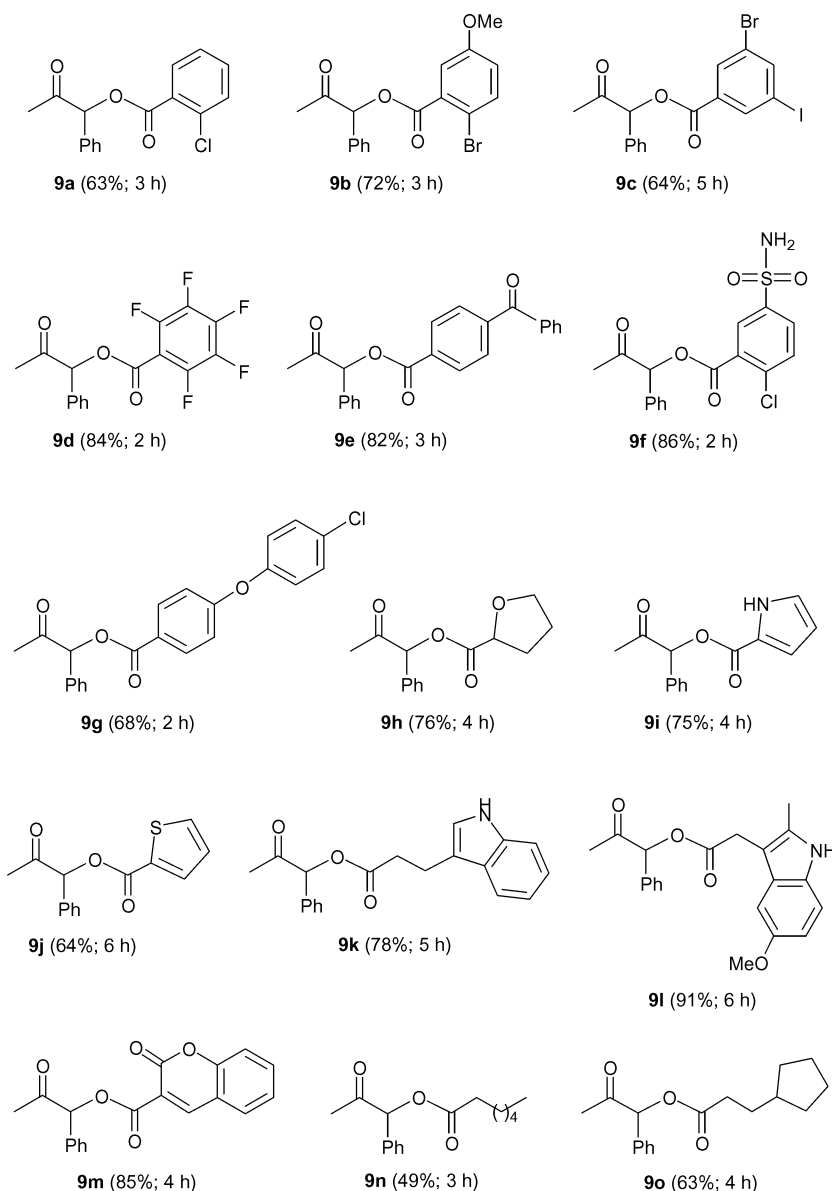


Fig. 2 Structures of the β -oxo esters **9a–o**.

and the resulting reaction mixture stirred at 100 °C for the time indicated (see Table 2, Schemes 3 and 4, or Fig. 2). The course of the reaction was monitored by regular sampling and analysis by GC. After elimination of the solvent under reduced pressure, the crude reaction mixture was purified by column chromatography over silica gel using an ethyl acetate–hexane mixture (1 : 10 v/v) as eluent. Compounds **2a**,³¹ **2k**,³² **2o**,^{9a} **2p**,^{9b} **2q**,^{9b} **2r**,^{9b} **7**²⁶ and **8**²⁷ have been previously described in the literature. Characterization data for the novel β -oxo esters synthesized in this work are as follows:

1-(1-Naphthyl)-2-oxopropyl benzoate 2b. Pale yellow solid; ¹H NMR (300.1 MHz, CDCl₃): δ 2.16 (s, 3H), 6.88 (s, 1H), 7.41–7.71 (m, 7H), 7.91–7.95 (m, 3H), 8.01–8.12 (m, 2H) ppm; ¹³C{¹H} NMR (75.47 MHz, CDCl₃): δ 26.3, 80.0, 123.9, 125.3, 126.2, 127.2, 128.3, 128.4, 128.9, 129.2, 129.5, 129.9, 130.3, 131.3, 133.4, 134.2, 165.7, 201.8 ppm; IR (nujol): ν 1716 and

1732 (C=O) cm⁻¹; GC-MS (EI, 70eV): m/z 304 (30%, M⁺), 261 (30), 105 (100), 77 (25); Elemental analysis calcd (%) for C₂₀H₁₆O₃: C 78.93, H 5.30; found: C 78.81, H 5.23.

1-(2-Naphthyl)-2-oxopropyl benzoate 2c. Pale yellow solid; ¹H NMR (300.1 MHz, CDCl₃): δ 2.24 (s, 3H), 6.38 (s, 1H), 7.45–7.63 (m, 6H), 7.89–7.94 (m, 3H), 8.02–8.17 (m, 3H) ppm; ¹³C{¹H} NMR (75.47 MHz, CDCl₃): δ 26.2, 81.4, 124.7, 126.7, 126.9, 127.7, 127.8, 128.1, 128.4, 129.1, 129.2, 129.9, 130.6, 131.1, 133.4, 133.5, 165.8, 201.8 ppm; IR (nujol): ν 1721 and 1738 (C=O) cm⁻¹; GC-MS (EI, 70eV): m/z 304 (30%, M⁺), 261 (30), 105 (100), 77 (25); Elemental analysis calcd (%) for C₂₀H₁₆O₃: C 78.93, H 5.30; found: C 78.77, H 5.36.

1-(2-Chlorophenyl)-2-oxopropyl benzoate 2d. Colourless oil; ¹H NMR (300.1 MHz, CDCl₃): δ 2.26 (s, 3H), 6.74 (s, 1H), 7.33–7.37 (m, 2H), 7.42–7.49 (m, 3H), 7.53–7.60 (m, 2H), 8.09–8.12 (m, 2H) ppm; ¹³C{¹H} NMR (75.47 MHz, CDCl₃): δ 26.8,

77.4, 127.5, 128.4, 129.1, 129.8, 129.9, 130.1, 130.6, 131.7, 133.5, 133.9, 165.5, 200.1 ppm; IR (neat): ν 1731 and 1785 (C=O) cm^{-1} ; GC-MS (EI, 70eV): m/z 253 (3%, $\text{M}^+ - \text{Cl}$), 245 (10), 211 (5), 105 (100), 77 (30); HRMS (ESI-TOF): m/z 289.063254 [$\text{M}^+ + \text{H}$], $\text{C}_{16}\text{H}_{14}\text{O}_3\text{Cl}$ requires 289.063147.

1-(3-Chlorophenyl)-2-oxopropyl benzoate 2e. Colourless oil; ^1H NMR (300.1 MHz, CDCl_3): δ 2.22 (s, 3H), 6.16 (s, 1H), 7.30–7.43 (m, 4H), 7.45–7.61 (m, 3H), 8.10–8.12 (m, 2H) ppm; $^{13}\text{C}\{^1\text{H}\}$ NMR (75.47 MHz, CDCl_3): δ 26.1, 80.4, 125.9, 127.7, 128.5, 128.9, 129.5, 129.9, 130.3, 133.6, 134.9, 135.2, 165.5, 201.4 ppm; IR (neat): ν 1706 and 1732 (C=O) cm^{-1} ; GC-MS (EI, 70eV): m/z 288 (1%, M^+), 245 (10), 211 (2), 105 (100), 77 (30); HRMS (ESI-TOF): m/z 289.063007 [$\text{M}^+ + \text{H}$], $\text{C}_{16}\text{H}_{14}\text{O}_3\text{Cl}$ requires 289.063147.

1-(4-Chlorophenyl)-2-oxopropyl benzoate 2f. Colourless oil; ^1H NMR (300.1 MHz, CDCl_3): δ 2.21 (s, 3H), 6.19 (s, 1H), 7.41–7.49 (m, 4H), 7.58–7.61 (m, 3H), 8.11–8.13 (m, 2H) ppm; $^{13}\text{C}\{^1\text{H}\}$ NMR (75.47 MHz, CDCl_3): δ 26.1, 80.5, 128.6, 129.2, 129.4, 129.9, 132.0, 132.1, 135.2, 135.5, 135.9, 165.7, 201.6 ppm; IR (neat): ν 1716 and 1737 (C=O) cm^{-1} ; GC-MS (EI, 70eV): m/z 288 (1%, M^+), 245 (10), 105 (100), 77 (30); HRMS (ESI-TOF): m/z 289.062991 [$\text{M}^+ + \text{H}$], $\text{C}_{16}\text{H}_{14}\text{O}_3\text{Cl}$ requires 289.063147.

1-Pentafluorophenyl-2-oxopropyl benzoate 2g. Orange oil; ^1H NMR (300.1 MHz, CDCl_3): δ 2.43 (s, 3H), 6.68 (s, 1H), 7.48–7.53 (m, 2H), 7.63–7.68 (m, 1H), 8.10–8.13 (m, 2H) ppm; $^{13}\text{C}\{^1\text{H}\}$ NMR (75.47 MHz, CDCl_3): δ 26.4, 70.3, 109.8 (m), 128.5, 128.7, 130.2, 134.1, 134.2, 135.8–147.3 (m), 164.9, 200.1 ppm; ^{19}F NMR (282.4 MHz, CDCl_3): δ –160.8 (m, 2F), –151.2 (t, $J = 22.0$ Hz, 1F), –136.6 (m, 2F) ppm; IR (neat): ν 1712 and 1731 (C=O) cm^{-1} ; GC-MS (EI, 70eV): m/z 344 (1%, M^+), 301 (30), 105 (100), 77 (25); HRMS (ESI-TOF): m/z 345.054946 [$\text{M}^+ + \text{H}$], $\text{C}_{16}\text{H}_{10}\text{F}_5\text{O}_3$ requires 345.055011.

1-(2-Methoxyphenyl)-2-oxopropyl benzoate 2h. Colourless oil; ^1H NMR (300.1 MHz, CDCl_3): δ 2.20 (s, 3H), 3.92 (s, 3H), 6.70 (s, 1H), 6.87–7.02 (m, 4H), 7.28–7.62 (m, 3H), 8.09–8.14 (m, 2H) ppm; $^{13}\text{C}\{^1\text{H}\}$ NMR (75.47 MHz, CDCl_3): δ 26.3, 55.6, 75.2, 111.1, 120.6, 121.1, 128.3, 128.4, 129.4, 129.9, 133.1, 133.7, 156.9, 171.7, 202.1 ppm; IR (neat): ν 1683 and 1716 (C=O) cm^{-1} ; GC-MS (EI, 70eV): m/z 284 (1%, M^+), 241 (10), 105 (100), 77 (30); HRMS (ESI-TOF): m/z 285.112721 [$\text{M}^+ + \text{H}$], $\text{C}_{17}\text{H}_{17}\text{O}_4$ requires 285.112684.

1-(3-Methoxyphenyl)-2-oxopropyl benzoate 2i. Colourless oil; ^1H NMR (300.1 MHz, CDCl_3): δ 2.21 (s, 3H), 3.84 (s, 3H), 6.18 (s, 1H), 6.94–7.12 (m, 4H), 7.35–7.61 (m, 3H), 8.11–8.14 (m, 2H) ppm; $^{13}\text{C}\{^1\text{H}\}$ NMR (75.47 MHz, CDCl_3): δ 25.9, 55.3, 81.1, 113.4, 114.7, 120.2, 128.4, 129.2, 129.9, 130.1, 133.4, 133.7, 159.9, 165.7, 201.7 ppm; IR (neat): ν 1704 and 1732 (C=O) cm^{-1} ; GC-MS (EI, 70eV): m/z 284 (1%, M^+), 241 (10), 105 (100), 77 (30); HRMS (ESI-TOF): m/z 285.112563 [$\text{M}^+ + \text{H}$], $\text{C}_{17}\text{H}_{17}\text{O}_4$ requires 285.112684.

1-(4-Methoxyphenyl)-2-oxopropyl benzoate 2j. Colourless oil; ^1H NMR (300.1 MHz, CDCl_3): δ 2.19 (s, 3H), 3.86 (s, 3H), 6.17 (s, 1H), 6.82–7.11 (m, 4H), 7.43–7.64 (m, 3H), 8.09–8.14 (m, 2H) ppm; $^{13}\text{C}\{^1\text{H}\}$ NMR (75.47 MHz, CDCl_3): δ 25.6, 55.1, 80.7, 114.0, 127.9, 129.1, 129.6, 129.8, 133.0, 133.6, 159.9, 171.9, 201.7 ppm; IR (neat): ν 1709 and 1738 (C=O) cm^{-1} ;

GC-MS (EI, 70eV): m/z 284 (1%, M^+), 241 (10), 105 (100), 77 (30); HRMS (ESI-TOF): m/z 285.112687 [$\text{M}^+ + \text{H}$], $\text{C}_{17}\text{H}_{17}\text{O}_4$ requires 285.112684.

1-Benzyl-2-oxopropyl benzoate 2l. Colourless oil; ^1H NMR (300.1 MHz, CDCl_3): δ 2.14 (s, 3H), 3.22 (m, 2H), 5.45 (dd, $J = 7.7$ and 5.1 Hz, 1H), 7.23–7.35 (m, 5H), 7.43–7.61 (m, 3H), 8.04 (m, 2H) ppm; $^{13}\text{C}\{^1\text{H}\}$ NMR (75.47 MHz, CDCl_3): δ 26.9, 36.9, 79.5, 127.1, 128.5, 128.6, 129.1, 129.4, 129.7, 133.5, 135.8, 165.9, 205.7 ppm; IR (neat): ν 1720 (br, C=O) cm^{-1} ; GC-MS (EI, 70eV): m/z 146 (40%, $\text{M}^+ - \text{PhCO}_2$), 105 (100), 77 (40); HRMS (ESI-TOF): m/z 269.117855 [$\text{M}^+ + \text{H}$], $\text{C}_{17}\text{H}_{17}\text{O}_3$ requires 269.117770.

1-Phenethyl-2-oxopropyl benzoate 2m. Colourless oil; ^1H NMR (300.1 MHz, CDCl_3): δ 2.24 (s, 3H), 2.30 (m, 2H), 2.85 (m, 2H), 5.27 (dd, $J = 6.0$ and 6.0 Hz, 1H), 7.22–7.35 (m, 5H), 7.49–7.54 (m, 2H), 7.65 (m, 1H), 8.13 (m, 2H) ppm; $^{13}\text{C}\{^1\text{H}\}$ NMR (75.47 MHz, CDCl_3): δ 26.2, 31.6, 32.1, 78.5, 126.4, 128.5, 128.6, 128.7, 129.3, 129.8, 133.5, 140.4, 166.0, 205.4 ppm; IR (neat): ν 1716 and 1734 (C=O) cm^{-1} ; GC-MS (EI, 70eV): m/z 282 (1%, M^+), 105 (100), 77 (25); HRMS (ESI-TOF): m/z 283.133166 [$\text{M}^+ + \text{H}$], $\text{C}_{18}\text{H}_{19}\text{O}_3$ requires 283.133420.

1-(1-Phenylethyl)-2-oxopropyl benzoate 2n. Colourless oil; ^1H NMR (300.1 MHz, CDCl_3): δ 1.51 (d, $J = 6.0$ Hz, 3H), 2.00 (s, 3H), 3.45 (m, 1H), 5.31 (d, $J = 5.7$ Hz, 1H), 7.26–7.35 (m, 5H), 7.47–7.65 (m, 3H), 8.10 (m, 2H) ppm; $^{13}\text{C}\{^1\text{H}\}$ NMR (75.47 MHz, CDCl_3): δ 16.1, 27.9, 41.2, 82.8, 127.7, 127.8, 128.4, 128.5, 128.7, 129.8, 133.5, 141.3, 166.0, 205.6 ppm; IR (neat): ν 1721 and 1743 (C=O) cm^{-1} ; GC-MS (EI, 70eV): m/z 239 (1%, $\text{M}^+ - \text{MeCO}$), 161 (15), 105 (100), 77 (25); HRMS (ESI-TOF): m/z 283.133276 [$\text{M}^+ + \text{H}$], $\text{C}_{18}\text{H}_{19}\text{O}_3$ requires 283.133420.

1-Acetyl-cycloheptyl benzoate 2s. Colourless oil; ^1H NMR (300.1 MHz, CDCl_3): δ 1.58–1.64 (m, 7H), 2.08–2.16 (m, 3H), 2.12 (s, 3H), 2.23–2.33 (m, 2H), 7.44–7.62 (m, 3H), 8.05 (m, 2H) ppm; $^{13}\text{C}\{^1\text{H}\}$ NMR (75.47 MHz, CDCl_3): δ 21.3, 23.6, 24.8, 27.7, 29.3, 89.3, 128.4, 129.7, 129.8, 133.3, 165.5, 206.9 ppm; IR (neat): ν 1716 (br, C=O) cm^{-1} ; GC-MS (EI, 70eV): m/z 231 (5%, $\text{M}^+ - 2\text{CH}_3$), 105 (100), 77 (20); HRMS (ESI-TOF): m/z 261.148865 [$\text{M}^+ + \text{H}$], $\text{C}_{16}\text{H}_{21}\text{O}_3$ requires 261.149070.

2-Acetyl-adamantan-2-yl benzoate 2t. Yellow oil; ^1H NMR (300.1 MHz, CDCl_3): δ 1.70–1.91 (m, 8H), 2.13 (s, 3H), 2.22 (m, 4H), 2.57 (br, 2H), 7.47–7.64 (m, 3H), 8.10 (d, $J = 7.2$ Hz, 2H) ppm; $^{13}\text{C}\{^1\text{H}\}$ NMR (75.47 MHz, CDCl_3): δ 24.1, 26.8, 26.9, 32.6, 33.7, 33.9, 37.7, 88.8, 128.6, 129.8, 130.0, 133.4, 165.2, 205.9 ppm; IR (neat): ν 1673 and 1722 (C=O) cm^{-1} ; GC-MS (EI, 70eV): m/z 255 (20%, $\text{M}^+ - \text{MeCO}$), 105 (100), 77 (30); HRMS (ESI-TOF): m/z 299.164630 [$\text{M}^+ + \text{H}$], $\text{C}_{19}\text{H}_{23}\text{O}_3$ requires 299.164720.

1-Phenyl-2-oxopropyl 2-chlorobenzoate 9a. Pale yellow oil; ^1H NMR (300.1 MHz, CDCl_3): δ 2.21 (s, 3H), 6.22 (s, 1H), 7.31–7.54 (m, 8H), 8.00 (m, 1H) ppm; $^{13}\text{C}\{^1\text{H}\}$ NMR (75.47 MHz, CDCl_3): δ 25.7, 81.3, 126.2, 127.6, 128.4, 128.7, 129.0, 130.7, 131.6, 132.5, 132.7, 133.8, 164.2, 200.9 ppm; IR (neat): ν 1738 (br, C=O) cm^{-1} ; GC-MS (EI, 70eV): m/z 245 (10%, $\text{M}^+ - \text{COMe}$), 139 (100), 111 (20), 75 (15); HRMS (ESI-TOF): m/z 289.063188 [$\text{M}^+ + \text{H}$], $\text{C}_{16}\text{H}_{14}\text{O}_3\text{Cl}$ requires 289.063147.

1-Phenyl-2-oxopropyl 2-bromo-5-methoxybenzoate 9b. Orange oil; $^1\text{H NMR}$ (300.1 MHz, CDCl_3): δ 2.22 (s, 3H), 3.84 (s, 3H), 6.22 (s, 1H), 6.92 (dd, $J = 8.7$ and 3.1 Hz, 1H), 7.43–7.58 (m, 7H) ppm; $^{13}\text{C}\{^1\text{H}\}$ NMR (75.47 MHz, CDCl_3): δ 26.2, 55.7, 81.9, 112.3, 117.2, 119.2, 128.1, 129.1, 129.5, 131.6, 132.8, 135.2, 158.6, 165.1, 201.2 ppm; IR (neat): ν 1730 (br, C=O) cm^{-1} ; GC-MS (EI, 70eV): m/z 364 (3%, M^+), 321 (10), 213 (100), 187 (10), 170 (10); HRMS (ESI-TOF): m/z 363.023211 [$\text{M}^+ + \text{H}$], $\text{C}_{17}\text{H}_{16}\text{O}_4\text{Br}$ requires 363.023202.

1-Phenyl-2-oxopropyl 3-bromo-5-iodobenzoate 9c. Orange oil; $^1\text{H NMR}$ (300.1 MHz, CDCl_3): δ 2.19 (s, 3H), 6.21 (s, 1H), 7.46–7.53 (m, 5H), 8.07 (dd, $J = 1.7$ and 1.7 Hz, 1H), 8.19 (dd, $J = 1.7$ and 1.7 Hz, 1H), 8.35 (dd, $J = 1.7$ and 1.7 Hz, 1H) ppm; $^{13}\text{C}\{^1\text{H}\}$ NMR (75.47 MHz, CDCl_3): δ 26.2, 81.8, 94.0, 123.0, 128.2, 129.3, 129.7, 132.1, 132.4, 132.6, 137.3, 144.2, 163.1, 200.6 ppm; IR (neat): ν 1716 and 1738 (C=O) cm^{-1} ; GC-MS (EI, 70eV): m/z 415 (20%, $\text{M}^+ - \text{MeCO}$), 309 (100), 281 (15), 182 (10), 156 (15); HRMS (ESI-TOF): m/z 458.909398 [$\text{M}^+ + \text{H}$], $\text{C}_{16}\text{H}_{13}\text{O}_3\text{BrI}$ requires 458.909284.

1-Phenyl-2-oxopropyl pentafluorobenzoate 9d. Orange oil; $^1\text{H NMR}$ (300.1 MHz, CDCl_3): δ 2.18 (s, 3H), 6.23 (s, 1H), 7.42–7.54 (m, 5H) ppm; $^{13}\text{C}\{^1\text{H}\}$ NMR (75.47 MHz, CDCl_3): δ 28.0, 84.7, 130.0, 130.7–134.1 (m), 138.2–149.7 (m), 160.3, 201.9 ppm; $^{19}\text{F NMR}$ (282.4 MHz, CDCl_3): δ –160.1 (m, 2F), –147.2 (m, 1F), –136.6 (m, 2F) ppm; IR (neat): ν 1739 (br, C=O) cm^{-1} ; GC-MS (EI, 70eV): m/z 301 (20%, $\text{M}^+ - \text{MeCO}$), 195 (100), 167 (10), 117 (5), 105 (5); HRMS (ESI-TOF): m/z 345.055126 [$\text{M}^+ + \text{H}$], $\text{C}_{16}\text{H}_{10}\text{F}_5\text{O}_3$ requires 345.055013.

1-Phenyl-2-oxopropyl 4-benzoylbenzoate 9e. Yellow oil; $^1\text{H NMR}$ (300.1 MHz, CDCl_3): δ 2.23 (s, 3H), 6.26 (s, 1H), 7.46–7.66 (m, 8H), 7.81–7.88 (m, 4H), 8.24 (d, $J = 8.3$ Hz, 2H) ppm; $^{13}\text{C}\{^1\text{H}\}$ NMR (75.47 MHz, CDCl_3): δ 26.2, 81.6, 128.1, 128.5, 129.2, 129.6, 129.8, 130.1, 132.3, 133.0, 133.1, 136.9, 141.8, 165.1, 195.9, 201.2 ppm; IR (neat): ν 1667, 1717 and 1738 (C=O) cm^{-1} ; GC-MS (EI, 70eV): m/z 315 (10%, $\text{M}^+ - \text{MeCO}$), 252 (5), 209 (100), 152 (10), 105 (20); HRMS (ESI-TOF): m/z 359.128577 [$\text{M}^+ + \text{H}$], $\text{C}_{23}\text{H}_{19}\text{O}_4$ requires 359.128334.

1-Phenyl-2-oxopropyl 2-chloro-5-sulfamoylbenzoate 9f. Yellow solid; $^1\text{H NMR}$ (300.1 MHz, CDCl_3): δ 2.16 (s, 3H), 5.44 (br, 2H), 6.22 (s, 1H), 7.43–7.59 (m, 6H), 8.16 (dd, $J = 8.3$ and 2.1 Hz, 1H), 8.73 (d, $J = 2.1$ Hz, 1H) ppm; $^{13}\text{C}\{^1\text{H}\}$ NMR (75.47 MHz, CDCl_3): δ 26.6, 82.4, 128.6, 129.1, 129.7, 130.2, 131.3, 132.4, 132.9, 134.9, 137.0, 140.5, 164.1, 201.4 ppm; IR (nujol): ν 1714 (br, C=O), 3390 (N–H) cm^{-1} ; GC-MS (EI, 70eV): m/z 324 (15%, $\text{M}^+ - \text{MeCO}$), 218 (100), 138 (10), 105 (15), 77 (20); Elemental analysis calcd (%) for $\text{C}_{16}\text{H}_{14}\text{O}_5\text{ClNS}$: C 52.25, H 3.84, N 3.81; found: C 52.33, H 3.96, N 3.70.

1-Phenyl-2-oxopropyl 4-(4-chlorophenoxy)benzoate 9g. Yellow oil; $^1\text{H NMR}$ (300.1 MHz, CDCl_3): δ 2.21 (s, 3H), 6.22 (s, 1H), 7.01 (m, 4H), 7.34–7.55 (m, 7H), 8.11 (m, 2H) ppm; $^{13}\text{C}\{^1\text{H}\}$ NMR (75.47 MHz, CDCl_3): δ 26.1, 81.3, 117.5, 121.3, 124.0, 128.0, 129.1, 129.4, 130.1, 132.2, 133.4, 154.2, 161.8, 165.2, 201.8 ppm; IR (neat): ν 1715 (br, C=O) cm^{-1} ; GC-MS (EI, 70eV): m/z 337 (5%, $\text{M}^+ - \text{MeCO}$), 231 (100), 168 (15), 139 (10), 105 (10); HRMS (ESI-TOF): m/z 381.089428 [$\text{M}^+ + \text{H}$], $\text{C}_{22}\text{H}_{18}\text{O}_4\text{Cl}$ requires 381.089363.

1-Phenyl-2-oxopropyl tetrahydrofuran-2-carboxylate 9h. Orange oil; $^1\text{H NMR}$ (300.1 MHz, CDCl_3): δ 1.89–2.04 (m, 2H), 2.15 (s, 3H), 2.26–2.40 (m, 2H), 3.92–4.11 (m, 2H), 4.59–4.67 (m, 1H), 6.03 (s, 1H), 7.42 (br, 5H) ppm; $^{13}\text{C}\{^1\text{H}\}$ NMR (75.47 MHz, CDCl_3): δ 25.1, 26.2, 30.3, 69.5, 76.3, 80.9, 128.2, 129.1, 129.4, 132.9, 172.8, 201.1 ppm; IR (neat): ν 1731 and 1755 (C=O) cm^{-1} ; GC-MS (EI, 70eV): m/z 205 (5%, $\text{M}^+ - \text{MeCO}$), 177 (10), 105 (10), 71 (100), 43 (50); HRMS (ESI-TOF): m/z 249.112745 [$\text{M}^+ + \text{H}$], $\text{C}_{14}\text{H}_{17}\text{O}_4$ requires 249.112692.

1-Phenyl-2-oxopropyl 1H-pyrrole-2-carboxylate 9i. Brown oil; $^1\text{H NMR}$ (300.1 MHz, CDCl_3): δ 2.20 (s, 3H), 6.16 (s, 1H), 6.31 (dd, $J = 6.5$ and 2.8 Hz, 1H), 7.00–7.09 (m, 2H), 7.42–7.53 (m, 5H), 9.24 (br, 1H) ppm; $^{13}\text{C}\{^1\text{H}\}$ NMR (75.47 MHz, CDCl_3): δ 26.0, 80.6, 110.7, 116.5, 123.7, 127.9, 128.1, 128.7, 129.3, 133.5, 160.0, 202.3 ppm; IR (nujol): ν 1732 (br, C=O), 3315 (NH) cm^{-1} ; GC-MS (EI, 70eV): m/z 200 (20%, $\text{M}^+ - \text{MeCO}$), 94 (100), 66 (20), 39 (20); HRMS (ESI-TOF): m/z 244.097459 [$\text{M}^+ + \text{H}$], $\text{C}_{14}\text{H}_{14}\text{O}_3\text{N}$ requires 244.097378.

1-Phenyl-2-oxopropyl thiophene-2-carboxylate 9j. Red oil; $^1\text{H NMR}$ (300.1 MHz, CDCl_3): δ 2.21 (s, 3H), 6.18 (s, 1H), 7.34 (dd, $J = 5.1$ and 3.1 Hz, 1H), 7.43–7.55 (m, 5H), 7.60 (dd, $J = 5.1$ and 1.1 Hz, 1H), 8.24 (dd, $J = 3.1$ and 1.1 Hz, 1H) ppm; $^{13}\text{C}\{^1\text{H}\}$ NMR (75.47 MHz, CDCl_3): δ 26.1, 81.0, 126.3, 127.9, 128.0, 129.1, 129.4, 132.6, 133.4, 133.8, 161.8, 201.8 ppm; IR (nujol): ν 1719 (br, C=O) cm^{-1} ; GC-MS (EI, 70eV): m/z 217 (20%, $\text{M}^+ - \text{MeCO}$), 111 (100), 83 (15), 39 (20); HRMS (ESI-TOF): m/z 261.05846 [$\text{M}^+ + \text{H}$], $\text{C}_{14}\text{H}_{13}\text{O}_3\text{S}$ requires 261.058541.

1-Phenyl-2-oxopropyl 3-(1H-indol-3-yl)propionate 9k. Orange oil; $^1\text{H NMR}$ (300.1 MHz, CDCl_3): δ 2.09 (s, 3H), 2.28 (m, 2H), 3.17 (t, $J = 7.3$ Hz, 2H), 5.99 (s, 1H), 7.09–7.39 (m, 9H), 7.60 (d, $J = 7.9$ Hz, 1H), 7.97 (br, 1H) ppm; $^{13}\text{C}\{^1\text{H}\}$ NMR (75.47 MHz, CDCl_3): δ 20.9, 26.4, 35.0, 81.3, 111.5, 115.1, 119.0, 119.7, 121.9, 122.5, 127.8, 128.4, 129.5, 129.7, 133.7, 136.7, 173.0, 202.3 ppm; IR (nujol): ν 1716 and 1738 (C=O), 3412 (NH) cm^{-1} ; GC-MS (EI, 70eV): m/z 321 (20%, M^+), 188 (10), 146 (10), 130 (100), 105 (10), 77 (10); HRMS (ESI-TOF): m/z 322.144280 [$\text{M}^+ + \text{H}$], $\text{C}_{20}\text{H}_{20}\text{O}_3\text{N}$ requires 322.144319.

1-Phenyl-2-oxopropyl (5-methoxy-2-methyl-1H-indol-3-yl)acetate 9l. Yellow oil; $^1\text{H NMR}$ (300.1 MHz, CDCl_3): δ 2.04 (s, 3H), 2.38 (s, 3H), 3.80 (s, 3H), 3.83 (s, 2H), 5.97 (s, 1H), 6.77 (dd, $J = 8.7$ and 2.5 Hz, 1H), 7.01 (d, $J = 2.5$ Hz, 1H), 7.13 (d, $J = 8.7$ Hz, 1H), 7.39 (br, 5H), 7.82 (br, 1H) ppm; $^{13}\text{C}\{^1\text{H}\}$ NMR (75.47 MHz, CDCl_3): δ 11.8, 25.9, 30.1, 55.8, 81.1, 100.2, 103.9, 111.0, 111.2, 127.9, 128.9, 129.0, 129.2, 130.1, 133.3, 133.7, 154.2, 171.2, 202.0 ppm; IR (nujol): ν 1719 (br, C=O), 3391 (NH) cm^{-1} ; GC-MS (EI, 70eV): m/z 351 (30%, M^+), 174 (100), 158 (15), 131 (15), 105 (10), 77 (10); HRMS (ESI-TOF): m/z 352.154709 [$\text{M}^+ + \text{H}$], $\text{C}_{21}\text{H}_{22}\text{O}_4\text{N}$ requires 352.154883.

1-Phenyl-2-oxopropyl 2-oxo-2H-chromene-3-carboxylate 9m. Orange oil; $^1\text{H NMR}$ (300.1 MHz, CDCl_3): δ 2.20 (s, 3H), 6.21 (s, 1H), 7.26–7.65 (m, 9H), 8.62 (s, 1H) ppm; $^{13}\text{C}\{^1\text{H}\}$ NMR (75.47 MHz, CDCl_3): δ 26.0, 81.7, 116.7, 117.0, 117.7, 124.9, 127.9, 129.1, 129.4, 129.7, 132.8, 134.7, 149.5, 155.2, 156.3, 162.0, 201.4 ppm; IR (nujol): ν 1713 (br, C=O) cm^{-1} ; GC-MS (EI, 70eV): m/z 280 (10%, $\text{M}^+ - \text{MeCO}$), 216 (10), 173 (100),

146 (20), 105 (15), 89 (20); HRMS (ESI-TOF): m/z 323.092216 [$M^+ + H$], $C_{19}H_{15}O_5$ requires 323.091949.

1-Phenyl-2-oxopropyl heptanoate 9n. Yellow oil; 1H NMR (300.1 MHz, $CDCl_3$): δ 0.87 (t, $J = 6.9$ Hz, 3H), 1.25–1.38 (m, 6H), 1.66 (m, 2H), 2.11 (s, 3H), 2.41 (m, 2H), 5.97 (s, 1H), 7.37–7.42 (m, 5H) ppm; $^{13}C\{^1H\}$ NMR (75.47 MHz, $CDCl_3$): δ 14.0, 22.4, 24.7, 26.1, 28.6, 31.3, 33.9, 80.7, 127.9, 129.0, 129.3, 133.3, 173.1, 201.8 ppm; IR (neat): ν 1734 (br, C=O) cm^{-1} ; GC-MS (EI, 70eV): m/z 219 (20%, $M^+ - MeCO$), 134 (10), 113 (100), 105 (20), 85 (15), 77 (10); HRMS (ESI-TOF): m/z 263.164689 [$M^+ + H$], $C_{16}H_{23}O_3$ requires 263.164725.

1-Phenyl-2-oxopropyl 3-cyclopentylpropionate 9o. Yellow oil; 1H NMR (300.1 MHz, $CDCl_3$): δ 1.10–1.89 (m, 11H), 2.11 (s, 3H), 2.47 (m, 2H), 5.97 (s, 1H), 7.40 (br, 5H) ppm; $^{13}C\{^1H\}$ NMR (75.47 MHz, $CDCl_3$): δ 24.6, 25.7, 30.5, 31.9, 32.8, 39.1, 80.3, 127.6, 128.6, 128.8, 132.8, 172.7, 201.4 ppm; IR (neat): ν 1768 (br, C=O) cm^{-1} ; GC-MS (EI, 70eV): m/z 274 (2%, M^+), 231 (40), 134 (10), 125 (100), 107 (60), 97 (10), 79 (50); HRMS (ESI-TOF): m/z 275.164641 [$M^+ + H$], $C_{17}H_{23}O_3$ requires 275.164724.

Acknowledgements

This work was supported by the Ministerio de Educación y Ciencia (MEC) of Spain (Projects CTQ2006-08485/BQU and Consolider Ingenio 2010 (CSD2007-00006)) and the Gobierno del Principado de Asturias (FICYT Project IB08-036). J.F. thanks MEC and the European Social Fund for the award of a PhD grant.

Notes and references

- For references on the use of esters units as protecting groups of alcohols, see: (a) P. J. Kocienski, *Protecting Groups*, Thieme Verlag, Stuttgart, 3rd edn, 2003; (b) T. W. Greene, P. G. M. Wuts, *Protective Groups in Organic Synthesis*, Wiley-Interscience, New York, 3rd edn, 1999.
- See, for example: (a) N. Kaila, K. Janz, S. DeBernardo, P. W. Bedard, R. T. Camphausen, S. Tam, D. H. H. Tsao, J. C. Keith, C. Nickerson-Nutter, A. Shilling, R. Young-Sciame and Qin Wang, *J. Med. Chem.*, 2007, **50**, 21; (b) J. F. Márquez Ruiz, G. Radics, H. Windle, H. O. Serra, A. L. Simplicio, K. Kedziora, P. G. Fallon, D. P. Kelleher and J. F. Gilmer, *J. Med. Chem.*, 2009, **52**, 3205.
- See, for example: (a) P. Ruggli and K. Knecht, *Helv. Chim. Acta*, 1944, **27**, 1108; (b) M. A. Ashraf, M. A. Jones, N. E. Kelly, A. Mullaney, J. S. Snaith and I. Williams, *Tetrahedron Lett.*, 2003, **44**, 3151.
- See, for example: T. Shono, Y. Matsumura and Y. Nakagawa, *J. Am. Chem. Soc.*, 1975, **97**, 6144.
- See, for example: T. Shinada, T. Kawakami, H. Sakai, I. Takada and Y. Ohfune, *Tetrahedron Lett.*, 1998, **39**, 3757.
- See, for example: (a) D. W. Hansen, R. Pappo and R. B. Garland, *J. Org. Chem.*, 1988, **53**, 4244; (b) P. Yates, R. S. Grewal and P. C. Hayes, *Can. J. Chem.*, 1988, **66**, 2805.
- See, for example: (a) G. W. K. Cavill and D. H. Solomon, *J. Chem. Soc.*, 1955, 4426; (b) A. S. Demir, M. Camkerten, H. Akgun, C. Tanyeli, A. S. Mahasneh and D. S. Watt, *Synth. Commun.*, 1990, **20**, 2279.
- (a) Ruthenium complexes have emerged in recent years as powerful tools in catalytic organic synthesis, with significant applications in atom-economic transformations. See, for example: *Ruthenium Catalysts and Fine Chemistry*, ed. C. Bruneau and P. H. Dixneuf, Springer-Verlag, Berlin, 2004; (b) *Ruthenium in Organic Synthesis*, ed. S.-I. Murahashi, Wiley-VCH, Weinheim, 2004; (c) B. M. Trost, M. U. Fredericksen and M. T. Rudd, *Angew. Chem., Int. Ed.*, 2005, **44**, 6630; (d) C. Bruneau and P. H. Dixneuf, *Angew. Chem., Int. Ed.*, 2006, **45**, 2176.
- (a) D. Devanne, C. Ruppini and P. H. Dixneuf, *J. Org. Chem.*, 1988, **53**, 925; (b) S. Costin, N. P. Rath and E. B. Bauer, *Adv. Synth. Catal.*, 2008, **350**, 2414.
- (a) C. Bruneau, Z. Kabouche, M. Neveux, B. Seiller and P. H. Dixneuf, *Inorg. Chim. Acta*, 1994, **222**, 155; (b) C. Darcel, C. Bruneau, P. H. Dixneuf and G. Neef, *J. Chem. Soc., Chem. Commun.*, 1994, 333.
- T. Mitsudo, Y. Hori, Y. Yamakawa and Y. Watanabe, *J. Org. Chem.*, 1987, **52**, 2230.
- For general reviews on metal-catalyzed addition of heteroatom-hydrogen bonds to alkynes, see: (a) F. Alonso, I. P. Beletskaya and M. Yus, *Chem. Rev.*, 2004, **104**, 3079; (b) M. Beller, J. Seayad, A. Tillack and H. Jiao, *Angew. Chem., Int. Ed.*, 2004, **43**, 3368.
- For specific accounts covering the use ruthenium catalysts in this type of transformations, see: (a) C. Bruneau, M. Neveux, Z. Kabouche, C. Ruppini and P. H. Dixneuf, *Synlett*, 1991, 755; (b) C. Fischmeister, C. Bruneau, and P. H. Dixneuf, in *Ruthenium in Organic Synthesis*, ed. S.-I. Murahashi, Wiley-VCH, Weinheim, 2004, pp.189-217.
- See, for example: (a) P. T. Anastas, and J. C. Warner, in *Green Chemistry: Theory and Practice*, Oxford University Press, Oxford, 1998; (b) A. S. Matlack, in *Introduction to Green Chemistry*, Marcel Dekker, New York, 2001; (c) M. Lancaster, in *Handbook of Green Chemistry and Technology*, eds. J. H. Clark, and D. J. Macquarrie, Blackwell Publishing, Abingdon, 2002; (d) M. Lancaster, in *Green Chemistry: An Introductory Text*, RSC Editions, London, 2002.
- See, for example: (a) W. M. Nelson, in *Green Solvents for Chemistry: Perspectives and Practice*, Oxford University Press, New York, 2003; (b) J. H. Clark and S. J. Taverner, *Org. Process Res. Dev.*, 2007, **11**, 149; (c) F. M. Kerton, in *Alternative Solvents for Green Chemistry*, RSC Publishing, Cambridge, 2009.
- See, for example: (a) C. J. Li, *Chem. Rev.*, 1993, **93**, 2023; (b) A. Lubineau, J. Auge and Y. Queneau, *Synthesis*, 1994, 741; (c) C. J. Li and T. H. Chan, in *Organic Reactions in Aqueous Media*, John Wiley & Sons, New York, 1997; (d) U. M. Lindström, *Chem. Rev.*, 2002, **102**, 2751; (e) C. J. Li, *Acc. Chem. Res.*, 2002, **35**, 533; (f) C. J. Li, *Chem. Rev.*, 2005, **105**, 3095; (g) C. K. Z. Andrade and L. M. Alves, *Curr. Org. Chem.*, 2005, **9**, 195; (h) C. J. Li and L. Chen, *Chem. Soc. Rev.*, 2006, **35**, 68; (i) L. Chen and C. J. Li, *Adv. Synth. Catal.*, 2006, **348**, 1459; (j) C. I. Herreras, X. Yao, Z. Li and C. J. Li, *Chem. Rev.*, 2007, **107**, 2546; (k) C. J. Li and T. H. Chan, in *Comprehensive Organic Reactions in Aqueous Media*, John Wiley & Sons, New Jersey, 2007; (l) *Organic Reactions in Water: Principles, Strategies and Applications*, ed. U. M. Lindström, Blackwell Publishing Ltd., Oxford, 2007.
- See, for example: (a) P. Kalck and F. Monteil, *Adv. Organomet. Chem.*, 1992, **34**, 219; (b) W. A. Herrmann and C. W. Kohlpaintner, *Angew. Chem., Int. Ed. Engl.*, 1993, **32**, 1524; (c) *Aqueous Organometallic Chemistry and Catalysis*, eds. I. T. Horváth and F. Joó, Kluwer, Dordrecht, 1995; (d) F. Joó and A. Kathó, *J. Mol. Catal. A: Chem.*, 1997, **116**, 3; (e) *Aqueous-Phase Organometallic Catalysis: Concepts and Applications*, eds. B. Cornils and W. A. Herrmann, Wiley-VCH, Weinheim, 1998; (f) B. E. Hanson, *Coord. Chem. Rev.*, 1999, **185–186**, 795; (g) F. Joó, in *Aqueous Organometallic Catalysis*, Kluwer, Dordrecht, 2001; (h) N. Pinault and D. W. Bruce, *Coord. Chem. Rev.*, 2003, **241**, 1; (i) C. A. M. Afonso, L. C. Branco, N. R. Candeias, P. M. P. Gois, N. M. T. Lourenço, N. M. M. Mateus and J. N. Rosa, *Chem. Commun.*, 2007, 2669.
- (a) V. Cadierno, S. E. García-Garrido and J. Gimeno, *Chem. Commun.*, 2004, 232; (b) V. Cadierno, P. Crochet, S. E. García-Garrido and J. Gimeno, *Dalton Trans.*, 2004, 3635; (c) V. Cadierno, S. E. García-Garrido, J. Gimeno and N. Nebra, *Chem. Commun.*, 2005, 4086; (d) V. Cadierno, S. E. García-Garrido, J. Gimeno, A. Varela-Álvarez and J. A. Sordo, *J. Am. Chem. Soc.*, 2006, **128**, 1360; (e) P. Crochet, J. Díez, M. A. Fernández-Zúmel and J. Gimeno, *Adv. Synth. Catal.*, 2006, **348**, 93; (f) A. E. Díaz-Álvarez, P. Crochet, M. Zablocka, C. Duhayon, V. Cadierno, J. Gimeno and J. P. Majoral, *Adv. Synth. Catal.*, 2006, **348**, 1671; (g) V. Cadierno, S. E. García-Garrido and J. Gimeno, *J. Am. Chem. Soc.*, 2006, **128**, 15094; (h) V. Cadierno, J. Francos, J. Gimeno and N. Nebra, *Chem. Commun.*, 2007, 2536; (i) V. Cadierno, J. Gimeno and N. Nebra, *Chem.-Eur. J.*, 2007, **13**, 6590; (j) A. E. Díaz-Álvarez, P. Crochet, M. Zablocka, C. Duhayon, V. Cadierno and J.-P. Majoral, *Eur. J. Inorg. Chem.*, 2008, 786; (k) V. Cadierno, P. Crochet and J. Gimeno, *Synlett*, 2008, 1105.

- 19 The abbreviations used for the hydrosoluble phosphines correspond to the following IUPAC names: PTA = 1,3,5-triaza-7-phosphatricyclo[3.3.1.1^{3,7}]decane; PTA-Bn = 1-benzyl-3,5-diaza-1-azonia-7-phosphatricyclo[3.3.1.1^{3,7}]decane chloride; DAPTA = 3,7-diacetyl-1,3,7-triaza-5-phosphabicyclo[3.3.1]nonane; TPPMS = 3-diphenylphosphanyl-benzenesulfonate sodium salt.
- 20 V. Cadierno, J. Francos and J. Gimeno, *Chem.–Eur. J.*, 2008, **14**, 6601.
- 21 As observed in our previous work on nitrile hydrations using catalysts **3a–6d**, no direct relationship between the solubility of these complexes in water and their catalytic activity exists. Detailed data about the solubility of **3a–6d** in water at 20 °C can be found in ref. 20.
- 22 For general reviews on the chemistry of transition-metal allenylidene complexes, see: (a) M. I. Bruce, *Chem. Rev.*, 1998, **98**, 2797; (b) V. Cadierno, M. P. Gamasa and J. Gimeno, *Eur. J. Inorg. Chem.*, 2001, 571; (c) V. Cadierno, P. Crochet and J. Gimeno, in *Metal vinylidenes and allenylidenes in catalysis: From reactivity to applications in synthesis*, ed. C. Bruneau and P. H. Dixneuf, Wiley-VCH, Weinheim, 2008, pp 61-98; (d) V. Cadierno and J. Gimeno, *Chem. Rev.*, 2009, **109**, 3512.
- 23 For specific examples of Ru-allenylidene C_α=C_β bond cleavage by water, with alkene release, see: (a) C. Bianchini, M. Peruzzini, F. Zanobini, C. López, I. de los Rios and A. Romerosa, *Chem. Commun.*, 1999, 443; (b) E. Bustelo and P. H. Dixneuf, *Adv. Synth. Catal.*, 2005, **347**, 393.
- 24 Ruthenium-catalyzed cleavage of the C≡C bond of propargylic alcohols to generate the corresponding alkenes and carbon monoxide has been described by R.-S. Liu, and co-workers: (a) S. Datta, C.-L. Chang, K.-L. Yeh and R.-S. Liu, *J. Am. Chem. Soc.*, 2003, **125**, 9294; (b) R.-S. Liu, *Synlett*, 2008, 801; (c) For a general review on catalytic reactions involving carbon-carbon triple bond cleavage, see: M. Tobisu and N. Chatani, *Chem. Soc. Rev.*, 2008, **37**, 300.
- 25 Addition of carboxylic acids to ethisterone and mestranol could be successfully achieved in organic media using [$\{\text{Ru}(\mu\text{-O}_2\text{CH}(\text{CO})_2(\text{PPh}_3)_2\}_2]$ as catalyst: see ref. 10b.
- 26 (a) A. Segaloff and R. B. Gabbard, *Steroids*, 1964, **4**, 433; (b) V. I. De Brabandere, L. M. Thienpont, D. Stöckl and A. P. De Leenheer, *J. Lipid Res.*, 1997, **38**, 780.
- 27 (a) R. Kirdani, R. I. Dorfman and W. R. Nes, *Steroids*, 1963, **1**, 219; (b) R. Kanojia, S. Rovinsky and I. Scheer, *Chem. Commun.*, 1971, 1581.
- 28 Formation of allenylidene-ruthenium(II) complexes from ethisterone and mestranol has been described: V. Cadierno, S. Conejero, M. P. Gamasa, J. Gimeno and M. A. Rodríguez, *Organometallics*, 2002, **21**, 203.
- 29 (a) M. M. Midland, *J. Org. Chem.*, 1975, **40**, 2250; (b) The secondary propargylic alcohol 1-pentafluorophenyl-2-propyn-1-ol **1g**, isolated as a yellow oil in 78% yield, has not been previously described. Characterization data for this new compound are as follows: ¹H NMR (300.1 MHz, CDCl₃): δ 2.66 (d, *J* = 2.4 Hz, 1H), 3.75 (br, 1H), 5.76 (d, *J* = 2.4 Hz, 1H) ppm; ¹³C{¹H} NMR (75.47 MHz, CDCl₃): δ 54.3, 74.8, 80.1, 114.1 (m), 135.7 (m), 139.6 (m), 143.3 (m) ppm; ¹⁹F NMR (282.4 MHz, CDCl₃): δ -161.7 (m, 2F), -153.8 (m, 1F), -143.6 (m, 2F) ppm; IR (neat): ν 2127 (C≡C), 3309 (br, OH and ≡C–H) cm⁻¹; GC-MS (EI, 70eV): *m/z* 222 (30%, M⁺), 203 (70) 194 (100), 174 (50), 143 (20), 117 (20), 99 (15), 53 (20).
- 30 (a) C. S. Allardyce, P. J. Dyson, D. J. Ellis and S. L. Heath, *Chem. Commun.*, 2001, 1396; (b) H. Horváth, G. Laurenczy and A. Kathó, *J. Organomet. Chem.*, 2004, **689**, 1036; (c) C. Scolaro, A. Bergamo, L. Brescacin, R. Delfino, M. Cocchietto, G. Laurenczy, T. J. Geldbach, G. Sava and P. J. Dyson, *J. Med. Chem.*, 2005, **48**, 4161; (d) J. Diez, M. P. Gamasa, E. Lastra, A. García-Fernández and M. P. Tarazona, *Eur. J. Inorg. Chem.*, 2006, 2855.
- 31 C. L. Stevens, W. Malik and R. Pratt, *J. Am. Chem. Soc.*, 1950, **72**, 4758.
- 32 M. B. Rubin and S. Inbar, *J. Org. Chem.*, 1988, **53**, 3355.

High performance magnetic separation of gold nanoparticles for catalytic oxidation of alcohols†

Rafael L. Oliveira,^a Pedro K. Kiyohara^b and Liane M. Rossi^{*a}

Received 14th August 2009, Accepted 30th September 2009

First published as an Advance Article on the web 29th October 2009

DOI: 10.1039/b916825g

We present the magnetic separation approach to facilitate the recovery of gold nanoparticle (AuNP) catalysts. The use of magnetically recoverable supports for the immobilization of AuNPs instead of traditional oxides, polymers or carbon based solids guarantees facile, clean, fast and efficient separation of the catalyst at the end of the reaction cycle. Magnetic separation can be considered an environmentally benign separation approach, since it minimizes the use of auxiliary substances and energy for achieving catalyst recovery. The catalyst preparation is based on the immobilization of Au³⁺ on the surface of core-shell silica-coated magnetite nanoparticles, followed by metal reduction using two different methods. AuNPs were prepared by thermal reduction in air and by hydrogen reduction at mild temperature. Interestingly, the mean particle size of the supported AuNPs was similar (*ca.* 5.9 nm), but the polydispersity of the samples is quite different. The catalytic activity of both catalysts in the aerobic oxidation of alcohols was investigated and a distinct selectivity for benzyl alcohol oxidation was observed.

Introduction

The development of new strategies for the recovery and recycling of catalysts, which minimizes the consumption of auxiliary substances, energy and time used in achieving separations can result in significant economical and environmental benefits.

Gold in the bulk form has been regarded as being chemically inert towards chemisorption of reactive molecules such as oxygen and hydrogen. Consequently, bulk gold was considered to be an uninteresting metal from the point of view of catalysis. However, the catalytic properties of gold are revealed when the size is reduced to few nanometers, particularly with dimension less than 10 nm.¹ The overall performance of gold nanoparticle (AuNP) catalysts highly depends on the size and shape of the nanoparticles, the structure and properties of the catalyst support and the gold-support interface interactions.² A variety of interesting catalytic properties of AuNPs in both oxidation and reduction reactions has been reported.¹⁻³ Despite this, little attention has been paid to possible difficulties arising from size reduction, and the challenges of separating the very small particles, most of the time in a colloidal equilibrium, from the products. In this regard, AuNPs have been dispersed on solid supports to increase the catalyst stability and to facilitate the catalyst recovery.³ As the size of the support decreases, separation using physical methods, such as filtration or centrifugation, becomes a difficult and time-consuming procedure.

Simple filtration is inefficient to accomplish product isolation in systems comprised of nanoparticles stabilized in solution or very thin solids. In these circumstances, an alternative that has drawn attention lately is the use of magnetically recoverable solid supports. Magnetic separation is easy, fast, clean and a very promising recovery tool for isolation of thin solids from the reaction medium. It can be considered an environmentally benign separation approach, since it minimizes the use of auxiliary substances and energy for achieving catalyst recovery. Magnetic supports, mainly composed of superparamagnetic nanoparticles, can be attracted to relatively low static magnetic field strengths and are easily recovered, since no residual magnetization is observed when the magnetic field is removed. The immobilization of homogeneous and NP-based catalysts on magnetically separable solid supports has been shown to be a powerful tool for catalyst recovery and recycling.⁴⁻⁷

We report herein the preparation of AuNPs supported on a magnetic solid that can be easily recovered from solution by applying an external magnetic field, while keeping good control over different parameters, such as particle size, size distribution and catalytic activity. The oxidation of alcohols was used to probe the catalytic activity of the catalyst. Catalytic oxidations are green alternatives to stoichiometric oxidations with permanganate, manganese dioxide and chromium(VI) reagents, major sources of waste, particularly in fine chemicals and pharmaceuticals manufacture.⁸

Experimental

Synthesis of silica-coated magnetite nanoparticles

The synthesis of oleic acid-coated Fe₃O₄ nanoparticles and the core-shell Fe₃O₄@SiO₂ composite was reported elsewhere.⁷ The solid was modified with amino groups by reaction with

^aInstituto de Química, Universidade de São Paulo, 05508-000, São Paulo, SP, Brazil. E-mail: lrossi@iq.usp.br; Fax: +55 11 3815 5579; Tel: +55 11 30912181

^bInstituto de Física, Universidade de São Paulo, 05508-090, São Paulo, SP, Brazil

† Electronic supplementary information (ESI) available: TEM and EDS analyses of the spent catalyst. See DOI: 10.1039/b916825g

3-aminopropyltriethoxysilane (APTES) in dry toluene under N_2 , to give the amino-functionalized support ($Fe_3O_4@SiO_2/NH_2$). The final solid was washed with toluene and dried at $100^\circ C$ for 20 h.

Synthesis of supported Au(0) nanoparticles

Supported AuNPs were prepared as follows: 50 mg of $Fe_3O_4@SiO_2/NH_2$ was added to 10 mL of an aqueous $HAuCl_4$ solution (1 g L^{-1} , pH=6). The mixture was stirred at $25^\circ C$ for 2 h. The solid was then magnetically collected from the solution and washed twice with hot distilled water. The Au(0)NPs were obtained by reduction of the Au(III) precursor either by thermal treatment (oven, $150^\circ C$ (constant), 8 h, in air) or by H_2 reduction (glass reactor, 650 mg 2, 3 mL cyclohexane, $80^\circ C$, 4 atm H_2 , 3 h). The color of the solid changes from brown to dark purple after formation of Au NPs.

Characterization methods

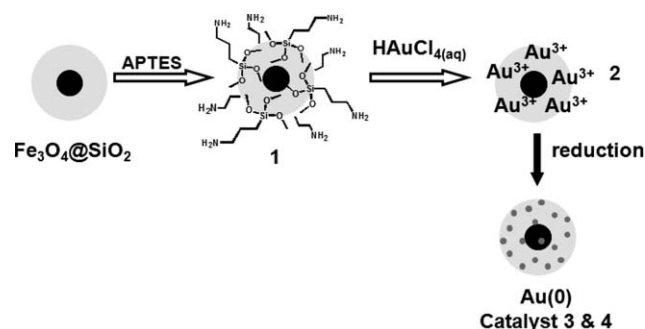
High-resolution transmission electron microscopy (HRTEM) and X-ray energy dispersive spectroscopy (EDS) were performed at the Laboratório Nacional de Luz Síncrotron (LNLS, Campinas, SP) using a Jeol-3010 ARP microscope, and conventional TEM images were performed using a Philips CM 200 microscope (IF-USP). Samples for TEM observations were prepared by placing a drop containing the nanoparticles in a carbon-coated copper grid. The histograms of the gold nanoparticles size distribution, assuming a spherical shape, were obtained from the measurement of the diameter of about 300 particles found in arbitrarily chosen areas of enlarged micrographs. The samples were observed in different regions of the Cu grid.

Catalytic experiments

All reactions were performed using a modified Fischer–Porter glass reactor loaded under a positive pressure of dry N_2 from a Schlenk line. Liquids and solutions were transferred *via* a syringe. In a typical reaction, the glass reactor was loaded with the supported Au(0)NPs catalyst (50 mg, $1.8\ \mu\text{mol Au}$), the substrate (1.5 mmol), and 2 mL of toluene. The reactor, immersed in an oil bath, was loaded with O_2 to the desired pressure. The temperature was maintained by an oil bath placed in a hot-stirring plate connected to a digital controller (ETS-D4 IKA). The reactions were conducted under magnetic stirring, using a Teflon-coated magnetic stir bar, for the desired time. The catalyst was magnetically recovered by placing a permanent magnet in the reactor wall and the products were collected with a syringe and analysed by gas chromatography (GC) and GC-MS. The isolated catalyst could be reused when a new amount of substrate was added.

Results and discussion

A schematic illustration of the step-by-step approach used for the preparation of gold catalysts composed of supported AuNPs on a magnetically recoverable solid is shown in Scheme 1. The magnetically recoverable support used in this study consists of core–shell silica-coated magnetite nanoparticles ($Fe_3O_4@SiO_2$) prepared following the procedure described recently.⁶ The



Scheme 1 Step-by-step preparation of magnetically recoverable AuNPs.

approach to prepare AuNPs is based on the uptake of Au^{3+} ions from $HAuCl_4$ aqueous solution by the silica-coated magnetic nanoparticles, previously functionalized with $-NH_2$ groups, followed by metal reduction under mild conditions. The amino-functionalized support (**1**) was loaded with 0.72 wt% of gold, as determined by atomic absorption analysis (ICP OES). It is interesting to notice that the non-functionalized support, when submitted to a similar metal solution, do not adsorb gold ions. The Au^{3+} -loaded magnetic solid (**2**) was used as precursor for the preparation of supported AuNPs either by thermal treatment (catalyst **3**) or by H_2 reduction (catalyst **4**). The formation of the AuNPs could be evidenced by the SPR bands at 567 nm (catalyst **3**) and 522 nm (catalyst **4**) observed in the UV-Vis spectra shown in Fig. 1.

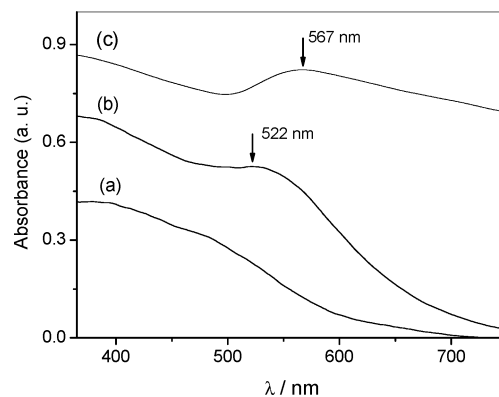


Fig. 1 UV-Vis spectra of ethanolic suspensions of $Fe_3O_4@SiO_2-NH_2$ **1** (a), Au(0) catalyst **4** (b) and Au(0) catalyst **3** (c).

The morphology of the supported AuNPs were examined by transmission electron microscopy (TEM), shown in Fig. 2a and b. The support is comprised of magnetic cores ($Fe_3O_4 \sim 10\text{ nm}$) spherically coated with silica (spheres of $\sim 40\text{ nm}$ in diameter). The mean diameter of the supported AuNPs in both catalysts was estimated at 5.9 nm with polydispersity of 18% for catalyst **4** and 32% for catalyst **3**. The AuNPs are fairly well-distributed over the support in both catalysts; however, the particle size distribution of catalyst **4** is sharper if compared to catalyst **3**, as can be seen in the size distribution histograms adjusted to lognormal functions presented in Fig. 2c–d. The SPR band of catalyst **4** appears at λ_{max} ca. 520 nm, which agrees with the higher monodispersity of the AuNPs. Moreover, the λ_{max} red shift of about 45 nm and the broadened optical spectrum of catalyst **3**

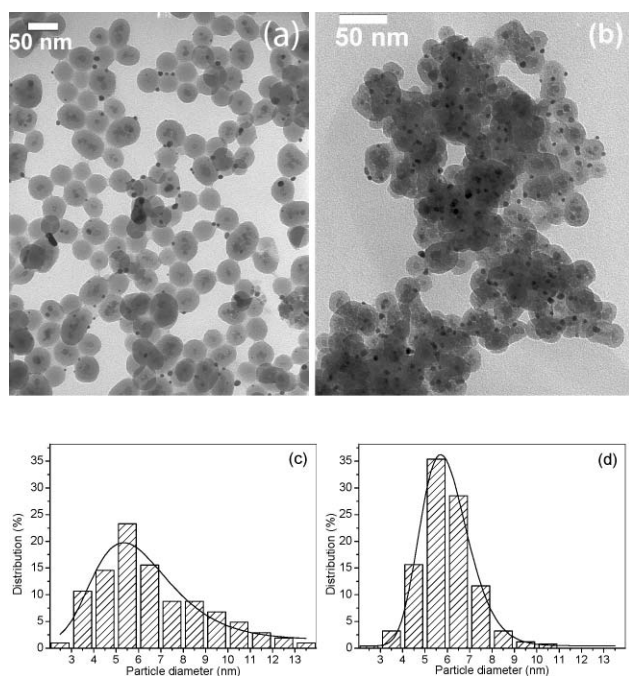


Fig. 2 TEM images of catalyst **3** (a) and catalyst **4** (b). Histogram showing particle size distribution and lognormal fitting of the AuNPs of catalyst **3** (c) and the AuNPs of catalyst **4** (d).

can be realized by aggregation of small particles, light scattering and lower overall quality of the supported nanoparticles.⁹

The distribution and composition of each nanoparticle of the nanocomposite was revealed by energy dispersive spectroscopy (EDS) analysis of the image shown in Fig. 3. The core nanoparticles were found to be exclusively composed of Fe atoms (Fig. 3b), and the darker nanoparticles of Au atoms (Fig. 3c), through a detailed EDS analysis of the image areas shown in box (b) and box (c), respectively. The EDS analysis shown in Fig. 3a corresponds to the whole nanocomposite which contains Fe, Au and Si (Cu from sample holder).

The magnetic properties of the $\text{Fe}_3\text{O}_4@\text{SiO}_2$ nanocomposite were investigated elsewhere.⁷ It displays excellent magnetic properties characterized by negligible coercivity and remanence, and very high saturation magnetization M_s at room temperature ($M_s \sim 69 \text{ emu g}^{-1}$ at 70 kOe). These magnetic properties describe a superparamagnetic material that responds to an external magnetic field but does not remain magnetized when the magnetic field is removed. Such materials can be easily concentrated from the solution with a magnet and immediately redispersed after removing the magnetic field, since the absence of remanence prevents aggregation of particles.

The catalytic oxidation of benzyl alcohol was used to probe the activity and recovery of the supported AuNPs in catalysts **3** and **4**. The first attempt to catalyze the oxidation of benzyl alcohol using our supported AuNPs was performed under atmospheric pressure of O_2 and no products (aldehyde or ester) were observed (Table 1, entry 1). It was also observed that in the absence of base, the catalyst was not efficient in catalyzing the selective oxidation of alcohols, even at 100 °C and 5 atm O_2 (Table 1, entry 2). The conversion increased to 75% (95% selectivity) as long as a small amount of K_2CO_3 was present (Table 1, entry 3). As it can be seen in Fig. 4, there is a strong dependence of the

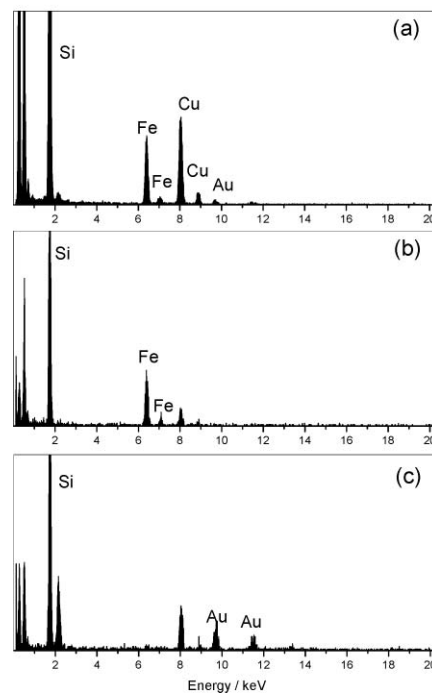
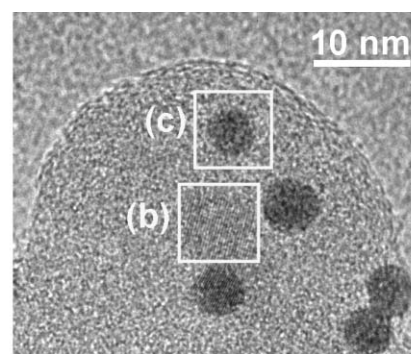


Fig. 3 HRTEM image and EDS analysis of the AuNP magnetically recoverable catalyst **4** in different areas of the image: (a) corresponds to the whole area, (b) corresponds to the iron oxide particle shown in box b and (c) corresponds to the gold particle shown in box c.

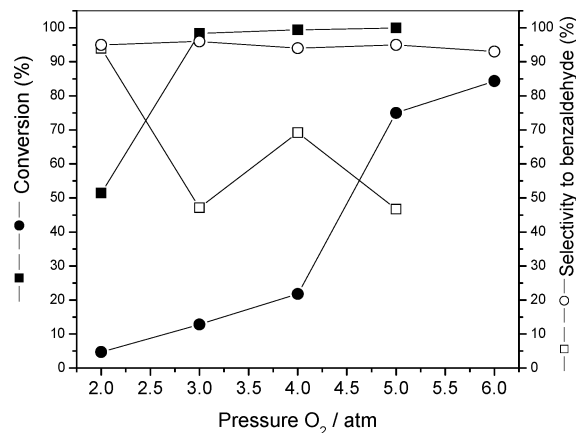


Fig. 4 Pressure dependence of the catalytic performance of supported AuNPs: catalyst **3** (circle) and catalyst **4** (square). Reaction conditions: 1.5 mmol of benzyl alcohol, 50 mg catalyst, 70 mg K_2CO_3 , 2 mL toluene, 100 °C, 6 h.

Table 1 Oxidation of alcohols ^a by magnetically recoverable Au NP catalyst

Entry	Catalyst	Substrate	<i>P</i> O ₂ (atm)	Conversion (%) ^b	Selectivity (%) ^b	
					Aldehyde or ketone	Ester (homocoupling)
1	3	Benzyl alcohol	— ^c	0.0	—	—
2 ^d	3	Benzyl alcohol	5	2.2	99	1
3	3	Benzyl alcohol	5	75	95	5
4	3	Benzyl alcohol	6	84.3	95	5
5	4	Benzyl alcohol	3	100	47	53
6	3	1-Phenyl ethanol	6	100	100	0
7	4	1-Phenyl ethanol	3	100	100	0
8	3	Cyclohexanol	6	31	100	0
9	4	Cyclohexanol	6	42	100	0

^a Reaction conditions: 1.5 mmol of substrate, 2 mL of toluene, 50 mg of catalyst (1.8 μmol Au), 70 mg K₂CO₃, 100 °C, reaction time 6 h. ^b Determined by GC-MS. ^c Bubbling O₂. ^d Without base.

oxidation reaction with the O₂ pressure for both catalysts **3** and **4**. Catalyst **3** is less active and requires higher pressure for the substrate conversion, but the selectivity was maintained in the pressure range studied. On the other hand, catalyst **4** is more active, reaching 100% conversion at 3 atm of O₂, but the high activity is accompanied by the drop of selectivity to benzaldehyde to *ca.* 50%. The oxidation reaction catalyzed by catalyst **3** is highly selective to benzaldehyde, found as the main product. It is also known that benzaldehyde can be further oxidized into benzoic acid, and, finally, benzyl alcohol and benzoic acid would interact and produce benzyl benzoate.¹⁰ In fact, benzyl benzoate was found as the only by-product in the oxidation of benzyl alcohol by catalysts **3** and **4**.

Secondary alcohols such as 1-phenyl ethanol and cyclohexanol (Table 1, entries 6–9) were also oxidized to the corresponding ketones with 100% selectivity. In all experiments, the catalyst was recovered by using a permanent magnet and the products were collected with a syringe and analysed by GC-MS.

Recycling experiments were examined for the catalytic oxidation of benzyl alcohol at 5 atm of O₂ and 100 °C using catalysts **3** and **4**. After the first reaction, the catalyst was recovered in the reactor wall by using a permanent magnet, the products were collected with a syringe, and the recovered catalyst was washed with ethanol (2 mL) inside the reactor, and dried under vacuum. The catalyst was reused in successive oxidation reactions by adding new portions of solvent, base and substrate. This procedure was repeated four times, however the supported AuNP catalyst **3** lost 50% of the initial conversion, considering the same reaction time. After the 4th cycle, the conversion of benzyl alcohol was 35% but the selectivity to aldehyde was maintained as shown in Fig. 5. The deactivation process of catalyst **4** is more severe than catalyst **3** under similar experimental conditions. The activity of 100% in the 1st run drops to less than 10% in the 4th run.

The low reusability of the catalyst is a point of concern. One of the key factors that must be considered is the possibility that the active metal would leach into the reaction mixture, especially in liquid phase oxidation reactions, because of the possible dissolution of metals by the reactants and, particularly, the carboxylic acid-type (by)products, thereby leading to catalyst deactivation. To address this possibility, the isolated products obtained after magnetic separation were analysed by

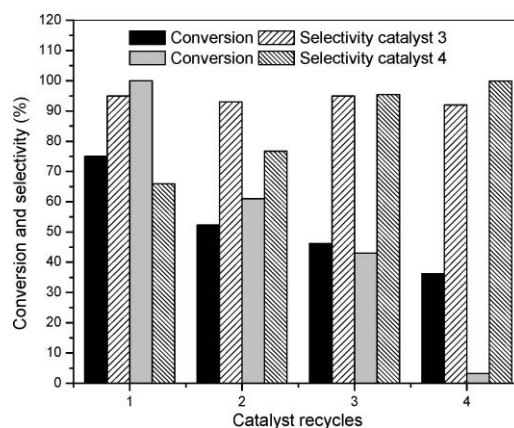


Fig. 5 Conversion and selectivity of the catalytic oxidation of benzyl alcohol to benzaldehyde using the magnetically recovered AuNP catalysts **3** and **4** (conditions similar to entry 3, Table 1).

atomic absorption analysis (ICP OES). Results have shown that negligible Au leaching of our catalysts occurs (less than the limit of quantitation of 2.5 ppb of Au). This demonstrates the high affinity of gold and our magnetic support, the high performance of the magnetic separation in the present catalytic system and, as a first conclusion, indicates that the catalyst deactivation is not related to metal loss. Another key factor to be considered is the stability of the catalyst support and nanoparticles when subjected to the reaction conditions. TEM images and EDS analysis of the spent catalysts (see ESI†, Fig. S1) and TEM image of the catalyst support subjected to basic reaction conditions (see ESI†, Fig. S2) provided supporting evidence for the catalyst deactivation under reuse. First, the morphology of the catalyst support (core-shell Fe₃O₄@SiO₂) has changed; the silica layer was strongly affected by the presence of base in the reaction medium and the catalyst support lost the spherical morphology, which caused aggregation. Second, large Au particles (~80 nm) were revealed in the TEM image of spent catalyst, which suggests the coalescence of the small, active gold particles into larger, less active or inactive particles. The growth of the Au particles, above the catalytic limit of about 10 nm,¹ can also be a consequence of the changes occurring in the catalyst support during the reaction. Therefore, the use of base associated with a silica-based catalyst support should be the main reason for the catalyst

deactivation. Another point that might be relevant concerns the presence of potassium as detected by EDS analysis. This is also a consequence of the use of base that can cause metal surface contamination.

It is also important to mention that some catalytic activity still remains even after the 4th reuse (*ca.* 50% for catalyst **3**), most probably because small particles are still present, as indicated by the TEM image.

Conclusions

We successfully prepared supported AuNP catalysts by the reduction of gold salts previously immobilized on a magnetically recoverable support. The method used in the reduction step for metal nanoparticle formation can be crucial in determining particle dispersion and distribution over the solid support and, consequently, the catalytic activity of the metal nanoparticles. In this work, two reduction methods were compared. Supported AuNPs were prepared by thermal reduction in air and by hydrogen reduction at mild temperature. Interestingly, the mean particle size was similar *ca.* 5.9 nm, but the polydispersity of the samples is quite different. The UV-Vis and TEM data of the AuNPs prepared by hydrogen reduction, catalyst **4**, suggest that a higher control over the particle dispersion was achieved by this reduction method. With respect to the catalytic activity, catalyst **4** is more active in the aerobic oxidation reactions, but less selective for the aldehyde product.

The catalysts reported here are very efficiently recovered by magnetic separation, with negligible Au leaching to the solution. This separation procedure is an efficient and green alternative to the conventional separation techniques used for the recovery of solids, such as filtration and centrifugation, since it is fast, clean, easy to scale-up and constitutes a waste minimization and low energy consumption procedure.

The use of base, K₂CO₃, was necessary to attain good catalytic activities in the oxidation of alcohols by our AuNPs catalysts, but seems to be responsible for the catalyst deactivation under reuse due to degradation of the catalyst support, which causes metal particles to grow beyond the catalytically active limit. The literature contains alternatives for the use of base in such reactions, such as the use of basic and redox supports^{39,10} or bimetallic Au–Pd alloys.^{2f} Additional experiments are in progress in our laboratory in order to synthesize and characterize magnetic catalysts comprised of supports and/or metal particles more resistant to base or, hopefully, active in the absence of base.

Acknowledgements

The authors are grateful to the Brazilian agencies FAPESP and CNPq for financial support and indebted to LNLS-Laboratório de Microscopia Eletrônica (Brazil) for HRTEM images and EDS analysis. The authors also acknowledge the Instituto Nacional de Ciência e Tecnologia de Catálise em Sistemas Moleculares e Nanoestruturados (INCT-CMN).

Notes and references

- (a) T. V. Choudhary and D. W. Goodman, *Top. Catal.*, 2002, **21**, 25; (b) T. V. Choudhary and D. W. Goodman, *Appl. Catal., A*, 2005, **291**, 32; (c) G. C. Bond and D. T. Thompson, *Catal. Rev. Sci. Eng.*, 1999, **41**, 319; (d) G. C. Bond and D. T. Thompson, *Appl. Catal., A*, 2006, **302**, 1; (e) G. J. Hutchings, *Catal. Today*, 2005, **100**, 55; (f) G. J. Hutchings and M. Haruta, *Appl. Catal., A*, 2005, **291**, 2; (g) M. Haruta, *Gold Bull.*, 2004, **37**, 27; (h) F. L. Didier Astruc and J. R. Aranzas, *Angew. Chem., Int. Ed.*, 2005, **44**, 7852 and references therein; (i) G. J. Hutchings, *Chem. Commun.*, 2008, 1148; (j) A. S. K. Hashmi and G. J. Hutchings, *Angew. Chem., Int. Ed.*, 2006, **45**, 7896.
- (a) N. Zheng and G. D. Stucky, *J. Am. Chem. Soc.*, 2006, **128**, 14278; (b) N. Zheng and G. D. Stucky, *Chem. Commun.*, 2007, 3862; (c) N. S. Patil, R. Jha, B. S. Uphade, S. K. Bhargava and V. R. Choudhary, *Appl. Catal., A*, 2004, **275**, 87; (d) A. Abad, P. Concepción, A. Corma and H. Garcia, *Angew. Chem., Int. Ed.*, 2005, **44**, 4066; (e) H. Tsunoyama, H. Sakurai and T. Tsukuda, *Chem. Phys. Lett.*, 2006, **429**, 528; (f) D. I. Enache, J. K. Edwards, P. Landon, B. Solsona-Espriu, A. F. Carley, A. A. Herzing, M. Watanabe, C. J. Kiely, D. W. Knight and G. J. Hutchings, *Science*, 2006, **311**, 362; (g) D. I. Enache, D. W. Knight and G. J. Hutchings, *Catal. Lett.*, 2005, **103**, 43.
- (a) M. Haruta, *CATTECH*, 2002, **6**, 102–115; (b) M. Haruta, *Catal. Today*, 1997, **36**, 153; (c) R. Zanella, S. Giorgio, C. R. Henry and C. Louis, *J. Phys. Chem. B*, 2002, **106**, 7634; (d) C. Aprile, A. Abad, H. Garcia and A. Corma, *J. Mater. Chem.*, 2005, **15**, 4408; (e) E. Taaring, Anders Theilgarard, J. M. Marchetti, K. Egeblad and C. H. Christensen, *Green Chem.*, 2008, **10**, 408; (f) M. Comotti, C. Della Pina, R. Matarrese and M. Rossi, *Angew. Chem., Int. Ed.*, 2004, **43**, 5812; (g) R. L. Oliveira, P. K. Kiyohara and L. M. Rossi, *Green Chem.*, 2009, **11**, 1366; (h) S. Biella, G. L. Castiglioni, C. Fumagalli, L. Patri and M. Rossi, *Catal. Today*, 2002, **72**, 43; (i) V. R. Choudhary, R. Jha and P. Jana, *Green Chem.*, 2007, **9**, 267; (j) H. Tsunoyama, T. Tsukuda and H. Sakurai, *Chem. Lett.*, 2007, **36**, 212; (k) S. Carrettin, P. McMorn, P. Jonhnston, K. Griffin and G. J. Hutchings, *Chem. Commun.*, 2002, 696; (l) S. Kim, S. W. Bae, J. S. Lee and J. Park, *Tetrahedron*, 2009, **65**, 1461; (m) C. Raptis, H. Garcia and M. Stratakis, *Angew. Chem., Int. Ed.*, 2009, **48**, 3133; (n) A. Abad, A. Corma and H. Garcia, *Chem.–Eur. J.*, 2008, **14**, 212; (o) J. Hu, L. Chen, K. Zhu, A. Suchopar and R. Richards, *Catal. Today*, 2007, **122**, 277; (p) J. Yang, Y. Guan, T. Verhoeven, R. van Santen, C. Li and E. J. M. Hensen, *Green Chem.*, 2009, **11**, 322; (q) S. Demirel, M. Lucas, J. Waerna, T. Salmi, D. Murzin and P. Claus, *Top. Catal.*, 2007, **44**, 299; (r) P. Haider and A. Baiker, *J. Catal.*, 2007, **248**, 175; (s) S. Biella and M. Rossi, *Chem. Commun.*, 2003, 378; (t) L. Patri and M. Rossi, *J. Catal.*, 1998, **176**, 552; (u) N. S. Patil, B. S. Uphade, P. Jana, R. S. Sonawane, S. K. Bhargava and V. R. Choudhary, *Catal. Lett.*, 2004, **94**, 89; (v) T. A. Nijhuis, E. Sacaliuc-Parvulescu, N. S. Govender, J. C. Schouten and B. M. Weckhuysen, *J. Catal.*, 2009, **265**, 161; (w) C. Aprile, A. Corma, M. E. Domine, H. Garcia and C. Mitchell, *J. Catal.*, 2009, **264**, 44; (x) V. R. Choudhary, N. S. Patil and S. K. Bhargava, *Catal. Lett.*, 2003, **89**, 55.
- For examples, see: (a) T.-J. Yoon, W. Lee, T.-S. Oh and J. K. Lee, *New J. Chem.*, 2003, **27**, 227; (b) P. D. Stevens, G. Li, J. Fan, M. Yen and Y. Gao, *Chem. Commun.*, 2005, 4435; (c) P. D. Stevens, G. Li, J. Fan, H. M. R. Gardimalla, M. Yen and Y. Gao, *Org. Lett.*, 2005, **7**, 2085; (d) A. Hu, G. T. Yee and W. Lin, *J. Am. Chem. Soc.*, 2005, **127**, 12486; (e) M. Kotani, T. Koike, K. Yamaguchi and N. Mizuno, *Green Chem.*, 2006, **8**, 735; (f) R. Abu-Reziq, H. Alper, D. Wang and M. L. Post, *J. Am. Chem. Soc.*, 2006, **128**, 5279; (g) D. K. Yi, S. S. Lee and J. Y. Ying, *Chem. Mater.*, 2006, **18**, 2459; (h) M. Kawamura and K. Sato, *Chem. Commun.*, 2006, 4718; (i) Y. Zheng, P. D. Stevens and Y. Gao, *J. Org. Chem.*, 2006, **71**, 537; (j) M. Kawamura and K. Sato, *Chem. Commun.*, 2007, 3404; (k) D. Guin, B. Baruwati and S. V. Manorama, *Org. Lett.*, 2007, **9**, 1419; (l) Z. Yinghuai, S. C. Peng, C. Emi, A. Zhenshun and R. A. Kemp, *Adv. Synth. Catal.*, 2007, **349**, 1917; (m) B. Baruwati, D. Guin and S. Manorama, *Org. Lett.*, 2007, **9**, 5377; (n) C. O. Dalaigh, S. A. Corr, Y. Gunko and S. J. Connon, *Angew. Chem., Int. Ed.*, 2007, **46**, 4329; (o) S. Luo, X. Zheng, H. Xu, X. Mi, L. Zhang and J.-P. Cheng, *Adv. Synth. Catal.*, 2007, **349**, 2431; (p) M. Shokouhimehr, Y. Piau, J. Kim and Y. Jang, *Angew. Chem., Int. Ed.*, 2007, **46**, 7039; (q) S. Z. Luo, X. X. Zheng and J.-P. Cheng, *Chem. Commun.*, 2008, 5719; (r) X. Zheng, S. Luo, L. Zhang and J.-P. Cheng, *Green Chem.*, 2009, **11**, 455; (s) B. Panella, A. Vargas and A. Baiker, *J. Catal.*, 2009, **261**, 88.

-
- 5 L. M. Rossi, F. P. Silva, L. L. R. Vono, P. K. Kiyohara, E. L. Duarte, R. Itri, R. Landers and G. Machado, *Green Chem.*, 2007, **9**, 379.
- 6 M. J. Jacinto, P. K. Kiyohara, S. H. Masunaga, R. F. Jardim and L. M. Rossi, *Appl. Catal., A*, 2008, **338**, 52.
- 7 M. J. Jacinto, O. H. C. F. Santos, R. F. Jardim, R. Landers and L. M. Rossi, *Appl. Catal., A*, 2009, **360**, 177.
- 8 (a) R. A. Sheldon, *Green Chem.*, 2007, **9**, 1273; (b) S. Caron, R. W. Dugger, S. G. Ruggeri, J. A. Ragan and D. H. B. Ripin, *Chem. Rev.*, 2006, **106**, 2943.
- 9 K. R. Brown, D. G. Walter and M. J. Natan, *Chem. Mater.*, 2000, **12**, 306.
- 10 V. R. Choudhary, A. Dhar, P. Jana, R. Jha and B. S. Uphade, *Green Chem.*, 2005, **7**, 768.

Perfluoro-tagged, phosphine-free palladium nanoparticles supported on silica gel: application to alkylation of aryl halides, Suzuki–Miyaura cross-coupling, and Heck reactions under aerobic conditions†

Roberta Bernini,^a Sandro Cacchi,^{*b} Giancarlo Fabrizi,^b Giovanni Forte,^c Francesco Petrucci,^c Alessandro Prastaro,^a Sandra Niembro,^d Alexandr Shafir^d and Adelina Vallribera^{*d}

Received 29th July 2009, Accepted 24th September 2009

First published as an Advance Article on the web 29th October 2009

DOI: 10.1039/b915465e

The utilization of perfluoro-tagged palladium nanoparticles immobilized on fluorosilica gel through fluorosilica–fluorosilica interactions (Pd_{np}-A/FSG) or through covalent bonding to silica gel (Pd_{np}-B) in the alkylation of aryl halides, in the Suzuki–Miyaura cross-coupling, as well as in the Heck reaction between methyl acrylate and aryl iodides is described. The reactions are carried out under aerobic and phosphine-free conditions with excellent to quantitative product yields in each case. The catalysts are easily recovered and reused several times without significant loss of activity. The alkylation of aryl halides (under copper-free conditions) and the Suzuki–Miyaura cross-coupling are carried out in water. The Heck reaction of methyl acrylate with aryl iodides is best performed in MeCN. The utilization of Pd_{np}-B in the synthesis of 2,3-disubstituted indoles from 2-(alkynyl)trifluoroacetanilides and aryl halides is also reported.

Introduction

Palladium catalysis has achieved an important place in the arsenal of the practising organic chemist.¹ Palladium catalysts are expensive, however, and this may limit their utilization in some cases. Furthermore, their use might result in palladium contamination of the desired isolated product, a significant problem for the pharmaceutical industry, which has to meet strict specifications to limit the presence of heavy metal impurities in active substances.² Immobilized palladium catalysts³ can provide a way to overcome these problems by allowing the palladium species to be separated, recovered, and reused, thus reducing palladium contamination of the isolated products. This approach would be exceedingly convenient in industrial applications as well as in cases when the reactions are carried out in multiple vessels for library generation.

A number of studies have been devoted to immobilizing palladium on inert support materials, including activated carbon, silica gel, polymers containing covalently-bound ligands, metal oxides, porous aluminosilicates, clays and other inorganic

materials, as well as microporous and mesoporous supports.⁴ Palladium has been microencapsulated in a polymeric coating,⁵ an efficient and cost-effective technique to ligate and retain palladium species. Aerogels, a new class of porous solids obtained *via* sol-gel processes coupled with supercritical drying of wet gels, have also been shown to exhibit a great potential for the preparation of heterogeneous catalysts.⁶

Recently, palladium nanoparticles have been shown to be stabilized by entrapment in perfluoro-tagged, phosphine-free compounds.⁷ This finding was somewhat unexpected, given that heavily fluorinated compounds are not expected to be the best constituents of protecting shields for nanoparticles (perfluorinated chains are indeed known to exhibit very small attractive interactions toward other materials and among themselves⁸). Thus, we were intrigued by the idea of immobilizing phosphine-free, perfluoro-tagged palladium nanoparticles on solid supports⁹ and evaluating the utilization of the immobilized catalyst in C–C bond forming reactions. A nice example of immobilizing perfluoro-tagged palladium has been reported by Bannwarth *et al.*¹⁰ who prepared several catalysts *via* adsorption of palladium(II) complexes containing perfluorinated phosphine ligands on fluorosilica gel (FSG) and showed the advantages of their utilization (separation and recovery of perfluoro-tagged palladium) in the Suzuki–Miyaura cross-coupling reaction in comparison with fluorosilica biphasic catalysis approaches using expensive and environmentally-persistent perfluorinated solvents. Phosphines, however, are often air-sensitive. In that sense, interesting results have been achieved in some cases by employing more efficient phosphines.¹¹ Such phosphines are not readily available, however, and some limits to their use in large-scale applications still remain. The development of efficient phosphine-free catalysts would provide obvious advantages in many synthetic applications. In this context, we observed

^aDipartimento A. B. A. C., Università della Tuscia e Consorzio Universitario “La Chimica per l’Ambiente”, Via S. Camillo De Lellis, 01100, Viterbo, Italy

^bDipartimento di Chimica e Tecnologie del Farmaco, Sapienza, Università di Roma, P.le A. Moro 5, 00185, Rome, Italy.
E-mail: sandro.cacchi@uniroma1.it; Fax: +39 (06) 4991 2780; Tel: +39 (06) 4991 2795

^cIstituto Superiore di Sanità, Viale Regina Elena 299, 00161, Rome, Italy

^dDepartment of Chemistry, Universitat Autònoma de Barcelona, Cerdanyola, 08193, Spain. E-mail: adelina.vallribera@uab.cat; Tel: +34 93 581 3045

† Electronic supplementary information (ESI) available: Experimental procedures and physical data of compounds. See DOI: 10.1039/b915465e

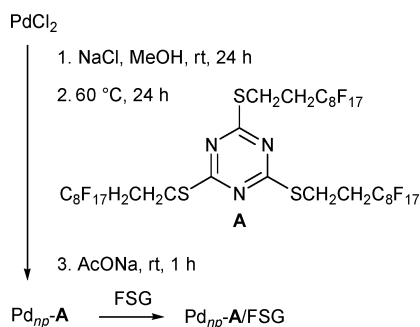
and previously communicated that immobilized phosphine-free, perfluoro-tagged palladium nanoparticles can be extremely efficient in catalyzing the alkylation of aryl halides (with palladium nanoparticles immobilized through covalent bonding to silica gel)¹² and the Heck reaction (with palladium nanoparticles immobilized on fluorosilica gel through fluorosilica–fluorosilica interactions¹³ as well as through covalent bonding to silica gel¹⁴).

We wish at this time to report full details of the utilization of this new immobilized phosphine-free palladium system in these two C–C bond-forming reactions. The alkylation of aryl halides and the Heck reaction have been extended to a larger number of substrates. The utilization of immobilized phosphine-free, perfluoro-tagged palladium nanoparticles through covalent bonding to silica gel in the Heck reaction as well as in the synthesis of 2,3-disubstituted indoles from 2-(alkynyl)trifluoroacetanilides and aryl halides have also been investigated. Furthermore, perfluoro-tagged palladium nanoparticles immobilized on fluorosilica gel through fluorosilica–fluorosilica interactions and through covalent bonding to silica gel have been used in the Suzuki–Miyaura cross-coupling.

Results and discussion

Preparation of phosphine-free, perfluoro-tagged palladium nanoparticles immobilized on FSG (Pd_{np}-A/FSG) and covalently bound to silica gel (Pd_{np}-B)

Phosphine-free, perfluoro-tagged palladium nanoparticles Pd_{np}-A (diameter 2.3 ± 0.7 nm; 13.4% palladium) were prepared as described previously for similar systems^{7e} by reduction of Na₂Pd₂Cl₆ (prepared *in situ* from PdCl₂ and NaCl) with methanol at 60 °C in the presence of compound A, a stabilizing agent featuring long perfluorinated chains, followed by the addition of AcONa (Scheme 1 and Fig. 1a). To prepare the immobilized catalyst, nanoparticles, Pd_{np}-A, were dissolved in perfluorooctane, and to this solution, commercially available FSG (C₈; 35–70 μm) was added and the solvent was evaporated, affording the immobilized catalyst (Pd_{np}-A/FSG) as an air stable powder. Transmission electron microscopy (TEM) of this material showed well-defined spherical particles dispersed in the silica matrix (Fig. 1b). The mean diameter of the nanoparticles was about 1.5 ± 0.7 nm.



Scheme 1 Synthesis of phosphine-free, perfluoro-tagged palladium nanoparticles Pd_{np}-A and their immobilization on fluorosilica gel (FSG).

Palladium nanoparticles stabilized by a perfluorinated compound covalently bound to silica gel were also prepared. This

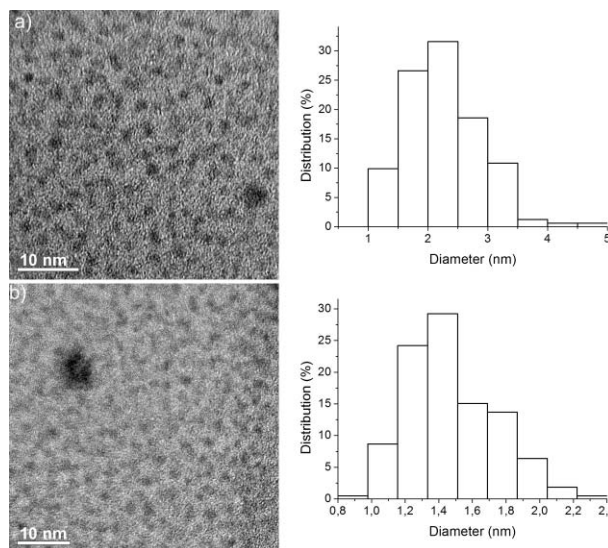
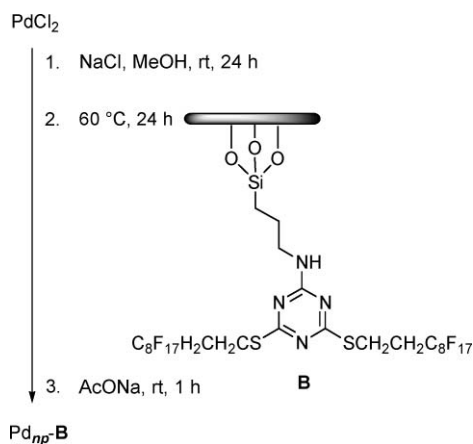


Fig. 1 (a) TEM image and particle size distribution histogram of Pd_{np}-A (particle size 2.3 ± 0.7 nm). (b) TEM image and particle size distribution histogram of Pd_{np}-A/FSG (particle size 1.5 ± 0.7 nm).

catalyst system (Pd_{np}-B), containing 3.47% of palladium in the form of nanoparticles with an average particle size of 3.9 ± 0.9 nm, was prepared by the sol-gel process described previously¹⁴ (Scheme 2).



Scheme 2 Synthesis of Pd_{np}-B.

Alkylation of aryl halides

We initiated our investigation by screening for reaction conditions under which the alkylation reaction would proceed in the presence of oxygen, and in the absence of copper and phosphine. Copper salts can induce Glaser-type homocoupling¹⁵ of terminal alkynes due to the oxidative coupling of copper acetylide intermediates when exposed to oxidative agents or air. In addition, the presence of two metals hinders the recovery and reuse of the expensive palladium catalysts (its recovery would be the best way to overcome cost-related problems).

Reactions were conducted in water. The use of water as the reaction medium is very attractive in organic synthesis for safety, economical, and environmental reasons.¹⁶ In addition, reactions involving water-insoluble substrates often benefit from

Table 1 The influence of solvents and bases on the reaction of phenylacetylene with 3-(trifluoromethyl)iodobenzene catalyzed by Pd_{np}-A/FSG^a

Entry	Base	% Yield of 3a ^b
1	K ₂ CO ₃	50
2	KOAc	50
3	Et ₂ NH	89
4	Et ₃ N	91
5	Piperidine	95
6	Pyrrrolidine	99

^a Reactions were carried out under aerobic conditions in 2 mL of water using 1 mmol of 3-(trifluoromethyl)iodobenzene, 1 mmol of phenylacetylene and 2 mmol of base in the presence of 0.1 mol% of Pd_{np}-A/FSG. ^b Yields are given for isolated products.

the hydrophobic effect when carried out in water due to its high dielectric constant and density.¹⁷ There are only a few reports of alkylation reactions of aryl halides in the presence of immobilized palladium catalysts under copper- and phosphine-free conditions in water¹⁸ or using water as cosolvent.¹⁹ Our recent report¹² showed that palladium nanoparticles can be successfully employed in the alkylation of aryl halides under these conditions.

Using the reaction of 3-(trifluoromethyl)iodobenzene with phenylacetylene as a probe for evaluating the reaction conditions (Table 1), we observed that the desired coupling product could be isolated in moderate yields after 5 h at 100 °C in water using Pd_{np}-A/FSG (catalyst loading 0.1 mol%), K₂CO₃ or KOAc as bases under aerobic conditions (entries 1 and 2). No homocoupling derivative was observed. We then tested nitrogen bases and found that an almost quantitative yield could be obtained with pyrrolidine (entry 6).

The coupled product was isolated in excellent yield under the optimized conditions [Pd_{np}-A/FSG (catalyst loading 0.1 mol%), H₂O, 100 °C, 5 h]. However, recycling studies revealed that Pd_{np}-A/FSG has a limited capacity to be reused. Indeed, a significant loss of activity was observed in the third run (Table 2, entry 1). Increasing the catalyst loading resulted in only a marginal increase in the number of runs that could be performed without a significant loss of activity (entries 2–4).

Although only trace amounts of palladium were detected in the water fraction obtained after the reaction (0.05–0.08 ppm by SF-ICP-MS), high levels of palladium (39–240 ppm) were

found in the crude isolated product. This is most likely due to the relative weakness of fluorine–fluorine interactions responsible for the binding of the Pd_{np}-A species to FSG, with the effect becoming most pronounced in the alkylation reaction (not observed in the Suzuki–Miyaura cross-coupling and Heck reaction, *vide infra*). Confirming this assumption, the ¹⁹F NMR analysis of the crude mixture obtained from the reaction of phenylacetylene with 3-(trifluoromethyl)iodobenzene after filtration revealed the presence of significant amounts of A, corresponding to an approximately 50% loss of the fluorine stabilizer A per run.

A possible explanation is that the leaching of palladium and the loss of activity in this reaction depends on the nature of reagents and products. Relatively strong interactions²⁰ might be established between palladium and alkyne (substrate/product). These interactions could favor the leaching of palladium that is removed from the solid support combined with the stabilizer A.

To circumvent the problems caused by the stabilizer leaching, we went on to investigate the use of material Pd_{np}-B, with the perfluoro-tagged palladium nanoparticles covalently linked to silica gel. The catalytic activity and stability of this catalyst was tested using our model system in water with a variety of bases (K₂CO₃, KOAc, pyrrolidine, piperidine, Et₂NH, and Et₃N). After some experimentation, we found that 3a could be isolated in 95% yield using 0.5 mol% of Pd_{np}-B and 2 equiv. of pyrrolidine at 100 °C for 1 h. Further studies revealed that the recyclability of this supported catalyst system was significantly superior to that of Pd_{np}-A/FSG (Table 2, entry 5). The Ostwald ripening process, where atoms detach from smaller clusters and reattach to bigger clusters,²¹ was not observed upon recycling. The material recovered after 11 runs was examined by TEM and showed nanoparticles of about 3.2 nm in diameter (Fig. 3).

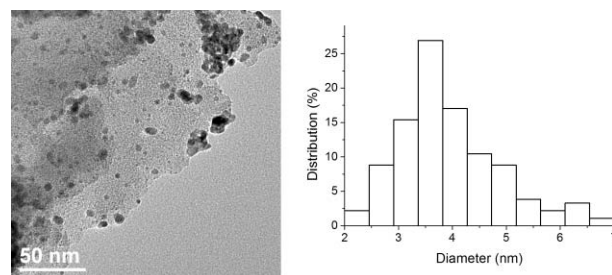


Fig. 2 TEM image and particle size distribution histogram of Pd_{np}-B (particle size 3.9 ± 0.9 nm).

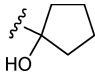
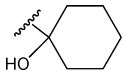
A variety of terminal alkynes and aryl halides were then subjected to the optimized conditions using both Pd_{np}-A/FSG (procedure A) and Pd_{np}-B (procedure B). As shown in Table 3,

Table 2 Recycling studies on the reaction of phenylacetylene with 3-(trifluoromethyl)iodobenzene using Pd_{np}-A/FSG or Pd_{np}-B^a

Entry	Catalyst	Loading	T/°C	Time/min	% Yield of 3a ^b	TON
1	Pd _{np} -A/FSG	0.1 mol%	100	120	95, 92, 50	2370
2		0.5 mol%	100	45	95, 96, 93, 83, 15	764
3		1.0 mol%	80	45	97, 92, 90, 80, 60	427
4		1.5 mol%	80	40	85, 92, 91, 95, 55	279
5	Pd _{np} -B	0.5 mol%	100	60	95, 90, 91, 86, 95, 92, 95, 90, 88, 86, 70	1956

^a Reactions were carried out under aerobic conditions in 2 mL of water using 1 mmol of 3-(trifluoromethyl)iodobenzene, 1 mmol of phenylacetylene and 2 mmol of pyrrolidine in the presence of Pd_{np}-A/FSG or Pd_{np}-B. ^b Yields are given for isolated products.

Table 3 The reaction of terminal alkynes **1** with aryl iodides and bromides **2** in the presence of Pd_{np}-A/FSG or Pd_{np}-B^a

		Pd _{np} -A/FSG or Pd _{np} -B pyrrolidine H ₂ O, 100 °C				
		R-C≡C- 1	+ ArX 2	R-C≡C-Ar 3		
Entry	Terminal Alkyne 1 R	ArX 2	Proc.	Time/h	% Yield of 3 ^b	
1	Ph	3-CF ₃ C ₆ H ₄ I	A	3	3a	95
2		3-CF ₃ C ₆ H ₄ I	A	3	3a	95 ^c
3		3-CF ₃ C ₆ H ₄ I	B	1	3a	95
4		4-EtO ₂ CC ₆ H ₄ I	A	5	3b	95
5		4-MeCOC ₆ H ₄ I	B	6	3c	80
6		4-NO ₂ C ₆ H ₄ I	A	5	3d	93
7		4-MeOC ₆ H ₄ -I	B	12	3e	90
8		4-CNC ₆ H ₄ I	A	6	3f	86
9		4-CNC ₆ H ₄ I	B	5	3f	88
10		PhI	A	24	3g	94
11		PhI	B	12	3g	70
12		3-Me-4-NO ₂ C ₆ H ₄ I	A	8	3h	86
13		2-NH ₂ C ₆ H ₄ I	B	24	3i	75
14	4-MeOC ₆ H ₄	4-CNC ₆ H ₄ I	A	5	3l	85
15		4-CNC ₆ H ₄ I	B	7	3l	95
16		2-MeC ₆ H ₄ I	A	29	3m	80
17		2-MeC ₆ H ₄ I	B	9	3m	90
18	4-CNC ₆ H ₄	3-CF ₃ C ₆ H ₄ I	A	2	3n	89
19		3-CF ₃ C ₆ H ₄ I	B	2	3n	99
20	4-MeCOC ₆ H ₄	4-CNC ₆ H ₄ I	A	4	3o	90
21		4-CNC ₆ H ₄ I	B	2	3o	99
22	4-CNC ₆ H ₄	4-MeOC ₆ H ₄ -I	A	3	3l	85
23		4-MeOC ₆ H ₄ -I	B	7	3l	25
24		3-CF ₃ C ₆ H ₄ I	A	2	3n	89
25		3-CF ₃ C ₆ H ₄ I	B	2	3n	99
26	2-MeC ₆ H ₄	4-CNC ₆ H ₄ I	A	44	3p	84
27		4-MeOC ₆ H ₄ -I	A	5	3m	85
28	HOCH ₂	4-CNC ₆ H ₄ I	B	24	3q	89
29		4-MeOC ₆ H ₄ -I	B	24	3r	87
30	HO(Me) ₂ C	4-MeOC ₆ H ₄ I	A	48	3s	83
31		4-CNC ₆ H ₄ I	A	24	3t	75
32	HO(Me)(Et)C	4-MeCOC ₆ H ₄ I	B	22	3u	90
33	HO(Me)(Ph)C	4-MeOC ₆ H ₄ I	B	24	3v	90
34		4-CNC ₆ H ₄ I	B	12	3z	95
35		4-MeCOC ₆ H ₄ I	B	14	3za	85
36		4-MeOC ₆ H ₄ I	B	24	3zb	87
37		4-MeCO-C ₆ H ₄ I	B	14	3zc	92
38		4-MeOC ₆ H ₄ I	B	18	3zd	89
39	Ph	4-MeCOC ₆ H ₄ Br	A	44	3c	50
40		4-MeCOC ₆ H ₄ Br	B	10	3c	80
41		3-CF ₃ C ₆ H ₄ Br	B	9	3a	91
42		4-MeOC ₆ H ₄ Br	B	48	3e	65
43		4-CNC ₆ H ₄ Br	A	24	3f	99
44		4-CNC ₆ H ₄ Br	B	8	3f	75
45		4-NO ₂ C ₆ H ₄ Br	A	24	3d	92

^a Reactions were carried out under aerobic conditions in 2 mL of water using 1 mmol of **2**, 1 mmol of **1**, 2 mmol of pyrrolidine with Pd_{np}-A/FSG (catalyst loading 0.1 mol%); procedure A) or with Pd_{np}-B (catalyst loading 0.5 mol%); procedure B). ^b Yields are given for isolated products. ^c In the presence of Pd_{np}-A/FSG (catalyst loading 0.5 mol%).

acetylenes bearing electron-rich and electron-poor aryl groups as well as alkyl substituents give coupling products in excellent yields employing aryl iodides, which in turn can accommodate electron-withdrawing and electron-donating substituents. Ortho substituents in the aryl halide are also tolerated (entries 13, 16, 17). With aryl bromides, longer reaction times are required to

obtain similar or slightly lower yields (compare entry 3 with entry 41, entry 5 with entry 40, entry 6 with entry 45, entry 7 with entry 42, entry 8 with entry 43, and entry 9 with entry 44).

The formation of **3i** (entry 13) is particularly attractive in that coupling products of this type are useful intermediates for the synthesis of indoles.²² We briefly investigated using

Table 4 Synthesis of 2,3-disubstituted indoles from 2-(phenylethynyl)trifluoroacetanilide and aryl iodides in the presence of Pd_{np}-B^a

Entry	ArI 2	Time/h	% Yield of 5 ^{b,c}	
1	PhI	9	82	5a
2	3-CF ₃ C ₆ H ₄ I	2	91 (90, 86, 87)	5b
3	4-CNC ₆ H ₄ I	4	84 (92, 90, 86)	5c
4	4-MeCOC ₆ H ₄ I	2	89 (91, 87)	5d
5	3-MeC ₆ H ₄ I	40	77	5e
6	4-MeOC ₆ H ₄ I	48	70	5f
7	4-ClC ₆ H ₄ I	5	96 (92, 83)	5g
8	4-NO ₂ C ₆ H ₄ I	4	90	5h

^a Reactions were carried out under aerobic conditions in 2 mL of MeCN using 1 mmol of **2**, 1 mmol of **4**, and 2 mmol of K₂CO₃ in the presence of Pd_{np}-B (catalyst loading 0.1 mol%). ^b Yields are given for isolated products. ^c Yields in parentheses refer to successive runs carried out with the recovered catalyst.

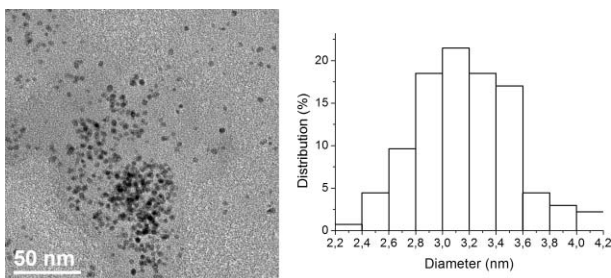


Fig. 3 TEM image and particle size distribution histogram of Pd_{np}-B after 11 runs (particle size 3.2 ± 0.4 nm).

Pd_{np}-B in the synthesis of 2,3-disubstituted indoles from 2-(phenylethynyl)trifluoroacetanilide and aryl iodides *via* the aminopalladation–reductive elimination protocol²³ (Table 4). Excellent yields are obtained with electron-poor aryl iodides. Lower reaction rates and slightly lower yields are observed with electron-rich aryl iodides.

Suzuki–Miyaura cross-coupling

We started this part of the study by examining the reaction of 4-iodobenzoic acid with 2-tolylboronic acid as the model system, using a material containing 20 mg of Pd_{np}-A per g of FSG (0.26% palladium) and catalyst loading down to 0.1 mol% in the presence of K₃PO₄ in water at 100 °C for 5 h.²⁴ Under these conditions, the corresponding cross-coupling product **7a** was isolated in 80% yield. The influence of bases on the reaction outcome was next investigated (Table 5). K₂CO₃ gave a higher yield (entry 2) while **7a** was isolated in moderate yield using KF (entry 3). Complete conversion could be obtained when the reaction was carried out in the presence of a 1 : 1 K₂CO₃/KF combination²⁶ (entry 4). An even higher reaction rate was observed under the same conditions using 0.1 mol% of Pd_{np}-B, giving **7a** in 99% yield after 1 h (entry 5).

Table 5 The influence of bases on the reaction of 4-iodobenzoic acid with 2-tolylboronic acid in water catalyzed by Pd_{np}-A/FSG or Pd_{np}-B^a

Entry	Catalyst	Base	Time/h	% Yield of 7a ^b
1	Pd _{np} -A/FSG	K ₃ PO ₄	5	80
2		K ₂ CO ₃	5	87
3		KF	5	64
4		K ₂ CO ₃ /KF (1 : 1)	5	99
5	Pd _{np} -B	K ₂ CO ₃ /KF (1 : 1)	1	99

^a Reactions were carried out under aerobic conditions in 2 mL of water using 1 mmol of 4-iodobenzoic acid, 1 mmol of 2-tolylboronic acid, 2 mmol of base in the presence of Pd_{np}-A/FSG or Pd_{np}-B (catalyst loading 0.1 mol%). ^b Yields are given for isolated products.

Recycling studies were then performed and revealed that both Pd_{np}-A/FSG and Pd_{np}-B could be reused several times without significant loss of activity (Table 6, entries 1 and 4). Further recycling studies were performed using lower palladium loading. Using materials containing 2 mg of Pd_{np}-A per g of FSG (0.026% palladium) with a palladium loading down to 0.01 mol% and 0.2 mg of Pd_{np}-A per g of FSG (0.0026% palladium) with a palladium loading down to 0.001 mol%, the cumulative turnover number (TON) over six and four runs is 55 300 and 333 000, respectively (entries 2 and 3). With Pd_{np}-B and a palladium loading down to 0.01% the cumulative turnover number over is 37 000 (entry 5).

The resistance of Pd_{np}-A/FSG and Pd_{np}-B to leaching was assessed for the same reaction (4-iodobenzoic acid and 2-tolylboronic acid). SF-ICP-MS analysis indicated the level of palladium species in water and in the raw product to be in the range of 1–2.4 and 3–23 ppb, respectively (Table 7). In addition, TEM analysis showed that, after 15 runs, the palladium nanoparticles are very similar in shape and size to those of the original catalyst system (compare Fig. 4a with Fig. 1 and Fig. 4b with Fig. 2).

The crucial role of fluoros–fluorop interactions with Pd_{np}-A/FSG was assessed by immobilizing Pd_{np}-A on standard reversed phase silica gel and using the resultant catalyst in our model reaction (4-iodobenzoic acid with 2-tolylboronic acid). Compound **7a** was obtained in 87% yield in the first run. However, a pronounced loss of activity was observed in the second run, which gave the cross-coupling product in 62% isolated yield.

Using the optimized conditions (K₂CO₃/KF 1 : 1, 100 °C, H₂O), we next explored the efficiency of Pd_{np}-A/FSG and Pd_{np}-B with other aryl iodides and bromides as well as arylboronic acids. As shown in Table 8, both precatalysts gave good to excellent results with aryl halides and arylboronic acids containing both electron-donating and electron-withdrawing substituents. The success with the electron-deficient arylboronic acids (entries 5, 30, 32, 33, and 34) is particularly noteworthy given that these compounds are often reluctant to give Suzuki–Miyaura products,²⁷ a tendency usually attributed to

Table 6 Recycling studies on the reaction of 4-iodobenzoic acid with 2-tolylboronic acid using Pd_{np}-A/FSG or Pd_{np}-B^a

Entry	Catalyst	Loading	% Yield of 7a	TON
1	Pd _{np} -A/FSG	0.1 mol%	99, 86, 84, 88, 91, 90, 86, 92, 87, 90, 90, 85, 84, 91, 93	13 360
2		0.01 mol%	98, 95, 99, 92, 99, 70	55 300
3		0.001 mol%	89, 85, 87, 72	333 000
4	Pd _{np} -B	0.1 mol%	99, 99, 91, 99, 97, 99, 97, 100, 95, 90, 92, 95, 90, 85, 85	14 130
5		0.01 mol%	97, 95, 90, 87	37 000

^a Reactions were carried out under aerobic conditions in 2 mL of water using 1 mmol of 4-iodobenzoic acid, 1 mmol of 2-tolylboronic acid, 2 mmol of K₂CO₃/KF (1 : 1) at 100 °C in the presence of Pd_{np}-A/FSG (5 h) or Pd_{np}-B (1 h). ^b Yields are given for isolated products.

Table 7 Palladium leaching in the reaction of 4-iodobenzoic acid with 2-tolylboronic acid using 0.1 mol% of Pd_{np}-A/FSG or Pd_{np}-B

Run	Pd leaching in water (ppb)		Pd leaching in the row product (ppb)	
	Pd _{np} -A/FSG	Pd _{np} -B	Pd _{np} -A/FSG	Pd _{np} -B
1	2.4	1	22.7	46
2	1.6	na	22.2	na
3	1.8	na	6.0	na
5	1	1	4.3	4.5
10	1	na	3.5	na
15	1	1	1.5	1

esters from methyl acrylate and aryl iodides. Iodobenzene was selected as the model system. A silica gel containing 100 mg of Pd_{np}-A per g of FSG (1.22% palladium) and a 0.6 mol% palladium loading was initially evaluated. The reaction, carried out in water in the presence of Et₃N, in air at 80 °C for 24 h, gave no evidence of **8a**. A slightly better result was obtained with *t*-butyl acrylate, the corresponding vinylic substitution product being isolated in 35% yield. Similarly, employing a 40% EtOH aqueous solution gave only a 3% conversion after 24 h. Gratifyingly, using DMF led to the formation of methyl cinnamate in almost quantitative yield. A similar result was obtained in the second run. However, a loss of activity was observed in the third run (85% yield) which became even more substantial in the fourth run (75% yield). Assuming that these results might be due to the leaching of palladium in DMF, we switched to the utilization of MeCN. After some experimentation we found that complete conversion could be reached in MeCN at 100 °C after 24 h using 20 mg of Pd_{np}-A per g of FSG and a catalyst loading down to 0.1 mol%. Methyl cinnamate was isolated in 90% yield. A similar result was obtained using 0.1 mol% of Pd_{np}-B under the same conditions. Methyl cinnamate was isolated in 93% yield.

Recycling studies showed that both Pd_{np}-A/FSG and Pd_{np}-B can be reused several times without significant loss of activity (Table 9). Using a material containing 3.3 mg of Pd_{np}-A per g of FSG (0.04% palladium) and a palladium loading down to 0.001 mol%, the cumulative turn-over number over three runs is 265 000 (entry 3). With Pd_{np}-B and a palladium loading down to 0.01 mol%, the cumulated turnover number over four runs is 36 100 (entry 4).

The resistance of Pd_{np}-A/FSG to leaching was assessed for the model reaction. SF-ICP-MS analysis indicated the level of palladium in the crude mixtures to be in the 2–7 ppm range. Agglomeration of nanoparticles was not observed upon recycling. The recovered material after the 15th run was examined by TEM showing nanoparticles of about 1.9 ± 0.3 nm (Fig. 5). Control

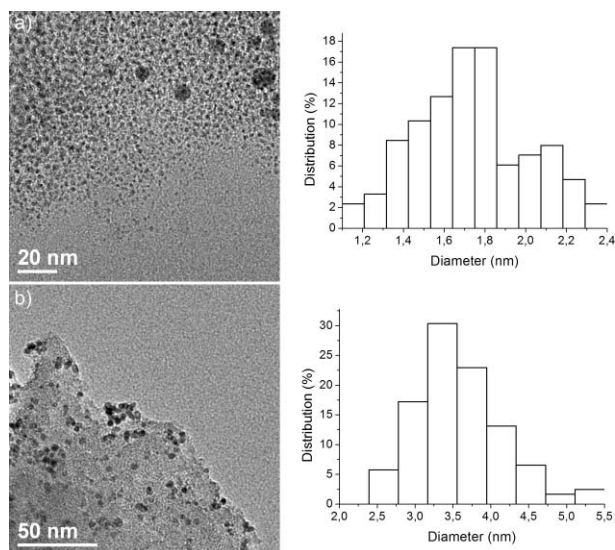


Fig. 4 (a) TEM image and particle size distribution histogram of Pd_{np}-A/FSG after the 15th run (particle size 1.7 ± 0.3). (b) TEM image and particle size distribution histogram of Pd_{np}-B after the 15th run (particle size 3.6 ± 0.6).

their lower nucleophilicity (in comparison to their electron-neutral or electron-rich analogues) and, consequently, slower transmetalation. *Ortho* methyl substituents are tolerated both in the aryl halide and the arylboronic acid component (entries 1, 2, 4, 13, 23, 29, 32). In addition, *ortho* functional groups such as -Br, -COOH, and -NO₂ are also well tolerated (entries 25, 33, 34).

Heck reaction

To explore the utilization of Pd_{np}-A/FSG and Pd_{np}-B in the Heck reaction, we decided to study the synthesis of cinnamate

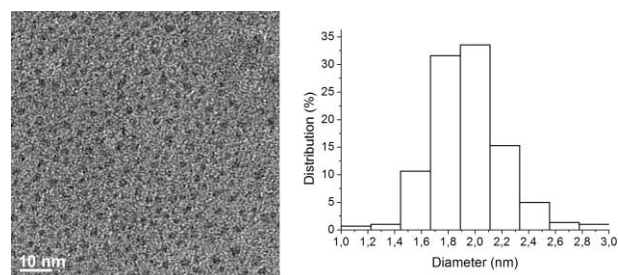
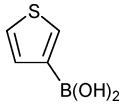
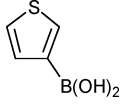


Fig. 5 TEM image and particle size distribution histogram of Pd_{np}-A/FSG after the 15th run (particle size 1.9 ± 0.3 nm).

Table 8 The reaction of arylboronic acids with aryl halides in the presence of Pd_{np}-A/FSG and Pd_{np}-B^a

Entry	ArX 2	ArX + Ar ¹ B(OH) ₂		Proc.	Time/h	Ar—Ar ¹	% Yield of 7 ^{b,c}
		2	6				
1	4-HO ₂ CC ₆ H ₄ I	2-MeC ₆ H ₄ B(OH) ₂	A	5		7a	99
2		2-MeC ₆ H ₄ B(OH) ₂	B	1		7a	99
3		4-F,3-MeC ₆ H ₃ B(OH) ₂	A	5		7b	72
4	4-MeOC ₆ H ₄ I	2-MeC ₆ H ₄ B(OH) ₂	A	24		7c	92
5		4-MeCOC ₆ H ₄ B(OH) ₂	B	5		7d	91
6	4-HO ₂ CC ₆ H ₄ Br	4-F,3-MeC ₆ H ₃ B(OH) ₂	A	44		7b	80
7		4-CF ₃ C ₆ H ₄ B(OH) ₂	A	7		7e	71
8		4-CF ₃ C ₆ H ₄ B(OH) ₂	B	8		7e	90(92)
9		PhB(OH) ₂	A	8		7f	72
10		PhB(OH) ₂	B	8		7f	91
11		4-MeOC ₆ H ₄ B(OH) ₂	A	6		7g	91(90)
12		4-MeOC ₆ H ₄ B(OH) ₂	B	8		7g	87
13		2-MeC ₆ H ₄ B(OH) ₂	B	5		7a	90
14		4-MeC ₆ H ₄ B(OH) ₂	B	5		7h	87
15	4-HO ₂ CC ₆ H ₄ I	4-MeOC ₆ H ₄ B(OH) ₂	A	5		7g	95(99)
16		4-CF ₃ C ₆ H ₄ B(OH) ₂	A	2		7e	94(99, 84)
17		4-MeC ₆ H ₄ B(OH) ₂	A	5		7h	99
18		PhB(OH) ₂	A	24		7f	83
19	4-MeOC ₆ H ₄ I	4-CF ₃ C ₆ H ₄ B(OH) ₂	A	24		7i	80
20	4-MeOC ₆ H ₄ Br	4-CF ₃ C ₆ H ₄ B(OH) ₂	B	24		7i	88(85)
21		4-MeCOC ₆ H ₄ B(OH) ₂	B	48		7d	80
22	PhI	4-CF ₃ C ₆ H ₄ -B(OH) ₂	A	24		7l	50
23		2-MeC ₆ H ₄ B(OH) ₂	B	9		7m	99
24	4-MeCOC ₆ H ₄ I	4-CF ₃ C ₆ H ₄ B(OH) ₂	A	8		7n	91
25		2-BrC ₆ H ₄ B(OH) ₂	B	48		7o	62
26	4-MeCOC ₆ H ₄ Br	4-CF ₃ C ₆ H ₄ B(OH) ₂	B	8		7n	92(93)
27		4-MeOC ₆ H ₄ B(OH) ₂	B	24		7d	84
28			B	5		7p	90
29	4-FC ₆ H ₄ I	2-MeC ₆ H ₄ B(OH) ₂	A	6		7q	89
30	4-CNC ₆ H ₄ I	4-MeCOC ₆ H ₄ B(OH) ₂	B	24		7r	87
31	4-MeOC ₆ H ₄ Br		B	16		7s	89
32	2-MeC ₆ H ₄ I	4-MeCOC ₆ H ₄ B(OH) ₂	B	6		7t	93
33	2-HO ₂ CC ₆ H ₄ I	4-MeCOC ₆ H ₄ B(OH) ₂	B	2		7a	80
34	2-NO ₂ ,4-MeC ₆ H ₄ I	4-MeCOC ₆ H ₄ B(OH) ₂	B	2		7u	87

^a Unless otherwise stated, reactions were carried out under aerobic conditions in 2 mL of water using 1 mmol of aryl halide, 1 mmol of arylboronic acid, 2 mmol of K₂CO₃/KF (1 : 1) at 100 °C in the presence of Pd_{np}-A/FSG (procedure A) or Pd_{np}-B (procedure B) (catalyst loading 0.1 mol%).
^b Yields are given for isolated products. ^c Yields in parentheses refer to successive runs carried out with the recovered catalyst.

Table 9 Recycling studies for the reaction of iodobenzene with methyl acrylate catalyzed by Pd_{np}-A/FSG or Pd_{np}-B^a

Entry	Catalyst loading	Time/h	T/°C	Yield% of 8a	TON
1	Pd _{np} -A/FSG 0.1 mol%	24	100	90(91), 96(90, 96(90), 93(86), 87(88), 89(95), 97(100), 96(99), 95(94), 98(95), 97, 90, 90, 84, 80	13 780
2	Pd _{np} -A/FSG 0.01 mol%	24	120	100, 96, 81, 97, 85	45 900
3	Pd _{np} -A/FSG 0.001 mol%	24	140	100, 82, 83	265 000
4	Pd _{np} -B 0.01 mol%	24	120	97, 94, 86, 84	36 100

^a Reactions were carried out under aerobic conditions in 2 mL of MeCN using 1 mmol of iodobenzene, 2 mmol of methyl acrylate, 3 mmol of Et₃N at 100 °C for 24 h in the presence of Pd_{np}-A/FSG or Pd_{np}-B. ^b Yields are given for isolated products. ^c Yields in parentheses refer to a second set of experiments

Table 10 Reaction of aryl iodides with methyl acrylate catalyzed by Pd_{np}-A/FSG or Pd_{np}-B^a

Entry	Aryl iodide 2	Procedure	Time/h	% Yield of 8 ^{b,c}	
1	PhI	A	24	90	8a
2	PhI	B	24	93	8a
3	4-MeCOC ₆ H ₄ I	A	5	89 (90)	8b
4	4-MeCOC ₆ H ₄ I	B	5	92	8b
5	4-MeOC ₆ H ₄ I	A	23	90 (70)	8c
6	4-MeOC ₆ H ₄ I	B	18	89	8c
7	4-MeC ₆ H ₄ I	A	23	90	8d
8	4-NO ₂ C ₆ H ₄ I	A	48	74 (65)	8e
9	3-CF ₃ C ₆ H ₄ I	A	6	93 (90)	8f
10	4-EtO ₂ CC ₆ H ₄ I	A	5	98	8g
11	3-Me-4-NO ₂ C ₆ H ₃ I	A	23	96	8h
12	2-NH ₂ C ₆ H ₄ I	A	48	84	8i
13	2-MeO ₂ CC ₆ H ₄ I	A	7	89	8j

^a Reactions were carried out under aerobic conditions in 2 mL of MeCN using 1 mmol of aryl iodide, 2 mmol of methyl acrylate, 3 mmol of Et₃N at 100 °C in the presence of Pd_{np}-A/FSG (procedure A) or Pd_{np}-B (procedure B) (catalyst loading 0.1 mol%). ^b Yields are given for isolated products. ^c Yields in parentheses are for the second run carried out with the recovered catalyst.

experiments were also carried out to assess whether leaching of the stabilizer **A** might take place under reaction conditions. ¹⁹F NMR analysis of the crude mixture produced in the reaction of methyl acrylate with 3-(trifluoromethyl)iodobenzene after filtration revealed the presence of small amounts of **A**, corresponding to a loss of about 5%. No evidence of fluorine was observed in the isolated vinylic substitution product.

As was the case with the Suzuki–Miyaura cross-coupling, the reusability of the catalyst system is strongly dependent on fluorine–fluorine interactions. Immobilizing Pd_{np}-A on standard reversed phase silica gel and using the resultant catalyst in the reaction of methyl acrylate with iodobenzene gave methyl cinnamate in 93% yield in the first run. However, a remarkable loss of activity was observed in the second run where the Heck product was isolated only in 59% yield.

We next evaluated the efficiency of Pd_{np}-A/FSG and Pd_{np}-B with other aryl iodides. The preparative results are summarized in Table 10.

We have not investigated in detail whether the nanoparticles on the solid surface are the actual catalyst or they are just a source that leaches active catalyst species²⁸ in all the reactions described in the present manuscript. Nevertheless, we observed that when methyl acrylate, *p*-iodoanisole and Et₃N were added to the crude mixture derived from the reaction of methyl acrylate with iodobenzene (after separation of the solid material), the corresponding vinylic substitution derivative could be isolated in 40% yield after 23 h at 100 °C. This result supports the notion that palladium species leached from the solid surface are, at least in part, responsible for the catalytic activity.

Conclusions

In conclusion, we have demonstrated that perfluoro-tagged palladium nanoparticles immobilized on fluorinated silica gel by fluorine–fluorine interactions (Pd_{np}-A/FSG) or linked to silica gel by covalent bonds (Pd_{np}-B) can be successfully used under

aerobic and phosphine-free conditions in the alkylation of aryl halides (under copper-free conditions), in the Suzuki–Miyaura cross-coupling, and in the Heck reaction of methyl acrylate with aryl iodides. The alkylation of aryl halides and the Suzuki–Miyaura cross-coupling are carried out in water. The Heck reaction of methyl acrylate with aryl iodides is best performed in MeCN. Pd_{np}-B can be successfully used in the synthesis of 2,3-disubstituted indoles from 2-(alkynyl)trifluoroacetanilides and aryl halides.

Both catalysts allow for the isolation of the desired products, usually in high to excellent yields. However, in the alkylation of aryl halides the use of Pd_{np}-B gives the best results in terms of recovery and reuse.

The supported palladium can be easily recovered and reused. The recovery involves centrifugation and decanting the solution in the presence of air, without any particular precaution.

Acknowledgements

This work was carried out in the framework of the National Projects “Stereoselezione in Sintesi Organica. Metodologie ed Applicazioni” supported by the Ministero dell’Università e della Ricerca (MUR) and by Sapienza, Università di Roma. Financial support from Ministerio de Ciencia e Innovación of Spain (Projects CTQ2008-05409-C02-01 and CTQ2005-04968-C02-01 and Consolider Ingenio 2010 (CSD2007-00006)) and DURSI-Generalitat de Catalunya (SGR 2005-00305 and SGR 2009-1441) are gratefully acknowledged. A.S. has been supported through a Ramon y Cajal contract from the Ministerio de Educación y Ciencia of Spain. S.N. acknowledges MICINN for a predoctoral fellowship.

Notes and references

- (a) J. Tsuji, *Palladium Reagents and Catalysts - Innovation in Organic Synthesis*, John Wiley & Sons, New York, 1995; (b) *Handbook of Organopalladium Chemistry for Organic Synthesis*, E. Negishi, Ed.;

- John Wiley & Sons, New York, 2002, Vols. 1 and 2; (c) J. Tsuji, *Palladium Reagents and Catalysts - New Perspectives for the 21st Century*, John Wiley & Sons, New York, 2004.
- C. E. Garret and K. Prasad, *Adv. Synth. Catal.*, 2004, **346**, 889.
 - For a review, see: S. V. Ley, I. R. Baxendale, R. N. Brem, P. S. Jackson, A. G. Leach, A. Longbottom, M. Nesi, J. S. Scott, R. I. Storer and S. J. Taylor, *J. Chem. Soc., Perkin Trans. 1*, 2000, 3815.
 - For some excellent recent reviews on the use of heterogeneous palladium catalysts in C–C bond forming reactions, see: (a) L. Yin and J. Liebscher, *Chem. Rev.*, 2007, **107**, 133; (b) M. Moreno-Mañas and R. Pleixats, *Acc. Chem. Res.*, 2003, **36**, 638.
 - For selected references, see: (a) R. Akiyama and S. Kobayashi, *Angew. Chem., Int. Ed.*, 2001, **40**, 3469; (b) C. Ramarao, S. V. Ley, S. C. Smith, I. M. Shirley and N. DeAlmeida, *Chem. Commun.*, 2002, 1132; (c) S. V. Ley, C. Ramarao, R. S. Gordon, A. B. Holmes, A. J. Morrison, I. F. McConvey, I. M. Shirley, S. C. Smith and M. D. Smith, *Chem. Commun.*, 2002, 1134; (d) N. Bremeyer, S. V. Ley, C. Ramarao, I. M. Shirley and S. C. Smith, *Synlett*, 2002, 1843; (e) S. V. Ley, C. Mitchell, D. Pears, C. Ramarao, J.-Q. Yu and W. Zhou, *Org. Lett.*, 2003, **5**, 4665.
 - (a) T. F. Bauman, G. A. Fox and J. H. Satcher, Jr., *Langmuir*, 2002, **18**, 7073; (b) T. F. Bauman and J. H. Satcher, Jr., *Chem. Mater.*, 2003, **15**, 3745; (c) F. J. Maldonado-Hódar, C. Moreno-Castilla and A. F. Pérez-Cadenas, *Microporous Mesoporous Mater.*, 2004, **69**, 119; (d) C. Moreno-Castilla and F. J. Maldonado-Hódar, *Carbon*, 2005, **43**, 455; (e) S. Martínez, A. Vallribera, C. L. Cotet, M. Popovici, L. Martín, A. Roig, M. Moreno-Mañas and E. Molins, *New J. Chem.*, 2005, **29**, 1342; (f) L. C. Cotet, M. Gich, A. Roig, I. C. Popescu, V. Cosoveanu, E. Molins and V. Danciu, *J. Non-Cryst. Solids*, 2006, **352**, 2772; (g) S. Cacchi, C. L. Cotet, G. Fabrizi, G. Forte, A. Goggiamani, L. Martín, S. Martínez, E. Molins, M. Moreno-Mañas, F. Petrucci, A. Roig and A. Vallribera, *Tetrahedron*, 2007, **63**, 2519; (h) R. Soler, S. Cacchi, G. Fabrizi, G. Forte, L. Martín, S. Martínez, E. Molins, M. Moreno-Mañas, F. Petrucci, A. Roig, R. M. Sebastián and A. Vallribera, *Synthesis*, 2007, 3068; (i) A. Vallribera, E. Molins, Aerogel supported nanoparticles in catalysis, in *Nanoparticles and Catalysis*, Wiley-VCH, 2008.
 - (a) M. Moreno-Mañas, R. Pleixats and S. Villarroya, *Organometallics*, 2001, **20**, 4524; (b) M. Moreno-Mañas, R. Pleixats and S. Villarroya, *Chem. Commun.*, 2002, 60; (c) M. Tristany, J. Courmarcel, P. Dieudonne, M. Moreno-Mañas, R. Pleixats, A. Rimola, M. Sodupe and S. Villarroya, *Chem. Mater.*, 2006, **18**, 716; (d) A. Serra-Muns, R. Soler, E. Badetti, P. de Mendoza, M. Moreno-Mañas, R. Pleixats, R. M. Sebastián and A. Vallribera, *New J. Chem.*, 2006, **30**, 1584; (e) S. Niembro, A. Vallribera and M. Moreno-Mañas, *New J. Chem.*, 2008, **32**, 94.
 - (a) *Organofluorine Chemistry. Principles and Commercial Applications*, R. E. Banks, B. E. Smart, J. C. Tatlow, Eds: Plenum, New York, 1994; (b) *Modern Fluoroorganic Chemistry*, P. Kirsch, Ed.: Wiley-VCH, Weinheim, 2004.
 - For selected recent reviews on fluorous catalysts, see: (a) J. A. Gladysz, R. Correa de Costa, In *The handbook of fluorous chemistry* J. Gladysz, A. D. P. Curran, I. T. Horvath, Eds.; Wiley-VCH, Weinheim, 2004, pp. 24-40, see especially sections 4.6 - 4.9; (b) D. P. Curran, In *The handbook of fluorous chemistry*, J. A. Gladysz, D. P. Curran, I. T. Horvath, Eds.; Wiley-VCH, Weinheim, 2004, pp. 101-127, see section 7.6; (c) S. Schneider, C. C. Tzschucke, W. Bannwarth, In *The handbook of fluorous chemistry*, J. A. Gladysz, D. P. Curran, I. T. Horvath, Eds.; Wiley-VCH, Weinheim, 2004, pp. 257-272; (d) D. P. Curran, K. Fischer and G. Moura-Letts, *Synlett*, 2004, 1379.
 - (a) C. C. Tzschucke, C. Markert, H. Glatz and W. Bannwarth, *Angew. Chem., Int. Ed.*, 2002, **41**, 4500; (b) C. C. Tzschucke and W. Bannwarth, *Helv. Chim. Acta*, 2004, **87**, 2882.
 - See, for example: (a) V. P. W. Böhm and W. A. Herrmann, *Eur. J. Org. Chem.*, 2000, 3679; (b) T. Hundertmark, A. F. Littke, S. L. Buchwald and G. C. Fu, *Org. Lett.*, 2000, **2**, 1729; (c) M. Eckhardt and G. C. Fu, *J. Am. Chem. Soc.*, 2003, **125**, 13642; (d) K. W. Anderson and S. L. Buchwald, *Angew. Chem., Int. Ed.*, 2005, **44**, 6173.
 - R. Bernini, S. Cacchi, G. Fabrizi, G. Forte, F. Petrucci, A. Prastaro, S. Niembro, A. Shafir and A. Vallribera, *Org. Biomol. Chem.*, 2009, **7**, 2270.
 - R. Bernini, S. Cacchi, G. Fabrizi, G. Forte, S. Niembro, F. Petrucci, R. Pleixats, A. Prastaro, R. M. Sebastian, R. Soler and M. Tristany, *Org. Lett.*, 2008, **10**, 561.
 - S. Niembro, A. Shafir, A. Vallribera and R. Alibes, *Org. Lett.*, 2008, **10**, 3215.
 - For selected references, see: (a) C. Glaser, *Ber. Dtsch. Chem. Ges.*, 1869, **2**, 422; (b) A. S. Hay, *J. Org. Chem.*, 1962, **27**, 3320; (c) R. Rossi, A. Carpita and C. Bigelli, *Tetrahedron Lett.*, 1985, **26**, 523; (d) N. G. Kundu, M. Pal and C. Chowdhury, *J. Chem. Res.*, 1993, 432; (e) A. Lei, M. Srivastava and X. Zhang, *J. Org. Chem.*, 2002, **67**, 1969 and references therein; (f) I. J. S. Fairlamb, P. S. Bauerlein, L. R. Marrison and J. M. Dickinson, *Chem. Commun.*, 2003, 632; (g) A. S. Batsanov, J. C. Collings, I. J. S. Fairlamb, J. P. Holland, J. A. K. Howard, Z. Lin, T. B. Marder, A. C. Parsons and R. M. Ward, *J. Org. Chem.*, 2005, **70**, 703; (h) for a review of alkyne coupling, see: P. Siemsen, R. C. Livingston and F. Diederich, *Angew. Chem., Int. Ed.*, 2000, **39**, 2632.
 - For a recent review on C–C bond forming reactions in aqueous media, see: C.-J. Li, *Chem. Rev.*, 2005, **105**, 3095.
 - M. Cai, Q. Xu, J. Sha and J. Molec, *J. Mol. Catal. A: Chem.*, 2007, **272**, 293.
 - (a) J. Gil-Moltó, S. Karlström and C. Nájera, *Tetrahedron*, 2005, **61**, 12168; (b) Z.-W. Ye and W.-B. Yi, *J. Fluorine Chem.*, 2008, **129**, 1124.
 - L. Djakovitch and P. Rollet, *Tetrahedron Lett.*, 2004, **45**, 1367.
 - M. Ahlqvist, G. Fabrizi, S. Cacchi and P.-O. Norrby, *Chem. Commun.*, 2005, 4196.
 - (a) A. Imre, D. L. Beke, E. Gontier-Moya, I. A. Szabo and E. Gillet, *Appl. Phys., A*, 2000, **71**, 19; (b) A. Howard, C. E. J. Mitchell and R. G. Egddell, *Surf. Sci.*, 2002, **515**, L504; (c) R. Narayanan and M. A. El-Sayed, *J. Am. Chem. Soc.*, 2003, **125**, 8340.
 - For some recent reviews, see: (a) G. Zeni and R. C. Larock, *Chem. Rev.*, 2004, **104**, 2285; (b) F. Alonso, I. P. Beletskaya and M. Yus, *Chem. Rev.*, 2004, **104**, 3079; (c) I. Nakamura and Y. Yamamoto, *Chem. Rev.*, 2004, **104**, 2127; (d) S. Cacchi and G. Fabrizi, *Chem. Rev.*, 2005, **105**, 2873; (e) G. R. Humphrey and J. T. Kuethe, *Chem. Rev.*, 2006, **106**, 2875; (f) L. Ackermann, *Synlett*, 2007, 5607; (g) K. Krüger, A. Tillack and M. Beller, *Adv. Synth. Catal.*, 2008, **350**, 2153.
 - (a) G. Battistuzzi, S. Cacchi and G. Fabrizi, *Eur. J. Org. Chem.*, 2002, 2671; (b) See also: S. Cacchi, G. Fabrizi and A. Goggiamani, *Adv. Synth. Catal.*, 2006, **348**, 1301 and the references cited therein.
 - While this manuscript was in preparation, a study of cross-coupling using the same catalyst system, Pd_{np}-A/FSG, was reported (L. Wang, C. Cai, *J. Mol. Catal. A: Chem.* 2009, **306**, 97). Reactions, however, were performed in the presence of Bu₄NBr (which may limit the degree of recycling of the catalyst system²⁵) and an increase of palladium nanoparticles to 5–10 nm (from the initial 2–3 nm) and a palladium leaching of 10 ppm was observed.
 - For some leading references on tetraalkylammonium-stabilized palladium nanoparticles, see: (a) M. T. Reetz, R. Breinbauer and K. Wanninger, *Tetrahedron Lett.*, 1996, **37**, 4499; (b) M. Beller, H. Fischer, K. Kühlein, C.-P. Reisinger and W. A. Herrmann, *J. Organomet. Chem.*, 1996, **520**, 257; (c) M. T. Reetz and M. Maase, *Adv. Mater.*, 1999, **11**, 773; (d) M. T. Reetz and E. Westermann, *Angew. Chem., Int. Ed.*, 2000, **39**, 165.
 - Interestingly, a similar result was obtained subjecting 4-iodobenzoic acid and potassium 4-methoxyphenyltrifluoroborate to 0.1 mol% of Pd_{np}-A/FSG at 100 °C in water in the presence of K₂CO₃, omitting KF. The corresponding diaryl derivative **7i** was isolated in 99% yield after 5 h (compare with the result reported in Table 8, entry 15).
 - T. E. Barder, S. D. Walker, J. R. Martinelli and S. L. Buchwald, *J. Am. Chem. Soc.*, 2005, **127**, 4685.
 - For a recent review on solid catalysts and on evidence for and against catalysis by solid surfaces vs. soluble species, see: (a) N. T. S. Phan, M. Van Der Sluys and C. W. Jones, *Adv. Synth. Catal.*, 2006, **348**, 609; (b) see also: ref. 9a and M. B. Thathagar, J. E. ten Elshof and G. Rothenberg, *Angew. Chem., Int. Ed.*, 2006, **45**, 2886.

Exploring the possibility of using a thermostable mutant of β -glucosidase for rapid hydrolysis of quercetin glucosides in hot water

Sofia Lindahl,^a Anna Ekman,^c Samiullah Khan,^b Christina Wennerberg,^b Pål Börjesson,^c Per J. R. Sjöberg,^a Eva Nordberg Karlsson^b and Charlotta Turner^{*a}

Received 11th June 2009, Accepted 28th September 2009

First published as an Advance Article on the web 4th November 2009

DOI: 10.1039/b920195p

The antioxidant quercetin was extracted from yellow onion waste and converted to its aglycone form by a combination of subcritical water extraction and enzymatic hydrolysis. The hydrolytic step was catalysed by a double residue (N221S, P342L) mutant of the thermostable β -glucosidase (*TnBgl1A*), isolated from the thermophile *Thermotoga neopolitana* and cloned and produced in *E. coli*. The activity of wt *TnBgl1A* was shown to be dependent on the position of the glucosylation on the quercetin backbone, favouring hydrolysis of quercetin-4'-glucoside over quercetin-3-glucoside. The mutated variant of the enzyme harboured a mutation in the +2 sub-site (N221S) and showed increased catalytic efficiency in quercetin-3-glucoside hydrolysis and also to a certain extent hydrolysis of quercetin-4'-glucoside. The mutated enzyme was used directly in yellow onion extracts, prepared by subcritical water extraction, resulting in complete hydrolysis of the glucosylated flavonoids quercetin-3,4'-diglucoside, quercetin-4'-glucoside, quercetin-3-glucoside, isorhamnetin-4'-glucoside and isorhamnetin-3,4'-diglucoside. To complete hydrolysis within five minutes, 3 mg of *TnBgl1A_N221S* was used per gramme of onion (dry weight). A life cycle assessment was done to compare the environmental impact of the new method with a conventional solid-liquid extraction-and-hydrolysis method utilising aqueous methanol and hydrochloric acid. Comparison of the methods showed that the new method is preferable regarding primary energy consumption and global warming potential. Another advantage of this method is that handling of toxic chemicals (methanol and HCl) is avoided. This shows that combined subcritical water extraction/enzyme hydrolysis is both a fast and sustainable method to obtain quercetin from onion waste.

Introduction

The agricultural, forestry, and food industries produce tonnes of waste materials and by-products every year, such as onion skin, apple peel, carrot waste and birch bark. In the case of onion, the amount of onion waste annually produced within the European Union is almost half a million tons.¹ The produced waste and by-products are today used in animal feed, or for composting, incineration or anaerobic digestion. However, these waste materials and by-products contain high-value compounds such as antioxidants that can be extracted before the waste reaches its final destination. Waste and by-products from fruits and vegetables are rich in antioxidants such as polyphenols, which have uses as additives in pharmaceuticals, food products and cosmetics. A large group of polyphenolic compounds are flavonoids. Quercetin (Q) is an example of a high-value flavonoid, and can for example be extracted from onion.^{2,3} Hence, it is of interest to be able to extract quercetin and

other flavonoids from waste and by-products since they possess antioxidative properties – studies have shown that they have positive effects against, for example, cancer⁴ and neurodegenerative diseases.⁵ These compounds are mainly present in glycosylated forms in fruits and vegetables. In onion, they mainly occur as quercetin-4'-glucoside (Q-4') and quercetin-3,4'-diglucoside (Q-3,4') (Fig. 1), but other types of quercetin glucosides as well as the aglycone form (Fig. 1) are also present, but at much lower concentrations.⁶

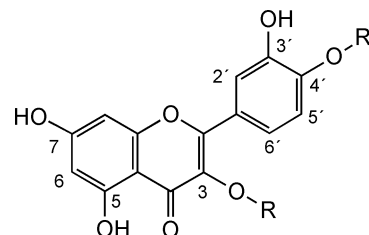


Fig. 1 Chemical structures of quercetin ($R, R' = H$), quercetin-3-glucoside ($R = \text{glucose}$ and $R' = H$), quercetin-4'-glucoside ($R = H$ and $R' = \text{glucose}$) and quercetin-3,4'-diglucoside ($R, R' = \text{glucose}$).

There are a number of different methods published on how to extract quercetin and quercetin glycosides from onion, of which the most commonly used technique is solid-liquid extraction with aqueous methanol as extraction solvent.^{6,7} The extraction

^aUppsala University, Department of Physical and Analytical Chemistry, Analytical Chemistry, P.O. Box 599, SE-751 24, Uppsala, Sweden.
E-mail: Charlotta.Turner@kemi.uu.se

^bLund University, Department of Biotechnology, P.O. Box 124, SE-221 00, Lund, Sweden

^cLund University, Department of Technology and Society, P.O. Box 118, SE-221 00, Lund, Sweden

of quercetin and quercetin glycosides is often combined with acid hydrolysis of the extracted glycosides. To catalyse the hydrolysis reaction, hydrochloric acid at high concentration is commonly used.⁷⁻¹⁰ Deglycosylation of the quercetin glycoside mixture obtained after extraction is advantageous for two reasons. Firstly, the glycosides are present in an extract at various concentrations, and by hydrolysing them to the quercetin aglycone, the quantitative determination is simplified. Secondly, the antioxidising power is in general higher for the deglycosylated form,¹¹ which we have also measured for quercetin species using the DPPH (2,2-diphenyl-1-picrylhydrazyl) method (data not shown). Hence, by hydrolysing the quercetin glucoside mixture, the potential value of the material is increased. A problem with acid-catalysed hydrolysis is that the conditions are harsh, resulting in degradation of compounds such as phenolic acids in the extract, and even degradation of the target molecule quercetin.⁸ Another drawback is that the acidity of the sample can cause problems in the analysis step. This is commonly performed by high performance liquid chromatography (HPLC), and the HPLC-column may be damaged by the extremely low pH of the sample. To overcome these problems, enzymatic hydrolysis is an alternative.^{3,10,12} β -Glucosidases catalyse hydrolysis of glucose linked to either a carbohydrate or non-carbohydrate moiety, and these enzymes have previously been shown to hydrolyse quercetin glucosides.^{3,10,13}

Turner *et al.*³ have described a subcritical water extraction method, followed by hydrolysis by thermostable β -glucosidase from *Thermotoga neapolitana* that yielded quercetin in the aglycone form from a yellow onion extract. The pressurised liquid extraction with water as a solvent was run at 120 °C and 50 bar, and the following enzymatic hydrolysis in water at 90 °C and pH 5.0. This method gave the same yield as a conventional solid-liquid extraction method, although one limitation in the hydrolysis step was that the enzyme had a low conversion rate of quercetin-3-glucoside (Q-3) to the aglycone form (Q), which was speculated to be due to steric hindrance (Fig. 1). It is well known that water at elevated temperature and pressure is an efficient, less polar solvent, similar to methanol.^{14,15} Use of a thermostable enzyme may allow a combination of the extraction with the hydrolysis step, without extensive cooling in-between. Moreover, the hydrolysis reaction will go faster due to increased diffusion rates. Other advantages using subcritical water extraction combined with enzymatic hydrolysis compared to conventional methanol extraction and acid hydrolysis include: (i) lower environmental load, as water is a more sustainable solvent than methanol, and hence no production or destruction facilities are needed; (ii) use of the onion waste as animal feed or as feedstock in biogas production after extraction and hydrolysis is still possible, since only a small fraction of the biomass is removed, and (iii) a significantly shorter total processing time per sample.

However, it is important to not just analyse qualitative parameters, like the exchange of a solvent with another, but to also quantify the environmental load of the method. For this purpose a standardised life cycle assessment (LCA) is an excellent tool allowing quantification of primary energy consumption and emissions.¹⁶ In LCA, fluxes of materials and energy are followed from the extraction of raw materials, production and handling of the product when it has become waste. The flows are quantified

and characterised to different environmental impact categories, of which Global Warming Potential (GWP) is one example. LCA can be used for several different purposes such as product and process development and for comparison of the environmental impact of different products and manufacturing processes. LCA is standardised according to ISO 14044.¹⁷

A long-term aim of our research is to develop a sustainable on-line extraction-biocatalysis system with high efficiency that can be used directly at the site of an industry that produces the waste, or alternatively at a plant taking care of waste products. As a first step, the aim of this study was to optimise the hydrolysis reaction with quercetin glucosides at an analytical level, and to improve the conversion of Q-3 to quercetin. A mutated β -glucosidase (*TnBgl1A_N221S*) was utilised in the hydrolysis and compared to the wild type (wt) enzyme, *TnBgl1A*. The optimised subcritical water extraction and enzymatic hydrolysis method was subsequently applied to a yellow onion extract, and the environmental performance of the developed processes, including greenhouse gas performance and energy efficiency, was assessed from a life cycle perspective.

Results and discussion

This paper focuses on use of the thermostable β -glucosidase, wt *TnBgl1A*, and a mutated variant of the same enzyme (termed *TnBgl1A_N221S*), as catalysts for deglycosylation of quercetin glucosides in a high-temperature step, coupled off-line to an environmentally sustainable, pressurised hot water method to extract the quercetin species. Previous work showed that the wild type, *TnBgl1A*, and a differently folded glucosidase (*TnBgl3B*), both efficiently hydrolysed the major quercetin glucoside in onion extracts, glucosylated at the 4'-position of the quercetin molecule (Q-4').³ However, the Q-3 in the extract was not efficiently deglycosylated under the conditions used.³ To further investigate the possibility of the enzyme to hydrolyse quercetin species glucosylated at the 3-position (Fig. 1), this work involves deglycosylation studies of standards of quercetin glucosides (Q-4', Q-3,4', and Q-3, see Fig. 1) over time with a special emphasis on Q-3, using both the wt and a variant of *TnBgl1A* mutated at two positions (residues 221 (N→S) and 342 (P→L)). Only one (residue 221) of the two mutated residues was judged to be important for specificity, as it is located at the substrate binding site (+2 sub-site), while the other (residue 342) is found on the surface on the reverse side (opposite the active site) of the enzyme.¹⁸ This variant was chosen from a set of mutants, as it both showed the highest turnover of the substrate *para*-nitrophenyl- β -D-glucopyranoside (*p*NPG), and based on a simple screening experiment, also higher conversion of Q-3 to quercetin.¹⁸ Finally, the mutated variant is utilized coupled with subcritical water extraction of onion waste, and the environmental performance of the method is evaluated.

HPLC-UV analysis

In order to follow the hydrolysis process, high selectivity in the detection method is needed. Direct spectrophotometric detection could be employed if (for example) in the hydrolysis of *p*NPG to *p*-nitrophenol (*p*NP), the substrate and products have clearly different absorption maxima. For quercetin and

quercetin glucosides there is no such difference in absorption maxima, and a separation step prior to detection with UV is necessary (although this is time-consuming).

The number of samples to be analysed with HPLC-UV is high, and to minimise the analysis time of each sample an isocratic elution profile was selected, with methanol–water (50 : 50) containing 0.13 M (0.5 vol%) formic acid as mobile phase. The isocratic elution profile used resulted in base-line separation of the analytes: Q-3,4'; Q-3; Q-4'; and quercetin (see Fig. 5b).

Hydrolysis of quercetin glucosides by wt *TnBgl1A*

In Fig. 2a,b, the relatively fast conversion of Q-4' by wt *TnBgl1A* is clearly shown. Using a 1 : 100 enzyme:substrate molar ratio, Q-4' was completely converted to Q within 5 min, while the same conditions for Q-3 resulted in only 70% conversion within

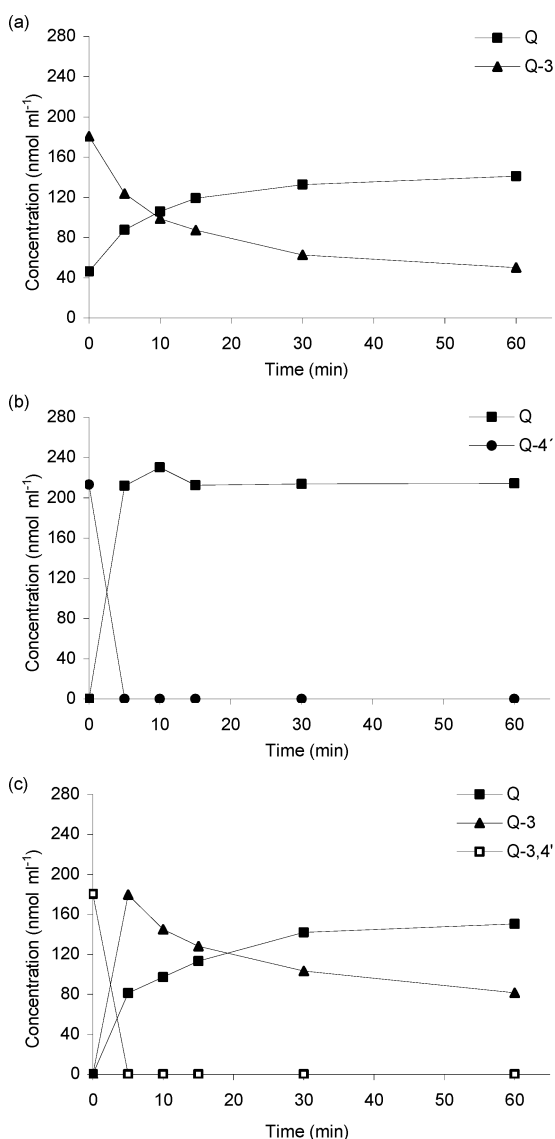


Fig. 2 Catalysis by *TnBgl1A* with (a) Q-3, (b) Q-4' and (c) Q-3,4'. 20 pmol of *TnBgl1A* and 200 nmol of substrate were used. Relative standard deviation (RSD) of the concentration values at the different sampling time points ranges between 0.3 and 20.6% ($n = 3$).

60 min. Enzymatic hydrolysis of the double glucosylated form (Q-3,4'), also showed that the 4'-glucosylation was completely hydrolysed within the 5 min interval, after which the remaining Q-3 was slowly deglycosylated to yield approximately 70% in the aglycone form (Fig. 2c). This shows that hydrolysis of the 4'-glucosylation is clearly favoured by wt *TnBgl1A*. Moreover, presence of Q-3 is not disturbing the deglycosylation at the 4'-position, and finally hydrolysis of Q-3 is possible but slow, which may be due to low affinity or steric hindrance for efficient binding of Q-3 in the active site. The homologous human β -glucosidase (hCBG), which has high specificity for Q-4' and quercetin-7-glucoside, does not hydrolyse 3-linked flavonoid glucosides,¹⁹ hence hydrolysis of this substrate by *TnBgl1A* suggests an interesting difference in the catalytic site.

Thermal stability and solubility of quercetin species

Self-hydrolysis of quercetin glucosides at high temperature was studied, and could be excluded since incubations of the quercetin glucosides at 95 °C for 1 h (the highest expected temperature for the enzyme catalysis), showed no thermal degradation of the glucosides (data not shown), and the biocatalyst was hence necessary.

A drawback with production of the more potent antioxidant Q (the deglycosylated form), is a decreased water solubility, and initial hydrolysis data showed that this decrease led to losses of the produced quercetin (data not shown). To avoid this, solubility tests were made, and the results revealed that concentrations of maximum 25 nmol ml⁻¹ of quercetin were soluble in the buffer at 95 °C. The highest concentration of quercetin species used in the remaining work was thus limited to 17 nmol ml⁻¹, to ensure full solubility of the produced quercetin.

Enzymatic hydrolysis of the different quercetin glucosides

To obtain quantitative data, a number of enzyme:substrate ratios for the wt *TnBgl1A* and mutated variant, *TnBgl1A_N221S*, were tested, using the substrates, Q-3 and Q-4', to find optimal ratios for determination of kinetic parameters. The detection method used requires sampling followed by quantification; hence the challenge was to find ratios where the initial reaction is neither too fast nor too slow. Indeed, the obtained results showed that different enzyme:substrate ratios were necessary for different enzyme/substrate combinations: for Q-3, 1 : 250-1250 and 1 : 2500-12500 for wt *TnBgl1A* and *TnBgl1A_N221S*, respectively, and for Q-4', 1 : 2500-12500 and 1 : 5000-250000 for wt *TnBgl1A* and *TnBgl1A_N221S*, respectively. The higher concentration required of the wt was in accordance with the higher turnover and specific activity reported for *TnBgl1A_N221S* (1700 s⁻¹ at 80 °C) as compared to the wt (485 s⁻¹ at 80 °C) for hydrolysis of pNPG.¹⁸

In Table 1 all kinetic data are summarised. As shown in Fig. 1, the glucose on Q-4' is situated at a position resulting in an extended molecule, while for Q-3 the glucose is in the middle of the flavonoid backbone resulting in a different overall shape, which may be sterically more difficult to accommodate in the active site. This is reflected in the higher K_m of Q-3 than for Q-4'. Furthermore, the K_m (Michaelis–Menten constant) value of *TnBgl1A_N221S* is lower for both Q-3 and Q-4' compared to the wt (Table 1), which indicates that the mutation has increased

Table 1 Kinetic studies of enzymes *TnBgl1A* and *TnBgl1A_N221S*, and the substrates Q-3 and Q-4' ($n = 3$). K_m – Michaelis–Menten constant, V_{max} – maximal conversion rate, k_{cat} – turnover number and k_{cat}/K_m – catalytic efficiency.

Enzyme	Substrate	K_m /mM	V_{max} /μmol min ⁻¹ mg ⁻¹	k_{cat} /s ⁻¹	(k_{cat}/K_m) /s ⁻¹ M ⁻¹
<i>TnBgl1A</i>	Q-3	0.129 ± 0.059	8.3 ± 2.1	7.2	55
	Q-4'	0.059 ± 0.026	8.3 ± 1.4	7.2	122
<i>TnBgl1A_N221S</i>	Q-3	0.046 ± 0.020	8.1 ± 1.3	7.1	154
	Q-4'	0.022 ± 0.015	7.1 ± 1.1	6.2	281

the affinity for both quercetin substrates. The effect is, however, especially pronounced for Q-3. The smaller size of the serine residue at position 221 may have reduced the steric hindrance of this molecule, leading to a better fit in the binding site resulting in higher catalytic efficiency. The maximal conversion rate (V_{max}) and the turnover number (k_{cat}) were in the same range for all enzyme and quercetin-substrate combinations, but as a consequence of the change in K_m the catalytic efficiency (k_{cat}/K_m) was higher for the mutant (see Table 1).

Despite the improved affinity for Q-3 using *TnBgl1A_N221S*, experiments with this variant at 95 °C showed a hydrolysis pattern with decreased deglycosylation rate at increasing incubation times (Fig. 3, 0–30 min). A second addition of the enzyme after 30 min restarted the reaction (Fig. 3, 30–65 min). To understand if this was a result of deactivation or product inhibition, thermal deactivation experiments of the enzyme in the absence of substrate, as well as incubations of the enzyme in the presence of products, were made (see below).

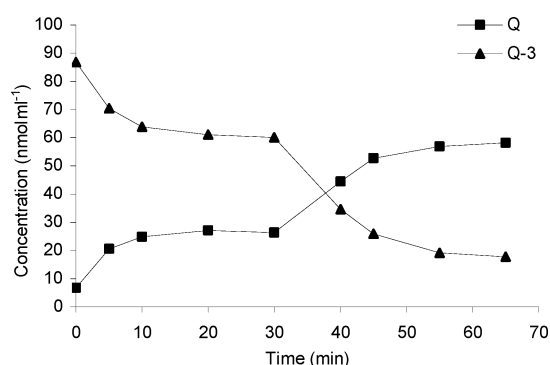


Fig. 3 A second addition of 20 pmol *TnBgl1A_N221S* 35 min after the first addition of 20 pmol *TnBgl1A_N221S*. RSD of the concentration values at the different sampling time points ranges between 0.4 and 16.9% ($n = 3$).

Thermal stability of the β-glucosidases *TnBgl1A* and *TnBgl1A_N221S*

The occurrence of irreversible thermal deactivation at 85, 90 and 95 °C was investigated to establish the tolerance of the enzymes to prolonged exposure to these temperatures (Table 2). Almost no enzymatic activity was lost for wt *TnBgl1A* during the first 30 min of incubation at 85 and 90 °C. Prolonged incubations up to 24 h fitted a first-order deactivation rate during the complete incubation period, resulting in a deactivation constant (k) of 0.027 h⁻¹ (at 90 °C). The half-life of the enzyme ($t_{1/2}$) could thus be calculated to exceed 10 h at 90 °C. A further 5 °C increase in temperature led to significant activity loss, giving a $t_{1/2}$ of 28 min (0.46 h, Table 2). The mutant *TnBgl1A_N221S* showed

Table 2 Irreversible thermal deactivation of *TnBgl1A* and *TnBgl1A_N221S*. k is the deactivation constant and $t_{1/2}$ is the half-life of the enzymes

T /°C	<i>TnBgl1A</i>		<i>TnBgl1A_N221S</i>	
	k /h ⁻¹	$t_{1/2}$ /h	k (h ⁻¹)	$t_{1/2}$ /h
85	0.018	20	0.029	7.0
90	0.027	11	0.040	6.4
95	0.73	0.46	1.51	0.23

a slightly higher deactivation rate, but both the wt and mutant were judged to be stable at temperatures up to 90 °C ($t_{1/2}$ of the mutant was approximately 6 h).

A larger difference was seen at 95 °C, where the deactivation constant (k) for the mutant was doubled, and its half-life reduced to 13 min (0.23 h, Table 2). Thermal transitions by differential scanning calorimetry have shown the apparent transition temperature (T_m) from the folded to unfolded state at 102.5 °C (wt) and 100.5 °C (mutant), respectively.¹⁸ However, inspection of the chromatograms showed that the starting point of the transition occurred around 95 °C (data not shown), explaining the reduced stability at this temperature. This sets a limitation in the time frame applicable for the hydrolysis reaction if a temperature of 95 °C is used, and should only be applied if the overall reaction time is short (≤ 10 min). This relatively high temperature was used in the kinetic study and the total reaction time was less than 5 min. A temperature of 95 °C was also used in the hydrolysis of the onion extract (with a total reaction time of 5 min) to minimise the temperature difference between extraction and hydrolysis temperatures in the process.

However, in longer studies of the deglycosylation, deactivation will be significant at temperatures above 90 °C. This means that the slow deglycosylation rate of Q-3 seen within the 30 min interval for the wt cannot be a consequence of deactivation, as this was run at 90 °C (Fig. 2), while in the reaction performed with the mutated variant at 95 °C, deactivation should be significant (Fig. 3).

Activation/inhibition of the enzyme

An experiment was set up to evaluate if the mutated enzyme was product-inhibited. In this experiment, glucose and quercetin, respectively, were added to *TnBgl1A_N221S* 18 min prior to adding a hydrolysable substrate (in this case Q-4'). Product inhibition acts on the enzyme, and the presence of substrate can hence be used to detect if inhibition has occurred after the pre-incubation. To avoid thermal deactivation, the temperature was set to 90 °C. The results in Fig. 4 show that most of the Q-4' was hydrolysed after 10 min with either quercetin or the control (just the buffer). Interestingly, incubations in the presence of glucose

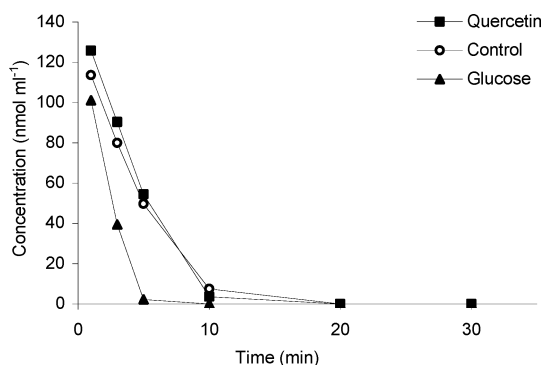


Fig. 4 The effect of incubation of *TnBgl1A_N221S* with glucose, quercetin and buffer (control) on the hydrolysis of Q-4'. RSD of the concentration values at the different sampling time points ranges between 0.3 and 6.1% ($n = 3$).

led to complete Q-4' hydrolysis after just 5 min. The conclusion is that there is no inhibition effect by either quercetin or glucose on the enzyme, but rather that glucose is an activator of the enzyme. An activating effect of glucose on the β -glucosidases from the glycoside hydrolase family 1 (GH1) is in accordance with results reported by other researchers,²⁰⁻²² and has previously been reported for wt *TnBgl1A*.^{18,21} This work shows that the activating effect of glucose also works for the mutated variant of the enzyme.

The activating effect of glucose may also explain the improved conversion of Q-3 to Q seen after the second addition of *TnBgl1A_N221S* (Fig. 3), where glucose released after the first enzyme addition is present in the reaction mixture. Currently, one can only speculate that glucose may prevent non-productive binding of the Q-3 or Q-4' substrate, for example by blocking a high affinity sub-site. To obtain proof of this suggestion, detailed studies on the binding affinity of the subsites of *TnBgl1A* will be necessary.

Application to an onion sample

Whole yellow onion was chopped and both the skin and the pulp was mixed and extracted using subcritical water at 120 °C and 50 bar as solvent. The result of the HPLC-UV analysis of the extract was that seven flavonoids were identified in the yellow onion extract – Q-4', Q-3, Q-3,4', quercetin, isorhamnetin-4'-glucoside (I-4'), isorhamnetin-3,4'-diglucoside (I-3,4') and isorhamnetin. Quercetin and the three quercetin glucosides were identified by comparing the retention time and elution order with standards, and isorhamnetin, I-4' and I-3,4' were identified based on the results by Turner *et al.*³ One of the peaks labelled "unknown" is most likely kaempferol, and this assumption is based on a previous study.³ Q-4' and Q-3,4' are the most abundant flavonoids identified in the yellow onion extract and this corresponds well to other publications of flavonoid content in yellow onion.^{3,6} Three different amounts of *TnBgl1A_N221S* were tested (20 pmol, 100 pmol and 3 nmol) (data not shown) resulting in the following method optimised for 1.2 ml of onion extract corresponding to 0.4 g of onion (50 mg dw); 3 nmol of *TnBgl1A_N221S*, reaction temperature of 95 °C, pH 5.0 and 5 min reaction time. Chromatograms of yellow onion extracts before and after enzymatic treatment at 95 °C can be seen in Fig. 5b and 5c. In Fig. 5a the amounts of quercetin and

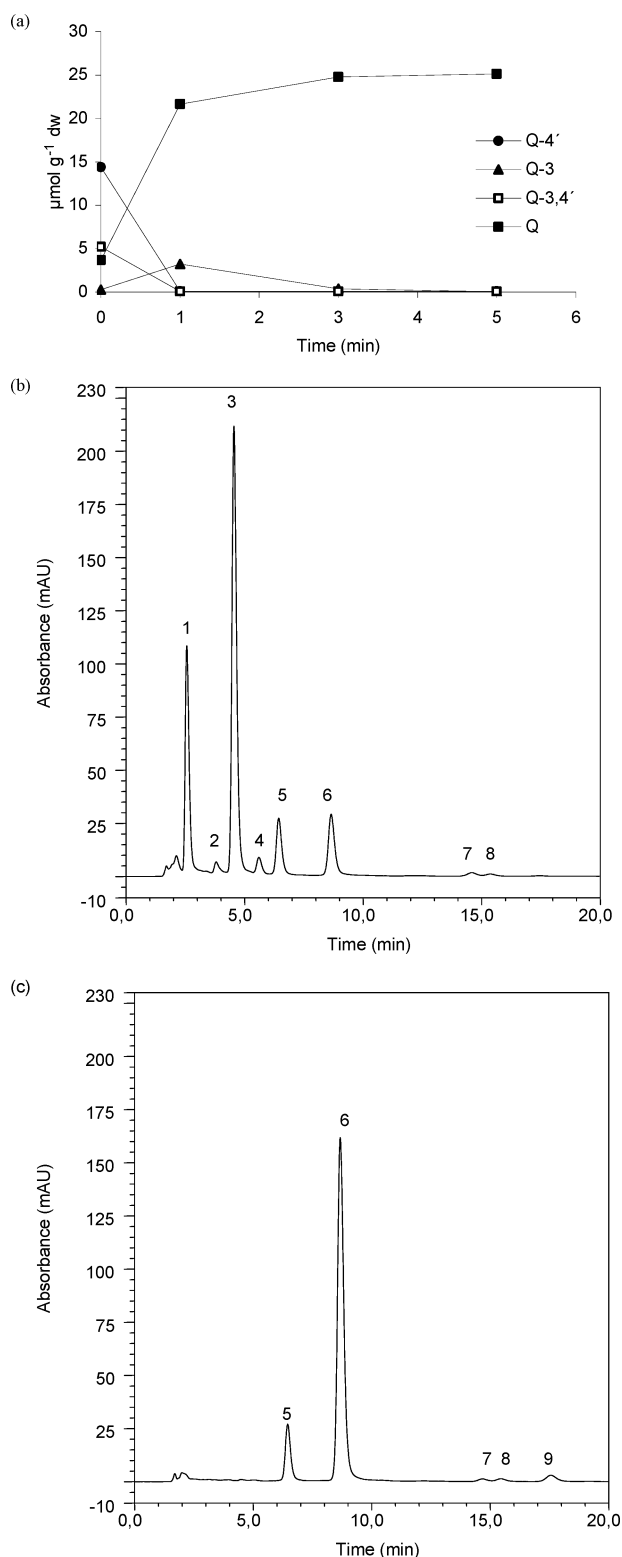


Fig. 5 HPLC-UV analysis of a yellow onion extract before and after enzyme treatment. Concentration change of Q-4', Q-3, Q-3,4' and Q during enzymatic reaction (a), RSD of concentration at the different sampling time points ranges between 0.8 and 10.6%, within the calibration curve range ($n = 3$). HPLC-UV chromatogram of yellow onion extract before addition of enzyme (b) and 5 min after addition of *TnBgl1A_N221S* (c). Peak labels; 1 (mix of Q-3,4' and I-3,4'), 2 (Q-3), 3 (Q-4'), 4 (I-4'), 5 (morin (IS)), 6 (Q), 7-8 (unknowns) and 9 (isorhamnetin).

Table 3 Primary energy consumption and emission of greenhouse gases relating to the manufacture of the compounds used in the extraction methods per 10 g of quercetin. Ranges of values are in brackets

Compounds	Primary energy (MJ kg ⁻¹ solvent/catalyst)	GWP (kg CO ₂ -eq kg ⁻¹ solvent/catalyst)	Primary energy/MJ	GWP (kg CO ₂ -eq)
Methanol ^a	1.5	17	46 (24–83)	550 (270–960)
HCl ^b	27	1.6	86 (46–160)	5.1 (2.7–9.4)
Enzyme ^c	110	9	0.33 (0.22–0.66)	0.027 (0.018–0.054)

^a Furnander.²³ ^b Boustead.²⁴ ^c Nielsen *et al.*²⁵

Table 4 Primary energy consumption and emissions of greenhouse gases relating to the heating needed in the extraction methods per 10 g of quercetin. Ranges of values are in brackets

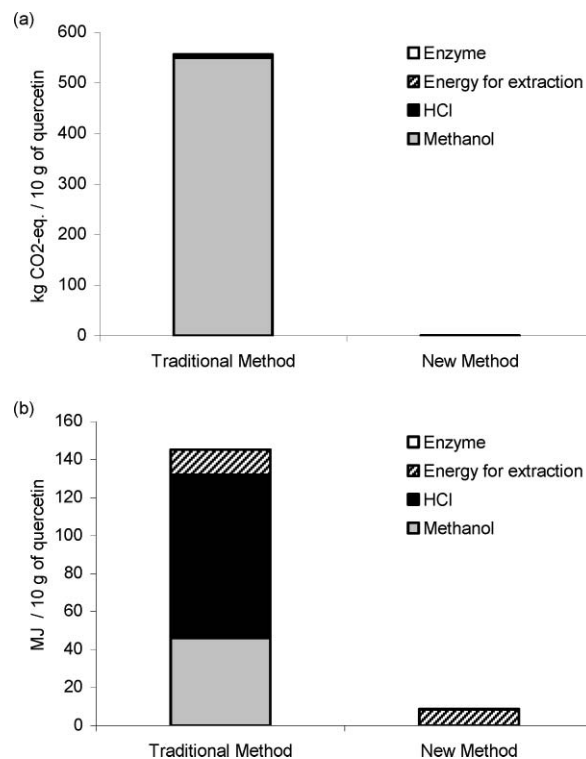
Extraction method	Heating/MJ	Extraction/kJ	Total energy/MJ	GWP (kg CO ₂ -eq)
Traditional method	13 (9.3–25)	70 (60–80)	13 (9.4–25)	1.3 (0.94–2.5)
New method	8.4 (4.2–15)	11 (8–13)	8.4 (4.2–15)	0.85 (0.42–1.5)

quercetin glucosides have been plotted as a function of sampling time points. Almost all the Q-4' and Q-3,4' have been hydrolysed after 1 min, while Q-3 concentration has increased, and after 5 min only trace amounts of glucosides are detected (Fig. 5c). Within the few minutes it takes to conduct the reaction of the yellow onion extract, *TnBg11A_N221S* maintains its activity, even though the reaction is done at 95 °C. The quercetin aglycone concentration increased at the same rate as the concentration of glucosides decreased. The increase in Q-3 concentration (after 1 min) shows that the presence of the glucosylation at this position does not limit the activity of the enzyme, but that accommodation of the substrate favours hydrolysis of glucose bound at the 4'-position. By comparing the peaks in Fig. 5b and 5c it is seen that after 5 min of reaction no I-4' or I-3,4' peaks are detected, but instead an isorhamnetin peak can be found. This indicates that *TnBg11A_N221S* also catalyses the hydrolysis of isorhamnetin glucosides to isorhamnetin. However, to confirm if it the enzyme catalyses the reaction, a study using isorhamnetin species standards should be done.

Environmental performance

The results from the environmental impact assessment are shown in Table 3 and 4. The traditional method with organic solvents leads to a significantly higher contribution to the GWP than the extraction with subcritical water. This is mainly due to the use of fossil methanol as a solvent, but also due to the larger amount of solvents needed per gramme of onion for the traditional method. Although clear differences in energy consumption can be seen for the two methods, energy for heating gives relatively small contributions to the overall environmental impact. The major input of primary energy is in the manufacture of HCl and methanol.

The environmental impact is summarised in Fig. 6. There are several uncertainties involved in the environmental assessment performed, such as the linear scaling-up of the laboratory methods. Furthermore, depending on the primary fuel used for producing heat (in this case natural gas), the contribution to the GWP will differ. However, despite these uncertainties, there are some “hot-spots” identified, supporting the conclusion

**Fig. 6** Total contribution to the GWP expressed as kg CO₂-equivalents per 10 g of quercetin, for the two extraction methods (a), and as total primary energy consumption, expressed as MJ per 10 g of quercetin, for the two extraction methods (b).

that subcritical water extraction is more favourable. These “hot-spots” are the effect of the use of fossil-fuel-derived methanol on GWP, and in addition the effect of the use of HCl on the primary energy consumption.

Experimental

Materials

Methanol and formic acid were purchased from Merck (Darmstadt, Germany). Quercetin dihydrate, quercetin

3- β -D-glucoside (Q-3), citric acid monohydrate, disodium hydrogen phosphate and *p*NPG were purchased from Sigma-Aldrich (Steinheim, Germany). Quercetin 4'-*O*- β -glucopyranoside (Q-4') and quercetin 3,4'-di-*O*- β -glucopyranoside (Q-3,4') were purchased from Polyphenols Laboratories AB (Sandnes, Norway). Ultrapure water (MilliQ) was used at all times.

Enzyme production and purification

The gene encoding wt *TnBgl1A* was cloned in pET22b(+), under control of the T7lac-promoter, as described by Turner *et al.*³ The *TnBgl1A_N221S* was obtained by site-directed mutagenesis using megaprimer PCR.¹⁸ The fragment encoding the mutated *TnBgl1A* was cloned in pET22b(+) (Novagen, Madison, WI, USA) under control of the T7lac-promoter, and transformed to *E. coli* BL21(DE3) for production.

Both enzymes were produced in 2.5 l batch cultivations, in strain BL21(DE3) after induction with isopropyl-1-thio- β -D-galactopyranoside (IPTG) (2 h), as described by Abou-Hachem *et al.*²⁶ The cells were harvested by centrifugation (10000g, 10 min, 4 °C). Cell pellets were resuspended in buffer (20 mM citrate-phosphate pH 5.6 for a single step heat treatment (80 °C, 30 min, used only for the irreversible deactivation studies)/or binding buffer (20 mM Tris-HCl, 20 mM imidazole, 0.75 M NaCl, pH 7.5) for a two-step procedure involving heat treatment (70 °C, 30 min) and immobilized metal ion affinity chromatography). The cell pellets were disintegrated by sonication (60 W cm⁻², 0.5 cycle, for 5 \times 3 min) with a UP400S sonicator (Dr. Hielscher, Stahnsdorf, Germany) while cooling in an ice-water mixture. The sonicated extracts were centrifuged at 25000g (20 min, 4 °C), and the resulting supernatants stored at 4 °C until purified.

After the heat treatment, the samples were again centrifuged (30 min at 25000g and 4 °C) for removal of denatured aggregated proteins. The supernatants obtained after heat treatment at 80 °C were used directly to study irreversible deactivation, while those treated at 70 °C were filtered (0.4 μ m pore size) and further purified by immobilised metal-ion affinity chromatography (IMAC).²⁷

Enzyme assays

The total protein concentrations were estimated using the bicinchoninic acid method (Sigma-Aldrich, Steinheim, Germany) or the Bradford protein assay (BioRad, Hercules, CA, USA) according to the manufacturers' instructions. Bovine serum albumin (BSA) was used as standard (in concentrations from 0.2 to 1.0 mg ml⁻¹). The absorbance was measured at 562 nm (bicinchoninic acid method) and 595 nm (Bradford method) using an Ultrospec 1000 (Pharmacia, Uppsala, Sweden). To estimate the purity of the enzyme, SDS-PAGE according to Laemmli²⁸ was used.

For thermal inactivation tests, the β -glucosidase activity was measured as the release of *p*NPG after 5 min incubations at 85 °C. To 960 μ l preheated substrate (2.92 mM *p*NPG dissolved in citrate-phosphate buffer pH 5.6), 40 μ l of enzyme solution was added, and the assay was performed as described in Turner *et al.*²⁹ Absorbance was measured at 405 nm using Ultrospec 1000 (Pharmacia). One Unit (U) for this substrate corresponds

to the amount of enzyme that will release 1 μ mol *p*-nitrophenol per minute under the described conditions.

Enzymatic hydrolysis of quercetin standards

In an initial activity screening, 200 nmol sample of Q-3, Q-4' and Q-3,4' dissolved in methanol (in triplicate) were evaporated, 1.0 ml of 100 mM citrate-phosphate buffer, pH 5.0, was added and the vials were heated at 90 °C until substrate dissolved. A 50 μ l fraction was collected and added to 450 μ l of mobile phase composed of methanol-water (50 : 50) and 0.13 M (0.5 vol%) formic acid (0 min fraction in Fig. 2). The reaction took place at 90 °C and the reaction was started by adding 20 pmol of wt *TnBgl1A*. 50 μ l fractions were collected and added to 450 μ l of mobile phase 1-60 min after addition of enzyme. Samples were analysed by HPLC-UV. Collection of fractions and enzyme addition was done with a 50 μ l GC-syringe. The fraction-collection procedure and enzyme addition were similar for all experiments described below, unless otherwise noted.

Thermal stability of the quercetin standards

Samples (150 nmol) of Q-3, Q-4' and Q-3,4' dissolved in methanol were evaporated, 1.5 ml of 100 mM citrate-phosphate buffer was added (triplicate samples for each glucoside) and the vials were heated at 95 °C until substrate was dissolved. Fractions were collected 10, 30 and 60 min after the first fraction collection. Fractions were collected and diluted as above. The samples were analysed by HPLC-UV.

Enzyme kinetics of the hydrolysis of Q-3 and Q-4'

To determine the kinetics of the hydrolysis reactions, 50-250 nmol samples of Q-3 and Q-4' dissolved in methanol were evaporated and re-dissolved as described above, and the volume of buffer used was 1.5 ml. Fractions were collected at 0, 1, 3, and 5 min after enzyme addition. The enzyme amounts used were 200 pmol of wt *TnBgl1A* and 20 pmol of *TnBgl1A_N221S* to Q-3 and 20 pmol of wt *TnBgl1A* and 10 pmol of *TnBgl1A_N221S* to Q-4'. Samples were analysed by HPLC-UV. The enzyme activity using Q-3 and Q-4' is expressed in Units (U). One U corresponds to the amount of enzyme required to release 1 μ mol quercetin per minute under the described conditions. Obtained data was analysed using Enzpack (Biosoft, UK), using a time-range allowing fit to the Michaelis-Menten curve. Kinetic constants were calculated using the Wilkinson non-linear regression method, supplied in the program.

Repeated enzyme additions at the applied conditions

A sample of Q-3 (triplicate of 150 nmol) in methanol was evaporated and re-dissolved as above at 95 °C. Fractions were collected at 0, 5, 10, 20 and 30 min after addition of 20 pmol *TnBgl1A_N221S*. 35 min after the first enzyme addition, the same amount of *TnBgl1A_N221S* was added and fractions were collected 40, 45, 55 and 65 min after the first enzyme addition. Samples were analysed by HPLC-UV.

Thermal stability of the enzymes in absence of substrate

Thermal stability of the enzymes was measured as irreversible deactivation. The heat-treated wt (*TnBgl1A*, 1.5 mg ml⁻¹, 29 μM) and mutant (*TnBgl1A_N221S*, 2.0 mg ml⁻¹, 38 μM) glucosidase were aliquoted into microcentrifuge tubes. These samples were incubated at 85, 90 and 95 °C, at time intervals ranging from 0 to 24 h. During the first 30 min, duplicate samples were withdrawn every 5 min, then samples were taken after 1, 2, 3, 4, 5, 18 and 24 h, and were chilled on ice (at least 30 min), centrifuged (13 000g, 30 min, 4 °C) and stored at 4 °C until activity analysis was performed. The inactivation kinetics of the different constructs was analysed assuming a first-order reaction rate. For a constant temperature:

$$A/A_0 = e^{-kt} \quad (1)$$

$$\ln A - \ln A_0 = -kt \quad (2)$$

where A_0 is the initial activity expressed in U ml⁻¹, A is the activity at time t , expressed as above, t (h) is the time, and k is the inactivation rate constant (h⁻¹). The linear regression line of the natural logarithm of the residual activity *versus* incubation time were obtained using Excel (Microsoft Office 2003). The half-life ($t_{1/2}$) at the respective temperature was obtained at $A = 0.5A_0$.

Product inhibition studies

Quercetin samples (triplicates of 100 nmol each) in methanol were evaporated and re-dissolved in 750 μl of 100 mM citrate–phosphate buffer pH 5.0, and the vials were heated at 90 °C until the quercetin had dissolved. Glucose (triplicates of 100 nmol) dissolved in 750 μl 100 mM citrate–phosphate buffer, pH 5.0, and controls containing 750 μl of 100 mM citrate–phosphate buffer pH 5.0, (triplicate) were also heated at 90 °C, and treated in the same way as the quercetin samples. *TnBgl1A_N221S* (10 pmol) was added to the vials and the samples were heated at 90 °C. Then, 18 min after addition of enzyme, pre-heated 100 nmol of Q-4' dissolved in 750 μl of 100 mM citrate–phosphate buffer, pH 5.0, was added to the vials. Fractions were collected as above, 1, 3, 5, 10, 20 and 30 min after addition of Q-4'. The first point in Fig. 4 is the 1 min fraction. Samples were analysed by HPLC-UV.

Subcritical water extraction

15–18 g of onion samples, in triplicate, were weighed into 33 ml stainless steel extraction cells containing a cellulose filter at the bottom. Extractions were performed on a Dionex ASE®-200 subcritical water extraction system (Dionex, Sunnyvale, CA, USA) using water as the only solvent as described by Turner *et al.*³ The pressure was set to 50 bar and the initial heating lasted

for 5 min. Extraction temperature was 120 °C and extraction time 15 min (three extraction cycles of 5 min each). Purging between extractions was performed with nitrogen. The extract was collected in 100 ml clear glass vials, cooled down to room temperature and diluted with degassed water to a total volume of 50 ml.

Enzymatic hydrolysis of onion extract

A 1.2 ml aliquot of onion extract, prepared by subcritical water extraction, was mixed with 300 μl of 100 mM citrate–phosphate buffer, pH 5.0, and heated at 95 °C until the sample components dissolved. Fractions were collected at 0, 1, 3, 5 and 10 min after addition of 3 nmol of *TnBgl1A_N221S*. Samples were analysed by HPLC-UV.

HPLC analysis

HPLC-UV analysis was performed using the chromatographic system UltiMate 3000 from Dionex (Germering, Germany). An Agilent Zorbax SB-C18 column (100 × 2.1 mm, 3.5 μm) was used for isocratic separation with a methanol–water (50 : 50) and formic acid (0.13 M, 0.5 vol%) mobile phase at a flow rate of 0.15 ml min⁻¹. The injection volume was 10 μl and detection was accomplished at 350 nm. Quantification of quercetin and its glucosides was performed using a five-point calibration curve of a quercetin dihydrate, Q-3, Q-4' and Q-3,4' standards at concentrations between 0.5 and 25 μg ml⁻¹. Each vial taken to analysis had a total volume of 500 μl.

Environmental impact assessment

The global warming potential (GWP) and primary energy consumption for the new and a traditional extraction method were assessed from a gate-to-gate perspective.^{16,30} The calculations are based on a functional unit of 10 g of quercetin. The new, subcritical water extraction method is described by Turner *et al.*³ (see Subcritical water extraction, above), while the enzymatic reaction method is described in this study (see Enzymatic hydrolysis of onion extract, above). The traditional method using methanol extraction and HCl-catalysed hydrolysis (80 °C for 2 h) is described by Hertog *et al.*⁷ and Nuutila *et al.*⁸ Extractions were scaled up linearly to produce 10 g of quercetin. The dry matter content in onion is around 13.5% and the quercetin content in onion is, on average, 13 mg g⁻¹ dry matter, varying between 7 and 25 mg g⁻¹ (see Table 5).³

Energy demand is calculated for heating and heat losses during extraction according to Welty *et al.*³¹ Extraction is set to be carried out in vessels of stainless steel insulated with mineral wool. Production of extraction equipment and generation of pressure are not considered in this study. A natural gas burner with 60% efficiency is set to be used for heating. Emissions due to

Table 5 Data for the extraction methods both producing 10 g of quercetin. Traditional method: 80 °C for 2 h. New method: extraction at 120 °C for 15 min and biocatalysis at 95 °C for 5 min. Ranges of values are in brackets

Extraction method	Onion/kg	Amount of solvent/kg	Amount of catalyst/kg	Total volume (dm ³)
Traditional method	5.7 (3.0–10.6)	Methanol: 31 (16–56)	HCl: 3.2 (1.7–5.9)	87 (41–150)
New method	5.7 (3.0–10.6)	Water: 13 (6.5–23)	Enzyme: 0.003 (0.002–0.006)	21 (9.4–33)

production and combustion of natural gas are from Uppenberg *et al.*³² The environmental impact of water is assumed to be insignificant.

Conclusions

In this paper, we have developed analytical methods to study the kinetics of a thermostable β -glucosidase (wt *TnBgl1A*), and a mutant of the same enzyme (*TnBgl1A_N221S*) towards Q-3 and Q-4'. We have also developed an off-line biocatalysis method, in which the hydrolysis of all quercetin glucosides present in yellow onion extract is completed within 5 min at 95 °C using only 3 nmol of enzyme per 1.3 μ mol of quercetin species. This study shows that *TnBgl1A_N221S* has higher activity towards both Q-3 and Q-4' compared to the wt *TnBgl1A*, *i.e.* a mutation of residue 221 at the +2 binding site of the enzyme does significantly affect substrate affinity, but this effect is higher for the Q-3 substrate. Another conclusion that can be drawn is that deactivation is significant at 95 °C, and to avoid this, the temperatures should be kept below 95 °C, if reactions are more than a few minutes long. To increase the hydrolysis rate of quercetin glucosides, addition of glucose can be considered. Future aspects include immobilisation of *TnBgl1A_N221S* onto a support material allowing recycling of the enzyme, and the use of an on-line flow system of hot water extraction and enzymatic hydrolysis of quercetin and quercetin glucosides from yellow onion waste and other potential by-products and waste. The immobilisation of the enzymes may also improve the thermostability of the enzymes.

From an environmental point of view, extraction with subcritical water followed by an enzymatic hydrolysis is to be preferred regarding primary energy consumption and global warming potential. Shorter extraction time and smaller volumes makes the process more energy-efficient, although a higher temperature and pressure have to be generated. Furthermore, avoiding the use of organic solvents from fossil origin, such as methanol, makes the subcritical water extraction more resource efficient and favourable from a greenhouse gas perspective. Handling of large quantities of toxic chemicals, such as HCl and methanol, is also avoided.

Abbreviations

Q	Quercetin
Q-3	Quercetin-3-glucoside
Q-4'	Quercetin-4'-glucoside
Q-3,4'	Quercetin-3,4'-diglucoside
pNPG	p-Nitrophenyl- β -D-glucopyranoside
pNP	p-Nitrophenol
BSA	Bovine serum albumin
GWP	Global warming potential
LCA	Life cycle assessment
I-4'	Isorhamnetin-4'-glucoside
I-3,4'	Isorhamnetin-3,4'-diglucoside
IPTG	Isopropyl-1-thio- β -D-galactopyranoside
dw	Dry weight
DPPH	2,2-Diphenyl-1-picrylhydrazyl
RSD	Relative standard deviation
IMAC	Immobilised metal-ion affinity chromatography

wt	Wild type
T_m	Transition temperature
GH1	Glycoside hydrolase family 1

Acknowledgements

The Swedish Research Council for Environment, Agricultural Sciences and Spatial Planning (FORMAS, 2006-1346); the Swedish Research Council (VR, 2006-4084 and 2006-6048); the Swedish International Development Cooperation Agency (SIDA, SWE-2005-473); the Swedish Foundation for Strategic Research (SSF, 2005 : 0073/13) and the Foundation for Strategic Environmental Research (MISTRA, Greenchem) are greatly acknowledged.

References

- 1 A. Schieber, F. C. Stintzing and R. Carle, *Trends Food Sci. Technol.*, 2001, **12**, 401–413.
- 2 M. G. L. Hertog, P. C. H. Hollman and M. B. Katan, *J. Agric. Food Chem.*, 1992, **40**, 2379–2383.
- 3 C. Turner, P. Turner, G. Jacobson, K. Almgren, M. Waldeback, P. Sjöberg, E. N. Karlsson and K. E. Markides, *Green Chem.*, 2006, **8**, 949–959.
- 4 A. Murakami, H. Ashida and J. Terao, *Cancer Lett.*, 2008, **269**, 315–325.
- 5 K. Ono, T. Hamaguchi, H. Naiki and M. Yamada, *Biochim. Biophys. Acta, Mol. Basis Dis.*, 2006, **1762**, 575–586.
- 6 K. R. Price and M. J. C. Rhodes, *J. Sci. Food Agric.*, 1997, **74**, 331–339.
- 7 M. G. L. Hertog, P. C. H. Hollman and D. P. Venema, *J. Agric. Food Chem.*, 1992, **40**, 1591–1598.
- 8 A. M. Nuutila, K. Kammiovirta and K. M. Oksman-Caldentey, *Food Chem.*, 2002, **76**, 519–525.
- 9 S. H. Hakkinen, S. O. Karenlampi, I. M. Heinonen, H. M. Mykkanen and A. R. Torronen, *J. Sci. Food Agric.*, 1998, **77**, 543–551.
- 10 J. B. Harborne, *Phytochemistry*, 1965, **4**, 107–120.
- 11 Y. K. Do, J. M. Kim, S. M. Chang, J. H. Hwang and W. S. Kim, in *International Conference on Biorefinery*, Elsevier Science Bv, Beijing, JAPAN, 2007, pp. 173–178.
- 12 F. Siewek and R. Galensa, *J. Chromatogr., A*, 1984, **294**, 385–389.
- 13 N. Lambert, P. A. Kroon, C. B. Faulds, G. W. Plumb, W. R. McLauchlan, A. J. Day and G. Williamson, *Biochim. Biophys. Acta, Protein Struct. Mol. Enzymol.*, 1999, **1435**, 110–116.
- 14 E. Ibanez, A. Kubatova, F. J. Senorans, S. Cavero, G. Reglero and S. B. Hawthorne, *J. Agric. Food Chem.*, 2003, **51**, 375–382.
- 15 K. Hartonen, K. Inkala, M. Kangas and M. L. Riekkola, *J. Chromatogr., A*, 1997, **785**, 219–226.
- 16 A. Azapagic, *Handbook of Green Chemistry and Technology*, Blackwell Science, Oxford, 2002, 62–85.
- 17 I. S. Organization, *Environmental management - Life cycle assesment - Requirements and guidelines*, ISO 14044, 2006.
- 18 S. Khan, T. Pozzo, C. Paul, S. Lindahl, C. Turner, and E. Nordberg Karlsson, 2009, unpublished work.
- 19 J. G. Berrin, W. R. McLauchlan, P. Needs, G. Williamson, A. Puigserver, P. A. Kroon and N. Juge, *Eur. J. Biochem.*, 2002, **269**, 249–258.
- 20 R. M. Wright, M. D. Yablonsky, Z. P. Shalita, A. K. Goyal and D. E. Eveleigh, *Appl. Environ. Microbiol.*, 1992, **58**, 3455–3465.
- 21 D. A. Yernool, J. K. McCarthy, D. E. Eveleigh and J. D. Bok, *J. Bacteriol.*, 2000, **182**, 5172–5179.
- 22 J. A. Perezpons, X. Rebordosa and E. Querol, *Biochim. Biophys. Acta, Protein Struct. Mol. Enzymol.*, 1995, **1251**, 145–153.
- 23 Å. Furnander, *Life Cycle Assessment of Dimethyl Ether as a Motor Fuel*, Chalmers University of Technology, Gothenburg, 1996.
- 24 I. Boustead, *Eco-Profiles of the European Plastic Industry - Hydrogen Chloride*, PlasticEurope - Association of Plastics Manufacturers, 2005.

-
- 25 P. H. Nielsen, K. M. Oxenboll and H. Wenzel, *Int. J. Life Cycle Assess.*, 2007, **12**, 432–438.
- 26 M. Abou-Hachem, F. Olsson and E. N. Karlsson, *Extremophiles*, 2003, **7**, 483–491.
- 27 P. Turner, D. Svensson, P. Adlercreutz and E. N. Karlsson, *J. Biotechnol.*, 2007, **130**, 67–74.
- 28 U. K. Laemmli, *Nature*, 1970, **227**, 680–685.
- 29 P. Turner, A. Pramhed, E. Kanders, M. Hedstrom, E. N. Karlsson and D. T. Logan, *Acta Crystallogr., Sect. F: Struct. Biol. Cryst. Commun.*, 2007, **63**, 802–806.
- 30 A. E. V. Petersson, L. M. Gustafsson, M. Nordblad, P. Borjesson, B. Mattiasson and P. Adlercreutz, *Green Chem.*, 2005, **7**, 837–843.
- 31 J. R. Welty, C. H. Wicks, R. E. Wilson and G. Rorrer, *Fundamentals of momentum, Heat and Mass Transfer*, John Wiley & Sons, Inc., 2001, 201–218.
- 32 S. Uppenberg, M. Almemark, M. Brandel, L.-G. Lindfors, H.-O. Marcus, H. Stripple, A. Wachtmeister and L. Zetterberg, *Miljöfaktabok för Bränslen Del 2*, IVL Swedish Environmental Research Institute Ltd., 2001.

A simple approach to reduce the environmental impact of olefin metathesis reactions: a green and renewable solvent compared to solvent-free reactions

Manuela Kniese^a and Michael A. R. Meier^{*a,b}

Received 24th June 2009, Accepted 8th October 2009

First published as an Advance Article on the web 5th November 2009

DOI: 10.1039/b921126h

Two widely-studied olefin metathesis reactions, the cross-metathesis of allyl benzene with *cis*-1,4-diacetoxy-2-butene and the ring closing metathesis of diethyl diallylmalonate, were studied under environmentally more benign reaction conditions. All studied catalysts allowed these reactions to be performed under bulk conditions, thus avoiding large amounts of solvent waste. Moreover, methyl decanoate, a fatty acid-derived, and thus renewable and non-toxic, solvent, was shown to be an environmentally friendly alternative solvent to the usually applied dichloromethane. Most interestingly, only the reactions performed under bulk conditions allowed a 25-fold catalyst loading reduction, thus offering the “greenest” alternative of the investigated reaction conditions.

Introduction

Since the development and continuous improvement of well defined, highly active and functional group-tolerant ruthenium based catalysts,^{1–11} olefin metathesis has found manifold possible applications in organic and polymer synthesis.^{12–16}

More recently, many methods for the reduction of the environmental impact of olefin metathesis reactions were reported in the literature. For instance, supported catalysts that facilitate catalyst removal and recycling were often reported.¹⁷ Similarly, procedures for the removal of homogenous catalysts from the reaction mixture are being developed.¹⁷ However, since the catalyst is not the only parameter that can influence the environmental impact of a reaction, many reports are available that describe olefin metathesis in alternative solvents. Most often, homogeneously-catalyzed metathesis reactions are carried out in dichloromethane (and, less frequently, in aromatic solvents) at high dilutions. Current investigations focus on the use of ionic liquids,^{18,19} water,²⁰ other environmentally friendly solvents,²¹ and supercritical fluids^{22,23} for olefin metathesis reactions. All of these investigations claim the use of less toxic solvents and/or an easier recycling of the catalyst as environmental advantages. However, it should be mentioned here that a certain solvent should not generally be considered as “green”, since all process parameters have to be carefully evaluated and compared (*e.g.* by using environmental factors) to each other before such a statement can be made.

Although the use of ruthenium based metathesis initiators under bulk conditions is a standard procedure for acyclic diene metathesis (ADMET) polymerization and, in some cases, for

ring-opening metathesis polymerization (ROMP), very little has been reported on olefin metathesis reactions to yield defined low molecular weight organic compounds under solvent-free conditions. In 2002, Grubbs *et al.* reported a solvent free cross-metathesis procedure for the synthesis of trisubstituted olefins.²⁴ Practically, a non-dimerizing cross-metathesis reaction partner, isobutylene or 2-methyl-2-butene in this case, was used in excess and acted as solvent for these reactions, allowing a 5-fold catalyst loading reduction (from 5 to 1%). Along the same lines, we observed that low catalyst loadings of 0.1–1% were sufficient for the quite challenging cross-metathesis reactions of allyl chloride²⁵ and methyl acrylate²⁶ with fatty acid derivatives under bulk conditions to yield renewable monomers for step-growth polymerizations. Here, an excess of allyl chloride or methyl acrylate also acted practically as the solvent, but it is important to note that these reactions did not proceed well when performed in dichloromethane or other organic solvents. Moreover, a solvent-free ring-closing metathesis procedure under microwave conditions with 1% of catalyst that provided quantitative conversions in many cases was recently reported.²⁷ Despite these promising observations, no detailed studies on the performance of ruthenium-based metathesis initiators under bulk conditions is available.

With the aim of reducing the environmental impact of the reaction conditions commonly applied in olefin metathesis reactions, we investigated the use of a fatty acid-derived (and thus renewable) solvent, as well as solvent-free conditions, in detail for two commonly-studied metathesis reactions with three frequently-studied highly active second generation catalysts (see Fig. 1). The studied reactions were the cross-metathesis (CM) of allyl benzene with *cis*-1,4-diacetoxy-2-butene and the ring closing metathesis (RCM) of diethyl diallylmalonate (see Fig. 2), since both reactions were suggested by Grubbs *et al.* as standard reactions for the evaluation of a new catalyst.²⁸ However, here we used these widely-studied reactions to evaluate and compare more environmentally friendly reaction conditions.

^aUniversity of Applied Sciences Oldenburg/Ostfriesland/Wilhelmshaven, Constantiaplatz 4, 26723, Emden, Germany

^bUniversity of Potsdam, Institute of Chemistry, Karl-Liebknecht-Str. 24–25, 14476, Golm, Germany. E-mail: michael.meier@uni-potsdam.de; Web: www.meier-michael.com

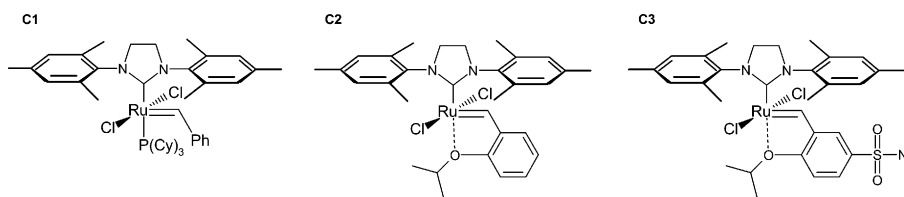


Fig. 1 Investigated second generation catalysts.

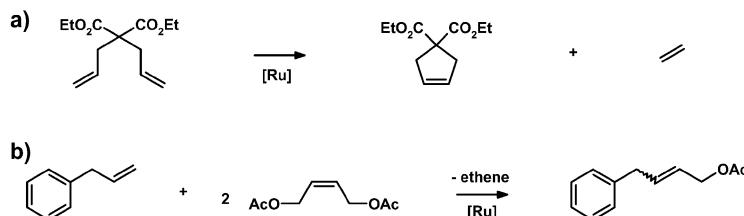


Fig. 2 Investigated metathesis reactions: (a) ring-closing metathesis of diethyl diallylmalonate; (b) cross-metathesis of allyl benzene with *cis*-1,4-diacetoxy-2-butene.

Results and discussion

We studied the CM of allyl benzene with *cis*-1,4-diacetoxy-2-butene and the RCM of diethyl diallylmalonate under bulk conditions and in a renewable and non-toxic solvent with the aim of reducing the environmental impact of metathesis reactions. Our findings were then compared to the conventionally-applied reaction conditions, e.g. reaction in the toxic solvent dichloromethane at high dilution.

In the case of the ring closing metathesis of diethyl diallylmalonate, Grubbs *et al.* suggested performing the reaction at a concentration of 0.1 mol L⁻¹ in dichloromethane (DCM) with a catalyst loading of 1% at 30 °C.²⁸ These conditions were suggested to test and evaluate new catalysts. We used these conditions as a starting point and as a reference for our target to minimize the environmental impact of olefin metathesis reactions. Thus, we performed this reaction in methyl decanoate (MD) and in bulk under otherwise unchanged conditions with catalysts **C1–C3**.

All reactions were performed in triplicate and the averaged results of these investigations are provided in Table 1. The

Table 1 Results of the RCM of diethyldiallyl malonate ($T = 30\text{ }^{\circ}\text{C}$, $t = 60\text{ min}$, reactions performed in triplicate; averaged results are given) using standard conditions with different solvents

Catalyst	Catalyst loading/mol% ^a	Solvent ^b	C/% ^c
C1	1.0	DCM	97.8
C1	1.0	MD	79.3
C1	1.0	none	88.1
C2	1.0	DCM	95.9
C2	1.0	MD	66.4
C2	1.0	none	99.5
C3	1.0	DCM	99.6
C3	1.0	MD	71.5
C3	1.0	none	99.4

^a Amount of catalyst in mol% relative to diethyldiallyl malonate.

^b DCM: dichloromethane ([diethyldiallyl malonate] = 0.1 mol L⁻¹); MD: methyl decanoate ([diethyldiallyl malonate] = 0.1 mol L⁻¹); none: reaction performed in bulk ([diethyldiallyl malonate] = 4.136 mol L⁻¹).

^c Conversion of diethyldiallyl malonate (by GC-MS).

reproducibility of these reactions was good (<3% standard deviation). Only the reactions performed in MD showed somewhat larger deviations (up to 5%). It is obvious that all investigated catalysts were able to catalyze the reaction, as expected and reported many times in the literature. The standard conditions at high dilution in DCM with 1% catalyst loading resulted in almost full conversion for all catalysts. MD gives somewhat poorer results for all catalysts and at all catalyst loadings, if compared to the reactions in DCM. Therefore, MD is generally suitable as a solvent for this RCM reaction, but somewhat less than DCM, if high conversions are desired. Nevertheless, the choice of MD can offer significant environmental benefits. More interestingly, with the exception of **C1**, the solvent-free conditions also show full conversions and thus offer an environmentally friendly alternative to the reactions performed in solvent.

In order to further reduce the environmental impact of these reactions, we investigated a 5-fold reduction in catalyst loading to 0.2 mol% (Table 2). We were pleased to still observe good to excellent results under these conditions in all solvent systems. Once more, the reactions performed in MD showed somewhat poorer results for all catalysts. However, the solvent-free reactions provided an advantage here, since the observed conversions remained high and were higher than in DCM in all cases.

Since diethyl diallylmalonate is an α,ω -diene one might expect ADMET as a side reaction, especially under these highly concentrated conditions. However, we did not observe the formation of oligomers or even polymers by GPC, ruling out this side reaction. Therefore, the RCM reactions with 0.2% of **C2** and **C3** avoid 46 L of toxic DCM per kg of obtained product without loss of catalyst activity. Inspired by these findings, we tried to reduce the loading of **C2** and **C3** even further to 0.04 mol%. **C2** was somewhat less active under these conditions than **C3**. Generally, this catalyst loading reduction resulted in decreased conversions, but **C3** remained highly active under bulk conditions. This is a very interesting and promising result, since not only does it save 46 L of DCM per kg of product, but also the amount of potentially toxic and expensive

Table 2 Results of the RCM of diethylallyl malonate ($T = 30\text{ }^{\circ}\text{C}$, $t = 60\text{ min}$, reactions performed in triplicate; averaged results are given) at reduced catalyst loadings

Catalyst	Catalyst loading/mol% ^a	Solvent ^b	C/% ^c
C1	0.2	DCM	76.4
C1	0.2	MD	60.8
C1	0.2	none	81.5
C2	0.2	DCM	86.5
C2	0.04	DCM	62.4
C2	0.2	MD	49.9
C2	0.2	none	99.4
C2	0.04	none	15.9
C3	0.2	DCM	94.9
C3	0.04	DCM	76.5
C3	0.2	MD	66.0
C3	0.2	none	99.6
C3	0.04	none	97.0

^a Amount of catalyst in mol% relative to diethylallyl malonate. ^b DCM: dichloromethane ([diethylallyl malonate] = 0.1 mol L^{-1}); MD: methyl decanoate ([diethylallyl malonate] = 0.1 mol L^{-1}); none: reaction performed in bulk ([diethylallyl malonate] = 4.136 mol L^{-1}). ^c Conversion of diethylallyl malonate (by GC-MS).

catalyst can be reduced at least 25-fold, compared to the classic literature conditions. Quite interestingly, the bulk reactions with low catalyst loadings showed a better reproducibility than the corresponding reactions in solvent, which is an additional advantage.

In order to evaluate if the above findings are only applicable to the investigated RCM reaction, or if they can be transferred to other metathesis reactions, we investigated the cross-metathesis of allyl benzene with *cis*-1,4-diacetoxy-2-butene in a similar set of experiments (see Table 3). Again, for these reactions, we used the reaction conditions suggested by Grubbs *et al.* as the starting point for our investigations: catalyst concentration of 2.5 mol%, 0.2 M allyl benzene in dichloromethane, 2 equivalents of *cis*-1,4-diacetoxy-2-butene, $25\text{ }^{\circ}\text{C}$.²⁸ In order to be able to compare the obtained results to the RCM reaction described above, we changed the concentration of allyl benzene to 0.1 M and left all other parameters unchanged. Starting from these conditions, we tested methyl decanoate and solventless reactions in a similar way as described above (Table 3). Under all reaction conditions,

Table 3 Results of the CM of allyl benzene with *cis*-1,4-diacetoxy-2-butene ($T = 25\text{ }^{\circ}\text{C}$, $t = 180\text{ min}$, reactions performed in triplicate; averaged results are given) using standard conditions with different solvents

Catalyst	Catalyst loading/mol% ^a	Solvent ^b	C/% ^c
C1	2.5	DCM	86.6
C1	2.5	MD	94.8
C1	2.5	none	85.8
C2	2.5	DCM	90.6
C2	2.5	MD	91.2
C2	2.5	none	90.6
C3	2.5	DCM	91.7
C3	2.5	MD	89.7
C3	2.5	none	90.2

^a Amount of catalyst in mol% relative to allyl benzene. ^b DCM: dichloromethane ([allyl benzene] = 0.1 mol L^{-1}); MD: methyl decanoate ([allyl benzene] = 0.1 mol L^{-1}); none: reaction performed in bulk ([allyl benzene] = 2.216 mol L^{-1}). ^c Conversion of allyl benzene (by GC)

Table 4 Results of the CM of allyl benzene with *cis*-1,4-diacetoxy-2-butene ($T = 25\text{ }^{\circ}\text{C}$, $t = 180\text{ min}$, reactions performed in triplicate; averaged results are given) at reduced catalyst loadings

Catalyst	Catalyst loading/mol% ^a	Solvent ^b	C/% ^c
C1	0.5	DCM	63.6
C1	0.5	MD	78.6
C1	0.5	none	81.9
C1	0.1	none	54.8
C2	0.5	DCM	87.7
C2	0.1	DCM	14.9
C2	0.5	MD	72.2
C2	0.5	none	88.4
C2	0.1	none	84.7
C3	0.5	DCM	71.7
C3	0.5	MD	79.7
C3	0.1	MD	35.9
C3	0.5	none	89.4
C3	0.1	none	81.8

^a amount of catalyst in mol% relative to allyl benzene; ^b DCM: dichloromethane ([allyl benzene] = 0.1 mol L^{-1}); MD: methyl decanoate ([allyl benzene] = 0.1 mol L^{-1}); none: reaction performed in bulk ([allyl benzene] = 2.216 mol L^{-1}); ^c Conversion of allyl benzene in % (by GC)

the observed formation of the allyl benzene self-metathesis product was below 1% and thus we will neglect this side-reaction in further discussions. The reproducibility was also good for these reactions ($< 3\%$ standard deviation). In contrast to the RCM reaction described above, MD is a very suitable solvent for this CM reaction for all catalysts and provides nearly full conversions of allyl benzene, similar to the reactions performed in DCM and in bulk. Thus, either an environmentally friendly and renewable solvent can be used for this reaction, or solvent-free conditions that avoid solvent waste completely may be chosen without losing catalyst activity.

Similar to the RCM reaction described above, a reduction in catalyst loadings led to decreased conversions (Table 4). This effect was more pronounced for solvent reactions than for the bulk reactions. Moreover, MD gives good results for all catalysts and all catalyst loadings, comparable to, and sometimes better than, the corresponding reactions in DCM. However, the solvent-free reaction conditions show the highest conversions for all catalysts and at all catalyst loadings. A further 5-fold reduction in catalyst loading was then attempted with all systems that provided conversions higher than 80% with a catalyst loading of 0.5%. These results are also presented in Table 4. A 25-fold reduction in catalyst loading while still maintaining high conversions was only possible under bulk conditions. These results clearly show that the most environmentally benign reaction conditions are once more the solvent-free conditions.

The *E*:*Z* ratio of the formed product was $\sim 9:1$, quite independent of the reaction conditions. The only exceptions were the reactions at high dilution and low catalyst loading in solvent, where the *E*:*Z* ratio was $\sim 4:1$. These observations are probably due to a deactivation of the catalyst, which is also in accordance with the low observed conversions under these reaction conditions (data not presented in Table 4). If the catalyst is deactivated, it cannot perform secondary metathesis reactions, which would equilibrate the product to the more stable *E* isomer.²⁸ Moreover, the *E*:*Z* ratio of the bulk reactions with C2 and C3 was again $\sim 9:1$, which is in agreement with the

high observed conversions for these reactions and, thus, the remaining high catalyst activity.

In summary, solvent-free conditions for this metathesis reaction also allowed for a straightforward 25-fold reduction of the amount of catalysts **C2** and **C3**. Moreover, MD was even better suited for this reaction than DCM and can provide a green alternative reaction medium, in case a solvent is required for the reaction. Furthermore, the solvent-free reactions showed significantly higher reproducibility, even at very low catalyst loadings.

Conclusions

The conclusions of these investigations are manifold. Most importantly, metathesis reactions in methyl decanoate and solvent-free metathesis reactions offer environmentally friendly alternatives to the commonly applied solvent dichloromethane. This finding seems to be of a general nature, but this has to be confirmed with different metathesis reactions in the future. In particular, the solvent free reaction conditions offer the most sustainable alternative by avoiding large amounts of solvent waste without losing catalyst activity. Along the same lines, only the bulk conditions allowed a straightforward 25-fold reduction of the amount of metathesis catalyst for both investigated metathesis reactions. This is not only interesting in terms of green chemistry, because large amounts of potentially toxic transition metal can be avoided, but also in terms of process economics, because the catalyst is by far the most expensive component of these reactions.

Experimental

Materials

Decanoic acid (Cognis, Edenor C10, 98%), methanol (VWR, 99%), sulfuric acid (Fluka, 95-97%), allylbenzene (Aldrich, 98%), *cis*-1,4-diacetoxy-2-butene (Aldrich, 95%), diethyl diallylmalonate (Aldrich, 98%), dichloromethane (Riedel-de Häen, 99.8%), tetradecane (Fluka, ≥99%), decane (Fluka, ≥99.8%), ethyl vinyl ether (Aldrich, 99%), tetrahydrofuran (Sigma, ≥99%), (1,3-*bis*-(2,4,6-trimethylphenyl)-2-imidazolidinylidene)-dichloro(*o*-isopropoxyphenyl-methylene)ruthenium (**C2**, Aldrich), benzylidene[1,3-*bis*-(2,4,6-trimethylphenyl)-2-imidazolidinylidene] dichloro (tricyclohexylphosphine) ruthenium (**C1**, Aldrich), and 1,3-*bis*-(2,4,6-trimethylphenyl)-4,5-dihydroimidazol-2-ylidene[2-(*i*-propoxy)-5-(*N,N*-dimethylaminosulfonyl)phenyl]methyleneruthenium(II)dichloride (**C3**, ABCR, 96%) were used as received. Methyl decanoate was prepared by esterification with methanol from the corresponding decanoic acid according to standard laboratory procedures.

Analytical equipment and methods. Thin layer chromatography (TLC) was performed on silica gel TLC-cards (layer thickness 0.20 mm, Fluka). Compounds were visualized by permanganate reagent. For column chromatography, silica gel 60 (0.035–0.070 mm, Fluka) was used.

¹H NMR spectra were recorded in CDCl₃ on a Bruker AVANCE DPX spectrometer operating at 300 (75.5) MHz. Chemical shifts (δ) are reported in parts per million relative to the internal standard tetramethylsilane (TMS, $\delta = 0.00$ ppm).

Analytical GC characterization of reaction mixtures was carried out with a Shimadzu GC-2010 equipped with a fused silica capillary column (Stabilwax®, 30 m × 0.25 mm × 0.25 μ m, Restek), using flame ionization detection. The oven temperature program was: initial temperature 50 °C, hold for 5 min, ramp at 10 °C min⁻¹ to 250 °C, hold for 5 min (total analysis time: 30 min, cross-metathesis of allylbenzene with *cis*-1,4-diacetoxy-2-butene). Measurements were performed in the split–split mode (split ratio 45:1) using hydrogen as the carrier gas (linear velocity of 31.4 cm s⁻¹ at 220 °C).

GC-MS (EI) chromatograms were recorded using a VARIAN 3900 GC instrument with a capillary column FactorFour™ VF-5ms (30 m × 0.25 mm × 0.25 μ m, Varian) and a Saturn 2100T ion trap mass detector. Scans were performed from 40 to 650 *m/z* at rate of 1.0 scan s⁻¹. The oven temperature program was: initial temperature 95 °C, hold for 1 min, ramp at 10 °C min⁻¹ to 200 °C, hold for 3 min (total analysis time: 14.5 min, ring-closing metathesis of diethyl diallylmalonate). The injector transfer line temperature was set to 250 °C. Measurements were performed in the splitless and split–split modes (split ratio 50:1) using helium as the carrier gas (flow rate 1.0 ml min⁻¹).

Mass spectra (ESI) were recorded on a VARIAN 500-MS ion trap mass spectrometer with the TurboDDST™ option installed. Samples were introduced by direct infusion with a syringe pump. Nitrogen served both as the nebulizer gas and the drying gas. Helium served as the cooling gas for the ion trap and collision gas for MSⁿ. Nitrogen was generated by a nitrogen generator Nitrox from Domnick Hunter.

Gel permeation chromatograms were measured on a SEC system LC-20A from Shimadzu equipped with a SIL-20A autosampler, PLgel 5 μ m MIXED-D column (Polymer Laboratories, 300 mm × 7.5 mm), and a RID-10A refractive index detector in THF (flow rate 1 ml min⁻¹) at 50 °C. All determinations of molar mass were performed relative to poly(methylmethacrylate) standards (Polymer Standards Service, *M_p* 102–981.000 Da).

Cross-metathesis reaction (general procedure). In a typical experiment, allylbenzene and *cis*-1,4-diacetoxy-2-butene were mixed at a molar ratio of 1:2 and dichloromethane or methyl decanoate was added in different amounts. Some experiments were also performed in bulk, without the addition of solvent. Reactions were carried out in parallel using a carousel reaction station™ RR98072 (Radleys Discovery Technologies, UK) under stirring at 25 °C. The solid catalyst (**C1–C3**) was then added to the solution, in the quantities of 0.1, 0.5 and 2.5 mol% of the educt allylbenzene. All reactions were carried out without a nitrogen atmosphere. Samples were taken periodically and quenched with an excess of ethyl vinyl ether in order to stop the metathesis reaction. Tetradecane was used as an internal standard in the samples with solvent and decane as external standards in the solvent-free samples for GC analysis. After this procedure, a conversion and composition analysis was performed by GC. For isolation of the cross-metathesis product, this procedure was performed with 1.175 ml (1.05 g, 0.0089 mol) allylbenzene, 2.828 ml (3.05 g, 0.018 mol) *cis*-1,4-diacetoxy-2-butene and 0.1627 g (2.5 mol %) of **C3**. The reaction mixture was stirred magnetically at 25 °C. After 25 h reaction time the compound was purified by column chromatography

on silica with a mixture of hexane and diethyl ether (1:10) as eluent.

4-Phenylbut-2-enyl acetate. MS (ESI-positive, CH₃OH, *m/z*): 213.1 (MNa⁺, calc. 213.1). ¹H NMR (300 MHz, CDCl₃): δ = 7.29–7.17 (m, 5H, C₆H₅), 5.91 (m, 1H, –CH=CH–), 5.62 (m, 1H, –CH=CH–), 4.54 (d, 2H, –CH₂–O–CO–), 3.39 (d, 2H, C₆H₅–CH₂–), 2.05 (s, 3H, –O–CO–CH₃).

Ring-closing metathesis reaction (general procedure). In a typical experiment, diethyl diallylmalonate and dichloromethane or methyl decanoate as solvent were mixed in different concentrations. Some experiments were also performed in bulk, without the addition of solvent. Reactions were carried out in parallel using a carousel reaction stationTM RR98072 (Radleys Discovery Technologies, UK) under stirring at 30 °C. The solid catalyst (C1–C3) was then added to the solution in the quantities of 0.04, 0.2 and 1.0 mol%. All reactions were carried out without a nitrogen atmosphere. Tetradecane was used as external standard for GC-MS analysis. Samples were taken periodically and quenched with an excess of ethyl vinyl ether in order to stop the ring-closing metathesis reaction. After this procedure, a conversion and composition analysis was performed by GC-MS. For isolation of the ring-closing metathesis product, this procedure was performed with 4 ml (3.98 g, 0.017 mol) diethyl diallylmalonate and 0.1037 g (1 mol %) of C2. The reaction mixture was stirred magnetically at 30 °C. After 25 h reaction time the compound was purified by column chromatography on silica with a mixture of hexane and diethyl ether (1:1) as eluate.

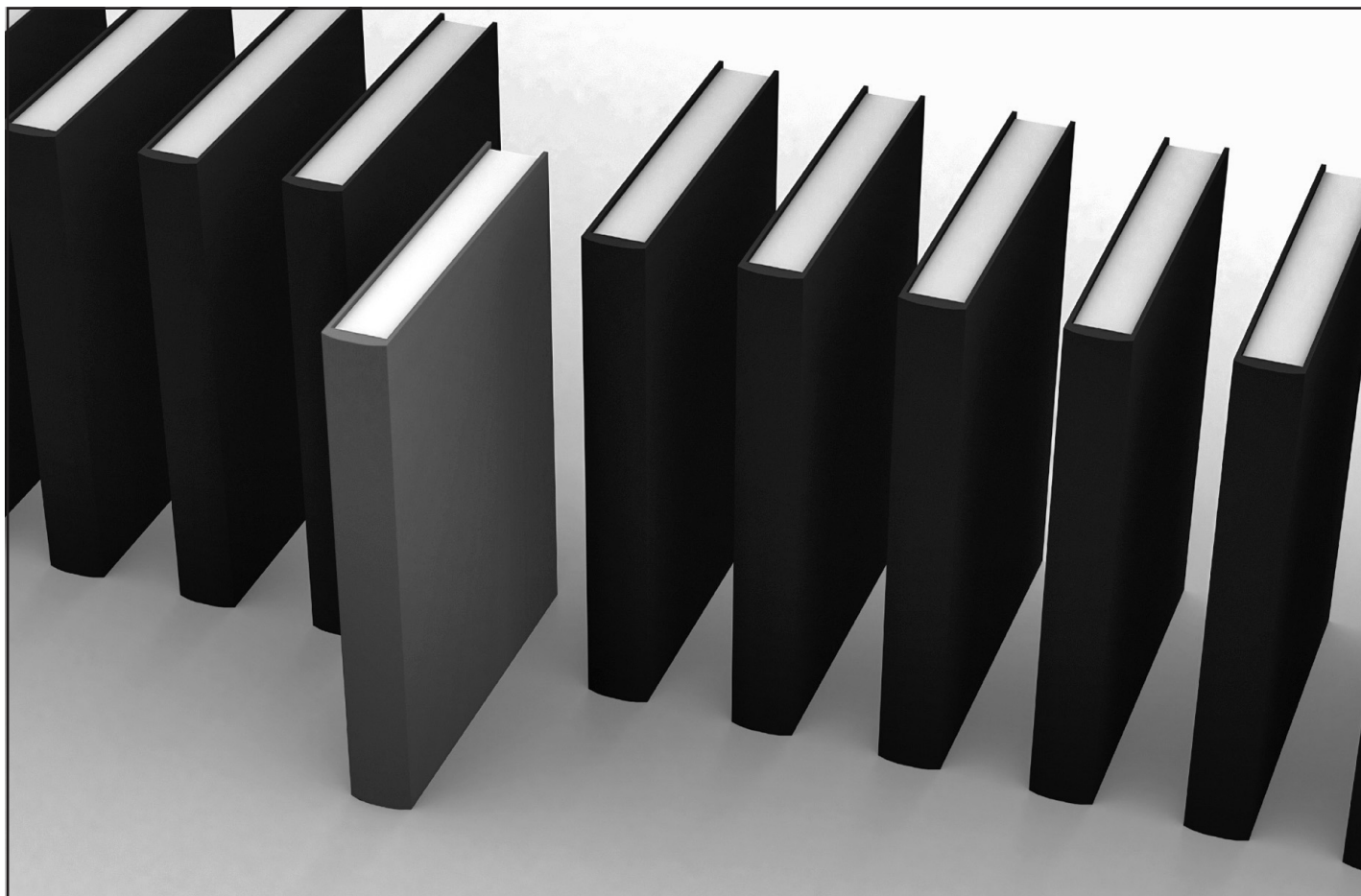
Diethyl cyclopent-3-ene-1,1-dicarboxylate. GC-MS (EI, *m/z*): 212.8 (M⁺, calc. 212.2). ¹H NMR (300 MHz, CDCl₃): δ = 5.60 (m, 2H, –CH₂–CH=CH–CH₂–), 4.20 (q, 4H, 2× –CO–O–CH₂–CH₃), 3.01 (d, 4H, –CH₂–CH=CH–CH₂–), 1.26 (t, 6H, 2× –CO–O–CH₂–CH₃).

Acknowledgements

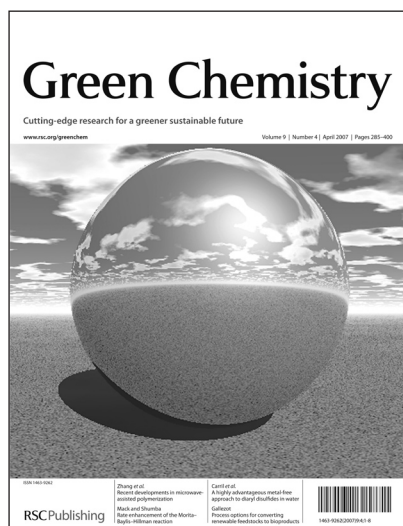
This project was partially financed by the German Federal Ministry of Food, Agriculture and Consumer Protection (represented by the Fachagentur nachwachsende Rohstoffe; FKZ 22026905). The authors thank the University of Oldenburg (Germany) for access to NMR facilities.

Notes and references

- S. T. Nguyen, L. K. Johnson, R. H. Grubbs and J. W. Ziller, *J. Am. Chem. Soc.*, 1992, **114**, 3974–3975.
- P. Schwab, R. H. Grubbs and J. W. Ziller, *J. Am. Chem. Soc.*, 1996, **118**, 100–110.
- P. Schwab, M. B. France, J. W. Ziller and R. H. Grubbs, *Angew. Chem., Int. Ed. Engl.*, 1995, **34**, 2039–2041.
- T. Weskamp, W. C. Schattenmann, M. Spiegler and W. A. Herrmann, *Angew. Chem., Int. Ed.*, 1998, **37**, 2490–2493.
- J. Huang, E. D. Stevens, S. P. Nolan and J. L. Peterson, *J. Am. Chem. Soc.*, 1999, **121**, 2674–2678.
- J. Huang, H.-J. Schanz, E. D. Stevens and S. P. Nolan, *Organometallics*, 1999, **18**, 5375–5380.
- L. Ackermann, A. Fürstner, T. Weskamp, F. J. Kohl and W. A. Herrmann, *Tetrahedron Lett.*, 1999, **40**, 4787–4790.
- T. Weskamp, F. J. Kohl, W. Hieringer, D. Gleich and W. A. Herrmann, *Angew. Chem., Int. Ed.*, 1999, **38**, 2416–2419.
- M. Scholl, S. Ding, C. W. Lee and R. H. Grubbs, *Org. Lett.*, 1999, **1**, 953–956.
- M. Scholl, T. M. Trnka, J. P. Morgan and R. H. Grubbs, *Tetrahedron Lett.*, 1999, **40**, 2247–2250.
- S. B. Garber, J. S. Kingsbury, B. L. Gray and A. H. Hoveyda, *J. Am. Chem. Soc.*, 2000, **122**, 8168–8179.
- A. Fürstner, *Angew. Chem., Int. Ed.*, 2000, **39**, 3012–3043.
- S. J. Connon and S. Blechert, *Angew. Chem., Int. Ed.*, 2003, **42**, 1900–1923.
- B. M. Novak, W. Risse and R. H. Grubbs, *Adv. Polym. Sci.*, 1992, **102**, 47–72.
- C. Slugovc, *Macromol. Rapid Commun.*, 2004, **25**, 1283–1297.
- T. W. Baughman and K. B. Wagener, *Adv. Polym. Sci.*, 2005, **176**, 1–42.
- H. Clavier, K. Grela, A. Kirschning, M. Mauduit and S. P. Nolan, *Angew. Chem., Int. Ed.*, 2007, **46**, 6786–6801.
- D. Sémeril, H. Olivier-Bourbigou, C. Bruneau and P. H. Dixneuf, *Chem. Commun.*, 2002, 146–147.
- Q. Yao and Y. Zhang, *Angew. Chem., Int. Ed.*, 2003, **42**, 3395–3398.
- D. Burtscher and K. Grela, *Angew. Chem., Int. Ed.*, 2009, **48**, 442–454.
- X. Miao, C. Fischmeister, C. Bruneau and P. H. Dixneuf, *ChemSusChem*, 2008, **1**, 813–816.
- A. Fürstner, L. Ackermann, K. Beck, H. Hori, D. Koch, K. Langemann, M. Liebl, C. Six and W. Leitner, *J. Am. Chem. Soc.*, 2001, **123**, 9000–9006.
- F. Michalek, D. Mäde, J. Rühle and W. Bannwarth, *Eur. J. Org. Chem.*, 2006, 577–581.
- A. K. Chatterjee, D. P. Sanders and R. H. Grubbs, *Org. Lett.*, 2002, **4**, 1939–1942.
- T. Jacobs, A. Rybak and M. A. R. Meier, *Appl. Catal., A*, 2009, **353**, 32–35.
- A. Rybak and M. A. R. Meier, *Green Chem.*, 2007, **9**, 1356–1361.
- G. V. Thanh and A. Loupy, *Tetrahedron Lett.*, 2003, **44**, 9091–9094.
- T. Ritter, A. Hejl, A. G. Wenzel, T. W. Funk and R. H. Grubbs, *Organometallics*, 2006, **25**, 5740–5745.



'Green Chemistry book of choice'



Why not take advantage of free book chapters from the RSC? Through our 'Green Chemistry book of choice' scheme *Green Chemistry* will regularly highlight a book from the RSC eBook Collection relevant to your research interests. Read the latest chapter today by visiting the *Green Chemistry* website.

The RSC eBook Collection offers:

- Over 900 new and existing books
- Fully searchable
- Unlimited access

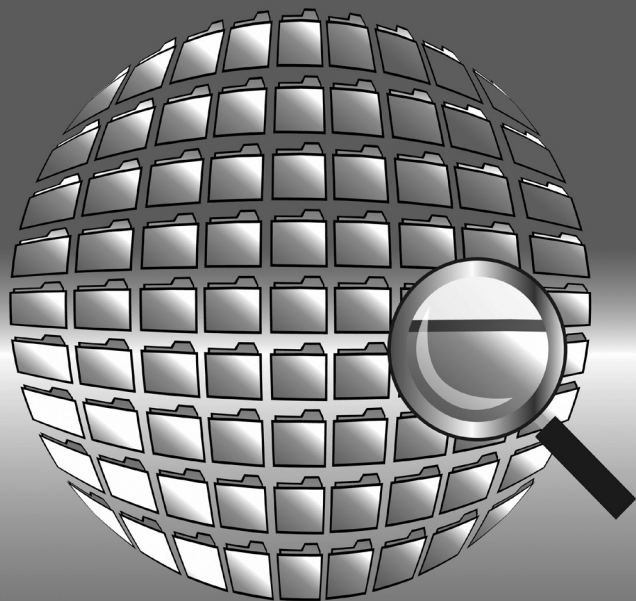
Why not take a look today? Go online to find out more!

RSC Publishing

www.rsc.org/greenchem

Registered Charity Number 207890

RSC Database and Current Awareness Products



- Abstracted from high quality sources
- Easy to use search functions
- Clearly displayed results
- Spanning the chemical sciences

for quick and easy searching

Graphical Databases

present search results in both text and graphical form. Titles include *Catalysts & Catalysed Reactions*, *Methods in Organic Synthesis* and *Natural Product Updates*.

Specialist Databases

review both academic and industrial literature on a wide range of hard to reach and unique information. Titles include *Chemical Hazards in Industry* and *Laboratory Hazards Bulletin*.

Analytical Abstracts

is the first stop for analytical scientists. Offering coverage on all areas of analytical and bioanalytical science. With a fresh new look, including improved search and results features, *Analytical Abstracts* offers an excellent online service.

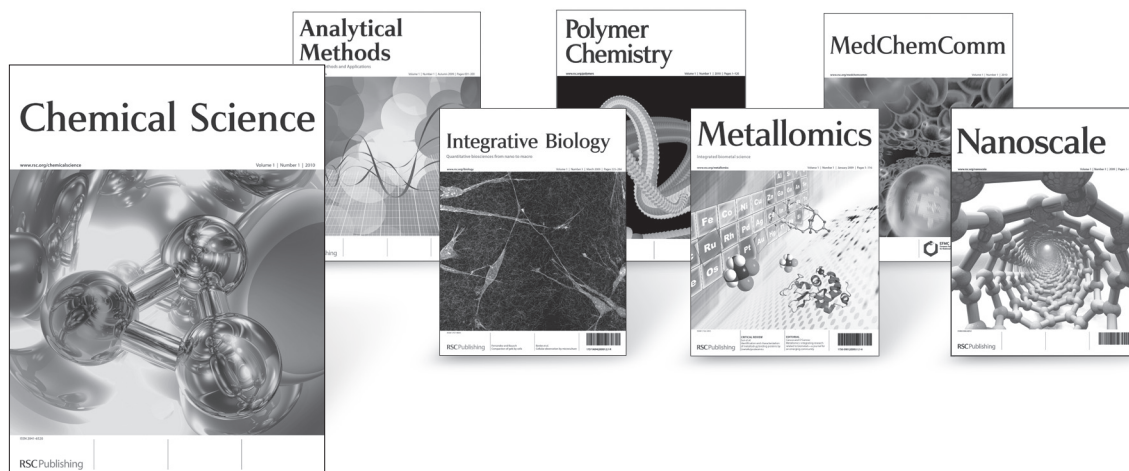
Find out more at

RSC Publishing

www.rsc.org/databases

Registered Charity Number 207890

Top science ...free institutional access



New for 2010

Chemical Science - a new journal presenting findings of exceptional significance from across the chemical sciences. www.rsc.org/chemicalscience

MedChemComm - focusing on medicinal chemistry research, including new studies related to biologically-active chemical or biochemical entities that can act as pharmacological agents with therapeutic potential or relevance. www.rsc.org/medchemcomm

Polymer Chemistry - publishing advances in polymer chemistry covering all aspects of synthetic and biological macromolecules, and related emerging areas. www.rsc.org/polymers

New for 2009

Analytical Methods - highlights new and improved methods for the practical application of analytical science. This monthly journal will communicate research in the advancement of analytical techniques for use by the wider scientific community. www.rsc.org/methods

Integrative Biology - focusing on quantitative multi-scale biology using enabling technologies and tools to exploit the convergence of biology with physics, chemistry, engineering, imaging and informatics. www.rsc.org/ibiology

Metallomics - covering the research fields related to metals in biological, environmental and clinical systems. www.rsc.org/metallomics

Nanoscale - publishing experimental and theoretical work across the breadth of nanoscience and nanotechnology. www.rsc.org/nanoscale

Free institutional access, managed by IP address, is available on all these titles. For more details, and to register, visit www.rsc.org/free_access_registration

For the highest impact – publish in Photochemical & Photobiological Sciences

The official journal of the European Photochemistry Association, the European Society for Photobiology, the Asia and Oceania Society for Photobiology and the Korean Society of Photoscience.

Photochemical & Photobiological Sciences (PPS) publishes high quality research on all aspects of photochemistry and photobiology, including elemental photochemical and photophysical processes, the interaction of light with living systems, environmental photochemistry, environmental photobiology, the use of light as a reagent, how light affects health, the use of light as a diagnostic tool and for curative purposes and areas in which light is a cost-effective catalyst.

PPS provides:

- High visibility with an impact factor of 2.144*
- Fast publication times
- RSC Manuscript Central submission system
- No page charges and free colour where it enhances the article

PPS has a strong themed issue programme, with contributions from key people in the relevant fields. Recent themed issues include:

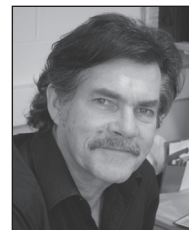
- Microscopy beyond imaging: space-resolved photochemistry and photobiology
- Photosynthesis from molecular perspectives – towards future energy production
- Issue dedicated to Professor NJ Turro

PPS publishes high impact research, recent papers include:

- Triplet-relaxation microscopy with bunched pulsed excitation by G Donnert, C Eggeling and SW Hell
- Mimicking the antenna system of green plants by G Calzaferri and K Lutkouskaya
- Time-resolved fluorescence microscopy by K Suhling, PNW French and D Phillips
- Effects of solar UV radiation on aquatic ecosystems and interactions with climate change by DP Hader, HD Kumar, RC Smith *et al.*
- Milestones in the development of photodynamic therapy and fluorescence diagnosis by A Juzeniene, Q Peng and J Moan
- Combining intracellular and secreted bioluminescent reporter proteins for multicolor cell-based assays by E Micheli, L Cevenini, L Mezzanotte *et al.*

*2008 Thomas Scientific (ISI) Journal Citation Reports

Editors-in-chief:



Rex Tyrrell
Bath, UK
Photobiology Editor



Frans De Schryver
Leuven, Belgium
Photochemistry Editor



060978

RSC Publishing



www.rsc.org/pps

Registered Charity Number 207890



Top Quality Bioscience Journals

Molecular BioSystems - a journal with a focus on the interface between chemistry and the -omic sciences and systems biology. www.molecularbiosystems.org

Organic & Biomolecular Chemistry - an international journal covering the breadth of synthetic, physical and biomolecular chemistry. www.rsc.org/obc

Natural Product Reports (NPR) - a critical review journal which stimulates progress in all areas of natural products research. www.rsc.org/npr

Photochemical & Photobiological Sciences - publishing high quality research on all aspects of photochemistry and photobiology, encouraging synergism between the two areas. www.rsc.org/pps

NEW for 2010

MedChemComm - focusing on medicinal chemistry research, including new studies related to biologically-active chemical or biochemical entities that can act as pharmacological agents with therapeutic potential or relevance. www.rsc.org/medchemcomm

NEW for 2009

Integrative Biology - a journal focusing on quantitative multi-scale biology using enabling technologies and tools to exploit the convergence of biology with physics, chemistry, engineering, imaging and informatics. www.rsc.org/ibiology

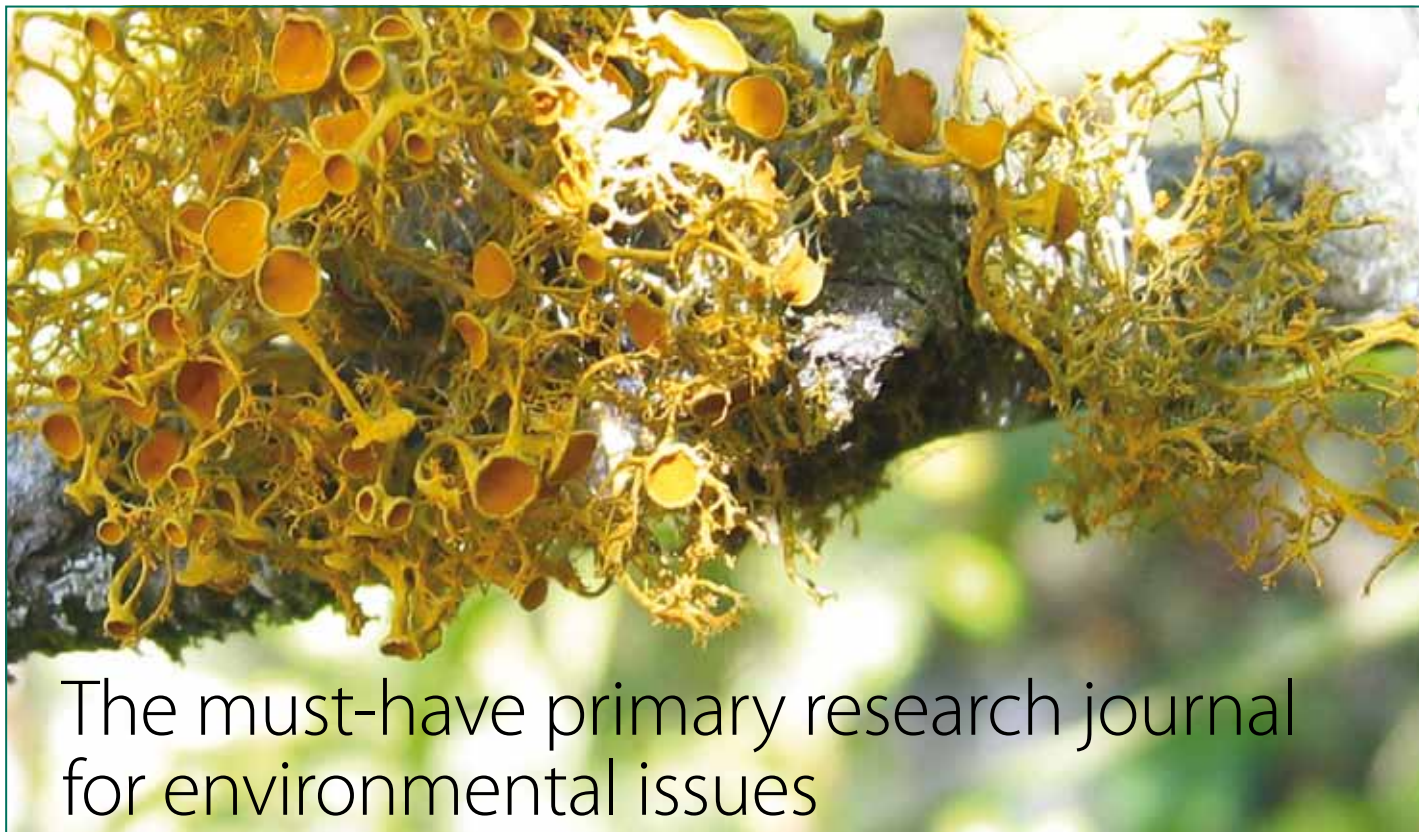
Metallomics - a journal covering the research fields related to metals in biological, environmental and clinical systems. www.rsc.org/metallomics

Take a look today!

RSC Publishing

www.rsc.org/journals

Registered Charity Number 207890



The must-have primary research journal for environmental issues

Comprehensive and high quality coverage of multidisciplinary, international research relating to the measurement, pathways, impact and management of contaminants in all environments.



- Impact factor: 1.99[†]
- Highly visible and cited in MEDLINE
- Dedicated to the measurement of natural and anthropogenic sources of pollution, with an insight into environmental processes and impacts

Submit your work to JEM today

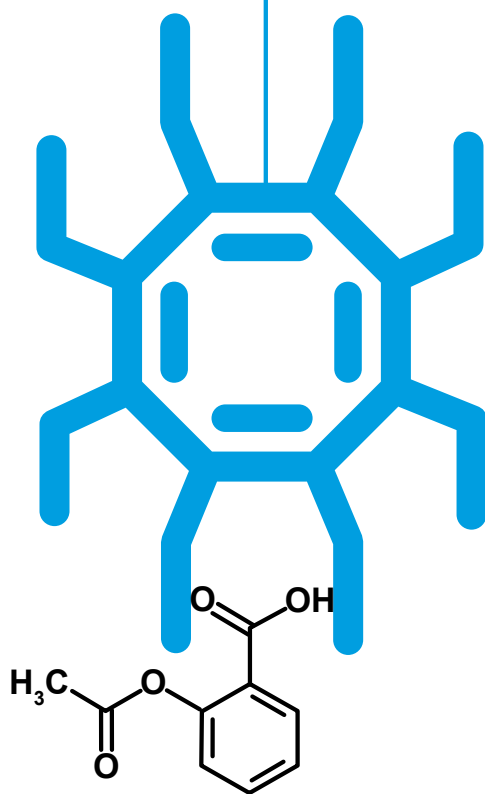
[†]2008 Thompson Scientific (ISI) Journal Citation Reports

RSC Publishing

www.rsc.org/jem

Registered Charity Number 207890

New adventures on the web



ChemSpider is a free online, structure centric community for chemists, providing fast access to millions of unique chemical entities, resources and information and the opportunity to collaborate with a world wide community of scientists. Rapidly becoming the richest single source of structure based chemistry information online, ChemSpider is a ground breaking initiative now supported by the RSC, the most innovative of chemical societies.

www.chemspider.com